Equilibrium and Non-Equilibrium Thermodynamics of Natural Gas Processing

Measurement and Modelling of Absorption of Carbon Dioxide
into Methyldiethanolamine Solutions at High Pressures

by

Even Solbraa

A Thesis Submitted for the Degree
of

Doktor Ingeniør

Norwegian University of Science and Technology
Department of Refrigeration and Air Conditioning

December 2002

Abstract

The objective of this work has been to study equilibrium and non-equilibrium situations during high pressure gas processing operations with emphasis on utilization of the high reservoir pressure. The well stream pressures of some of the condensate and gas fields in the North Sea are well above 200 bar. Currently the gas is expanded to a specified processing condition, typically 40-70 bar, before it is recompressed to the transportation conditions. It would be a considerable environmental and economic advantage to be able to process the natural gas at the well stream pressure. Knowledge of thermodynamic- and kinetic properties of natural gas systems at high pressures is needed to be able to design new high pressure process equipment.

Nowadays, reactive absorption into a methyldiethanolamine (MDEA) solution in a packed bed is a frequently used method to perform acid gas treating. The carbon dioxide removal process on the Sleipner field in the North Sea uses an aqueous MDEA solution and the operation pressure is about 100 bar. The planed carbon dioxide removal process for the Snøhvit field in the Barents Sea is the use of an activated MDEA solution.

The aim of this work has been to study high-pressure effects related to the removal of carbon dioxide from natural gas. Both modelling and experimental work on high-pressure non-equilibrium situations in gas processing operations have been done.

Few experimental measurements of mass transfer in high pressure fluid systems have been published. In this work a wetted wall column that can operate at pressures up to 200 bar was designed and constructed. The wetted wall column is a pipe made of stainless steel where the liquid is distributed as a thin liquid film on the inner pipewall while the gas flows co- or concurrent in the centre of the pipe. The experiments can be carried out with a well-defined interphase area and with relatively simple fluid mechanics. In this way we are able to isolate the effects we want to study in a simple and effective way.

Experiments where carbon dioxide was absorbed into water and MDEA solutions were performed at pressures up to 150 bar and at temperatures 25 and 40°C. Nitrogen was used as an inert gas in all experiments.

A general non-equilibrium simulation program (NeqSim) has been developed. The simulation program was implemented in the object-oriented programming language Java. Effort was taken to find an optimal object-oriented design. Despite the increasing popularity of object-oriented programming languages such as Java and C++, few publications have discussed how to implement thermodynamic and fluid mechanic models. A design for implementation of thermodynamic, mass transfer and fluid mechanic calculations in an object-oriented framework is presented in this work.

NeqSim is based on rigorous thermodynamic and fluid mechanic models. Parameter fitting routines are implemented in the simulation tool and thermodynamic-, mass transfer- and fluid mechanic models were fitted to public available experimental data.

Two electrolyte equations of state were developed and implemented in the computer code. The electrolyte equations of state were used to model the thermodynamic properties of the fluid systems considered in this work (non-electrolyte, electrolyte and weak-electrolyte systems).

i

The first electrolyte equation of state (electrolyte ScRK-EOS) was based on a model previously developed by Furst and Renon (1993). The molecular part of the equation was based on a cubic equation of state (Scwarzentruber et.al. (1989)'s modification of the Redlich-Kwong EOS) with the Huron-Vidal mixing rule. Three ionic terms were added to this equation – a short-range ionic term, a long-range ionic term (MSA) and a Born term. The thermodynamic model has the advantage that it reduces to a standard cubic equation of state if no ions are present in the solution, and that public available interaction parameters used in the Huron-Vidal mixing rule could be utilized. The originality of this electrolyte equation of state is the use of the Huron-Vidal mixing rule and the addition of a Born term. Compared to electrolyte models based on equations for the gibbs excess energy, the electrolyte equation of state has the advantage that the extrapolation to higher pressures and solubility calculations of supercritical components is less cumbersome. The electrolyte equation of state was able to correlate and predict equilibrium properties of CO_2-MDEA-water solutions with a good precision. It was also able to correlate high pressure data of systems of methane-CO_2-MDEA and water.

The second thermodynamic model (electrolyte CPA-EOS) evaluated in this work is a model where the molecular interactions are modelled with the CPA (cubic plus association) equation of state (Kontogeorgios et.al., 1999) with a classical one-parameter Van der Walls mixing rule. This model has the advantage that few binary interaction parameters have to be used (even for non-ideal solutions), and that its extrapolation capability to higher pressures is expected to be good. In the CPA model the same ionic terms are used as in the electrolyte ScRK-EOS.

A general non-equilibrium two-fluid model was implemented in the simulation program developed in this work. The heat- and mass-transfer calculations were done using an advanced multicomponent mass transfer model based on non-equilibrium thermodynamics. The mass transfer model is flexible and able to simulate many types of non-equilibrium processes we find in the petroleum industry. A model for reactive mass transfer using enhancement factors was implemented for the calculation of mass transfer of CO_2 into amine solutions. The mass transfer model was fitted to the available mass transfer data found in the open literature.

The simulation program was used to analyse and perform parameter fitting to the high pressure experimental data obtained during this work. The mathematical models used in NeqSim were capable of representing the experimental data of this work with a good precision. From the experimental and modelling work done, we could conclude that the mass transfer model regressed to pure low-pressure data also was able to represent the high-pressure mass transfer data with an acceptable precision. Thus the extrapolation capability of the model to high pressures was good.

For a given partial pressure of CO_2 in the natural gas, calculations show a decreased CO_2 capturing capacity of aqueous MDEA solutions at increased natural gas system pressure. A reduction up to 40% (at 200 bar) compared to low pressure capacity is estimated. The pressure effects can be modelled correctly by using suitable thermodynamic models for the liquid and gas. In a practical situation, the partial pressure of CO_2 in the natural gas will be proportional to the total pressure. In these situations, it is shown that the CO_2 capturing capacity of the MDEA solution will be increased at rising total pressures up to 200 bar. However, the increased capacity is not as large as we would expect from the higher CO_2 partial pressure in the gas.

The reaction kinetics of CO_2 with MDEA is shown to be relatively unaffected by the total pressure when nitrogen is used as inert gas. It is however important that the effects of thermodynamic and kinetic non- ideality in the gas and liquid phase are modelled in a consistent way.

Using the simulation program NeqSim – some selected high-pressure non-equilibrium processes (e.g. absorption, pipe flow) have been studied. It is demonstrated that the model is capable of simulating equilibrium- and non-equilibrium processes important to the process- and petroleum industry.

Preface

This work was accomplished at the Department of Refrigeration and Air- Conditioning at the Norwegian University of Science and Technology (NTNU). The study started in November 1998 and ended in June 2002 and was financed by Statoil ASA and the Norwegian Research Council. My primary supervisor has been professor Ole Jørgen Nydal from the Department of Refrigeration and Air Conditioning at NTNU. My two other supervisors have been professor Geir Owren from the Department of Refrigeration and Air Conditioning at NTNU and Dr. Arne Fredheim from Statoil Research Centre.

I would like to express my thankfulness to all my supervisors for their support and helpfulness throughout this challenging and exciting period.

I'm very thankful to Kirsti Tangvik, Inger-Marie Malvik, Bjørn Magnus Berg and Sigbjørn Svenes from Statoil Research Centre for their helpfulness and good leadership during my years at Statoil. Their active support of my work has inspired me and made me feel that I was working on something useful and important.

I would like to thank Stig Jørgensen, Øyvind Olsen, Geir Kojedal and Arnfinn Killingberg for all help with the design and for carrying out the mechanical work on the experimental equipment. A big thank to Toril Haugum for helping me doing gas chromatography work.

Further thanks are due to my fellow Ph.D students and colleges at NTNU for making this department an interesting place to spend time. Thanks to the administrative people at the department of refrigeration and air-conditioning for helping with the administrative work during these years.

Finally, thanks to Solveig and my family for always supporting me in my work.

Trondheim, December 2002

Even Solbraa

Table of Contents

Nomenclature

Latin letters

a	Activity	-
A	Area	m^2
a	Vector of Fitted Parameters eq. (7.9)	-
A	Atom Element Matrix	-
a	Attractive Term in Equation of State	Jm^3/mol
A	Chemical Affinity eq. (4.10)	-
A	Debye Huckel Parameter eq. (3.83)	-
a	Effective Packing Area	m^2/m^3
A	Helmholtz Energy	J
B	Ion Pair Interaction Parameter eq. (3.87)	-
b	Repulsive Term in Equation of State	m^3/mol
c	Molar Concentration	mol/m^3
cov	Covariance eq. (7.19)	-
corr	Correlation eq. (7.20)	-
D	Dielectric Constant	-
D	Effective/Ficks Diffusion Coefficient	m^2/sec
$Ð$	Maxwell Stefan Diffusion Coefficient	m^2/sec
d	Molecular Drag eq. (4.23)	-
d	Nominal Packing Diameter	m
d	Pipe Diameter	m
e	Electron Charge (1.60219·10^{-19})	C
E	Enhancement Factor eq. (4.38)	-
E	Reaction Activation Energy	J/mol
f	Fanning Friction Factor	-
F	Faraday Constant (96484.6)	C/mol
F	Force Vector	N/m^3
f	fugacity	bar
F	Reduced Residual Helmholtz Energy	-
g	CPA-Radial Distribution Function	-
G	Gibbs Energy	J
g	Gravity (9.81)	m/sec^2
H	Enthalpy	J
h	Heat Transfer Coefficient	J/m^{2}sec
Ha	Hatta Number eq. (4.78)	-
I	Ionic Strength eq. (3.82)	-
J	Flux Vector	mol/m^{2}sec
j	Mass Flux	kg/m^{2}sek
J	Molar Flux	mol/m^{2}sek
k	Boltzman's Constant (1.38066·10^{-23})	J/K
K	Chemical Equilibrium Constant	-
k	Interaction Parameter in EOS	-
k	Mass Transfer Coefficient	m/sec
k	Reaction Rate Constant	kcal/mol
$\not{k}$	Maxwell Stefan Mass Transfer Coefficient	m/sec
L	Onsager Coefficient eq. (4.17)	-
m	Mass Transfer Rate	kg/msec

m	Molality	mol/liter
M	Molecular Weight	kg/mol
N	Avagadro Constant ($6.02205 \cdot 10^{23}$)	1/mol
n	Mol Number Vector	-
N	Mole Numbers	mol
N	Total Molar Mass Transfer	mol/m^{2}sec
P	Pressure	Pa
P	Probability eq. (7.3)	-
Q	Heat Flux From Surroundings	-
q	Heat Flux	J/m^{2}sec
Q	Heat Transfer	J
Q	Incomplete Gamma Function eq. (7.6)	-
q	Ionic Charge	C
r	Reaction rate	mol/m^{3}sec
R	Universal Gas Constant	J/Kmol
Re	Reynolds Number	-
S	Contact Length	-
S	Entropy	J/K
Sc	Schidmt Number	-
Sh	Sherwood Number	-
St	Stanton Number eq. (4.47)	-
T	Temperature	K
U	Heat Transfer Coefficient eq. (5.13)	W/m^{2}sec
U	Internal Energy	J
U	Pair Interaction Potential eq. (3.92)	-
u	Velocity Vector	m/sec
u	Velocity	m/sec
V	Volume	m^3
$\overline{V}$	Molar Volume	m^3/mol
W	Electrolyte Interaction Parameter eq. (3.97)	-
W	Work	J
x	Liquid Mol Fraction	-
X	Mole Fraction used in CPA-EOS	-
y	Gas Mol Fraction	-
Z	Compressibility Factor	-
z	Ionic Charge Number (eg. +1 for Na$^+$)	-
z	Mol Fraction Based on Total System	-

Greek letters

ω	Acentric Factor	-
γ	Activity Coefficient	-
μ	Chemical Potential	J/mol
ε	CPA Energy Parameter	-
ρ	Density	kg/m^3
ε	Electric Permitivity	-
ε	Surface Roughness	m
π	Pi (3.14159)	-
ϕ	Electrical Potential	V

ε	Electrolyte EOS Parameter eq. (3.98)	-
α	Electrolyte MSA Parameter	-
Γ	Electrolyte Shielding Parameter	-
σ	Entropy Production Rate eq. (4.19)	
σ	Standard Deviation	-
δ	Film Thickness eq. (4.36)	m
Ξ	Finite Flux Correction Factor eq. (4.52)	
φ	Fugacity Coefficient eq. (3.13)	-
ω	Mass Fraction	-
Φ	Molar Flux Correction Factor eq. (4.57)	
σ	Molecular/Ionic Diameter	m
Γ	Non-Ideality Correction Factor eq. (4.27)	-
λ	Pitzer Binary Ionic Interaction Coefficient	-
λ	Ionic Parameter in Electrolyte EOS eq.(8.14)	-
Λ	Pitzer Ternary Ionic Interaction Coefficient	-
α	NRTL Non-Randomness Parameter	-
α	Phase Fraction	-
τ	NRTL Energy Parameter	-
Φ	Osmotic Coefficient	-
Π	Viscous Force Tensor	-
α	Correction for the a parameter	-
Δ	CPA-parameter	-
Δ	Delta	-
ν	Stochiometric Coefficient	-
τ	Shear Force	N/m^2
χ^2	Chi-Square eq. (7.5)	-

Subscripts

a	Anion
c	Cation
c	Critical Value
i,j,k	Index
i	Interface
w	Wall
g	Gas
l	Liquid
P	Constant Pressure
s	Solvent
surr/s	Surroundings
q	Heat
h	Hydraulic
T	Constant Temperature
w	Water
$\pm$	Mean Ionic
sur	Surroundings
r	Reduced Value
2t, 2	Second Order

xiii

ideal, seg, chain, assoc	Ideal Gas, Segregation, Chain Formation, Association
SR	Short Range
LR	Long Range

Superscripts

1,2	Phase Number
IG	Ideal Gas
r	Residual
∞	Infinite
E	Excess
V	Vapour
L	Liquid
*	Equilibrium State

1 Introduction

The removal of acid gases from gas streams, commonly referred to as acid gas treating, and also gas sweetening, is an important industrial process. Acid gasses are removed from natural gas before it is transported as sales-gas to the customer. This is done to achieve the specification on the sales-gas, and to obtain a price as high as possible. In some cases it is necessary to remove acid gases upstream to prevent corrosion of transport pipelines and process equipment. The two most common acid gases are carbon dioxide (CO_2) and hydrogen sulfide (H_2S).

Hydrogen sulfide or carbon dioxide concentrations in the gas streams vary widely, from several parts per million to 50 percent by volume of the gas stream. Cleanup specifications also vary widely depending on the process and nature of the impurity.

The primary operation of acid gas treating process generally falls into one of three categories (Kohl and Nielsen, 1997): absorption into a liquid, adsorption on a solid and chemical conversion to another compound. This work falls under the category of absorption into a liquid.

Today's conventional technology for acid gas removal operates at pressures between 40-70 bar. The transportation pressures in the sub-sea gas pipelines in the North Sea are up to about 200 bar. This means that after processing of the well stream gas (dew point control and acid gas treating), the gas has to be recompressed before it is sent into the transport pipelines. The recompression work is considerable.

The well stream pressures of some of the Norwegian condensate and gas fields are well above 200 bar. Currently the gas is expanded to a specified processing condition before it is recompressed to the transportation conditions. It would be an important environmental and economic advantage to be able to process the natural gas at well stream pressures. The savings in both process equipment-costs and energy consumption would be considerable.

In 1998 the national Norwegian oil company, Statoil, initiated a research programme on high pressure gas processing (dew point control and acid gas treating). Statoil's goal is to be able to process and transport their natural gas at as high pressure as possible. This means that most of the gas processing should be done at pressures up to 200 bar. As part of this research programme three ph.d works related to high pressure gas processing were started. Two of these ph.d works were related to removal the of carbon dioxide from natural gas at high pressures: one on equilibrium thermodynamics of carbon dioxide in solvents used for gas treating (Addicks, 2002), and another one on non-equilibrium thermodynamics during high pressure removal of carbon dioxide (this work). The third ph.d work was related to high-pressure adsorption processes (Christiansen, 2001).

Today, computer-aided process simulation is nearly universally recognized as an essential tool in the chemical process industries. Indeed, simulation software plays a key role in: process development – to study process alternatives, assess feasibility and preliminary economics, and interpret pilot-plant data; process design to optimise hardware and flow-sheets, estimate equipment and operating costs, and investigate feedstock flexibility; and plant operation- to reduce energy use, increase yield and improve pollution control.

1

Simulation programs have traditionally been used as design tools (together with experience and rules of thumb) in the design of new acid gas processing equipment. Today's process simulation programs are often based on low-pressure experimental data, and very often on simple empirical models. The extrapolation capability of such models to higher operation pressures is questionable. To be able to rely on the results from such simulation programs, the mathematical models (thermodynamics, kinetics, fluid mechanics) have to be validated against reliable experimental data at operational conditions. Few experimental data are reported in the literature at pressures higher than 100 bar. The results from this work will hopefully lessen this gap.

1.1 Topic of Thesis

This thesis presents results from experimental, theoretical and modelling work on mass transfer in high-pressure fluid systems (up to 200 bar). The experimental and theoretical investigations presented in this thesis are related to the removal of CO_2 at well stream conditions into aqueous methyldiethanoleamine solutions (weak electrolyte solution).

During the period 1998-2002 the author has developed a general non-equilibrium simulation computer program. The mass transfer models used in this program are based on the high-pressure experimental data obtained in this work.

1.1.1 Experimental Work on High Pressure Mass Transfer

Experimental investigation of mass transfer and kinetics during absorption of CO_2 into a chemical solvent (MDEA) was done at pressures between 50 and 150 bar and at temperatures 25 and 40 °C. A custom-made high-pressure wetted wall column was designed and fabricated in connection with this research.

High-pressure equilibrium data for methane-CO_2-MDEA-water systems were measured in a separate study (Addicks, 2002) related to this work. The thermodynamic model developed in this work is fitted to these high-pressure equilibrium data.

1.1.2 Modelling of Equilibrium and Non-Equilibrium Processes

For non-ideal liquids containing electrolytes, Gibbs Excess energy models have traditionally been used to calculate thermodynamic properties of the liquid phase. Such GE-models are developed for low-pressure systems, but are often used at higher pressures by the introduction of a pointing correction. The use of such models for high-pressure calculation is cumbersome.

Furst and Renon (1993) and Chunxi and Furst (2000) suggested using an electrolyte equation of state for the calculation of thermodynamic properties of acid gas solutions. Such a model is much more suited to use for high-pressure equilibrium- and solubility calculations of inert gas components. The model is expected to have good extrapolation capabilities to high pressures and temperatures.

In this work a new electrolyte equation of state, based on the model of Furst and Renon (1993), has been developed. The model has been used to predict the osmotic and activity coefficient of water–salt systems, as well as for the weak electrolyte system CO_2, MDEA and water.

A general multicomponent, non-equilibrium two fluid model for the calculation of mass transfer in high-pressure gas processing operations is proposed and implemented in a computer program called NeqSim. The non-equilibrium model is based on the assumption that the resistance to mass transfer is limited to the gas and liquid film near the interface (two-film-model), and assumes local equilibrium at the gas-liquid interface. Multicomponent molecular interactions are corrected for in both the liquid and gas film using the Maxwell-Stefan theories. Chemical reactions in the liquid film are accounted for using enhancement factors. The analytical equations used to calculate enhancement factors are fitted to the experimental data obtained in this work.

A general parameter-fitting model was developed to perform regression to the experimental data available. The parameters used in the thermodynamic model implemented in this study were regressed to available solubility data of carbon dioxide in MDEA-water solutions. The mass transfer model was regressed to available non-equilibrium data. The model was checked and fitted to the high-pressure experimental data obtained in this work.

An experimental database for published experimental thermodynamic and physical properties data has been created for CO_2, MDEA and water systems. The thermodynamic and physical properties models developed and implemented in this work have been fitted to these data.

1.1.3 Main Contributions

- New experimental equipment used to measure mass transfer and reaction kinetics at pressures up to 200 bar and under controllable conditions was designed and constructed. The equipment is unique because of the possibility of the high operation pressure.
- New experimental high-pressure mass transfer data for CO_2 in MDEA-water solutions are provided. The presented experimental data are unique because they are measured at pressures up to 150 bar.
- An electrolyte equation of state developed by other workers, Furst and Renon (1993), is extended and used to model the thermodynamic properties and the solubility of CO_2 in MDEA-water solutions. The model gives accurate results for the calculation of solubility of CO_2 and methane in the liquid phase.
- An electrolyte equation of state based on the CPA-EOS was developed and used to model thermodynamic properties of aqueous salt solutions.
- A general non-equilibrium model has been developed and implemented in a computer program called NeqSim. The simulation program can be used to predict non-equilibrium mass transfer processes in high-pressure process equipment.

1.2 Structure of the Thesis

This thesis is divided into a theory/model development section and a section related to the experimental data and data regression. A short description of the chapters of the thesis is presented below:

Chapter 1
Introduction – a short introduction to the work that has been done

Chapter 2-5
Theoretical review and new modelling

Chapter 6
Introduction to the non-equilibrium simulator NeqSim

Chapter 7-10
Experimental results and parameter regression

Chapter 11
Case studies. Simulation of non-equilibrium processes using NeqSim

Chapter 12
Summary and Conclusions

Many of the figures you will find in this thesis have been created using the simulator NeqSim. NeqSim simulations are executed through scripts written in a scripting language (Python). The scripts used to generate the data/figures are given in appendix G and the name of the corresponding script is given in the text under each figure. The reader can download NeqSim from the web (http://www.stud.ntnu.no/~solbraa/neqsim), and recreate the figures and data easily. An introduction to NeqSim is given in chapter 6 and a manual can be downloaded from the web page.

Performing process simulation calculations typically involves a lot of mathematical models. These models can be thermodynamic-, physical property-, non-equilibrium- or fluid mechanics models. When we fit parameters to a mass transfer model or a fluid mechanic model – we typically need to rely on a thermodynamic and physical property model. It is important to notice that when we fit parameters to a new model – the parameters will be strictly valid only in combination with the other models used. In this work the parameter fitting has been done in all models (thermodynamic, physical properties, mass transfer and fluid mechanics). It is important to note that an error in one of the fundamental models – would give an error when fitting parameters in models that are based on this model.

The experimental work presented in this thesis has earlier been presented at the AICHE Annual Meeting 2000 in Los Angeles (Solbraa et.al, 2000) and at the IGRC conference 2001 in Amsterdam (Solbraa et.al., 2001). An article on thermodynamic modelling of electrolyte solutions, based on the electrolyte equations of states implemented in this work, is being prepared.

2 Natural Gas Processing

The processing of natural gas consists of the separation of some of the components present at the well exit, such as water, acid gases and heavy hydrocarbons, to adjust the gas to transport or commercial specifications.

The distribution of these operations between the field and the delivery point is dictated by economic considerations. It is usually preferable to conduct on the production site operations that make the gas transportable.

The natural gas chain can be divided into separation, transport and distribution. An introduction to important operations in the gas chain is given by Rojey et.al.(1997). The first processing step separates the liquid fractions that may be contained in the well stream: liquid hydrocarbon fraction and uncombined water. The next processing step depends on the transport system adopted. Natural gas and its different fractions can be transported in various forms:

- Compressed natural gas (CNG, gas pipeline)
- Liquefied natural gas (LNG)
- Liquefied petroleum gas (LPG)
- Chemicals (methanol, ammonia, urea)

Some natural gas components must be extracted either for reasons imposed by the subsequent production or transport steps, or to comply with commercial or regulatory specifications. It may accordingly be necessary to remove at least partially:

- Hydrogen sulfide which is toxic and corrosive
- Carbon dioxide which is corrosive, has no heating value and can crystallize in a cryogenic process
- Mercury, which is toxic and corrosive, mainly with aluminium-based alloys
- Water, leading to the formation of hydrates and corrosion
- Heavy hydrocarbons, condensing in transport systems
- Nitrogen, with no heating value

The specifications to be met for the processed gas are related to the transport conditions or to the conditions of use (commercial gas). Gas from the Sleipner field in the North Sea is distributed as sales gas through sub sea pipelines to the European market. The Sleipner well stream contains about 10 mol% CO_2 and is reduced to about 2.5% in the absorber unit. The gas from the Snøhvit field in the Barents Sea will be transported as LNG, and this gas must be treated to a CO_2 content of less than 50 ppm (to prevent out freezing of solid CO_2 when liquefying the gas).

2.1 Purification Operations

The control of water, acid gas and heavy-hydrocarbon content is achieved by processing operations, which serve to purify the natural gas by separating the components to be removed from the processed gas.

5

These operations make use of various separation process; solvent absorption, adsorption, fractionation by cooling and gas permeation.

Apart from gas permeation, the separation processes used are all based on the principle of a phase change: the component to be separated is selectively transferred from the gas phase to a liquid or solid phase. All separation operations are performed by generating a non-equilibrium situation in the fluid system, resulting in spontaneous mass transfer and separation of the components. It is of crucial importance to understand the underlying physics of the non-equilibrium phenomena occurring, and to be able to model it correctly.

2.1.1 Solvent Absorption

Absorption by a solvent is the technique most commonly used to process natural gas. The basic principle of the absorption process is illustrated in Figure 2-1.
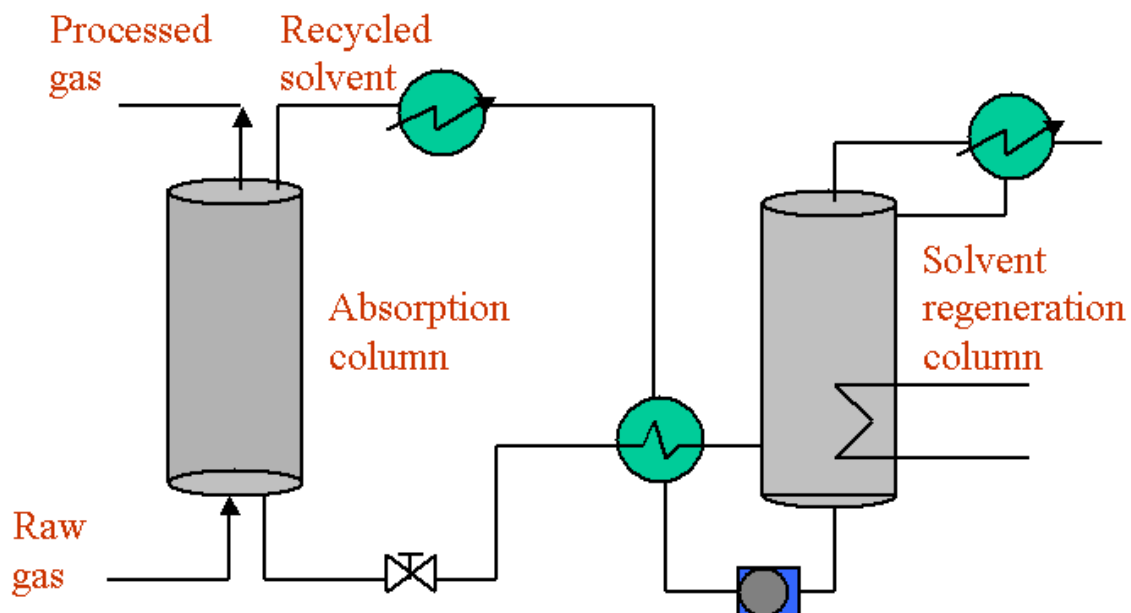
Figure 2-1 Schematic view of an absorption process

The gas to be processed is contacted in counter current flow with a selective solvent in a plate or packed column. If the solvent introduced at the top of the column is pure, the solvent circulation rate and the number of plates or the height of the packing in the column can be set to obtain a gas purity at the exit that corresponds to the specification. The solvent leaving the absorption column is sent to a distillation column for regeneration, generally operating at lower pressure. After regeneration, the solvent is recycled. It passes through a heat exchanger, designed to bring it to a temperature close to the temperature range in which the absorption column operates. Before going to the absorption column it usually goes through an additional cooling step.

2.2 Fluid Mechanic Behavior in Gas Processing Operations

Two methods have traditionally been used for large-scale gas processing simulation. Relatively advanced models have been used for one- and two-phase pipe-flow (the phenomenological two fluid model), while more or less empirical models have been used for gas processing operations in trayed and packed beds. The pressure drop in a packed bed has e.g. been calculated from pure empirical correlations.

Important parameters in both pipe flow and absorption towers are interfacial properties (surface tension, interface friction, wetting of surfaces), entrainment of liquid droplets in gas (liquid carryover), flooding and loading conditions, and bubbles in liquid.

In the modeling of gas processing operations it is important to simplify the fluid mechanical behavior and find similarities in flow patterns. Generally we can divide the fluid flow in gas processing units and in multiphase pipes into two main flow patterns: dispersed- and stratified flow. These flow patterns are illustrated in Figure 2-2. The basis for the model developed in this work is that all operations related to gas transport and processing can be modeled as either dispersed or stratified flow using a general two-fluid model.
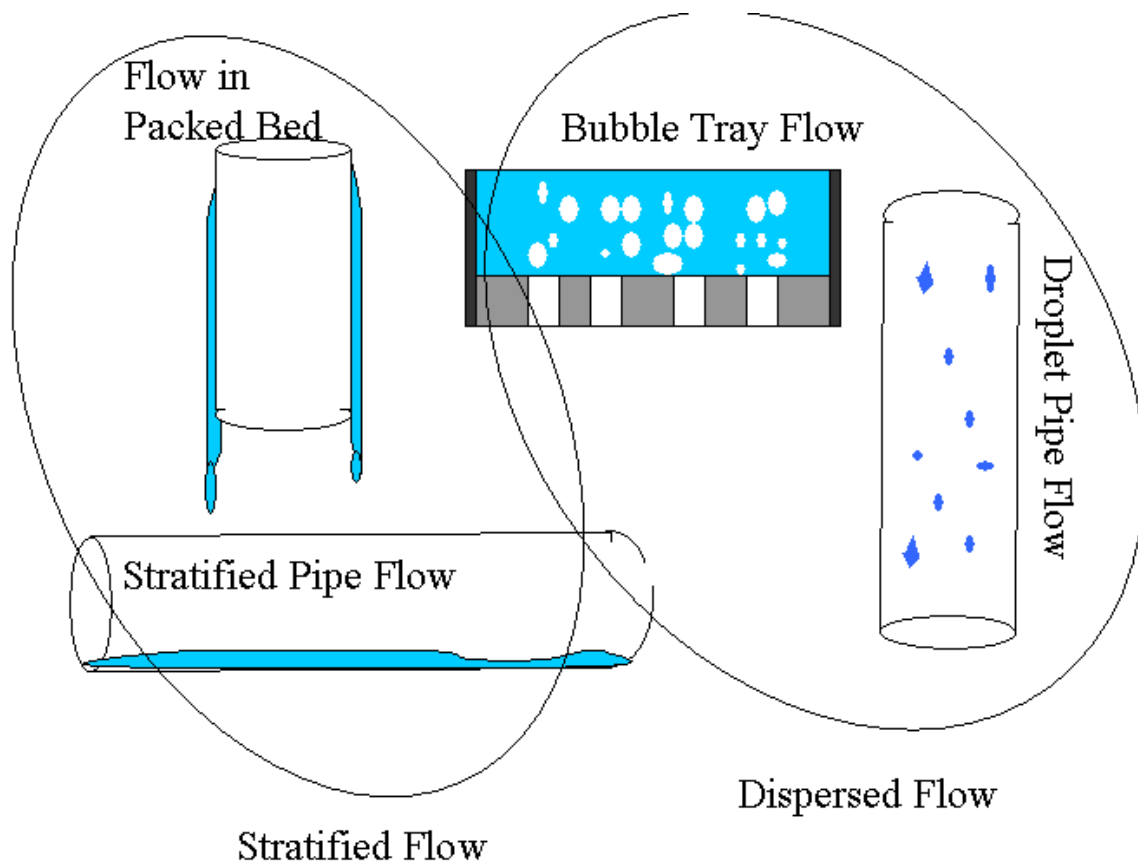
Figure 2-2 Flow patterns in natural gas processing

2.3 Modelling of Absorption Processes

Details of the procedure often used in the design of absorption equipment are explained in basic books on process design such as Perry and Green (1998) and Geankoplis (1993). The design of counter current absorbers normally involves the following steps:

- Selection of the type of contactor, including trays or packing
- Calculation of heat and material balances
- Estimation of required column height (number of trays / height of packing) based on mass transfer analysis
- Calculation of required column diameter based on gas and liquid flow rates and hydraulic considerations
- Mechanical design of hardware

The key data required in the design of absorbers are the physical, thermal, and transport properties of the gases and liquids involved; vapour/liquid equilibrium data; and, if chemical reactions are involved, reaction rate data. Configuration data of the trays and packing are also required.

The design of absorbers typically involves a computer-assisted, tray-by-tray or continuous, heat and material balance calculation to determine the required number of equilibrium stages or the height of packing. The required number of actual trays is related to the required number of equilibrium stages by estimated tray efficiency.

2.3.1 The Traditional Way of Modelling of Absorption Units

To facilitate the use of computers in the design of absorbers, Kesler and Wankat (1988) have converted a number of commonly used correlations to equation form. These include O'Connell's overall tray efficiency correlation (1946), Fair's flooding correlation for sieve tray columns (Fair, 1961), Hughmark and O'Connell's correlation relating to pressure drop of gas through a dry tray (Hughmark et.al.,1957), Fair's correlation for tray weeping (Fair, 1963), and Eckert's correlation for flooding in a packed tower (Eckert, 1970).

The most common way of modelling absorption and distillation processes is the use of equilibrium stage methods with tray efficiencies for trayed columns, and height and number of transfer units for packed columns. The equilibrium stage model assumes that the gas leaving a tray is in equilibrium with the liquid leaving the tray in a counter current direction.

This type of modelling has some major disadvantages. It is often based on purely empirical correlations found from low-pressure air-water experimental data, and the extrapolation capability is therefore questionable. The methods are unsuitable to be extended to multicomponent mixtures since each of the components will give different stage efficiencies and heights of a transfer unit.

The number of theoretical trays can be calculated with the simulation program developed in this work – NeqSim, and an example of this for absorption of CO_2 from a binary gas mixture in water is given in Figure 2-3. To find the actual number of trays we would have to multiply by a tray efficiency.

Physical Solvent Absorption Modeling

Countercurrent absorption of CO_2 from methane
Temperature and pressure: 40°C and 30 bar
Inlet gas: methane: 450 NL/min CO_2: 50NL/min
Inlet liquid: water 200 kg/min
Gas spec out: 1.0 % CO_2
Number of theoretical stages: ≈ 1.25
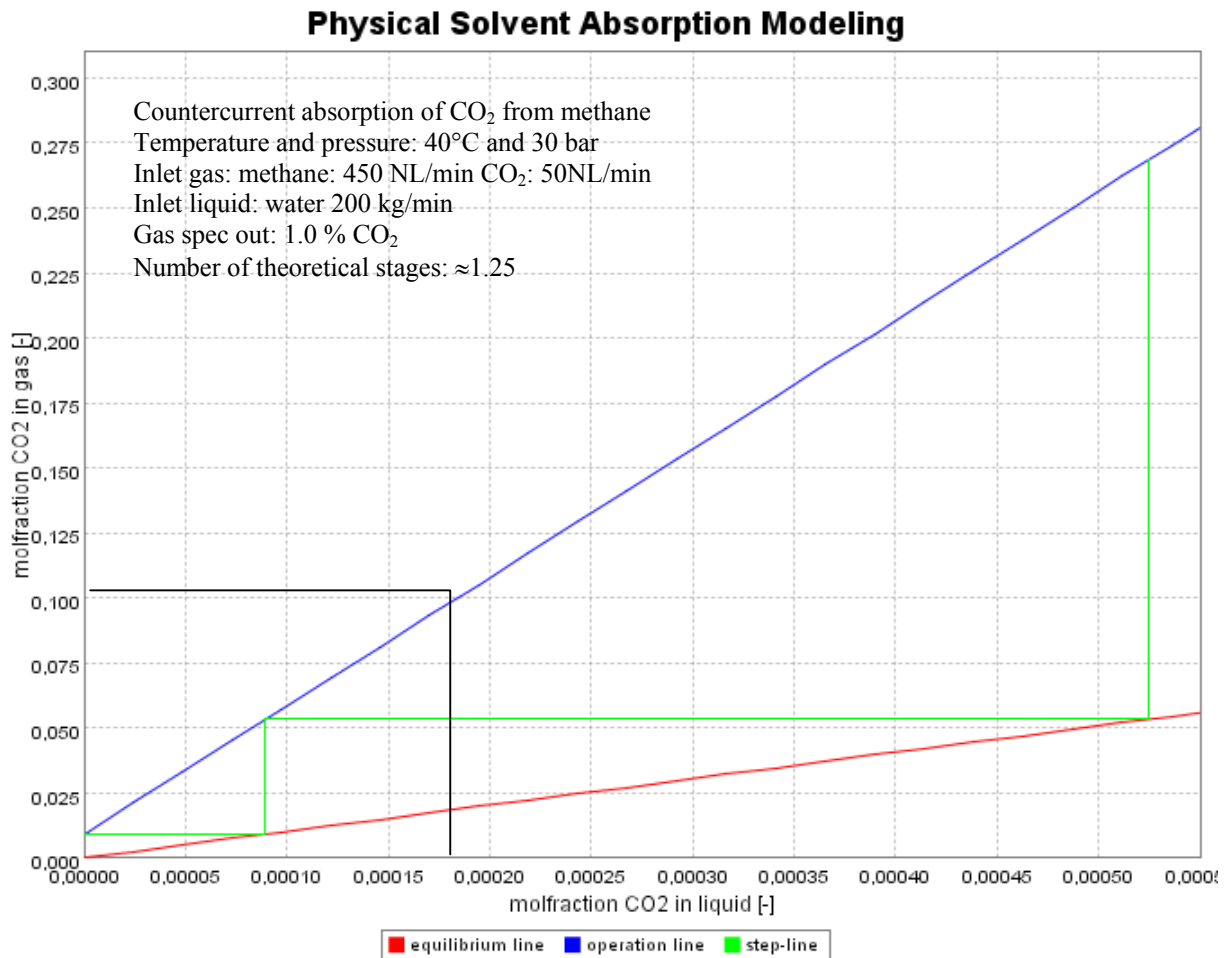
Figure 2-3 Traditional modeling of absorption units using equilibrium stages
        Script: tray.py, p. 303

2.3.2 Rate Based Modelling of Absorption Processes

The limitation of conventional equilibrium stage-stage efficiency calculations has been recognized for a long time.

More recently, a non-equilibrium stage (trayed columns) and a non-equilibrium continuous model (packed beds) have been developed. This non-equilibrium model can be solved numerically with a computer, which considers the actual trays or sections of packing and performs heat and material balances for each phase based on mass and heat transfer rates (Krishnamurthy and Taylor, 1985a/b). This type of modelling is often called the rate-based model. The model makes use of correlations, such as those for the individual mass transfer coefficients for liquid and gas, and interphase contact area to predict the actual performance of small sections of packing or on a tray. The approach does not involve HTU/NTU or HETP (height equivalent of a theoretical plate); in fact, the attainment of equilibrium is assumed to occur only at the gas liquid interface and not in the products of a theoretical stage. Generalized correlations for estimating the individual mass transfer coefficients have been proposed by Onda et.al. (1968), Bolles and Fair (1982) and Bravo and Fair (1982). In the rate-based model, separate material balances are made for gas and liquid phases in each packing section; these are coupled by interface mass transfer rates, which must be equal in each phase at the interface.

The non-equilibrium model of Krishnamarthy and Taylor (1985) considered energy and material balances for each component.

2.3.3 The Multicomponent Non-Equilibrium Two-Fluid Model

The rate based model made us able to simulate complicated absorption processes more accurate than we were able to do earlier using the equilibrium stage approach. In the rate based model the mass conservation equations are solved using a Newton-Raphson technique. A simplified fluid mechanic model is normally used. This is done since the fluid mechanics in a packed bed often is so complicated that it is hard to model it accurately. Such simplified fluid mechanic models are not suitable for doing transient simulations.

In this work a non-equilibrium two fluid model has been developed. It is based on the 1-dimensional two fluid model commonly used in multiphase pipe flow simulators (e.g. OLGA), but also considers conservation of each component. The mass fluxes between the phases are calculated with models similar to those often used in the rate base approach – the Maxwell-Stefan equations. This model can easily be extended to simulate time dependent processes.

2.4 Acid Gas Removal

Hydrogen sulfide and carbon dioxide are the main acid gases, which have to be removed from natural gas. Acid gas removal is a very important industrial operation, which has been described in many books; see e.g. Kohl and Nielsen (1997), Astarita et.al. (1983) and Danckwerts (1970). The most widely used processes to sweeten natural gas are those using alkanolamines, and of the alkanolamines a common one is methyldiethanolamine (MDEA). An absorption process using MDEA for the removal of CO_2 from the natural gas is used on the Sleipner field in the North Sea. A process using activated MDEA is also planed implemented to treat the natural gas from the Snøhvit field in the Barents Sea.

2.4.1 Acid Gas Absorption Processes Based on Physical Solvents

The processes based on physical solvents offer the advantage of requiring little or no heat to desorb the acid gases. On the other hand, they are sensitive to the presence of heavy hydrocarbons in the gas, which are absorbed by the solvent and then desorbed with the acid gases. The use of a process based on a physical solvent is favoured by the following conditions:

- Gas available at relatively high pressure
- Low concentration of heavy hydrocarbons in the feed
- High acid gas content in feed
- Desired H_2S/CO_2 selectivity

The absorption steps are carried out in a tray or packed column. Regeneration is performed by successive expansions, stripping by a neutral gas or reboiling of the solution. The Selexol process is an example of a physical solvent process (Jason and Homme, 1984).

2.4.2 Absorption Processes Based on Amine Solutions

An introduction to the chemistry of alkanolamines is given in appendix E. In this section a brief description of gas treating with alkanolamines is presented.

The basic building block of amines is the ammonia molecule NH_3. By replacing one or more of the hydrogen atoms with other functional groups we can create various types of amines. By replacing the hydrogen atoms with alcohol functional groups we can create alkanolamines. Due to the nitrous group alkanolamines form basic aqueous solutions. The alcoholic groups make the alkanolamines water-soluble.

Amines act by chemical affinity due to their basic charater. Monoethanolamine (MEA), diethanolamine (DEA), diglycolamine (DGA), diisopropanolamine (DIPA) and methydiethanolamine (MDEA) are used to sweeten natural gas. Thus prefix "mono", "di" or "tri" indicates the degree of substitution around the nitrogen atom. Thus if R denotes the functional group $HOCH_2CH_2$-, monoethanolamine has the chemical formula RNH_2., diethanolamine R_2NH and triethanol amine R_3N.

The reaction between H_2S and the alkanolamines can generally be represented by

$$2RNH_2 + H_2S \underset{k_{-1}}{\overset{k_2}{\rightleftharpoons}} \left(RNH_3\right)_2 S \qquad (2.1)$$

$$\left(RNH_3\right)_2 S + H_2S \underset{k_{-1}}{\overset{k_2}{\rightleftharpoons}} 2RNH_3HS \qquad (2.2)$$
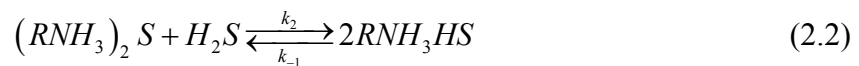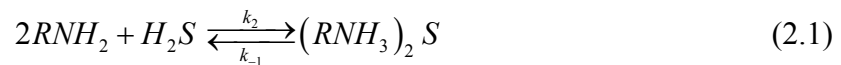
The reactions are direct and fast, and occur with primary, secondary and tertiary amines.

Compared with the instantaneous proton transfer reaction when H_2S reacts with an alkanolamine, the reaction between CO_2 and alkanolamines is more complex, and the reaction rate depends highly on the structure of the alkanolamine molecule. Amines react with carbon dioxide by two types of reactions.

Formation of carbonate and bicarbonate

$$2\, RNH_2 + CO_2 + H_2O \underset{k_{-1}}{\overset{k_2}{\rightleftharpoons}} \left(RNH_3\right)_2 CO_3 \qquad (2.3)$$

$$\left(RNH_3\right)_2 CO_3 + CO_2 + H_2O \underset{k_{-1}}{\overset{k_2}{\rightleftharpoons}} 2\, RNH_3HCO_3 \qquad (2.4)$$

Formation of carbamate

$$2\, RNH_2 + CO_2 \underset{k_{-1}}{\overset{k_2}{\rightleftharpoons}} RNHCOONH_3R \qquad (2.5)$$
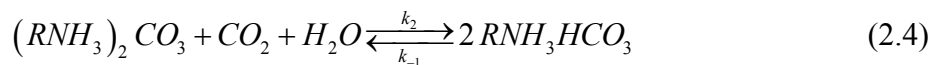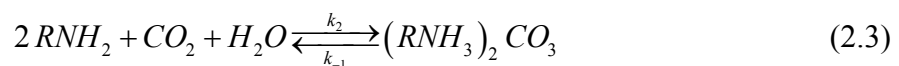
Reactions (2.3) and (2.4) are slow, because carbon dioxide must form carbonic acid with water (slow reaction) before reacting with the amine. Reaction (2.5) is relatively fast. With tertiary amines (e.g. MDEA, TEA) reaction (2.5) is impossible.

2.4.3 Absorption of CO$_2$ into MDEA Solutions

Methyldiethanolamine (MDEA) is today the most used tertiary amine for acid gas removal (Rojey et.al., 1997). The reaction between CO$_2$ and H$_2$S in MDEA solutions can be represented as

$$H_2S + MDEA \xrightleftharpoons[k_{-2}]{k_2} HS^- + MDEA^+ \qquad (2.6)$$

$$CO_2 + MDEA + H_2O \xrightleftharpoons[k_{-2}]{k_2} HCO_3^- + MDEA^+ \qquad (2.7)$$
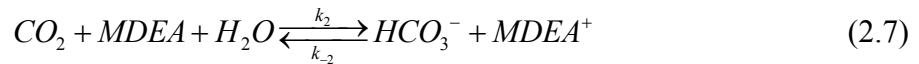
The reaction between H$_2$S and MDEA is very fast, while the reaction with CO$_2$ is relatively slow.

MDEA allows selective absorption of H$_2$S in the presence of CO$_2$ – because of the reaction rate difference for CO$_2$ and H$_2$S with MDEA. When the correct additives/activators are used, MDEA offers several advantages over other amines also for bulk CO$_2$ removal. An important reason for this is the relatively low heat of absorption of CO$_2$ into MDEA solutions.

A detailed discussion of the reaction kinetics of CO$_2$ in MDEA-solutions is given in appendix E.

The reaction rate for CO$_2$ in a MDEA-solution can be calculated from

$$r_{CO_2} = k_2 [CO_2][MDEA] - \frac{K_r}{k_2} [HCO_3^-][MDEA+] \qquad (2.8)$$

where k_2 is the second order reaction rate constant and K_r is the chemical equilibrium constant for the reaction between CO$_2$ and MDEA-solutions. The reaction rate constant is normally given using an Arrenihus type of equation

$$k_2 = k_{2(T=313K)} \exp\left\{ -\frac{E_a}{R}\left(\frac{1}{T} - \frac{1}{313K} \right) \right\} \qquad (2.9)$$

When experimental data from the literature are regressed simultaneously, the following correlation can be obtained (Pacheco, 1998);

$$k_{2(T=313K)} = 6.28 \pm 1.62 \, m^3 / kmol \, s$$
$$E_a = 48.9 \pm 6 \, kJ / mol \qquad (2.10)$$

Figure 2-4 shows the rate constant as calculated from equation (2.9) and (2.10).
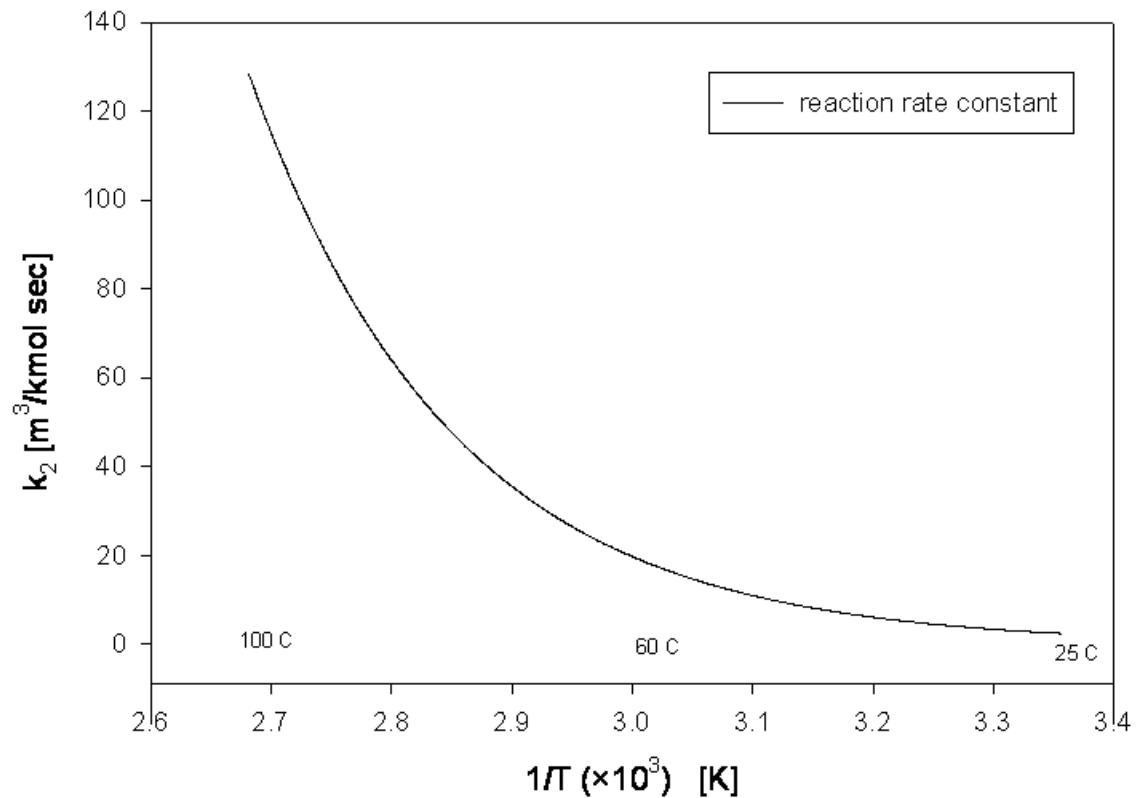
Figure 2-4 Reaction rate constant for reaction between CO$_2$ and aqueous MDEA calculated from eq. (2.9).

2.4.4 Modelling of Reactive Acid Gas Removal

The traditional modelling of reactive absorption has been cumbersome and primarily based on empirical data. Such procedures have proven to be adequate for plants designed essentially for complete removal of acid gases from natural gas streams, because an overly conservative design, with a few extra trays or extra length of packing, could only improve performance. This is not true for selective absorption because too many trays can destroy selectivity. We also see that it is getting more and more important to operate the process equipment as effective as possible – accurate process simulation tools would help us to operate it effectively.

In Figure 2-5 the operation line and equilibrium line for the absorption of CO$_2$ from a gas stream using a MDEA-solution are created using NeqSim. On the x-axis we have the sum of mole fractions of CO$_2$ in molecular and ionic form in the solution. We see that the equilibrium line will be curved due to the chemical reactions occurring in the liquid phase. The stage efficiencies for reactive absorption are typically low. In Figure 2-5 the molefraction on the x-axis represents the sum of the free and chemically combined carbon dioxide (CO$_2$ and HCO$_3^-$).
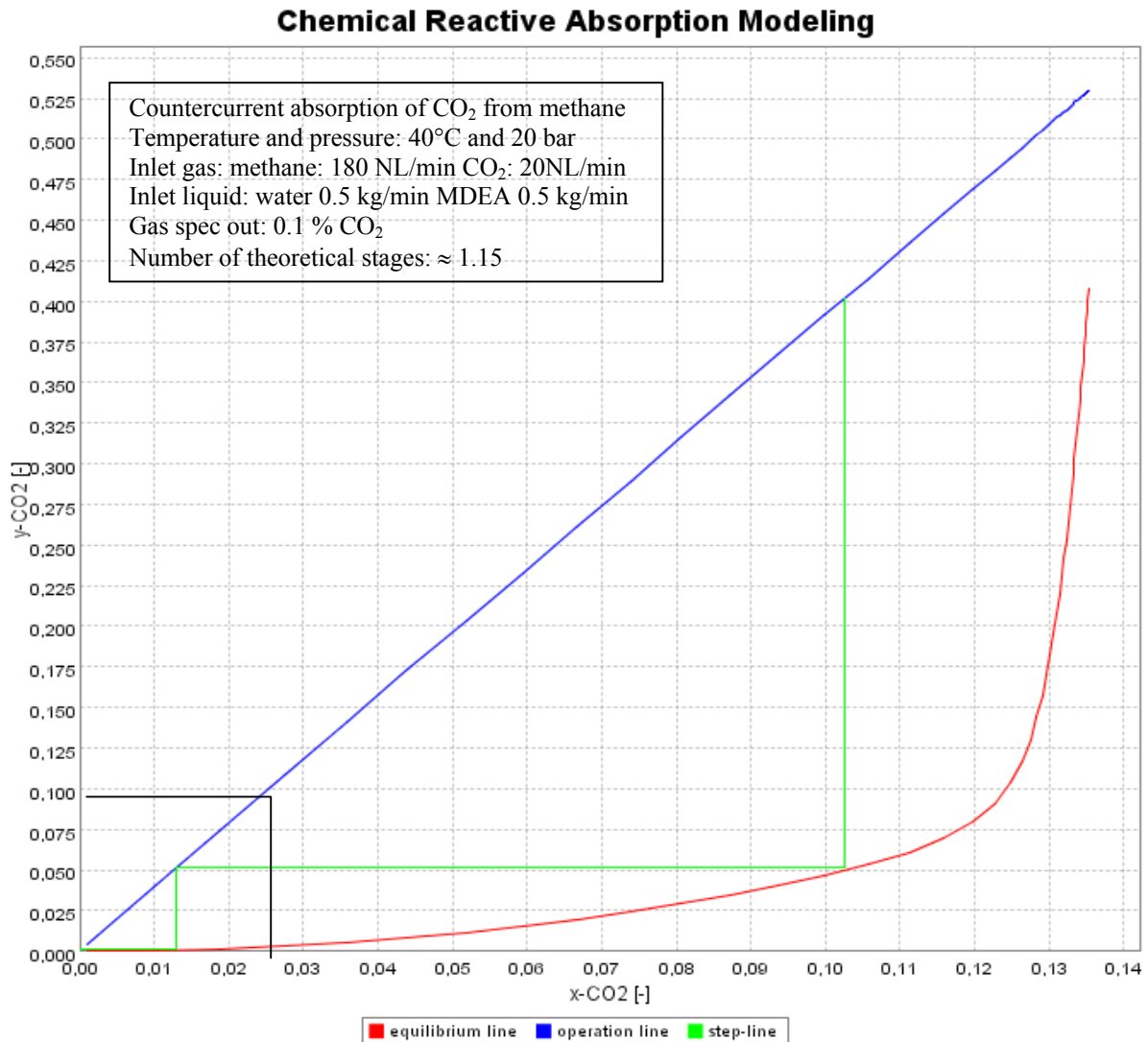
Figure 2-5 Tradition modeling of chemical absorption units using equilibrium stages
Script: tray-amine.py, p. 304

If we compare the physical absorption case from Figure 2-3 with the chemical absorption case in Figure 2-5, we see that much less solvent circulation rate is required for reactive absorption and that we reach very low CO_2 contents after few ideal stages. It is important to remember that the stage efficiency generally is low for reactive absorption into MDEA solutions and that a relatively large amount of energy is required for CO_2-stripping. The use of stage efficiencies in reactive absorption is cumbersome and many times erroneous. The gas and liquid leaving a stage will often be far from equilibrium and stage efficiencies are difficult to estimate accurately.

When the rate based modelling of Krishnamurthy and Taylor (1985) was introduced a more fundamental approach could be utilized. This approach involved the use of enhancement factors for reactive mass transfer. The enhancement factor describes the local effect of reactions on the mass transfer rate and can be calculated based on fundamental knowledge of the reaction rate constants and fluid mechanics. Examples of how to use and calculate the enhancement factor are given in chapter 4.

2.5 Future Trends in Gas Processing

The removal of CO_2 from gas streams will be an important challenge also for future work on gas processing. Because of the intensive activity to achieve CO_2 free energy from natural gas fired power plants, the removal of CO_2 from flue gas is an enormous challenge now days. Many researchers are working in this area and large resources are used to develop effective CO_2 capturing processes. The alkanolamine process is an attractive alternative also in such processes.

The transportation pressures in sub-sea gas pipelines in the North Sea are up to about 200 bar. The conventional technology for acid gas removal operates at pressures between 40-70 bar. Currently the gas is expanded to a specified processing condition before it is recompressed to the transportation conditions. It would be a considerable environmental and economic advantage to be able to process the natural gas at well stream pressures. As the economical margins in the gas industry are getting lower we will probably see that the operating pressure of gas processing plants will rise.

For economical reasons it would be advantageous to process the well stream as early as possible. Well stream processing is a challenge that will be important in the future. The basic phenomena occurring in gas processing units, such as entrainment and flooding, are complicated and highly 3-dimensional. Effort is being taken to study these phenomena on a laboratory scale. A better understanding of such processes will make us prepared to design process equipments that can operate at very high pressures.

2.6 Future Trends in Modelling and Simulation

The process simulation tools will probably be of increased importance in future design of gas processing equipment. As the mathematical models are getting better – the simulation results will be of great value for the designer and the operator of such equipment – and better process design and operation can be achieved.

Simulation tools for offshore pipelines (e.g. OLGA) will possibly be integrated into dynamic process simulation tools (e.g. HYSYS), and the effect of transient operation can be studied. Computer networks will make us able to communicate with other process systems. Online simulators and internet technology based programming languages such as Java can be used.

We will probably see that more and more of the mathematical models used in simulators are of a fundamental art. As the computers are getting faster we will probably see increased use of first principle modelling such as CFD-simulations.

As the computers are getting faster it will be possible to integrate process simulation tools with rigorous pipeline simulation tools. When this is done it will be possible to simulate the whole gas transportation and processing chain in one tool, and it will be possible to study the effect of transients in pipelines (e.g. liquid slugs) on the operation of the process plant.

The simulation tool developed in this work (NeqSim) integrates common process simulation operations such as separators, mixers and heat exchangers with process equipment that are modelled with more rigorous fluid mechanic models (e.g. multiphase pipelines). The computational speed of NeqSim is still to slow to be able to simulate transients in large process systems.

2.7 The Process Design Procedure

When we are doing experimental and modelling work it is important to keep in mind the design- and implementation procedure of new technology. Our final goal is to provide new environmental-, compact- and cost-effective solutions. The design procedure is illustrated in Figure 2-6. New process design will normally come from a combination of experience and mathematical modelling/simulation.
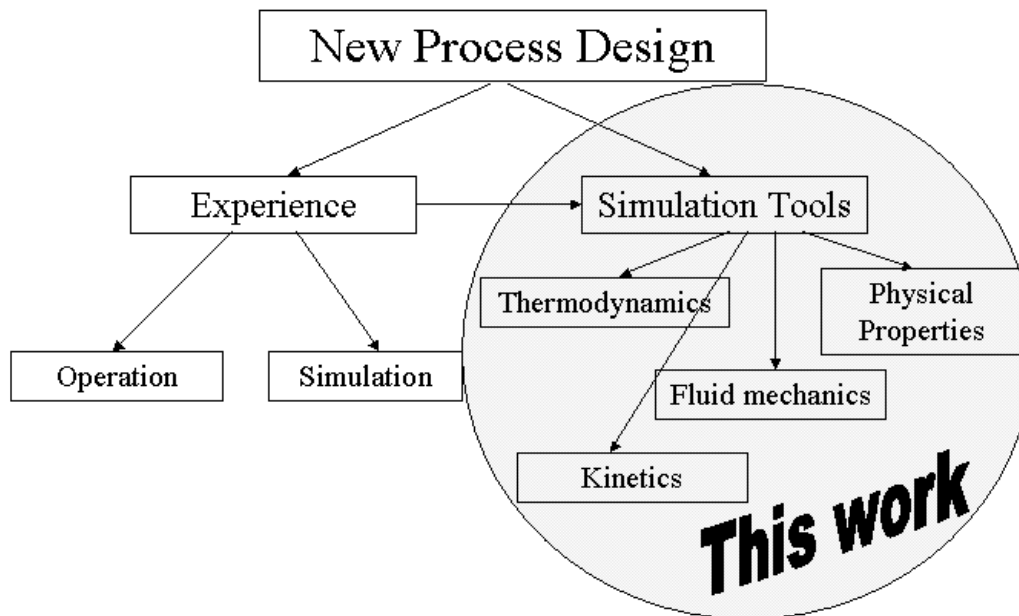
Figure 2-6 The design procedure for new process solutions

The goal of the high-pressure gas processing activity related to this work is to process the gas at extremely high pressures (optimally at well stream pressure). This work contributes to the need of qualified models and experimental data for use in new design. Finally, the simulation models developed are implemented in a simulation program that can be helpful in the search for optimal process solutions.

3 Equilibrium Thermodynamics

Equilibrium thermodynamics is important also when we want to simulate non-equilibrium processes. In most mass transfer models thermodynamic equilibrium is assumed to exist locally at the interface. In a multiphase-, multicomponent system, chemical equilibrium is established when the mass transfer from one phase to the other is equal in each direction. This is called dynamic equilibrium, and is characterized by zero entropy production. When a system is out of equilibrium, mass transfer between the phases will try to establish a new equilibrium situation. The driving force for mass transfer is proportional to how far the system is from thermodynamic equilibrium. Thus the modelling of thermodynamic equilibrium properties is important also when we want to calculate the driving force for mass transfer.

The thermodynamic models used for the calculation of equilibrium and thermodynamic properties of a fluid are important in process simulation programs. Accurate modelling of thermodynamic and physical properties such as enthalpy, density, surface tension and diffusivity are of vital importance in such process calculations.

The intention of this chapter is to present a general introduction to thermodynamic modelling, with emphasis on electrolyte solutions. First classical (e.g. SRK) and more resent (e.g. CPA) equations of states are reviewed and compared for the calculation of pure component density and vapour pressure. The equations of state are next used to correlate mutual solubility data of supercritical gasses and water – and the different mixing- and combination rules are compared. The most promising equations of state and mixing rules are then extended to electrolyte systems by introducing specific ionic terms. Two different electrolyte equations of state (electrolyte ScRK-EoS and electrolyte CPA-EoS) based on a model originally proposed by Furst and Renon (1993) are presented.

The derivation of the governing equation for the calculation of thermodynamic properties is based on an approach proposed by Michelsen and Mollerup (1986) and Mollerup and Michelsen (1992) using the reduced Helmholtz energy and its derivatives.

3.1 Governing Equations of Thermodynamics

In this section the governing relations for the calculation of thermodynamic equilibrium are derived. A general introduction to equilibrium thermodynamics is given in Prausnitz et.al (1999) and Sandler (1989).

From the 1. and 2. law of thermodynamics, for a general, homogeneous, thermodynamic system, we have;

The first law of thermodynamics - conservation of energy

$$dU = dQ - dW \tag{3.1}$$

The second law of thermodynamics – entropy production

17

$$dS \geq \frac{dQ}{T_S} \qquad (3.2)$$

These two basic laws of thermodynamics form the basis for the calculation of phase equilibrium in fluid systems. Two useful definitions are the Gibbs free energy (G) and the Helmholtz free energy (A).

$$G = H - TS \qquad (3.3)$$
$$A = U - TS \qquad (3.4)$$

From equations (3.1)-(3.4) one can show that

- The inner energy (U) has a minimum at a given volume and pressure
- The enthalpy (H) has a minimum at a given entropy and pressure
- The Helmholtz free energy (A) has a minimum at a given volume and pressure
- The Gibbs free energy (G) has a minimum at a given pressure and temperature

Since the Gibbs free energy involves temperature and pressure, two easily measurable properties, this is a preferable way to define the equilibrium state – in particular when we look at chemical equilibrium.

3.1.1 The Chemical Potential

If we combine equation (3.1), (3.2) and (3.3) we get

$$dG \leq V\,dP - S\,dT \qquad (3.5)$$

For an open system we have to consider the change in composition of the system

$$dG \leq V\,dP - S\,dT + \sum_{i=1}^{n} \left(\frac{\partial G}{\partial N_i} \right)_{T,P,n_j} dN_i \qquad (3.6)$$

For an isobaric and isothermal process, we get

$$dG \leq \sum_{i=1}^{n} \left(\frac{\partial G}{\partial N_i} \right)_{T,P,n_j} dN_i \qquad (3.7)$$

This means that a system at a given temperature and pressure is at equilibrium when the total Gibbs energy is at a minimum. This important information can be used to express the equilibrium state of homogeneous (one-phase) and heterogeneous (multi-phase) multi-component systems.

The chemical potential is defined as

$$\mu_i = \left(\frac{\partial G}{\partial N_i} \right)_{T,P,n_j} = \left(\frac{\partial A}{\partial N_i} \right)_{T,V,n_j} \qquad (3.8)$$

At chemical equilibrium the chemical potential for a component will be uniform in the whole system. When two phases are in contact and at thermodynamic equilibrium, the chemical potential of a component will be the same in both phases

$$\mu_i^1 = \mu_i^2 \tag{3.9}$$

This equation forms the basis when we want to calculate the composition of a multiphase system at thermodynamic equilibrium.

3.1.2 The Fugacity Coefficient

Use of the chemical potential to define the equilibrium state will often lead to mathematical difficulties. We therefore introduce the fugacity, f. The fugacity is a "pseudo-pressure", and is defined as

$$d\mu_i = \mu_i\left(T, P, x_i\right) - \mu_i^{IG}\left(T, P = 1\right) = RT\, d\left(\ln f\right)_T \tag{3.10}$$

where $\left(\dfrac{f}{P}\right) \to 1$ when $P \to 0$ and $\mu_i^{IG}(T, P = 1)$ is the chemical potential for the component

at the hypothetical standard state as an ideal gas at 1 bar. This definition is normalized so that the fugacity will be equal to the pressure, when the pressure goes to zero. The relation between fugacity and chemical potential provides a conceptual aid in performing the translation from thermodynamic to physical variables. It is difficult to visualize the chemical potential, but the fugacity is less so. Fugacity is a "corrected pressure"; for a component in a mixture of ideal gases it is equal to the partial pressure of that component.

If we combine the definition of the fugacity with equation (3.9), the equilibrium state is defined by

$$f_i^1 = f_i^2 \tag{3.11}$$

We define the fugacity coefficient as

$$\varphi_i = \frac{f_i}{P_i} \tag{3.12}$$

where P_i is the partial pressure of component i. Combining equation (3.12), (3.10) and (3.8) we get

$$RT \ln \varphi_i = \left(\frac{\partial}{\partial n_i} G^r\left(T, P, \mathbf{n}\right)\right)_{T, P, n_j} = \left(\frac{\partial}{\partial n_i} A^r\left(T, V, \mathbf{n}\right)\right)_{T, V, n} - RT \ln Z \tag{3.13}$$

Where the residual Gibbs energy (G^r) and residual Helmholtz energy (A^r) are the difference between the true value and a value where we assume it as an ideal gas. This is one of the key equations in equilibrium thermodynamics and it shows that the logarithm of the fugacity coefficient is most readily calculated as the partial derivative of the residual Gibbs function at state (T,P,$\mathbf{n}$) or the residual Helmholtz function at state (T,V,$\mathbf{n}$).

3.1.3 The Activity Coefficient

The ideal solution fugacity and chemical potential are calculated from

$$f_i(T,P,\mathbf{n}) = x_i \cdot f_i(T,P) \tag{3.14}$$

$$\mu_i(T,P,\mathbf{n}) = \mu_i(T,P) + RT \ln x_i \tag{3.15}$$

We see that the fugacity of a component in the solution is a linear function of the mole fraction. The ideal solution is a conventional hypotetical state which no solution strictly follow. Real solutions are non-ideal solutions. In the non-ideal solution we can calculate the fugacity from

$$f_i(T,P,\mathbf{n}) = x_i \gamma_i(T,P,\mathbf{n}) f_i(T,P) \tag{3.16}$$

or

$$\mu_i(T,P,\mathbf{n}) - \mu(T,P) = RT \ln\left(\gamma_i(T,P,\mathbf{n}) x_i\right) \tag{3.17}$$

where γ_i is the activity coefficient and is equal to 1 for ideal solutions. The relation between the chemical potential and the fugacity coefficient is given as,

$$\mu_i(T,P,x_i) - \mu_i^{IG}(T,P=1) = RT \ln\left(\varphi_i(T,P,\mathbf{n}) x_i\right) \tag{3.18}$$

Sometimes we need to calculate activity coefficients from relations for the fugacity coefficient. This will typically be the case when we use an equation of state to calculate the activity. The activity coefficient with reference state as a pure solvent can be calculated from the relation

$$\frac{\mu_i(T,P,x_i) - \mu_i(T,P)}{RT} = \ln\left(x_i \gamma_i\right) = \frac{\mu_i(T,P,x_i) - \mu_i^{IG}(T,P=1)}{RT} - \frac{\mu_i(T,P) - \mu_i^{IG}(T,P=1)}{RT}$$
$$= \ln x_i \varphi_i(T,P,x_i) - \ln \varphi_i(T,P) = \ln \frac{x_i \varphi_i(T,P,x_i)}{\varphi_i(T,P)} \tag{3.19}$$

Wee see that the activity coefficient with reference state pure solvent (symmetric) is given by

$$\gamma_i = \frac{\varphi_i(T,P,x_i)}{\varphi_{i,pure}(T,P)} \tag{3.20}$$

With a similar argumentation we can show that the activity coefficient with reference state at infinite dilution (unsymmetrical) can be calculated as

$$\gamma_i^{\infty} = \frac{\varphi_i(T,P,x_i)}{\varphi_i(T,P,x_i \to 0)} \tag{3.21}$$

The calculation of the activity coefficient from an equation of state is utilized in the chemical equilibrium calculations performed in this work. The use of activity coefficients is often necessary in weak electrolyte solutions – since the reaction equilibrium constant often is given for an ideal solution (all activities equal to 1).

3.2 Thermodynamic Equilibrium Calculations

Calculation of phase equilibrium is of importance for dimensioning of multistage separations cascades, as well as for single stage units. Satisfactory predictions of multiphase equilibrium require the adequate thermodynamic models for fluid phase are available.

3.2.1 Physical Equilibrium

The phase equilibrium criteria is expressed by equation (3.11) as

$$f_i^1 = f_i^2$$

In this work we use use the fugacity coefficient to calculate the fugacities, and the equilibrium criteria is

$$\varphi_i^g y_i P = \varphi_i^l x_i P \tag{3.22}$$

where we can calculate the fugacity coefficient of both gas and liquid from an equation for the residual Helmholtz energy (equation (3.13)). In this work we use equations of state to calculate the fugacity. When we use equations of state the model used to calculate thermodynamic properties for the liquid and gas phase is the same – and gives us some advantages compared to the traditional gamma-phi approach (using a GE-model for the liquid phase). Supercritical components such as methane and nitrogen can easily be added – and it is able to calculate the critical point of a solution (Michelsen et.al., 2000).

3.2.2 Chemical Equilibrium

The calculation of chemical equilibrium is in many ways similar to the calculation of phase equilibrium. In both cases the equilibrium state corresponds to a global minimum of the Gibbs energy subject to a set of material balance constrains.

Chemical equilibrium is commonly expressed in two ways. The Gibbs free energy is minimized at equilibrium yielding

$$\partial G = \sum_{i=1}^{n} \mu_i \partial n_i = 0 \tag{3.23}$$

where the chemical potential is expressed as

$$\mu_i = \mu_i^0 + RT \ln\left(\gamma_i x_i\right) \tag{3.24}$$

A more common definition is the definition of the equilibrium constant

$$\prod_{i=1}^{n}(\gamma_i x_i)^{v_i} = K = \exp\left(\frac{\Delta G^0}{RT}\right) \tag{3.25}$$

ΔG^0 is calculated from μ^0 and is generally a function of temperature only. The equilibrium constant K will consequently be a function of temperature only, when defined reference state for all components are used.

The activity coefficients in equation (3.24) can be calculated from a model for the fugacity coefficient, using equation (3.21). For the reaction between CO_2 and an aqeous MDEA solution we have (equation 2.7).

$$CO_2 + MDEA + H_2O \underset{k_{-2}}{\overset{k_2}{\rightleftharpoons}} HCO_3^- + MDEA^+$$
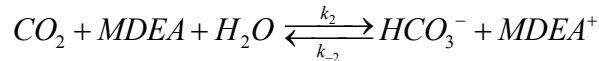
The chemical equilibrium relation is

$$K_{CO_2-MDEA} = \frac{[HCO_3^-][MDEA^+]}{[CO_2][H_2O][MDEA]} \cdot \frac{[\gamma_{HCO_3^-}][\gamma_{MDEA^+}]}{[\gamma_{CO_2}][\gamma_{H_2O}][\gamma_{MDEA}]} \tag{3.26}$$

In this study the reference state for the calculation of activity coefficients for CO_2 and ions are at infinite dilution in water (unsymmetrical activity coefficient in water), while the reference state for water and MDEA is as pure component at the system temperature and pressure (symmetric activity coefficient). In general we choose the unsymmetrical reference state in water for ions and supercritical components, and pure component reference sate for sub-critical molecular components.

3.3 Equations of State

Equations of state play an important role in chemical engineering design, and they have assumed an expanding role in the study of the phase equilibria of fluids and fluid mixtures. In this section an introduction to equations of state based on the review article of Wei and Sadus (2000) is presented. Originally, equations of state were used mainly for pure components. When first applied to mixtures, they were used only for nonpolar (Soave, 1972; Peng and Robinson, 1976) and slightly polar compounds (Huron et.al., 1978). Subsequently, equations of state have developed rapidly for the calculation of phase equilibria in non-polar mixtures. There are many advantages in using equations of state for phase equilibria calculations. Equations of state can be used typically over wide ranges of temperatures and pressures, and they can be applied to mixtures of diverse components, ranging from the light gases to heavy liquids. They can be used to calculate vapour-liquid equilibria, liquid-liquid, and supercritical fluid phase equilibria without any conceptual difficulties. The calculation of phase equilibria has been discussed extensively elsewhere (Sandler 1994, Michelsen et.al. 2000).

The van der Walls equation of state was the first equation to predict vapour-liquid coexistence. Later, the Redlich-Kwong equation of state (Redlich and Kwong, 1949) improved the accuracy of the van der Waals equation by introducing temperature-dependence for the attractive term. Soave (1972) and Peng and Robinson (1976) proposed additional modifications to more accurately predict the vapour pressure, liquid density, and equilibria ratios. In later work the attractive term in the Redlich and Kwong model has been modified to

represent the vapour pressures of polar non-ideal components (Schwartzentruber and Renon (1989), Mathias (1983)).

In addition of modelling small molecules, considerably emphasis has been placed recently on modelling chain-like molecules. Based on the theories of Prigogine (1957) and Flory (1965), other workers (Beret and Prausnitz, 1975; Donohue and Prausnitz, 1978) developed a perturbed hard chain theory (PHCT) equation of state for chain molecules. To take into account the increase in attractions due to dipolar and quadrupolar forces, Vilmalchand and Donohue (1985) obtaines fairly accurate multipolar mixture calculations by using the perturbed anisotropic chain theory (PACT). Ikonomu and Donohue (1986) extended PACT to obtain an equation of state which takes into account the existence of hydrogen bounding, namely, the associated perturbed anisotropic chain theory (APACT) equation of state.

Advances in statistical mechanics and an increased computer power have allowed the development of equations of state based on molecular principles that are accurate for real fluids and mixtures. Using Wertheim's theory (Wertheim, 1984a,b), Chapman et.al. (1990) and Huang and Radosz (1990) developed the statistical associating fluid theory (SAFT) which is accurate for pure fluids and mixtures containing associating fluids. Recently, various modified versions, such as LJ-SAFT (Banaszak et.al. 1994) and VR-SAFT (Gill-Villegas et.al., 1997) have been developed. A common feature of many newly developed equation of state is the increasing use of insights gained from molecular simulation to improve the accuracy of the underlying model.

In this section some of the most common and some more resent equations of state will be reviewed and tested for their capability to predict thermodynamic properties of pure components. The components we will consider are methane, CO_2, nitrogen, water and MDEA. In section 3.4 mixing rules will be reviewed and evaluated.

3.3.1 Equation of State for Simple Molecules

The van der Waals equation of state, proposed in 1873, was the first equation capable of representing vapour-liquid coexistence. The VdW equation of state is given by

$$Z = \frac{\overline{V}}{\overline{V} - b} - \frac{a}{RT\overline{V}}$$

(3.27)

where Z is the compressibility factor $Z = P\overline{V}/RT$, T is temperature, $\overline{V}$ is the molar volume, P is the pressure, and R is the molar universal gas constant. The parameter a is a measure of the attractive forces between the molecules, and the parameter b is the covolume occupied by the molecules (if the molecules are represented by hard-spheres of diameter σ, then $b = 2\pi N\sigma^3/3$). The a and b parameters can be obtained from the critical properties of the fluid. The van der Waals equation can be regarded as a "hard–sphere (repulsive) + attractive" term equation of state composed from the contribution of repulsive and attractive intermolecular interactions, respectively. It gives a quantitative description of the vapour and liquid phases and phase transitions but it is rarely sufficient accurate for critical properties and phase equilibrium calculations. The van der Waals equation gives a qualitatively correct description of fluid properties and phase behaviour of fluids, but has a critical compressibility factor of 0.375 (true values for hydrocarbons between 0.24 and 0.29) and thus gives a pure

correlation of densities in the critical region. The van der Waals equation has been superseded by a large number of other, more accurate equations of state. More than hundred different equations of state have been published since van der Waals proposed his equation of state in 1873. Many of these equations can be categorized in terms of modifications to the basic van der Waals model.

Perhaps, the most important model for the modification of the van der Waals equation of state is the Redlich-Kwong equation (Redlich and Kwong, 1949). It retains the original van der Waals hard sphere term with the addition of a temperature-dependent attractive term

$$Z = \frac{\overline{V}}{\overline{V} - b} - \frac{a}{RT^{1.5}\left(\overline{V} + b\right)} \tag{3.28}$$

For pure substances, the equations parameters a and b are usually expressed as

$$a = 0.4278 \frac{R^2 T_c^{2.5}}{P_c}$$
$$b = 0.0867 \frac{RT_c}{P_c} \tag{3.29}$$

Carnahan and Starling (1972) used the Redlich-Kwong equation of state to calculate the gas-phase enthalpies for a varity of substances, many of which are polar and/or not spherically symmetric. Their results showed that the Redlich-Kwong equation is a significant improvement over the van der Waals equation. Abbott (1979) also concluded that the Redlich-Kwong equation performed relatively well for the simple fluids Ar, Kr and Xe (where the acentric factor is equal to zero), bit did not perform well for complex fluid with nonzero acentric factors.

In Figure 3-1 the vapour pressure and density of CO_2 have been calculated using the RK-EOS. CO_2 has an acentric factor of 0.23 and we see that the deviations to the experimental data are relatively high both for vapour pressures and densities.
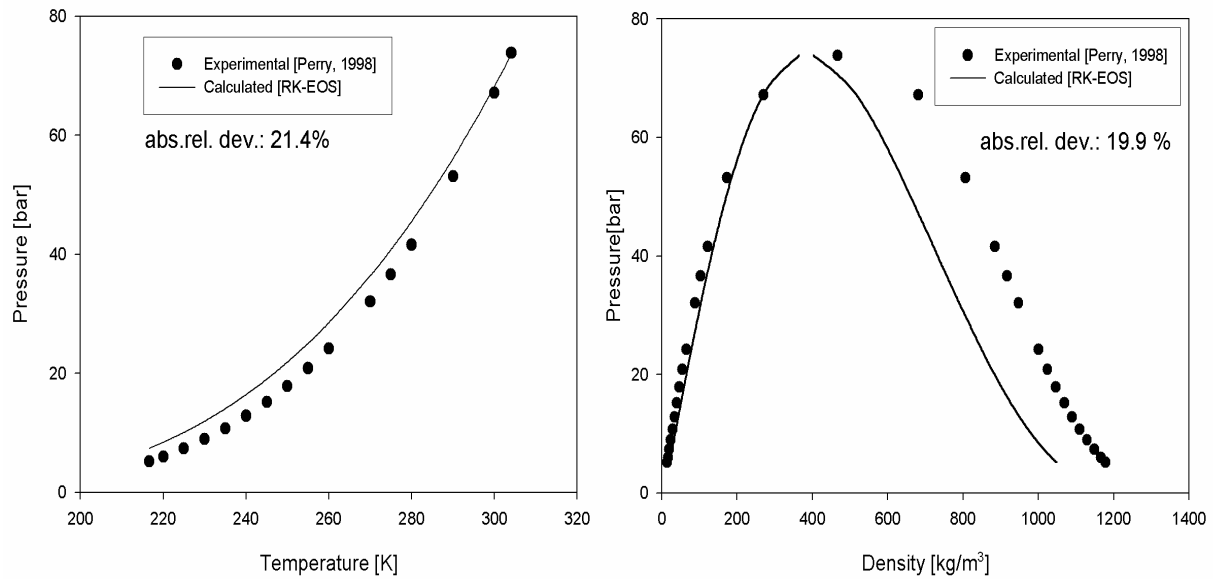
Figure 3-1 CO₂ vapour pressure and density calculated using the RK-EOS
          Script: bubp.py, p. 305

The success of the Redlich-Kwong equation has been the impetus for many further empirical improvements. Soave (1972) suggested replacing the term $a/T^{1.5}$ with a more general temperature-dependent term a(T), that is

$$Z = \frac{\overline{V}}{\overline{V} - b} - \frac{a(T)}{RT(\overline{V} + b)}$$ (3.30)

where

$$a(T) = 0.4274\left(\frac{R^2 T_c^2}{P_c}\right)\left\{1 + m\left[1 - \left(\frac{T}{T_c}\right)^{0.5}\right]\right\}^2$$

$$m = 0.480 + 1.57\omega - 0.176\omega^2$$ (3.31)

$$b = 0.08664\frac{RT_c}{P_c}$$

and ω is the acentric factor. To test the accuracy of Soave-Redlich-Kwong (SRK) equation, the vapour pressures of a number of hydrocarbons and several binary systems were calculated and compared with experimental data (Soave, 1972). In contrast to the original Reidlich-Kwong equation, Soave's modification fitted the experimental curve well and was able to predict the phase behaviour of mixtures in the critical region. Elliot and Daubert (1985) reported accurate correlations of vapor-liquid equilibria with the Soave equation for 95 binary systems containing hydrocarbon, hydrogen, nitrogen, hydrogen sulfide, carbon monoxide, and carbon dioxide. Elliot and Daubert (1987) also showed that the Soave equation improved the accuracy of the calculated critical properties of these mixtures. Accurate results were also

obtained for calculations of the vapor-liquid equilibrium of symmetric mixtures and methane containing mixtures.

In Figure 3-2 and Figure 3-3 the vapour pressure and saturated densities of methane and water calculated from the SRK-EOS are compared to experimental data. We can see that the predictions for the simple molecule methane are relatively good, while the calculations for the polar component water are poor.

The calculation of the liquid density will be better if we introduce a volume correction factor – such as the one proposed by Peneloux et.al (1982). Penloux shows that multicomponent VLE is unaltered by introducing the correction term as a mole fraction average.

$$\overline{V} = \overline{V}_{SRK} - \sum_{i=1}^{n} x_i c_i \qquad (3.32)$$

where $\overline{V}_{SRK}$ is the molar volume calculated from the SRK-EOS (eq. (3.30)) and c_i is the component dependent volume-shift parameter. When volume shift is introduced to the EOS for mixtures, the resulting expression for fugacity is

$$f_{i,SRK-Penloux} = f_{i,SRK} \exp\left(-c_i \frac{P}{RT}\right) \qquad (3.33)$$

Phase equilibria calculations are not affected by the volume correction if we use the same model for both phases. Applications that require direct use of fugacity (e.g chemical equilibrium calculations of this work and phi-gamma approaches) must include the volume-translation coefficient in the fugacity expression to be thermodynamic consistent. Even if the density calculation becomes more accurate, the calculation of the absolute fugacity will in general be worse when we introduce such volume corrections to the SRK-EOS (Michelsen et.al., 2000).
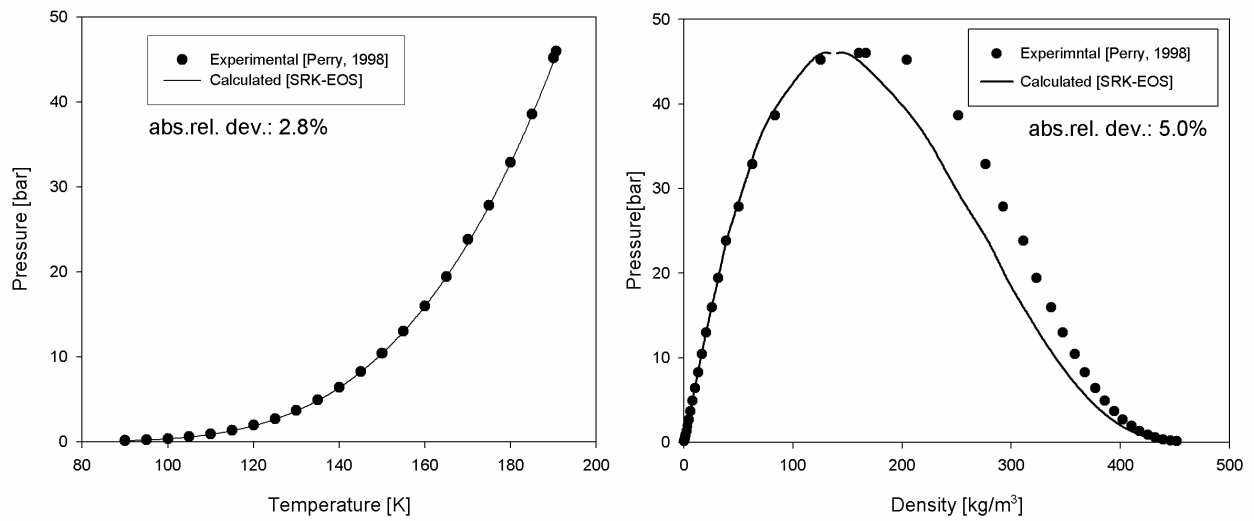
Figure 3-2 Vapour pressure and density of methane calculated using the SRK-EOS
Script: bubp.py, p. 305
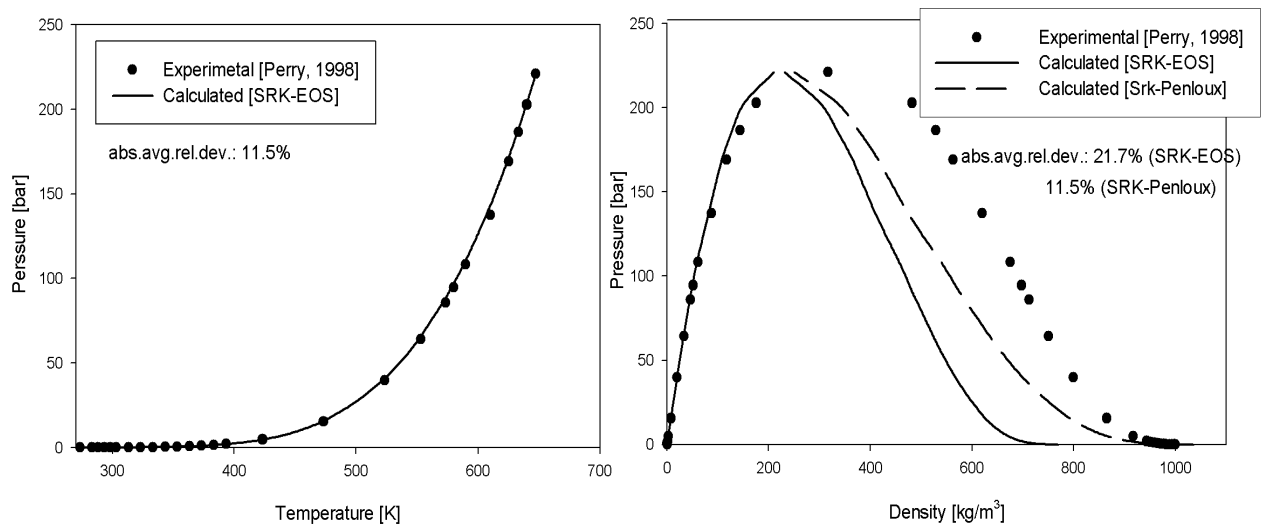
Figure 3-3 Vapour pressure and density of water calculated using the SRK-EOS
Script: bubp.py, p. 305

Peng and Robinson (1976) redefined a(T) as

$$a(T) = 0.45724 \left(\frac{R^2 T_c^2}{P_c} \right) \left\{ 1 + k \left[1 - \left(\frac{T}{T_c} \right)^{0.5} \right] \right\}^2$$

$$k = 0.37464 + 1.5422\omega - 0.26922\omega^2 \tag{3.34}$$

$$b = 0.07780 \frac{RT_c}{P_c}$$

Recognizing that the critical compressibility factor of the Redlich-Kwong equation (Z_c=0.333) is overestimated, they also proposed a different volume dependence

$$Z = \frac{\overline{V}}{\overline{V}-b} - \frac{a(T)\overline{V}}{RT\left[\overline{V}\left(\overline{V}+b\right)+b\left(\overline{V}-b\right)\right]} \qquad (3.35)$$

The Peng-Robinson (PR) equation of state slightly improves the prediction of liquid volumes and predicts a critical compressibility factor of Z_c=0.307. The prediction of the critical fugacity with the PR-EOS is generally less accurate then predictions with the SRK-EOS (Michelsen and Mollerup, 2000).

In Figure 3-4 vapour pressures and densities of water have been calculated using the Peng-Robinson equation of state. We can see that the liquid density is more accurately calculated than with the Soave-Redlich-Kwong model, but that it still deviates considerably from the experimental values.

The Peng-Robinson and Soave-Redlich-Kwong equations are used widely in industry. The advantages of these equations are that they can accurately and easily represent the relation among temperature, pressure, and phase composition in binary and multicomponent systems. They only require critical properties and acentric factor for the generalized parameters. Little computer time is needed and good phase equilibrium correlations can be obtained. However, the success of these modifications is restricted to the estimation of vapour pressure. The calculated saturated liquid volumes are not improved and are invariably higher than experimental measurements.
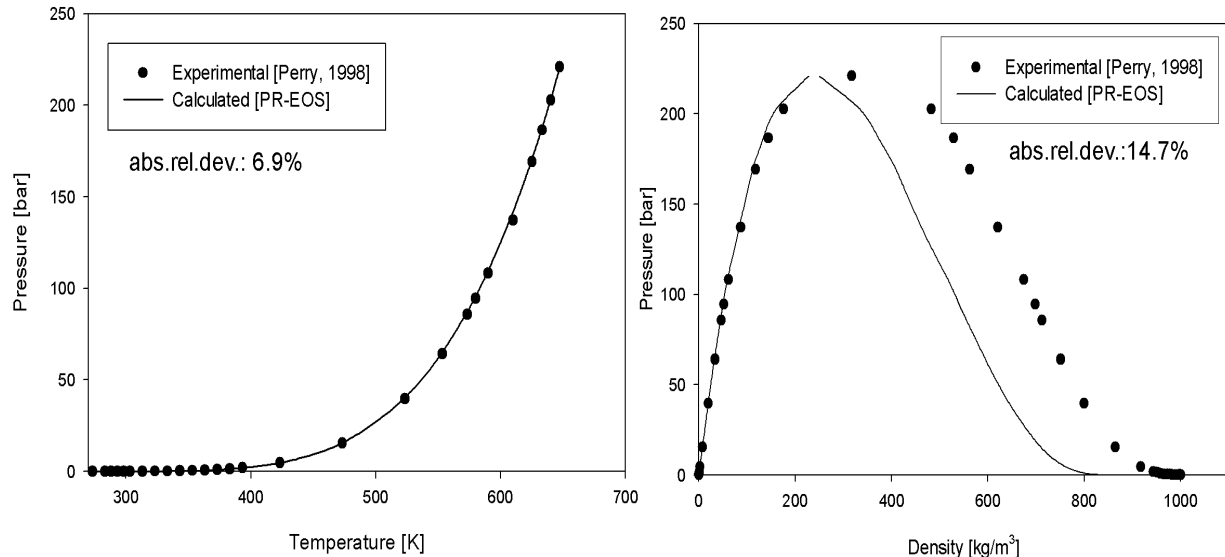
Figure 3-4 Vapour pressure and density of water calculated using the PR-EOS
        Script: bubp.py, p. 305

For polar components the SRK and PR gives bad results also for the vapour pressure. Many modifications have been proposed to give better predictions for polar components. One such model is the Schwartzentruber & Renon (1989) model (ScRK) – which introduce an alternative temperature dependence in the attractive term in the SRK equation of state.

$$a(T) = 0.4274 \left(\frac{R^2 T_c^2}{P_c} \right) \left\{ 1 + m \left(1 - T_r^{0.5} \right) - p_1 \left(1 - T_r \right) \left(1 + p_2 T_r + p_3 T_r^2 \right) \right\}^2 \qquad \text{for } T_r < 1$$

$$m = 0.48508 + 1.55191 \omega - 0.15613 \omega^2$$

$$a(T) = 0.4274 \left(\frac{R^2 T_c^2}{P_c} \right) \left\{ \exp \left[c \left(1 - T_r^d \right) \right] \right\}^2 \qquad \qquad \text{for } T_r > 1$$

$$d = 1 + \omega/2 - p_1 \left(1 + p_2 + p_3 \right)$$

$$c = 1 - 1/d$$

In general the Schwartzentruber & Renon (ScRK-EOS) expression offers a more flexible temperature dependence than the classical expression. It can therefore be used to represent more complicated pure component vapour pressure curves than what is possible with the classical expression. Parameters p_1, p_2 and p_3 can either be fitted to experimental vapour pressures or derived from the Antoine parameters of the pure components. They are set to zero for non-polar molecules.

In Figure 3-5 the vapour pressure and density of water predicted with the ScRK-EOS are compared to experimental data. We see that the vapour pressure is calculated very accurately – while the calculation of the liquid density still is inaccurate.
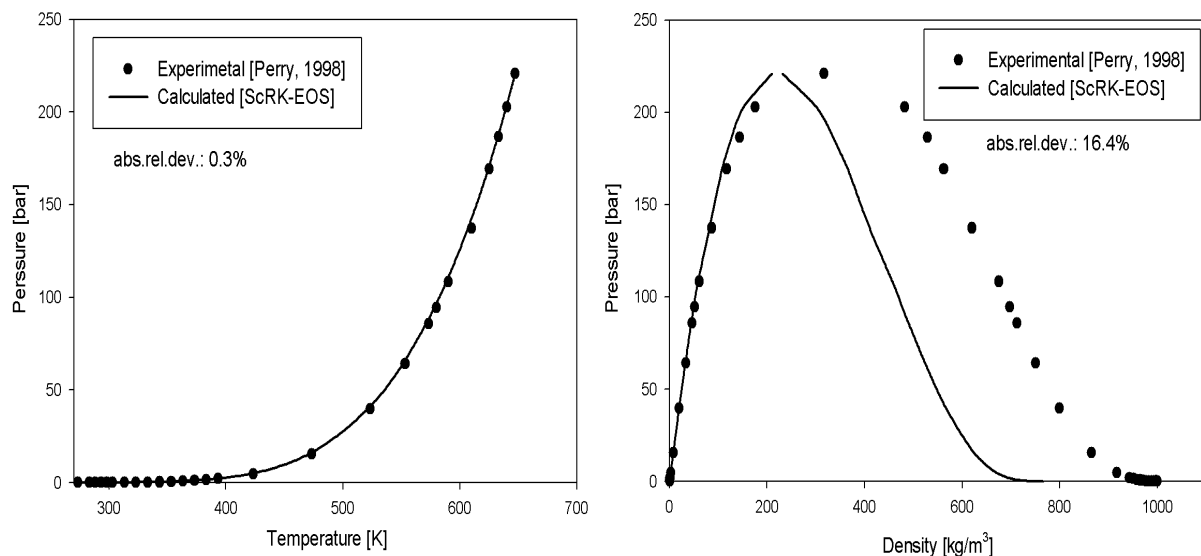
Figure 3-5 Vapour pressure and density of water calculated using the ScRK-EOS
Script: bubp.py, p. 305

3.3.2 Equations of State Based on Statistical Associating Fluid Theory

A more fundamental model, compared to the cubic equations of state, to account for the association and/or solvation is the statistical associating fluid theory (SAFT). The SAFT equation and its application was recently reviewed by Muller and Gubbins (2001). By extending Wertheims's (1984a,b) theory, Chapman et.al. (1988, 1990) proposed a general statistical associating fluid theory approach. Huang and Radosz (1990) developed the SAFT equation of state. The SAFT equation of state accounts for hard sphere repulsive forces,

dispersion forces, chain formation (for nonspherical molecules) and association, and it is presented as a sum, of four contributions to the Helmholtz function

$$\frac{A}{RT} = \frac{A_{ideal}}{RT} + \frac{A_{seg}}{RT} + \frac{A_{chain}}{RT} + \frac{A_{assoc}}{RT} \tag{3.36}$$

where A and A_{ideal} are the total Helmholtz function and the ideal gas Helmhotz function at the same temperature and density. The SAFT equation of state has been successfully used to model phase behaviour and thermodynamic properties of simple and complex fluid and fluid mixtures.

Kontogeorgis et.al. (1996) presented an equation of state suitable for describing associating fluids. The equation combines the simplicity of a cubic equation of state (the Soave-Redlich-Kwong), and the theoretical background of the perturbation theory employed for the association part. The resulting equation, called cubic plus association (CPA) equation of state, was given by

$$Z = \frac{\overline{V}}{\overline{V} - b_{CPA}} - \frac{a_{CPA}(T)}{RT(\overline{V} - b_{CPA})} + \rho \sum_{\alpha} \left(\frac{1}{X_{\alpha}} - \frac{1}{2} \right) \frac{\partial X_{\alpha}}{\partial \rho} \tag{3.37}$$

where the physical term is that of the Soave-Redlich-Kwong equation of state and the associating term is taken from SAFT equation (Huang and Radosz, 1990). The summation in the association term is over all association sites and the mole fraction not bounded at site A (X^{Ai}) is defined by

$$X^{A_i} = \left(1 + \rho \sum_j \sum_{B_j} x_j X^{B_j} \Delta^{A_i B_j} \right)^{-1}$$

$$\Delta^{A_i B_j} = g_{ij} \left[\exp\left(\frac{\varepsilon^{A_i B_j}}{RT} \right) - 1 \right] b_{CPA,ij} \beta^{A_i B_j} \tag{3.38}$$

where $\Delta^{A_i B_j}$ is the association strength, $\varepsilon^{A_i B_j}$ the association energy, $\beta^{A_i B_j}$ the association volume and $b_{CPA,ij} = \frac{1}{2}\left(b_{CPA,i} + b_{CPA,j} \right)$. The radial distribution function g_{ij} is given by

$$g_{ij} = \frac{2 - \frac{b_{CPA}}{4\overline{V}}}{2\left(1 - \frac{b_{CPA}}{4\overline{V}} \right)^3} \tag{3.39}$$

Finally the attractive term of the SRK-EOS is defined using a Soave-type temperature dependency,

$$a_{CPA}(T) = a_{CPA}\left(1 + m_{CPA}\left(1 - \sqrt{T_R} \right) \right)^2 \tag{3.40}$$

The pure component parameters that have to be fitted to vapour pressure and saturation density data are b_{CPA}, a_{CPA}, m_{CPA}, ε^{AB} and β^{AB}. Kontogeorgis et.al. (1996) applied this equation of state to pure components and obtained good correlations of both vapour pressures and saturated liquid volumes for primary-alcohols, phenol, tertbutyl alcohol, triethylene glycol and water. The equation has also been applied to mixtures of hydrocarbons and water – with success (Voutasas et.al., 1999).

Huang and Radosz (1990) have classified eight different association schemes. In this work we have employed the so called 2B (CO_2) and 4C (water and MDEA) association schemes, which are hereafter explained. These association schemes are obtained from molecular considerations where oxygen is assumed to have two association sites and hydrogen one association site.

The 2B association scheme:
$$\Delta^{AA} = \Delta^{BB} = 0$$
$$\Delta^{AB} \neq 0$$

The 4C association scheme:
$$\Delta^{AA} = \Delta^{AB} = \Delta^{BB} = \Delta^{CC} = \Delta^{CD} = \Delta^{DD} = 0$$
$$\Delta^{AC} = \Delta^{AD} = \Delta^{BC} = \Delta^{BD} \neq 0$$

In this work the association models (CPA-EOS) were implemented in the NeqSim computer code using a procedure suggested by Michelsen and Hendriks (2001). The thermodynamic properties and its derivatives could be found in a simple and effective way using the Michelsen Q-function procedure.

In Figure 3-6 and Figure 3-7 the vapour pressure and density of carbon dioxide and water were calculated using the CPA-EOS. We can see that the density predictions are much more accurate than with any of the earlier used equations of state. We also see that the critical point seems to be over-predicted, this is a known problem related to the SAFT based equations of state (Pfohl O. and Budich, M., 2001). The parameters used in the CPA-EOS will be presented in later chapters.
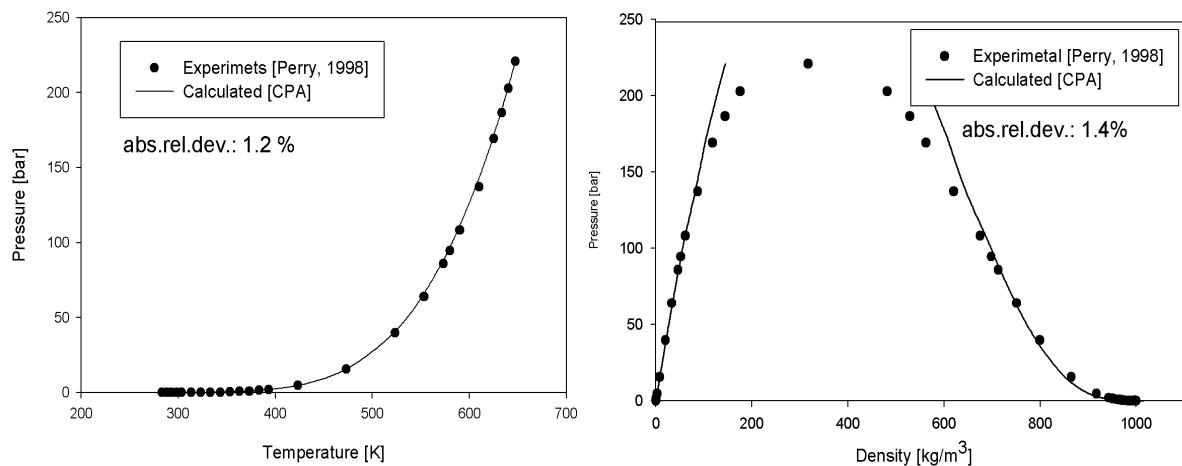
Figure 3-6 Vapour pressure and density of water calculated using the CPA-EOS
        Script: bubp.py, p. 305
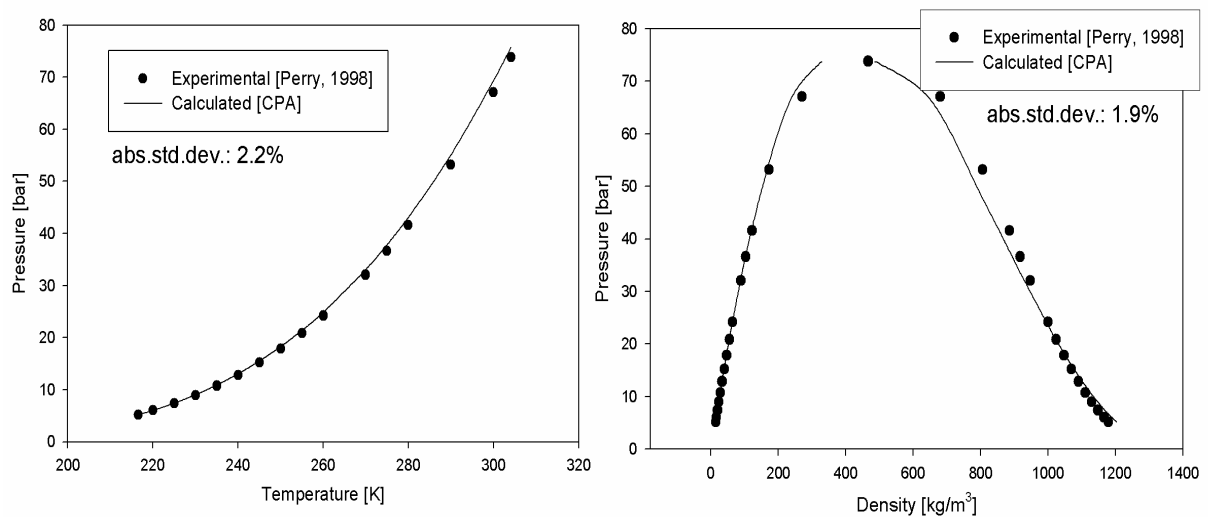
Figure 3-7 Vapour pressure and density of CO$_2$ calculated using the CPA-EOS
        Script: bubp.py, p. 305

3.3.3 Evaluation of EOS-Models for the Calculation of Pure Component Properties

An evaluation of pure component vapour pressure and densities predicted with the different EOS-models presented earlier is given in Table 3-1. The parameters used in the equations are given in the chapter on thermodynamic modelling (chapter 8) for amine systems.

Table 3-1 Absolute average relative deviation[1) [%] between experimental and calculated vapour pressures and densities with different equation of states

Component	RK	SRK	PR	ScRK[2)]	CPA[3)]	Experimental Data
Methane						Perry (1998),
vapour pressure:	15.6	2.8	**0.9**	2.8	-	Borgnakke et. al (1997)
liquid density:	**5.8**	6.5	8.1	6.5	-	
gas density:	17.7	3.9	**1.5**	4.6	-	
Nitrogen						Perry (1998),
vapour pressure:	10.1	1.7	**0.5**	2.2	-	Borgnakke et. al (1997)
liquid density:	4.5	4.2	4.5	**4.1**	-	
gas density:	11.8	3.3	**2.3**	3.8	-	
CO_2						Perry (1998),
vapour pressure:	21.4	0.3	0.8	**0.2**	2.2	Borgnakke et. al (1997)
liquid density:	14.9	11.6	4.0	11.5	**1.9**	
gas density:	24.9	3.2	2.5	3.5	**1.9**	
MDEA						Noll et.al. (1998)
vapour pressure:	>>100	83.3	67.2	5.1	**4.2**	
liquid density:	20.8	13.3	3.16	14.4	**1.1**	
gas density:	-	-	-	-	-	
Water						Perry (1998),
vapour pressure:	>>100	11.5	6.9	**0.3**	1.2	Borgnakke et. al (1997)
liquid density:	30.7	27.8	18.8	27.8	**1.1**	
gas density:	>>100	15.5	10.6	5.9	**1.7**	

[1)] Deviation (%) = 100 x (experimental-calculated)/experimental
[2)] The polar coefficients in the ScRK-EOS coefficients were fitted for water, CO_2 and MDEA
[3)] The coefficients in the CPA-EOS were fitted to experimental data

The RK-EOS generally gives larger deviations for both vapour pressures and densities than the other models. All the cubic equations of state (RK/SRK/PR/ScRK) give erroneous results for the liquid density for the polar component water. The introduction of a volume correction parameter can reduce this error – but will affect the chemical equilibrium calculations for the system. Of the classical cubic equations of state considered here, the Peng-Robinson model gives the best overall results for vapour pressures and densities for the systems considered.

For polar components the advanced CPA model generally gives the best results if we look at the average deviation of vapour pressure and density. The CPA-model has the advantage that it can be reduced to the classic SRK-EOS for non-polar components (by setting the number of associating sites to zero). The models will be evaluated for calculation of phase equilibrium for binary systems in the next section.

The ScRK-EOS and the CPA-EOS are the only models that are able to calculate vapour pressure of MDEA with an acceptable accuracy (5.1% and 4.2% absolute average deviation).

3.4 Mixing Rules

The great utility of equations of state is for phase equilibrium involving mixtures. The assumption inherent in such a calculation is that the same equation of state used for pure fluids can be used for mixtures if we have a satisfactory way to obtain the mixture parameters. This is achieved commonly by using mixing rules and combining rules, which relates the

properties of pure components to that of the mixture. The discussion will be limited to the extension of a and b parameters. These two parameters have a real physical significance and are common to many realistic equations of state.

The simplest possible mixing rule is a linear average of the equation of state parameters

$$a = \sum_i x_i a_i \qquad (3.41)$$

$$b = \sum_i x_i b_i \qquad (3.42)$$

Equation (3.42) is sometimes employed because of its simplicity, but (3.41) is rarely used because it does not account for the important role of unlike interaction in binary fluids. Consequently, employing both equations (3.41) and (3.42) would lead to poor agreement of theory with experiment.

3.4.1 Van der Waals Mixing Rules

The most widely used mixing rules are the Van der Waals one fluid proscriptions

$$a = \sum_i \sum_j x_i x_j a_{ij} \qquad (3.43)$$

$$b = \sum_i \sum_j x_i x_j b_{ij} \qquad (3.44)$$

where a_{ii} and b_{ii} are the constants of the equation for pure component i, and cross parameters a_{ij} and b_{ij} ($i \neq j$) are determined by an approximate combining rule or without binary parameters. The most common way of calculating a_{ij} and b_{ij} is

$$a_{ij} = \sqrt{a_i a_j} \left(1 - k_{ij} \right) \qquad (3.45)$$

$$b_{ij} = \frac{b_i + b_j}{2} \qquad (3.46)$$

where k_{ij} is a binary interaction parameter.

Equations (3.43) and (3.44) are based on the implicit assumption that radial distribution function of the component molecules are identical, and they both explicitly contain a contribution from interactions between dissimilar molecules. A comparison (Harismiadis et.al., 1991) with computer simulation has concluded that the van der Waals mixing rules are reliable for mixtures exhibiting up to a eight-fold difference in the size of the component molecules.

In this work it is important to accurately calculate the solubility of CO_2 in liquids over a large temperature and pressure range. Water and CO_2 are both polar (permanent dipole and quadrupole), but they are dissimilar molecules. In Figure 3-8 the results from the regression to CO_2 solubility data in water are presented. From the figure we can conclude that the van der Waals mixing rule is not able to give the correct temperature dependence for the CO_2 solubility in water over a wide temperature range. The classical mixing rules are also not able to predict mutual solubilities of CO_2 and water. If we fit the binary interaction coefficient to

CO_2 solubility data we get an interaction coefficient of about -0.13 while if we fit to water solubility in CO_2 we get a value of about 0.15.
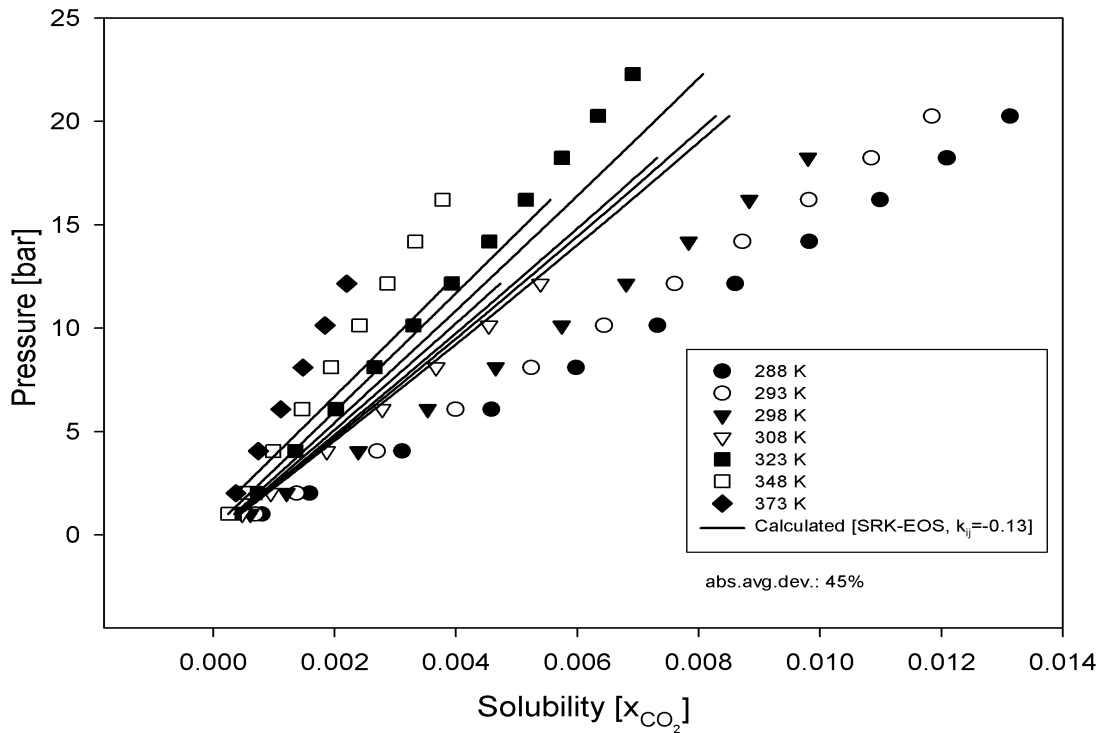
Figure 3-8 Calculation of CO_2 solubility in water using classical mixing rule. Experimental data from Houghton (1957). *Script: TPflash.py, p. 306*

3.4.2 Improved Van der Waals Mixing Rules

Many workers have proposed modifications for the van der Waals proscriptions. A common approach is to include composition-dependent binary interaction parameters to the attractive parameter in the van der Waals mixing rule and leave the b parameter rule unchanged.

Adachi and Sugie (1986) kept the functional form of the van der Waals mixing rule, left b parameter unchanged, and added an additional composition dependence and parameters to the a parameter in their van der Waals one-fluid mixing rule

$$a = \sum_i \sum_j x_i x_j a_{ij} \tag{3.47}$$

$$a_{ij} = \left(a_i a_j\right)^{1/2} \left[1 - l_{ij} - m_{ij}\left(x_i - x_j\right)\right] \tag{3.48}$$

Adachi and Sugie (1986) showed that their mixing rule could be applied to the binary and ternary systems containing strongly polar substances. The introduction of composition dependent interaction coefficients may violate homogeneity, and we may get the Michelsen Kistenmacher syndrome (Michelsen and Kistenmacher, 1990).

3.4.3 Mixing Rules From Excess Gibbs Energy Models

For binary pairs of components of which at least one is polar, the classical mixing rules are often insufficient. Huron and Vidal (1979) suggested a method for deriving mixing rules for equations of state from excess Gibbs energy models. Their method relies on three assumptions. First, the excess Gibbs energy calculated from an equation of state at infinite pressure equals an excess Gibbs energy calculated from a liquid phase activity coefficient model. Secondly, the covolume parameter b equals the volume V at infinite pressure. Third, the excess volume is zero. By using the SRK-EOS and applying the common linear mixing rule for the volume parameter b, the resulting expression for the parameter a is

$$a = b \left(\sum_{i=1}^{N} \left(z_i \frac{a_i}{b_i} \right) - \frac{G_\infty^E}{\ln 2} \right) \tag{3.49}$$

where G_∞^E is the excess Gibbs energy at infinite pressure. G_∞^E is found using a modified NRTL (Renon and Prauznitz ,1968) mixing rule

$$\frac{G_\infty^E}{RT} = \sum_{i=1}^{N} z_i \frac{\displaystyle\sum_{j=1}^{N} \tau_{ji} b_j z_j \exp(-\alpha_{ji} \tau_{ji})}{\displaystyle\sum_{k=1}^{N} b_k z_k \exp(-\alpha_{ki} \tau_{ki})} \tag{3.50}$$

where α_{ji} is a non-randomness parameter, i.e. a parameter for taking into account that the mole fraction of molecules of type i around a molecule of type j may deviate from the overall mole fraction of molecules of type i in the mixture. When α_{ji} is zero, the mixture is completely random. The τ - parameter is defined by the following expression

$$\tau_{ji} = \frac{g_{ji} - g_{ii}}{RT} \tag{3.51}$$

where g_{ji} is an energy parameter characteristic of the j-i interaction. In this work the g-parameters are temperature dependent and given by

$$\begin{aligned} g_{ij} - g_{jj} &= \left(g_{ij}' - g_{jj}' \right) + T \left(g_{ij}'' - g_{jj}'' \right) \\ g_{ji} - g_{ii} &= \left(g_{ji}' - g_{ii}' \right) + T \left(g_{ji}'' - g_{ii}'' \right) \end{aligned} \tag{3.52}$$

The parameter b entering into the expression for G_∞^E is the b-parameter of the SRK-equation. The classical mixing rule is still used for the b-parameter.

For a binary pair in which can be described by the classical van der Waals mixing rule, the local composition will not deviate from the overall composition and α_{ij} should be chosen to 0. By further selecting the following expressions for the interaction energy parameters, the Huron-Vidal mixing rules reduces to the classical van der Walls mixing rule.

$$g_{ii} = -\frac{a_i}{b_i}\left(\ln 2\right)$$

$$g_{ij} = -2\frac{\sqrt{b_i b_j}}{b_i + b_j}\sqrt{g_{ii}g_{jj}}\left(1 - k_{ij}\right)$$

(3.53)

Huron and Vidal (1979) showed that their mixing rule yields good results from non-ideal mixtures. Soave (1984) found the Huron-Vidal mixing rule represented an improvement over the classical quadratic mixing rules and made it possible to correlate vapour-liquid equilibria for highly non-ideal systems with good accuracy. The Huron Vidal mixing rule has also been applied to a varity of polar and asymmetric systems (Heidemann and Rizvi, 1986).

Figure 3-9 presents the results from calculations were the Huron-Vidal mixing rule was used with the SRK-EOS to model the solubility of carbon dioxide in water. From the figure we can see that the accuracy of the predictions is very good – but we should remember that we use more binary interaction parameters than for the classical van der Waals mixing rule used earlier.
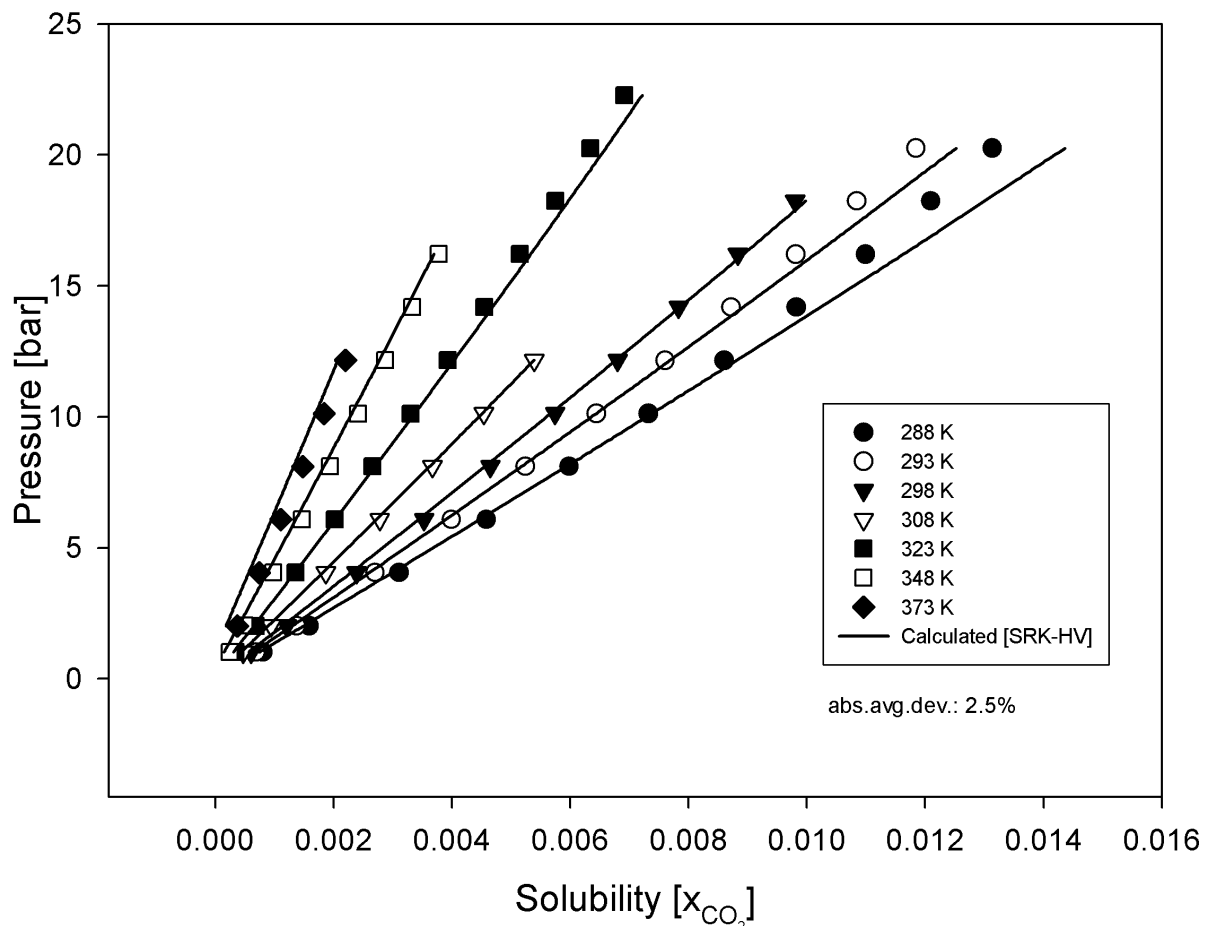
Figure 3-9 Calculation of CO₂ solubility in water using Huron-Vidal mixing rules. Experimental data from Houghton (1957). *Script: TPflash.py, p. 306*

The Huron-Vidal mixing rule is also capable of predicting the water solubility in gasses with a high accuracy (using the parameters fitted to mutual solubility data). In Figure 3-10 the

calculated water solubility in methane gas using the ScRK-EOS with the Huron Vidal mixing rule is compared to experimental data of Gillespie et.al. (1982) for a water-methane system. The model is capable of accurately representing the experimental data.
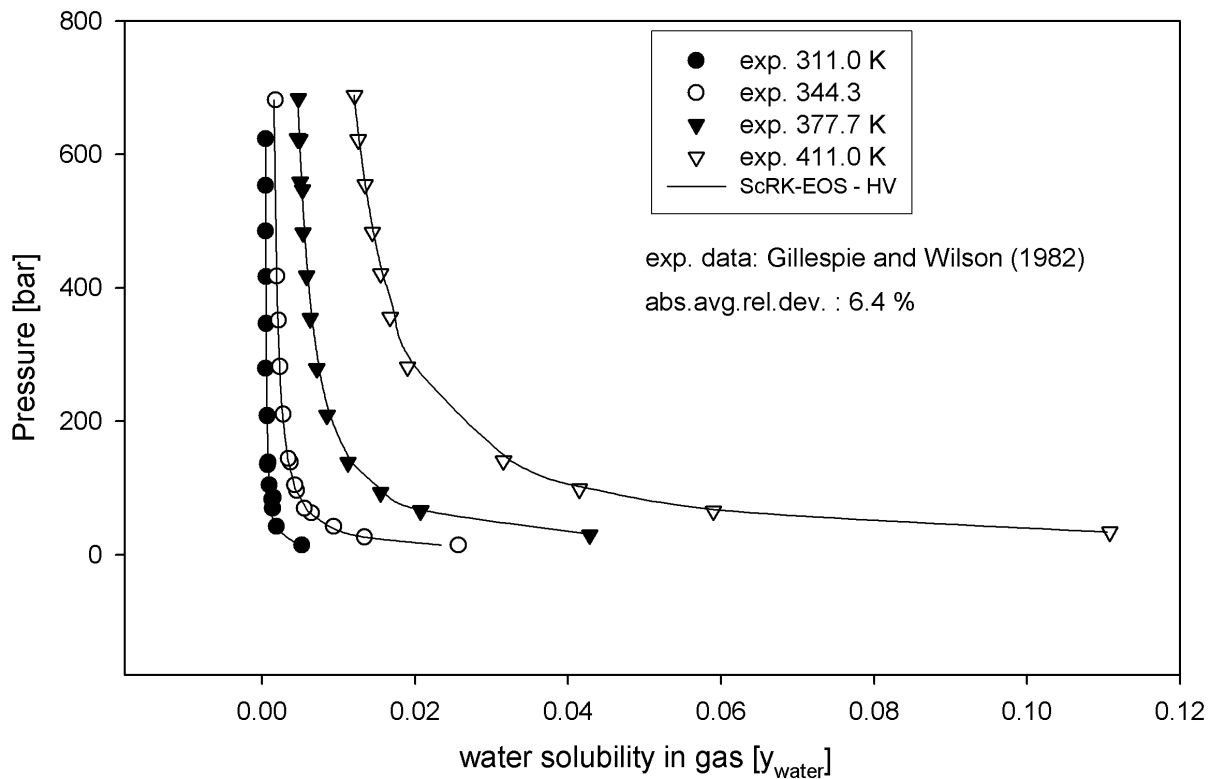
Figure 3-10 Water solubility in methane calculated with the Huron-Vidal mixing rule
Script: TPflash.py, p. 306

Using the Huron-Vial mixing rule described in this section we can generally model both solubilities of gasses in liquids and liquids in gasses with a high accuracy.

A weakness of the Huron-Vidal mixing rule is that the equation of state excess Gibbs energy at near atmospheric pressures differs from that at infinite pressure. The parameters in the Huron-Vidal are equal to parameters of the GE-model fitted to infinite pressure data. Most public available parameters for GE-models are obtained from low-pressure experimental data. Therefore, the Huron-Vidal mixing rule has a difficulty in dealing with low pressure data without refitting the parameters in the GE-models.

Mollerup (1986) modified equation (3.49) by retaining that the excess volume is zero but evaluating the mixture parameter a directly from the zero pressure excess free energy expression. Using a reference pressure of zero and the Soave-Redlich-Kwong equation of state the concepts of Mollerup were implemented by Michelsen (1990). Michelsen (Michelsen 1990, Dahl and Michelsen, 1990) repeated the matching procedure of Huron-Vidal resulting in the following mixing rule called the modified Huron-Vidal first order (MHV1)

$$\alpha = \sum_{i=1}^{n} x_i \alpha_i + \frac{1}{q_1} \left[\frac{G^E}{RT} + \sum_{i=1}^{n} x_i \ln\left(\frac{b}{b_i}\right) \right] \tag{3.54}$$

where

$$\alpha = {a}\big/{bRT}$$

$$b = \sum_{i=1}^{n} x_i b_i \tag{3.55}$$

$$\alpha_i = {a_i}\big/{b_i RT}$$

with the recommended value of q_1=-0.593. In addition, Dahl and Michelsen (1990) derived an alternative mixing rule referred to as the modified Huron-Vidal second-order (MHV2)

$$q_1\left(\alpha - \sum_{i=1}^{n} x_i \alpha_i\right) + q_2\left(\alpha^2 - \sum_{i=1}^{n} x_i \alpha_i^2\right) = \frac{G^E}{RT} + \sum_{i=1}^{n} x_i \ln\left(\frac{b}{b_i}\right) \tag{3.56}$$

with suggested values of q_1=-0.478 and q_2=-0.0047.

Dahl and Michelsen investigated the ability of MHV2 to predict high-pressure vapor-liquid equilibria when used in combination with the parameter table of modified UNIFAC (Larsen et.al., 1987). They concluded that satisfactory results were obtained for the mixtures investigated.

Generally, the use of the infinite pressure or zero pressure standard states for mixing in the equation of state will lead to inconsistencies with the statistical mechanical result that the second order virial coefficient must be a quadratic function of composition.

Wong and Sandler (1992) used the Helmholtz function to develop mixing rules to satisfy the second virial condition. For mixture parameters of an equation of state, a and b are

$$a = b\left[\sum_{i=1}^{n} x_i \frac{a_i}{b_i} + \frac{A_\infty^E}{C}\right] \tag{3.57}$$

$$b = \frac{\displaystyle\sum_i \sum_j x_i x_j \left(b - \frac{a}{RT}\right)_{ij}}{1 + \dfrac{A_\infty^E}{RT} - \displaystyle\sum_{i=1}^{n} x_i\left(\dfrac{a_i}{b_i RT}\right)} \tag{3.58}$$

where C is a constant dependent on the equation of state selected (for example, C is equal to $1/\sqrt{2}\ln\left(\sqrt{2}-1\right)$ for the Peng-Robinson equation of state) and A_∞^E is the excess Helmholtz function at infinite pressure, and

$$\left(b - \frac{a}{RT}\right)_{ij} = \frac{\left(1 - k_{ij}\right)}{2}\left[\left(b_i - \frac{a_i}{RT}\right) + \left(b_j - \frac{a_j}{RT}\right)\right] \tag{3.59}$$

where k_{ij} is a binary interaction parameter. The Helmholtz excess energy is relatively independent of pressure, and generally we can set $A_\infty^E = A^E$ (equal to excess energy at low

pressure). This leads to the important result that low pressure excess models (e.g UNIQUAQ, NRTL, UNIFAC(predictive)) and parameters can be used directly in the Wong-Sandler mixing rule.

Wong and Sandler tested the mixing rules (3.57) and (3.58), and concluded that they were reasonably accurate in describing both simple and complex phase behaviour of binary and ternary systems for the diverse systems they considered. The mixing rules can be applied at temperatures and pressures that greatly exceed the experimental data used to obtain the parameters.

To go smoothly from activity coefficient-like behaviour to the classical van der Waals one fluid mixing rule, Orbey and Sandler (1995) slightly reformulated the Wong-Sandler mixing rules by rewriting the cross second virial term given in equation (3.59) by

$$\left(b - \frac{a}{RT}\right)_{ij} = \frac{\left(b_i + b_j\right)}{2} - \frac{\sqrt{a_i a_j}\left(1 - k_{ij}\right)}{RT} \qquad (3.60)$$

while retaining the basic equations (3.57) and (3.58). Orbey and Sandler tested five binary systems and one ternary mixture and showed that this new mixing rule was capable of both correlating and predicting the vapour-liquid of various complex binary mixtures accurately over wide ranges of temperature and pressure and that it can be useful for accurate predictions of multicomponent vapour-liquid equilibria.

In Figure 3-11 vapour pressures of a binary mixture of methanol and water have been calculated with the SRK-EOS with the Wong-Sandler mixing rule (NRTL-GE model) and compared to calculations with the NRTL model. The parameters for the NRTL-model were the same in both models. We see that the SRK-EOS with the Wong-Sandler mixing rule is able to recreate the results from the NRTL model with a reasonable accuracy – using the same set of low-pressure parameters in the NRTL-model.
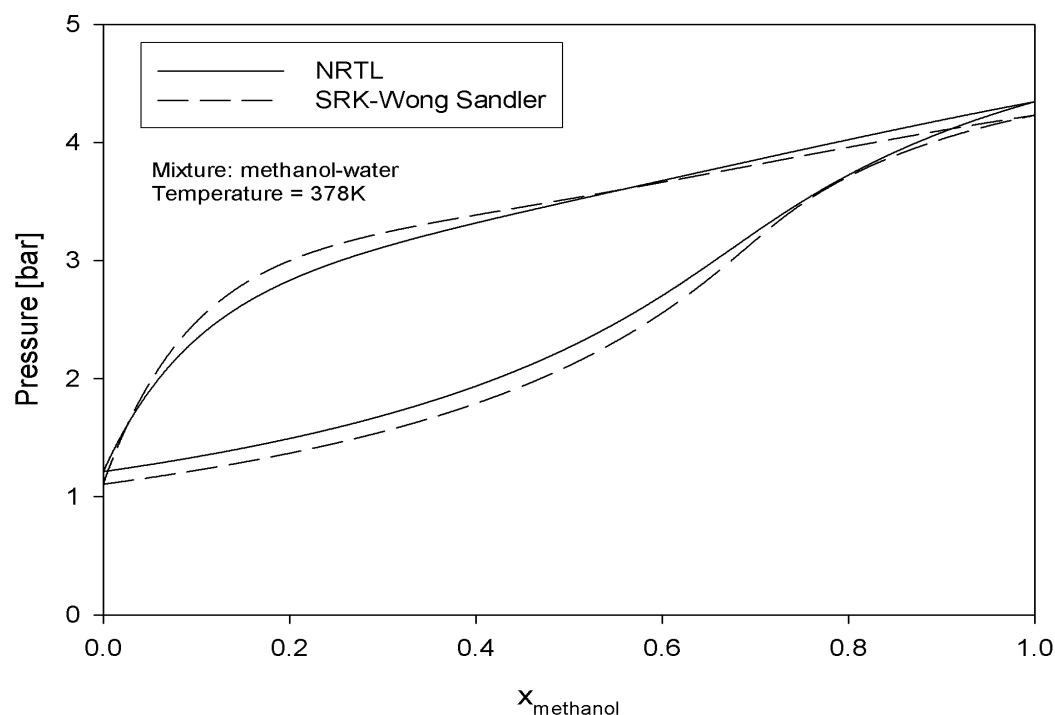
Figure 3-11 Vapour pressure of a binary mixture of methanol and water at 378 K calculated using the SRK-EOS with WS-mixing rule. *Script: TPflash.py, p. 306*

Several other mixing rules have been proposed (Heidemann and Kokal, 1990, Soave, 1992; Holderbaum and Gmehling, 1991) based on excess free energy expressions.

3.4.4 Combining Rules for Cross Association in the CPA-EOS

In systems with more than one associating component (such as water/alcohol systems), crossaccosiation occurs in the CPA-EOS model. In this case we need combining rules for the cross-association energy and volume parameters $\varepsilon^{A_iB_j}$ and $\beta^{A_iB_j}$. In this work the combination rules proposed by Voutsas et.al. (1999) were implemented.

$$\varepsilon^{A_iB_j} = \frac{\varepsilon^{A_i} + \varepsilon^{B_j}}{2}, \ \beta^{A_iB_j} = \sqrt{\beta^{A_i}\beta^{B_j}} \tag{3.61}$$

3.4.5 Evaluation of Models for the Calculation of Mutual Solubility

For this work the calculation of gas solubility in water is of crucial importance. In other situations the water solubility in gas is important (e.g. dew-point calculations). The equations of state and mixing rules presented earlier were fitted to the experimental data collected from the open literature, and a comparison of the mixing rules is given in Table 3-2. The fitting procedure, the experimental data used for regression and the final parameters obtained are described in chapter 8.

Table 3-2 Absolute average deviations (%) between experimental data and different models for the calculation of solubility of gasses in water and water in gas.

Gas	No.points used for fitting[1]	SRK + classic	SRK-HV[2]	ScRK-HV	PR-HV	SRK-WS	CPA + classic
Number of Fitted Parameters		**1**	**4**	**4**	**4**	**5**	**1**
Nitrogen							
nitrogen in water	13	>>100	**3.0**	7.1	4.3	8.7	29.7
water in nitrogen	78	32.2	**8.1**	17.6	10.0	11.6	28.2
CO_2							
CO_2 in water	43	>>100	6.0	6.1	**5.8**	7.6	12.0
water in CO_2	57	45.0	13.5	**10.6**	11.8	15.4	22.5
Methane							
methane in water	176	>>100	6.4	**5.5**	5.9	7.6	31.8
water in methane	215	52.2	13.1	10.6	**10.1**	10.4	14.1

1) See chapter 8 for references to the actual experimental data used in the fitting
2) The α parameter in the Huron Vidal and Wong Sandler mixing rule was not fitted

We see that the Huron-Vidal and the Wong-Sandler mixing rules perform similarly and very good for all components – but with more parameters than the other models. The big advantage of the Huron-Vidal mixing rule is that it can easily be reduced to the classical mixing rules for interaction between non-polar components. This is important when we are going to simulate gas mixtures with many hydrocarbon components.

It seems as if the Huron-Vidal mixing rule is able to calculate the mutual solubility of all gas-water systems considered here with a high accuracy. The SRK equation of state model with the classical mixing rule is not able to calculate both liquid and gas solubility. When fitting this model to dew point data – the calculated gas solubility in the liquid will be off by many orders of magnitude compared to the experimental values.

The CPA-EOS with the classical mixing rule performs much better than the SRK-EOS with the same mixing rule. The correlation of mutual solubility has a relatively low absolute average deviation. The average deviation in the correlation of CO_2 solubility in water is still too high to be acceptable (12.0%) for amine solutions. More advanced mixing rules used in with CPA-EOS could eventually compensate for this.

3.5 The Reduced Helmholtz Energy Calculated From an Equation of State

The pressure equation is often denoted an equation of state. Given a pressure equation

$$P = P(T, V, \mathbf{n}) \qquad (3.62)$$

where V is the total volume and $\mathbf{n}$ is the vector of mixture mole numbers. The usual textbook approach to calculate mixture fugacity coefficients is by means of an integral, i.e.

$$RT \ln \varphi_i = \int_0^P \left(\bar{V}_i - \frac{RT}{P} \right) dP = -\int_\infty^V \left(\left(\frac{\partial P}{\partial n_i} \right)_{T,V,n_j} - \frac{RT}{V} \right) dV - RT \ln Z \qquad (3.63)$$

where Z is the compressibility factor, $Z = PV/nRT$. However, interchange of the order of integration and differentiation in equation (3.63) leads to an equivalent, but more convenient expression

$$RT \ln \varphi_i = -\frac{\partial}{\partial n_i} \int_\infty^V \left(P - \frac{nRT}{V} \right) dV - RT \ln Z$$

$$= \frac{\partial A^r (T,V,\mathbf{n})}{\partial n_i} - RT \ln Z \qquad (3.64)$$

where

$$A^r (T,V,\mathbf{n}) = -\int_\infty^V \left(P - \frac{nRT}{V} \right) dV \qquad (3.65)$$

$A^r(T,V,\mathbf{n})$ is the residual Helmholtz function, i.e. the Helmholtz function of the mixture given as a function of temperature T, total volume V, and the vector of mixture mole numbers $\mathbf{n}$ minus that of the equivalent ideal gas mixture at the same state variables (T,V,$\mathbf{n}$).

The expression for the residual Helmholtz energy is a key equation in equilibrium thermodynamics because all other residual properties are calculable as partial derivatives in the independent variables T,V and n. In particular it is important to recognize that mole numbers rather than mole fractions are the independent variables. Derivatives with respect to mole fractions are best avoided as they require a definition of the "dependent" mole fraction and in addition lead to more complex expressions missing many important symmetry properties.

The pressure equation itself, normally used to define the "equation of state", is actually just one of these derivatives given by

$$P = -\left(\frac{\partial A^r (T,V,\mathbf{n})}{\partial V} \right)_{T,P} + \frac{nRT}{V} \qquad (3.66)$$

To modify a thermodynamic model, it is by far most convenient and safer to introduce such modifications directly in the expression for $A^r (T,V,\mathbf{n})$ remembering that modifications should depend only on T, V and $\mathbf{n}$ to preserve the homogeneity of the residual function. This approach reduces the risk of errors and inconsistencies or misconceptions such as "pressure dependent interaction coefficients".

In addition many models concepts relate directly to the Helmholtz function rather than to pressure equation. This applies for example to a corresponding states model, to a 'chemical' model, and to models based on statistical thermodynamics where the Helmholtz function is given directly in terms of canonical partition function.

3.6 Derivation of Thermodynamic Properties Using the Reduced Residual Helmholtz Energy

The calculation of thermodynamic properties is a problem that is discussed in many textbooks. Most approaches derive one property at a time – and it is no simple way to implement it effectively in a computer program. Michelsen and Mollerup (1986) have proposed a way of calculating all the thermodynamic properties based on the reduced Helmholtz energy.

$$F = \frac{A^r(T,V,n)}{RT} \qquad (3.67)$$

Where A^r is the residual Helmholtz energy.

In appendix A it is shown how the thermodynamic properties of a solution can be calculated from an expression for the reduced Helmholtz energy. In appendix B a general method for integrating mixing rules based on GE-models is given. By using these methods for implementing new models – one saves time and reduces chances for errors in the computer code.

The approach described above and in appendix for the calculation of thermodynamic properties was used in the modelling work for this thesis. In this way many different models could be implemented in the same computer code with a minimal effort.

3.7 Thermodynamic Modelling of Electrolyte Solutions

Although the thermodynamic properties of electrolyte solutions can be discussed in terms of chemical potentials and activities in much the same way as solutions of non-electrolytes, they have a number of distinctive features. One is the presence of strong interactions between ions in solution, which means that deviations from ideality are marked even in quite dilute systems. Therefore, we must equip our selves with means of dealing with activity coefficients that differ significantly from 1. A second feature is that, because many reactions of ions involve the transfer of electrons, they can be studied (und utilized) by allowing them to take place in an electrochemical cell.

3.7.1 The Thermodynamic Properties of Ions in Solution

Many of the concepts described for the non-electrolyte modelling carry over without change into the discussion of electrolyte solutions. The equations derived earlier in this chapter and in appendix A and B are valid for non-electrolyte systems as well as for electrolyte systems. The difference in the treatment of electrolyte systems arises from the presence of ions in the electrolyte solutions, which causes long range interactions due to columbic forces. Because of these long range interactions it is necessary to develop different models (or alternatively to add more terms) for the calculation of activity coefficients of electrolyte systems.

3.7.2 Concentration Scales

Different concentration scales are used in the description of electrolyte systems and the activity coefficients are different depending on the scale used. If the mole fraction scale is used the activity coefficients are called rational activity coefficients. If molality m (mol solute/kg solvent) is used they are called molal or practical activity coefficients.

For the calculation of chemical potential on the molality scale we use

$$\mu_i = \mu_i^\circ + RT \ln\left(m_i \gamma_i^\circ\right) \tag{3.68}$$

where the product $m_i \gamma_i^\circ$ is the ionic activity.

3.7.3 Ion Activities

Interactions between ions are so strong that the approximation of replacing activities by molalities is valid only in very dilute solutions (less than 10^{-3} mol/kg in total ion concentration) and in precise work activities themselves must be used.

We know that the chemical potential of a solute in a real solution is related to its activity by

$$\mu = \mu^0 + RT \ln a \tag{3.69}$$

where the standard state is a hypothetical solution with molality $m^0 = 1$ mol/kg in which the ions are behaving ideally. The activity is related to the molality, by

$$a = \frac{\gamma^\circ m}{m^0} \tag{3.70}$$

where the activity coefficient γ° depends on the composition, molality, and temperature of the solution. As the solution approaches ideality (in the sense of obeying Henry's law) at low molalities, the activity coefficient tends towards 1:

$$\gamma^\circ \to 1 \ and \ a \to m/m^0 \ as \ m \to 0 \tag{3.71}$$

Because all deviations from ideality are carried in the activity coefficient, the chemical potential can be written

$$\mu = \mu^0 + RT \ln m + RT \ln \gamma^\circ = \mu^{ideal} + RT \ln \gamma^\circ \tag{3.72}$$

where μ^{ideal} is the chemical potential of the ideal-dilute solution of the same molality.

3.7.4 Mean Ionic Activity Coefficients

If the chemical potential of a univalent cation M^+ is denoted μ_+ and that of a univalent anion X^- is denoted μ_-, the Gibbs energy of the ions in the electrically neutral solution is the sum of these partial molar quatities. The molar Gibbs energy for a real solution is

$$G_m = \mu_+ + \mu_- = \mu_+^{ideal} + \mu_-^{ideal} + RT \ln \gamma_+^\circ + RT \ln \gamma_-^\circ$$
$$= G_m^{ideal} + RT \ln \gamma_+^\circ \gamma_-^\circ \qquad (3.73)$$

All deviations from ideality are contained in the last term.

There is no experimental way of separating the product $\gamma_+^\circ \gamma_-^\circ$ into contributions from the cations and the anions. The best we can do experimentally is to assign responsibility for the non-ideality equally to both kinds of ions. Therefore for a 1:1-electrolyte, we introduce the mean activity coefficient as the geometric mean of the individual coefficients:

$$\gamma_\pm = \left(\gamma_+^\circ \gamma_-^\circ \right)^{1/2} \qquad (3.74)$$

and express the individual chemical potentials of the ions as

$$\mu_+ = \mu_+^{ideal} + RT \ln \gamma_\pm$$
$$\mu_- = \mu_-^{ideal} + RT \ln \gamma_\pm \qquad (3.75)$$

The sum of these two chemical potentials is the same as before (3.73), but now the non-idealities are shared equally.

This approach can be generalized to the case of a compound M_pX_q that dissolves to give a solution of p cations and q anions from each formula unit. The molar Gibbs energy of the ions is the sum of their partial molar Gibbs energies:

$$G_m = p\mu_+ + q\mu_- = G_m^{ideal} + pRT \ln \gamma_+^\circ + qRT \ln \gamma_-^\circ \qquad (3.76)$$

if we introduce the mean activity coefficient

$$\gamma_\pm = \left(\gamma_+^{\circ p} \gamma_-^{\circ q} \right)^{1/s} \qquad s = q + p \qquad (3.77)$$

and write the chemical potentials of each ion as

$$\mu_i = \mu_i^{ideal} + RT \ln \gamma_\pm \qquad (3.78)$$

we get the same expression as in equation (3.76) for G_m when we write

$$G = p\mu_+ + q\mu_- \qquad (3.79)$$

However, both types of ion now share equal responsibility for the non-ideality.

The advantage of using the mean ionic activity coefficient is that it can be measured directly in an electrochemical cell. It is however no conceptual problem of using individual activity coefficient of the ions in modelling work – but we are not able to measure them individually. In modelling work we often derive the ionic activity coefficients from an expression for the excess Gibbs energy of a solution. Using such models the individual activity coefficients can

be calculated directly. Individual activity coefficients were used in this work for the modelling of the weak electrolyte system CO_2-MDEA-water.

3.7.5 The Osmotic Coefficient

For electrolyte solutions solvent activity is close to unity and does not reflect the strong non ideality of the systems. To overcome this problem Bjerrum in 1909 introduced the osmotic coefficient Φ, which shows the deviation from ideality stronger than the activity coefficient of the solvent.

$$\Phi = \frac{-\ln\left(m_s \gamma_s\right)}{M_s \sum_i \nu_{ion,i} m_{ion,i}} = -\left[\left(\frac{\mu_s - \mu_s^0}{RT}\right) - \left(\frac{\mu_s - \mu_s^0}{RT}\right)^{ref}\right] \frac{x_s}{\sum_j x_j} \tag{3.80}$$

In Figure 3-12 the osmotic coefficient and the mean ionic activity coefficient of a NaCl solution are calculated with the electrolyte ScRK-EOS developed in this work and compared to experimental data. The mean ionic activity coefficient is generally more difficult to estimate accurately than the osmotic coefficient.
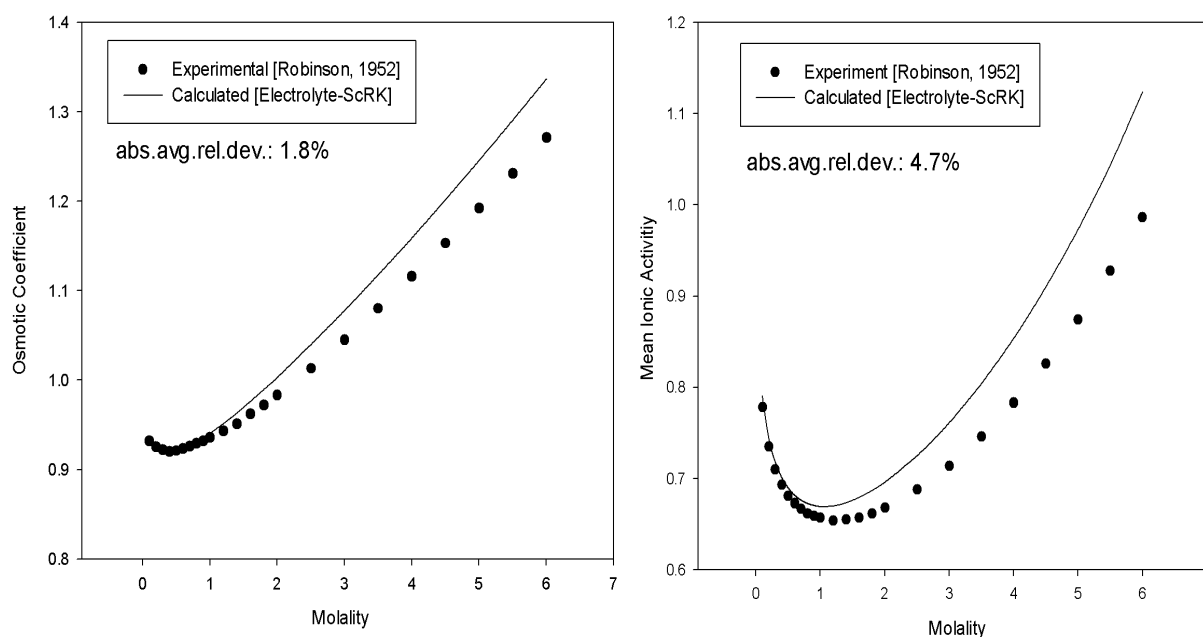
Figure 3-12 Mean ionic activity- and osmotic coefficient of a NaCl solution calculated using the electrolyte ScRK-EOS developed in this work. *Script: electrolyte.py, p. 307*

3.7.6 Review: The Development of Activity Coefficient Models for Electrolyte Solutions

The electrostatic interactions between ions in a solution are strong and have a long-range characteristic. This makes the electrolyte solutions very difficult to model. For many years, the textbooks avoided the subject of electrolyte solutions. The earliest attempt to systematically attack the problem went to Svante Arrenius in 1887. It was Peter Debye and Erick Huckel in 1923, which presented the first significant model for the activity coefficient

of electrolyte solution. By considering the ionic components as point charges and the solvent as a dielectric medium, they obtained the Debye-Huckel limiting law:

$$\ln \gamma_i = -A z_i^2 \sqrt{I}$$
$$\ln \gamma_{\pm} = -A |z_+ z_-| \sqrt{I}$$

$$(3.81)$$

where I is the ionic strength defined as

$$I = \frac{1}{2} \sum_{i=1}^{n} m_i z_i^2$$

$$(3.82)$$

and A is the Debye Huckel parameter, a function of solvent density (ρ_s), solvent dielectric constant (D_s), and temperature. The parameter A was given as

$$A = \frac{1}{2.303} \left(\frac{e}{\sqrt{D_s kT}} \right)^3 \sqrt{\frac{2\pi \rho_s N_{Av}}{1000}}$$

$$(3.83)$$

where N_{Av} is the Avagadro's number, e is the electronic charge, and k is the Boltzmann's constant.

Due to the assumptions and simplifications the Debye Huckel limiting law is valid only for very dilute solutions of ionic strength 0.001 molal (mol/kg solvent) or less. Recognizing this, Debye and Huckel proposed the extended Debye Huckel equation by taking account of the distance of closest approach and the effect of concentration on the dielectric constant.

$$\ln \gamma_{\pm} = -\frac{A |z_+ z_-| \sqrt{I}}{1 + \sigma \sqrt{I}}$$

$$(3.84)$$

where the σ is the closest approach between ions. Guntelberg (1926) suggested a simplified extended Debye Huckel equation.

$$\ln \gamma_{\pm} = -\frac{A |z_+ z_-| \sqrt{I}}{1 + \sqrt{I}}$$

$$(3.85)$$

This version of Debye Huckel equation holds quite well up to an ionic concentration of 0.1 molal. However, this ionic strength is still far too low for practical industrial applications. In this series of equations the only interaction that was taken into consideration was the electrostatic long-range interaction among the charged species. This is only true when the ionic concentration is low. When the ionic concentration is low the distance between a pair of ions is far enough to neglect the short-range interaction. Recognizing this, later studies tried to correct this shortcoming by assuming the non-ideality of the solution can be attributed by independent contributions. Interactions like ion-dipole, dipole-dipole and hydrogen bounding are significant only at close range and their effects drop rapidly as the separation distance between ions increase. Therefore for simplification, all these contributions are lumped into a short-range contribution. Based on this assumption, later models tried to consider the short-range interaction by combining binary, and sometimes ternary interaction parameters in their

equations. The concepts of these interaction parameters were originally developed from non-electrolyte systems.

A comparison between the variants of the Debye Huckel model and the electrolyte equation of state developed in this work is presented in Figure 3-13. It is easily seen that the Debye Huckel model gives poor results at high salt concentrations.
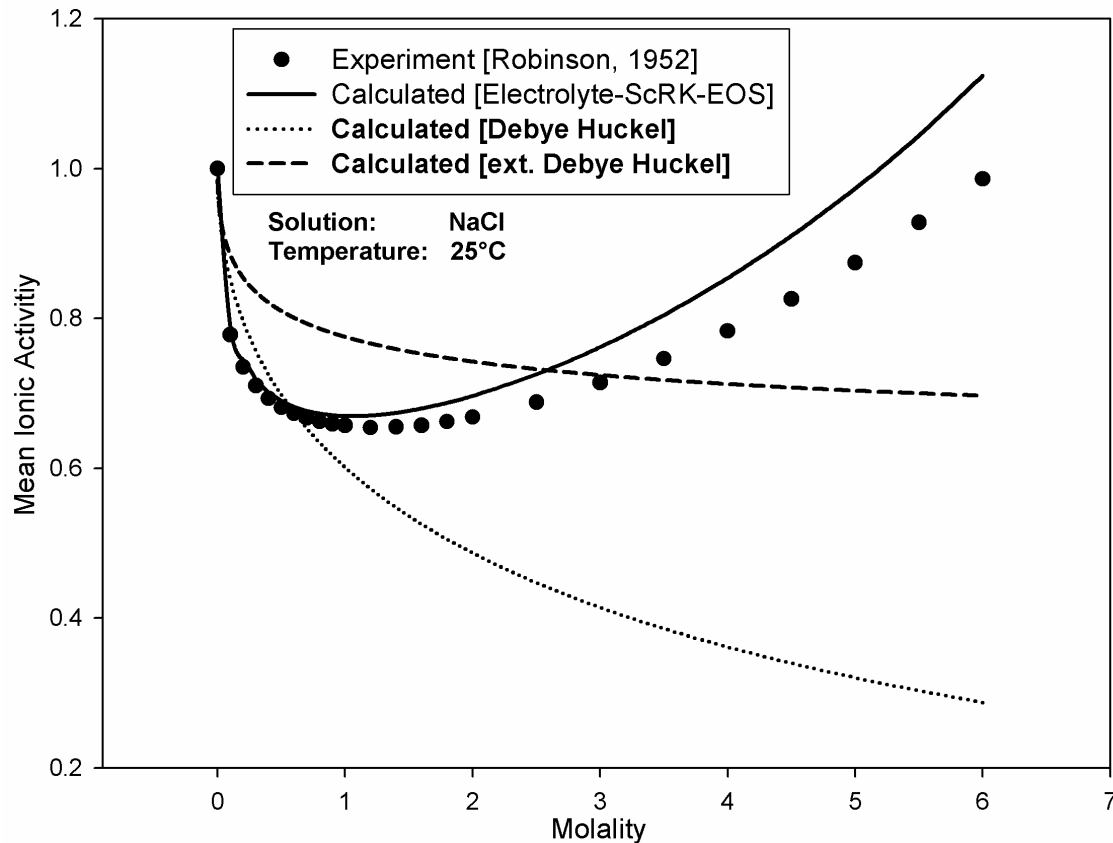
Figure 3-13 Calculated mean ionic activity coefficient for an aqueous NaCl solution using the Debye Huckel model and the electrolyte ScRK-EOS developed in this work. *Script: electrolyte.py, p. 307*

In 1935 and 1955, Guggenheim proposed his improved version of Debye Huckel equation by adding the second virial coefficients (binary interaction parameter). The mean activity coefficient for an electrolyte with cation c and anion a is:

$$\ln \gamma_{c,a} = -\frac{A|z_c z_a|\sqrt{I}}{1+\sqrt{I}} + \frac{2v_c}{v_c+v_a}\sum_a \beta_{c,a}m_a + \frac{2v_a}{v_c+v_a}\sum_c \beta_{c,a}m_c \qquad (3.86)$$

where v_a and v_c are number of anions and cations of the electrolyte, $\beta_{c,a}$ is coefficient for the interaction between c and a. In their 1955 paper, Guggenheim and Turgeon provided β's value for many electrolytes. For 1-1, 1-2, and 2-1 electrolytes, accurate calculations can be obtained up to 0.1 M (molarity [mole/liter solution]).

L.A. Bromley published a paper (1972) in witch he demonstrated that the pair interaction parameter $\beta_{c,a}$, in the Guggenheim's equation may be approximated by the values for the individual ions, β_c and β_a, for 1-1 electrolytes:

$$\beta_{c,a} = \beta_c + \beta_a \tag{3.87}$$

Bromley (1973) proposed a correlation for aqueous electrolyte systems. For a single salt solution, it is expressed as

$$\ln \gamma_{\pm} = \frac{A|z_+ z_-|\sqrt{I}}{1+\sqrt{I}} + \frac{(0.06 + 0.6B)|z_+ z_- I|}{\left(1 + \frac{1.5I}{|z_+ z_-|}\right)^2} + BI \tag{3.88}$$

B is constant for ionic interaction and its value for different electrolytes can be found in the same paper. For strong electrolytes, this equation can give good results up to 6 molal.

Pitzer (Pitzer 1973, Pitzer and Kim 1974, Pitzer 1980, Pitzer 1991) presented a series of papers dealing with electrolyte thermodynamic properties. From their analyses they found that the ion-ion short-range interactions are important and are dependent in the ionic strength. They proposed their model by taking into account both binary and ternary inter-ion interactions. The theory can be expressed in terms of excess Gibbs free energy as

$$\frac{G_E}{RT} = w_w f(I) + \frac{1}{n_W} \sum_i \sum_j \lambda_{i,j}(I) n_i n_j + \frac{1}{n_W^2} \sum_i \sum_j \sum_k \Lambda_{i,j,k} n_i n_j n_k \tag{3.89}$$

where w_w is the kilo gram of water, $\lambda_{i,j}(I)$ is the ionic strength dependent coefficient of binary interaction between ion i and ion j, and $\Lambda_{i,j,k}$ is the coefficient of tertiary interaction among ions i, j, and k. In activity coefficient form

$$\ln \gamma_i = \frac{z_i^2}{2} \frac{df(I)}{dI} + 2\sum_j \lambda_{i,j}(I) m_j + \frac{z_i}{2} \sum_j \sum_k \frac{d\lambda_{i,j}(I)}{dI} m_j m_k + 3\sum_j \sum_k \Lambda_{i,j,k} m_j m_k \tag{3.90}$$

This model has proven to be highly successful for many electrolyte systems up to ionic strength of 6 molal.

All of the above mentioned models ignored the solvent. The solvent was taken into account through its dielectric constant in the solution medium.

Chen et.al. (1979), presented an extension of Pitzer's model by adding the molecular contribution on the excess Gibbs free energy. They tested the validity of the model by correlating VLE experimental data for three systems. They successfully reproduced the aqueous hydrochloride solution data up to 18 molal and aqueous K_2CO_3-CO_2 systems up to 40 percent K_2CO_3. In 1982, Chen et.al. proposed their new model by combining the local composition concept with Pitzer's model. In this model, excess Gibbs free energy is divided into two contributions, long range and short-range interactions. They adopted the extended Debye-Huckel equation proposed by Pitzer (1973, 1980) to deal with the long-range forces. Meanwhile, they characterized the short-range interactions by the concept of local composition, originally developed for non-electrolyte systems. The activity coefficient of each species can be expressed as

$$\ln \gamma_i = \ln {\gamma_i}^{PDH} + \ln {\gamma_i}^{LC} \tag{3.91}$$

where the superscript PDH stands for Pitzer-Debye-Huckel and LC means local composition. They utilized the non-random two-liquid (NRTL) model, by Renon and Prausnitz (1968), for the LC term. Their model worked well for some strong electrolytes up to 6 molal. In 1986, they successfully tested their model to some weak electrolyte solutions.

Another route to the study of properties of electrolyte solution is based on the mean spherical approximation (MSA) theory (Blum and Høye, 1977). In the MSA theory, the solvent molecules are removed and replaced by a dielectric continuum. This idealization of ionic solution is called the primitive model. In the model, the ions are considered as charged spheres of different sizes immersed in a dielectric medium. The interaction potential between two ions i and j is given by

$$
\begin{aligned}
U_{i,j} &= +\infty \qquad r \le \sigma_{ij} \\
U_{i,j} &= \frac{q_i q_j}{Dr} \qquad r > \sigma_{ij}
\end{aligned}
\tag{3.92}
$$

where q_i and q_j are the charges on i and j, D is the dielectric constant, r is the distance between i and j, and σ_{ij} is the average of collision diameter of i and j, $\left(\sigma_i + \sigma_j\right)/2$. By assigning pair correlation function g_{ij} and direct correlation function C_{ij},

$$
\begin{aligned}
g_{ij}(r) &= 0 \qquad\qquad r \le \sigma_{ij} \\
C_{ij}(r) &= -\frac{q_i q_j}{DkT}\frac{1}{r} \qquad r > \sigma_{ij}
\end{aligned}
\tag{3.93}
$$

one can solve Ornstein-Zernik (OZ) (Lee, 1988) equation

$$h_{ij}\left(r,r^{'}\right) - C_{ij}\left(r,r'\right) \equiv \sum_k \rho_k \int ds\, C_{ik}\left(r,s\right) h_{ij}\left(s,r'\right) \tag{3.94}$$

MSA was first solved for the restricted primitive model. In the restricted primitive model the sizes of anion and cation are assumed to be equal (Waisman and Lebowitz, 1972). Blum (1975); Blum and Hoye (1977) generalized it to the non-restricted primitive model, where the ionic sizes are not necessarily equal. Plache and Renon (1981) generalized MSA to a non-primitive model and applied it to simple electrolyte solutions and polar substances. They could reproduce the experimental data up to 6 molal. In 1985 Ball et.al. derived an equation of state based on the MSA-model developed by Planche and Renon, and were able to derive an analytical model for the thermodynamic properties of ionic solutions. The model was used to correlate ionic solution data up to 6 molal.

Furst and Renon (1993) derived an equation of state for electrolyte solutions based on the work of Ball et.al. and Plance et.al. The model was based on the ScRK-EOS and added two additional terms for electrolyte interactions. They could predict the activity and osmotic coefficient of salt solutions up to 6 molal. In this work an electrolyte equation of state based on Furst and Renons model was developed (electrolyte ScRK-EOS).
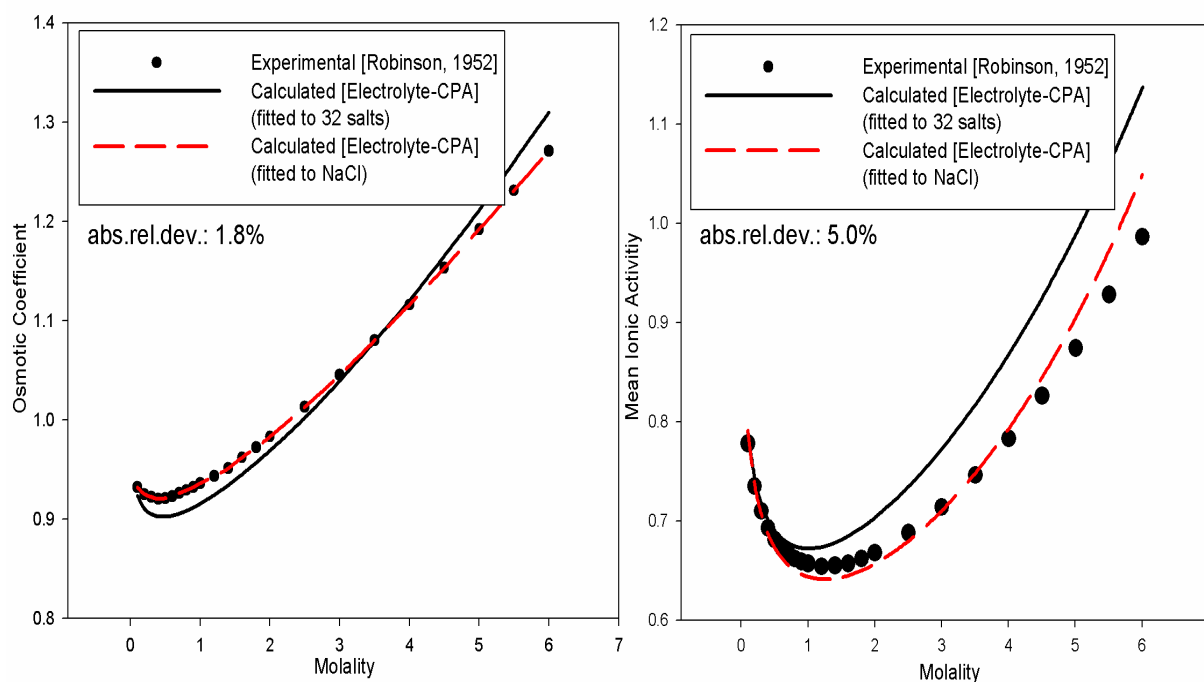
Figure 3-14 Osmotic coefficient and activity coefficients calculated with electrolyte-CPA model implemented in this work. *Script: electrolyte.py, p. 307*

In 1998 Wu and Prausnitz developed an electrolyte model based on the Peng-Robinson EOS plus an association term taken from the CPA-EOS. A simplified MSA and a Born term were used to represent ionic contributions. In this work an electrolyte equation of state (electrolyte CPA-EOS) based on the CPA model is developed. In this model the electrolyte terms are equal to those used in the electrolyte ScRK-EOS. Figure 3-14 gives an illustration of the performance of this model for an aqueous solution of NaCl. We can see that both the osmotic coefficient and the mean ionic activity coefficient are calculated with an acceptable accuracy up to 6 molal. The model is described in detail later in this chapter.

3.7.7 Review: The Development of Thermodynamic Models for Acid Gas Treating

The acid gas sweetening process has been studied for decades. Countless papers on experimental data, model development and plant operations can be found in the literature. The goal of the present section is to give a systematic review of the relevant studies in the past. In fact, the central issue in thermodynamics studies in the past was focused on the activity coefficient model.

The non-ideality of a solution occurs because of differences in the properties of its constituents. Solutions containing similar species, like benzene-toluene, behave almost like ideal solutions. However in the aqueous alkanolamine solution loaded with sour components, interactions and associations between ions, solvent, co-solvent(s), and different functional groups make the solution highly non-ideal.

The first attempt to correlate the solubility data for CO_2-ethanol-water systems was made by Mason and Dodge (1936). It was a plain curve fitting approach. In 1949, Van Krevlen et.al.

developed a model to predict partial pressure of H_2S and NH_3 over an aqueous solutions. In their model, a pseudo-equilibrium constant, which contains no activity coefficients and is a function of ionic strength, was used. Dankwerst and McNeil (1967) adopt Van Krevlen's approach to predict the CO_2 pressure over carbonate solutions. The most serious limitation of this model is that the ionic strength alone is insufficient to determine the concentration dependency of the pseudo-equilibrium constants. Kent and Eisenberg (1976) modified the Dankwerst and McNeil approach and calculated the equilibrium solubility of H_2S-alkanolamine-water systems. They adopted the published equilibrium constants from the literature for all reactions, except the protonation and carbamation of amines. They treated these two values as adjustable parameters and forced the calculated pressure to match the experimental data. This model is only valid in very narrow loading range from 0.2 to 0.7 mole of acid gas/mol of amine. When used as a predictive tool, this model gives significant deviation from experimental values. The model is unsuccessful for tertiary amines because they do not form carbamates and, as a result, one of the adjustable parameters is missing for tertiary systems.

Atwood et.al. (1957) proposed a model to calculate the equilibria of H_2S-amine-water system. In their calculations, they introduced the mean activity coefficients. The activity coefficients of all ionic species are assumed to be equal. This model was utilized Klyamer and Kolesnikova (1972) for CO_2-amine-water systems, and generalized by Klyamer et.al. (1973) for H_2S-CO_2-amine-water calculations. The activity coefficients are dependent on the ionic strength of solution only and were calculated by Debye-Huckel's limiting law, eq. (3.81).

Edwards et.al. (1975) developed a thermodynamic model to calculate the vapour liquid equilibrium of sour water system. They adopted the Guggenheim's equation (eq. (3.86)) for activity coefficient calculation. In their development, in addition to the ion-ion long range and short range interactions, they also included the short range ion-molecule and molecule-molecule interactions. This model is thermodynamically more rigorous than those developed earlier. However, the calculations were limited to low concentration of electrolyte and low temperature (below 80°C). In 1978, Edwards et.al. extended their previous work by replacing the Guggenheim's equation with Pitzer's equation (Eq. (3.90)). This time their calculation range had been improved up to 10 to 20 molal and 0 to 170°C.

Deshmukh and Mather (1981) applied Guggenheim's equation (Eq. (3.86)) to develop another model for H_2S and CO_2 in aqueous MEA systems. The binary interaction parameters have been fitted for H_2S-MEA-water and CO_2-MEA-water VLE systems. In 1985, Chakravarty extended Deshmukh and Mather's model to different amine systems, including DEA, MDEA, and DIPA. They also calculated the VLE for acid gas in aqueous mixed amine systems. By adjusting selected binary interaction parameters and carbamation equilibrium constants, they fitted their calculation to the extensive body of data reported in the literature. Weiland et.al. (1993) also adopted this model and a new set of parameters were obtained by regression.

Austgen (1989) adopted the electrolyte-NRTL model (Chen et.al 1982) for acid gas-alkanolamine systems. A rigorous thermodynamic framework had been developed. The adjustable parameters including the binary interaction parameters and ternary (molecule-ion pair) interaction parameter had been regressed to fit binary (amine-water) and ternary (acid-gas, amine and water) systems. They also adjusted the carbamation equilibrium constant in their calculation. Prediction of mixed acid gases in aqueous amines and CO_2 in aqueous amine blends were also made. However, for some systems, the parameters used in binary interaction were different from those used in ternary ones. Chang et.al. (1993) tried to refit

their binary parameter by adding new data on freezing point measurements in their data. Posey and Rochelle (1994) measured the amine-water binary heat of mixing data, combined with total pressure, freezing point depressing data for their electrolyte-NRTL binary parameters regression. A new parameter set was given. Addicks (2002) fitted parameters in the electrolyte NRTL-model to high pressure experimental data for methane, CO_2, water and MDEA.

Li and Mather (1994) presented a new model applying the new Pitzer equation (1991). For short range interaction, instead of only consider ion-ion interactions in the orginal (1973) equation, the new Pitzer equation takes into account interactions between all species. Li and Mather correlated the data for carbon dioxide in aqueous MDEA and aqueous MEA systems. Binary and ternary interaction parameters were obtained from regression. Prediction of the VLE of carbon dioxide in aqueous MDEA-MEA blends was also made in their work. The errors in prediction were greater than 30%.

Oscarson et.al. (1995) developed a thermodynamic model for VLE and enthalpy calculation of solution of acid gases in aqueous alkanolamine solutions. They used Pitzer equation as modified by Edwards et.al (1978). They needed to add some postulated ion-pair formation in their model to fit the experimental data within acceptable error. It is still unknown if the ion-pair formation are true or just fitting.

Vallee et.al. (1999) developed a model based on the Furst and Renon electrolyte equation of state (Furst & Renon, 1993). They were able to develop a model for aqueous solutions of DEA who were able to correlate and predict the equilibrium CO_2 partial pressure over a wide range of loadings and temperatures. The model was later used by Chunxi and Furst (2000) to model CO_2 and H_2S partial pressures over aqueous solutions of MDEA.

A model based on the Furst and Renon EOS (1993) has been developed and implemented in this work. In Figure 3-15 the calculated activity and speciation of a CO_2-MDEA-water solution is given as function of loading (mol CO_2/mol amine).

Button and Gubbins (1999) use the SAFT equation of state to model the vapour-liquid equilibria of CO_2, water and MEA or DEA. Unlike the models discussed earlier in this section, the SAFT-EOS does not require any knowledge of the chemical reactions in the liquid phase. Instead the reactions are incorporated in the association term by allocating association cites to the molecules. It is not clear from the article of Button and Gubbins how accurate the model correlates the experimental data.
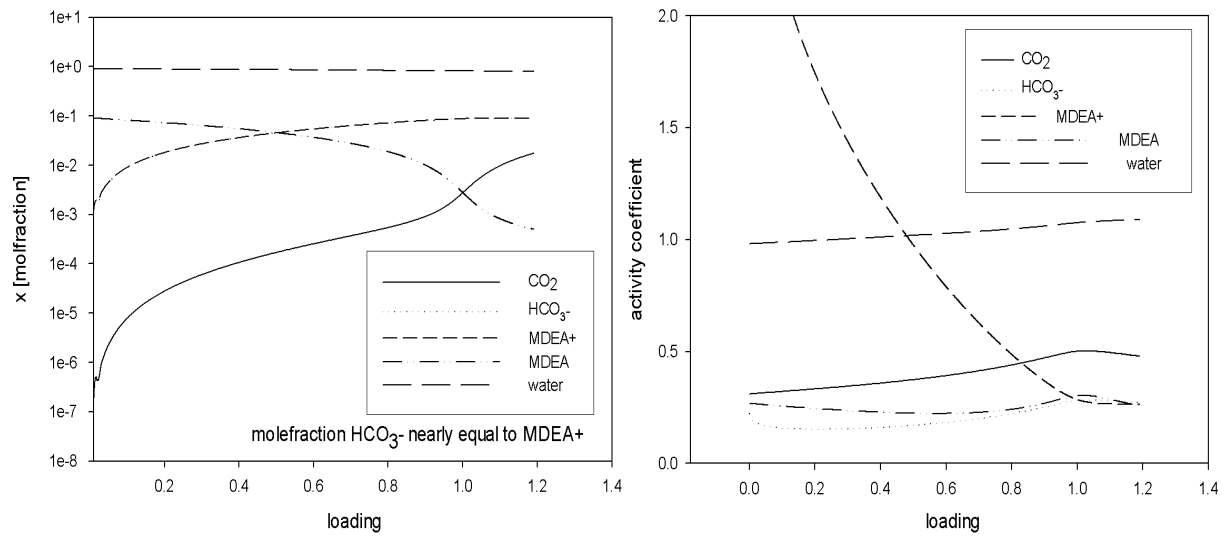
Figure 3-15 Speciation of a CO_2 , MDEA (30wt%) and water solution at 313K calculated from the electrolyte ScRK-EOS developed in this work. *Script: electrolyte-MDEA.py, p. 308*

3.8 The Electrolyte Equation of State

Most models for the representation of non-ideality in electrolyte solutions use the formalism of excess Gibbs energy. Few attempts to use Helmholtz free energy expressions and derived equations of state have been published. This is in contrast to the noticeable developments of the equation of state approach in the representation of non-electrolyte solutions. As new precise equation of state of non-electrolyte solutions are now available for the representation of equilibrium properties, it become useful to develop methods extending the applications of those EOS to the representation of the thermodynamic properties where electrolytes are dissolved.

The electrolyte equation of state presented by Furst and Renon (1993) was derived from an expression of the Helmholtz energy including a non-electrolyte part and two terms devoted to the representations specific to the ions. The originality of their approach was the use of an equation of state (Schwartzentruber Redlich-Kwong EOS) previously developed for modelling non-electrolyte systems. This means that we can use our thermodynamic models for non-electrolyte systems – and add terms specific to ionic components. This is advantageous because the model reduces to the chosen EOS if no ions are present.

The molar Helmholtz Energy is developed as the sum of (Born term added in this work):

$$\left(\frac{A-A^0}{RT}\right) = \left(\frac{A-A^0}{RT}\right)_{RF} + \left(\frac{A-A^0}{RT}\right)_{SR1} + \left(\frac{A-A^0}{RT}\right)_{SR2} + \left(\frac{A-A^0}{RT}\right)_{LR} + \left(\frac{A-A^0}{RT}\right)_{BORN} \quad (3.95)$$

where the two first terms are the ones obtained from the cubic equation of state (appendix A),

$$\left(\frac{A-A^0}{RT}\right)_{RF} + \left(\frac{A-A^0}{RT}\right)_{SR1} = -n \cdot g\left(V, B(n)\right) - \frac{D(n,T)}{T} f\left(V, B(n)\right) \quad (3.96)$$

A-A^0 is the residual of the Helmholtz energy and corresponds to the F-function given in equation (3.67). The functions g and f are dependent on the equation of state used. For cubic equations of state the expressions for the different terms in this equation (3.96) and its derivatives are given in Michelsen and Mollerup (2000). All of the equations of state discussed earlier in this chapter could in principle be used to model the RF and the SR1 term in equation (3.96). The last three terms (ionic contributions) of equation (3.95) and the derivatives are given here and in appendix C.

The SR2 term of equation (3.96) is a short range term specific to interactions involving ionic species.

$$\left(\frac{A - A^0}{RT} \right)_{SR2} = -\sum_k \sum_l \frac{n_k n_l W_{kl}}{V (1 - \varepsilon_3)}$$

(3.97)

where at least one of k and l is an ion. W_{kl} is an ion-ion or ion-molecule interaction parameter. ε_3 is calculated from,

$$\varepsilon_3 = \frac{N\pi}{6} \sum_k \frac{n_k \sigma_k^3}{V}$$

(3.98)

where k is over all species and σ_k is the molecular- or ionic diameter. The ion-molecule/ion-ion interaction parameter W is an adjustable parameter. A model for calculating the values of these interaction parameters is described in section 8.3.

The SR2 term may be considered as a simplified form of the corresponding term in Plance and Ball's MSA model (Plance and Renon (1981), Ball et. al. (1985)). The fact that a short range interaction term specific to ionic species is added to the equivalent term in an equation of state is justified by the fact that the short-range interactions between ions and polar molecular species are very different from the corresponding interactions in nonelectrolyte solutions.

The long-range ion-ion interaction term is given by a simplified MSA term (Planche et.al 1980, Ball et. al. 1985),

$$\left(\frac{A - A^0}{RT} \right)_{LR} = -\frac{\alpha_{LR}^2}{4\pi} \sum_i \frac{n_i Z_i^2 \Gamma}{1 + \Gamma \sigma_i} + \frac{\Gamma^3 V}{3\pi N}$$

Where the shielding parameter Γ is given implicitly by the equation

$$4\Gamma^2 = \alpha_{LR}^2 \sum_i \frac{n_i}{V} \left(\frac{Z_i}{1 + \Gamma \sigma_i} \right)^2$$

with,

$$\alpha_{LR}^2 = \frac{e^2 N}{\varepsilon_0 DRT}$$

where ε_0 is the dielectric permitivity of free space. The dielectric constant is calculated from

$$D = 1 + (D_s - 1)\frac{\left(1 - \varepsilon_3^{''}\right)}{\left(1 + \dfrac{\varepsilon_3^{''}}{2}\right)}$$

In this equation $\varepsilon_3^{''}$ is similar to ε_3 defined in equation (3.98) but the sum is only over ions. The shielding parameter is calculated by a Newton approach, and is normally found in a few iterations with 0 as an initial guess. The solvent dielectric constant is given as

$$D_s = \frac{\sum\limits_i n_i D_i}{\sum\limits_i n_i} \qquad (3.99)$$

where the summation is only over molecular components.

The Born term is given as,

$$\left(\frac{A - A^0}{RT}\right)_{BORN} = \frac{Ne^2}{4\pi\varepsilon_0 RT}\left(\frac{1}{D_s} - 1\right)\sum_i \frac{n_i Z_i^2}{\sigma_i^*}$$

In this work the ionic volume in this equation $\left(\sigma_i^*\right)$ is the same as used earlier in the SR2 term $\left(\sigma_i\right)$. The Born term does not give contribution to the activity coefficient of ions for pure component solvents, but gives a contribution to the fugacity coefficient. The contribution of the Born term is a strong function of the dielectric constant of the solvent, D_s. This term is the reason for the low solubility of ions in the gas phase (low dielectric constant). It is because of this term that few ions exist in the gas phase. Furst and Renon did not use the Born term in their original publication (1993) – though it has been added in a later article on LLE in electrolyte systems. The Born term is important if you want to model the gas and liquid with the same model – because it contributes in such a way that it keeps the ions in the liquid phase. For a mixed solvent it would give a contribution to the activity coefficient of an ion – and will therefore be important in the modelling of MDEA-water solutions when we use infinite dilution in pure water as the reference state for ions.

The partial derivatives of the F-functions used for calculating thermodynamic properties for the electrolyte terms in the electrolyte equation of state are given in appendix C.

In this work two different equations of state were used to model the non-electrolyte part of equation (3.95). In the first model the ScRK-EOS with the Huron-Vidal mixing rule was used to model molecular interactions, and in the second model the CPA model was used to model these interactions. The models will be referred to as the electrolyte ScRK-EOS and the electrolyte CPA-EOS.

In Figure 3-16 the osmotic coefficient for selected salt solutions are calculated using the electrolyte ScRK-EOS – and compared to experimental data of Robinson et.al. (1952). We

see that the electrolyte model generally gives good results. The modelling work to the experimental data is described in chapter 8.
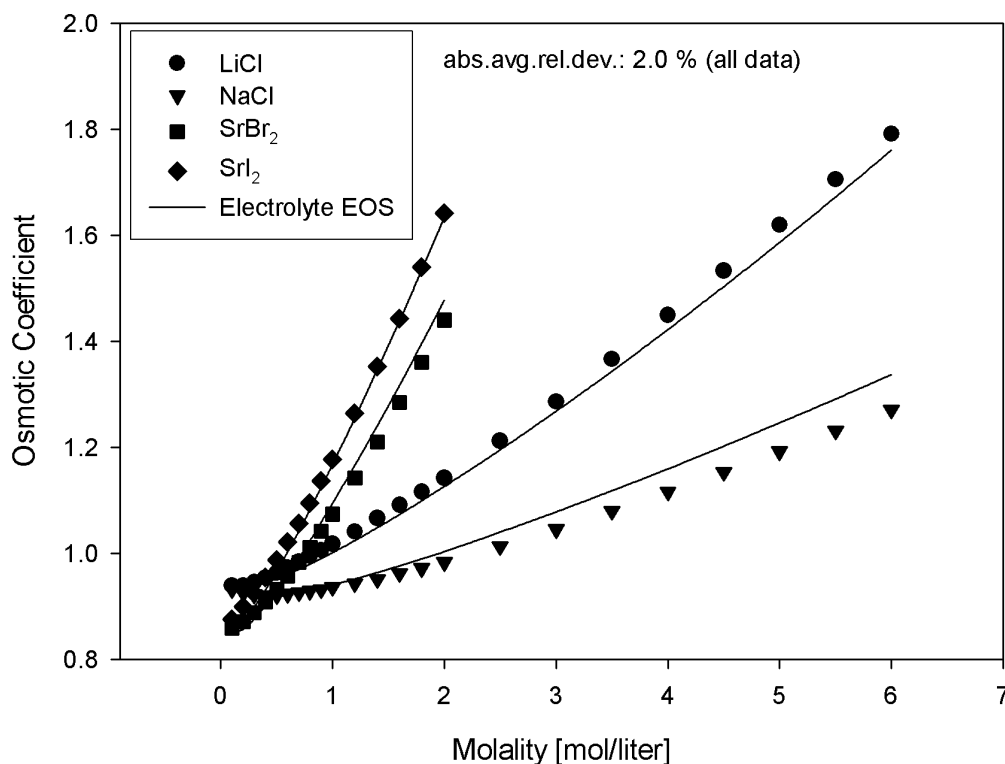
Figure 3-16 Osmotic coefficients of salt solutions calculated using the electrolyte ScRK-EOS
Script: electrolyte.py, p. 307

3.8.1 Evaluation of Variants of the Electrolyte Equation of State

In this work two different variants of the electrolyte equation of state have been implemented. Both models are extensions of the electrolyte EOS proposed by Furst and Renon in 1993 as was described in last section. In both models a Born term has been added to the original model. The Born terms corrects for the gibbs energy of charging the ion into the solvent medium - and is the main reason for large differences in fugacity of ions in liquids and gasses. With the introduction of the Born term both vapour and liquid can be calculated with the same model.

In the first electrolyte EOS implemented in this work the physical term in the EOS is the Schwartzentruber EOS (as was used by Furst and Renon in 1993) with the Huron-Vidal mixing rule (Chunxi .et.al. (2000) used the Wong Sandler mixing rule). In the second model developed in this work, the CPA-EOS was used to model molecular interactions with a classical Van der Waals mixing rule. The ionic terms were described in last section. The modelling procedure for the two electrolyte equations is illustrated in Figure 3-17.
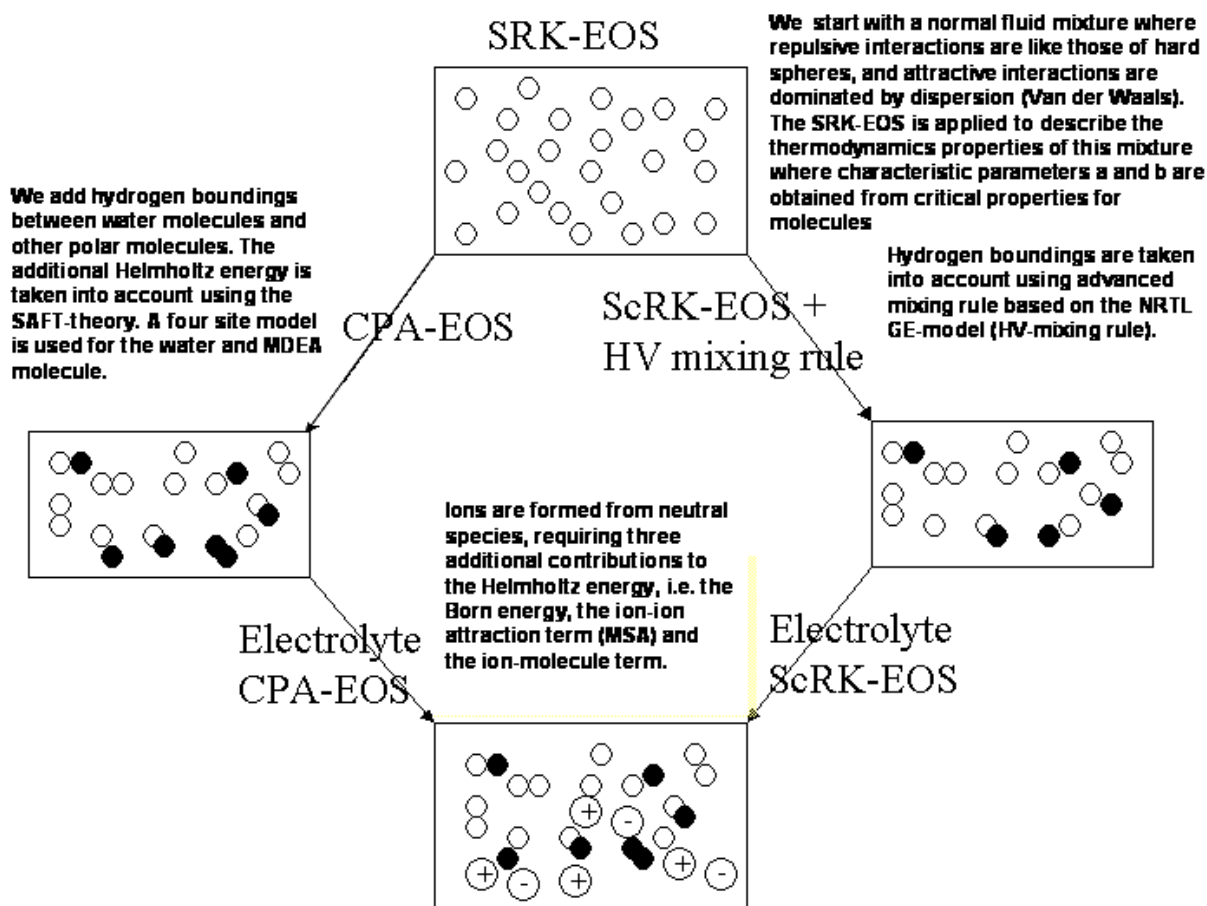
Figure 3-17 Development of the electrolyte equations of state

The models were fitted to experimental osmotic coefficient data of 28 halide salt solutions. Five parameters were fitted to all the experimental data in the molality range 0.1-6. The fitting procedure and the resulting parameters are given in chapter 8. Comparisons between the two electrolyte models are given in Table 3-3.

Table 3-3 Evaluation of different electrolyte models for the calculation osmotic coefficient and mean ionic coefficient for 28 halide salt solutions[1]

Model	No. of experimental points used in fitting	Osmotic coefficient abs.avg.rel.dev [%]	Mean ionic activity abs.avg.rel.dev [%]	Experimental data
Electrolyte ScRK-EOS	230	2.1	5.5	Robinson (1952)
Electrolyte CPA-EOS	230	2.3	4.9	Robinson (1952)

[1] Salt concentrations: 0.1-6.0 molal. Salt solutions: NH_4Cl, LiCl, LiBr, LiI, NaCl, NaBr, NaI, KCl, KBr, KI, KBr, KI, RbCl, RbBr, RbI, CsCl, CsBr, CsI, $MgCl_2$, $MgBr_2$, MgI_2, $CaCl_2$, $CaBr_2$, MgI_2, $CaCl_2$, $CaBr_2$, CaI_2, $SrCl_2$, $SrBr_2$, SrI_2, $BaCl_2$, $BaBr_2$, BaI_2

From Table 3-3 we see that both the electrolyte ScRK-EOS and the electrolyte CPA-EOS are able to represent the osmotic coefficients and activity coefficient of aqueous salt solutions with good accuracy. As was shown earlier the solubility of CO_2 in water could not be

calculated accurately with the CPA-EOS with the one-parameter classical mixing rule. For the calculation of solutions of CO_2-MDEA and water we expect the electrolyte ScRK-EOS with the Huron Vidal mixing rule to be the most accurate (but with more fitted parameters).

The density of ionic solutions is calculated directly from the electrolyte equation of state. A comparison between calculated and experimental measured densities for a NaCl-solution is given in Figure 3-18. We see that the calculated density is accurate for low-concentrations of NaCl. For higher concentration the deviation increases – but the deviation is always relatively low. We see that the accuracy of the calculated densities with the electrolyte-CPA-EOS and the electrolyte-ScRK-EOS with volume correction are about the same.
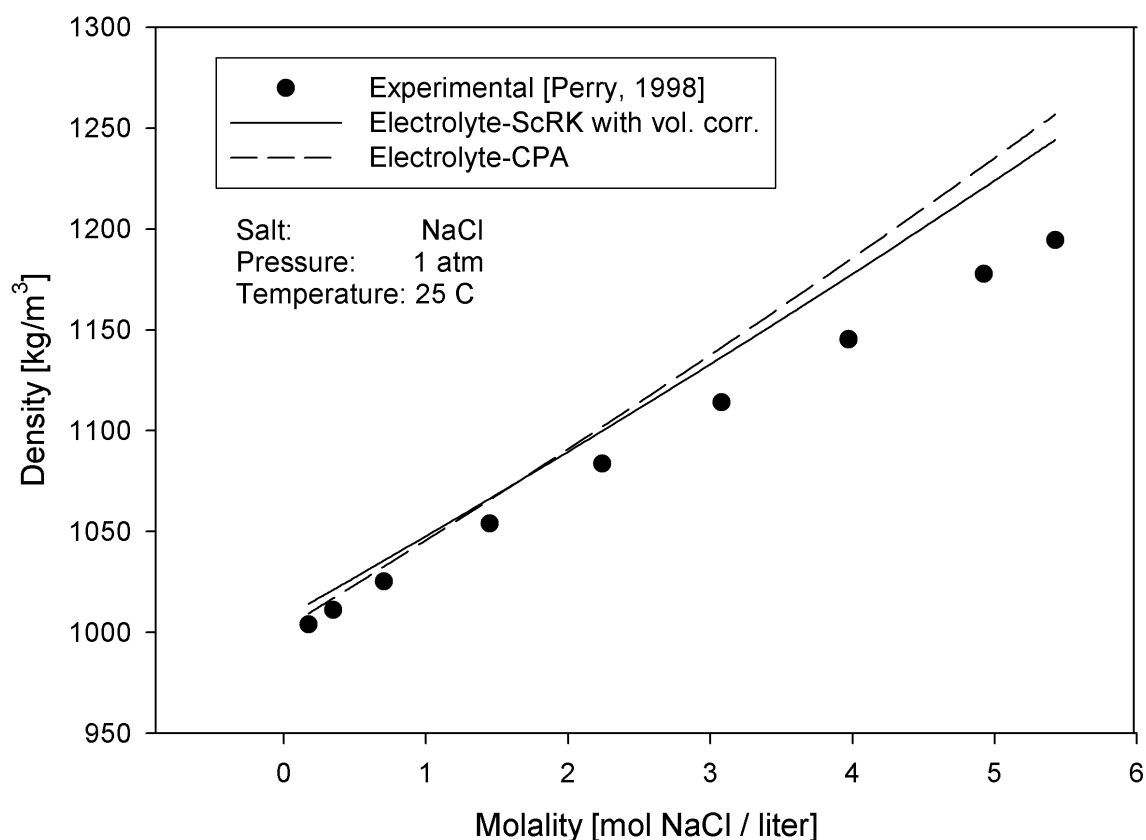
Figure 3-18 Calculated and experimental density of an aqueous NaCl solution
         Script: electrolyte.py, p. 307

3.9 *Weak Electrolyte Solutions*

Weak electrolytes are substances that dissociate only to a small extent in aqueous solution, and therefore produce relatively few ions when dissolved in water. The most common weak electrolytes are weak acids and weak bases. MDEA is a weak base.

3.9.1 Equilibrium Constants in CO_2-MDEA-Water Solutions

In this work the possible reactions in a mixture of CO_2-MDEA and water had to be accounted for in a chemical equilibrium algorithm. The reactions to be considered in the system CO_2, MDEA and water are:

$$2H_2O \rightleftarrows H_3O^+ + OH^- \tag{3.100}$$

$$2H_2O + CO_2 \rightleftarrows HCO_3^- + H_3O^+ \tag{3.101}$$

$$H_2O + HCO_3^- \rightleftarrows CO_3^= + H_3O^+ \tag{3.102}$$

$$H_2O + MDEA^+ \rightleftarrows H_3O^+ + MDEA \tag{3.103}$$
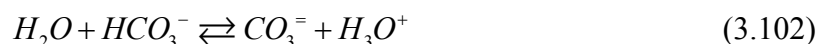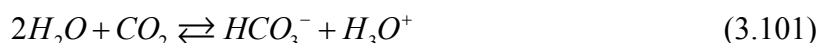
The temperature dependency of the equilibrium constants on the mole fraction scale is expressed by:

$$\ln K_x = C_1 + \frac{C_2}{T} + C_3 \ln T \tag{3.104}$$

The constants of this equation are given in Table 3-4 together with literature sources from where they are taken.

For MDEA we will always have a low formation of bicarbonate (for loadings of practical interest), and equation (3.102) can often be neglected. In this case we can write the total reaction equilibrium as

$$MDEA + H_2O + CO_2 \rightleftarrows HCO_3^- + MDEA^+ \tag{3.105}$$
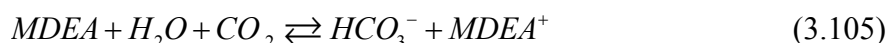
In this work all chemical equilibrium calculations have been done using equation (3.105).

Table 3-4 Constants for calculation of the equilibrium constant K

Reaction	C_1	C_2	C_3	T [°C]	Reference
(3.100)	132.899	-13445.9	-22.4773	0-225	Posey (1995)
(3.101)	231.465	-12092.1	-36.7816	0-225	Posey (1995)
(3.102)	216.049	-12431.7	-35.4819	0-225	Posey (1995)
(3.103)	-56.2	-4044.8	7.848	25-146	Posey (1995)
(3.105)	287.665	-8047.3	-44.6296	25-146	Calculated

3.9.2 Calculation of Reference Potentials From Chemical Equilibrium Constants

The Greiner algorithm adopted in this work for calculating the equilibrium composition of the system utilizes standard potentials, μ^0, for all species participating in the independent set of chemical reactions. However, for several of the components of the system CO_2-amine-water, standard state chemical potentials are not available in the literature. Fortunately, equilibrium constants for all participating reactions (reaction (3.100)-(3.103)) are available. The equation

$$RT \quad \ln\left(K_{xj}\right) = -\sum_{i=1}^{N} \upsilon_{ij} \mu_i^0 = \Delta G_T^0 \qquad j = 1, 2, ..R \tag{3.106}$$

provides a connection between standard state chemical potentials for the components participating in a reaction and the equilibrium constant for the reaction. Where R is the number of reactions and N is the number of components participating in reaction j.

The problem is to determine a suitable vector μ^0 for K_x. It is easy to show that any vector μ^0 which satisfies equation (3.106) can be used to determine the equilibrium composition of the

system by the Greiner algorithm (nonstoichiometric). Such a vector, μ^0, is said to be consistent with the equilibrium constant K_x.

Equation (3.106) represents a system of R equations in N unknowns. Since N is generally greater than R, there are an infinite number of vectors, μ^0 that are consistent with the j values of K_x. One such vector results from setting N minus R values of, μ^0 to zero and using equation (3.106) to solve for the remaining values. In vector notation, this can be written as

$$\left(\frac{N^T}{I}\right)\mu^0 = -RT\left(\frac{\ln K}{0}\right) \quad (3.107)$$

where μ^0 is a N x 1 column vector, N^T is a transposed N x R matrix with elements υ_{ij}, I is a (N-R) x N identity matrix, K is an R x 1 column vector of equilibrium constants. This method has been adopted in this work for determining a consistent set of μ^0.

3.10 Reaction Check Algorithm

In the computer program developed during this work an automatically reaction check algorithm was implemented. The chemical reaction check algorithm searches a database for possible reactions that can occur – given an initial set of molecular components. If all reactants or products of a reaction are present – the reaction is added– and new components are added to the system (reaction products). In this way only the molecular components have to be added to a system when we want to evaluate weak electrolyte systems (ions are added automatically by the reaction check algorithm). This is an advantage when complicated and coupled reactions can occur.

If any reactions are found – the reactive and inert components are sorted. To ensure stability and convergence of chemical equilibrium algorithms it is advantageous to specify primary components. The primary components are effectively found from algorithms developed by Myers and Myers (1986) and Castier et.al (1988). The computational algorithm implemented in the computer code developed in this work is based on their work.

3.11 Chemical Equilibrium Algorithm

The calculation of chemical reaction equilibrium at specified temperature and pressure is in many ways similar to the calculation of phase equilibrium. In both cases the equilibrium state corresponds to a global minimum of the Gibbs energy subject to a set of material balance constrains. An excellent introduction to chemical equilibrium calculations is given in Smith and Missen (1991).

The chemical equilibrium algorithm implemented in this work is a generalized Rand method – developed by Greiner (1991). This algorithm has the advantage over the classical Rand method (Smith and Missen, 1991) – that it accounts explicitly for non-ideal behaviour. In this section a short description of the Greiners method is presented.

In phase equilibrium calculations for a given feed at specified temperature and pressure a material balance must be satisfied for each component in the mixture, the total amount in the combined product phases being identical to the feed. When chemical reactions occur,

additional degrees of freedom are available, resulting in a set of material balance constraints, which is smaller than the number of components in the mixture.

The mixture compositions at chemical equilibrium at constant T and P satisfies the condition of minimum Gibbs energy,

$$Min \quad G \ = \ Min \quad \sum_i n_i \mu_i \tag{3.108}$$

subject to a set of M<C material constraint. In addition we must require that

$$n_i > 0, \quad i = 1, 2, ... C \tag{3.109}$$

The element (atom) conservation constraints can be written on a vector-matrix form

$$\mathbf{An = b} \tag{3.110}$$

where $\mathbf{A}$ is the element (atom) matrix and b_k is the total amount of element k in the reaction mixture (see Smith and Missen, 1991). The matrix $\mathbf{A}$ has M = C-R rows, where R is the number of independent chemical reactions. The M rows of $\mathbf{A}$ must be linearly independent.

When ionic species are present in solution the last row of $\mathbf{A}$ (one row extra compared to non-ionic systems) contain the ionic charge number of each component. The electroneutrality criterion of the solution reduces the degrees of freedom (R) by one. The last element of the $\mathbf{b}$ vector will be zero, because of electroneutrality of the total solution.

3.11.1   Solution by Constrained Optimisation

The constraints defined by eqn. (3.110) can be incorporated into a Gibbs energy minimization algorithm by means of Lagrange multipliers, λ_k. We find it preferable to work with the reduced Gibbs energy and form the augmented objective function,

$$L(n, \lambda) = \sum_i n_i \frac{\mu_i}{RT} - \sum_j \lambda_j \left(\sum_i A_{ji} n_i - b_j \right) \tag{3.111}$$

At the minimum it is required that the derivatives of the Lagrange function are equal to zero:

$$
\begin{aligned}
\frac{\partial L}{\partial n_i} &= \frac{\mu_i}{RT} - \sum_j A_{ji} \lambda_j = 0 \\
\frac{\partial L}{\partial \lambda_j} &= -\sum_j A_{ji} n_i + b_j = 0
\end{aligned}
\tag{3.112}
$$

which yields a total of C+M equations to determine the C+M variables.

3.11.2   The Greiner-Rand Method

The classical Rand method was developed for ideal solutions (Smith and Missen, 1991), but a general variant is due to Greiner (1991), which accounts explicitly for non-ideal behaviour.

The chemical potential is written as:

$$\frac{\mu_i}{RT} = \frac{\mu_i^0}{RT} + \ln \frac{n_i}{n_t} + \ln \varphi_i + \ln P \tag{3.113}$$

where $n_t = \sum_i n_i$. The working equations (3.112), are linearized around the current composition estimate:

$$\frac{\mu_i}{RT} + \sum_k \frac{\partial}{\partial n_k}\left(\frac{\mu_i}{RT}\right)\Delta n_k + \frac{\partial}{\partial n_t}\left(\frac{\mu_i}{RT}\right)\Delta n_t - \sum_j \lambda_j A_{ji} = 0$$

or from the definition of the chemical potential,

$$\frac{\mu_i}{RT} + \sum_k M_{ik}\Delta n_k - \frac{1}{n_t}\Delta n_t - \sum_{k=1}^n \lambda_j A_{ij} = 0 \tag{3.114}$$

where $M_{ik} = \frac{1}{n_i}\delta_{ik} + \frac{\partial \ln \varphi_i}{\partial n_k}$. This equation is solved for the correction vector,

$$\Delta \mathbf{n} = \mathbf{M}^{-1}\left(\mathbf{A}^T\boldsymbol{\lambda} - \boldsymbol{\mu_i}\right) + \mathbf{n}s \tag{3.115}$$

where $s = \Delta n_t / n_t$ and we have utilized that $\mathbf{Mn} = 1$. The correction vector must satisfy the M+1 relations:

$$\begin{aligned}\mathbf{A}\Delta\mathbf{n} &= 0\\ \mathbf{1^T}\Delta\mathbf{n} - \Delta n_t &= 0\end{aligned} \tag{3.116}$$

Substitution of equation (3.115) into equation (3.116) finally yield the set of working equations:

$$\begin{pmatrix} \mathbf{AM}^{-1}\mathbf{A}^T & \mathbf{b} \\ \mathbf{b}^T & \mathbf{0} \end{pmatrix}\begin{pmatrix} \boldsymbol{\lambda} \\ s \end{pmatrix} = \frac{1}{RT}\begin{pmatrix} \mathbf{AM}^{-1}\boldsymbol{\mu} \\ \mathbf{n}^T\boldsymbol{\mu} \end{pmatrix} \tag{3.117}$$

These are solved for the Lagrange multipliers and for s, and the correction to the composition vector is subsequently calculated from equation (3.115). In the case of an ideal solution the matrix $\mathbf{M}$ becomes diagonal, and we recover the classical Rand method. For a deeper introduction to computational chemical equilibrium algorithms see Michelsen and Mollerup (2000).

3.12 TP-Flash Algorithm

The TP-flash algorithm implemented in this work is based on the work of Michelsen (1982a/b, 1994). It is a general multiphase flash algorithm – that solves for chemical

equilibrium of all phases in an inner loop. The physical equilibrium (phase-equilibrium) is calculated using accelerated successive substitution – or alternatively second order methods.

After convergence the stability of the phases is checked. If the system is not stable – a new phase is added – and new multiphase flash calculations are done. The algorithm is illustrated in Figure 3-19.
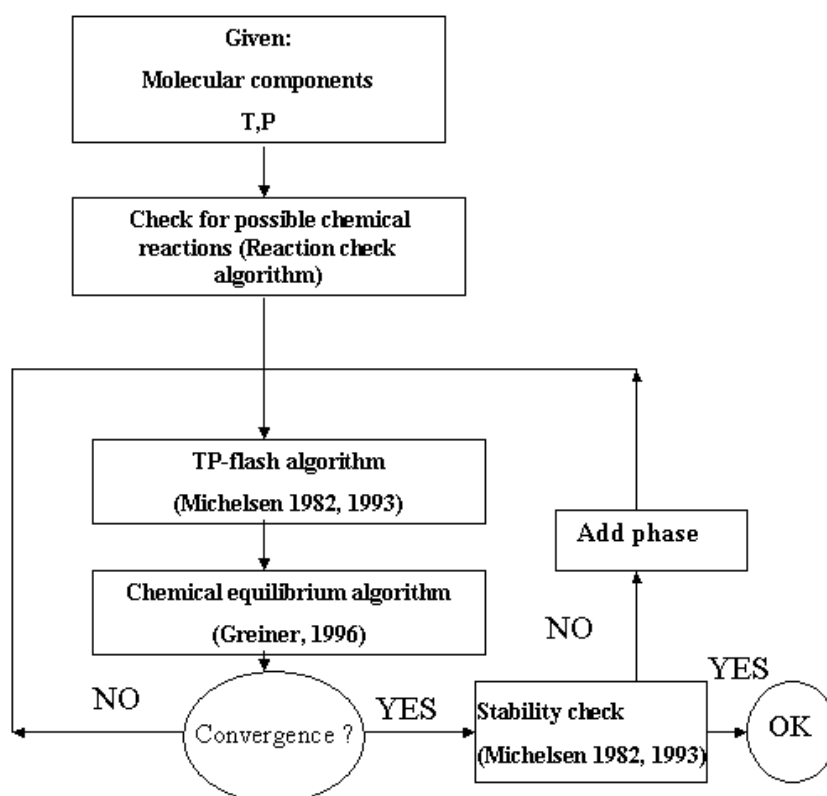
Figure 3-19 Reactive/Non-reactive TP-flash algorithm

3.13 Reactive Bubble Point Flash Algorithm

The bubble point flash algorithm is based on the traditional bubble point flash algorithm – as given in many general textbooks in thermodynamics. The chemical equilibrium calculations are done in an inner loop. Iterations are performed until both the chemical and bubble point-algorithm have converged.

3.14 Convergence Analysis

In Table 3-5 an example of the number of iterations needed and the computational time for typical physical+chemical equilibrium calculations is presented. We see that the computational time used when we have chemical equilibrium calculations and non-ideal systems – will be relatively long. This means solving large process flow-sheets can be very time-consuming.

Table 3-5 Convergence analysis of chemical equilibrium algorithm

System	T,P	Chemical equilibrium	Physical equilibrium	Time for 1000 calculations
CO_2,water (assume no reactions)	298 K, 10 bar	No	Yes	2.5 sec
CO_2,water (reactive)	298 K, 10 bar	Yes	Yes	10.1 sec
CH_4,CO_2,water,MDEA	298 K, 10 bar	Yes	Yes	32.5 sec

Chemical equilibrium calculations can in many practical situations be disregarded. An example is the phase equilibrium calculation of a CO_2-water system. A negligible amount of CO_2 dissociates into bicarbonate – and we may often assume that only molecular CO_2 will be present in the water phase. In a situation were we want to calculate the pH of a CO_2-water system – a chemical equilibrium algorithm is necessary. An example of such a calculation with the electrolyte ScRK-EOS is given in Figure 3-20. The pH of the water is given as function of pressure in the gas phase.
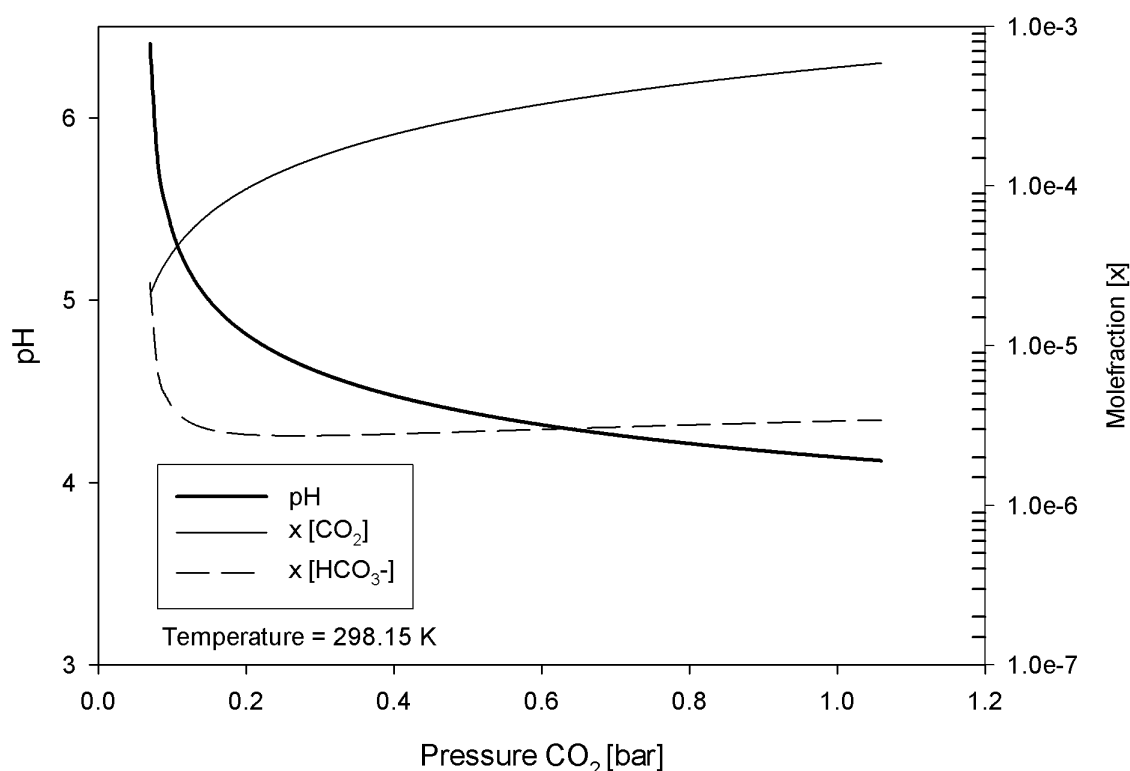
Figure 3-20 pH and speciation of carbon dioxide in water calculated from the chemical equilibrium algorithm. *Script: TPflash.py, p. 306*

3.15 Discussion and Summary - Thermodynamic Modelling

In this chapter thermodynamic modelling using equation of states has been in focus. Two (electrolyte) equations of states have been developed.

The first one is the electrolyte Schwarzentruber Redlich Kwong Equation of State (electrolyte ScRK-EOS) that is based on the electrolyte equation of state originally proposed by Furst and Renon (1993). In this work a Born term has been added – so that the same model could be used for all phases. The Huron Vidal mixing rule was used to model molecular interactions for interaction between components of different chemical nature. The advantage of using the Huron-Vidal mixing rule (compared to the Wong-Sandler mixing rule used by Chunxi and Furst (2000)), is that it can easily reduce to the classical Van der Waals mixing rule and this gives flexibility for multicomponent hydrocarbon mixtures.

The ScRK-EOS with the Huron Vidal mixing rule seems to be promising for modelling solubility's of CO_2 in water. The electrolyte ScRK-EOS was also able to calculate osmotic and mean ionic activity coefficients for many different salt solutions.

The second electrolyte EOS developed in this study was also based on the electrolyte equation of state originally proposed by Furst and Renon (1993). The molecular interactions were modelled using the CPA-EOS with the classical Van der Waals mixing rule. The ionic terms were the same as the ones used by Furst and Renon with the addition of a Born term. This equation was referred to as the electrolyte CPA-EOS.

The CPA-EOS using only one interaction parameter had problems representing the solubility data of CO_2 in water at all temperatures, but was able to calculate both osmotic- and mean ionic activity coefficients of aqueous salt solutions with a good accuracy.

Both the electrolyte ScRK-EOS and the electrolyte CPA-EOS will be used for thermodynamic modelling and parameter fitting in chapter 8.

4 Interphase Mass Transfer in Reactive Electrolyte Mixtures

This chapter gives a brief introduction to non-equilibrium thermodynamics and mass transfer. The intention of this chapter is to derive the basic equations of mass transfer with chemical reactions, which has been implemented in NeqSim. Traditional approaches to mass transfer in gas treating models have been based on Fick's law. In this chapter a mass transfer model for gas treating is derived from the theory of irreversible thermodynamics – which has a more theoretically sound basis than Fick's law.

In many cases Fick's law will be sufficient – either because it is theoretically valid (for some cases it can be derived from non-equilibrium thermodynamics) – or the process we model is simply so complicated that a rigorous application of irreversible thermodynamics is not convenient. Anyway, irreversible thermodynamics serves as a good theoretical background when we introduce simplifications in our models.

A general way of calculating finite flux mass transfer coefficients for multicomponent mixtures in non-ideal systems is presented. The basic theory behind analogies for heat and mass transfer is presented – and equations for calculating heat and mass transfer coefficients for different multiphase systems are given.

4.1 Irreversible Thermodynamics

In this section a general introduction to irreversible thermodynamics is given. For a deeper understanding of the concepts of non-equilibrium thermodynamics the reader is referred to de Groot and Mazur (1984). In the derivation of the basic laws of irreversible thermodynamics, we use general equations on a consistent vector based format. In section 4.2 and later a simplified non-vector based mathematical notification is used.

4.1.1 The Equations of Change for Multi Component Systems

The starting point of the deduction of the governing equations of irreversible thermodynamics is the conservation laws for components, total mass, momentum and energy. These conservation laws are derived and presented in most standard textbooks on fluid mechanics. In this work they are given in the same form as presented in the works of de Groot and Mazur (1984) and Bird et. al (2002). For a deeper insight into these conservation laws and the basic equations of irreversible thermodynamics - the reader is referred to the work of de Groot and Mazur (1984). The centre of mass velocity (barycentric velocity) is used in this derivation, and the substantial derivative is given by

$$\frac{D}{Dt} = \frac{\partial}{\partial t} + \mathbf{u} \cdot grad$$

The conservation law for a component in a system is given by

$$\rho \frac{D\omega_k}{Dt} = -div\,\mathbf{J_k} + \sum_{j=1}^{R} \upsilon_{kj} r_j \quad , \quad (k = 1, 2, ..., n) \tag{4.1}$$

where n is number of components and R is number of reactions and υ is the stocihometric coefficient. $\upsilon_{kj}r_j$ is the production of k per unit volume in the j'th reaction. $\mathbf{J_k}$ is the diffusive fluxes relative to the barycentric velocity and ω_k is the mass fraction of component k. Note that $\sum_{k=1}^{n} \mathbf{J_k} = 0$.

Conservation of the total mass is given as

$$\frac{D\rho}{Dt} = -\rho \, div \, \mathbf{u} \tag{4.2}$$

Conservation of momentum

$$\rho \frac{D\mathbf{u}}{Dt} = -Div \, \mathbf{P_{tens}} + \sum_k \rho_k \mathbf{F_k} \tag{4.3}$$

where $\mathbf{P_{tens}}$ is the pressure tensor resulting from the short range interactions between particles of the system, whereas $\mathbf{F_k}$ contains the external forces as well as possible contribution from long range interactions in the system. The pressure tensor $\mathbf{P_{tens}}$ is normally split into a hydrostatic part ($P\mathbf{I}$) and a tensor ($\mathbf{\Pi}$) (Bird et.al., 2002), where $\mathbf{I}$ is the unit matrix.

The balance equation for kinetic energy is obtained when multiplying equation (4.3) by the velocity

$$\rho \frac{D \tfrac{1}{2}\mathbf{u}^2}{Dt} = -div \left(\mathbf{P_{tens}} \cdot \mathbf{u} \right) + \mathbf{P_{tens}} : Grad \, \mathbf{u} + \sum_k \rho_k \mathbf{F_k} \cdot \mathbf{u} \tag{4.4}$$

The conservation of energy follows from the first law of thermodynamics

$$\frac{DU}{Dt} = \frac{D\mathbf{J_q}}{Dt} - P\frac{d\mathbf{u}}{dt} - \bar{V}\,\mathbf{\Pi} : Grad \, \mathbf{u} + \bar{V}\sum_k \mathbf{J_k} \cdot \mathbf{F_k} \tag{4.5}$$

where $\bar{V}$ is the molar volume, U is the internal energy and $\mathbf{J_q}$ is the total heat flux vector.

4.1.2 The Entropy Production Rate

The variation of entropy may be written as the sum of two terms

$$dS = d_e S + \sigma \tag{4.6}$$

where $d_e S$ is the entropy supplied to the system by its surroundings, and σ the entropy produced inside the system. The entropy balance equation is

$$\rho \frac{DS}{Dt} = -\left(div \, \mathbf{J_s} \right) + \sigma \tag{4.7}$$

where $\mathbf{J_s}$ is the entropy flux. The equation above is often referred to as the Jaumann's entropy balance equation (Curtiss and Bird, 1999).

The change in entropy for a system is given by a well-known equation from equilibrium thermodynamics (the Gibbs equation)

$$dU = TdS - pdV + \sum_i \left(\frac{G_i}{M_i} \right) d\omega_i \qquad (4.8)$$

This equation is valid for systems at equilibrium, but will be used for non-equilibrium systems where we assume local thermodynamic equilibrium (Kjelstrup and Bedaux, 2002). If we combine this equation with the equations given in the last section (conservation of components, total mass, momentum and energy), we get the following equation for the change in entropy

$$\rho \frac{DS}{Dt} = -\frac{div\,\mathbf{J_q}}{T} - \frac{1}{T}\mathbf{\Pi} : Grad\,\mathbf{u} + \frac{1}{T}\sum_{k=1}^{n} \mathbf{J_k} \cdot \mathbf{F_k} + \frac{1}{T}\sum_{k=1}^{n} \mu_k\,div\,\mathbf{J_k} - \frac{1}{T}\sum_{j=1}^{R} r_j A_j \qquad (4.9)$$

where we use the chemical affinities of chemical reactions (j=1,2,..,R) defined by

$$A_j = \sum_{k=1}^{n} \upsilon_{kj}\mu_k, \quad \left(j = 1, 2, ..., R \right) \qquad (4.10)$$

and μ_k is the chemical potential of component k. It is easy to cast equation (4.9) into a form of a balance equation for entropy

$$\rho \frac{DS}{Dt} = -div \left(\frac{\mathbf{J_q} - \sum_k \mu_k \mathbf{J_k}}{T} \right) - \frac{1}{T^2}\mathbf{J_q} \cdot grad\,T - \frac{1}{T}\sum_{k=1}^{n}\mathbf{J_k}\left(T\,grad\frac{\mu_k}{T} - \mathbf{F_k} \right) - \frac{1}{T}\mathbf{\Pi} : Grad\,\mathbf{u} - \frac{1}{T}\sum_{j=1}^{R} r_j A_j \quad (4.11)$$

If we compare this equation with equation (4.7), we get for the entropy flux:

$$\mathbf{J_s} = \frac{1}{T}\left(\mathbf{J_q} - \sum_{k=1}^{n} \mu_k \mathbf{J_k} \right) \qquad (4.12)$$

For the entropy production rate we get

$$\sigma = -\frac{1}{T^2}\mathbf{J_q} \cdot grad\,T - \frac{1}{T}\sum_{k=1}^{n}\mathbf{J_k} \cdot \left(T\,grad\frac{\mu_k}{T} - \mathbf{F_k} \right) - \frac{1}{T}\mathbf{\Pi} : Grad\,\mathbf{u} - \frac{1}{T}\sum_{j=1}^{R} r_j A_j \geq 0 \quad (4.13)$$

We now use the thermodynamic relation (de Grooth et.al., 1984)

$$T\,d\left(\frac{\mu_k}{T} \right) = \left(d\mu_k \right)_{T,P} + \frac{\bar{V}_k}{M_k}dP - \frac{h_k}{T}dT \qquad (4.14)$$

where h_k and $\overline{V}_k$ is the partial specific enthalpy and volume of component k. We also introduce the pure conductive heat flux

$$\mathbf{J}_{\mathbf{q}}^{'} = \mathbf{J}_{\mathbf{q}} - \sum_{k=1}^{n} h_k \mathbf{J}_{\mathbf{k}} \tag{4.15}$$

Inserting equation (4.14) and (4.15) into equation (4.13) we get

$$\sigma = -\frac{1}{T^2}\mathbf{J}_{\mathbf{q}}^{'} \cdot grad\, T - \frac{1}{T}\sum_{k=1}^{n}\mathbf{J}_{\mathbf{k}} \cdot \left(\left| grad\, \mu_k \right|_{T,P} + \frac{\overline{V}_i}{M_i}\nabla P - \mathbf{F}_{\mathbf{k}} \right) - \frac{1}{T}\mathbf{\Pi}:Grad\,\mathbf{u} - \frac{1}{T}\sum_{j=1}^{R} r_j A_j \geq 0 \quad (4.16)$$

This equation is the basis for deriving the basic equations for the calculation diffusive heat and mass fluxes in irreversible thermodynamics. We have expressed the entropy production rate in terms of conjugate fluxes and forces. The only assumption used so far, is the assumption of local thermodynamic equilibrium. This assumption is valid in most situations of practical interest (Kjelstrup et.al., 2002).

The flux equations in irreversible thermodynamics are obtained from the entropy production rate, σ. Once the entropy production rate has been determined, one knows a complete set of independent thermodynamic forces and their conjugate fluxes. We can now write the fluxes, J_i, as a linear function if all forces, $\mathbf{X}_{\mathbf{k}}$,

$$\mathbf{J}_{\mathbf{i}} = \sum_{k} L_{ik}\mathbf{X}_{\mathbf{k}} \tag{4.17}$$

The coefficients L_{ij} are the Onsager conductivities. When the coefficients L_{ij} are known, we know how the different processes are coupled to one another. The Onsagers coefficients can be shown (Onsager, 1931) to always fulfil the conditions

$$\begin{aligned} L_{ii} &\geq 0 \\ L_{ik} &= L_{ki} \end{aligned} \tag{4.18}$$

which are often referred to the Onsagers reciprocal relations.

4.1.3 The Driving Force of Molecular Diffusion

From equation (4.16) we see that entropy production resulting from pure molecular diffusion is given as

$$T \cdot \sigma_{diff} = -\sum_{k=1}^{n}\mathbf{J}_{\mathbf{k}} \cdot \left(\left| grad\, \mu_k \right|_{T,P} + \frac{\overline{V}_k}{M_k}\nabla P - \mathbf{F}_{\mathbf{k}} \right) \tag{4.19}$$

Since $\sum \mathbf{J}_k = 0$ we can add an arbitrary vector to equation (4.19) (Taylor and Krishna, 1993). We add the vector

$$-\frac{1}{\rho_k}\nabla P + \sum_{k=1}^{n}\omega_k \mathbf{F}_{\mathbf{k}}$$

Equation (4.19) can now be written

$$ T \cdot \sigma_{diff} = -\sum_{k=1}^{n} \mathbf{J_k} \cdot \left(\frac{\nabla_{T,P}\mu_k}{M_k} + \frac{\overline{V}_k}{M_k}\nabla P - \frac{1}{\rho_k}\nabla P + \sum_{j=1}^{n} \omega_j \mathbf{F_j} - \mathbf{F_k} \right) \tag{4.20} $$

or

$$ \sigma_{diff} = -c_t R \sum_{k=1}^{n} d_k \cdot (\mathbf{u_k} - \mathbf{u}) \geq 0 \tag{4.21} $$

where we have used the relations $\mathbf{J_k} = \rho_k (\mathbf{u_k} - \mathbf{u})$ and

$$ c_t RT d_k = c_k \nabla_{T,P}\mu_k + (\phi_k - \omega_k)\nabla P - \rho_k \left(\mathbf{F_k} - \sum_{j=1}^{n} \omega_j \mathbf{F_j} \right) \tag{4.22} $$

where ϕ_k is the volume fraction of species k and c_t is the total molar concentration. The physical interpretation of $c_t RT d_k$ is that it represents the force acting on component k per unit volume of mixture tending to move component k relative to the solution. Equation (4.22) shows that a pressure gradient can effect separation in a mixture provided there is a difference in volume and mass fractions.

4.2 The Maxwell-Stefan Equations

The generalized Maxwell-Stefan equations argues from a semi-theoretical point of view that the general driving force for molecular diffusion of equation (4.22) can be calculated from

$$ d_i = \sum_{k \neq i} \frac{x_i x_k}{\mathcal{D}_{ik}} \left(\frac{J_k}{\rho_k} - \frac{J_i}{\rho_i} \right) + \sum_{k} \frac{x_i x_k}{\mathcal{D}_{ik}} \left(\frac{D_k^T}{\rho_k} - \frac{D_i^T}{\rho_i} \right)(\nabla \ln T) \tag{4.23} $$

where molecular diffusion due to temperature gradients (the Doufour effect) is included. The Doufour effect is often neglected – and will be so in this work. Equation (4.23) was derived from the basic theory of irreversible thermodynamics by Bird et.al. (1999).. Only n-1 of the flux equations are independent. It will prove convenient to cast the equations in a n-1 dimensional matrix form. The resulting matrix form is (Taylor and Krishna, 1993)

$$ (J) = -c_t [B]^{-1}(d) \tag{4.24} $$

Where the B matrix is given as

$$ B_{ii} = \frac{x_i}{\mathcal{D}_{in}} + \sum_{\substack{k=1 \\ i \neq `k}}^{n} \frac{x_k}{\mathcal{D}_{ik}} $$

$$ B_{ij} = -x_i \left(\frac{1}{\mathcal{D}_{ij}} - \frac{1}{\mathcal{D}_{in}} \right) \; i \neq j \; and \; i,j = 1,2,...,n-1 \tag{4.25} $$

where $\mathcal{D}_{ij}$ is the binary Maxwell-Stefan diffusion coefficient for diffusion of component i in component j. From Onsagers relations we can show the Maxwell-Stefan diffusion coefficients obey $\mathcal{D}_{ij} = \mathcal{D}_{ji}$ and are always larger than 0.

If we neglect the contribution of temperature gradients on the rate of molecular diffusion and we assume no contribution from external forces, equation (4.24) can be written

$$-\frac{x_i}{RT}\nabla_{T,P}\mu_i = \sum_{j=1}^{n}\frac{x_j J_i - x_i J_j}{c_t \mathcal{D}_{ij}} = \sum_{j=1}^{n}\frac{x_j N_i - x_i N_j}{c_t \mathcal{D}_{ij}} \qquad (4.26)$$

This equation is the Maxwell-Stefan relation for diffusion in multicomponent systems.

For a multicomponent system, the thermodynamic factor Γ_{ij} relates the chemical potential of a component to the activity coefficient. The thermodynamic factor can be calculated from

$$\frac{x_i}{RT}\nabla_{T,P}\mu_i = \sum_{j=1}^{n-1}\Gamma_{ij}\nabla x_j \quad where \quad \Gamma_{ij} = \delta_{ij} + x_i \frac{\partial \ln \gamma_i}{\partial x_j} \qquad i = 1,2,...,n-1 \qquad (4.27)$$

Equation (4.26) can be combined with equation (4.27) to represent the Maxwell-Stefan diffusion equations for multicomponent systems in a n-1 dimensional matrix form:

$$-c_t[\Gamma](\nabla x) = [B](J) \quad or \quad (J) = -c_t[\Gamma][B]^{-1}(\nabla x) \qquad (4.28)$$

where the symbols [] and () represents matrices and vectors respectively. The elements of the matrix $[B]$ can be calculated from equation (4.25).

Analogous to the Fick's law for binary diffusion, a matrix of Ficks diffusivities [D] can be defined as,

$$(J) = -c_t[B]^{-1}[\Gamma](\nabla x) = -c_t[D](\nabla x) \qquad (4.29)$$

where $[D] = [B]^{-1}[\Gamma]$. Equation (4.29) constitutes the proper generalization of the Fick's law for diffusion in multicomponent mixtures. The elements D_{ij} of the matrix of Ficks diffusivities $[D]$ are not to be confused with the binary diffusion coefficients in equation (4.25); they may take positive or negative values and, in general they are not symmetric ($D_{ij} \neq D_{ji}$).

4.2.1 Maxwell-Stefan Equations for Multi Component Mass Transfer in Electrolyte Systems

In many cases of practical interest the pressure gradient is negligibly small and this term may therefore be neglected in eqn. (4.22). For diffusion of charged species the external body force F_i is given by

$$F_i = -z_i F \nabla \phi \qquad (4.30)$$

where $\nabla\phi$ is the gradient in electrical potential, F the Faraday constant and z is the electronic charge number (eg. +1 for Na^+ and –1 for Cl^-). Except in regions close to the surfaces where there will be charge separation (double layer phenomena), the condition of electroneutrality

$$\sum_{i=1}^{n} z_i c_i = 0 \tag{4.31}$$

is met and therefore the expression for the expression for the driving force d_i simplifies to

$$d_i = \frac{x_i}{RT}\nabla_{T,P}\mu_i + x_i z_i \frac{F}{RT}\nabla\phi \tag{4.32}$$

For dilute solutions the above equation combined with equation (4.24) reduce to (Taylor and Krishna, 1993)

$$J_i = -c_t D_{in}\nabla x_i - c_i z_i D_{in}\frac{F}{RT}\nabla\phi \quad i = 1,2,..,n-1 \tag{4.33}$$

which is the Nernst-Planck equation commonly used to describe mass transport in electrolyte solutions.

We can approximate the driving force by linear composition and electrostatic potential profiles over the range of interest

$$d_i = \frac{x_i}{RT}\frac{\Delta_{T,P}\mu_i}{\delta} + x_i z_i \frac{F}{RT}\frac{\Delta\phi}{\delta} \tag{4.34}$$

where δ is the film thickness. The contribution from the electrostatic potential are often neglectable compared to the chemical potential (weak electrolyte systems). In this work the contribution from the gradient in electrostatic potential was neglected, therefore the only driving force for molecular diffusion considered is the gradient in chemical potential.

$$d_i = \frac{x_i}{RT}\frac{\Delta_{T,P}\mu_i}{\delta} \tag{4.35}$$

In future non-equilibrium modelling it is easy to extend this model with other driving forces such as electrical- and gravitational forces.

4.2.2 Maxwell-Stefan Equations Using Mass Transfer Coefficients

We define the Maxwell Stefan mass transfer coefficient as

$$k_{ij} = \frac{Ð_{ij}}{\delta} \tag{4.36}$$

If we introduce these Maxwell Stefan mass transfer coefficients into equation (4.25) and use the driving force defined in equation (4.35) we get on a n-1 dimensional format

$$\sum_{k \neq i} \frac{x_i x_k}{k_{ik}} \left(\frac{J_k}{\rho_k} - \frac{J_i}{\rho_i} \right) = \frac{x_i}{RT} \Delta_{T,P} \mu$$

On a more convenient form, we get on a n-1 dimensional form

$$(J) = -c_t [\Gamma][R]^{-1} (\Delta x) \tag{4.37}$$

Where the R matrix is given as

$$R_{ii} = \frac{x_i}{k_{in}} + \sum_{\substack{k=1 \\ i \neq k}}^{n} \frac{x_k}{k_{ik}}$$

$$R_{ij} = -x_i \left(\frac{1}{k_{ij}} - \frac{1}{k_{in}} \right)$$

This is the form of the Maxwell-Stefan equation that will be used in this work. The film thickness defined in equation (4.36) is normally hard to estimate. The easiest way would be to estimate the binary Maxwell-Stefan mass transfer coefficients from analogies and empirical equations using the Maxwell-Stefan diffusion coefficients. The analogies and empirical equations used in this work are described later in this chapter.

4.2.3 The Generalized Maxwell Stefan Equations for Reactive Electrolyte Mixtures

The equations derived in last section are valid for diffusion in electrolyte solutions. These equations can still be used when reactions occur simultaneously, because reactions does not couple with the other forces responsible for the diffusion. This is because of Curie's principle that states that forces of different tensorial order do not couple (de Groth and Mazur, 1983).

We define the enhancement factor E_i as the difference between the mass transfer flux with reaction to that without reactions – where we have the same driving force.

$$E_i = \frac{J_{i,reactive}}{J_{i,non\ reactive}} \tag{4.38}$$

If we introduce this enhancement factor into the generalized Maxwell Stefan equations for mass transfer, we can write equation (4.37) as

$$(J) = -c_t (E)[\Gamma][B]^{-1} (\Delta x) \tag{4.39}$$

The expressions for the enhancement factors and the mass transfer coefficients will be given later in the thesis. The enhancement factor can be calculated from a numerical solution of the boundary layer accounting for all reactions and viscous forces. For relatively simple reactions (e.g. first order reactions) analytical relations for the enhancement factor can be derived.

Analytical expressions for the enhancement factor are derived for slow, fast and infinite fast reactions with respect to mass transfer by Astarita et.al. (1983). Such analytical expressions using the effective diffusivity approach were used in this work. The calculation of effective diffusion coefficient and mass transfer coefficient is therefore important. It is important to realize that the effective diffusivity approach is only used for enhancement factor calculations. The full matrix mass transfer calculation (equation (4.39)) is used to calculate the mass transfer fluxes.

4.3 Effective Diffusivity Methods

The effective diffusion coefficient of a multicomponent system can be defined by a relationship analogous to Fick's law for binary systems

$$J_i = -c_t D_{i,eff} \nabla x_i \quad or \quad N_i = -c_t D_{i,eff} \nabla x_i + x_i \sum_{k=1}^{n} N_k \tag{4.40}$$

Solving equation (4.40) for ∇x_i and equating the result to the composition gradient obtained from the Maxwell-Stefan equation, the following relationship between effective and the Maxwell-Stefan diffusivities is obtained (Bird et. al., 2002):

$$D_{i,eff} = \frac{N_i - x_i N_t}{N_t \sum_{\substack{j=1 \\ j \neq i}}^{n} \frac{x_j}{Ð_{ij}} - x_i \sum_{\substack{j=1 \\ j \neq i}}^{n} \frac{N_t}{Ð_{ij}}} \tag{4.41}$$

This complicated relationship indicates that, in principle, the effective diffusion coefficients are not bounded, i.e., they can be negative as well as positive. This in turns implies that the effective diffusion coefficients as defined by equation (4.40) do not, in general, have the physical significance of a diffusion coefficient in a binary system. However, in practical applications equation (4.41) is rarely used, instead, correlations based on experimental data or simpler approximations are employed.

Other simpler relationships between the effective diffusion coefficients and the Maxwell-Stefan binary diffusion coefficients have been used. For instance Taylor and Krishna (1993) report the relationship

$$\frac{1}{D_{i,eff}} = \frac{x_i}{Ð_{in}} + \sum_{\substack{k=1 \\ k \neq i}}^{n} \frac{x_k}{Ð_{ik}} \tag{4.42}$$

which corresponds to $D_{i,eff} = 1/B_{ii}$ with B_{ii} determined by equation (4.25). This approximation is equivalent to neglecting the off-diagonal elements of the matrix $[B]$ in the calculation of the diffusive fluxes using equation (4.25).

The diffusive flux can be also be defined in terms of effective mass transfer coefficients by a expression similar to equation (4.36)

$$J_i = c_t k_{i,eff} \Delta x_i \tag{4.43}$$

Like its multicomponent counterpart the effective mass transfer coefficient is defined as $k_{i,eff} = D_{i,eff} \big/ \delta$ but in practice the effective mass transfer coefficients are calculated from empirical correlations using effective diffusivities. When there is a need to compare mass transfer rates calculated from an effective diffusivity approach to those calculated by a more rigorous multicomponent formulation like the Maxwell Stefan approach, the effective mass transfer coefficients are calculated from binary mass transfer coefficients using relationships equivalents to equation (4.42), but substituting diffusivities by mass transfer coefficients, i.e.,

$$\frac{1}{k_{i,eff}} = \frac{x_i}{k_{in}} + \sum_{\substack{k=1 \\ k \neq i}}^{n} \frac{x_k}{k_{ik}} \tag{4.44}$$

Frank et. al. (1995a/b) used a relationship similar to equation (4.44) to estimate effective mass transfer coefficients when comparing the Maxwell-Stefan and pseudo-binary approaches to mass transfer.

In this work the effective diffusivities and mass transfer coefficients were used to estimate enhancement factors in reactive mixtures.

4.3.1 When is Multicomponent Interaction Effects Important ?

The importance of the interaction effects on mass transfer depends on the specific conditions of each system and it is difficult to establish general criteria to determine when the diffusional interactions are unimportant and, therefore, when an effective diffusivity approach can be used. Krishna and Wesselingh (1997) indicate that interaction phenomena occur routinely in multicomponent mass transfer processes like absorption and distillation. In mass transfer equipments, such as trayed and packed columns, the drivingforce of a given component Δx_i could change sign along column. This is unlikely especially for components with intermediate volatility. For these components the drivingforce should assume vanishing small values at some positions. When this situation occurs, the flux of that component is strongly influenced by the fluxes of the others. This in turns leads to the "odd" behaviour like, reverse and osmotic transport, and transport barrier (Taylor and Krishna, 1993). Under these circumstances the component efficiencies are unbounded and can assume values greater than 100% and either sign.

4.4 Mass Transfer in Multiphase Fluid Systems

Convective mass transfer is defined as the coupling between molecular diffusion and bulkflow. If a fluid flows relative to another, and the two phases are out of thermodynamic equilibrium, concentration boundary-layers will develop. The boundary-layer is the layer from the interface where $x = x_{i,int}$, to the bulkfluid where $x = x_{i,b}$ (where x_i is molar fraction of component i). The convective mass transfer is described by the mechanisms in this boundary-layer. For a binary ideal gas the mass transfer rate of component A is calculated from

$$J_A = k_A \left(x_{A,int} - x_{A,b} \right) \tag{4.45}$$

where k_A is the mass transfer coefficient.

4.4.1 The Mass Transfer Coefficient

The convective mass transfer coefficient is dependent on fluid properties, surface properties and geometry and convective movements in the boundary layer.

We normally assume no-slip at the fluid interface (y=0). This means that there is no relative movement between the liquid and gas at the interface. The mass transfer occurs only by molecular diffusion. A combination of Fick's law and equation (4.45) gives us an expression for the mass transfer coefficient.

$$k_A = \frac{-c_t D_A \left.\frac{\partial x_A}{\partial y}\right|_{y=0}}{x_{A,\text{int}} - x_{A,bulk}} \tag{4.46}$$

An analytical equation for calculating this mass transfer coefficient is found for a lot of different types of flows.

4.4.2 Analogy's Between Heat and Mass Transfer

Many problems related to heat- and mass transfer are driven by transport phenomena of energy and mass near an interface (Figure 4-1).
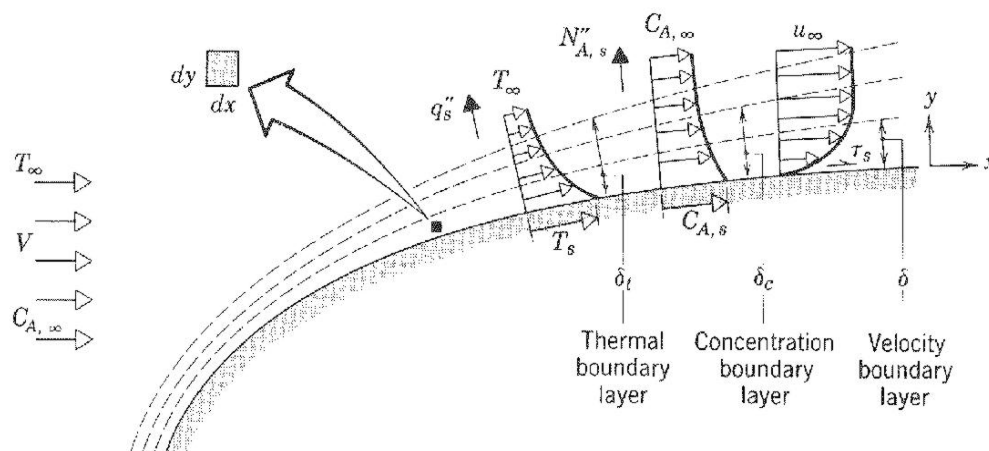
Figure 4-1 Transfer of momentum, energy and mass near an interface (Bird et.al, 2002)

Two processes are analogous if the dimensionless equations that describes the process are on the same form. We can show that the conservation equations of energy and components are analogous (see Figure 4-2).

BOUNDARY LAYER	CONSERVATION EQUATION	BOUNDARY CONDITIONS		SIMILARITY PARAMETER(S)
		WALL	FREE STREAM	
Velocity	$u^* \dfrac{\partial u^*}{\partial x^*} + v^* \dfrac{\partial u^*}{\partial y^*} = -\dfrac{dp^*}{dx^*} + \dfrac{\nu}{VL}\dfrac{\partial^2 u^*}{\partial y^{*2}}$ (6.57)	$u^*(x^*,0) = 0$ $v^*(x^*,0) = 0$	$u^*(x^*,\infty) = \dfrac{u_\infty(x^*)}{V}$ (6.60)	Re_L
Thermal	$u^* \dfrac{\partial T^*}{\partial x^*} + v^* \dfrac{\partial T^*}{\partial y^*} = \dfrac{\alpha}{VL}\dfrac{\partial^2 T^*}{\partial y^{*2}}$ (6.58)	$T^*(x^*,0) = 0$	$T^*(x^*,\infty) = 1$ (6.61)	Re_L, Pr
Concentration	$u^* \dfrac{\partial C_A^*}{\partial x^*} + v^* \dfrac{\partial C_A^*}{\partial y^*} = \dfrac{D_{AB}}{VL}\dfrac{\partial^2 C_A^*}{\partial y^{*2}}$ (6.59)	$C_A^*(x^*,0) = 0$	$C_A^*(x^*,\infty) = 1$ (6.62)	Re_L, Sc

Figure 4-2 Analog equations of momentum, heat and mass transfer

The conservation laws for heat and mass transfer are the same with different dimensionless groups. This means that the relations that we use for heat transfer can be used for mass transfer, and the other way. This is done by changing the corresponding dimensionless groups as given in Table 4-1.

Table 4-1 Corresponding groups for heat and mass transfer

Heat Transfer	Mass Transfer
$Nu_x = \dfrac{h_q L}{k}$	$Sh_x = \dfrac{k_m L}{D}$
$Pr = \dfrac{\nu}{\alpha}$	$Sc = \dfrac{\nu}{D}$
$St = \dfrac{h_q}{\rho c_p \bar{u}}$	$St = \dfrac{k_m}{\bar{u}}$
T	ρ
α	D

Where D is the diffusion coefficient, k the conductivity, h_q the heat transfer coefficient, k_m the mass transfer coefficient and $\bar{u}$ the mean velocity. α is the molecular thermal diffusivity and is calculated from $k/\rho c_p$.

4.4.3 The Theory Behind Analogies

Analogies between wall shear force and heat transfer
The Reynolds analogy for heat transfer is derived from turbulent boundary layer theory. Reynolds (1874) assumed that at a solid interface no turbulence can form. In this area viscous forces could only be transferred by molecular shear forces (not eddies) and heat transfer had to be driven by conduction (not turbulent convection). This is illustrated in Figure 4-3.
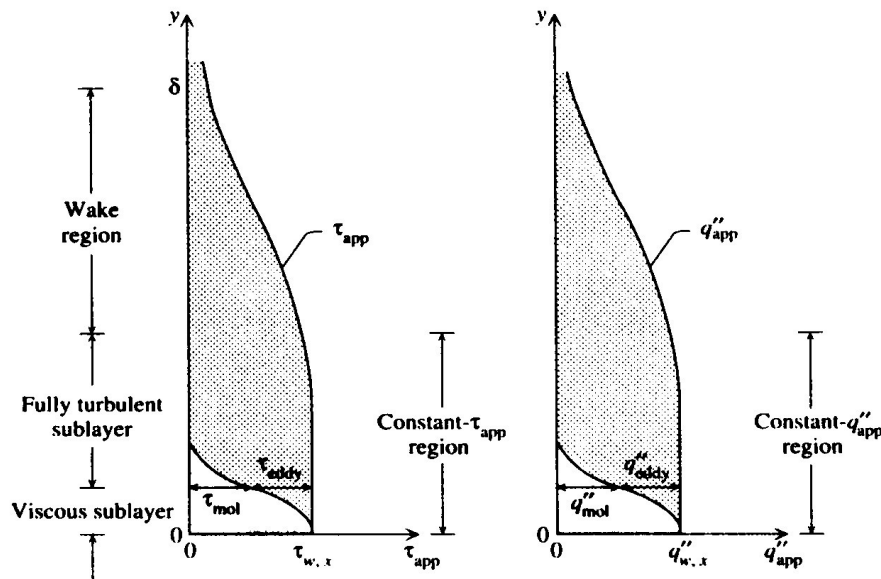
Figure 4-3 Transfer of shear forces and heat near an interface (Bird et.al., 2002)

The Reynolds analogy was derived based on an assumption of a fluid with a Schmidt number of 1. The Reynolds analogy is usually written as

$$St = \frac{k_m}{\bar{u}} = \frac{f}{2} \tag{4.47}$$

where f is the fanning friction factor and $\bar{u}$ is the mean velocity. This means that if we know the friction factor at the interphase – we can calculate the heat or mass transfer coefficient.

To take account of fluids whose Schmidt number is not unity, Chilton-Colburn suggested the empirical equation (Colburn, 1964)

$$St = \frac{1}{2} f \cdot Sc^{-2/3} \tag{4.48}$$

For turbulent flow in a pipe the fanning friction factor can be approximated by (Bejan, 1993)

$$f \cong 0.079 \, \text{Re}^{-1/4} \tag{4.49}$$

Inserting this friction factor into equation (4.48) we get

$$Sh = \frac{1}{2} \cdot f \cdot \text{Re} \, \text{Pr}^{1/3} = 0.028 \, \text{Re}^{3/4} \, Sc^{1/3} \tag{4.50}$$

This is a correlation often used when we want to calculate mass transfer between the pipe wall and a fluid at high Reynolds numbers. The corresponding equation for heat transfer is also often used to calculate heat transfer between fluid and pipewall. Equation (4.50) shows that the mass- and heat transfer coefficient can be estimated from knowledge of the friction factor. Alternatively the friction factor can be estimated from knowledge of the mass- transfer coefficient.

Similar models could also be used for calculating mass transfer coefficients in multiphase fluid systems. In these cases interphase friction factors would have to be used. For a fluid-fluid boundary layer the assumption of pure molecular diffusion at the interface is more questionable. We know that waves and rippling will affect the mass transfer at the interface.

4.4.4 Models for Mass Transfer Coefficients in Gasses and Liquids

In this section the characteristic equations commonly used in many mass transfer processes are given. They can be derived from analogies as described in last section – or they can be fitted to experimental data. The empirical correlations given in Table 4-2 will be used through out the thesis for calculating the binary Maxwell-Stefan mass transfer coefficients, $\hbar_{AB}$ (using the Maxwell-Stefan diffusivities $Ð_{AB}$) and effective mass transfer coefficients k_{AB} (using Ficks diffusivities D_{AB} or $D_{eff.}$).

Table 4-2 Selected mass transfer correlations for fluid-fluid interfaces (Cussler, 1997)

Physical situation	Basic equation				Key variables	Remarks
Liquid in a packed tower	$\dfrac{k_{AB}d}{D_{AB}} = 25\left(\dfrac{d \cdot U_{liq}^{sup}}{v_{liq}}\right)^{0.45}\left(\dfrac{v_{liq}}{D_{AB}}\right)^{0.5}$				d = nominal packing size	U^{sup}= superficial velocity
Gas in a packed tower	$\dfrac{k_{AB}d}{a\,D_{AB}} = 3.6\left(\dfrac{U_{gas}^{sup}}{av_{gas}}\right)^{0.70}\left(\dfrac{v_{gas}}{D_{AB}}\right)^{0.33}\left(ad\right)^{-2.0}$				a = packing area per bed volume d = nominal packing size	
Turbulent flow through circular tube	$\dfrac{k_{AB}d}{D_{AB}} = 0.026\left(\dfrac{d \cdot U^{sup}}{v}\right)^{0.93}\left(\dfrac{v}{D_{AB}}\right)^{1/3}$				d = pipe diameter	
Falling liquid film in wetted wall column	$k_{AB}^{*} = \left(\dfrac{k_{AB}}{D_{AB}}\right)\cdot\left(\dfrac{v^2}{g}\right)^{1/3} = K \cdot Re^{a}\,Sc^{b}$ Regime / Reynolds Number / K / a / b Laminar / Re<300 / $1.099\cdot10^{-2}$ / 0.3955 / 0.5 Laminar-Wavy / 300<Re<1600 / $2.995\cdot10^{-2}$ / 0.2134 / 0.5 Turbulent-Wavy / 1600<Re / $9.77\cdot10^{-4}$ / 0.6804 / 0.5					Equations regressed by Yih.et.al (1982)
Stirred cell gas phase	$Sh = 0.023\cdot Re^{0.8}\,Sc^{0.5}$				$Re = \dfrac{O_r}{r}$ Where O_r = stirring rate [rpm] and r stirrer diameter	Equation regressed by Versteeg (1986)
Stirred cell liquid phase	$Sh = 0.026\cdot Re^{0.67}\,Sc^{0.33}$				$Re = \dfrac{O_r}{r}$ Where O_r = stirring rate [rpm] and r stirrer diameter	Equation regressed by Versteeg (1986)

The Maxwell-Stefan mass transfer coefficient for use in multicomponent mass transfer is calculated from the same equation – but by using the Maxwell-Stefan diffusion coefficients in the equations given in the table above.

4.4.5 Example – Mass Transfer in a Stirred Cell

To illustrate the mass transfer model described in the previous sections we consider a stirred cell as illustrated in the Figure 4-4. A stirred cell is typically an autoclave with stirring in the upper and lower part (gas and liquid). The stirred cell is initially filled with 5 normal litre pure CO_2 gas at 10 bar with a stirrer speed of 50 rpm. The gas is suddenly brought into contact with 0.2 kg water in the cell (fast injection of water). Mass transfer between the gas and the liquid will start immediately. Water will vaporize into the gas and CO_2 will dissolve in the water. After a relatively long time the liquid and gas will come to equilibrium. In this example we want to evaluate the molar fluxes of water and CO_2 and the concentration of water and CO_2 as function of time. The temperature of the system is 40°C.

We will use the SRK-EOS with the Huron-Vidal mixing rule to model the thermodynamics of the system. The NeqSim script for this simple simulation case is:

```python
# script: simple-flux.py
system = thermo('srk', temperature=313.15, pressure=10.0)
addComponent(system,'CO2', 5.0, 'Nlitre/min', 0)
addComponent(system,'water', 0.2, 'kg/min', 1)
mixingRule(system,'HV')

cellgeometry = geometry.stirredcell(0.05)
cell = node.stirredcell(system,cellgeometry)
cell.setStirrerSpeed(50.0/60.0)
cell.setDt(0.05)

cell.getFluidBoundary().useFiniteFluxCorrection(1)
cell.getFluidBoundary().useThermodynamicCorrections(1)

# Iterates a specified number of time-steps
for i in range(3000):
        flow.solve(cell,noneq=1,heattrans=0,masstrans=1)
        print 'time ', i*cell.getDt()/60.0, \
        ' x_CO2 ', cell.getBulkSystem().getPhase(1).getComponent(0).getx(),\
        ' flux_CO2 ', cell.getMolarMassTransferRate(0),\
        cell.update()
```
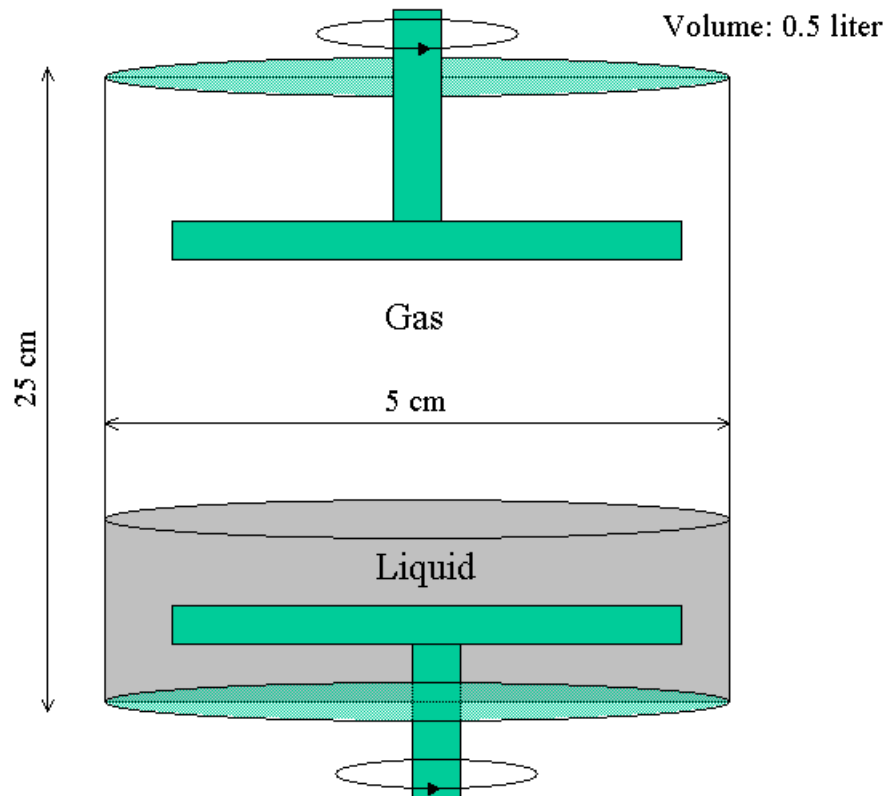
Figure 4-4 Illustration of the stirred cell with stirring in both liquid and gas

Using the equations given in Table 4-2 for calculating the binary low-flux Maxwell-Stefan mass transfer coefficients for a stirred cell in combination with equation (4.37), the diffusive fluxes of all components are calculated as function of time.

In Figure 4-5 and Figure 4-6 the results of the calculations for the stirred cell are given. We see that water has a high mass transfer rate – mainly due to that the low mass transfer resistance on the gas side. CO_2 has a relatively low mass transfer rate because of the high mass transfer resistance on the liquid side (low diffusivity in liquids). From Figure 4-5 we see that it takes about 10 seconds to vaporize the water into the gas, while it takes about 5 minutes to dissolve the CO_2 (obtaining thermodynamic equilibrium).
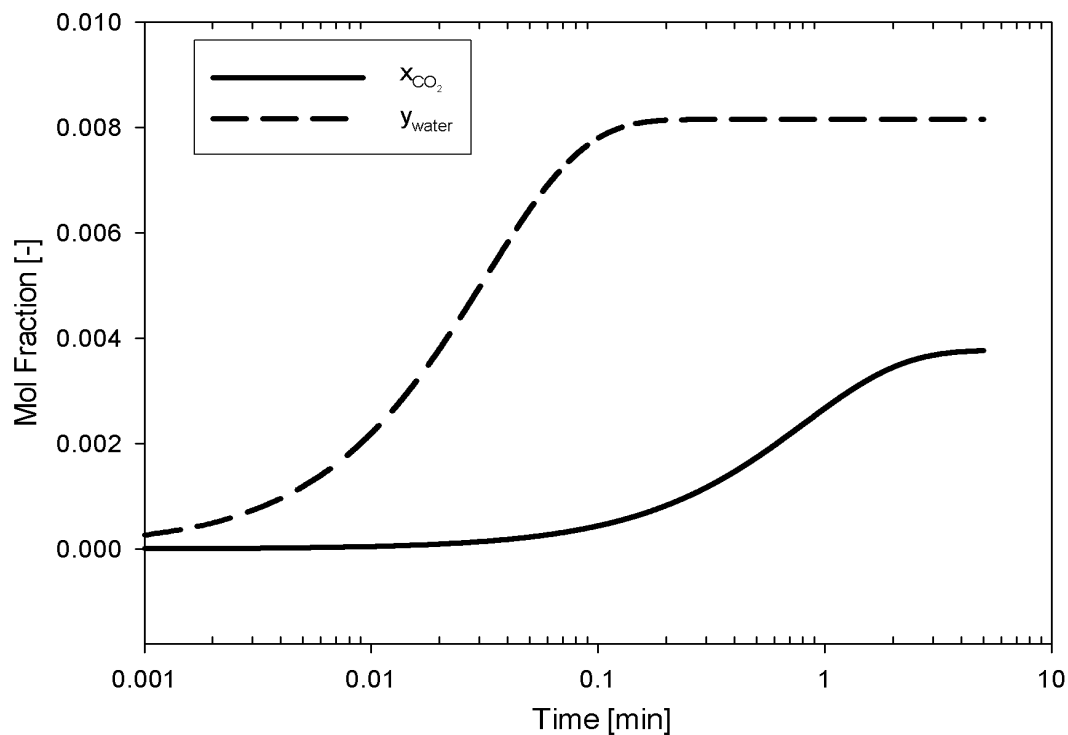
Figure 4-5 Simulation of mass transfer of CO_2 and water in a stirred cell. Calculated molar fractions of CO_2 in liquid and water in gas as function of time. *Script: simple-flux.py, p. 82*
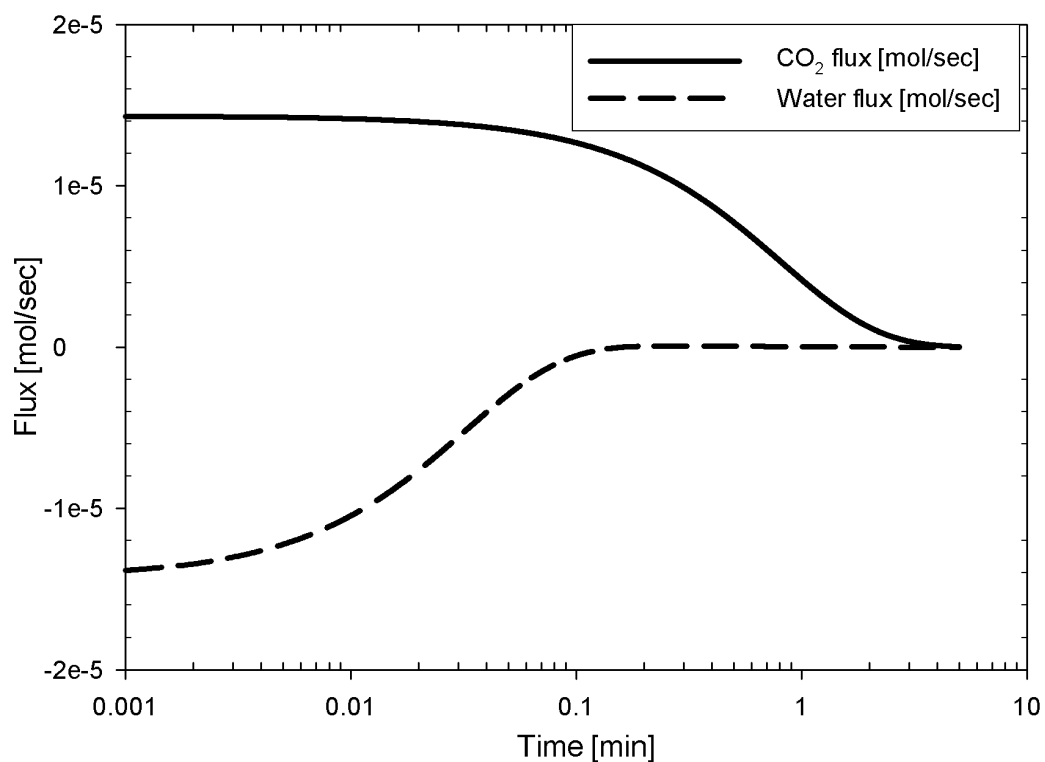
Figure 4-6 Simulation of mass transfer of CO_2 and water in a stirred cell. Calculated molar mass transfer rate of CO_2 in water and water in CO_2 as function of time. *Script: simple-flux.py, p. 82*

Using the equations given in this chapter the mass fluxes for many simple multiphase systems can be estimated. In many situations the mass transfer model described here needs to be combined with fluid mechanical models. Such types of calculations will be considered in chapter 5.

4.5 Finite Flux Corrections to the Mass Transfer Coefficient

During the process of mass transfer through an interface, the composition and velocity profiles are affected by the diffusion process. In equation (4.46) the mass transfer coefficient is defined for the limit of vanishing small mass transfer rates (N_1, $N_2 \rightarrow 0$) in order to avoid introducing the distortions in the definitions of the mass transfer coefficient. The mass transfer coefficients defined by equation (4.46) are called the low-flux mass transfer coefficients. The low-flux mass transfer coefficients are the ones that are usually available from empirical correlations of mass transfer data and from mass transfer analogies. Examples of such equations for the low flux mass transfer coefficients were given in Table 4-2. In this section we define the finite flux mass transfer coefficient. This mass transfer coefficient of a component A in a two-component ideal gas is written as

$$k_A^* = \left(\frac{N_A - x_A N_t}{c_t \left(x_{A,bulk} - x_{A,\mathrm{int}} \right)} \right) = \left(\frac{J_A}{c_t \Delta x_A} \right) \tag{4.51}$$

where the superscript * indicates that the mass transfer coefficient corresponds to conditions of finite mass transfer rates.

For the calculation of the mass transfer rate (flux), the finite flux mass transfer coefficient k_A^* is needed. This coefficient is related to the zero-flux coefficient by the general relation:

$$k_A^* = k_A \Xi_A \tag{4.52}$$

with Ξ_A being the correction factor that accounts for the effect of finite fluxes on k_A. The correction factor depends on the composition profiles and total mass transfer rates and, consequently, it is directly related to the model used to describe the hydrodynamics of the mass transfer process.

In multicomponent systems, the mass transfer rates of each species are better expressed in matrix form:

$$(J) = (N) - (x_b) N_t = c_t \left[k^* \right] (x_b - x_i) \tag{4.53}$$

where $\left[k^* \right]$ is a matrix of finite flux mass transfer coefficients. The finite flux mass transfer coefficients are related to the low flux coefficients by a relation equivalent to equation (4.52)

$$\left[k^* \right] = [k][\Xi] \tag{4.54}$$

The matrix of low flux mass transfer coefficients [k] may be expressed in terms of the Maxwell-Stefan mass transfer coefficient matrix [R] as (see equation (4.37))

$$[k] = [\Gamma][R]^{-1} \tag{4.55}$$

High net transfer rates across phase boundaries distort the boundary-layer profiles of velocity and temperature as well as species concentration, and they alter the boundary layer thickness. Both of these effects tend to increase friction factors and the heat and mass transfer coefficients, if the mass transfer is toward the boundary, and to reduce them in the reverse situation. The magnitudes of such changes are dependent on the system geometry, boundary conditions, and the magnitude of the governing parameters such as the Reynolds-, Prandtl-, and Schmidt numbers, and they are accompanied by the effects of changes in physical properties. They can also either increase or decrease the hydrodynamic stability. Accurate allowance for the effects of net mass transfer thus requires extensive calculation and/or experimentation. A relative simple model for incorporating this effect was implemented in the mass transfer model developed in this work, and will be presented in the next section.

Bird et. al. (2002) calculated the effect of mass transfer on the velocity-, temperature- and composition profile in a laminar boundary layer of a two-component ideal gas stream. By analytically solving the conservation laws of momentum, energy and components they obtained the results as illustrated in Figure 4-7 and Figure 4-8. In the figures the thickness of the boundary layer is given as a function of the dimension groups.

$$\Pi_v = \frac{v_x}{v_\infty} \qquad \Pi_T = \frac{T - T_0}{T_\infty - T_0} \qquad \Pi_{AB} = \frac{\omega_A - \omega_{A0}}{\omega_{A\infty} - \omega_{A0}}$$

and

$$\wedge_v = \frac{v}{v} \quad \wedge_T = \frac{v}{\alpha} = \mathrm{Pr} \quad \wedge_\omega = \frac{v}{D_A} = Sc$$
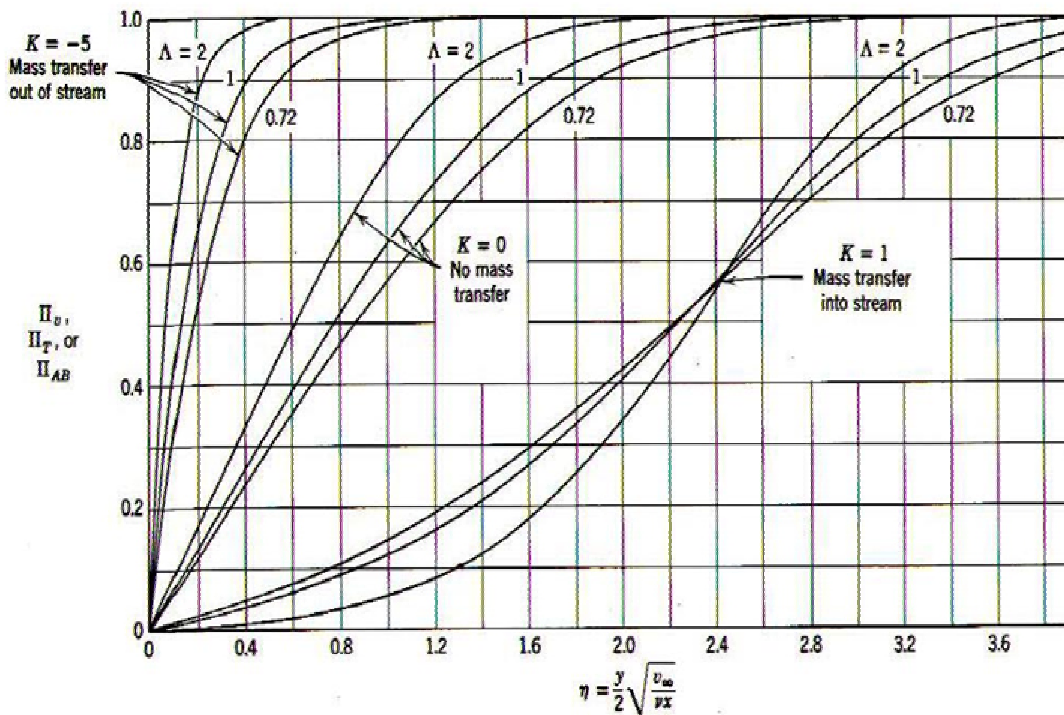
Figure 4-7 Dimensionless boundary layer thickness for finite mass transfer rates (Bird et.al., 2002)
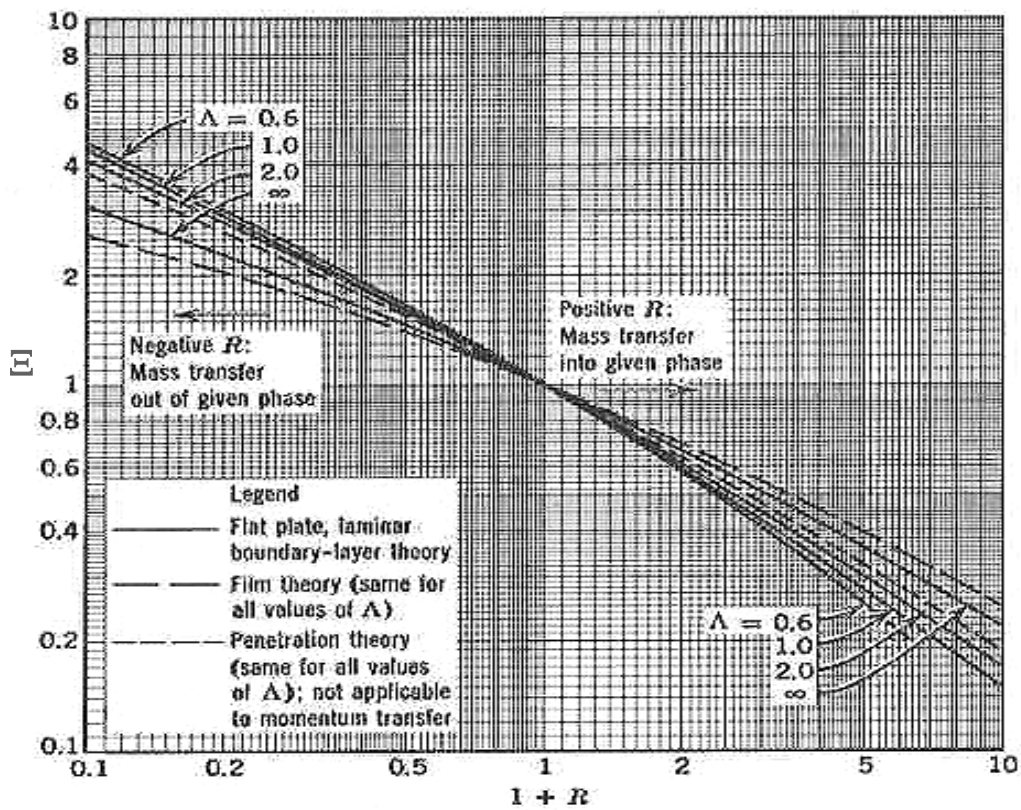
Figure 4-8 Values for the correction factor (Ξ) to the mass transfer coefficient (Bird et.al., 2002)

From Figure 4-8 we see that the correction factor (Ξ) is smaller than one for mass transfer into a given phase, while it is larger than one for mass transfer out of the phase. This is a consequence of the thinner boundary layer when we have mass transfer out of the stream (see Figure 4-7). This means that the total mass transfer coefficient will be larger if the mass transfer is out of a given phase than if the opposite is the situation. For large mass transfer rates the effect will be considerable and thus important to incorporate into a non-equilibrium model.

4.5.1 Calculation of Correction Factors for Finite Mass Transfer Rates

The correction factors presented in this section have been derived from film theory. The derivation can be found in Taylor and Krishna (1993).

The correction factor matrix can be calculated from

$$[\Xi] = \frac{[\Phi]\exp[\Phi]}{\exp[\Phi]-[I]} \tag{4.56}$$

We write the elements of the rate factor matrix $[\Phi]$ in terms of these binary Maxwell Stefan mass transfer coefficients.

$$\Phi_{ii} = \frac{N_i}{c_t k_{in}} + \sum_{\substack{k=1 \\ k \neq i}}^{n} \frac{N_k}{c_t k_{ik}} \tag{4.57}$$

$$\Phi_{ij} = -N_i \left(\frac{1}{c_t k_{ij}} - \frac{1}{c_t k_{in}} \right) \quad i \neq j \text{ and } i, j = 1, 2, ..., n-1 \tag{4.58}$$

The computation of the fluxes N_i from equation (4.53) involves an iterative procedure, partly because the N_i themselves are needed for the evaluation of the matrix of correction factors $[\Phi]$.

The method of successive substitution can be very effective when computing the N_i from equation (4.53) when the mole fractions at both ends of the diffusion path are known. In practice, we start from an initial guess of the fluxes N_i and compute the rate factor matrix $[\Phi]$. The correction factor matrix $[\Xi]$ may be calculated from an application of Sylvester's expansion formula (see e.g. Taylor and Krishna, 1993).

$$[\Xi] = \sum_{i=1}^{m} \hat{\Xi}_i \left\{ \prod_{\substack{j=1 \\ j \neq i}}^{m} \frac{[\Phi] - \hat{\Phi}_j [I]}{\prod_{\substack{j=1 \\ j \neq i}}^{m} \left(\hat{\Phi}_i - \hat{\Phi}_j \right)} \right\} \tag{4.59}$$

where m is the number of distinct eigenvalues of $[\Phi]$ $(m \leq n-1)$. The eigenvalue functions $\hat{\Xi}_i$ are given by

$$\hat{\Xi} = \frac{\hat{\Phi}_i \exp \hat{\Phi}_i}{\exp \hat{\Phi}_i - 1} \qquad (4.60)$$

The fluxes can be calculated from equation (4.53). The new estimates of the fluxes N_i are used to recalculate $[\Phi]$ and the procedure is repeated until convergence is obtained.

The procedure described above for calculating the finite mass transfer coefficient was implemented in the computer code developed in this work.

4.5.2 Calculation of the Non-Ideality Corrections

In this work we use the equations of state as described in chapter 3 to model the thermodynamic properties of fluid systems. In such cases it is convenient to calculate the non-ideality corrections form expressions for the fugacity coefficient. In this work we use the expression,

$$\Gamma_{ij} = \delta_{ij} + x_i \frac{\partial \ln \varphi_i}{\partial x_j}\bigg|_{T,P} \qquad (4.61)$$

When we use the non-ideal correction factor, the total mass transfer rate is calculated from

$$(J) = (N) - (x_b) N_t = c_t \left[k^* \right] (x_b - x_i) = c_t [\Gamma][\Xi][R]^{-1} (x_b - x_i) \qquad (4.62)$$

For mass transfer in a case of multicomponent, non-ideal, reactive finite flux mass transfer we have

$$(J\ ) = (N) - (x_b) N_t = c_t (E) \left[k^* \right] (x_b - x_i) = c_t (E) [\Gamma][\Xi][R]^{-1} (x_b - x_i) \qquad (4.63)$$

where R is calculated from equation (4.37) using the Maxwell-Stefan mass transfer coefficients.

4.5.3 Example – Evaluation of Influence of Mass Transfer Corrections

To test the effect of using finite flux and non-ideality corrections for a typical non-equilibrium case of interest in this work, a case study calculation was done. Consider the stirred cell and the case described in Figure 4-4 and section 4.4. We will simulate a case where methanol and water evaporates into CO_2 gas in the stirred cell. We consider a case where the temperature is 60°C and the initial gas is 5 litre pure CO_2 at 1 bar pressure. The initial composition of the liquid is 0.15 kg water and 0.10 kg methanol. The stirring rate is 50 rpm in both liquid and gas.

Mass transfer between the gas and the liquid will start immediately after a fast injection of the liquid solution. Water and methanol will vaporize into the gas and CO_2 will dissolve in the liquid. After a time the liquid and gas will come to equilibrium. In this example we want to evaluate the concentrations and molar fluxes of water and methanol as function of time. We

want to see if the finite flux correction and the thermodynamic non-ideality corrections have considerable effect.

We will use the SRK-EOS with the Huron-Vidal mixing rule to model the thermodynamics of the system. The NeqSim script for this simulation case is:

```python
# simple-flux2.py
system = thermo('srk', 342.15, 1.0)
addComponent(system,'CO2', 5.00, 'Nlitre/min',0)
addComponent(system,'methanol', 0.100, 'kg/min',1)
addComponent(system,'water', 0.150, 'kg/min',1)
mixingRule(system,'HV')

cellgeometry = geometry.stirredcell(0.05)
cell = node.stirredcell(system,cellgeometry)
cell.setStirrerSpeed(50.0/60.0)
cell.setDt(0.05)

cell.setInterphaseModelType(1)
cell.getFluidBoundary().useFiniteFluxCorrection(1,0)
cell.getFluidBoundary().useFiniteFluxCorrection(1,1)
cell.getFluidBoundary().useThermodynamicCorrections(0,0)
cell.getFluidBoundary().useThermodynamicCorrections(0,1)

# Iterates a specified number of time-steps
for i in range(7000):
        flow.solve(cell,heattrans=0,masstrans=1)
        print 'time ', i*cell.getDt()/60.0, \
        ' y_methanol ',
         cell.getBulkSystem().getPhase(0).getComponent(1).getx(),\
        ' flux_methanol ', cell.getMolarMassTransferRate(1)
        cell.update()
```

Using the equations given in Table 4-2 for calculating the binary low-flux Maxwell-Stefan mass transfer coefficients for a stirred cell in combination with equation (4.37), the diffusive fluxes and concentration profiles of all components are calculated as function of time. The diffusion coefficients are calculated from the empirical models described in appendix D.

The results are presented in Figure 4-9 and Figure 4-10. We see that the gas will be saturated with methanol and water after about 1 minute. We can see that the effects of non-ideality and finite mass transfer fluxes have a relatively large influence on the results. In the calculations where we used finite flux and non-ideality corrections – we see that we get a peak in water concentration after a short while. This peek is not observed if the corrections were not included. We conclude that for this case the use finite flux- and non-ideality corrections were important.

A closer investigation would show that the finite mass transfer correction was the main reason for the difference from the ideal case. As expected we can see that the finite flux correction reduces the methanol mass transfer rate (mass transfer into the gas phase). For this case, the mass transfer was high enough to affect the concentration profiles of water and methanol considerably.

The mass transfer model developed in this work uses thermodynamic- and finite flux corrections by default. All simulations done further on in this thesis have included these correction terms.
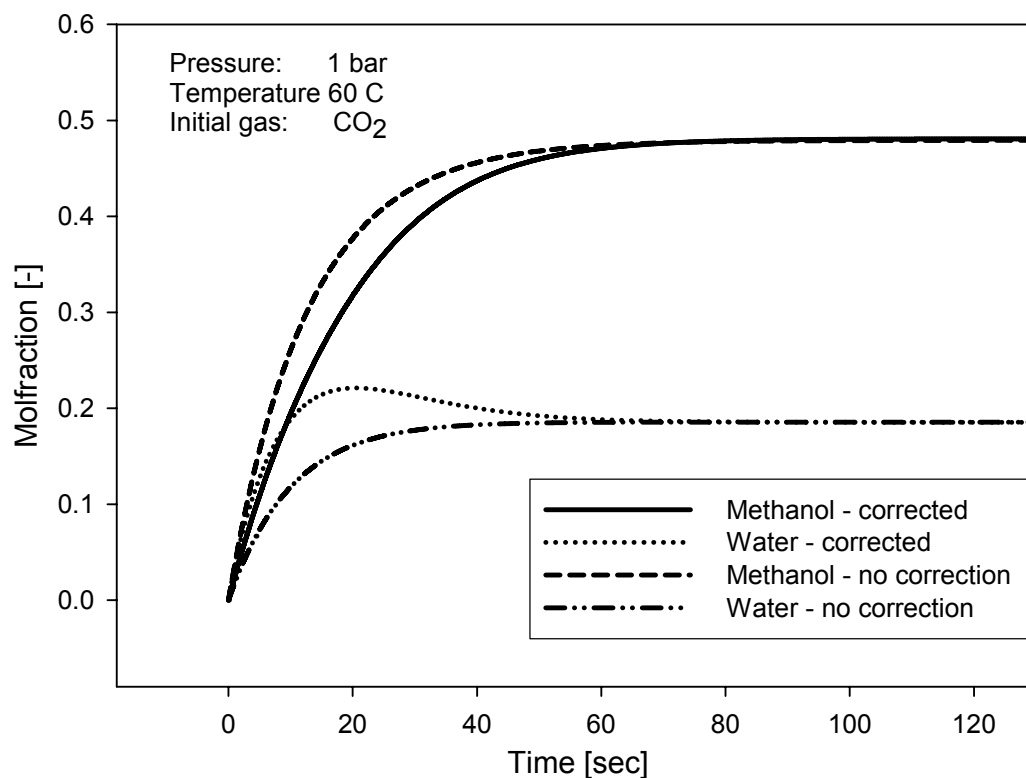
Figure 4-9 Simulation of mass transfer of methanol and water into CO_2 in a stirred cell. Calculated molar concentrations of methanol and water in the gas as function of time are given. *Script: simple-flux2.py, p. 90*
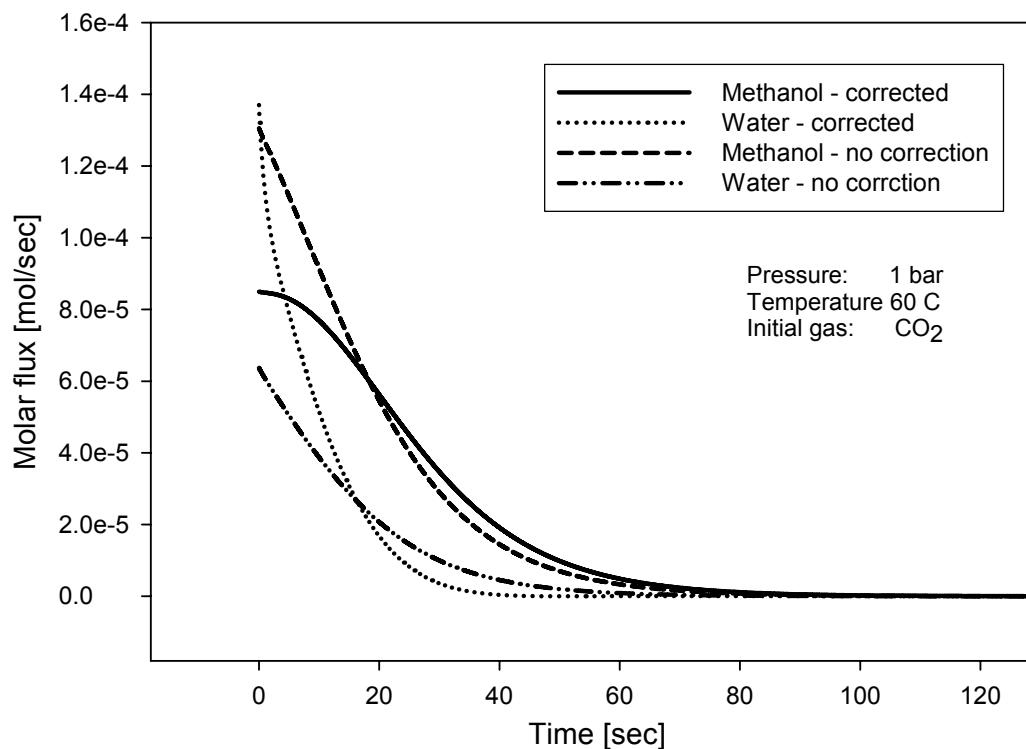
Figure 4-10 Simulation of mass transfer of methanol and water into CO_2 in a stirred cell. Calculated molar fluxes of methanol and water as function of time are given. *Script: simple-flux2.py, p. 90*

To check that the mass transfer model calculates the correct equilibrium state, an equilibrium TPflash was done. The result of the TPflash calculation is presented in Figure 4-11. By comparing the results of the mass transfer calculations and the equilibrium calculation, we conclude that the correct equilibrium composition is reached (final vapour fraction of methanol is about 0.46 and water 0.18).

System-Report	Phase 1	Phase 2	Phase 3	Unit
CO2	3.458E-1	1.22993E-4		[-]
methanol	4.67061E-1	2.5728E-1		[-]
water	1.87139E-1	7.42597E-1		[-]
Density	1.19177E0	9.46915E2		[kg/m^3]
PhaseFraction	5.0388E-2	9.49612E-1		[-]
MolarMass	3.35555E1	2.16271E1		[kg/kmol]
Cp	1.25584E0	1.85289E0		[kJ/kg*K]
Viscosity	1.43795E-5	4.90856E-4		[kg/m*sec]
Conductivity	2.28825E-2	6.66573E-1		[W/m*K]
Pressure	1.0	1.0		[bar]
Temperature	342.15	342.15		[K]

Figure 4-11 Equilibrium state of CO_2, methanol and water at 60°C and 1 bar
        Script: TPflash.py, p. 306

4.5.4 Numerical Computation of the Fluxes

The heat and mass fluxes are calculated subsequently. The following (3n) equations are solved for the mass fluxes:

- n independent equilibrium relations at the interphase
- 2 summations of mole fractions at the liquid-gas interphase
- n-1 rate equation at the liquid interface
- n-1 rate equations at the gas interface

where n is the number of components. We define x and y as the liquid and gas composition at the interface and N_i is the molar flux of component i.

We have the (3n) unknown variables, z:

$$z_i \;=\; y_i \quad i = 1..n$$
$$z_{i+n} \;=\; x_i \quad i = 1..n$$
$$z_{i+2n} \;=\; N_i \quad i = 1..n$$

The (3n) equations are:

$$f_i = \ln\left(\varphi_i^{gas} y_i\right) - \ln\left(\varphi_i^{liq} x_i\right) \quad i = 1..n$$

$$f_i = 1 - \sum_{j=1}^{n} x_i \qquad\qquad i = n+1$$

$$f_i = 1 - \sum_{j=1}^{n} y_i \qquad\qquad i = n+2 \qquad\qquad (4.64)$$

$$f_i = N_i + c_t^{liq}(E)\left[k_{liq}^*\right]\Delta x_i - x_i^{bulk} N_{tot} \quad i = (n+3)..2n+1$$

$$f_i = N_i - c_t^{gas}\left[k_{gas}^*\right]\Delta y_i - y_i^{bulk} N_{tot} \quad i = (2n+2)..3n$$

where $N_{tot} = \sum_{i=1}^{n} N_i$ and we have assumed that reactions can only occur in the liquid phase. These equations can be effectively solved using a Newton-Raphson method.

4.5.5 Interphase Heat Transfer Calculations

When modelling processes such as gas absorption and distillation it is essential to consider the transport across the phase boundary and the continuity of mass and energy flux. Reactive gas absorption is a typical exothermal process. In some absorption systems the temperature rise is not significant and therefore isothermal operation can be assumed. However, in some processes of physical absorption and in most reactive absorption situations the thermal effects are large and the heat released can be responsible for a significant increase in temperature of the liquid and vapour (Zarzycki and Chacuk, 1993). These thermal effects in turn affect the transport and physiochemical properties and therefore the mass transfer kinetics.

The theory presented in this section on interfacial transport phenomena has been developed by Krishna (1977) and Taylor and Krishna (1993). Though the analysis given below is developed for liquid-vapour interface transport, the formalism is generally valid for all two-phase systems.

At the vapour-liquid interface we have continuity of the component molar fluxes:

$$N_i^L = N_i = N_i^V \qquad\qquad (4.65)$$

and the total molar fluxes N_t:

$$N_t^L = N_t = N_t^V \qquad\qquad (4.66)$$

where N_i^L and N_i^V are the normal components of the molar flux N_i at the interface. These fluxes are composed of diffusive and convective contributions as

$$N_i^L = J_i^L + x_i N_t^L = N_i = J_i^V + y_i N_t^V = N_i^V \qquad\qquad (4.67)$$

We also have continuity of the energy flux across the vapour-liquid interface:

$$J_q^V = J_q^L = J_q \qquad\qquad (4.68)$$

where J_q^V and J_q^L are the normal components of the energy flux at the interface. The energy flux can be defined as follows (eq. (4.15)):

$$J_q = J_q^{'} + \sum_{i=1}^{n} \bar{H}_i N_i \qquad (4.69)$$

where $J_q^{'}$ represents the purely conductive heat flux and the second term accounts for the convective enthalpy transfer due to the diffusing species. The conductive heat flux $J_q^{'}$ plays a role analogous to the molar diffusion flux J_i.

Considering equation (4.68), the energy transfer across the interface can be expressed as:

$$J_q^{'V} + \sum_{i=1}^{n} \bar{N}_i^V \bar{H}_i^V \left(T^V \right) = J_q^{'L} + \sum_{i=1}^{n} \bar{N}_i^L \bar{H}_i^L \left(T^L \right) \qquad (4.70)$$

with the conductive heat fluxes in the two phases given by

$$J_q^{'V} = h_V^* \left(T^V - T^i \right)$$
$$J_q^{'L} = h_L^* \left(T^L - T^i \right) \qquad (4.71)$$

where h_L^* and h_V^* are the finite flux heat transfer coefficients in the vapour and liquid respectively, and T^i is the temperature at the vapour-liquid interface. Analogous to the finite mass transfer coefficient, the finite flux heat transfer coefficient can be calculated from

$$h_V^* = h_V \frac{\Phi_H^V}{\exp\left(\Phi_H^V\right) - 1} \qquad (4.72)$$

where h_v is the low flux heat transfer coefficient and can be calculated from heat transfer analogies or empirical equations. From film theory we can show (Taylor and Krishna, 1993) that Φ_H^V is given as

$$\Phi_H^V = \sum_{i=1}^{n} \frac{N_i C_{pi}}{h_V} \qquad (4.73)$$

where C_{pi} is the partial specific heat capacity.

In the model developed in this work equation (4.70) is solved simultaneously with equation (4.64). Although computation of coupled heat and mass fluxes can be calculated relatively effective using the Newton-Raphson technique described earlier – such mass transfer calculations will be resource demanding in multiphase flow calculations. Flux calculations are often repeated thousands of times and will often lead to slow simulation programs.

4.6 Effect of Chemical Reaction on Mass Transfer of CO_2 into Aqueous Amine Solutions

In this section, the theory of mass and heat transfer accompanied with chemical reactions in gas-liquid systems is reviewed. The Ficks's law and Maxwell-Stefan approaches to mass transfer will be compared and discussed in detail. The effects of chemical reactions on mass transfer with emphasis on the chemistry of the reactions between CO_2 with alkanolamines will be described. Previous work in these areas is discussed.

Vanni and Baldi (1991), Valerio and Vanni (1994), Frank et.al. (1995) and Pacheco (1998) have studied the problem of mass transfer with simultaneous chemical reactions when the mass transfer problem is described by the Maxwell-Stefan approach. These researchers compared the predictions of the more rigorous multicomponent approach with estimates of interfacial mass transfer rates using a pseudo-binary approach based on Fickian diffusion. The film model was adopted by these researchers to describe the hydrodynamics at the interface. Frank et. al. (1995) studied a more general situation where a chemical reaction of the following form takes place in the liquid phase:

$$v_A A + v_B B \underset{k_{-2}}{\overset{k_2}{\rightleftharpoons}} v_C C + v_D D \tag{4.74}$$

with a reaction rate given by $R\left(kmol/m^3 \sec\right) = k_2 [A]^a [B]^b - k_{-2} [C]^c [D]^d$ where [A] is the molar concentration of component A. The conservation equation for the liquid phase is given by

$$\frac{dN_i}{d\eta} = v_i R \delta \tag{4.75}$$

where η is the dimensionless distance in the film defined as $\eta = x/\delta$. When a thermodynamic ideal solution is assumed, an expression equivalent to equation (4.24) can be used to relate the molar fluxes of the different components with the concentration driving force:

$$\frac{dx_i}{d\eta} = \sum_{\substack{j=1 \\ j \neq i}}^{n} \frac{x_i N_i - x_i N_t}{c_t \mathcal{k}_{ij}} \tag{4.76}$$

The system of differential equations (4.75) and (4.76) along with the appropriate boundary conditions can be solved numerically. Frank and co-workers compared molar fluxes for the diffusing gas (component A) calculated using this numerical solution with the interfacial fluxes obtained using the enhancement factor approach based on Fickian diffusion;

$$N_A = E_A N_{A,no \; reaction} \tag{4.77}$$

This comparison was performed only for irreversible reactions of the form $A \rightarrow C$ (1,1 order). The enhancement factor for the diffusing gas was calculated using relationships between Hatta number and the enhancement factor derived for the case when Fick's formulation for mass and heat transfer is used. The Hatta number is expressed by:

$$Ha = \frac{\sqrt{k_1 D_{A,eff}}}{k_{A,eff}}$$

(4.78)

where k_1 is the first order or pseudo-first order reaction constant. The effective mass transfer coefficient $k_{A,eff}$ was estimated using a relationship similar to equation (4.44). The interfacial mass transfer flux in the absence of chemical reactions was calculated using an approximate analytical solution of the Maxwell-Stefan equations (equation (4.39)). Comparison between the two theories indicated that even when the Maxwell-Stefan theory is used to describe the mass transfer process, the enhancement factor follows the same functionality with respect to the Hatta number as it is derived on the basis on the basis of Fick's law. This result was obtained using a wide range of conditions with respect to diffusion rates (both equal and different binary mass transfer coefficients) and reaction kinetics. Mass transfer with reversible chemical reaction was also modelled using the Maxwell-Stefan approach, but no comparison was made with the enhancement factor theory.

The work of Vanni and Baldi (1991) is somewhat similar to the contribution of Frank et.al. (1995), but they assumed that the reaction product is soluble in both the liquid and vapour phases. These researchers derived approximate expressions for the enhancement factors that account for the diffusion interactions in the framework of the Maxwell-Stefan theory. Valerio and Vanni (1994) addressed the problem of mass transfer accompanied with chemical reactions in non-ideal multicomponent systems. The effect of non-ideal diffusion kinetics was evaluated for first order and instantaneous reactions. The Maxwell-Stefan diffusivities are calculated from infinite dilution diffusion coefficients corrected for composition effects for concentrated solutions. This composition dependence of the Maxwell-Stefan diffusivities is one source of non-ideality on the diffusion kinetics. The other source of non-ideality on the diffusion kinetics arise from the use of chemical potential gradients rather that molar composition gradients as the driving force for mass transfer. The effect of non-ideal thermodynamics on the kinetics of diffusion is reflected on the matrix $[\Gamma]$ (see equation (4.62)). To evaluate the matrix of thermodynamic factors $[\Gamma]$, a model that relates the activity or the fugacity coefficient of the different components with composition is needed. Valerio and Vanni (1994) adopted the multicomponent Marguels model. In this work the equations of state derived in the previous chapter are used.

Valerio and Vanni (1994) defined three different ranges for the infinite dilution activity coefficients of component i in component j $\left(\gamma_{ij}^{\infty}\right)$ in order to study the effect of thermodynamic non-ideality on the predictions of the interfacial fluxes of diffusing gas. For moderately non-ideal systems $(0.2 < \left(\gamma_{ij}^{\infty}\right) < 5.0)$ the difference between the interfacial flux of the diffusing gas calculated considering the non-ideal thermodynamic to that neglecting the effect of the non-ideality was always less than 10%. This range of $\left(\gamma_{ij}^{\infty}\right)$ is representative of several actual systems with significant non-ideal behaviour. For systems where the thermodynamic non-ideality was even more significant $(0.05 < \left(\gamma_{ij}^{\infty}\right) < 20.0)$, the difference between the calculated interfacial fluxes was usually less than 15%. In these calculations the thermodynamic non-ideality of the solutions affected not only the diffusion kinetics but also the reaction kinetics.

The effect of the composition dependence on the Maxwell-Stefan diffusion coefficients was shown to be negligible even in concentrated solutions. Only when the infinite dilution diffusion coefficients differ by more than a factor of four from each other, the interfacial flux of the diffusing gas is affected by more than 15% with respect to the ideal solution. The authors indicated that for most gas-liquid systems the infinite dilution diffusion coefficients do not differ from each other by more than a factor of two. Under this conditions the diffusional non-ideality accounts for less than 3% of the interfacial flux. Therefore, the surprising conclusion of the work by Valerio and Vanni (1994) is that non-ideal diffusion and non-ideal thermodynamics affect the interfacial fluxes in gas-liquid reactive systems only in very highly non-ideal solutions, excluding most systems of practical interest.

The nonideality of the CO_2-MDEA-water system can be estimated by calculating the activity coefficients of the individual components and ions in solution, as was done in Figure 3-15 for a 30wt% MDEA solution at 40°C. We can see that the activity coefficients of the molecules and ions varies from about 0.2 to 2 and corresponds to a situation where the thermodynamic non-idelaity effect will be less than 10% (Valerio and Vanni, 1994).

In this work the non-ideality and finite flux corrections were included in all calculations – even though the importance of these terms are questionable. The calculation of the enhancement factors were based on the effective mass- and diffusion coefficient method – as was shown by Frank et.al. (1995) to give accurate results for reactive mass transfer.

4.7 Gas-Liquid Reactions and Surface Renewal Theory – Calculation of the Enhancement Factor

Different models have been developed in order to describe the interfacial hydrodynamics of gas-liquid systems. Film theory, penetration and surface renewal theories, and eddy diffusivity theories are among the models more commonly studied and used. A thorough comparison between these models was conducted by Glasscock and Rochelle (1989). Both penetration and surface renewal theories are unsteady-state theories and are generally accepted as being more accurate than film theory for mass transfer at turbulent gas-liquid interfaces (Danckwerst (1970), Glasscock and Rochelle (1989)). In the present work the Danckwerst surface renewal theory was adopted in the reaction-diffusion modelling to describe the hydrodynamics at the vapour-liquid interface (for calculating the enhancement factor).

The Danckwerst model of mass transfer is one of the surface-renewal models that take as their basis the replacement at intervals of elements of liquid at the surface by liquid from the interior which has the local mean bulk concentration. Thus, the surface-renewal models visualize the surface of an agitated liquid or a liquid flowing over a packing, as a mosaic of elements which have been exposed to the gas for different lengths of time (or have different "ages"), and which will therefore be absorbing at different specific rates. The Danckwerst model assumes that the chance of an element of surface being replaced with fresh liquid is independent of the length of time for which it has been exposed. This leads to a distribution of surface "ages" in which the fraction of the surface which at any given instant has been exposed to the surface for times between θ and $(\theta+d\theta)$ is $se^{-s\theta}d\theta$. Where s is the fraction of the area of surface which is replaced with fresh liquid in unit time.

If N is the instantaneous rate of absorption per unit area of surface which has been exposed for time θ, the average rate of absorption per unit area of surface which has been exposed for

time θ, the average rate of absorption into the surface is the value of N averaged over all elements of the surface, having ages between 0 and ∞:

$$\bar{N} = s\int_0^\infty N(\theta)e^{-s\theta}d\theta \qquad (4.79)$$

For physical absorption the rate of mass transfer of spieces A per unit area of surface is $\left([A]_i - [A]_0\right)\sqrt{D_A/\pi\theta}$ (Danckwerst, 1970). Therefore, the average mass transfer rate is given by:

$$\bar{N} = \left([A]_i - [A]_0\right)s\sqrt{D_A/\pi}\int_0^\infty \frac{e^{-s\theta}}{\sqrt{\theta}}d\theta$$
$$\bar{N} = \left([A]_i - [A]_0\right)\sqrt{D_A s} \qquad (4.80)$$

From this equation it can be seen that in Danckwerst model the physical mass transfer coefficient is given by $k_L^0 = \sqrt{D_A s}$. The Danckwerst model estimates the mass transfer coefficient to be proportional to the square root of the diffusion coefficient. This is in contradiction to the film model who gives a linear relationship. From experimental experience we know that the true value falls somewhere between these two estimates.

Similarly as the average rate of absorption is given by equation (4.79), the average concentration of a given component at a distance x below the surface is

$$\left[\bar{A}\right]_x = s\int_0^\infty [A]_{x,\theta}e^{-s\theta}d\theta \qquad (4.81)$$

where $[A]_{x,\theta}$ is the instantaneous concentration at a distance x below the vapour-liquid interface at time θ after first exposure to the surface to the gas. Equations (4.80) and (4.81) represents the "s-multiplied" Laplace transform of the instantaneous absorption rate and instantaneous concentration, respectively. DeCoursey and Thring (1989) and DeCoursey (1992) used the property that the time-mean fluxes and concentrations are equal to the respective "s-multiplied" Laplace transform in order to simplify the solution of the diffusion-reaction equations using the Danckwerst surface renewal model for the interfacial hydrodynamics.

For physical absorption, the mass balance of the diffusing gas A can be expressed as:

$$D_A\frac{\partial^2[A]}{\partial x^2} - \frac{\partial[A]}{\partial t} = 0 \qquad (4.82)$$

with the initial and boundary conditions:

$$[A] = [A]_0 \qquad x > 0, t = 0$$
$$[A] = [A]_i \qquad x = 0, t > 0$$
$$[A] = [A]_0 \qquad x \to \infty, t > 0$$

where $[A]_0$ and $[A]_1$ are the concentrations at the liquid bulk and vapour-liquid interface, respectively.

Applying the s-multiplied Laplace transform to equation (4.82), the following expression is obtained:

$$D_A \frac{d^2[\overline{A}]}{dx^2} - s\left\{[\overline{A}] - [\overline{A}]_0\right\} = 0 \qquad (4.83)$$

with

$$[\overline{A}] = [\overline{A}]_i \qquad x = 0, t > 0$$
$$[\overline{A}] = [\overline{A}]_0 \qquad x = \infty, t > 0$$

where the time mean concentration $[\overline{A}]$ is given by equation (4.81). Similarly, when a first order reaction $(R = k_1[A])$ takes place in the liquid phase with the initial and boundary conditions:

$$[A] = [A]_0 \qquad x > 0, t = 0$$
$$[A] = [A]_i \qquad x = 0, t > 0$$
$$[A] = 0 \qquad x \to \infty, t > 0$$

the solution of the diffusion-reaction equation is the following

$$[\overline{A}] = [A]_i \exp\left\{-\frac{x E_A k_{L,A}^0}{D_A}\right\} \qquad (4.84)$$

where the enhancement factor for the interfacial flux of A, E_A, is given by:

$$E_A = \sqrt{1 + \frac{k_1 D_A}{k_{L,A}^0{}^2}} \qquad (4.85)$$

The results given by equations (4.84) and (4.85) led DeCoursey and Thring (1989) and DeCoursey (1992) to consider that an approximate solution of the governing diffusion-reaction equation for reversible second-order chemical reaction of the form

$$A + v_b B \underset{k_{-2}}{\overset{k_2}{\rightleftarrows}} v_c C + v_d D \qquad R = k_2[A][B]^b - k_{-2}[C]^c[D]^d \qquad (4.86)$$

can be given by:

$$\left[\bar{A}\right] - \left[\bar{A}\right]_0 = \left(\left[A\right]_i - \left[\bar{A}\right]_0\right) \exp\left\{-\frac{x E_A k_{L,A}^0}{D_A}\right\} \tag{4.87}$$

where E_A, the enhancement factor for the interfacial flux of A, accounts not only for the effect of forward chemical reaction, but also for the reversibility and the diffusion limitations of the reactants and reaction products. The functionality of E_A with respect to the diffusion and reaction kinetics, and the equilibria is found in such a way that equation (4.87) satisfies exactly the diffusion-reaction equation at the interface, but only approximately elsewhere. Equation (4.87) is exact in value and slope at the interface and liquid bulk for a second order reaction, but it deviates from the true profile in-between. The diffusion-reaction equation is satisfied exactly at the interface but only approximately elsewhere because, under most conditions, the reaction rate and diffusion process closest to the interface has the greatest influence on the mass transfer enhancement. Also the condition of zero flux at the interface of the reactants (different from A) and reaction products makes their gradients close to zero at the interface.

Equation (4.87) provides the appropriate representation of the interfacial flux, as

$$\bar{N}_A = -D_A \left(\frac{d\left[\bar{A}\right]}{dx}\right)_{x=0} = E_A k_{L,A}^0 \left(\left[A\right]_i - \left[A\right]_0\right) \tag{4.88}$$

where it was assumed that the interfacial molar flux of the diffusing gas is equal to its diffusive flux. This assumption is justified considering that, under most conditions, the mole fraction of the absorbing gas in the liquid phase is quite low which makes the contribution of the convective term $\left(x_A N_t\right)$ negligible.

4.7.1 Enhancement Factors for Slow and Infinite Fast Reactions

In the last sections the equations used to calculate enhancement factor for reactions in the fast reaction regime were derived. We normally divide the reaction regimes into the slow, fast and infinite fast reaction regime with respect to the fluid mechanics. For slow reactions the kinetics in the liquid film are so slow that the mass transfer rate is unaffected (E=1). For infinitely fast reactions the reactions occurs so fast that the reactants and products can't coexists. In this case the mass transfer rate will be limited by diffusion of reactants and products in the liquid film. For a comprehensive review of calculation methods for enhancement factors for different reaction regimes – the reader is referred to Astarita et.al. (1983) and Perry (1998). For complicated and reversible reactions we often have to use numerical methods with full discretisation of the liquid boundary layer. Such calculations will be very time-consuming.

4.7.2 Example – Calculation of the Enhancement Factor During Absorption of CO_2 into Aqueous MDEA in a Stirred Cell

Consider again the system described in section 4.4. In this example we fill the cell with a 50 wt% solution of MDEA at 25°C. The gas consists of pure CO_2 at 10 bar. We would like to

estimate the enhancement factor for CO_2 in this system. By regulating the stirrer speed the liquid Reynolds number (and thus the mass transfer coefficient and Hatta number) can be varied.

In Figure 4-12 the initial enhancement factor for CO_2 in the MDEA solution was estimated using the equations given in this chapter. We can see that the enhancement factor reaches a constant value at low stirring rates (Reynolds numbers) – because of diffusion limitation of the reactants. At higher stirring rates – the enhancement factor drops – because of a rise in the convective forces. CO_2 reacts relatively slow in MDEA solutions – and the enhancement factor is always relatively low.
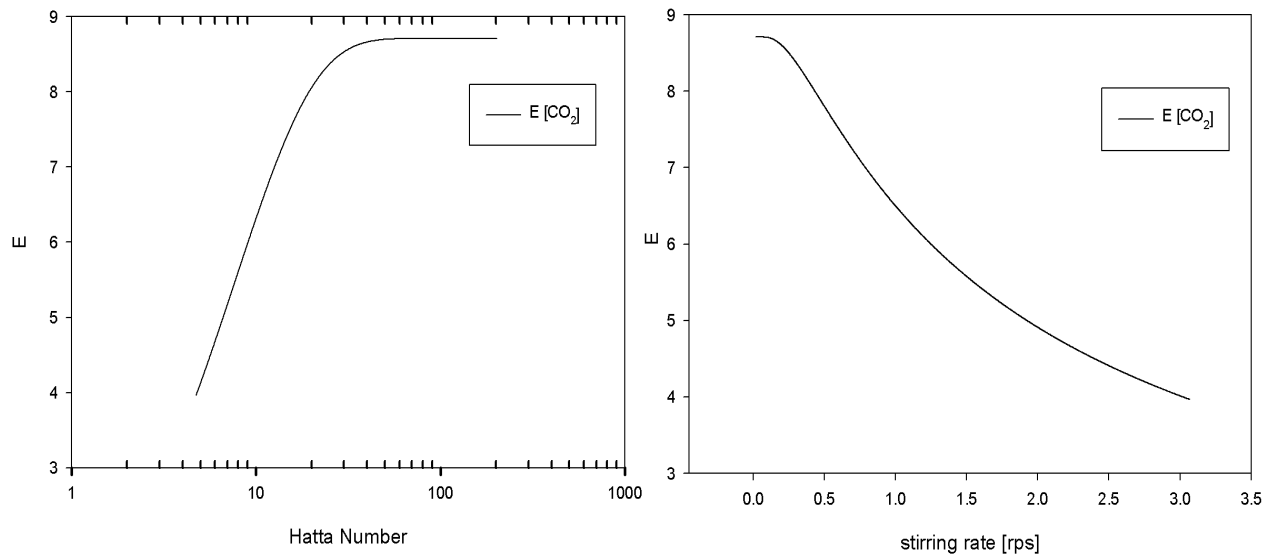
Figure 4-12 Calculated enhancement factors for CO_2 as function of stirring rate in a stirred cell for a 50wt% MDEA solution at 25°C. *Script: enhancement.py, p. 309*

4.8 Kinetics of Gas-Liquid Reactions: Reactive Absorption of CO_2 and H_2S in Aqueous Alkanolamines

When reacting with CO_2, sterically unhindered primary and secondary alkanolamines form stable carbamate ions. On the other hand, since tertiary alkanolamine molecules do not have the N-H bounds, their reaction with CO_2 produces only bicarbonate and carbonate ions.

Primary amines like MEA and DGA are noted for their fast reaction rates with CO_2. Secondary amines like DEA have intermediate reaction rates, and finally MDEA, being a tertiary amine, has much slower reaction rate with CO_2. Primary and secondary amines react with CO_2 to form carbamate:

$$CO_2 + R_2NH + H_2O \underset{k_{-2}}{\overset{k_2}{\rightleftharpoons}} R_2NCOO^- + H_3O^+ \tag{4.89}$$

Depending on the stability of the carbamate, it may revert to bicarbonate:

$$R_2NCOO^- + H_2O \underset{k_{-2}}{\overset{k_2}{\rightleftharpoons}} R_2NH + HCO_3^- \tag{4.90}$$
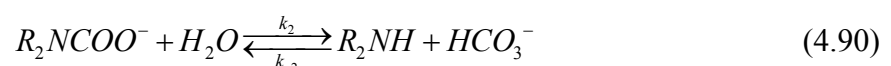
Danckwerst (1979) proposed that the carbamate formation may involve the formation of an intermediate zwitterion (a locally ionic, net neutral, molecule). Blauhoff et. al. (1984) reported that this mechanism can be used to reconcile much of the kinetic data available, especially for DEA. Crichfeld et.al. (1987) introduced reversibility into the mechanism. This mechanism is as follows:

$$CO_2 + R_2NH \underset{k_{-1}}{\overset{k_2}{\rightleftharpoons}} R_2NH^-COO^- \ (zwitterion)$$

$$R_2NH^-COO^- + B \underset{k_{-2}}{\overset{k_2}{\rightleftharpoons}} R_2NCOO^- + B_1H^+$$

(4.91)
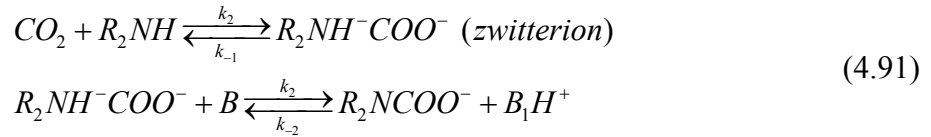
where B_1 designates any speices in solution that can act as a base to abstract the proton from the zwitterions in the second relation step. When pseudo-steady state approximation for the zwitterions is applied, the following expression is obtained for the rate of reaction of CO_2 (Crichfield and Rochelle, 1987):

$$R_{CO_2} = \frac{k_2[R_2NH]\left\{[CO_2]-[CO_2]^*\right\}}{1 + \dfrac{k_{-1}}{\sum k_{in}[B_1]}}$$

(4.92)

In equation (4.92), $[CO_2]^*$ is the equilibrium concentration of CO_2 and the summation is over all the bases in solution. For the amine system, the species that can abstract the proton from the zwitterions (B_i) are OH^-, water and the amines themselves.

When the rate of the second step represented in equation (4.91) is much faster than the reverse of the zwitterions formulation (that is, when the first step is the controlling mechanism), the rate expression (4.92) reduces to

$$R_{CO_2} = k_2[R_2NH]\left\{[CO_2]-[CO_2]^*\right\}$$

(4.93)

A rate expression equivalent to equation (4.93) was used by Hagewieche et.al. (1995) to describe the rate of reaction between MEA and CO_2 when modelling reactive absorption of CO_2 in unloaded solutions of MEA and MDEA.

Tertiary amines, unlike primary and secondary amines, cannot form carbamates and so they react with CO_2 by acting as a source of hydroxide, but there is evidence that the enhanced CO_2 absorption cannot be explained with the hydroxine reaction alone. Donaldson and Nguyen (1980) proposed that the enhanced absorption rates can be explained by a base catalysis of the CO_2 hydration. The essence of this catalysis is assumed to be a hydrogen bounding between the free amine and water which increases the reactivity of water towards CO_2.

For the specific reaction between CO_2 and MDEA, different researchers (Crichfield, 1988; Versteeg et.al., 1990; Glasscock, 1990; Rinker et.al. 1995) agree that a second order reversible reaction describes the experimental data. In the present work the following rate expression was used:

$$R_{CO_2} = k_2 [R_3N][CO_2] - k_{-2}[R_3NH^+][HCO_3^-] \qquad (4.94)$$

When a mixture of chemical solvents is used, the equilibrium concentration of CO_2, $[CO_2]^*$, is that which makes the total reaction rate equal to zero. For instance, for an aqueous solution of a primary and tertiary amine, the reaction rate of CO_2, can be expressed as:

$$R_{CO_2} = (k_{2p}[R_2NH] + k_{2t}[R_3N])\{[CO_2] - [CO_2]^*\} \qquad (4.95)$$

with $[CO_2]^*$ defining, therefore, a global equilibrium. This is the reaction rate model used in the modelling work of this study. We see that an accurate thermodynamic model is important to get the chemical equilibrium concentration $[CO_2]^*$ correct.

4.8.1 Calculation of the Enhancement Factor

From equation (4.95) and equation (4.85) it follows that the enhancement factor can be calculated as

$$E_A = \sqrt{1 + \frac{(k_{2p}[R_2NH] + k_{2t}[R_3N])D_{A,eff}}{k_{A,eff}^2}} \qquad (4.96)$$

This is the equation used to calculate the enhancement factor implemented in the simulation model developed in this work. The model can be used for calculation of the enhancement factor in both non-activated and activated MDEA solutions.

4.8.2 Calculation of Mass Transfer in a CO_2-MDEA-solution

From equation (4.96) and equation (4.63) we see that the mass transfer in the liquid phase can be calculated from

$$(J) = c_t(E)[k^*](x_b - x_i) \qquad (4.97)$$

where E_i is assumed to be unity for all components except for CO_2. The enhancement factor for CO_2 is calculated from

$$E_{CO_2} = \sqrt{1 + \frac{(k_{2t}[MDEA])D_{CO_2,eff}}{k_{CO_2,eff}^2}} \qquad (4.98)$$

The second order rate constant for the reaction between CO_2 and the MDEA-solution can be calculated from an Arrenihus type of equation, as was described in chapter 2, equation (2.9).

The model described above was used to model the experimental data of this work, and will also be used to simulate absorption of CO_2 in MDEA in packed beds.

4.9   Temperature Bulges and Reactive Absorption

In counter-current reactive absorption processes the enthalpy change due to absorption and reaction of the diffusing gas can cause a significant rise of the temperature of the liquid especially towards the bottom of the column where the interfacial fluxes are usually larger. Consequently, the liquid solvent (e.g. water) vaporizes. This increase in the temperature of the liquid is accompanied by an increase of the temperature of the vapour as well due to the contribution of the conductive heat transfer. However, towards the top of the column the vapour encounters a cooler incoming solvent, and therefore the vapour tends to condense. This interaction between convective enthalpy transfer of the diffusing gases, the enthalpy of vaporization-condensation of the liquid, and the conductive heat transfer between the vapour and liquid phases, can lead to the development of a temperature bulge at some point along the column.

Different researchers (Raal and Khurnana, 1973; Astarita et. al., 1983; Krishnamurthy et. al., 1986) have reported the existence of significant heat effects and temperature bulges both in physical and reactive absorption processes. Astarita et.al. (1983), for instance, illustrated a case of simultaneous absorption of CO_2 and H_2S in a solution of monoethanolamine/diethyleneglycol/water. With a high acid gas concentration, the measured temperature rise was over 40°C in the high temperature zone (temperature bulge).

In Figure 4-13 the temperature profile is calculated using the model developed in this work for absorption of CO_2 in an aqueous MDEA-solution. We see a typical temperature bulge in the lower part of the absorption tower. The simulated case is described in a case study reported in chapter 11.
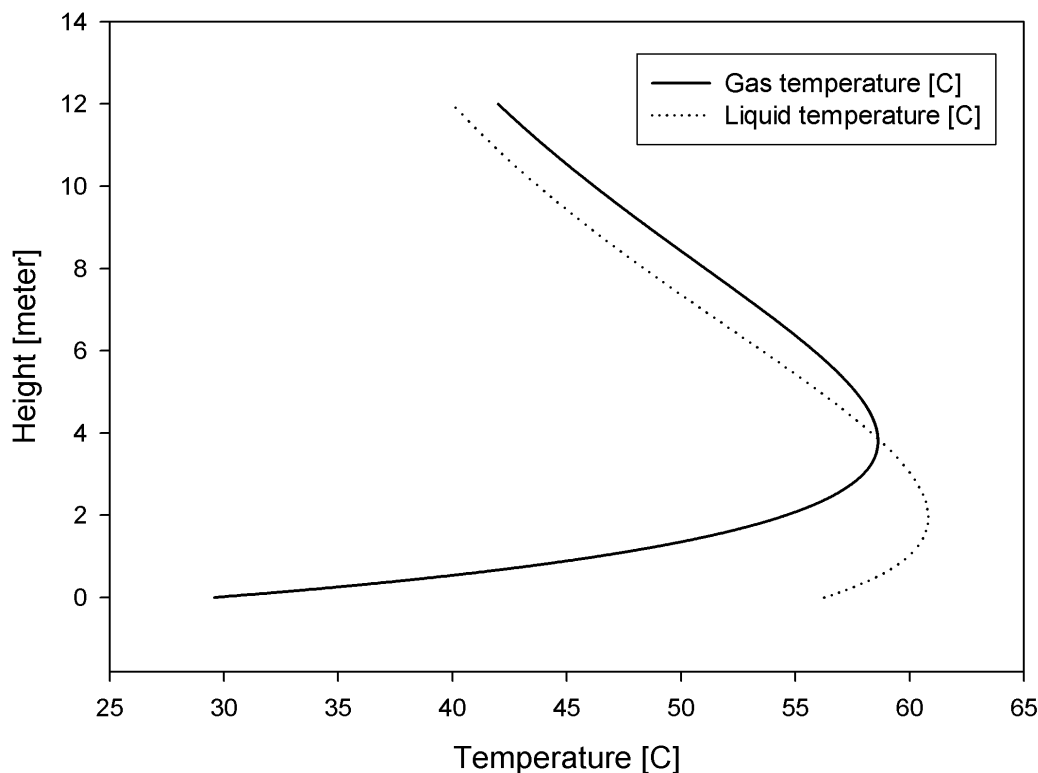
Figure 4-13 Temperature bulge for reactive absorption of CO_2 in a packed tower.
        Script: reactive-absorption.py, p. 317

4.10 Discussion and Summary – Non-Equilibrium Modelling

In this chapter a general non-equilibrium model has been developed. The model is based on the generalized Maxwell-Stefan equations. The resistance to mass transfer is considered to be restricted to the liquid and gas film. Local thermodynamic equilibrium is assumed to exist at the interface.

Thermodynamic non-ideality is corrected for using the thermodynamic models developed in chapter 3. Ackerman's correction factors are used to calculate the influence of finite mass transfer rates on the mass transfer coefficients.

Chemical reactions in the liquid film are modelled using enhancement factors. The enhancement factors are calculated using the penetration theory in combination with the effective diffusion- and mass transfer coefficient approach. This model is valid for relatively simple reactions. For coupled and reversible (e.g. when activators are added) an advanced numerical calculation scheme for the enhancement factors should be implemented.

The non-equilibrium model implemented in this work should be general and suitable for modelling many of the most common non-equilibrium processes we find in the process- and petroleum industry.

The non-equilibrium model described in this chapter was implemented in the NeqSim computer program. This program was used to model the experimental mass transfer data obtained during this work.

5 The Generalized Non-Equilibrium Two Fluid Model

Many processes in the petroleum industry involve the flow of a gas and a liquid in contact. In flowing hydrocarbon systems the changes in pressure and temperature along the pipeline will lead to mass transfer between the phases. The importance of this mass transfer in computational flow models vary with the flow conditions and the type of system studied. The mass transfer terms are often not significant in cases where mass transfer rates are small compared to the flow rate of the free phases. This will typically be for oil and gas flow in long multiphase pipelines where the pressure and temperature changes relatively slow. In mass- and heat transfer equipment such as heat exchangers and absorption columns – this mass transfer term is of crucial importance.

Two phase flow can often be treated as separated flow or dispersed flow. In separated flow the gas and the liquid have a well-defined interface (stratified-/annular flow) while for dispersed flow the interface is not defined (bubble-/droplet flow). In two phase pipe flow simulation codes – the modelling of both dispersed and stratified flow can be done using the same mathematical model – but with different closure relations. One of the most known commercial multiphase pipe flow simulators, OLGA, is based on a variant of the two fluid model (Bendiksen et.al., 1991).

This chapter gives a description of a general non-equilibrium, multi-component, two-fluid model. It is general because it is developed from an assumption that all types of multiphase flows can be modelled with the same equations – but with different closure relations. It uses conservation laws for each component in both liquid and gas – so we are able to track the composition of the liquid and gas. The interphase mass transfer rate is calculated with the multicomponent mass transfer model described in chapter 4. The thermodynamic properties are calculated with the thermodynamic models described in chapter 3 and the physical properties can be calculated with methods taken from Reid et. al. (1988). The methods used to calculate physical properties for amine systems are described in appendix D.

In section 5.1 the basic equations of the non-equilibrium two fluid model are described. Chapter 5.2 describes the closure relations used for pipe flow and flow in packed beds. Chapter 5.3 gives a short description of the numerical implementation.

5.1 Conservation Laws

The fluid mechanical model developed in this work uses a transient and 1-dimensional basis for all conservation laws (averaged over the pipe cross-section). An introduction to 1-dimensional modelling of two phase flow was presented by Wallis (1969) and the basic theory and equations of the two-fluid model was presented by Ishi (1975).

The non-equilibrium two fluid model is built up of 4+2n conservation equations, where n is the number of components. We have

- Conservation of mass for liquid and gas
- Conservation of momentum for liquid and gas
- Conservation of energy for liquid and gas
- n-1 independent conservation equations for components for liquid and gas

URN:NBN:no-3363

Droplet-field (entrainment / deposition) was not implemented in this work, but can easily be added in future versions of the computer code.

In the following sections the conservations equations for total mass, components, momentum and energy are given. In Figure 5-1 some of the characteristic parameters used in the two-fluid model are illustrated.
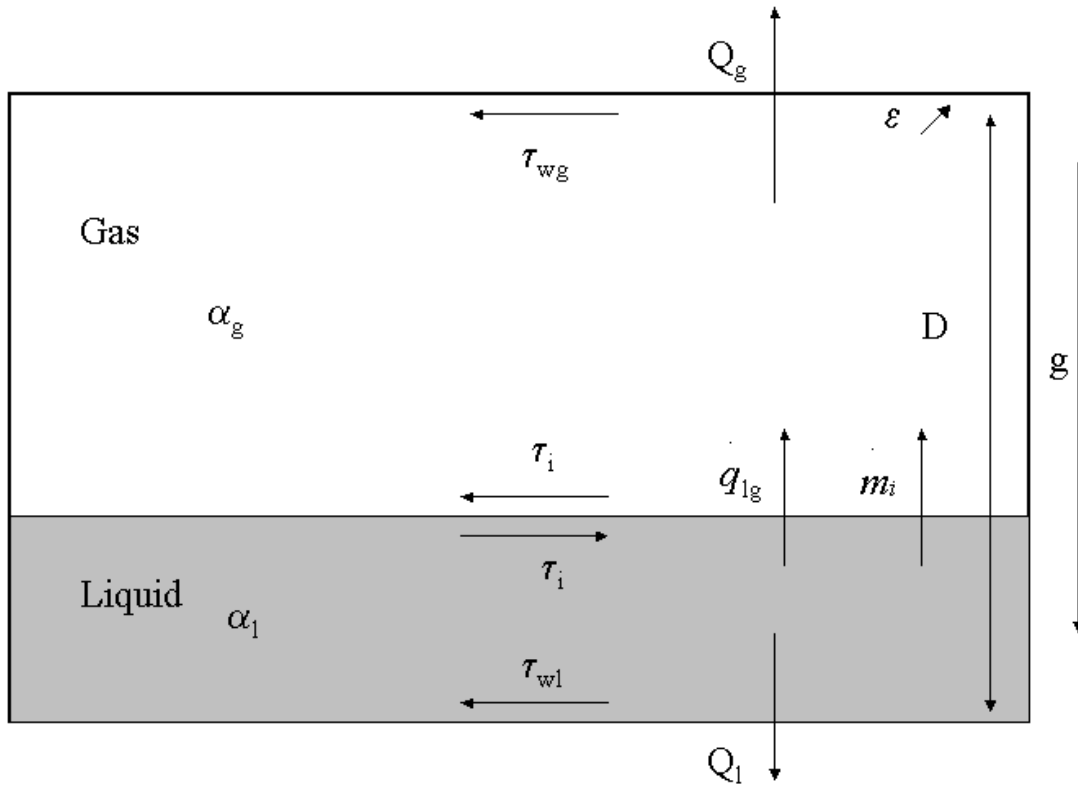
Figure 5-1 Illustration of symbols used in the conservation equations for the non-equilibrium two-fluid model

Variable	Description	Unit
$\dot{m}$	Mass transfer	$kg/m \cdot \sec$
τ_i	Interfacial liquid-gas shear stress	N/m^2
τ_{wg}	Wall-gas shear stress	N/m^2
τ_{wl}	Wall-liquid shear stress	N/m^2
α_l	Liquid phase fraction (holdup) $\left(A_l/A\right)$	-
α_g	Gas phase fraction $\left(A_g/A\right)$	-
Q	Heat flux from surroundings	$J/m \cdot \sec$

$\dot{q}_{lg}$	Interphase heat flux	$J\!\!\left/\!\!{m \cdot \sec}\right.$
D	Pipe diameter	m
ε	Surface roughness	m
g	Gravity	$m\!\!\left/\!\!{\sec^2}\right.$

5.1.1 Conservation of Mass

Separate conservation equations are applied for gas and liquid, which may be coupled through interphase mass transfer.

The conservation equations for total mass for the liquid and gas phase are given as,

$$\frac{\partial \rho_l \alpha_l A}{\partial t} + \frac{\partial \left(\rho_l \alpha_l u_l A \right)}{\partial x} = -\dot{m}_{mt\,lg}$$

$$\frac{\partial \rho_g \alpha_g A}{\partial t} + \frac{\partial \left(\rho_g \alpha_g u_g A \right)}{\partial x} = \dot{m}_{mt\,lg}$$

(5.1)

where α is the phase fraction defined as $\alpha_l = \dfrac{A_l}{A}$ and $\dot{m}_{mt\,lg} = \sum_i \dot{m}_{i,lg}$. The total mass flux

has unit $\left[\dfrac{kg}{m\,sek} \right]$. The total mass transfer between the gas and liquid was calculated from the

multicomponent mass transfer model described in chapter 4. All mass transfer terms are calculated in the barycentric frame of reference. Taylor and Krishna (1993) describe how to convert fluxes between different frames of reference.

5.1.2 Conservation of Momentum

The conservation of momentum for the liquid and gas is calculated from

$$\frac{\partial \rho_l u_l \alpha_l A}{\partial t} + \frac{\partial \left(\rho_l u_l^2 \alpha_l A \right)}{\partial x} = -\dot{m}_{mt\,lg}\, u_i - \alpha_l A \frac{\partial P}{\partial x} + \alpha_l A \rho_l g_x - S_{lw} \tau_{lw} + S_i \tau_i$$

$$\frac{\partial \rho_g u_g \alpha_g A}{\partial t} + \frac{\partial \left(\rho_g u_g^2 \alpha_g A \right)}{\partial x} = \dot{m}_{mt\,lg}\, u_i - \alpha_g A \frac{\partial P}{\partial x} + \alpha_g A \rho_g g_x - S_{gw} \tau_{gw} - S_i \tau_i$$

(5.2)

where S is the cross-sectional contact length between two phases or the wall, and is calculated from the physical geometry of the process equipment and from the knowledge of the gas and liquid flow pattern. The frictional terms τ are calculated for both wall friction and interphase friction. The derivations of these equations are given in Fuchs (1997).

5.1.3 Conservation of Energy

The conservation of energy is considered for both the liquid and gas phase. In some situations the gas and liquid will not be in thermal equilibrium that leads to a spontaneous interphase heat flux. Such a situation will typically exist for reactive absorption of CO_2 into amine solutions – where the heat of reaction in the liquid phase is important.

$$\frac{\partial \alpha_l A \rho_l \left(\overline{U}_l + gz \right)}{\partial t} + \frac{\partial \alpha_l A \rho_l u_l \left(\overline{H} + gz \right)}{\partial x} = -\dot{q}_{lg} + Q_l$$

$$\frac{\partial \alpha_g A \rho_g \left(\overline{U}_g + gz \right)}{\partial t} + \frac{\partial \alpha_g A \rho_g u_g \left(\overline{H} + gz \right)}{\partial x} = \dot{q}_{lg} + Q_g$$

(5.3)

where $\overline{U}$ and $\overline{H}$ are the specific internal energy and enthalpy of the fluid. Q is the heat transfer from the surroundings and q is the interphase heat transfer. The interphase heat transfer can be calculated from the model described in chapter 4 and has unit $\left[\dfrac{J}{m\,sek} \right]$. The method used for calculation of heat transfer from the surroundings will be described later in this chapter.

5.1.4 Conservation of Components

In this work we consider conservation of components in both the liquid and gas phase. The conservation equations used are on the form

$$\frac{\partial \omega_{i,l} \rho_l \alpha_l A}{\partial t} + \frac{\partial \left(\omega_{i,l} \rho_l \alpha_l u_l A \right)}{\partial x} = -\dot{m}_{i,lg}$$

$$\frac{\partial \omega_{i,g} \rho_g \alpha_g A}{\partial t} + \frac{\partial \left(\omega_{i,g} \rho_g \alpha_g u_g A \right)}{\partial x} = \dot{m}_{i,lg}$$

(5.4)

where $\dot{m}_{i,lg}$ is the mass transfer of component i between the liquid and gas, and is calculated from the methods described in chapter 4. The mass flux has unit $\left[\dfrac{kg}{m\,sek} \right]$ and ω_i is the mass fraction of component i. The mass transfer m_i is the sum of a convective and diffusive term. It is important to note that reaction terms are not included in this equation. The effects of chemical reactions are lumped into the model for calculating the mass fluxes by using an enhancement factor as described earlier. It is assumed that the reaction is completed in the liquid film and that the bulk liquid is in chemical equilibrium.

In systems where longitudinal dispersion is important, a dispersion term must be added to equation (5.4). Modelling of molecular dispersion processes has been thoroughly documented by Levenspiel (1999). In this work a dispersion term was added in case study 1 in chapter 11 (tracking of CO_2-concentration along a pipeline).

5.2 Closure Relations

The conservation equations as given in equation (5.1) to (5.4) are independent of the flow pattern. The two-fluid model involves a number of parameters that have to be estimated to solve the system of equations. To calculate these parameters we need constitutive laws that after the physical meaning can be classified as

- Constitutive equations of state
- Mechanical constitutive laws

- Constitutive laws for energy

The parameters U_g, U_l, H_g, H_l, ρ_g and ρ_l are only functions of temperature and pressure of the gas and liquid and are calculated from the thermodynamic models described in chapter 3. The mass- and heat transfer fluxes are calculated from the models described in chapter 4. The models used to calculate physical properties of amine solutions are described in appendix D. In the computer program developed in this work the physical properties of fluid systems not containing amines are calculated using standard methods from Reid et. al. (1988).

The interphase and wall shear forces τ and the interphase contact lengths S must be estimated from knowledge of the flow field and mechanistic relations. Models for these mechanistic parameters are given in the following sub-chapters.

5.2.1 Interphase and Wall Shear Forces

We need to calculate interphase shear between the fluid and the wall and the shear between the liquid and the gas. The gas-wall shear stress is calculated from

$$\tau_{gw} = f_w \cdot \rho_g \frac{u_g^2}{2} \tag{5.5}$$

where we have used the fanning friction factor f_w. The interphasial shear stress can similarly be calculated from

$$\tau_i = f_i \cdot \rho_g \frac{\left(u_g - u_i\right)^2}{2} \tag{5.6}$$

where u_i is the interphase velocity. The interphase velocity can for simplicity be assumed to be the same as the liquid velocity. f_i is the fanning friction factor for the interphase. A correlation we can use to estimate the friction factor between a fluid and the wall is the Håland (1983) correlation

$$\frac{1}{2\sqrt{f_w}} = -1.8 \cdot \log_{10}\left[\frac{6.9}{\text{Re}} + \left(\frac{\varepsilon}{3.7 \cdot D_h}\right)^{1.11}\right] \tag{5.7}$$

where Re is the Reynolds number based on hydraulic diameter D_h and ε is the roughness of the pipewall. The Håland equation is an explicit approximation of the well-known Colebrook equation. The interphase friction factor can be estimated from an empirical correlation given by Wallis (1969)

$$\left(\frac{f_i}{f_{wg}}\right) = \left[1 + 75\alpha_l\right] \tag{5.8}$$

where f_{wg} is the friction factor between the gas and the wall and α_l is the liquid phase fraction (holdup).

The Reynolds number is defined as

$$\mathrm{Re} = \frac{u \rho D_h}{\mu} \qquad (5.9)$$

where D_h is the hydraulic diameter and is calculated from

$$D_h = \frac{4 \cdot occupied\ area}{length\ of\ wetted\ perferi} \qquad (5.10)$$

5.2.2 Interphase Contact Length in Separated Two-Phase Pipe Flow

The interphase contact length must be calculated from the knowledge of the flow pattern and the velocities of the gas and liquid. For annular and stratified two-phase pipe flow the interphase contact lengths S_g, S_l and S_i can be calculated from the following geometrical relations

$$S_l = \theta \cdot D,\ S_g = \pi D - S_l,\ S_i = D \cdot \sin \theta \qquad (5.11)$$

where θ (see Figure 5-2) can be calculated from the trigonometric approximation

$$\theta = \pi \alpha_l + \left(\frac{3\pi}{2} \right)^{1/3} \left(1 - 2\alpha_l + \alpha_l^{1/3} - \alpha_g^{1/3} \right) \qquad (5.12)$$
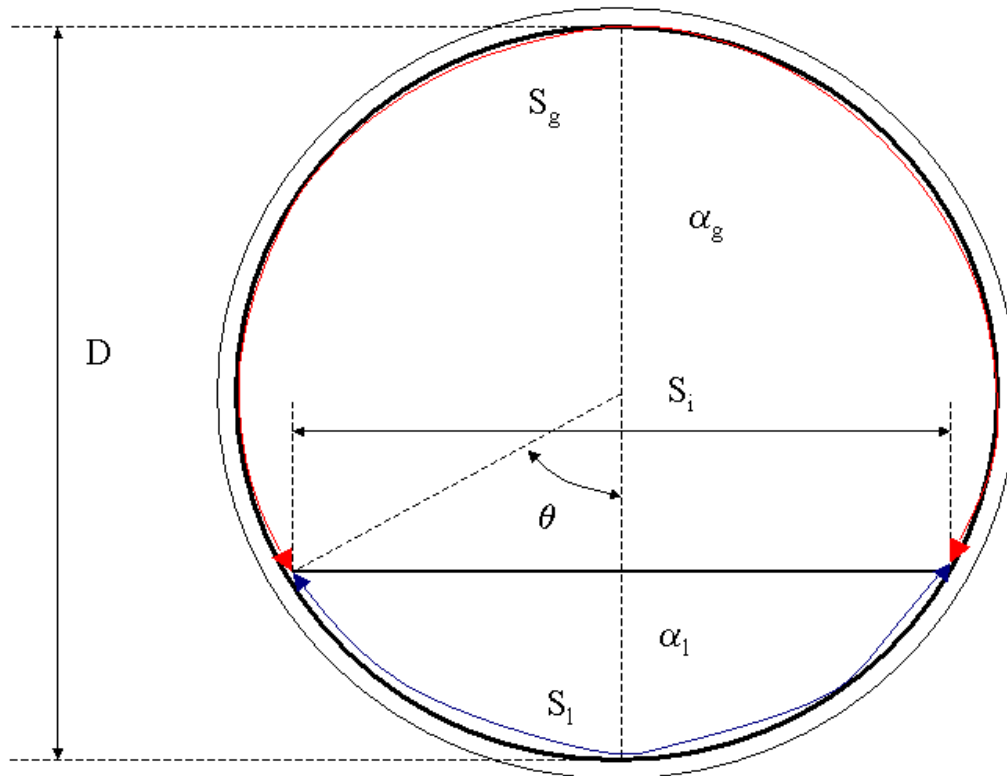
Figure 5-2 Geometric parameters for separated flows

5.2.3 Interphase Contact Area and Length in Packed Beds

For flow in packed bed absorbers we have to calculate the interphase contact length from knowledge of the interphase area pr. volume of packing. Such interphase area data for different types of packings are given in Table 5-1 (Billet, 1995).

Table 5-1 Interphase contact areas for different random packings (Billet, 1995)

Packing type	Material	Size [mm]	Packing area $\left[\dfrac{m^2}{m^3}\right]$	Void Fraction of Packing $\left[\dfrac{m^3}{m^3}\right]$
Pall Ring	Metal	50	112.6	0.951
		38	149.6	0.952
		25	223.5	0.954
Raschig Ring	Ceramic	25	185.4	0.662
Hiflow Ring	Metal	50	92.3	0.977
		25	202.9	0.962

Interphase contact areas for many types of packings are stored in the Access database developed in this work, and are directly available when running simulations with the computer program developed.

An example of a mass transfer calculation done where CO_2 is absorbed into water in a packed bed is illustrated in the following NeqSim script and in Figure 5-3 and Figure 5-4. Two cases

for absorption in a packed bed filled with packing material of different size are compared. In one case 25 mm pallrings were used (Figure 5-3) while in the other case 50 mm pallrings were used (Figure 5-4). From the results (and Table 5-1) we see that the interphase contact area is higher for small packing sizes (223.5 m^2/m^3 for 25 mm- and 112.6 m^2/m^3 for 50 mm nominal size). The mass transfer flux of CO_2 is however highest for the largest packing (0.0041 mol/m^2sec for 25 mm- and 0.0063 mol/m^2sec for 50 mm nominal size). The reason for this is that the liquid mass transfer coefficient is higher for the largest packing. The best packing must be selected from many considerations where interphase area and mass transfer properties are among the most important. The ability to prevent flooding and entrainment in the packed tower is another important property of the packing.

```python
#packing-flux.py
system = thermo('srk', 298.15, 10.0)
addComponent(system,'methane', 10000.0, 'Nlitre/min', 0)
addComponent(system,'CO2', 1000.0, 'Nlitre/min', 0)
addComponent(system,'water', 100.0, 'kg/min', 1)
mixingRule(system,'HV')
newdatabase(system)

geometry2 = geometry.packedbed(diameter=0.5)
geometry2.setPackingType("pallring","metal",25)
flowtest = node.packedbed(system,geometry2)
flowtest.setLengthOfNode(1.0)

flow.solve(flowtest,heattrans=0,masstrans=1)
flow.show(flowtest,'pallring-25mm')
```

	Phase 1	Phase 2	Phase 3	Unit
methane	9,09091E-1	7,36387E-32		[-] bulk
CO2	9,09091E-2	7,36387E-33		[-] bulk
water	1,23453E-29	1E0		[-] bulk
methane	9,11004E-1	2,09117E-4		[-] interface
CO2	8,65513E-2	4,50765E-4		[-] interface
water	2,44508E-3	9,9934E-1		[-] interface
methane	1,93639E-3	1,93639E-3		[mol/sec*m^2]
CO2	4,11557E-3	4,11557E-3		[mol/sec*m^2]
water	-2,46863E-3	-2,46863E-3		[mol/sec*m^2]
Reynolds Nu...	2,68281E2	4,33139E1		[-]
Velocity	9,26581E-2	8,38476E-3		[m/sec]
Heat Flux	0E0	0E0		[J/sec*m^2]
Pressure	10.0	10.0		[bar]
Bulk Tempera...	298.15	298.15		[K]
Interface Tem...	298.15	298.15		[K]
Interface Area	2,19421E2	2,19421E2		[m^2]
Node	pallring-25mm	pallring-25mm		-

Figure 5-3 Calculated fluxes in an absorber packed with 25 mm Pallrings.
Script: packing-flux.py, p. 113

	Phase 1	Phase 2	Phase 3	Unit
methane	9,09091E-1	7,36387E-32		[-] bulk
CO2	9,09091E-2	7,36387E-33		[-] bulk
water	1,23453E-29	1E0		[-] bulk
methane	9,14649E-1	2,09947E-4		[-] interface
CO2	8,29061E-2	4,31734E-4		[-] interface
water	2,44526E-3	9,99358E-1		[-] interface
methane	3,08683E-3	3,08683E-3		[mol/sec*m^2]
CO2	6,2589E-3	6,2589E-3		[mol/sec*m^2]
water	-1,97963E-3	-1,97963E-3		[mol/sec*m^2]
Reynolds Nu...	5,32511E2	8,59738E1		[-]
Velocity	9,26581E-2	8,38476E-3		[m/sec]
Heat Flux	0E0	0E0		[J/sec*m^2]
Pressure	10.0	10.0		[bar]
Bulk Tempera...	298.15	298.15		[K]
Interface Tem...	298.15	298.15		[K]
Interface Area	1,10545E2	1,10545E2		[m^2]
Node	pallring-50mm	pallring-50mm		-

Figure 5-4 Calculated fluxes in an absorber packed with 50 mm Pallrings
Script: packing-flux.py, p. 113

5.2.4 Heat Transfer Calculations

In the model used in this work the heat transfer from the surroundings to the fluid was calculated from the equation

$$Q_f = A_{fw} U_{fs} \left(T_f - T_{sur} \right) \tag{5.13}$$

where U_{fs} is the heat transfer coefficient from the fluid to the surroundings and A_{fw} is the fluid wall contact area. The heat transfer coefficient U_{fs} is calculated from considering contributions from heat transfer resistance in the fluid, wall and surroundings.

The interphase heat transfer was calculated using standard analogies between heat and mass transfer. These methods were described in chapter 4.

5.2.5 Example – Vertical Annular Two-Phase Flow

The equations given earlier in this chapter can be used to calculate the fluid mechanical state for transient two-phase stratified flow in pipes. In this work it was important to be able to simulate steady state vertical annular gas-liquid flow. To give an example of such a simulation we consider the vertical film flow as illustrated in Figure 5-5.
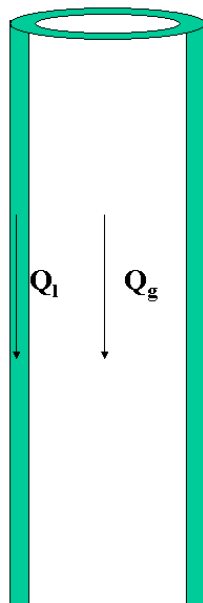
Figure 5-5 Annular co-current flow of a liquid and a gas

We will consider a case where the water film flows in contact with methane and CO_2 gas at 10 bar pressure and 25°C on the wall of a 2.5 cm inner diameter pipe. The gas circulation rate is kept constant at 200 Nl/min while the water circulation rate is varied between 0.3-1.2 liter/min. We use the models described in this chapter to calculate the holdup and the liquid velocity. The NeqSim-script used to simulate this case is given in the following text box.

```
# filmflow.py
system = thermo('srk', temperature=298.15, pressure=10.0)
addComponent(system,'methane', 100.0, 'Nlitre/min', 0)
addComponent(system,'CO2', 100.0, 'Nlitre/min', 0)
addComponent(system,'water', 1.5, 'kg/min', 1)

geometry2 = geometry.pipe(diameter=0.025, rough=0.005)
flowtest = node.twophase(system,geometry2,'annular')
flowtest.setLengthOfNode(0.1)
flow.solve(flowtest,heattrans=0,masstrans=1)
print 'liquid phase fraction ', flowtest.getPhaseFraction(1)
show(flowtest)
```

The result of the calculation is illustrated in Figure 5-6. We see that the holdup and liquid velocity increases with water circulation rate. The case simulated is a typical situation for the experimental equipment used in this work – a high pressure wetted wall column (described in chapter 9). The two fluid model described above will be used to calculate the fluid mechanical variables when modelling and parameter fitting to the experimental data obtained in this work.
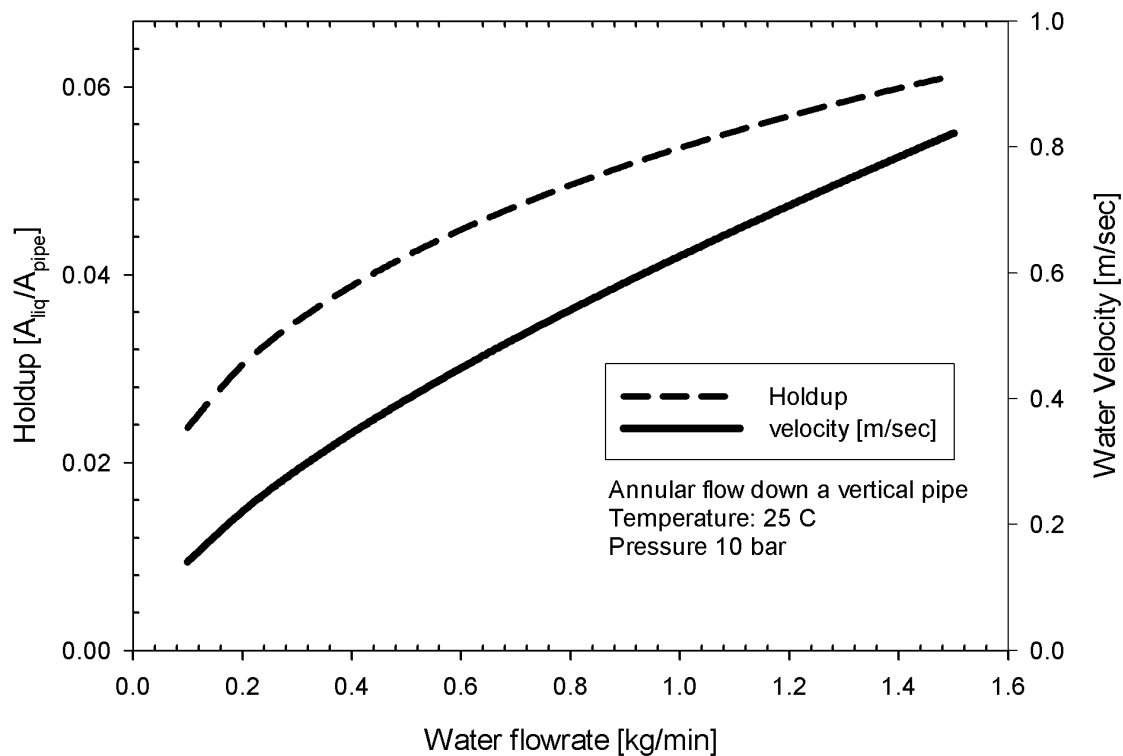
Figure 5-6 Calculated holdup and liquid velocity from the two fluid model described in this chapter.
Script: filmflow.py, p. 116

5.3 Numerical Implementation

To solve the conservation equations numerically we use a finite-volume discretisation of the conservation laws. The general conservation law can be written as (Patankar (1980), Versteeg and Malalasekera (1995))

$$\frac{\partial(\rho\phi)}{\partial t} + div(\rho\phi u) = div(\Gamma \cdot grad\,\phi) + S_\phi \tag{5.14}$$

This equation is the general transport equation for the property ϕ. The equation consists of four terms: the rate of change, the convective term, the diffusive term and the production term. All the general conservation equations (mass, momentum, energy and species) can be written in this general form.

To get the well-known finite-volume implementation we must integrate in space and time.

$$\int_{\Delta t}\frac{\partial}{\partial t}\left(\int_{CV}(\rho\phi)dV\right)dt + \int_{\Delta t}\int_A n\cdot(\rho\phi u)dA\,dt = \int_{\Delta t}\int_A n\cdot(\Gamma_\phi\cdot grad\,\phi)dAdt + \int_{\Delta t}\int_A S_\phi dVdt \tag{5.15}$$

It is convenient to define the two variables F and D to represent the convective transport per unit area and diffusion transport at cell interfaces. The equations for F and D are dependent on which conservation equation we are considering (see e.g. Versteeg et.al., 1995). We divide the geometry into cells and use an indexing scheme where the center node is P, the east node E and the west node W (Figure 5-7).
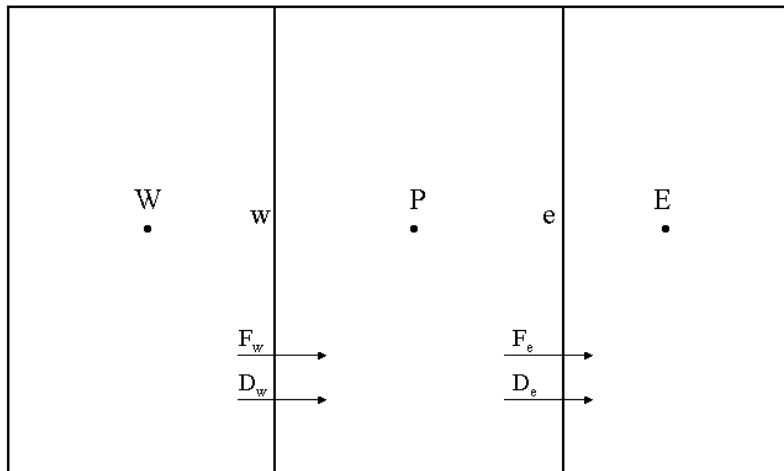
Figure 5-7 Numerical implementation and grid

The general conservation equation for a cell is given by

$$a_P\phi_P = a_W\phi_W + a_E\phi_E + S_u \tag{5.16}$$

Where

$$a_P = a_W + a_E + (F_e - F_w) + S_P \tag{5.17}$$

a_E and a_W are given in the table below for different numerical schemes. S is a source term for the considered property (e.g. chemical reactions). Dependent on which numerical scheme we want to use, the coefficients a_w and a_E are calculated from the equations given in Table 5-2.

Table 5-2 Coefficients a_w and a_E for different numerical schemes

Numerical Scheme	a_W	a_E
Central differencing	$Dw + Fw/2$	$D_e - F_e/2$
Upwind differencing	$D_w + \max(F_w, 0)$	$D_e + \max(-F_e, 0)$
Hybrid differencing	$\max[F_w, (D_w + F_w/2), 0]$	$\max[-Fe, (D_e - F_e/2), 0]$
Power law	$D_w \cdot \max[0, (1-0.1*|Pe_w|)^5] + \max(F_w, 0)$	$D_e \cdot \max[0, (1-0.1*|Pe_e|)^5] + \max(-F_e, 0)$

The equations given in this chapter were first implemented in the computer code for a transient 1-fluid pure gas model. This transient 1-phase model has been used to simulate a multicomponent transient case study described in chapter 11 (tracking of CO_2 along a pipeline). This model could be solved using the above numerical schemes with success (upwind differencing scheme). The same scheme was tested for the two-fluid model described in this chapter – but stability problems made the model little robust. These stability problems are currently being worked on. At the moment only a stationary model of the above-described two-fluid model is working well.

5.4 Summary – a Non-Equilibrium Two Fluid Model

The general non-equilibrium two fluid model described in this chapter was implemented in a Java computer code. Thermodynamic, physical properties and mass transfer fluxes were calculated using the models described earlier in the thesis.

The non-equilibrium two fluid model can be used to model many types of process equipment involving one or two phases. Different closure relations must be used for each type of process.

The non-equilibrium two fluid model was used to model the fluid flow in the experimental equipment used in this work. The experimental equipment was modelled as stationary vertical annular two-phase flow with closure relations (wall/interphase friction) described in this chapter.

6 NeqSim – a General Non-Equilibrium Simulator

Simulation programs are important tools used in design and operation of process plants. Most process simulation tools are based on equilibrium thermodynamic models. Few simulation programs use the rate-based approach for calculating mass transfer in process equipment – even though the rate based approach has many advantages compared to the equilibrium mass transfer models. The reason for the popularity of such equilibrium based models is the speed and stability of such calculations.

The modelling activity of this work has been conducted with two primary goals in mind;

- Develop a computer code/program that is easy to extend and reuse
- Develop a general non-equilibrium process simulation tool that focus on non-equilibrium simulation, but also is able to solve general equilibrium processes

Effort was taken to avoid the traditional way of doing modelling work, where we often see that;

- Code works only for the specific problem
- Code is never used after finishing the modelling work
- New students and researchers use a lot of time to develop code others have programmed before

Most implementations of thermodynamic routines have been done in procedural languages such as Fortran and C. Such languages are highly optimised and it is thus possible to create high performance programs. The increasing complexity of thermodynamic models, however, calls for a systematic approach in order to avoid inefficient or even incorrect codes. Michelsen and Mollerup (1986) developed a systematic method to calculate thermodynamic properties based on their F-functions (Reduced Helmholtz Energy). This method for calculating thermodynamic properties is described in appendix A. Michelsen and Mollerups method made it possible to build up a thermodynamic library where it is easy to change or implement new thermodynamic models. This modular approach is the standard way of implementing thermodynamic models in computer codes today, but traditionally these codes have been written in procedural languages. It would be a great improvement if this modular approach was implemented in a language that supported object oriented programming, such as C++ or Java.

In this work the Michelsen and Mollerup (1986) method of implementing thermodynamic properties calculations has been implemented in the object-oriented language Java. The object-oriented design of this library is described in this chapter. It will hopefully be useful for other researchers who want to implement thermodynamic models in an object-oriented language. The thermodynamic models described in chapter 3 were all implemented in this common framework.

The non-equilibrium two fluid model described in chapter 5 was implemented in NeqSim to be able to simulate mass- and heat transfer processes in process equipment. The two-fluid model was implemented in an object-oriented design. All fluid mechanic processes are modelled using the same base equations (conservation laws), and new process equipment is

easily added. The design of the fluid-mechanic package developed during this work will be described in this chapter.

Steady state process plant operations and networks can easily be simulated in NeqSim. All process plant equipment are implemented as objects – and new ones are easily added. The unit process operations are solved in a sequential order where successive substitution is used to converge the whole process plant simulation.

A graphical user interface (GUI) was made using the Java Swing package. A scripting language (Python) is embedded in the NeqSim simulator and no compilation step has to be done to run a simulation. Using the toolbars in the NeqSim-GUI simple process simulations can be done without manually having to write the scripts. The graphical user interface will be described in this chapter – and a user manual can be downloaded from the NeqSim homepage.

A statistical package was implemented in the computer code. The statistical package makes it easy to fit models to experimental data. These statistical models were used to fit parameters to the experimental data obtained in this work. The statistical package is described in the next chapter.

A short description of NeqSim can be given on a keyword format as;

- General modelling tool for non-equilibrium and equilibrium processes
- Based on rigorous thermodynamic models (equations of state for non-electrolytes and electrolytes)
- Fluid mechanics based the on the one- or two fluid model
- Implemented in an object oriented language (Java/Python object oriented design where everything is an object)
- Suitable for being used as a modelling tool (general parameter fitting routines implemented)
- Validated against experimental data (equilibrium/non-equilibrium)

The NeqSim program (source code/executables) can be downloaded from the NeqSim homepage, http://www.stud.ntnu.no/~solbraa/neqsim. On the homepage a user manual can also be downloaded.

A screenshot of the NeqSim GUI is shown in Figure 6-1.
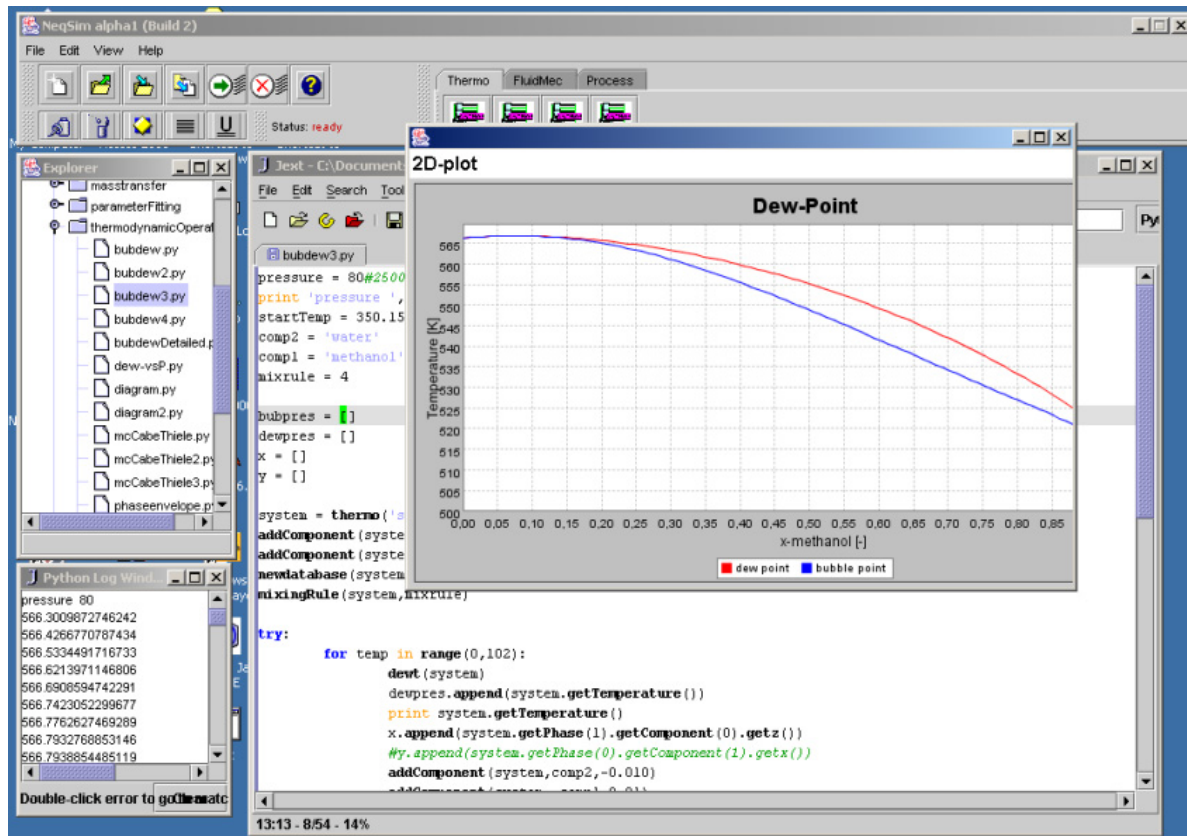
Figure 6-1 Screenshot of the NeqSim GUI.

6.1 Object Oriented Programming Languages

Today the most common object-oriented languages are C++ and Java. Object-oriented programs are made up of objects. An object packages both data and the procedures that operate on that data. The procedures are typically called methods or operations. An object performs an operation when it receives a request (or message) from a client.

Requests are the only way to get an object to execute an operation. Operations are the only way to change an object's internal data. Because of these restrictions, the object's internal state is said to be encapsulated; it cannot be accessed directly, and its representation is invisible from outside the object.

The hard part about object-oriented design is decomposing a system into objects. The task is difficult because many factors come into play; encapsulation, granularity, dependency, flexibility, performance, evolution, reusability, and on and on.

In the next sections an object-oriented design for process simulation calculation is presented. The object-oriented structure has been developed and implemented in the Java programming language. This design has proven to give a relatively fast executable code in which it is easy to extend and implement new mathematical models.

Designing object–oriented software is hard, and designing, reusable object–oriented software is even harder. You must find pertinent objects, factor them into classes at the right granularity, define class interfaces and inheritance hierarchies, and establish key relationships among them. The design should be specific to the problem at hand but also general enough to

address future problems and requirements. You also want to avoid redesign, or at least minimize it.

Guidance for finding object-oriented design can be found in Gamma et.al. (1995) and Cooper (2000).

6.2 Object Oriented Design of NeqSim

NeqSim is a dynamic process simulator designed to simulate the most common processes we find in the petroleum industry. This chapter is intended to give a short introduction to the design and use of NeqSim. The object-oriented design of NeqSim is graphically visualized in Figure 6-2. At the moment NeqSim is based on six modules

- Thermodynamic module

- Fluid mechanics module

- Statistical module

- Physical properties module

- Graphical user interface module

- Process plant module

The object hierarchy is built up in an intuitive manner. A typical process simulation case involves one or more process plant objects (ref. Figure 6-2). A process plant object holds a vector of process equipment. A process equipment object has an instance of a fluid mechanics system object. The fluid mechanic system object defines what kind of conservation laws and thermodynamic equations that describe the system. A fluid mechanic system (e.g. a pipe), is built up of legs and nodes. Each node has an instance of a thermodynamic system object. The thermodynamic system object defines the thermodynamic models used for the actual node (e.g. the EOS) and the composition of the fluid in the node. A thermodynamic system holds a vector of phase objects – and a phase object holds a vector of molecular component objects. The phase object has an instance of a physical property object, a mixing rule object and a chemical reaction object.

By active use of polymorphism in object oriented programming, the flexibility in the combination of models (eg. thermodynamic-, fluid mechanic- and physical property models) is kept as high as possible.
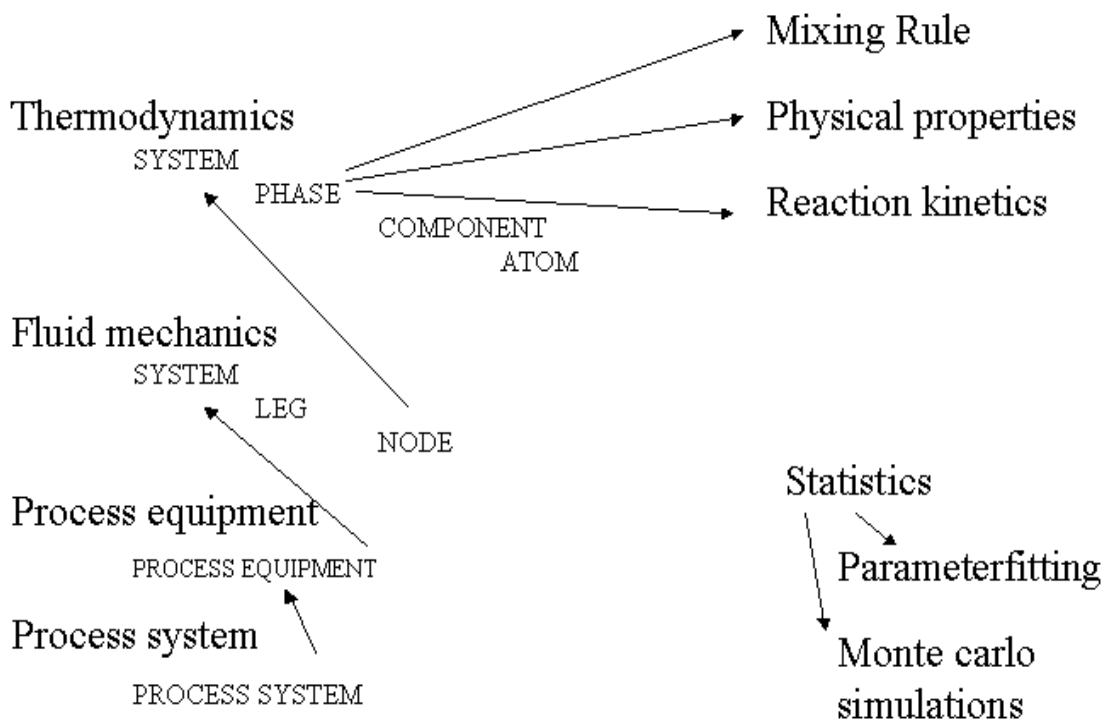
Figure 6-2 Object oriented design of NeqSim

6.3 Object-Oriented Implementation of the Thermodynamic Library

Calculations that can be done using the thermodynamic models and routines implemented in NeqSim are

- Flash calculations (TP, PH, PS,..)
- Creation of thermodynamic charts
- Thermodynamics of reactive mixtures
- Freezing point/hydrate calculations
- Calculation of thermodynamic properties of electrolyte systems (weak and strong)
- Dew-/bubble point calculations
- pH-value calculation
- Multiphase flash calculations
- …

The thermodynamic models in NeqSim are built upon well known design patterns in object oriented programming (e.g. the factory method patterns described by Gamma et.al., 1995). The object-oriented design changed somewhat during the first two years of programming, but is now in a flexible and satisfying form. This design has proven to generate a relatively fast code where it is easy to implement new mathematical models.

The main packages in the thermodynamic library are illustrated in Figure 6-3.
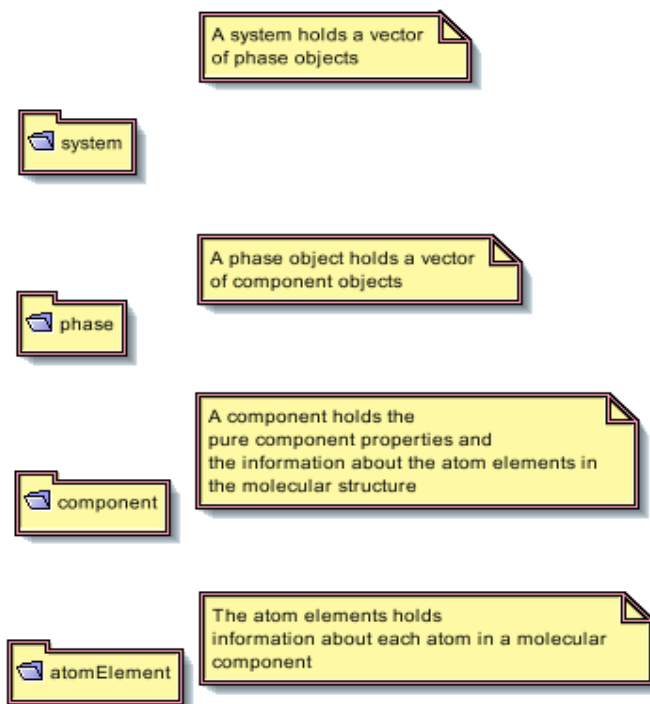
Figure 6-3 Main packages in the thermodynamic library

The main packages are system, phase and component. When you create a thermodynamic system object – you would typically create an instance of an object that implements the methods defined in the SystemInterface class. All models that implement/inherit from this base class – can perform the same operations – independent of which models they are based on. Active use of polymorphism creates an easy extendable and maintainable code.
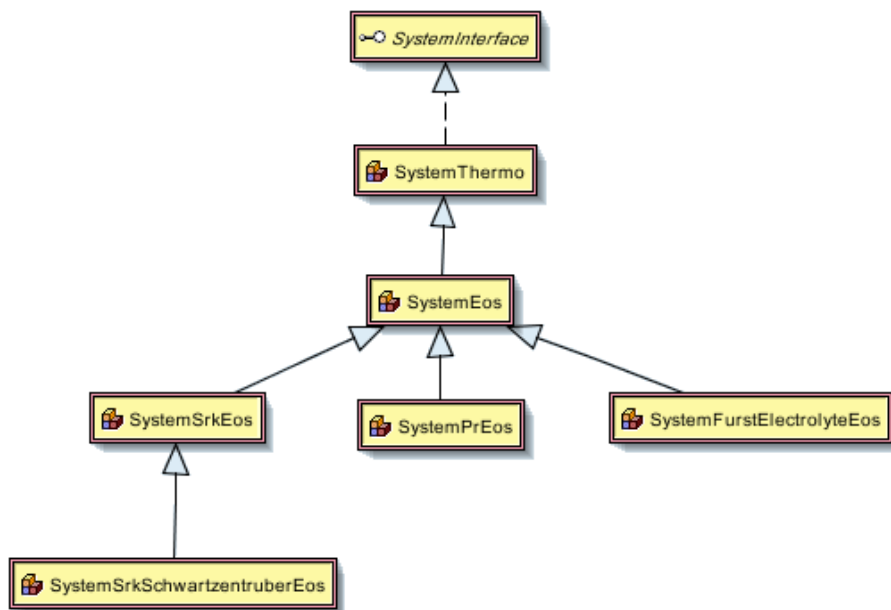
Figure 6-4 The system package

A system object holds a vector of phase objects (any number). The number of phase-objects is dependent on the thermodynamic state of the system. In principle a system can hold any number of phases.

The phase package is built up of objects as illustrated in Figure 6-5.
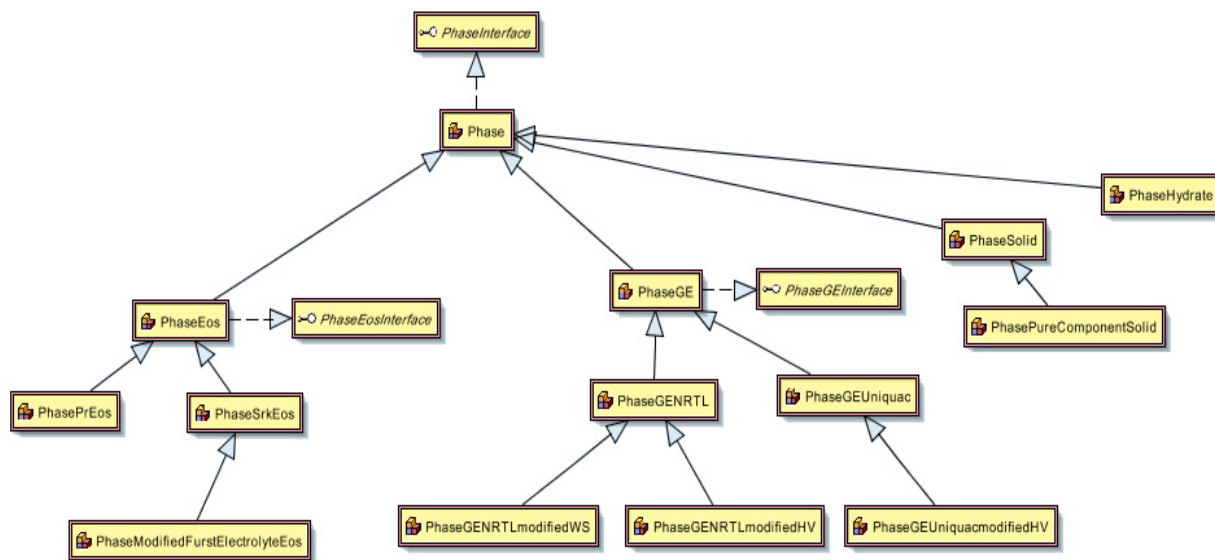
Figure 6-5 The structure of the phase package

A phase object holds a vector of components. The phase-object can hold any number of components. A phase object also holds the mixing rule object. All mixing rules are defined in

a single object as inner classes. The mixing rules currently implemented in the mixing rule class are:

- Classic mixing rule w/wo interaction parameters
- Huron-Vidal mixing rule
- Wong-Sandler mixing rule
- Electrolyte mixing rule
- CPA combinational rules (own object)

The component package is built up of objects as illustrated in Figure 6-6.
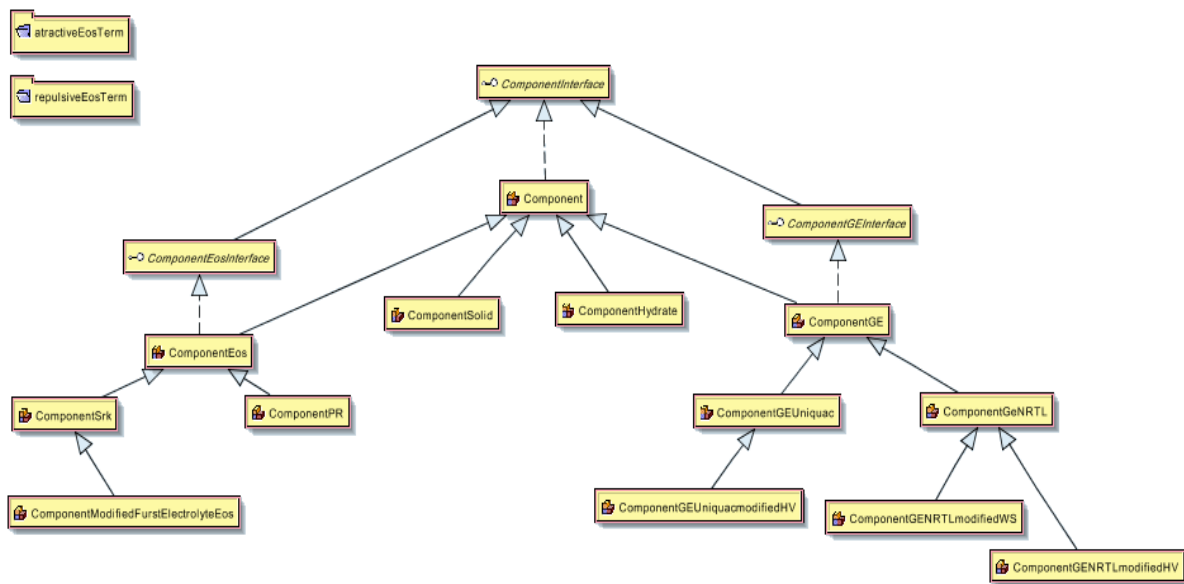
Figure 6-6 The structure of the Component package

The component object holds all the data that is specific to a component. The component properties are read from a database (Access-database).

It is easy to extend the program with new types of systems, phases and components. All the diagrams above implements an interface in the top of the object hierarchy – and this interface specify which methods it must define. Normally few lines of code have to be typed into new objects when you add new models. You will typically inherit from objects already defined in the hierarchy – and most of the code is already written.

Normally new thermodynamic models would be implemented in the Java programming language. For fast and easy testing of new models it however is possible to use the scripting language (Python). An example of adding an easy thermodynamic model (Raults law for liquid phase and ideal gas law for gas phase) using the scripting window – is given in appendix G (thermoModel.py, p.310).

6.3.1 Thermodynamic Operations

The thermodynamic operations are defined in its own object hierarchy. Some of the methods defined in the thermodynamic operation object are illustrated in Figure 6-7.
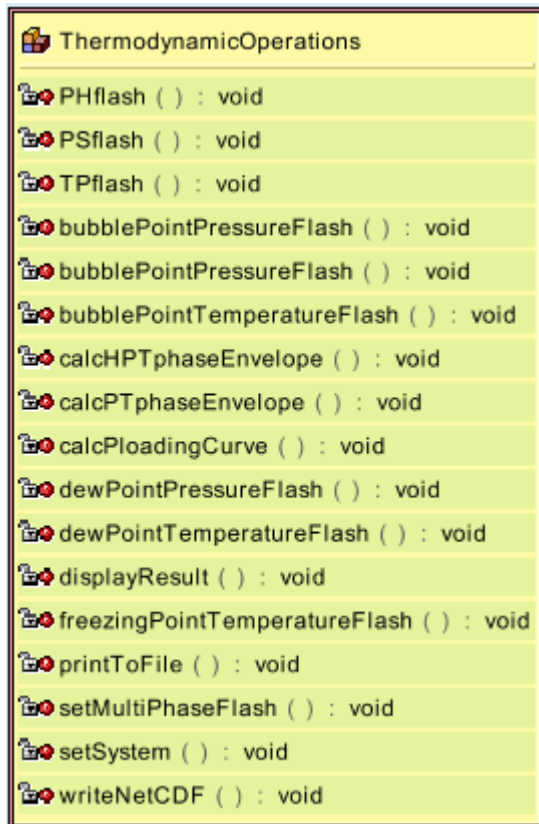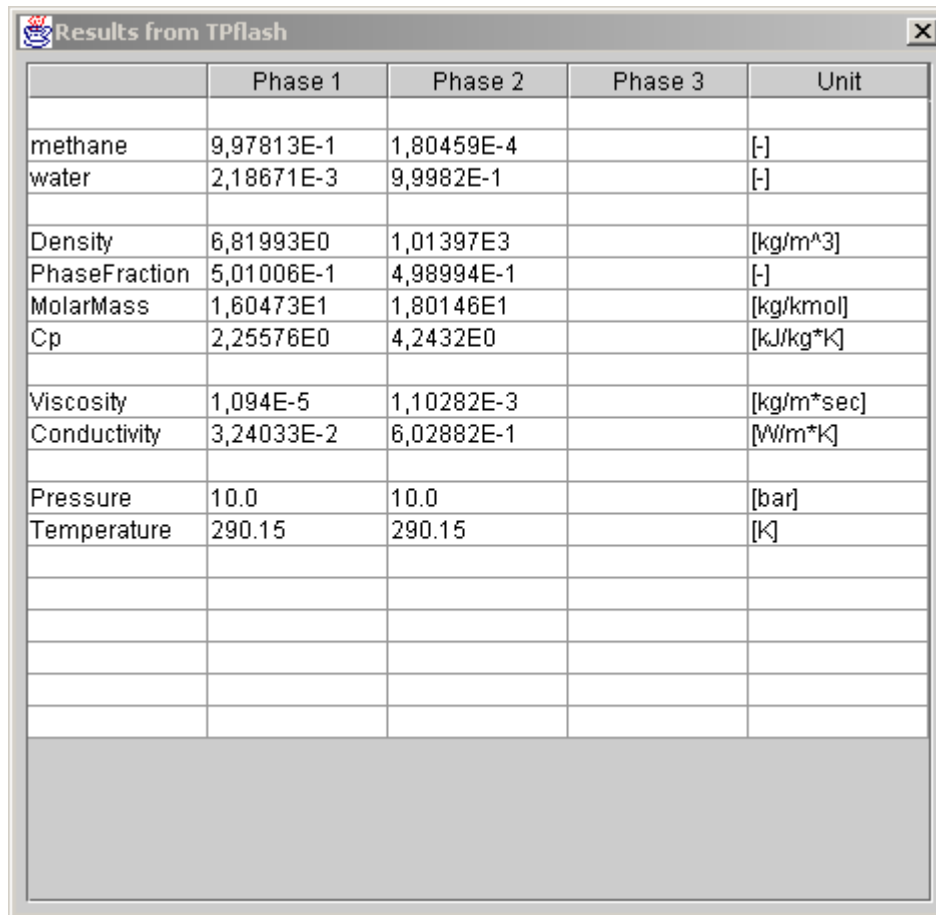
Figure 6-7 Thermodynamic operations

New thermodynamic operations are frequently added. An updated list of the available operations is available in the NeqSim documentation.

6.3.2 Examples of Thermodynamic Calculations

A simple example of a thermodynamic calculation is given in the textbox below. This shows how a simple TPflash is done from java (not Python!). The displayResult method will display the results shown in the Figure 6-8.

```
SystemInterface testSystem = new SystemSrk (290.15, 10.00);
ThermodynamicOperations testOps = new
ThermodynamicOperations(testSystem);
testSystem.addComponent("methane", 50);
testSystem.addComponent("water", 50);
testSystem.setMixingRule(4);
testOps.TPflash();
testOps.displayResult();
```

Results from TPflash	Phase 1	Phase 2	Phase 3	Unit
methane	9,97813E-1	1,80459E-4		[-]
water	2,18671E-3	9,9982E-1		[-]
Density	6,81993E0	1,01397E3		[kg/m^3]
PhaseFraction	5,01006E-1	4,98994E-1		[-]
MolarMass	1,60473E1	1,80146E1		[kg/kmol]
Cp	2,25576E0	4,2432E0		[kJ/kg*K]
Viscosity	1,094E-5	1,10282E-3		[kg/m*sec]
Conductivity	3,24033E-2	6,02882E-1		[W/m*K]
Pressure	10.0	10.0		[bar]
Temperature	290.15	290.15		[K]

Figure 6-8 Result-dialog from flash.
            Script: TPflash.py

Because Java-code has to be compiled it can be inflexible to work in Java. NeqSim embeds Python as a scripting language – and by using this scripting language fast and direct use of the thermodynamic models can be done.

The flash calculation done above will look as shown in the following textbox when written in Python – and can be executed directly by pressing the run-button in the GUI.

```
# TPflash.py
system = thermo('srk', 290.15, 10.0)
addComponent(system,'methane', 50)
addComponent(system, water, 50)
newdatabase(system)
TPflash(system)
show(system)
```

In Figure 6-9 a thermodynamic property chart for a typical Norwegian natural gas containing CO_2 has been created using the SRK-EOS. The script to create such a diagram is given in appendix G (natgas-chart.py, p. 311). Bubble- and dew-point lines, lines of constant molar density, enthalpy and entropy are displayed in the figure.
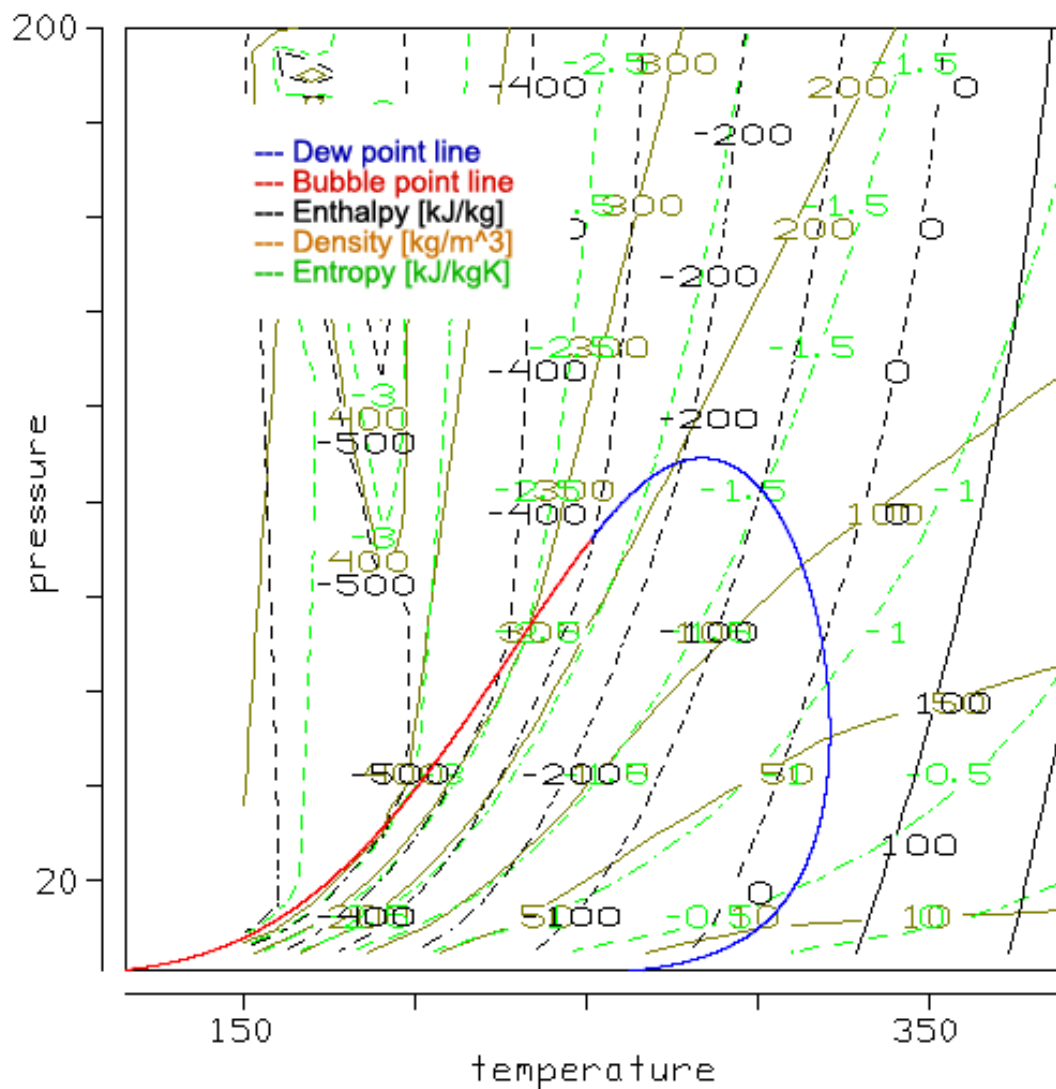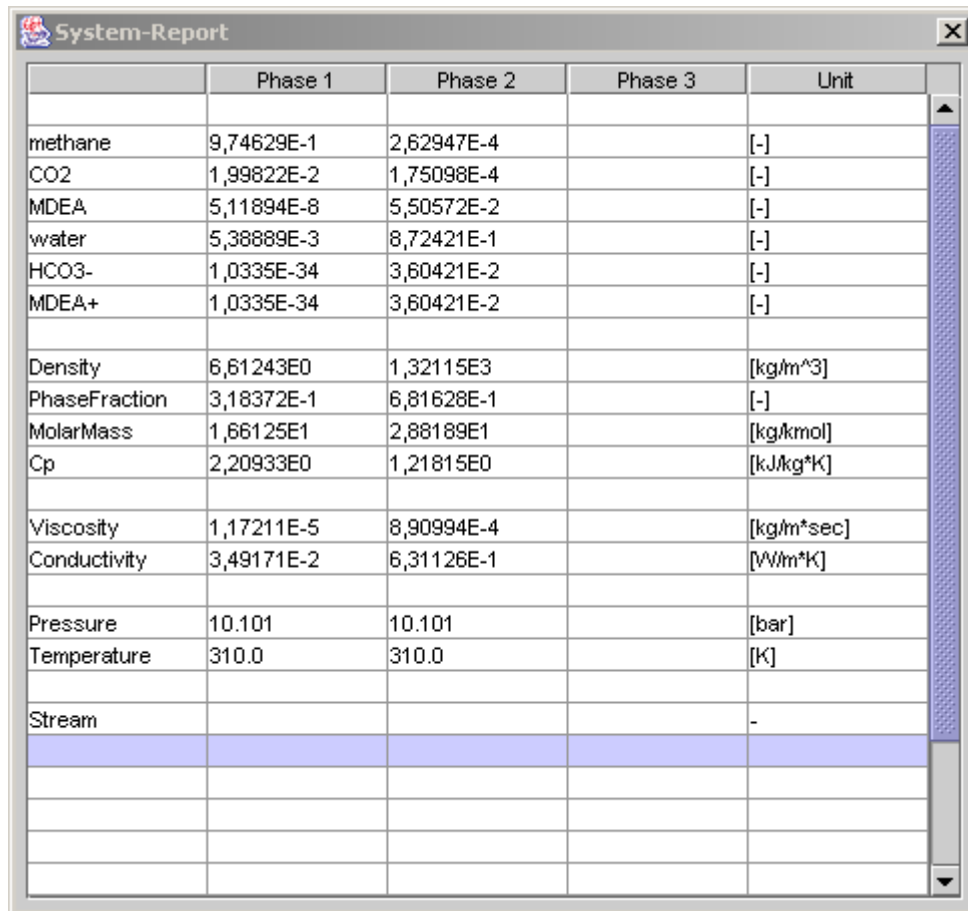
Figure 6-9 Thermodynamic property diagram for an untreated natural gas containing 8.87mol% CO$_2$ calculated with the SRK-EOS (chart.py). Molar composition (%): N$_2$ (0.64), CO$_2$ (8.87), methane (72.9), ethane (9.55), propane (5.0), i-butane (0.55), n-butane (1.04), n-pentane (0.5), n-heptane (0.64).
Script: natgas-chart.py, p. 311

An example of a reactive TPflash calculation for a mixture of methane, CO$_2$, water and MDEA is illustrated in the script given below. When performing reactive calculations in weak electrolyte systems – NeqSim will check for possible chemical reactions and add components that can form from these reactions. The reaction check algorithm was described in chapter 3. The result from the calculation is given in Figure 6-10.

```
# el-TPflash.py
system = thermo('electrolyte',310.0, 10.101)
addComponent(system,'methane',0.5)
addComponent(system,'CO2',0.05)
addComponent(system,'MDEA',0.1)
addComponent(system,'water',1.0)
reactionCheck(system)
newdatabase(system)

mixingRule(system,4)
TPflash(system)
show(system)
```

	Phase 1	Phase 2	Phase 3	Unit
methane	9,74629E-1	2,62947E-4		[-]
CO2	1,99822E-2	1,75098E-4		[-]
MDEA	5,11894E-8	5,50572E-2		[-]
water	5,38889E-3	8,72421E-1		[-]
HCO3-	1,0335E-34	3,60421E-2		[-]
MDEA+	1,0335E-34	3,60421E-2		[-]
Density	6,61243E0	1,32115E3		[kg/m^3]
PhaseFraction	3,18372E-1	6,81628E-1		[-]
MolarMass	1,66125E1	2,88189E1		[kg/kmol]
Cp	2,20933E0	1,21815E0		[kJ/kg*K]
Viscosity	1,17211E-5	8,90994E-4		[kg/m*sec]
Conductivity	3,49171E-2	6,31126E-1		[W/m*K]
Pressure	10.101	10.101		[bar]
Temperature	310.0	310.0		[K]
Stream				-

Figure 6-10 Results from running a TPflash calculation for a methane, CO_2, water and MDEA system.
Script: el-TPflash.py, p. 129

6.4 Object Oriented Design of the Fluid Mechanic Package

The fluid mechanics package is a relatively complicated and large library. The library will only be described very briefly here.

The fluid mechanic package is based on the general one- and two fluid model described in chapter 5. The same model is used for all kinds of process equipment (with different closure relations). The numerical calculations can be computational demanding – and long computational times often occurs when we use this module. All fluid mechanical calculations are done with a one-dimensional one- or two fluid model (depending on the number of phases present). The non-equilibrium two-fluid model was described in chapter 5.

Typical process equipment we can simulate with the fluid mechanical module are

- Pipe flow (one– and two phase)
- Reactor flow (absorption, distillation)
- Heat Exchanger flow

All types of flows are modelled with the transient one- or two fluid model. A staggered grid is used in the discretisation of all process equipment.

6.4.1 The Object Oriented Design of the Fluid Mechanic Library

The implemented object oriented design of the fluid mechanics package is constructed straight forward and relatively intuitively. A general fluid mechanics object/flow system (e.g. a pipe) is built up of legs and nodes. The number of legs and nodes is dependent on the complexity of the geometry of the system (e.g. the height profile of the pipe).

• **Nodes**
- holds an instance of a **thermodynamic system object**
- holds an instance of a **geometry object** describing the geometry and characteristics of the process equipment
- holds an instance **interphase transport coefficient object** describing the equations used to calculate interphase friction-, mass- and heat transfer coefficients
- holds an instance interphase **heat- and mass transfer object** describing the model used to calculate interphase heat- and mass transfer fluxes
• **Legs**
- holds a vector of node objects
• **Flow System**
- holds a vector of leg objects
• **Flow Solver**
- operates on a flow system object. Can return both stationary and dynamic simulation results.

The main packages in the fluid mechanics library are illustrated in Figure 6-11.
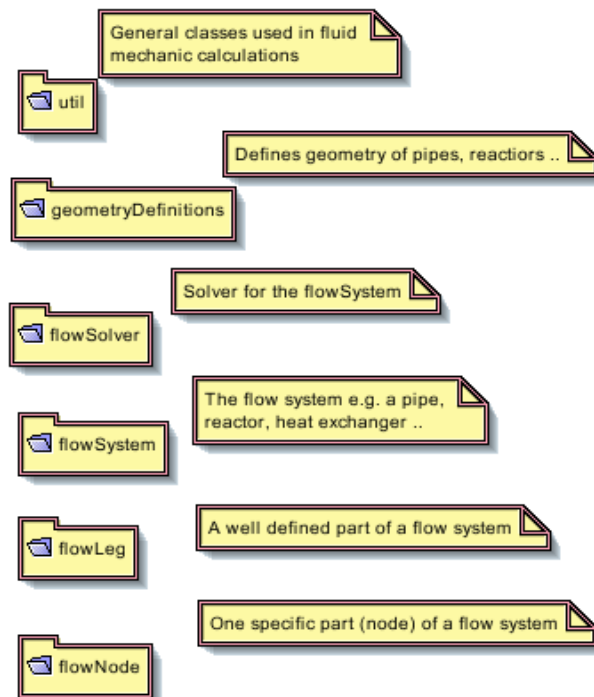
Figure 6-11 The fluid mechanics package

6.4.2 Example of a Fluid Mechanic Calculation

An example of calculating the pressure, velocity and temperature profile along a one-phase gas pipeline is illustrated in the following script,

```
# pipeflow.py
systemName = SystemSrkEos(298.0, 200.0)
systemName.addComponent("methane", 50, "MSm^3/day")
systemName.addComponent("CO2", 0.5, "MSm^3/day")
stream1 = stream(systemName,"stream 1")

legHeights =            [0,0]
legPositions =          [0.0, 720000.0]
pipeDiameters =         [1.025, 1.025]
outerTemperature =      [295.0, 295.0]
pipeWallRoughness =     [1e-5, 1e-5]
pipe = pipeline(stream1, legPositions, pipeDiameters, legHeights,
outerTemperature, pipeWallRoughness)
pipe.setNumberOfNodesInLeg(100)
pipe.setOutputFileName('c:/steadysim.nc')
run()
```

The calculated pressure profile is given in Figure 6-12.
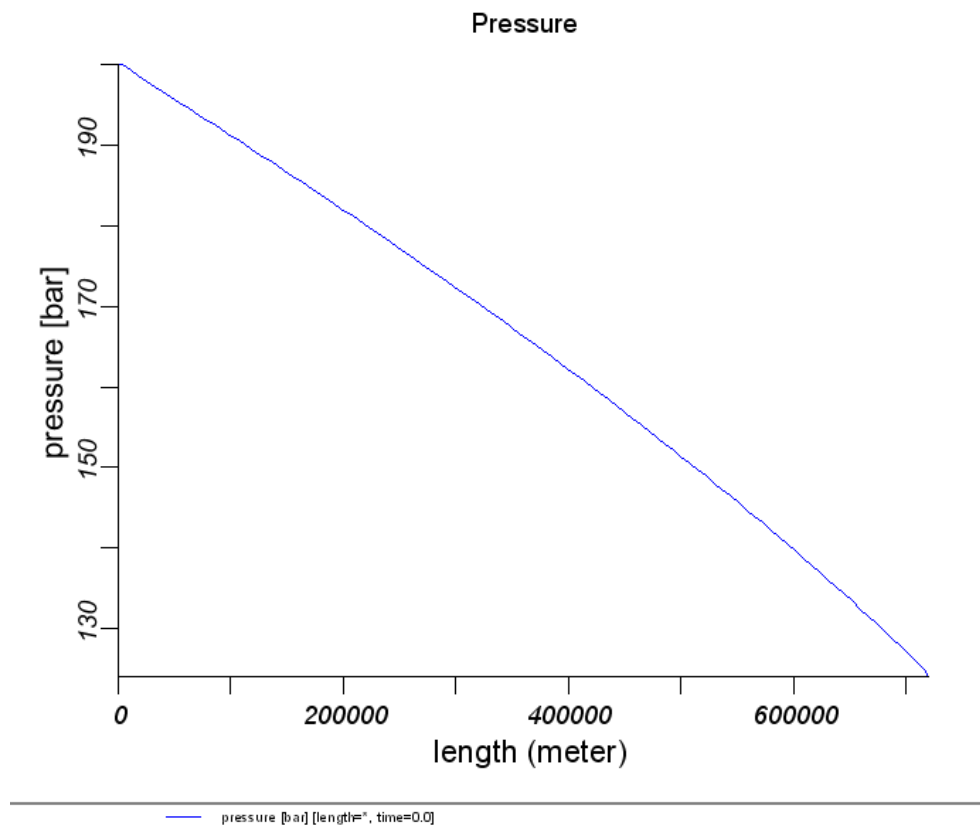
Figure 6-12 Pressure profile along a gas pipeline.
        Script: pipeflow.py, p. 233

More advanced use of the fluid mechanical package is described in the case studies reported in chapter 11.

6.5 Object Oriented Design of a Process Plant Simulation Package

The final goal of the NeqSim program is to use it as an evaluation and optimalization tool for process plants. A process plant is created by instantiating a process system object. A process system object holds a reference to a vector of process equipment objects. The structure of the process simulation package is illustrated in Figure 6-13.
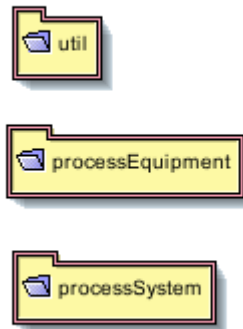
Figure 6-13 Structure of the process simulation package

The process equipment package is implemented as shown graphically in Figure 6-14. New process equipment can easily be added. All process equipment objects must implement a common interface that specifies methods the objects have to define (e.g. the run() method). New process equipment can easily be added – but the methods specified in the common interface have to be implemented.
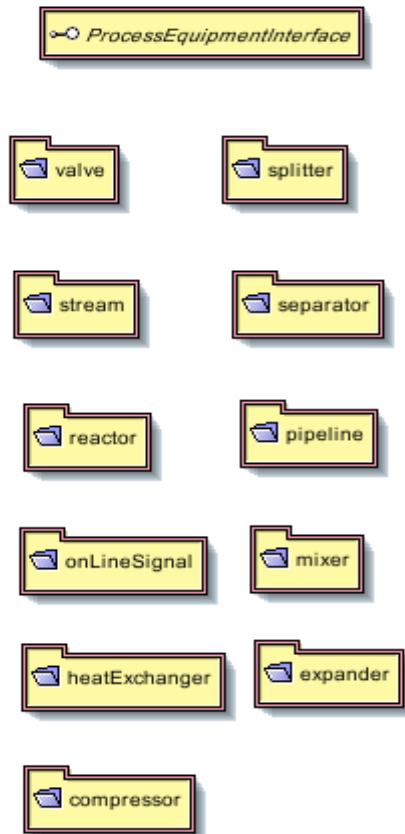
Figure 6-14 The process equipment package

Normally both equilibrium and non-equilibrium process equipment are added. The equilibrium process is what you find in common process simulators – and the non-equilibrium process is what is special for the NeqSim simulator. In non-equilibrium process equipment the non-equilibrium two fluid model described in chapter 5 is used to model the process.

Steady state process plant operations and networks can be simulated in NeqSim (a dynamic model is planned implemented). The unit process operations are solved in a sequential order where successive substitution is used to converge the whole process plant simulation.

An example of a script describing a small process plant is given below and illustrates how process equipment are simulated and connected with streams.

```python
# process-sim.py
systemName = SystemSrkEos(321.0, 92.6)
systemName.addComponent("methane", 0.95)
systemName.addComponent("water",  0.01)
systemName.setMixingRule(2)
newdatabase(systemName)

systemName2 = SystemSrkEos((273.15+4.3), 92.6)
systemName2.addComponent("methane",  0.9465)
systemName2.addComponent("water",  0.01)
systemName2.setMixingRule(2)

stream1 = stream(systemName,"stream 1")
stream2 = stream(systemName2,"stream 2")

separator1 = separator(stream1)
separator2 = separator(stream2)

stream3 = stream(separator1.getGasOutStream(),"TrollA_gasOut")
stream4 = stream(separator2.getGasOutStream(),"TrollWGP_gasOut")

mixer1 = mixer("mixer1")
mixer1.addStream(stream3)
mixer1.addStream(stream4)

stream5 = stream(mixer1.getOutStream(),"mixerOut")

neqheater1 = neqheater(stream5, "heater1")
neqheater1.setdT(-2.5)

stream6 = stream(neqheater1.getOutStream(),"heaterOutEqui")
stream7 =  neqstream(neqheater1.getOutStream(),"heaterOutNeq")
print "tot ant mol" , stream7.getMolarRate()

run()
processTools.view()
```

More examples of use of the process simulation package are given in the case studies in chapter 11.

6.6 Numerical Calculations and Visualization with NeqSim

Most of the figures and calculations done during this work have been created with NeqSim. The scripts used to do the calculations are given in appendix G. In this section a short description of the graphical user interface (GUI) is given.

6.6.1 The NeqSim GUI

The NeqSim GUI (graphical user interface) is programmed using the Java Swing Toolkit. The user interface is built up of four main components. These four components are:

- The script editor
- The toolbars (thermodynamic-, process-, and fluid mechanics toolbar)
- The file explorer (python script explorer)
- The main frame

NeqSim uses some open source tools for graphical visualization of data. These tools are:

- VisAd (3D-visualization + animations)
- JFreeChart (2D – graphs)
- NetCDF (data handeling in a binary file format)
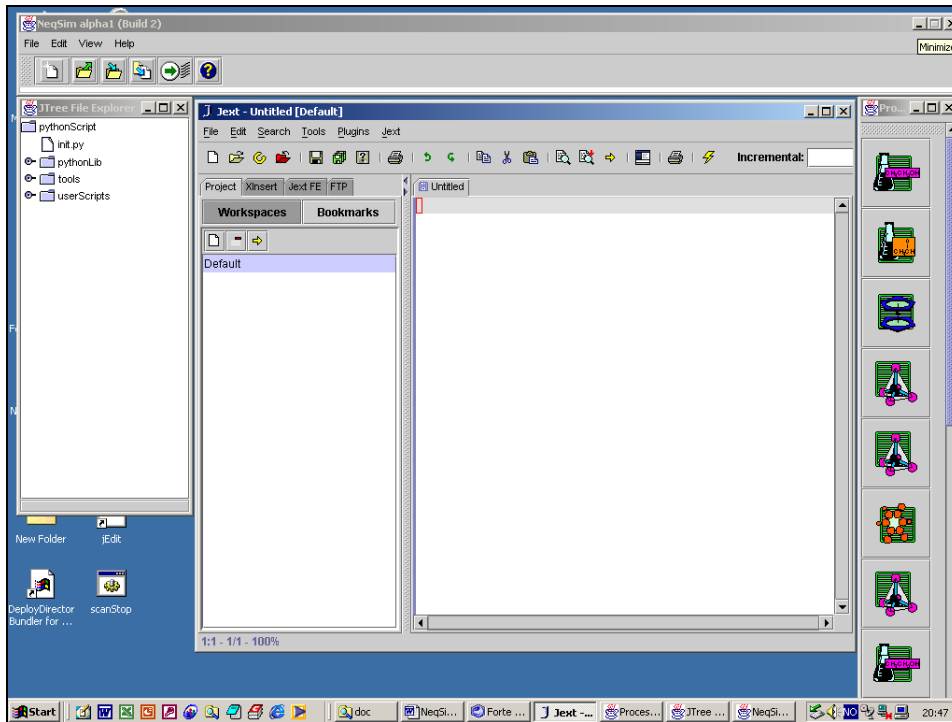
Figure 6-15 The NeqSim GUI

A screenshot of NeqSim is given in Figure 6-15. The script-editor is used to make NeqSim scripts (Python). The scripts can be written by the user or made automatically by using the toolbars. The scripts are executed by clicking the run-button in the main frame.

6.6.2 The Python Scripting Language

The scripting language used in NeqSim is Python (www.python.org). Python is an interpreted, easy, powerful and object oriented language. The python interpreter used in NeqSim is Jython (www.jython.org) – an interpreter written in the Java programming language. In this way it is easy to use existing Java libraries in Python – you are even able to inherit from your Java objects in your Python scripts.

Python is an easy to learn, powerful programming language. It has efficient high-level data structures and a simple but effective approach to object-oriented programming. Python's elegant syntax and dynamic typing, together with its interpreted nature, makes it an ideal language for scripting and rapid application development in many areas on most platforms.

6.6.3 The Matlab Toolbox

NeqSim can be used as a toolbox in Matlab. You can create a Python script in NeqSim – and run it in Matlab directly without modifications. In this way you are able to use the built in functions in Matlab – in combination with NeqSim. It is convenient to make the script in NeqSim – and to use it in Matlab – if you want to use some toolboxes or some of the graphing

capabilities of Matlab. Optimisation of process plants created in NeqSim – can easily be done in Matlab using built-in optimisation routines.

6.7 Summary – NeqSim: a Non-Equilibrium Simulator

A general non-equilibrium simulation tool was developed and implemented in the Java programming language. The mathematical fluid mechanic-, thermodynamic-, mass transfer- and physical properties models implemented in the program are described in this thesis.

A graphical user interface is distributed to make the use of the program as easy as possible. The toolbars in the graphical user interphase and the scripting language make it fast and easy to create new simulation scripts. Process equipment can be simulated and put together to form process plants. The process plant simulations can only be solved in steady state operation at the moment – a transient model is planned implemented in a future version.

NeqSim is constantly under development – and the latest updates and documentation can be downloaded from the homepage http://www.stud.ntnu.no/~solbraa/neqsim.

7 Experimental Parameter Fitting

All measurements are subject to some uncertainties, and no model will be able to fit the data perfectly. Error analysis is the study of experimental uncertainties, its two main functions being to allow us to estimate how large the experimental uncertainties are, and to reduce them if possible.

To evaluate parameters from experimental data and perform experimental uncertainty analysis, a statistical package was implemented in NeqSim. The statistical parameter fitting procedures were implemented in an object-oriented way – so that parameter fitting to new models could be calculated fast and easily. The parameter-fitting model implemented in the NeqSim computer code is based on the Levenberg-Marquardt method, as presented by Press et.al. (1999). The theoretical background presented in this chapter is also based on the descriptions given by Press.

Monte-Carlo simulation routines were implemented in the computer code. The Monte-Carlo routines were used to calculate confidence intervals of estimated parameters and to evaluate the influence of experimental measurement errors on the final model.

In this chapter an introduction to data modelling and parameter fitting is presented. A description of the priniciples and numerical implementation of Monte Carlo models are given at the end of the chapter. Section 7.6 gives a presentation of the object-oriented implementation of the statistical package. The background the theory to this chapter is described in more detail in books by Press et.al. (1999), Taylor (1997) and Box et.al. (1978).

7.1 Introduction to Experimental Parameter Fitting

Given a set of observations, one often wants to condense and summarize the data by fitting it to a "model" that depends on adjustable parameters. Sometimes the model is simply a convenient class of functions, such as polynomials or Gussians, and the fit supplies the appropriate coefficients. Other times, the model's parameters come from some underlying theory that the data is supposed to satisfy. Both kind of fitting are done in this work; the thermodynamic and fluid mechanics models are based on basic theory of thermodynamics and fluid dynamics and are often complicated models, while some of the physical property models are pure polynomial correlations. Generally we can say that the capability to extrapolate is better with the models that are based on scientific theory.

A general process simulation tool uses a number of equations and mathematical models. We use models for physical properties (viscosities, conductivities, diffusivity, surface tension), thermodynamic models (equations of state) and fluid mechanical models (interphase friction, mass transfer coefficients). The general modelling procedure is illustrated in Figure 7-1.

138
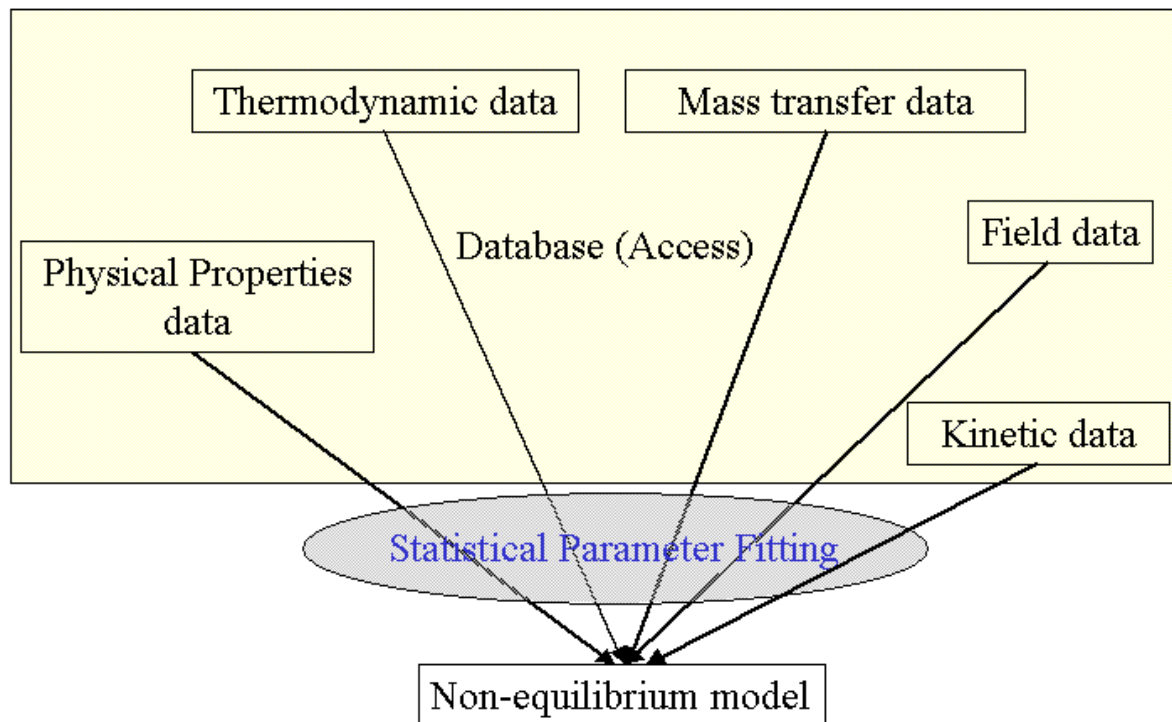
Figure 7-1 Strategy for parameter fitting

The basic approach in all cases is usually the same: You use a function (merit-function) that measures the agreement between the experimental data and the model with a particular choice of parameters. Thus, typically the experimental data never exactly fit the model that is being used - even when that model is correct.

We usually also need to know the accuracy with which parameters are determined by the data set. In other words, we need to know the errors of the fitted parameters – this information we usually obtain from the experimental error analysis.

Finally, it is not uncommon in fitting to discover that the merit function is not unimodal with a single minimum. In some cases, we may be interested in global rather than local minima. Finding the global minima is often difficult. One method is to try many different initial guesses for the parameters – and search until we are sure we have found a global minima. This was the method used when fitting parameters for the models during this work.

It is important to remember that fitting of parameters is not the end-all of parameter estimation. To be genuinely useful, a fitting procedure must provide:

- Parameters
- Error estimates on the parameters
- A statistical measure of the goodness-of-fit

When the third item suggests that the model is an unlikely match to the data, then items one and two are probably worthless.

It is the intention of this chapter to present a parameter fitting model that is easily an effectively applied to fit parameters to thermodynamic-, physical property- and fluid mechanical models. The routines should return parameters, uncertainties in parameters and goodness of the fit. It should be easy to fit parameters to new models when they are introduced in the computer program. Finally, the parameter fitting algorithm must be stable and effective, since such calculations can be computational demanding.

7.2 Least Squares Fitting and Error Analysis

In this section an introduction to least squares fitting based on Press et.al. (1999) is presented. Suppose we are fitting N data points $(x_i; y_i)$ $(i = 1, ..., N)$ to a model that has M adjustable parameters a_j $(j = 1,...,M)$. The model predicts a functional relationship between the measured independent and dependent variables,

$$y(x) = y(x; a_1,...,a_M) \tag{7.1}$$

where the dependence on the parameters is indicated explicitly on the right-hand side. The familiar least-squares fit is expressed as,

$$\text{minimize over } a_1...a_M: \quad \sum_{i=1}^{N}[y_i - y(x_i; a_1,...,a_M)]^2 \tag{7.2}$$

Given a particular data set of x_i's and y_i's, we have the intuitive feeling that some parameter sets $a_1...a_M$ are very unlikely — those for which the model function $y(x)$ looks nothing like the data - while others may be very likely - those that closely resemble the data.

We can turn the question around, and ask, "Given a particular set of parameters, what is the probability that this data set could have occurred?". If the y_i's take on continuous values, the probability will always be zero unless we add the phrase, "...plus or minus some fixed Δy on each data point." If the probability of obtaining the data set is infinitesimally small, then we can conclude that the parameters under consideration are "unlikely" to be right. Conversely, our intuition tells us that the data set should not be too improbable for the correct choice of parameters.

We identify the probability of the data given the parameters (which is a mathematically computable number), as the likelihood of the parameters given the data. Once we make this intuitive identification, however, it is only a small further step to decide to fit for the parameters $a_1...a_M$ precisely by finding those values that maximize the likelihood defined in the above way. This form of parameter estimation is maximum likelihood estimation.

Suppose that each data point y_i has a measurement error that is independently random and distributed as a normal (Gaussian) distribution around the "true" model $y(x)$. And suppose that the standard deviations σ of these normal distributions are the same for all points. From statistical theory we then obtain that the probability of the data set is the product of the probabilities of each point (see Press et.al., 1999),

$$P \propto \prod_{i=1}^{N} e^{-\frac{1}{2}\left(\frac{y_i - y(x_i)}{\sigma}\right)^2} \Delta y \tag{7.3}$$

Notice that there is a factor Δy in each term in the product. Maximizing (7.3) is equivalent to maximizing its logarithm, or minimizing the negative of its logarithm, namely,

$$\left[\sum_{i=1}^{N} \frac{\left[y_i - y(x_i)\right]^2}{2\sigma^2} \right] - N \log \Delta y \tag{7.4}$$

Since N, σ, and Δy are all constants, minimizing this equation is equivalent to minimizing (7.2).

What we see is that least-squares fitting is a maximum likelihood estimation of the fitted parameters if the measurement errors are independent and normally distributed with constant standard deviation. No assumption about the linearity or nonlinearity of the model $y(x; a_1 \ldots)$ in its parameters $a_1 \ldots a_M$ was made.

Sometimes the deviations from a normal distribution are easy to understand and quantify. For example, in measurements obtained by counting events, the measurement errors are usually distributed as a Poisson distribution. When the number of counts going into one data point is large, the Poisson distribution converges towards a Gaussian. However, the convergence is not uniform when measured in fractional accuracy. The more standard deviations out on the tail of the distribution, the larger the number of counts must be before a value close to the Gaussian is realized. The sign of the effect is always the same: The Gaussian predicts that "tail" events are much less likely than they actually (by Poisson) are. This causes such events, when they occur, to skew a least-squares fit much more than they ought.

Other times, the deviations from a normal distribution are not so easy to understand in detail. Experimental points are occasionally just way off. Perhaps the power flickered during a point's measurement, or someone wrote down a wrong number. Points like this are called outliers. They can easily turn a least-squares fit on otherwise adequate data into nonsense. Their probability of occurrence in the assumed Gaussian model is so small that the maximum likelihood estimator is willing to distort the whole curve to try to bring them, mistakenly, into line.

Measurements are also susceptible to systematic errors that will not go away with any amount of averaging. For example, the calibration of pressure transducer might depend on its temperature. If we take all our measurements at the same wrong temperature, then no amount of averaging or numerical processing will correct for this unrecognized systematic error.

When performing parameter fitting using a maximum likelihood models it is important to keep in mind the underlying assumptions that the errors are assumed to be normally distributed and the possibility of outliers and systematic errors. Because outliers can have a large and erroneous effects on estimated parameters, automatic identification of outliers is an important part of parameter fitting routines. This could be done by excluding points with large deviations (e.g. >100%) from the calculated values – but care must always be taken.

7.3 Chi-Square Fitting

If each data point $(x_i; y_i)$ has its own, known standard deviation σ_i, then equation (7.3) is modified only by putting a subscript i on the symbol σ. That subscript also propagates docilely into (7.4), so that the maximum likelihood estimate of the model parameters is obtained by minimizing the quantity

$$\chi^2 = \sum_{i=1}^{N} \left(\frac{y_i - y(x_i; a_1 ... a_M)}{\sigma_i} \right)^2 \tag{7.5}$$

called the "chi-square". The quantity χ^2 is correspondingly a sum of N squares of normally distributed quantities, each normalized to unit variance.

Once we have adjusted the $a_1 ... a_M$ to minimize the value of χ^2, the terms in the sum are not all statistically independent. For models that are linear in the a's, however, it turns out that the probability distribution for different values of χ^2 at its minimum can nevertheless be derived analytically, and is the chi-square distribution for N - M degrees of freedom. This probability function using the incomplete gamma function

$$Q\left(\chi^2 \middle| v\right) = Q\left(\frac{v}{2}, \frac{\chi^2}{2} \right) \tag{7.6}$$

This function gives the probability that the chi-square should exceed a particular value χ^2 by chance, where $v = N - M$ is the number of degrees of freedom. It is quite common, and usually not too wrong, to assume that the chi-square distribution holds even for models that are not strictly linear in the a's.

This computed probability gives a quantitative measure for the goodness-of-fit of the model. If Q is a very small probability for some particular data set, then the apparent discrepancies are unlikely to be chance fluctuations. Much more probably either:

- The model is wrong—can be statistically rejected
- The size of the measurement errors σ_i are really larger than stated

The chi-square probability Q does not directly measure the credibility of the assumption that the measurement errors are normally distributed. It assumes they are. In most, but not all, cases, however, the effect of nonnormal errors is to create an abundance of outlier points. These decrease the probability Q, so that we get the important conclusion that the measurement errors may not be normally distributed.

A rule of thumb is that a "typical" value of χ^2 for a "moderately" good fit is $\chi^2 \approx v$. More precise is the statement that the χ^2 statistic has a mean v and a standard deviation $\sqrt{2v}$, and, asymptotically for large v, becomes normally distributed.

If we happen to know the actual distribution law of your measurement errors, then it is possible to Monte Carlo simulate some data sets drawn from a particular model. You can then subject these synthetic data sets to your actual fitting procedure, so as to determine both the probability distribution of the χ^2 statistic, and also the accuracy with which the model parameters are reproduced by the fit.

In some cases the uncertainties associated with a set of measurements are not known in advance, and considerations related to χ^2 fitting are used to derive a value for σ. If we assume that all measurements have the same standard deviation, $\sigma_i = \sigma$, and that the model does fit well, then we can proceed by first assigning an arbitrary constant σ to all points, next fitting for the model parameters by minimizing χ^2, and finally recomputing.

$$\sigma^2 = \sum_{i=1}^{N} \left[y_i - y(x_i) \right]^2 \Big/ N - M \tag{7.7}$$

Alternatively we can assume a standard deviation of $\sigma_i = y_i/100$ (1% of measured value) for all points. In this case we get

$$\chi^2 = \sum_{i=1}^{N} \left(\frac{y_i - y(x_i; a_1 ... a_M)}{y_i/100} \right)^2$$

Obviously, this approach prohibits an independent assessment of goodness-of-fit, a fact occasionally missed by its adherents. When, however, the measurement error is not known, this approach at least allows some kind of error bar to be assigned to the points. This procedure was used in this work when the uncertainty in the experimental data points was unknown.

If we take the derivative of equation (7.5) with respect to the parameters a_k, we obtain equations that must hold at the chi-square minimum,

$$0 = \sum_{i=1}^{N} \left(\frac{y_i - y(x_i)}{\sigma_i^2} \right) \left(\frac{\partial y(x_i; ... a_k ...)}{\partial a_k} \right) \tag{7.8}$$

This equation is, in general, a set of M nonlinear equations for the M unknown a_k.

We usually divide non-linear and linear parameter fitting routines. The linear parameter fitting routines are faster and simpler – and more stable – but we very often need to use non-linear parameter fitting. Only a non-linear method was implemented in this work – this nonlinear model can however be used for fitting parameters to linear models.

7.4 Non-Linear Parameter Fitting

Consider fitting a model that depends nonlinearly on the set of M unknown parameters a_k where k = 1,2,..,M. We define a χ^2 merit function and determine best-fit parameters by its minimization. With nonlinear dependences the minimization must proceed iteratively. Given

trial values for the parameters, we develop a procedure that improves the trial solution. The procedure is then repeated until χ^2 stops (or effectively stops) decreasing.

The model to be fitted is

$$y = y(x; \boldsymbol{a}) \tag{7.9}$$

and the χ^2 merit function is

$$\chi^2(\mathbf{a}) = \sum_{i=1}^{N} \left(\frac{y_i - y(x_i; \mathbf{a})}{\sigma_i} \right)^2 \tag{7.10}$$

The gradient of χ^2 with respect to the parameters $\mathbf{a}$, which will be zero at the χ^2 minimum, has components

$$\frac{\partial \chi^2}{\partial a_k} = -2 \sum_{i=1}^{N} \frac{\left[y_i - y(x_i; \mathbf{a}) \right]}{\sigma_i^2} \frac{\partial y(x_i; \mathbf{a})}{\partial a_k} \qquad k = 1, 2, .., M \tag{7.11}$$

Taking an additional partial derivative gives

$$\frac{\partial^2 \chi^2}{\partial a_k \partial a_l} = 2 \sum_{i=1}^{N} \frac{1}{\sigma_i^2} \left[\frac{\partial y(x_i; \mathbf{a})}{\partial a_k} \frac{\partial y(x_i; \mathbf{a})}{\partial a_l} - \left[y_i - y(x_i; \mathbf{a}) \right] \frac{\partial^2 y(x_i; \mathbf{a})}{\partial a_l \partial a_k} \right] \tag{7.12}$$

It is conventional to remove the factors of 2 by defining

$$\beta_k \equiv -\frac{1}{2} \frac{\partial \chi^2}{\partial a_k} \qquad \alpha_{kl} = \frac{1}{2} \frac{\partial^2 \chi^2}{\partial a_k \partial a_l} \tag{7.13}$$

we can write up the set of linear equations

$$\sum_{i=1}^{M} \alpha_{kl} \delta a_l = \beta_k \tag{7.14}$$

This set is solved for the increments δa_l that, added to the current approximation, give the next approximation. In the context of least squares, the matrix $[\alpha]$, equal to one-half times the Hessian matrix, is usually called the curvature matrix.

Note that the components α_{kl} of the Hessian matrix (7.12) depend both on the first derivatives and on the second derivatives of the basis functions with respect to their parameters. Some treatments proceed to ignore the second derivative without comment – and this was also done in this work. Inclusion of the second-derivative term can in fact be destabilizing if the model fits badly or is contaminated by outlier points that are unlikely to be offset by compensating points of opposite sign. From this point on, we will always use as the definition of α_{kl} the formula

$$\alpha_{kl} = \sum_{i=1}^{N} \frac{1}{\sigma_i^{\,2}} \left[\frac{\partial y\left(x_i; \mathbf{a}\right)}{\partial a_k} \frac{\partial y\left(x_i; \mathbf{a}\right)}{\partial a_l} \right] \qquad (7.15)$$

A minor (or even major) fiddling with $\left[\alpha\right]$ has no effect at all on what final set of parameters **a** is reached, but affects only the iterative route that is taken in getting there. The condition at the χ^2 minimum, that $\beta_k = 0$ for all k, is independent of how $\left[\alpha\right]$ is defined.

7.4.1 The Levenberg-Marquardt Method

A popular method for numerical implementation of the above equations will be described in this section – and is often referred to as the Levenberg-Marquardt method. Marquardt (1963) put forth an elegant method, related to an earlier suggestion of Levenberg, for varying smoothly between the extremes of the inverse-Hessian method (7.14) and the steepest descent method. The latter method is used far from the minimum, switching continuously to the former as the minimum is approached. This Levenberg-Marquardt method works very well in practice and has become the standard of nonlinear least-squares routines.

The quantity χ^2 is nondimensional, i.e., is a pure number; this is evident from its definition (7.10). On the other hand, β_k has the dimensions of $1/a_k$, which may well be dimensional. The constant of proportionality between β_k and ∂a_k must have the dimensions of $a_k^{\,2}$. If we consider the components of $[\alpha]$ we see that there is only one obvious quantity with these dimensions, and that is $1/\alpha_{kk}$, the reciprocal of the diagonal element. So that must set the scale of the constant. But that scale might itself be too big. We divide the constant by some (nondimensional) fudge factor λ, with the possibility of setting $\lambda \gg 1$ to cut down the step.

$$\partial a_l = \frac{1}{\lambda \alpha_{ll}} \qquad or \qquad \lambda \alpha_{ll} \partial a_l = \beta_l \qquad (7.16)$$

It is necessary that all be positive, and this is guaranteed by equation (7.15).

Equations (7.16) and (7.14) can be combined if we define a new matrix α' by the following prescription

$$\begin{aligned} \alpha'_{jj} &\equiv \alpha_{jj}\left(1 + \lambda\right) \\ \alpha'_{jk} &\equiv \alpha_{jk} \end{aligned} \qquad (7.17)$$

and then replace both (7.16) and (7.14) by

$$\sum_{i=1}^{M} \alpha'_{kl} \delta a_l = \beta_k \qquad (7.18)$$

When λ is very large, the matrix α is forced into being diagonally dominant, so equation (7.18) goes over to be identical to (7.16). On the other hand, as λ approaches zero, equation (7.18) goes over to (7.14).

Given an initial guess for the set of fitted parameters **a**, the Levenberg-Marquardt recipe is:

- Compute $\chi^2(\mathbf{a})$
- Pick a modest value for λ, say $= 0.001$
- (*) Solve the linear equations (7.18) for $\delta\mathbf{a}$ and evaluate $\chi^2(\mathbf{a} + \delta\mathbf{a})$.
- If $\chi^2(\mathbf{a}+\delta\mathbf{a})>\chi^2(\mathbf{a})$, increase λ by a factor of 10 (or any other substantial factor) and go back to (*).
- If $\chi^2(\mathbf{a}+\delta\mathbf{a})<\chi^2(\mathbf{a})$, decrease λ by a factor of 10, update the trial solution $\mathbf{a} \leftarrow \mathbf{a} + \delta\mathbf{a}$, and go back to (*).

Iterating to convergence (to machine accuracy or to the round off limit) is generally wasteful and unnecessary since the minimum is at best only a statistical estimate of the parameters **a**. In practice, one might as well stop iterating on the first or second occasion that χ^2 decreases by a negligible amount, say either less than 0.01 absolutely or some fractional amount like 10^{-3}.

When the acceptable minimum has been found, one set $\lambda = 0$ and compute the matrix

$$[cov] \equiv [\alpha]^{-1} \qquad (7.19)$$

which is the estimated covariance matrix of the standard errors in the fitted parameters **a.** The correlation between parameters i and j is calculated from

$$corr_{i,j} = \frac{cov_{i,j}}{\sqrt{cov_{i,i} \cdot cov_{j,j}}} \qquad (7.20)$$

It is important to always keep the correlation between parameters low. High correlation between parameters gives an indication that some parameters may be redundant.

The object-oriented implementation of chi-square calculations implemented in this work is illustrated in Figure 7-2. A sample set object is built up of a list of sample point objects (experimental values with corresponding mathematical models). A sample set can hold many types of sample point objects (e.g both density- and vapour pressure data with corresponding models). This makes the models flexible, and it is easy to fit parameters to different kinds of experimental data.
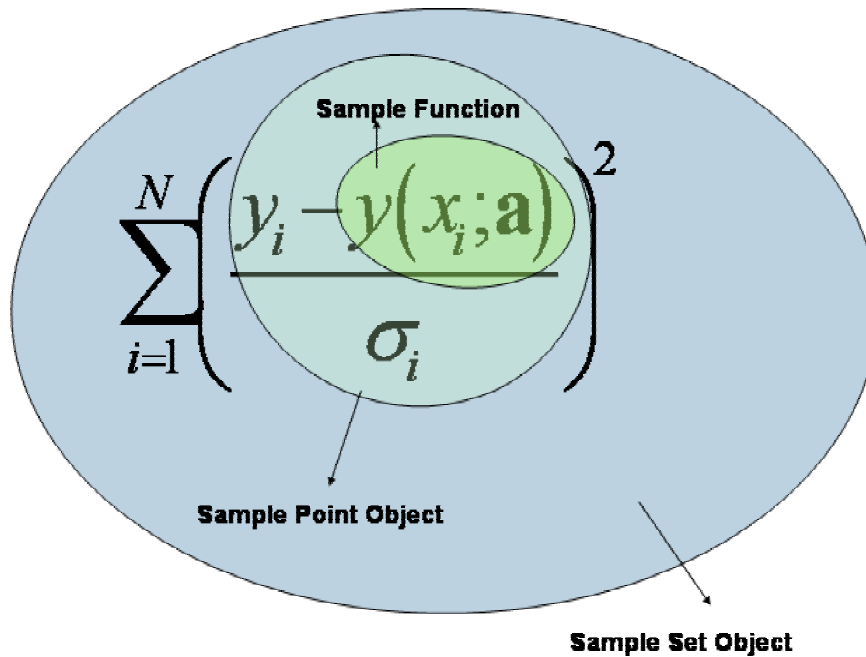
Figure 7-2 Object-oriented implementation of the Shi-Square function

In the figures below an example of parameter fitting with NeqSim is given. In the particular case studied, the acentric factor is fitted to pure component vapor pressure data of water. In the first text box a function class is created which calculates the vapor pressure corresponding to an estimated acentric factor. In the second textbox a sample set object is created by reading experimental data and the corresponding functions into sample objects. The Levenberg-Marquardt method object, representing the algorithm described in this chapter, works on any sample set object. In Figure 7-3 the output from the fitting procedure is given.

Creating a function class (parameterFit.py)

```python
class fitFunctionVapPres(LevenbergMarquardtFunction):

        def calcValue(self, dependentValues):
                self.system.setTemperature(dependentValues[0])
                self.system.init(0)
                self.system.init(1)
                self.thermoOps.bubblePointPressureFlash(0)
                return self.system.getPressure()

        def calcTrueVale(self, val):
                return val

        def setFittingParams(self, i, value):
                self.params[i] = value
                LevenbergMarquardtFunction.getSystem(self).getPhases()[0].
                getComponents()[i].setAcentricFactor(value)
                LevenbergMarquardtFunction.getSystem(self).getPhases()[1].getComp
                onents()[i].setAcentricFactor(value)
```

Creating a simulation set

```
dataSet = database.getResultSet("NeqSimDataBase",  "SELECT * FROM
PureComponentVapourPressures WHERE ComponentName='water' AND
VapourPressure<20");

try:
            while dataSet.next():
                function = fitFunctionDens()
                function.setInitialGuess(guess)
                testSystem = SystemSrkEos(280, 1.001)
              testSystem.addComponent(dataSet.getString("Name",100))
                newdatabase(testSystem)
                temperature = float(dataSet.getString("Temperature"))
                testSystem.setTemperature(temperature)
                standardDeviation1 =  [0.01]
                sample1 = [testSystem.getTemperature()]
                dens = float(dataSet.getString("liquiddensity"))
                dev = float(dataSet.getString("StandardDeviation"))
                sample = SampleValue(dens, dens/100.0,
                   sample1, standardDeviation1)
                sample.setFunction(function)
                sample.setReference(dataSet.getString("Reference"))
                sample.setThermodynamicSystem(testSystem)
                sampleList.append(sample)
```
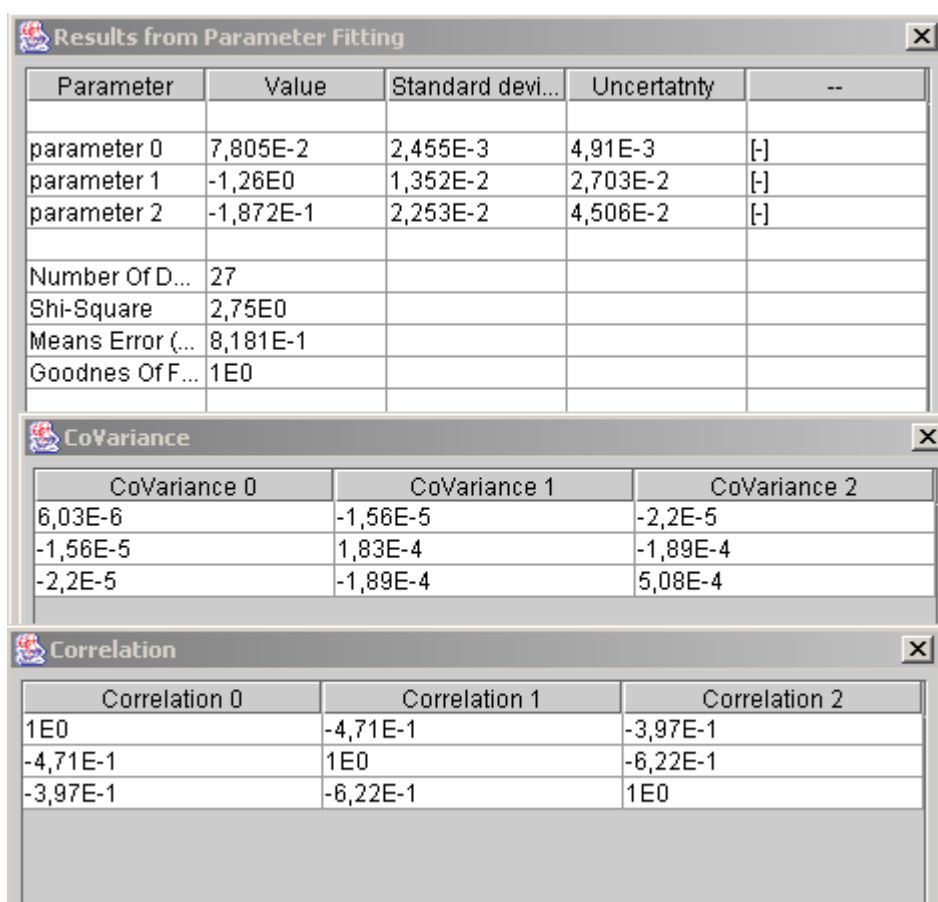
Results from Parameter Fitting

Parameter	Value	Standard devi...	Uncertatnty	--
parameter 0	7,805E-2	2,455E-3	4,91E-3	[-]
parameter 1	-1,26E0	1,352E-2	2,703E-2	[-]
parameter 2	-1,872E-1	2,253E-2	4,506E-2	[-]
Number Of D...	27			
Shi-Square	2,75E0			
Means Error (...	8,181E-1			
Goodnes Of F...	1E0			

CoVariance

CoVariance 0	CoVariance 1	CoVariance 2
6,03E-6	-1,56E-5	-2,2E-5
-1,56E-5	1,83E-4	-1,89E-4
-2,2E-5	-1,89E-4	5,08E-4

Correlation

Correlation 0	Correlation 1	Correlation 2
1E0	-4,71E-1	-3,97E-1
-4,71E-1	1E0	-6,22E-1
-3,97E-1	-6,22E-1	1E0

Figure 7-3 Output from parameter fitting routine in NeqSim.
            Script: parameterFit.py, p. 147

7.5 Confidence Limits on Estimated Model Parameters

Several times we have to make statements about the standard errors, or uncertainties, in a set of M estimated parameters **a**. In this section further information about how quantitative confidence limits on fitted parameters can be estimated is presented.

Figure 7-4 shows the conceptual scheme of an experiment that "measures" a set of parameters. There is some underlying true set of parameters $\mathbf{a}_{\text{true}}$ that are known to "be true" but hidden from the experimenter. These true parameters are statistically realized, along with random measurement errors, as a measured data set, which we will symbolize as $D_{(0)}$. The data set $D_{(0)}$ is known to the experimenter. We fit the data to a model by χ^2 minimization or some other technique, and obtains measured, i.e., fitted, values for the parameters, which we denote $\mathbf{a}_{(0)}$.
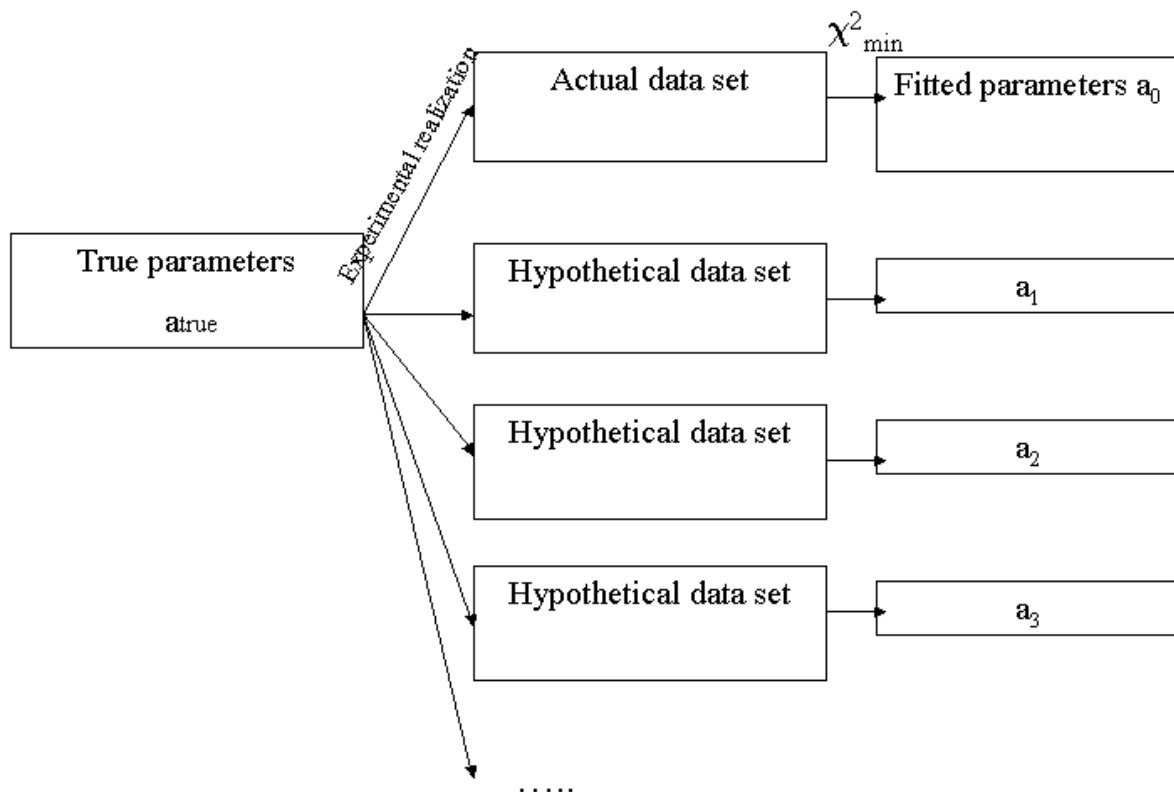
Figure 7-4 A statistical universe of data sets from an underlying model.

Because measurement errors have a random component, $D_{(0)}$ is not a unique realization of the true parameters $\mathbf{a}_{\text{true}}$. Rather, there are infinitely many other realizations of the true parameters as "hypothetical data sets" each of which could have been the one measured, but happened not to be. These can be symbolized by $D_{(1)}, D_{(2)}, \ldots$. Each one, had it been realized, would have given a slightly different set of fitted parameters, $\mathbf{a}_{(1)}, \mathbf{a}_{(2)}, \ldots$, respectively. These parameter sets $\mathbf{a}_{(i)}$ therefore occur with some probability distribution in the M-dimensional space of all possible parameter sets **a**. The actual measured set **a**(0) is one member drawn from this distribution.

Even more interesting than the probability distribution of $\mathbf{a}_{(i)}$ would be the distribution of the difference $\mathbf{a}(i) - \mathbf{a}_{true}$. This distribution differs from the former one by a translation that puts Mother Nature's true value at the origin. If we knew this distribution, we would know everything that there is to know about the quantitative uncertainties in our experimental measurement $\mathbf{a}_{(0)}$.

Our intension is to try to find some way of estimating or approximating the probability distribution of $\mathbf{a}_{(i)} - \mathbf{a}_{\underline{true}}$ without knowing $\mathbf{a}_{true}$ and without having available to us an infinite universe of hypothetical data sets.

7.5.1 Monte Carlo Simulation of Synthetic Data Sets

Although the measured parameter set $\mathbf{a}_{(0)}$ is not the true one, we consider a fictitious world in which it was the true one. Since we hope that our measured parameters are not too wrong, we hope that that fictitious world is not too different from the actual world with parameters $\mathbf{a}_{true}$. We assume that the shape of the probability distribution $\mathbf{a}_{(i)} - \mathbf{a}_{(0)}$ in the fictitious world is the same, or very nearly the same, as the shape of the probability distribution $\mathbf{a}_{(i)} - \mathbf{a}_{true}$ in the real world.

Notice that we are not assuming that $\mathbf{a}_{(0)}$ and $\mathbf{a}_{true}$ are equal. We are only assuming that the way in which random errors enter the experiment and data analysis does not vary rapidly as a function of $\mathbf{a}_{true}$, so that $\mathbf{a}_{(0)}$ can serve as a reasonable surrogate.

Now, often, the distribution of $\mathbf{a}_{(i)} - \mathbf{a}_{(0)}$ in the fictitious world is within our power to calculate. If we know something about the process that generated our data, given an assumed set of parameters $\mathbf{a}_{(0)}$, then we can usually figure out how to simulate our own sets of "synthetic" realizations of these parameters as "synthetic data sets." The procedure is to draw random numbers from appropriate distributions so as to mimic our best understanding of the underlying process and measurement errors in our apparatus. With such random draws, we construct data sets with exactly the same numbers of measured points, and precisely the same values of all control (independent) variables, as our actual data set $D_{(0)}$. We call these simulated data sets $D_{(1)}; D_{(2)} \ldots$. By construction these are supposed to have exactly the same statistical relationship to $\mathbf{a}(0)$ as the $D_{(i)}$'s have to $\mathbf{a}_{true}$.

Next, for each $D_{(j)}$, we perform exactly the same procedure for estimation of parameters, e.g., χ^2 minimization, as was performed on the actual data to get the parameters $\mathbf{a}_{(0)}$, giving simulated measured parameters $\mathbf{a}_{(1)}, \mathbf{a}_{(2)}, \ldots \mathbf{a}_{(n)}$. Each simulated measured parameter set yields a point $\mathbf{a}_{(i)} - \mathbf{a}_{(0)}$. Simulate enough data sets and enough derived simulated measured parameters, and you map out the desired probability distribution in M dimensions. This is what we call a Mote Carlo simulation. Not only is one able to characterize the errors of parameter estimation in a very precise way; one can also try out on the computer different methods of parameter estimation, or different data reduction techniques, and seek to minimize the uncertainty of the result according to any desired criteria.

Monte Carlo simulations can be performed on all data sets if the standard deviations/uncertainties of the experimental datapoints are available. NeqSim uses a statistical library (Colt-Library) to generate new sample sets from the experimental data, standard deviations and corresponding error distributions. If we have measured a set of pure component vapour pressures of water with a known standard deviation and error distribution, new datasets are easily generated. In Figure 7-5 the acentric factor for water has been Monte

Carlo simulated. In the case studied, 50 new datasets were generated from an initial experimental data set with a corresponding error estimate. From Figure 7-5 it is possible to estimate the uncertainty and confidence interval of the estimated acentric factor.
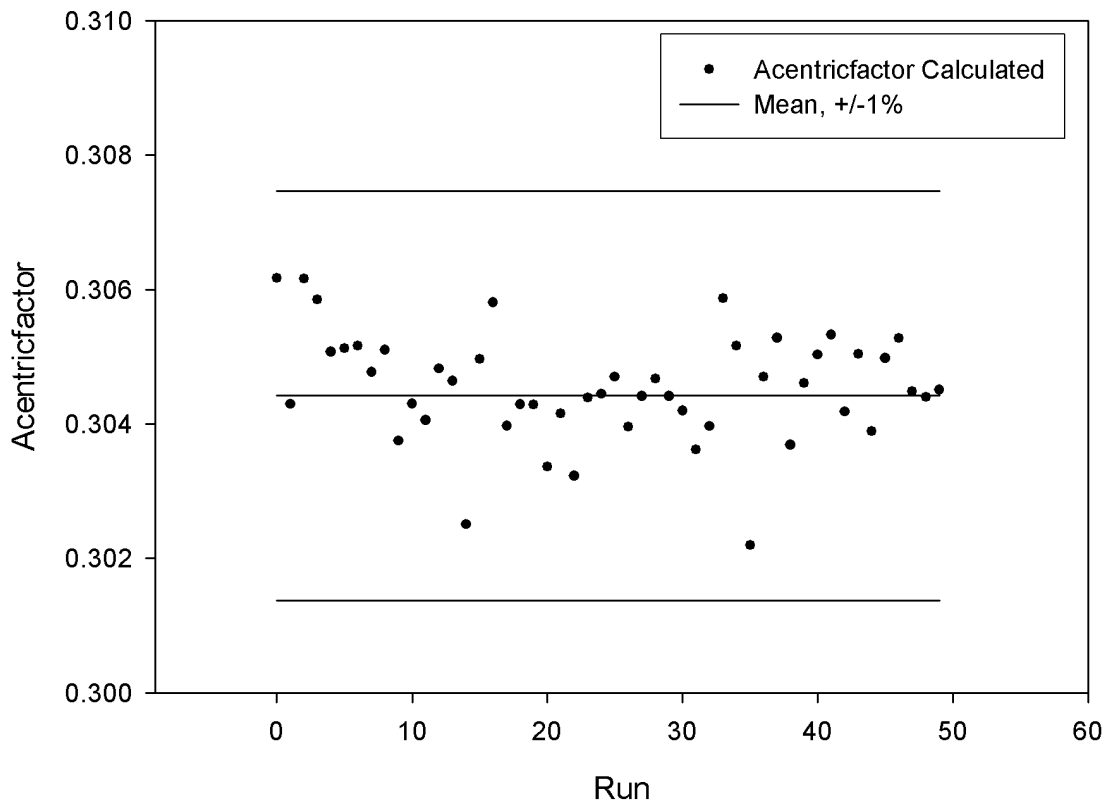

Figure 7-5 Monte Carlo simulation of acentric factor for water

7.6 *Object Oriented Implementation of Parameter Fitting Routines*

In this work the Levenberg-Marquardt method as described earlier in this chapter was implemented in Java – based on an object oriented design. There are many advantages of implementing the statistical calculations in an object-oriented language. The statistical models can be made both fast, general and maintainable.

NeqSim will calculate the parameters, covariance matrix and the confidence interval for the parameters. In the modeling work related to this thesis - these statistical routines have been used to fit parameters. The advantage of the procedure presented here is that it returns both confidence intervals for the parameters and an estimate of the goodness of the fit (Q) and thus the applicability of the model.

7.6.1 Object Oriented Implementation of the Levenberg Marquardt Method

The object-oriented design used in this work is illustrated in Figure 7-6.
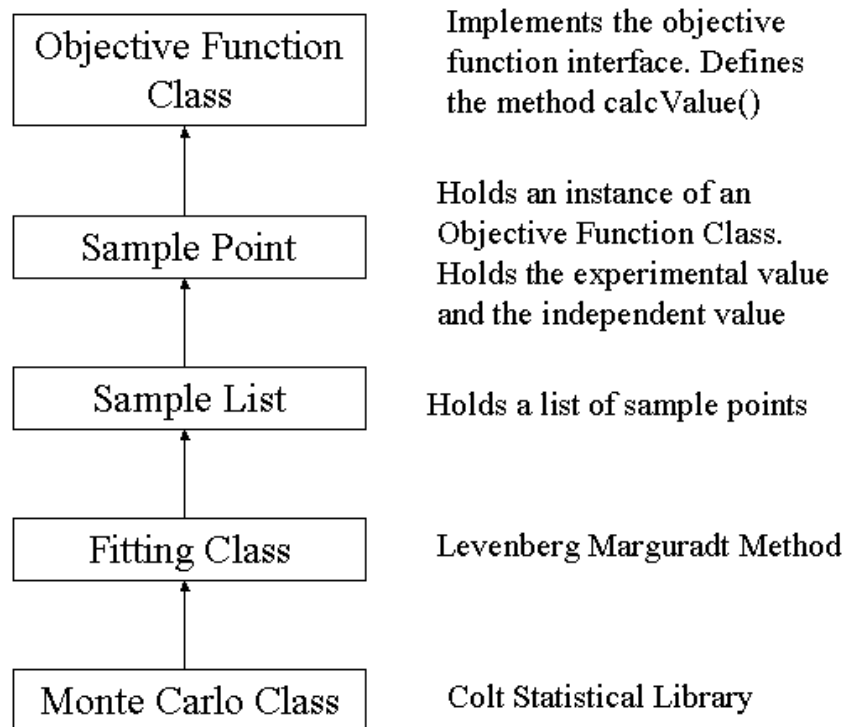
Figure 7-6 Object Oriented design of the Levenberg-Marquardt method

The fitting class holds a list of sample point objects. The sample point object holds an objective function object and the experimental value (and independent values and standard deviations for the experimental the value). The objective function object implements the objective function interface and must define the method calcValue() that returns the calculated value corresponding to the sample point. A sample list can hold different types of sample points (e.g. density and vapor pressure). Monte Carlo simulations to estimate uncertainties in fitted parameters can be done on any sample set – if the experimental standard deviations/uncertainties are available.

7.6.2 Example of Parameter Fitting with NeqSim

In this section a short example is given for parameter fitting to vapor pressure data for water. This is a rather simple calculation – but serves as an example of the parameter fitting models. One of the powerful applications of the object-oriented implementation of the parameter fitting routines – is the ability to use many objective functions. A data set object holds a vector of data point objects – and these data point objects have a reference to its own objective function. Because the objective function is instantiated in each data object we can fit to many types of data. This is useful when we fit parameters in the CPA-EOS to both vapor pressure and density data. This means that two different objective functions have to be used. The "chi-square" function we have to minimize becomes

$$\chi^2 = \sum_{i=1}^{N_\rho}\left(\frac{\rho_{i,\exp} - \rho_{model}\left(T_i;a_1...a_M\right)}{\sigma_{i,\rho}}\right)^2 + \sum_{i=1}^{N_{vap\,P}}\left(\frac{vap\,P_{i,\exp} - vap\,P_{model}\left(T_i;a_1...a_M\right)}{\sigma_{i,vap\,P}}\right)^2 \quad (7.21)$$

where T is the temperature and **a** is the parameters to be fitted (5 parameters in the CPA-model) and where the densities are both vapour and liquid densities.

The objects used when fitting parameters to the CPA model are illustrated in the Figure 7-7.
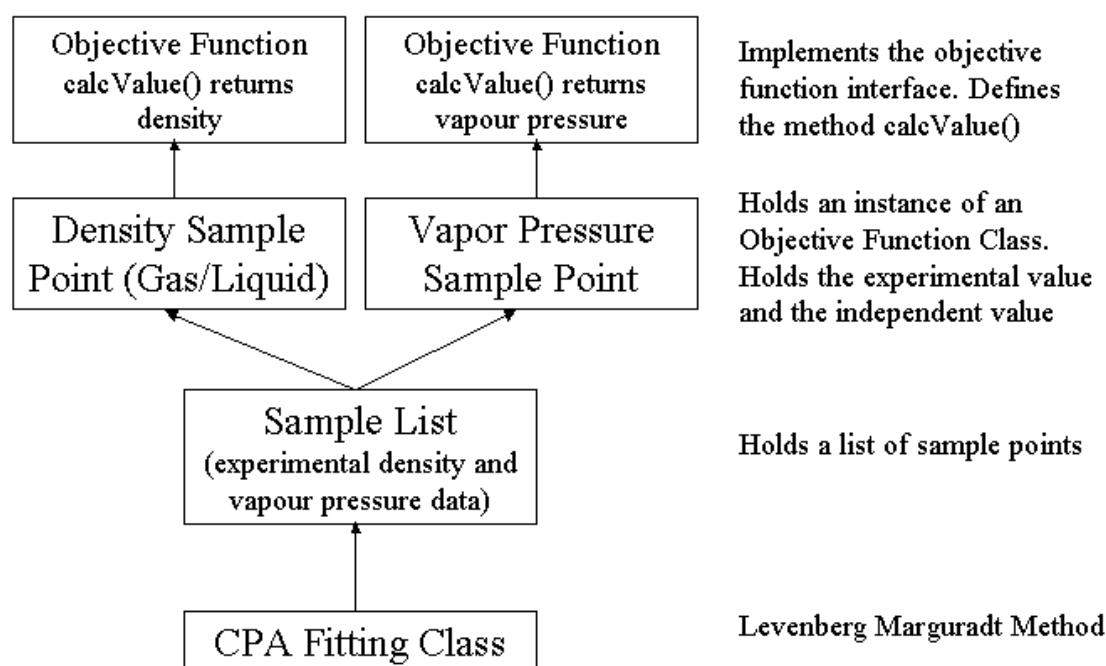
Figure 7-7 Objects used when fitting parameters to the CPA-EOS to pure component vapor pressure and density data

The script used to do parameter fitting to the CPA-EOS is given in appendix G (CPA-fit.py, p. 312).

7.7 *Experimental Uncertainty Analysis*

The analysis of uncertainties is a vital part of any scientific experiment, and error analysis is therefore an important part of all experimental work. A result of a given measurement is only an estimate of the specific value of the quantity subject to the measurement. The result is therefore complete only when supplemented with a quantitative uncertainty. The errors are commonly divided into groups (Taylor, 1997):

- **Spurious errors (outliers)**
  These are errors related to human errors or instrument malfunction. Such errors should

not be incorporated into any statistical analysis and the measurement should be discarded. These errors however can be difficult to detect.

- **Random errors**
  Random errors are referred to as precision or experimental errors. They are caused by numerous small, independent influences, which prevent measurement system from delivering the same measured value for repeated measurements with the same input values. The magnitude of the deviation is quantified as a statistical uncertainty.

- **Constant systematic errors**
  Systematic uncertainty is fixed and gives a constant output being either too high or too low compared to the true value. The uncertainties in question may be known, and can be corrected for by calibration, or they may be of unknown magnitude and sign.

- **Variable errors**
  These errors are identified when output of an instrument varies in the operating range of the instrument. An example of this is flow measurements, where the error increases as the flow rate decreases against the lower limit. Variable systematic errors may also occur where digital measurements are taken continuously with varying quantity. The uncertainty in the measurement due to its digital resolution then depends on the order of the final digit.

7.7.1 Propagation of Errors

When the measurement results have a functional dependency of several variables, of the form,

$$y = f\left(x_1, x_2, x_3, ..., x_n\right) \tag{7.22}$$

If $x_1, x_2, ... x_n$ are measured with uncertainties $\delta x_1, \delta x_2, ... \delta x_n$ and the measured values are used to compute the function y. If uncertainties in $x_1, x_2, ... x_n$ are independent and random, then the uncertainty in y is

$$\delta y = \sqrt{\left(\frac{\partial y}{\partial x_1}\delta x_1\right)^2 + \left(\frac{\partial y}{\partial x_2}\delta x_2\right)^2 + ... + \left(\frac{\partial y}{\partial x_n}\delta x_n\right)^2} \tag{7.23}$$

In any case, it is never larger than the ordinary sum

$$\delta y = \left|\frac{\partial y}{\partial x_1}\right|\delta x_1 + \left|\frac{\partial y}{\partial x_2}\right|\delta x_2 + ... + \left|\frac{\partial y}{\partial x_n}\right|\delta x_n \tag{7.24}$$

This method of error analysis was used for error estimation of the experimental results obtained in this work. The error analysis related to the experiments done during this work is presented in appendix H.

By doing Monte Carlo simulations with NeqSim it is easy to check the importance of parameters and the effect they have on error propagation for the experiment (see MonteCarlo.py, p.319). This is typically done in situations where you suspect some measurements to introduce large errors.

7.8 Summary - Experimental Parameter Fitting

A general model (the Levenberg-Marquardt method) for doing parameter fitting to experimental data was described in this chapter and implemented in the computer code developed during this work. The parameter-fitting package was implemented using an object oriented design basis – so that parameter fitting could be done to any model in a simple and effective way. Multiple objective functions are easy and straightforward to use. In this way a mathematical model can be fitted to many types of experimental data.

A general method to perform Monte Carlo simulations on experimental data sets is presented, and the method was implemented in the computer code developed. Monte Carlo simulation is a powerful technique to evaluate uncertainties in parameters fitted to experimental data – and is valuable in estimating uncertainties in regressed parameters.

8 Parameter Estimation for the Electrolyte Equation of State

Most of the thermodynamic models used in simulation programs involve parameters that need to be fitted to experimental data. The numbers of parameters that need to be fitted vary widely between the models – and one generally prefers models with few parameters. It is also preferable to fit as few binary- and ternary interaction parameters as possible.

The thermodynamic models used in this work are two different electrolyte equations of state. These two equations were described in chapter 3. The models consist of three main contributions to the Helmholtz energy; a traditional cubic equation of state, a short-range ion-ion and ion-molecule term and a long-range term for inter-ionic forces. One model uses the ScRK EOS with the Huron Vidal mixing rule to model the molecular interactions, while the other model uses the CPA-EOS to describe such interactions. Both models use the short range and long-range ionic interactions as described by Furst and Renon (1993) plus an additional Born term.

The main molecular components considered in this work have been methane, nitrogen, CO_2, water and MDEA. These components were used in both the modelling and in the experimental work described in this thesis.

The application of a thermodynamic model for the calculation of VLE in the case of inert- and acid gases in MDEA and water solutions implies the knowledge of several pure- and binary component parameters relative to the molecular compounds. These parameters were found by fitting the models to experimental data and are given in this chapter.

It is important to remember that all experimental data points will have uncertainties, and that the parameters we find also will have some uncertainties. A good parameter regression routine should give both parameters, the uncertainties in the parameters and the goodness of the model you try to fit. The model that was used for parameter fitting during this work was the Levenberg-Marquardt method as described in chapter 7. When we use the Levenberg-Marquardt method we need to know the standard deviation (uncertainties) in the experimental data points. Most articles and books where the experimental data are collected from give a value for the uncertainty. For some of the experimental data used, we had to estimate the experimental uncertainty. All experimental data used for parameterfitting during this work are stored in the Access database distributed with NeqSim.

Some of the estimated parameters are reported with a 95% confidence interval. This means that there is a 95 percent chance that the true parameters will fall within this region around the measured value.

$$p = p \pm \delta p$$

where $\pm \delta p$ is the 95% confidence interval. The absolute relative deviation and the bias deviation are calculated from

$$abs.avg.rel.dev = \frac{1}{n}\sum_{i=1}^{n}\left|\frac{y_{i,calc}-y_{i,\exp}}{y_{i,\exp}}\right|\cdot 100\% \tag{8.1}$$

156

$$bias.rel.dev = \frac{1}{n}\sum_{i=1}^{n}\frac{y_{i,calc} - y_{i,\exp}}{y_{i,\exp}} \cdot 100\% \tag{8.2}$$

where n is the number of experimental points.

8.1 Molecular Parameters

In chapter 3 different equations of state were evaluated. In this chapter the ScRK-EOS and the CPA-EOS will be used to model non-electrolyte systems – and parameters for the models will be regressed to experimental data. For non-polar mixtures we often use the classical mixing rules – but for mixtures with polar components, we have to apply more accurate mixing rules. Such a mixing rule is the Huron-Vidal mixing rule as described in chapter 3. In this work the classical van der Waals one parameter classical mixing rule was used with the CPA-EOS, while the Huron-Vidal mixing rule with a temperature dependent NRTL-model (described later in this chapter) was used for the ScRK-EOS.

In the first part of this chapter the parameters used in the non-electrolyte part of the models will be given / fitted to experimental data. In the last part of the chapter the parameters related to the electrolyte terms in the models will be estimated.

8.1.1 Critical Data

Most equations of state need information about critical properties and acentric factors of all molecular components. The critical properties and the acentric factors used in this work are given in Table 8-1. The pure component critical data was taken from Perry (1998) and Chunxi et.al. (2000). These critical parameters are used in the ScRK-EOS. In the CPA-model the critical pressure and the acentric factor for polar components are not used directly in the model (because the a, b and m parameters are fitted to vapour pressure and density data).

Table 8-1 Pure component parameters used in the ScRK-EOS

Solvent	Water	MDEA	CO$_2$	Methane	Nitrogen
T$_c$ [K]	647.3	677.8	304.2	190.5	126.2
P$_c$ [bar]	220.9	38.76	73.76	45.39	33.94
ω	0.344	1.242	0.225	0.008	0.04
M [gr/mol]	18.01	119.16	44.01	16.04	28.01

8.1.2 Calculation of Pure Component Vapour Pressures

As we are working with systems of polar components – we know that a model that uses only critical data and the acentric factor – such as the SRK-EOS - is not able to represent the vapour pressures accurately (see chapter 3). The ScRK model as proposed by Schwartzentruber and Renon (1989) has three additional parameters in the attractive term of the EOS. The ScRK-EOS model uses three polar parameters (p_1, p_2, p_3), which are determined by fitting to pure component vapour pressure data,

$$\sqrt{\alpha(T_r)} = 1 + m(\omega)\left(1 - \sqrt{T_r}\right) - p_1\left(1 - T_r\right)\left(1 + p_2 T_r + p_3 T_r^2\right) \tag{8.3}$$

and

$$m(\omega) = 0.48508 + 1.5519\omega - 0.15613\omega^2 \tag{8.4}$$

For non-polar components the parameters p are set to zero.

A lot of experimental data are available for vapour pressures of the polar molecules CO_2, water and MDEA. In this work the experimental data of Noll et.al. (1998) for vapour pressures of MDEA and the data of Perry (1998) and Borgnakke (1997) for water and CO_2 were used to estimate these parameters. In Table 8-2 the results from fitting the parameters to vapour pressure data of water, CO_2, and MDEA are given. For methane and nitrogen the parameters in the ScRK-EOS were set to zero.

The objective function used in the parameter fitting procedure was

$$\chi^2 = \sum_{i=1}^{n} \left(\frac{P_{i,\exp}(T) - P_{bub}(T; p_1, p_2, p_3)}{\sigma_{i,\exp}} \right)^2 \tag{8.5}$$

The standard deviation was set to $P_{i,\exp}/100$ if no experimental uncertainty was specified in the reference.

Table 8-2 Pure component parameters used in the ScRK-EOS

Component	p_1	p_2	p_3	Temperature-range [K]	AAD [%]	Experimental Data Sources
Water	0.074	-0.945	-0.699	273-647	0.6	Perry (1998) Borgnakke (1997)
MDEA	0.521	-1.152	-0.014	293-402	5.0	Noll et.al.(1998)
CO$_2$	0.0246	-1.261	0	138-304	0.2	Perry (1998) Borgnakke (1997)
Methane	0	0	0	-	-	-
Nitrogen	0	0	0	-	-	-

The results of the ScRK-EOS are compared with experimental vapour pressure data of water and MDEA in Figure 8-1 and Figure 8-2. We see that the model is capable of representing the vapour pressure of pure components with high precision.

In the CPA-EOS the parameters a_{CPA}, b_{CPA}, m_{CPA}, ε^{AB} and β^{AB} are fitted to vapour pressure and density data of pure components. The 4C association scheme suggested by Yakoumis et.al. (1998) was used for water. The same association scheme was used for MDEA. CO_2 was assumed to have 2 association sites (association scheme 2B of Huang and Radosz, 1990). CO_2 was also modelled by setting the number of association sites to zero. In this case the CPA-EOS reduced to the classic SRK-EOS for calculating thermodynamic properties of CO_2.

In this work the CPA-model was only used to model aqueous strong electrolyte salt system. The CPA-EOS was not able to calculate the solubility of CO_2 in water over a large

temperature range (see chapter 3) – and was therefore not found suitable for calculating thermodynamic properties of mixtures of CO_2, MDEA and water.

Table 8-3 Pure component parameters used in the CPA-EOS

Solvent	Water	MDEA	CO$_2$
a_{CPA} [bar dm^6 mol^{-2}]	0.855	25.846	3.437
b_{CPA} [dm^3 mol^{-1}]	1.440	10.751	2.706
m_{CPA} [-]	1.224	1.364	0.805
ε^{AB} [bar dm^3 mol^{-1}]	162.01	120.00	50.00
β^{AB} [dm^3]	$8.71 \cdot 10^{-2}$	$5.41 \cdot 10^{-2}$	$1.16 \cdot 10^{-3}$
Association scheme	4C	4C	2B
T_r, range	0.4-0.9	0.4-0.9	0.4-0.9
AAD ΔP [%]	0.9	4.2	2.2
AAD $\Delta \rho$ [%]	1.2	1.1	1.9

The pure component parameters in the CPA-EOS were fitted to vapour pressures and densities of water, MDEA and CO_2. The objective function used to fit the CPA parameters was given in equation (7.21). The estimated parameters are given in Table 8-3. We see that accurate correlations are obtained for both liquid densities and vapour pressures. For non-polar components such as methane and nitrogen we would normally set the number of association sites to zero. In this case the CPA-EOS reduces to the SRK-EOS (we choose not to fit the a, b and m parameters).

The ability of equation of states to reproduce experimental vapour pressure- and density data was illustrated in Figure 3-1 to Figure 3-7 in chapter 3. The accuracy of the models was reported in Table 3-1. Generally we see that the ScRK-EOS is able to reproduce the vapour pressure of both polar and non-polar components with a high precession. The calculation of liquid densities is generally erroneous using the ScRK-EOS. The CPA-EOS is able to reproduce both vapour pressure and density data of polar components with a good precision.
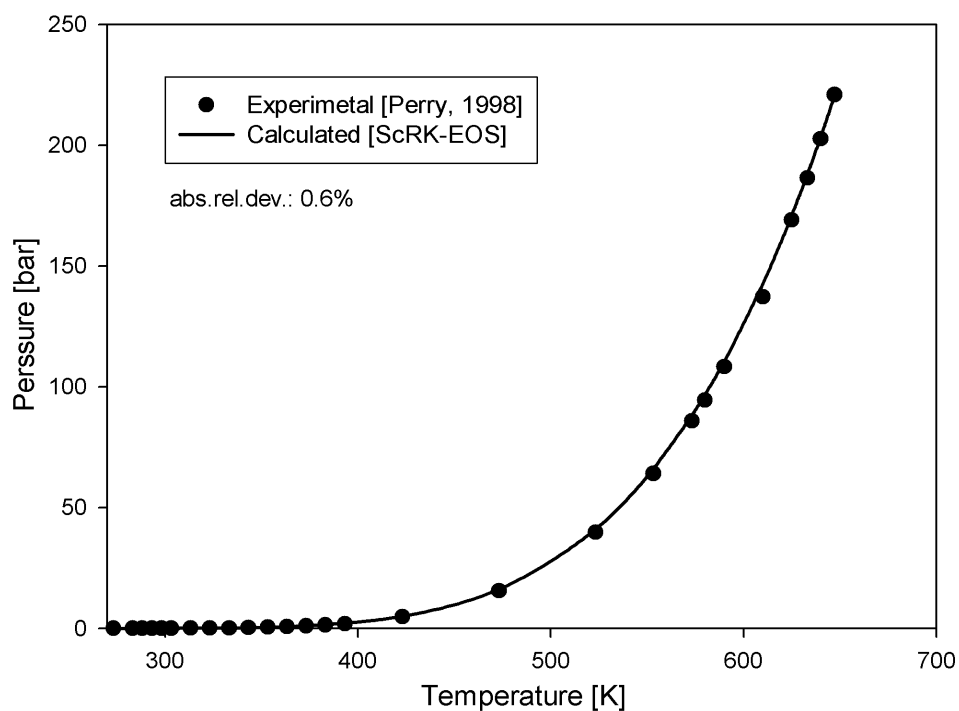
Figure 8-1 The ScRK-EOS fitted to experimental vapour pressures of water.
Script: bubp.py, p. 305.
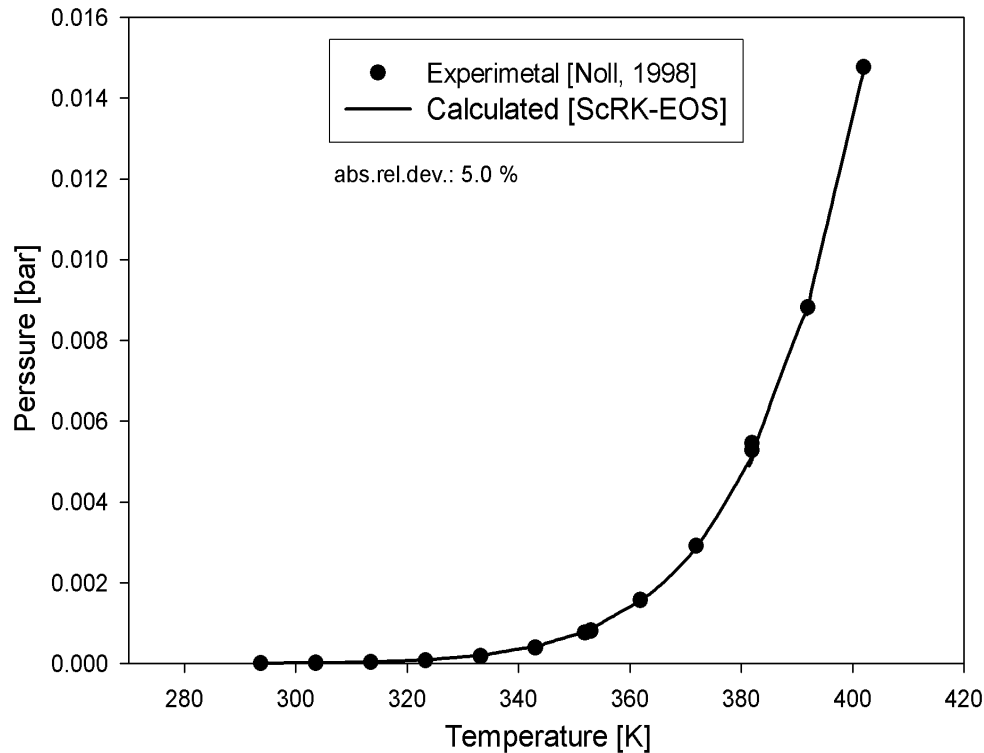
Figure 8-2 The ScRK-EOS fitted to experimental vapour pressures of MDEA
Script: bubp.py, p. 305.

8.2 Fitting of Binary Interaction Parameters

When we are working with mixtures, we need mixing rules in our equations of state. For ideal mixtures such as light hydrocarbons classical mixing rules are sufficient, but for mixtures of non-ideal components such as water and MDEA we need more accurate and flexible mixing rules. Such a mixing rule is the Huron and Vidal mixing rule (1979) as was introduced in chapter 3.

An advantage of using the Huron-Vidal mixing rule is that some commercial simulation packages such as PVTsim from Calsep use this mixing rule as standard – so that parameters for many molecular components are available. Another advantage is that the mixing rule can easily be reduced to the classical for non-polar components (see chapter 3).

8.2.1 The Huron-Vidal NRTL Interaction Coefficients

The calculations of the attractive parameters of the short-range term of the ScRK-EOS of the equation of state involve various parameters, which depend on the mixing rule chosen. In this work we used the mixing rule proposed by Huron and Vidal (1979) with temperature dependent interaction coefficients.

For binary pairs of components of which at least one is polar, the classical mixing rules are often insufficient. The Huron-Vidal attractive parameter mixing rule takes the form

$$a = b \left(\sum_{i=1}^{N} \left(z_i \frac{a_i}{b_i} \right) - \frac{G_\infty^E}{\ln 2} \right) \tag{8.6}$$

where G_∞^E is the excess Gibbs energy at infinite pressure. G_∞^E is found using a modified NRTL mixing rule

$$\frac{G_\infty^E}{RT} = \sum_{i=1}^{N} z_i \frac{\displaystyle\sum_{j=1}^{N} \tau_{ji} b_j z_j \exp(-\alpha_{ji} \tau_{ji})}{\displaystyle\sum_{k=1}^{N} b_k z_k \exp(-\alpha_{ki} \tau_{ki})} \tag{8.7}$$

where α_{ji} is a non-randomness parameter, i.e. a parameter for taking into account that the mole fraction of molecules of type i around a molecule of type j may deviate from the overall mole fraction of molecules of type i in the mixture. When α_{ji} is zero, the mixture is completely random. The τ - parameter is defined by the following expression

$$\tau_{ji} = \frac{g_{ji} - g_{ii}}{RT} \tag{8.8}$$

where g_{ji} is an energy parameter characteristic of the j-i interaction. The g-parameters are temperature dependent and given by the expression

$$g_{ji} - g_{ii} = \left(g_{ji}' - g_{ii}' \right) + T \left(g_{ji}'' - g_{ii}'' \right) \tag{8.9}$$

The parameter b entering into the expression for G_∞^E is the b-parameter of the SRK-equation. The classical mixing rule is still used for the b-parameter (see chapter 3).

For a binary pair, which can be described using the classical mixing rule, the local composition will not deviate from the overall composition, i.e. α_{ji} should be chosen equal to zero. By further selecting the following expressions for the interaction energy parameters

$$g_{ii} = -\frac{a_i}{b_i}\ln 2$$

$$g_{ji} = -2\frac{\sqrt{b_i b_j}}{b_i + b_j}\left(g_{ii}\ g_{jj}\right)^{0.5}\left(1 - k_{ij}\right)$$

(8.10)

the Huron-Vidal mixing rule reduces to the classical one. When the Huron-Vidal mixing rule is used, the latter expressions are therefore used for g_{ji} and g_{ii} of binary pairs, which do not require the advanced mixing rule.

8.2.2 Regression of Huron-Vidal Parameters

The binary interaction parameters needed in the Huron-Vidal mixing rule (g'_{ji}, g'_{ii}, g''_{ji}, g''_{ji} and α_{ij}) for mixtures of methane, nitrogen, CO_2, water and MDEA were fitted to available experimental data from the literature (Table 8-4). Five binary parameters were fitted for each molecular pair. The accuracy of the fit and the parameters found are reported in Table 8-5 and Table 8-6. The merit function used for parameter fitting to solubility data was

$$\chi^2 = \sum_{i=1}^{n}\left(\frac{x_{i,\exp} - x_{calc}(T,P)}{\sigma_{i,\exp}}\right)^2 + \sum_{j=1}^{m}\left(\frac{y_{i,\exp} - y_{calc}(T,P)}{\sigma_{j,\exp}}\right)^2$$

(8.11)

where n is the number of experimental gas solubility data in water and m is the number of experimental points for water in gas.

A literature search was performed to collect available mutual solubility data for gasses (methane, CO_2 and nitrogen) and water. Large amount of data for the systems methane-water and CO_2-water are published. Less experimental data were available for nitrogen-water systems. The experimental data used for parameter regression are referred in Table 8-4.

The binary interaction parameters for CO_2 and water systems were found by fitting parameters to solubility data of CO_2 in water and water in CO_2. The parameters were regressed to large amounts of the published mutual solubility data for CO_2 and water (a total of 222 data points) in the temperature range 289-533 K and pressure range 6.9-1500 bar. The ScRK-EOS was able to correlate all data with a good precision. An absolute average deviation of 6.1% for the solubility of CO_2 in liquid water was achieved, while a deviation of 10.6% for the solubility of water in gaseous CO_2 was obtained. The predictability of the model was evaluated by comparing to the experimental solubility data for CO_2 in water of Houghton et.al. (1957). The calculated solubility is compared to experimental values in Figure 8-3. The absolute average deviation between the model and experimental data was 2.5%, which shows that the predictions done with the model are good.

Following Chang's remark (Chang, Posey and Rochelle, 1993) the representation of gas solubility of CO_2 at low loadings is sensitive to the value of binary water-MDEA interaction parameters. Two types of data concerning the binary water and MDEA system have been obtained in the open literature: the first concerns total equilibrium pressures and is mainly restricted to intermediate and high temperatures and to concentrated MDEA aqueous solutions; the second one is related to water activity as deduced from the measuring of freezing point and is available at low temperatures and for dilute MDEA aqueous solutions. Consequently the combination of the reported water activity with these two methods covers a wide range of temperatures and MDEA concentrations with reliable precision. The binary ScRK-EOS Huron-Vidal interaction parameters for MDEA and water were fitted to the available activity coefficients for MDEA in water and water in MDEA over a large temperature range. The experimental data could be represented with an absolute average deviation of 2.3%. Examples of calculated activity coefficients of MDEA and water are given in Figure 8-5. In Figure 8-6 the model is compared to experimental values for freezing point depression in MDEA-water solutions.

The binary interaction parameters for methane and water were fitted to available mutual solubility data. A total of 400 experimental data points in the temperature range 274-589K and pressure range 3.5-689 bar were used for regression. References to the experimental data used and the parameters found are reported in Table 8-4 and Table 8-5. The experimental data could be represented by the ScRK-EOS with the Huron-Vidal mixing rule with an absolute average deviation of 7.6% (all points). An absolute average deviation of 5% was obtained for the solubility of methane in water while a deviation of 10.6% was achieved for the water solubility in the gaseous methane. The predictability of the model was tested by comparing to the experimental solubility data for methane in water of Culberson et.al. (1951). These data could be represented with an absolute average deviation of 5%. The calculated solubility is compared to experimental values in Figure 8-4.

Parameter regression was done to the nitrogen-water system. Less experimental data were available, and a somewhat larger average deviation between model and experiments were obtained (7.2% for nitrogen in water and 17.6% for water in nitrogen).

Table 8-4 Pressure and temperature intervals for experimental values used for parameter fitting

Gas	Solubility type	References	Min P [bar]	Max P [bar]	Min T [K]	Max T [K]	No. of points
Nitrogen	N_2 in H_2O	12	3.4	137.9	311	589	16
	H_2O in N_2	4,12,13	3.4	137.9	250	589	81
Methane	CH_4 in H_2O	1,3,6-8,14	3.5	689	274	589	181
	H_2O in CH_4	1-6,8,9,15	5	689	253	589	219
CO_2	CO_2 in H_2O	1,11	6.9	1500	289	533	100
	H_2O in CO_2	1,11,16	6.9	1500	289	533	122

References:

1.   Gillespie Paul, Wilson Grant. Vapor-Liquid and Liquid-Liquid Equilibria:Water-Methane,Water-Carbon Dioxide, Water-Hydrogen Sulfide, Water-nPentane, Water-Methane-nPentane. Research Report RR-48. 1982.

2.   Olds R., Sage B. and Lacey W. Phase Equilibria in Hydrocarbon Systems: Composition of the Dew-Point Gas of the Methane-Water System. Industrial and Engineering Chemistry. 1942; 34(10):1223-1227.

3.   Yarim-Agaev et al. Zhurnal Prikladnor Khimii. 1985; 58:165-168.

4.   Rigby M. and Prausnitz J.M. Solubility of Water in Compressed Nitrogen, Argon and Methane. The Journal of Physical Chemistry. 1968; 72(1):330-334.

5.   Yokoyama C., Wakana S. Kaminishi G. and Takahashi S. Vapor-Liquid Equilibria in the Methane-Diethylene Glycol-Water System at 298.5 and 323.15 K. J. Chem. Eng. Data. 1988; 33:274-276.

6.   Althaus Klaus. Messung und Berechnung von Wassergehalten kohlenwasserstoffhaltiger Gasgemische. Düsseldorf: 1999.

7.   Lekvam, Knut and Bishnoi, P. Raj. Dissolution of methane in water at low temperatures and intermediate pressures . Fluid Phase Equilib. 1997; 131(1-2):297-309. ISSN: 0378-3812.

8.   Crovetto R., Fernandez-Prini R. and Maria Laura Japas. Solubilities of inert gases and methane in H2o and in D2O in the temperature range of 300 to 600 K. J. Chem. Phys. 1982; 76(2):1077-1086.

9.   Sharma S.C. Equilibrium Water Content of Gaseous Mixtures: The University of Oklahoma; 1969.

10.   Culberson O., McKetta J. The solubility of methane in water at pressures to 10000 psia. Petrol. Trans. AIME. 1951; 192:223-226.

11.   Takenouchi S. and Kennedy G. The binary system H2O-CO2 at High Temperatures and Pressures. American Journal of Science. 1964; 262:1055-1074.

12.   Gillespie Paul, Wilson Grant. Vapor-Liquid Equilibrium Data on Water-Substitute Gas Components: N2-H2O, H2-H2O, CO-H2O, H2-CO-H2O, and H2S-H2O. Research Report RR-41. 1980.

13.   Blanco S., Avila S. Velasco I. Rauzy E. and Otin S. Water dew points of binary nitrogen+water and propane+water mixtures. Measurements and correlation. Fluid Phase Equilibria. 1999; 161:107-117.

14.   Davis E., McKetta J. Solubility of methane in water. Petrol. Ref. 1960:205-206.

15.   Kosyakov N., Ivenka B. Krishtopa P. Solubility of moisture in compressed argon, methane, and helium at low temperatures. Russian Journal of Applied Chemistry. 1979; 52(4):922-923.

16.   Coan C.R., and King A. D. Solubility of water in compressed carbon dioxide, nitrous oxide and ethane. Evidence for hydration of carbon dioxide and nitrous oxide in the gas phase. J. Am. Chem. Soc. 1971; 93:1857.

Table 8-5 ScRK-EOS Huron Vidal interaction parameters for binary mixtures

Binary pair	$\left(g_{12}^{'} - g_{22}^{'}\right)/R(K)$	$\left(g_{21}^{'} - g_{11}^{'}\right)/R(K)$	$\left(g_{12}^{''} - g_{22}^{''}\right)/R(K)$	$\left(g_{21}^{''} - g_{11}^{''}\right)/R(K)$	α_{ij}
CO$_2$-Water	3626	-2241	3.91	-3.16	0.03
Methane-Water	4875	-123.6	-6.55	2.14	0.15
Nitrogen-Water	4898	-112	-8.0	4.92	0.08
MDEA-Water	-1461	1201	5.89	-7.24	0.21

Table 8-6 Absolute average percentage deviations on fitted sets

Gas	Solubility type	No. of points used for fitting	Abs.avg. dev. ScRK-HV [%]
Nitrogen	N$_2$ in H$_2$O	13	7.2
	H$_2$O in N$_2$	78	17.6
Methane	CH$_4$ in H$_2$O	176	5.0
	H$_2$O in CH$_4$	215	10.6
CO$_2$	CO$_2$ in H$_2$O	43	5.8
	H$_2$O in CO$_2$	57	10.6

The interactions between non-polar components – were modelled using the classic Van der Waals one-parameter mixing rule. Because the Huron Vidal mixing rule is reduced to the classical Van der Waals mixing rule for specific choice of NRTL parameters. Such interactions are straight forward to implement in the mathmatical model. The interaction parameters used for non-polar components were taken from Prausnitz et.al. (1999) and Reid et.al. (1988). The interactions coefficients used in this work are given in Table 8-7.

Table 8-7 Interaction parameter used for simple interactions (HV reduced to classic mixing rule)

Binary pair	k$_{ij}$	Ref.
Methane-CO$_2$	0.12	Prausnitz et.al. (1999) Reid et.al. (1988)
CO$_2$-MDEA	0.2	Guessed
CO$_2$-Nitrogen	0.11	Prausnitz et.al. (1999) Reid et.al. (1988)
Methane-Nitrogen	0.02	Prausnitz et.al. (1999) Reid et.al. (1988)

From the data regression performed, we can see that the mutual solubility of methane, CO$_2$, and nitrogen in water can be predicted with a good accuracy using the ScRK-EOS with the Huron-Vidal mixing rule. This is in contrast to the classical mixing rule that is generally not able to predict mutual solubility of dissimilar pair of components. The activity coefficient of

binary mixtures of water and MDEA could be represented with a high accuracy with the Huron-Vidal mixing rule.

It is important to be aware of the relatively large number of binary interaction parameters used in the Huron Vidal mixing rule used here (5 parameters). A NRTL-GE model with temperature independent interaction coefficients has 3 parameters, but is not able to correlate the mutual solubility of gasses in water over large temperature ranges. The most promising model with respect to few binary interaction parameters is the CPA-model with a one-parameter classical mixing rule. This model was introduced in chapter 3, and parameters are fitted in the following section.
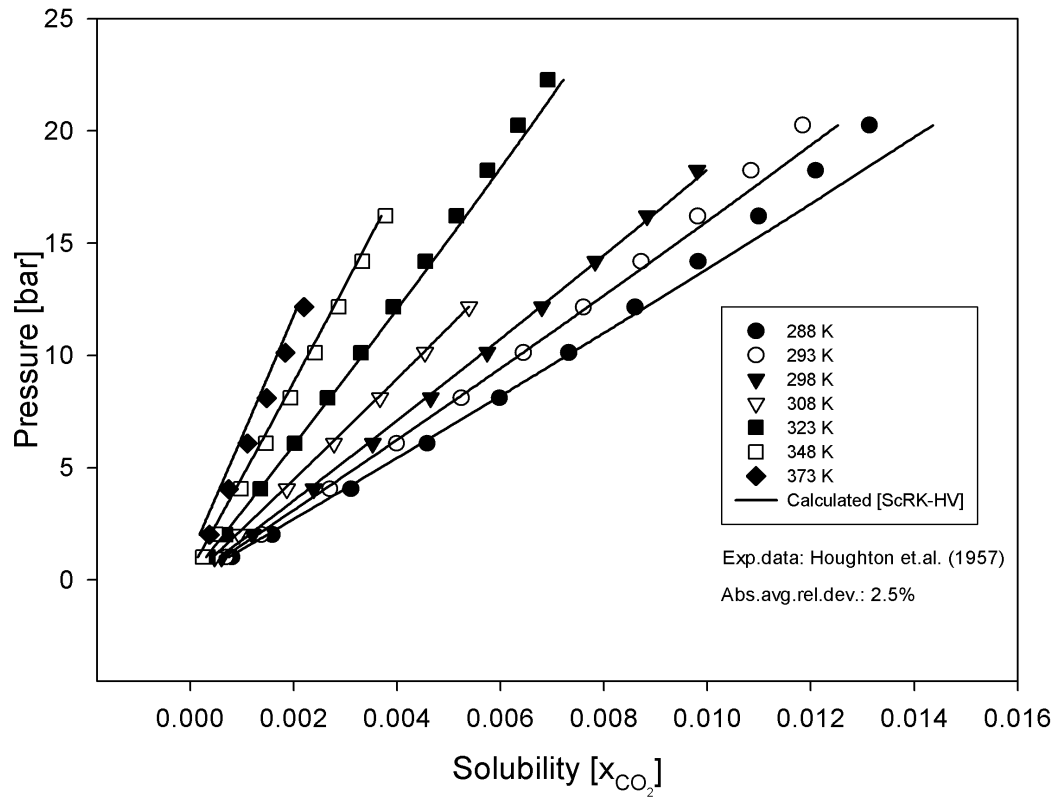
Figure 8-3 Predictions of the solubility of CO₂ in water calculated with the ScRK-EoS with the Huron-Vidal mixing rule. *Script: TPflash.py, p. 306.*
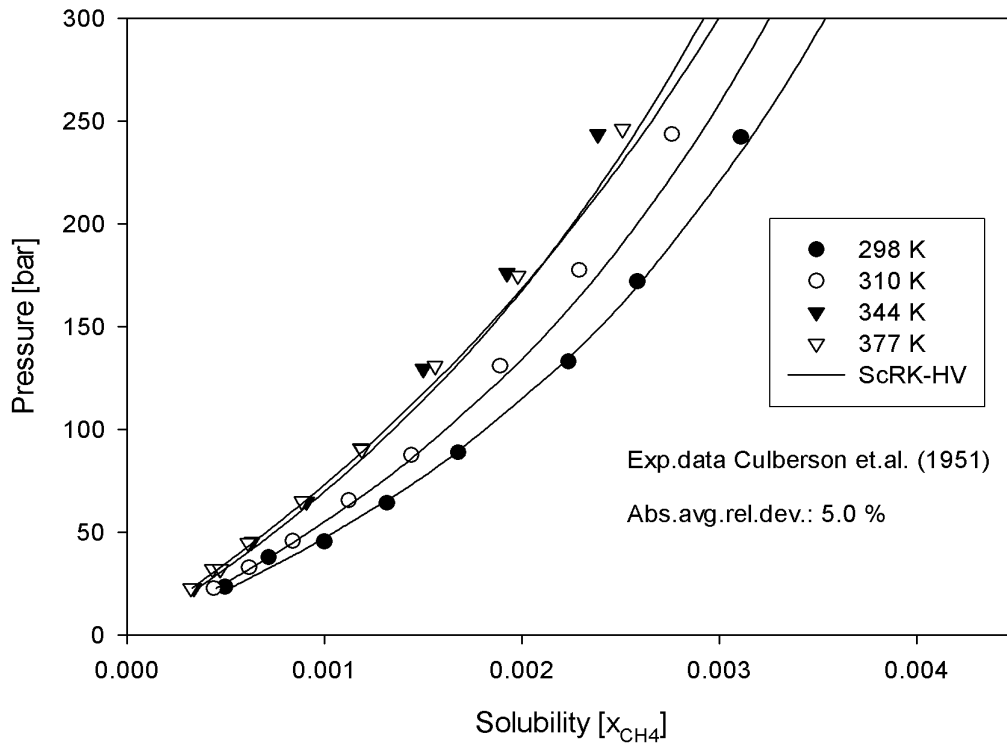
Figure 8-4 Predictions of the solubility of methane in water calculated with the ScRK-EoS with the Huron-Vidal mixing rule. *Script: TPflash.py, p. 306.*
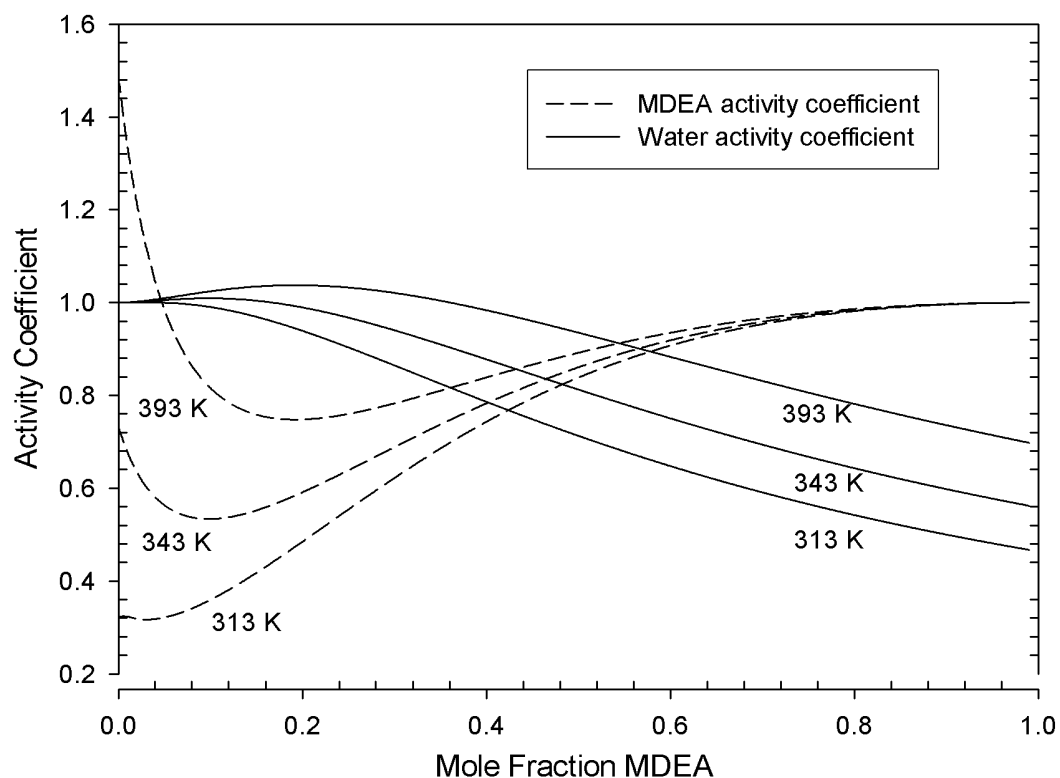
Figure 8-5 Activity coefficients (symmetric) of MDEA and water calculated with the ScRK-EOS with the Huron-Vidal mixing rule. *Script: activityCalc.py, p. 313.*
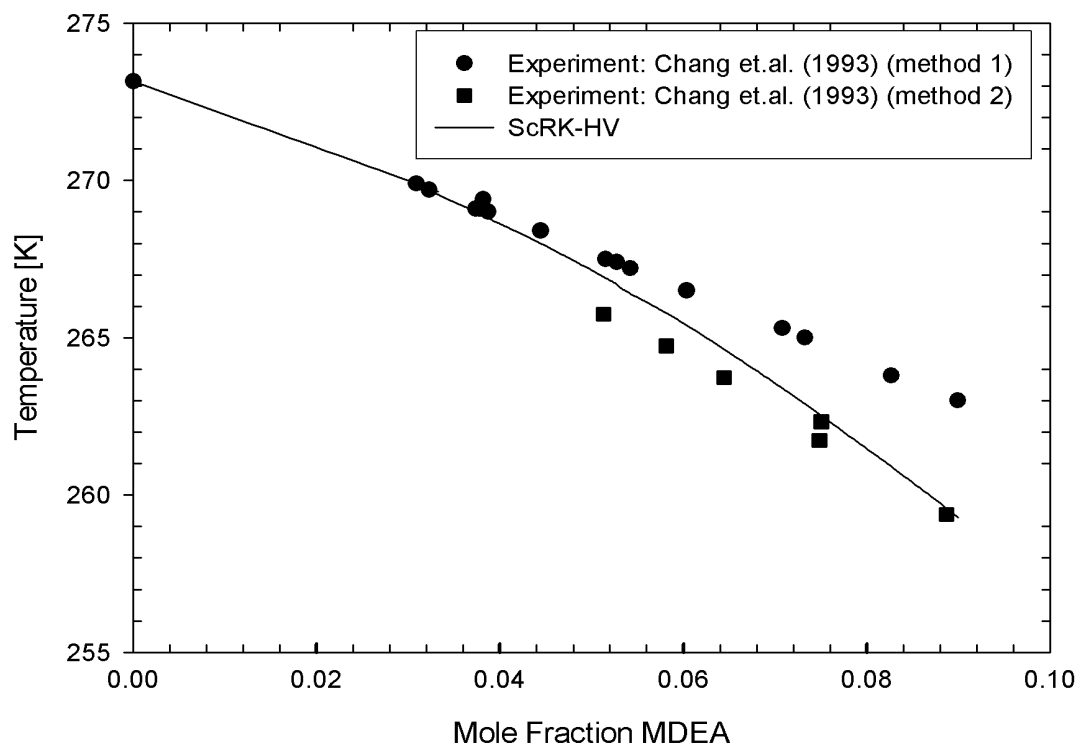
Figure 8-6 Experimental and calculated freezing points for a water-MDEA solution using the ScRK-EOS with the Huron Vidal mixing rule. *Script: freeze.py, p. 314.*

From Figure 8-3 to Figure 8-6 we see that the ScRK-EOS with Huron-Vidal mixing rules is a flexible model that is capable of representing the experimental data of the non-ideal systems considered here with a high precession.

8.2.3 Regression of CPA Interaction Parameters

The experimental data for mutual solubility of gasses and water described in Table 8-3 were used to regress binary CPA-interaction coefficients. The gaseous components (methane, nitrogen, ethane and propane) were modelled using the classical SRK-EoS (no cross association). Two different methods for representing thermodynamic properties of CO_2 were tested for the modelling of the mutual solubility in CO_2-water systems. In the first method CO_2 is represented by the CPA-EOS with two association sites (scheme 2B). In the second method CO_2 is modelled without association (reduces to classic SRK- and PR-EOS). The results from the regression are given in Table 8-8 and Table 8-9. Regression of interaction coefficients for ethane and propane with water was done in addition to the interactions considered earlier. Figure 8-7 illustrates a typical result from the correlation of experimental mutual solubility data (Kobayashi et.al., 1953) of propane and water.

Two different versions of the CPA-EoS were used. The first was based on the SRK-EoS while the other was based on the PR-EoS. The results from the data correlation using the SRK and the PR based versions of the CPA-EOS are given in Table 8-8 and Table 8-9. Because we use the classical one-parameter mixing rule, only one binary interaction parameter was fitted to the mutual solubility data.

Table 8-8: CPA interaction parameters for binary mixtures of water and the indicated second component. Average deviation of calculated mutual solubility (gas in water and water in gas) indicated in the right column.

Second component		k_{ij}	abs.avg.rel.dev[1]. [%]
CH$_4$	CPA-SRK	0.037	**20.7**
	CPA-PR	0.161	21.9
N$_2$	CPA-SRK	-0.010	**16.4**
	CPA-PR	0.241	19.4
CO$_2$ (association scheme 2B)	CPA-SRK	-0.052	**18.5**
	CPA-PR	0.014	20.6
CO$_2$ (no association)	CPA-SRK	-0.052	**18.5**
	CPA-PR	0.014	20.6
C$_2$H$_6$	CPA-SRK	0.055	**16.6**
	CPA-PR	0,133	18.2
C$_3$H$_8$	CPA-SRK	0.012	**14.3**
	CPA-PR	0,123	16.2

---

[1] Deviation (%) = 100 x (experimental-calculated)/experimental

Table 8-9: Absolute average percentage deviations on fitted set. The experimental data sources are the same as presented in Table 8-4.

| Gas		No.points used for fitting	%abs.avg. dev. CPA-SRK	%bias.avg. dev. CPA-SRK	%abs.avg. dev. CPA-PR	%bias.avg. dev. CPA-PR
N_2	N_2 in H_2O	13	**29.7**	-0.34	31.1	-21.3
	H_2O in N_2	78	28.2	26.3	**25.5**	22.4
CH_4	CH_4 in H_2O	176	**31.8**	2.0	35.5	2.1
	H_2O in CH_4	215	**14.1**	3.9	14.3	-0.1
CO_2[1]	CO_2 in H_2O	43	**12.0**	-0.2	17.5	-0.8
	H_2O in CO_2	57	**22.5**	-22.5	22.7	-22.7
CO_2[2]	CO_2 in H_2O	43	**12.0**	-0.2	17.5	-0.8
	H_2O in CO_2	57	**22.5**	-22.5	22.7	-22.7
C_2H_6	C_2H_6 in H_2O	38	**29.6**	-0.6	32.1	-12.0
	H_2O in C_2H_6	59	**23.4**	5.7	28.2	-0.8
C_3H_8	C_3H_8 in H_2O	142	**24.6**	-8.7	28.6	-6.7
	H_2O in C_3H_8	161	10.6	6.8	**10.4**	5.5

[1] CO_2 modelled using association scheme 2B
[2] CO_2 modelled without association

From table Table 8-9 we see that the correlation generally is less accurate then what we obtained using the ScRK-EOS with the Huron Vidal mixing rule. This is not surprising since the number of binary interaction parameters is reduced from five to one. The CPA-EOS based on the Soave Redlich Kwing model gives on average slightly better results than the version based on the Peng Robinson EOS.

The average deviation of the correlated CO_2 solubility in water is 12% (w/wo association modelling for CO_2) - which is too high to be useful for further modelling of CO_2-water-amine systems.

Generally, we see that the water solubility in the gaseous phase is correlated more accurate than the hydrocarbon content in the aqueous phase. The reason for this is probably that the SAFT-type of thermodynamic models (including the CPA-model) are not considering the hydrophobic effect, and are thus not able to predict the solubility of hydrocarbons accurate (Wu and Prausnitz, 1998). Further work should be done on representing the hydrophobic effect in water-hydrocarbon systems.
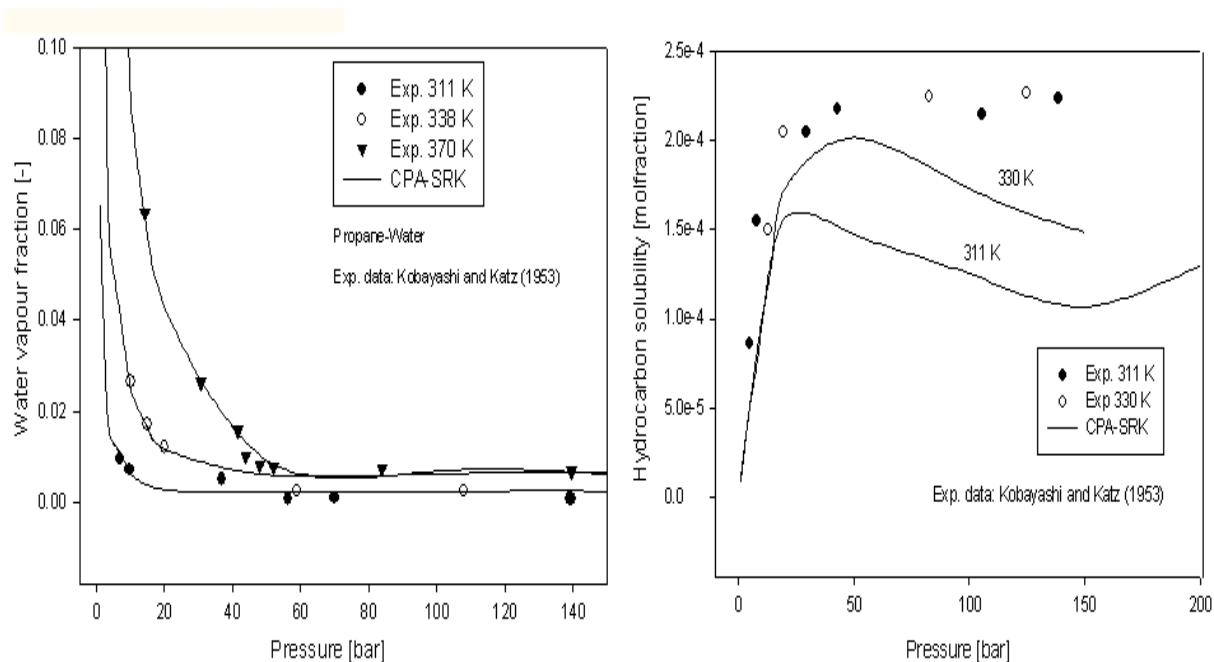
Figure 8-7 Correlation of the mutual solubility of propane and water using the CPA-EoS.
Script: TPflash.py, p. 306

8.3 Fitting of Ionic Parameters

In the electrolyte ScRK-EOS and CPA-EOS three terms specific to ions were added to the non-electrolyte model. The ionic terms were respectively a short range ionic term, a long range ionic term and the Born term. These ionic terms introduces new pure- and binary component parameters that we need to fit to experimental data.

Important parameters in the ionic terms of the electrolyte equations of state are ionic and molecular diameters, the dielectric constant, the ionic interaction coefficients W_{ij} and the shielding parameter in the electrolyte MSA term.

Furst and Renon (1993) suggested correlating the ionic interaction coefficients W_{ij} to the cationic Stokes- and the anionic Pauling diameter. In this way they obtained a fully predictive model. This was also done in this work – and the relationships between ionic diameters and the interaction coefficients were fitted to experimental measured osmotic coefficients of aqueous salt solutions.

8.3.1 Molecular and Ionic Diameters

The molecular and ionic diameters are needed in the short-range ionic term in the electrolyte equation of state (equation (3.97)). The diameters we use for molecular components are the Lennard-Jones diameters reported in literature. For many of the most common molecular components these molecular diameters are given by Reid et.al (1988), but as in the case of the MDEA no values were published. The molecular diameter of MDEA was estimated from the equation

$$\sigma_{MDEA} = \sigma_{H_2O} \left(\frac{b_{MDEA}}{b_{H_2O}} \right)^{1/3} = 4.5 \times 10^{-10} \ m \qquad (8.12)$$

considering that both covolume and diameter reflect the molecular size, the usual SRK-EOS formulation being used for the calculation of the MDEA covolume. This was also done by Chunxi et.al. (2000). The molecular diameters used in this work are presented in Table 8-10.

Table 8-10 Molecular diameters used in the electrolyte equation of state

Component	σ $[10^{-10}m]$	Ref.
CO$_2$	2.34	Reid et.al (1988)
Methane	2.52	Reid et.al (1988)
Water	2.52	Reid et.al (1988)
MDEA	4.50	Equation (8.12)
Nitrogen	2.30	Reid et.al (1988)

For ionic compounds, the diameters are deduced from the values of the ionic covolumes b_i by the relation

$$\sigma_i = \sqrt[3]{\frac{6b_i}{N\pi}} \qquad (8.13)$$

The ionic covolumes are calculated from the equations proposed by Furst and Renon (1993)

$$b_c = \lambda_1 \left(\sigma_c^S \right)^3 + \lambda_2$$
$$b_a = \lambda_1 \left(\sigma_a^P \right)^3 + \lambda_2 \qquad (8.14)$$

where subscript a means anion and c cation. σ^S and σ^P are the Stokes- and the Pauling diameter. Furthermore the interaction parameters between cations and water (W_{cw}) and between cations and anions (W_{ca}) can been related to σ_c^S and σ_a^P by

$$W_{cw} = \lambda_3 \sigma_c^S + \lambda_4$$
$$W_{ca} = \lambda_5 \left(\sigma_c^S + \sigma_a^P \right)^4 + \lambda_6 \qquad (8.15)$$

Using these relationships the electrolyte equation of state is fully predictive – and no ionic interaction coefficients are needed. An important step is to estimate the values of the coefficients λ. Furst and Renon (1993) fit these coefficients to osmotic coefficient data, and the same procedure was followed in this work.

In this work the cationic Stokes diameter of MDEA$^+$ was set equal to the molecular diameter of MDEA (4.50Å). The anionic Pauling diameter of HCO$_3^-$ is 3.36 Å.

8.3.2 Fitting of Pure Component Ionic Parameters

The ionic parameters in the Furst and Renon model are λ_1-λ_6. In their original paper Furst and Renon (1993) fitted these parameters to 28 aqueous strong electrolytes (halides). The same experimental data (Robinson and Stokes, 1952) were used for data regression in this work. The six ionic parameters were refitted to experimental osmotic coefficient data of 28 different strong electrolyte solutions. Because we use different terms for the molecular interactions in the electrolyte ScRK-EOS and the electrolyte CPA-EOS – we will get different values for the ionic coefficients. The ionic parameters were fitted for both the electrolyte ScRK-EOS and the CPA-EOS model. The osmotic coefficients for the 28 salt systems considered could be calculated with an absolute average deviation of 2.1% for the electrolyte ScRK-EOS and an average deviation of 2.3% with the electrolyte-CPA model. The experimental electrolyte systems used, average deviations and the regressed values for the parameters are given in Table 8-11 and Table 8-12.

The merit function used for data regression was

$$\chi^2 = \sum_{j=1}^{n} \left(\frac{\phi_{\exp,j} - \phi_{calc}\left(T,P,m_j\right)}{\sigma_{\exp,j}} \right)^2 \tag{8.16}$$

where ϕ is the osmotic coefficient and m the molal salt concentration. The model is not fitted to experimental activity coefficient data, and the calculated mean ionic activity coefficients are therefore predicted. The standard deviation was set to $\phi/100$ for all experimental points.

Table 8-11 Comparison of electrolyte ScRK-EOS and CPA-EOS for Representation of Osmotic Coefficients of Halide Solutions. Data of Robinson et.al. (1952).

Electrolyte	Molality Range	abs.avg.dev [%] (Electrolyte ScRK-EOS)	abs.avg.dev [%] (Electrolyte CPA)
NH_4Cl	0.1 - 6.0	1.5	1.7
LiCl	0.1 - 6.0	1.4	1.3
LiBr	0.1 - 6.0	0.8	0.9
LiI	0.1 – 3.0	1.3	1.4
NaCl	0.1 – 6.0	1.8	1.8
NaBr	0.1 – 4.0	0.8	0.8
NaI	0.1 – 3.5	0.8	0.9
KCl	0.1 – 4.5	2.0	2.0
KBr	0.1 – 5.5	2.1	2.2
KI	0.1 – 4.5	2.7	2.7
RbCl	0.1 – 5.0	2.0	2.0
RbBr	0.1 – 5.0	0.3	0.3
RbI	0.1 – 5.0	1.7	1.8
CsCl	0.1 – 6.0	1.3	1.5
CsBr	0.1 – 5.0	3.6	3.2
CsI	0.1 – 3.0	5.5	4.9
$MgCl_2$	0.1 – 3.0	2.8	2.9
$MgBr_2$	0.1 – 3.0	1.3	1.5
MgI_2	0.1 – 3.0	1.1	1.0
$CaCl_2$	0.1 – 3.0	1.3	1.6

Electrolyte	Molality Range	abs.avg.dev [%] (Electrolyte ScRK-EOS)	abs.avg.dev [%] (Electrolyte CPA)
$CaBr_2$	0.1 – 3.0	4.9	5.0
CaI_2	0.1 – 2.0	3.9	3.7
$SrCl_2$	0.1 – 4.0	5.2	5.0
$SrBr_2$	0.1 – 2.0	1.7	1.6
SrI_2	0.1 – 2.0	1.3	1.3
$BaCl_2$	0.1 - 1.8	1.3	1.3
$BaBr_2$	0.1 – 2.0	2.1	1.9
BaI_2	0.1 – 2.0	2.3	2.4
Average		**2.1**	**2.3**

Table 8-12 Values of the ionic coefficient fitted to osmotic coefficients of the 28 halide salt systems

Parameter	Value el. ScRK-EOS	Value el. CPA-EOS
λ_1	$1.117 \cdot 10^{-7}$	$1.609 \cdot 10^{-7}$
λ_2	$5.377 \cdot 10^{-6}$	$3.005 \cdot 10^{-6}$
λ_3	$6.992 \cdot 10^{-5}$	$3.815 \cdot 10^{-5}$
λ_4	$4.398 \cdot 10^{-6}$	$1.219 \cdot 10^{5}$
λ_5	$-6.060 \cdot 10^{-8}$	$-3.910 \cdot 10^{-8}$
λ_6	$-2.180 \cdot 10^{-5}$	$2.610 \cdot 10^{-8}$

The absolute average deviation of the ScRK and the CPA is nearly equal to the deviation obtained by Furst and Renon (1993) – and comparable to other electrolyte models. It is however important to note that the present model will be predictive if we know the ionic diameters of the salt ions. The ionic parameters λ_3-λ_6 are solvent dependent – and must in general be fitted to ionic solutions in the actual solvent.

In Figure 8-8 and Figure 8-9 the calculated osmotic- and activity coefficients of selected salt systems (LiCl, NaCl, $SrBr_2$, SrI) are compared to experimental data. A good accuracy is obtained for all salts considered here. Even the predicted mean activity coefficients can be represented with a good accuracy as can be seen from Figure 8-9. We thus conclude that the models are capable of representing thermodynamic properties of electrolyte solutions with an acceptable precision. Thermodynamic properties of new aqueous salt solutions can be predicted by knowledge of ionic Sokes and Pauling diameters.
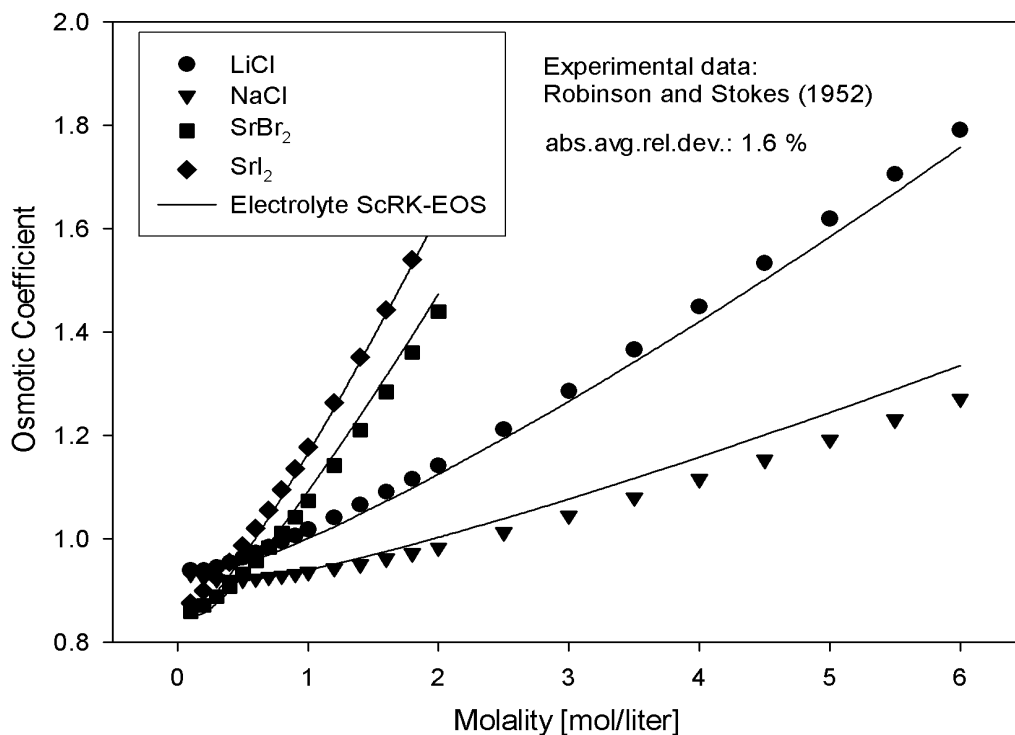
Figure 8-8 Calculation of osmotic coefficients of salt solutions using the electrolyte ScRK-EOS.
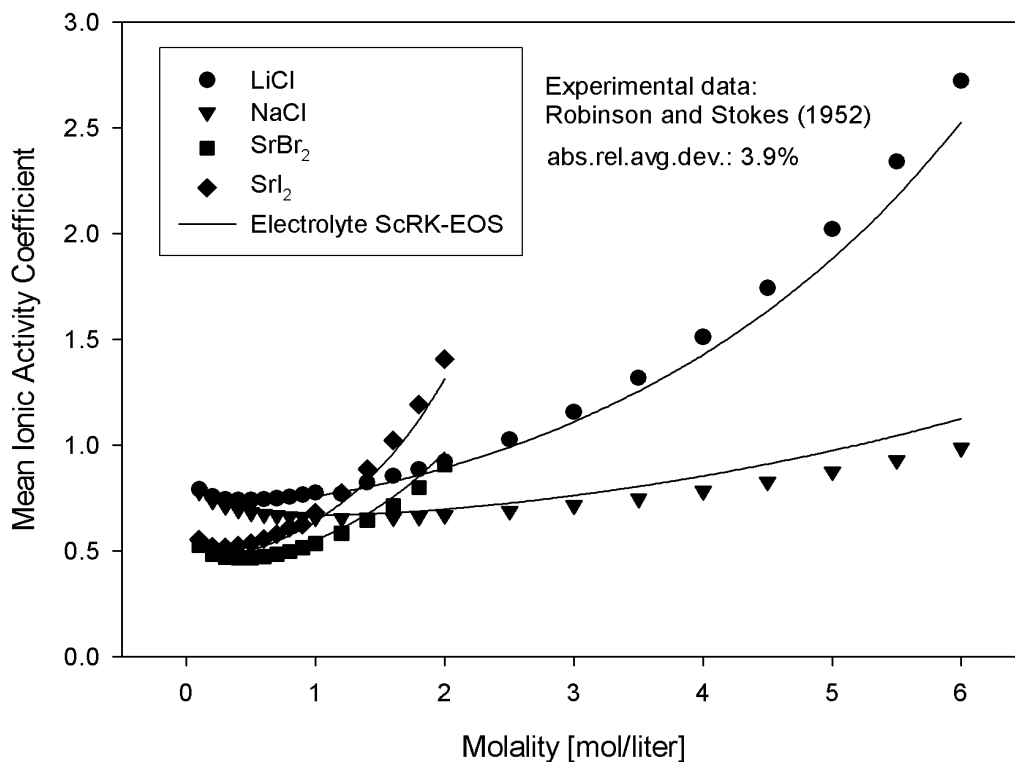*Script: electrolyte.py, p. 307.*

Figure 8-9 Calculation of mean ionic activity coefficients of salt solutions using the electrolyte ScRK-EOS.
Script: electrolyte.py, p. 307.

From Figure 8-8 and Figure 8-9 and Table 8-11 we see that the electrolyte ScRK-EOS and CPA-EOS are able to represent the experimental data with a good accuracy. The liquid densities are more accurately calculated with the electrolyte CPA-EOS model, but by introducing a volume correction in the ScRK-EOS the liquid density can be calculated with an acceptable accuracy also with this model. This was illustrated in Figure 3-18 for a NaCl-solution.

The mean ionic activity coefficients could be calculated with a high accuracy for all the salt systems considered. Figure 8-9 gives a typical illustration of the deviation between experimental ionic activity coefficient data and the model for some selected salts.

Electrolyte thermodynamic models have a wide applicability related to natural gas processing operations. The electrolyte model developed could e.g. been used for predicting scale precipitation in natural gas systems. The model can easily be extended to mixed solvent systems – and could e.g. be used for modelling salt precipitation in natural gas systems where glycol is used as hydrate inhibitor.

8.3.3 Prediction of Pure Component Dielectric Constants

As we are working with electrolyte systems, the dielectric constant D of the electrolyte solution must be introduced in the ionic long-range term of the models. The pure solvent dielectric constant was assumed to have the following temperature dependence

$$D_n = d^{(0)} + \frac{d^{(1)}}{T} + d^{(2)}T + d^{(3)}T^2 + d^{(4)}T^3 \qquad (8.17)$$

where the solvent-dependent coefficients $d^{(0)}$-$d^{(4)}$ are listed in Table 8-13 for the components considered in this work. In this work the values fitted by Chunxi et.al. (2000) were used. Chunxi fitted the coefficients in the model to the experimental data of Akhadow (1981) for water and those of Austgen (1989) for MDEA.

Table 8-13 Parameters used in the model for the dielectric constant

Component	$d^{(0)}$	$d^{(1)}$	$d^{(2)}$	$d^{(3)}$	$d^{(4)}$	Temperature-Range (°C)
Water	-19.29	$2.98\cdot10^4$	$-1.96\cdot10^{-2}$	$1.31\cdot10^{-4}$	$3.11\cdot10^{-7}$	0-300
MDEA	8.16	$8.90\cdot10^3$	0	0	0	0-300
CO_2	2.0	0	0	0	0	-
Methane	2.0	0	0	0	0	-
Nitrogen	2.0	0	0	0	0	-

8.3.4 The Mixture Dielectric Constant

The molecular part of the dielectric constant is itself obtained taking into account the contribution of the various molecular species through a function of mole fraction. A linear mixing rule is used to calculate the dielectric constant for a molecular solution

$$D_s = \sum_{i=1}^{n} x_i D_i \tag{8.18}$$

We see that we need no binary interaction parameters for the chosen model. Wang and Anderko (2001) have recently published a discussion and review of methods for calculating the dielectric constant of mixed solvent ionic solutions.

When we have ions in the solution, the dielectric constant is calculated using Pottel's equation

$$D = 1 + (D_s - 1)\left(\frac{1 - \varepsilon_3^{"}}{1 + \dfrac{\varepsilon_3^{"}}{2}}\right) \tag{8.19}$$

where $\varepsilon_3^{"}$ is calculated from the equations given in chapter 3. We also here see that no extra binary parameters are needed in the model for the dielectric constant of the ionic solution.

8.3.5 Fitting of Binary Ionic Interaction Coefficients

The ionic interaction parameter W_{ij} can be calculated for cation-anion interactions and for cation-water interaction using equation (8.15). For MDEA-water solutions the use of this correlation is questionable because we can consider the system a mixed solvent one and, in this case the solvation characteristics of $MDEA^+$ are expected to depend on the solvent composition (Zuo and Furst, 1998).

In this work the ionic interaction coefficients involving $MDEA^+$ were fitted to experimental data. No temperature dependence of the ionic parameters W_{ij} was assumed. The coefficients

$$W_{MDEA^+\text{-Water}}, \quad W_{MDEA^+\text{-MDEA}}, \quad W_{MDEA^+\text{-}HCO_3^-}, \quad W_{MDEA^+\text{-}CO_2}$$

were fitted to vapour pressure data for CO_2, MDEA and water and will be reported in the next sections.

8.4 Correlation of Salting out Effects of CO_2

When an appreciable amount of salt dissolves in a liquid, it significantly affects that liquid's vapour pressure. This can be quantified be the value of the osmotic coefficient of water. Further, the dissolved salt affects the solubility of a gas (or liquid) in that solvent and finally; if the solvent is a mixture of two volatile components, the dissolved salt influences the composition of the vapour in equilibrium with the solvent mixture.

The solubility of a gas in a salt solution is usually less than in salt-free water; this solubility decrease is called salting-out. Salting out effects affects the solubility of CO_2 in amine solutions in a high degree. At moderately and high loadings these effects will be very important. To evaluate the electrolyte ScRK-EOS's ability to model salting out effects of CO_2, the model was regressed to the experimental data of Kiepe et.al. (2002). Kiepe measured the solubility of CO_2 in aqueous electrolyte solutions of NaCl and KCl. The range of experimental data is summarized in Table 8-14. The salting out effects can easily be seen in

Figure 8-10 where the solubility of CO_2 at varying salt concentrations and total pressures at 40°C is presented.

From Table 8-14 we see that the model is able to correlate the data with an acceptable precision (average abs. deviation of 8.6%). We see that the fitted ionic interaction coefficient ($W_{NaCl-CO2}$) varies in a considerable degree with temperature (different values at 40°C and 80°C). Application of temperature dependent ionic interaction coefficients should therefore be considered – but as we shall see good results are obtained even without using temperature dependent parameters for CO_2-water-MDEA systems.

Table 8-14 Results from regression of electrolyte ScRK-EOS to the experimental data of Kiepe et.al. (2002)

Gas	Electrolyte	Molality	Temp. [°C]	Pressure [bar]	No. Points	$W_{NaCl-CO2}$	Abs.dev. [%]	Bias.dev. [%]
CO_2	NaCl	0.52, 2.5, 4.0	40	1 – 92	36	$8.1 \cdot 10^{-6}$	4.8	3.0
CO_2	NaCl	0.5, 2.5, 4.0	80	1-101	34	$5.4 \cdot 10^{-5}$	9.2	-6.3
CO_2	KCl	0.5, 2.5, 4.0	40	1-100	45	$-6.5 \cdot 10^{-6}$	6.3	-0.9
CO_2	KCl	0.5, 2.5, 4.0	80	1-100	46	$2.67 \cdot 10^{-5}$	14.3	-9.5
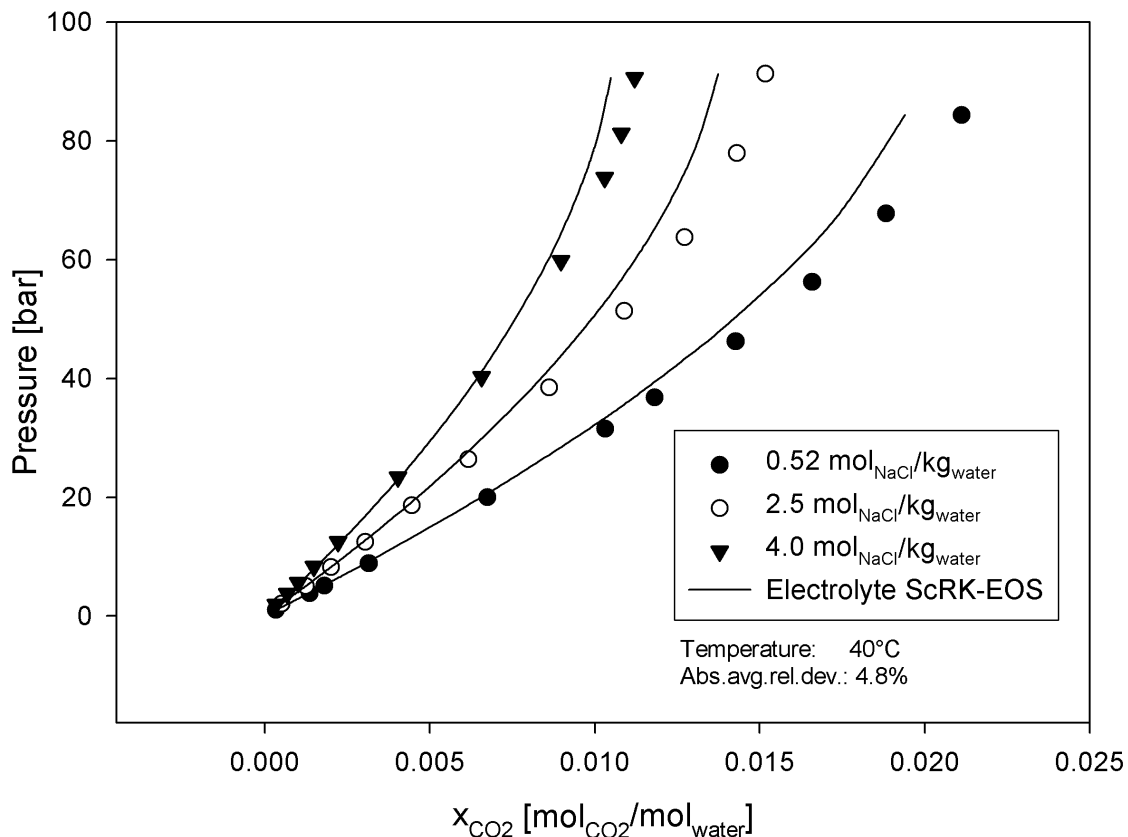
Figure 8-10 Solubility of CO_2 in an aqueous NaCl solution. Experimental data from Kiepe et.al (2002).
Script: TPflash.py, p. 306

8.5 Fitting of Ionic Interaction Coefficients to Vapour Pressures of CO_2-MDEA-Water Systems

The interaction parameters W_{ij} for $MDEA^+$-MDEA, $MDEA^+$-Water, $MDEA^+$-HCO_3^- and $MDEA^+$-CO_2 were fitted to ternary CO_2, MDEA and water data over a large temperature range (298 – 393 K). In this work a subset of the ternary CO_2, MDEA and water data presented by Chunxi et.al. (2000) was used for regression of the ionic interaction parameters. Chunxi checked the data presented in their paper for self – and mutual consistency. In self – consistency test it was examined if the partial pressure curves of CO_2 at specified temperature and MDEA concentration have a shape as expected. With the mutual consistency test values from different sources at similar conditions were compared with each other. Chunxi expects the data to follow three trends:

- At very low loading a linear relation between the logarithm of the partial pressure and the gas loading exists.
- At fixed loading and temperature, the acid gas partial pressure increases with MDEA concentration.
- At specified loading and MDEA concentrations, the acid gas partial pressure increases with the temperature.

The data set used by Chunxi for parameter regression passed the test and therefore it was also used in this work.

Chunxi et.al. (2000) used their electrolyte EOS to calculate VLE of the system CO_2, water and MDEA. They give average relative deviations for the data used in their parameter regression. This deviation goes for the different data sets from 12.7% for the data from Bahiri (1984) up to 41.2% for the data from Austgen et.al. (1989). They did not report the accuracy of predictions done with their model.

In Table 8-15 the experimental data used and the goodness of the fit are reported. A comparison between some experimental data points and the model is given in Figure 8-11 (Rho et.al., 1997), Figure 8-12 (Austgen (1989) and Jou (1982) at 313K) and Figure 8-13 (Kuranov (1996) at 373K). Table 8-16 reports the values obtained for the interaction parameters found by regressing the electrolyte ScRK-EOS model to all the experimental data. An absolute average deviation of 26% was achieved when regressing the four ionic interaction coefficients to all the experimental data reported in Table 8-15. The average deviation for the different data sets used for fitting goes from 11.3% for the data from Rho et.al. (1997) up to 31.4% for the data from Mac Gregor and Mather (1991). This is similar deviations (on average) as was reported by Chunxi et.al. (2000).

The electrolyte CPA-EOS was not used for CO_2-MDEA-water systems since it was not able to calculate the solubility of CO_2 in water over a large temperature range with an acceptable accuracy (ref. chapter 3).

The objective function used for parameter regression was

$$\chi^2 = \sum_{i=1}^{n} \left(\frac{P_{CO_2 \exp,i} - P_{CO_2 calc}(T,P)}{\sigma_{CO_2 \exp,i}} \right)^2 \tag{8.20}$$

The standard deviation was set to $P_{CO_2\,exp}/50$ if no value was reported in the literature.

Table 8-15 Description of the data used for fitting ionic parameters of CO_2-MDEA-Water systems and of the average deviation obtained in the data regression. Literature references to the experimental data are presented below the table.

Ref.	MDEA (wt%)	Temperature (K)	Loading range (mol CO_2/mol amine)	Number of points	AAD (%)
Jou et.al. (1993)	35	313, 373	0.005-0.795	35	26.5
Jou et.al. (1982)	23.4	298,313,343,373,393	0.0009-1.833	54	29.6
	48.9	298,313,343,373,393	0.0001-1.381	55	28.4
Austgen et.al. (1991)	23.4	313	0.006-0.842	9	21.0
	48.9	313	0.04-0.671	5	21.0
Chakma and Meisen (1987)	19.8, 48.9	373	0.04-1.304	17	18.8
Bahiri (1984)	20.0	311, 339	0.157-1.336	44	12.8
Kuranov (1996)	18.8-19.2	313, 333, 373, 393	0.209-1.316	33	16.3
	32.1	313, 333, 373, 393	0.195-1.157	34	23.2
Rho et.al. (1997)	5.0	323, 348, 373	0.03-0.684	19	16.4
	20.5	323, 348, 373	0.026-0.847	31	11.3
Mac Gregor and Mather (1991)	23.4	313	0.124-1.203	5	31.4
Average Deviation					**26%**

References:

1.   Jou, F.Y., Carrol, J.J., Mather, A.E., Otto, F.D., *The Solubility of Carbon Dioxide and Hydrogen Sulfide in 35wt% Aqueous Methyldiethanolamine Solutions*, Can. J.Chem.Engr., Vol. 71, p.264, 1993.

2.   Jou, F.Y., Mather, A.E., Otto, F.D., *Solubility of H_2S and CO_2 in Aqueous MDEA Solutions*, Ind.Eng.Chem., Proc.Design.Dev., Vol. 21, p. 539, 1982.

3.   Austgen, D.M., Rochelle, G.T., Chen, C.C., *Model of Vapour-Liquid Equilibria for Aqueous Acid Gas-Alkanolamine Systems, 2. Representation of H_2S and CO_2 solubility in Aqueous MDEA and CO_2 solubility in Aqueous Mixtures of MDEA with MEA and DEA*, Ind.Eng.Chem.Res., Vol. 30, p. 543, 1991.

4.   Chakma, A., Meisen, A., *Solubility of Aqueous Methyldiethanolamine and N,N-Bis(hydroxyethyl) Piperazine Solutions*, Ind.Eng.Chem.Res., Vol. 26, p.2461, 1987.

5.   Bahiri, A.M, *Experimental equilibrium Between Acid Gases and Ethanolamine Solutions*, Ph.D. dissertation of Oklahoma Stat University, 1984.

6.   Kuranov, G., Rumpf, G., Smirnova, N.A., Maurer, G., *Solubility of Single Gases Carbon Dioxide and Hydrogen Sulfide in Aqueous Solutions of N-Methyldiethanolamine in Temperature Range 313-413K at Pressures up to 5 MPa*, Ind.Eng.Chem.Res., Vol. 71, p.264, 1996.

7.   Rho, S.W., Yoo, K.P., Lee, J.S., Nam, S.C., Son, J.E., Min, B.M., *Solubility of CO_2 in Aqueous Methyldiethanolamine Solutions*, J.Chem.Eng.Eng.Data, Vol. 42, p.1161, 1997.

8.   Mac Gregor, R.J., Mather, A.E., *Equilibrium Solubility of H₂S and CO₂ and their Mixtures in a Mixed Solvent*, Can.J.Chem.Engr., Vol. 69, p. 1357, 1991.

Table 8-16 Ionic interaction parameters involving MDEA$^+$

Interaction	W_{ij} ($\cdot 10^4$)
MDEA$^+$-water	1.054
MDEA$^+$-CO$_2$	0.135
MDEA$^+$-MDEA	1.055
MDEA$^+$-HCO$_3^-$	-1.049

From Table 8-15 and Figure 8-11 to Figure 8-13 we see that all the experimental data sets can be estimated with an absolute average deviation between 10-40%. Compared to other models used to calculate vapour pressures of CO$_2$-MDEA-water solutions (eg. Austgen, 1989) the results obtained here are comparable. It is important to note that the numbers of parameters fitted are generally less than in previously published electrolyte models. The deviations obtained using the electrolyte ScRK-EOS are comparable to deviations between the experimental data obtained by different experimenters – and we thus conclude that the model is applicable for such weak electrolyte systems.

Predictions done with the model were compared to some experimental data of Bahiri (1982) at 298 K and 323 K and Lemoine (2000) at 298K. The absolute average deviation between the model and these data was 30% (Bahiri) and 15.6% (Lemoine). The experimental and the calculated data are given in Figure 8-14 and Figure 8-15. From Figure 8-14 we see that at high loadings the partial pressure of CO$_2$ is under-predicted.
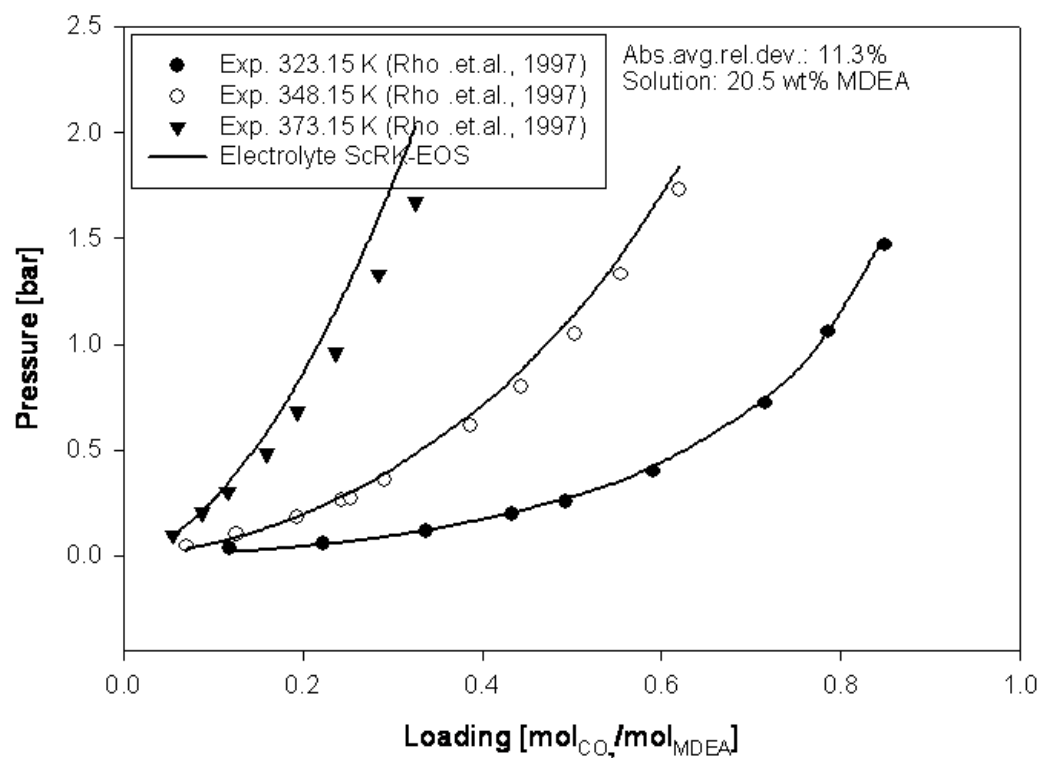
Figure 8-11 Experimental (Rho et.al, 1997) and calculated (electrolyte-ScRK) partial pressures of CO$_2$ over aqueous MDEA (20.5 wt%) solutions at 313, 348 and 373K. *Script: pubp_amine.py, p. 315*
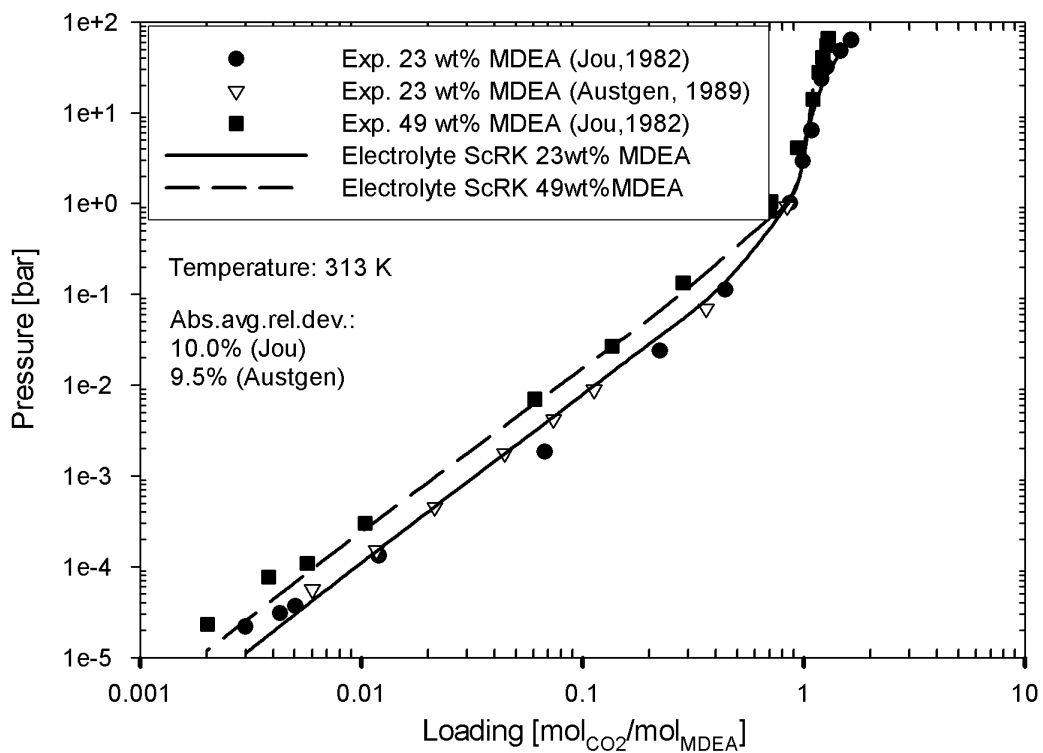
Figure 8-12 Experimental (Jou, 1982 and Austgen , 1989) and calculated (electrolyte-ScRK) partial pressures of CO_2 for a CO_2, MDEA and water solution at 313K. *Script: pubp_amine.py, p. 315*
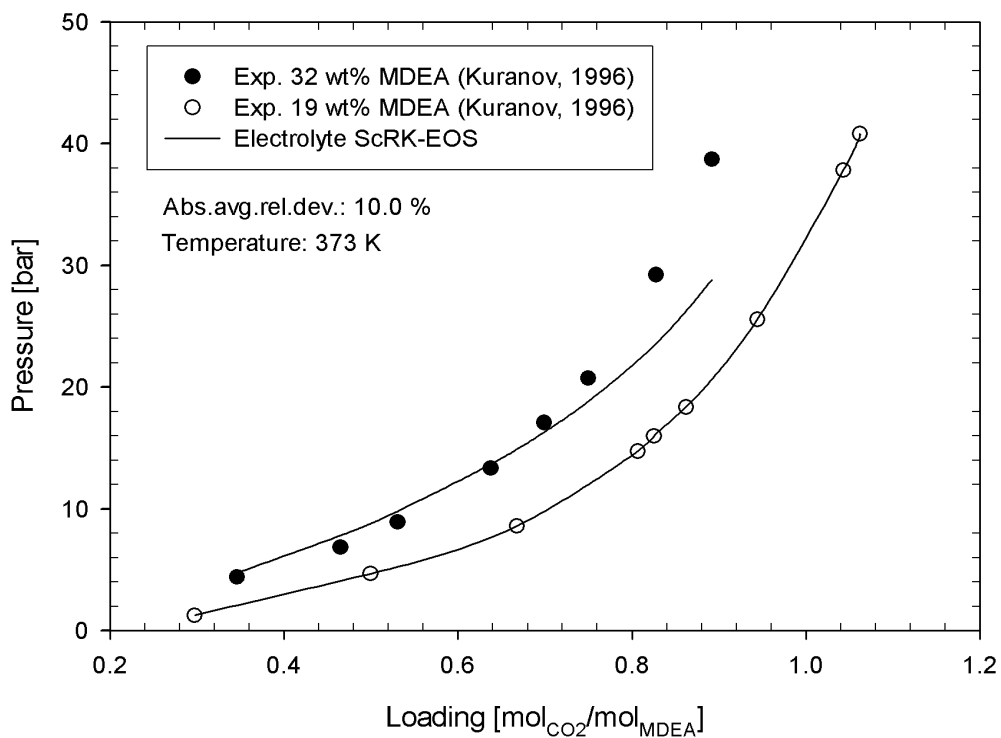
Figure 8-13 Experimental (Kuranov 1996) and calculated (electrolyte-ScRK) partial pressures of CO_2 for a CO_2, MDEA and water solution at 373K. *Script: pubp_amine.py, p. 315*

182

Figure 8-14 Experimental (Bahiri, 1982) and predicted (electrolyte-ScRK) partial pressures of CO₂ for a CO₂, MDEA and water solution at 298 and 323K. *Script: pubp_amine.py, p. 315*

Figure 8-15 Experimental (Lemoine, 2000) and predicted (electrolyte-ScRK) partial pressures of CO₂ for a CO₂, MDEA and water solution at 298 K. *Script: pubp_amine.py, p. 315*

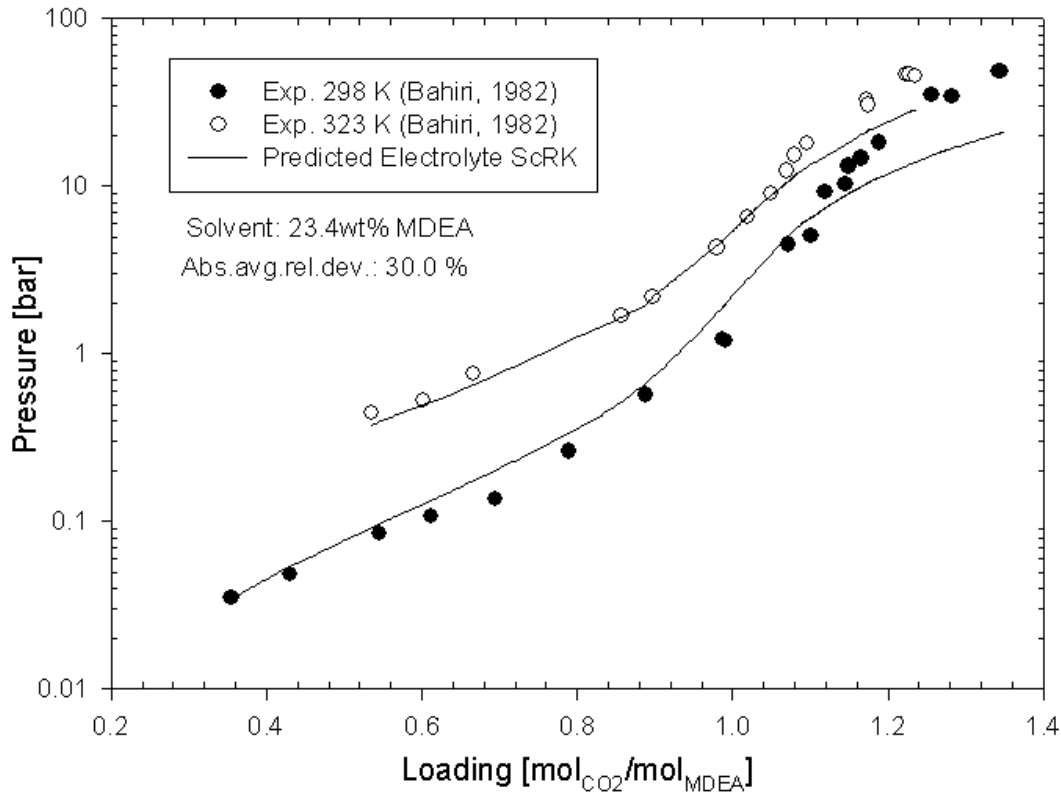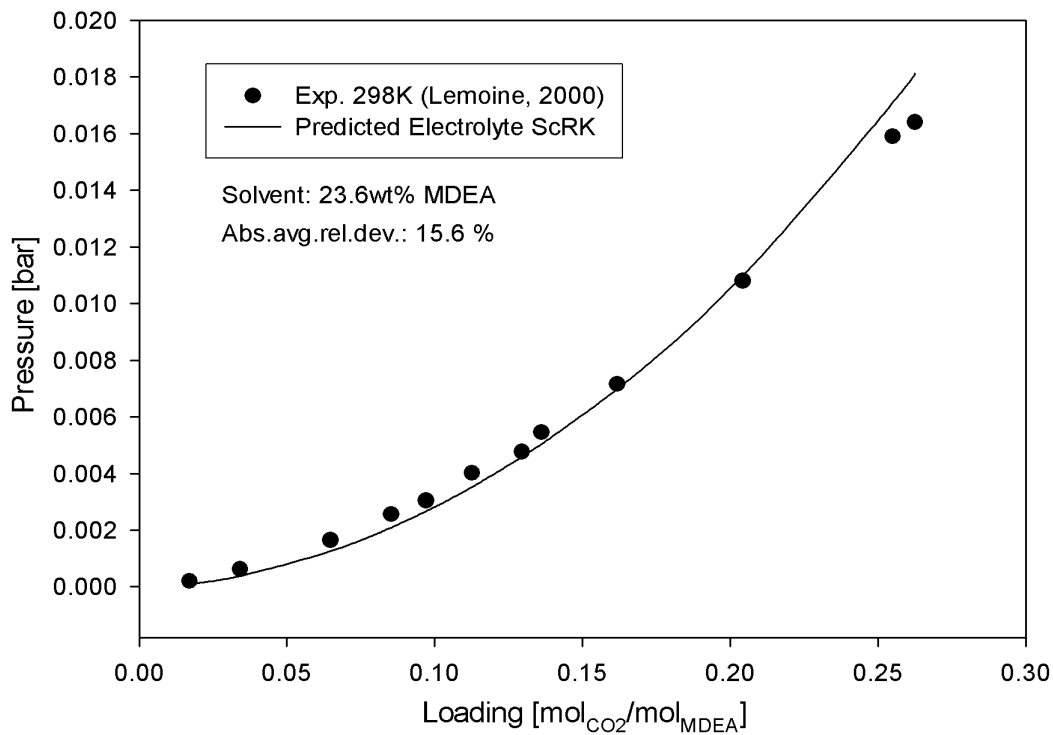## 8.6 Simultaneous Solubility of Methane and CO₂ in Aqueous MDEA Solutions

The main advantage of using an equation of state for modelling of amine solutions – will probably be when we want to study the solubility of hydrocarbons in the liquid phase. In an equation of state supercritical components can be added in a consistent way. For the electrolyte ScRK-EOS only one ionic parameter has to be fitted per inert component we want to use. For methane the ionic interaction coefficient $W_{MDEA^+\text{-methane}}$ must be fitted to solubility data in MDEA solutions.

Few experimental data have been published in the open literature for the solubility of methane in solutions of CO_2, MDEA and water. To the author's knowledge the only solubility data published are the data of Addicks (2002). Addicks measured the solubility of methane in CO_2, MDEA (30 and 50wt%) and water solutions at pressures up to 200 bar and temperatures 40 and 80°C. In this work the electrolyte ScRK-EOS was fitted to represent the data reported by Addicks. The only parameter fitted was the ionic interaction coefficient between $MDEA^+$ and methane, $W_{MDEA^+\text{-methane}}$. The data measured by Addicks (2002) are presented in Figure 8-16 taken from Addicks et.al., 2002b.

30wt% MDEA 313K

P	liquid-phase comp		vapor-phase comp	
	CO_2	CH_4	CO_2	CH_4
bar	mol/mol$_{MDEA}$	mol/mol$_{MDEA}$	mol/mol	mol/mol
100	0.2586	0.0264	0.0011	0.9989
100	0.6203	0.0257	0.0048	0.9952
150	0.6256	0.0331	0.0039	0.9961
150	0.9887	0.0256	0.1411	0.8589
150	1.0062	0.0247	0.1424	0.8576
200	1.0285	0.0295	0.1365	0.8635
200	1.0243	0.0284	0.1428	0.8572
200	0.9086	0.0353	0.0298	0.9702
200	0.9687	0.0339	0.0544	0.9456

30wt% MDEA 353K

P	liquid-phase comp		vapor-phase comp	
	CO_2	CH_4	CO_2	CH_4
bar	mol/mol$_{MDEA}$	mol/mol$_{MDEA}$	mol/mol	mol/mol
100	0.6895	0.0234	0.0778	0.9222
100	0.7713	0.0222	0.1056	0.8944
100	0.8347	0.0206	0.1441	0.8559
150	0.7365	0.0323	0.0631	0.9369
150	0.8736	0.0289	0.1343	0.8657
200	0.7593	0.0367	0.0594	0.9406
150	0.8122	0.0311	0.0928	0.9072
200	0.8288	0.0378	0.0875	0.9125
200	0.9690	0.0275	0.1455	0.8545

50wt% MDEA 313K

P	liquid-phase comp		vapor-phase comp	
	CO_2	CH_4	CO_2	CH_4
bar	mol/mol$_{MDEA}$	mol/mol$_{MDEA}$	mol/mol	mol/mol
100	0.5815	0.0114	0.0124	0.9876
200	0.8128	0.0158	0.0488	0.9512
100	0.9232	0.0074	0.2627	0.7373
200	0.9426	0.0116	0.2533	0.7457

50wt% MDEA 353K

P	liquid-phase comp		vapor-phase comp	
	CO_2	CH_4	CO_2	CH_4
bar	mol/mol$_{MDEA}$	mol/mol$_{MDEA}$	mol/mol	mol/mol
100	0.2762	0.0188	0.0243	0.9757
150	0.2935	0.0257	0.0187	0.9813
200	0.3037	0.0315	0.0159	0.9841
100	0.4091	0.0187	0.0467	0.9533
200	0.4364	0.0270	0.0314	0.9686
100	0.5713	0.0112	0.0948	0.9052
200	0.6134	0.0204	0.0687	0.9313
100	0.7026	0.0114	0.1712	0.8288
200	0.7569	0.0209	0.1364	0.8636

Figure 8-16 Experimental solubility data of methane and CO₂ in aqueous MDEA solutions from Addicks et.al. (2002b).

The electrolyte ScRK-EOS was fitted to experimental measured equilibrium total pressure and CO_2 partial pressure data. The objective function used for parameter regression was

$$\chi^2 = \sum_{i=1}^{n}\left(\frac{P_{tot\,exp,i} - P_{tot\,calc}(T,P)}{\sigma_{exp,i}}\right)^2 + \sum_{j=1}^{m}\left(\frac{P_{CO_2\,exp} - P_{CO_2\,calc}(T,P)}{\sigma_{exp,j}}\right)^2 \qquad (8.21)$$

The standard deviation was set to 2% of the experimental total pressure and CO_2 partial pressure. In Table 8-17 a description of the data used for regression and the accuracy of the fit are reported. Both the absolute average deviation for the total pressure, the partial pressure of CO_2 and the solubility of methane in the liquid phase are presented. The fitted ionic interaction coefficient is given in Table 8-18. The absolute average deviation of the correlated total pressure (comparison of experimental total pressure and calculated bubble point pressure) was 12.1% (40°C) and 14.6% (80°C). The deviation between the measured and calculated partial pressure of CO_2 in the gas phase was 51% (40°C) and 15.4% (80°C).

The hydrocarbon loss to the amine solution will be of importance in process design. The experimental measured solubilites of methane in the liquid solution were compared to the calculated values using the electrolyte ScRK-EOS. The average deviation for the solubility of methane in the liquid phase is 7% (313K, 30 and 50wt% MDEA) and 5% (353K, 30 and 50wt% MDEA). This shows that we are able to calculate the methane solubility in the amine solutions with a satisfying accuracy.

In Figure 8-17 to Figure 8-20 the calculated bubble point pressures of the liquid solution are compared to the measured total pressure. In Figure 8-21 to Figure 8-24 the calculated partial pressures of CO_2 are compared to the experimental values. In Figure 8-25 and Figure 8-26 the calculated solubility of methane in the liquid solution is compared to the experimental values of Addicks.

The regressed interaction parameter W is given in Table 8-18. From Figure 8-21 we see that the model under-predicts the partial pressure of CO_2 in the gas. The under prediction is considerable for the 50wt% MDEA solution at 40°C (see Figure 8-22). Due to the limited number of experimental data points, it is hard to decide wether the reason for the deviation is due to the model or the experimental data.

Table 8-17 Comparison of experimental data of Addicks (2002) and model correlation for methane, CO_2, MDEA and water mixtures

Ref.	Temperature [K]	Pressure [bar]	MDEA [wt%]	Loading range	Number of points	AAD P_{tot} [%]	AAD P_{CO2} [%]	AAD (x_{CH4}) [%]
Addicks	313	100-200	30,50	0.2-1.1	13	12.1	51.0	7.0
(2002)	353	100-200	30,50	0.2-1.1	18	14.6	15.4	5.0

Table 8-18 Ionic interaction parameters involving MDEA$^+$ and methane

Interaction	W_{ij} ($\cdot 10^3$)
MDEA$^+$-methane	1.23

The classical Van der Waals one-parameter mixing rule was used to model methane-CO_2 molecular interactions. The binary interaction parameter $k_{CO2-methane}$ was fixed to a value of 0.12. This binary interaction parameter describes the interaction between methane and CO_2. A higher value indicate weaker attractive interaction forces (less CO_2 in the gas phase), while a lower (or negative) value indicate stronger attractive forces (more CO_2 in the gas phase). A correct modelling of the CO_2-methane interaction parameter will be of crucial importance in high pressure modelling of high pressure CO_2 removal processes.

In Figure 8-25 and Figure 8-26 the experimental and calculated solubility of methane in the liquid solution is given as a function of loading. The well known salting out effect can be observed. At higher loadings more salts will be present in the liquid phase ($MDEA^+$ and HCO_3^-) and less methane will dissolve in the liquid.

Hydrocarbon loss to the amine solution can be a serious problem in high pressure acid gas treating. The simultaneous solubility of methane and CO_2 in amine solutions is therefore important to calculate accurately. The electrolyte ScRK-EOS developed here is shown to be able to represent the solubility of methane with a high accuracy. The model should be further developed to be able to represent the solubility of heavier hydrocarbons (ethane, propane) in amine solutions.
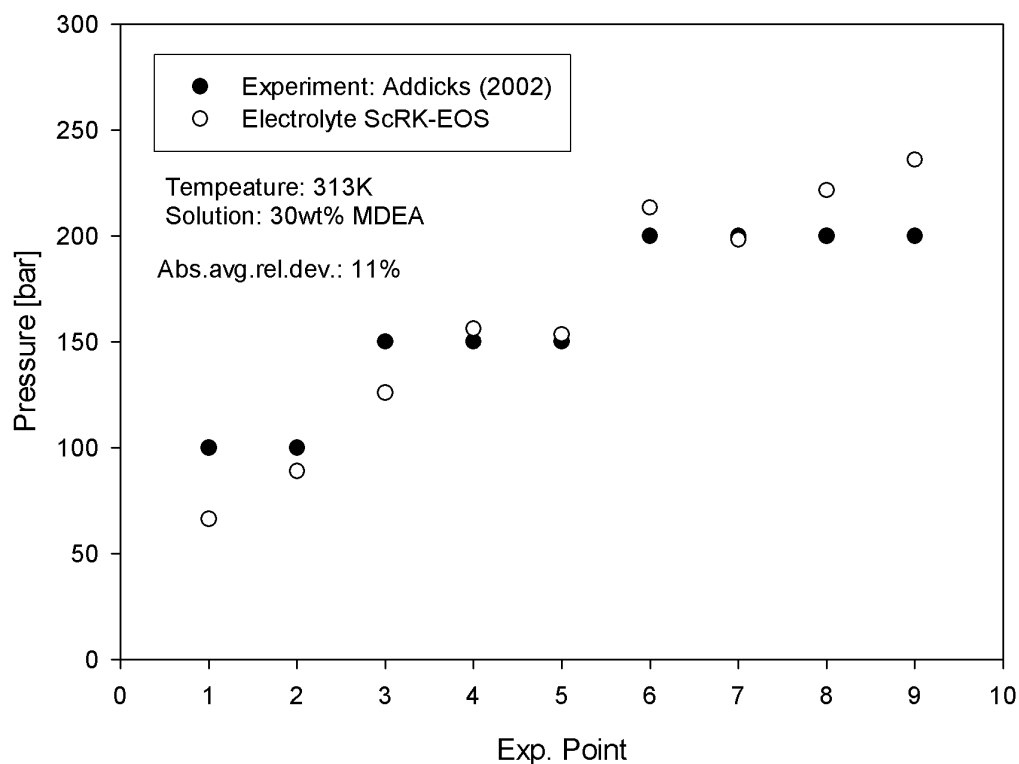
Figure 8-17 Experimental (Addicks, 2002) and calculated (electrolyte-ScRK) bubble point pressures of methane, CO₂, MDEA (30wt% in water) and water solutions at 313K. *Script: pubp_amine.py, p. 315*
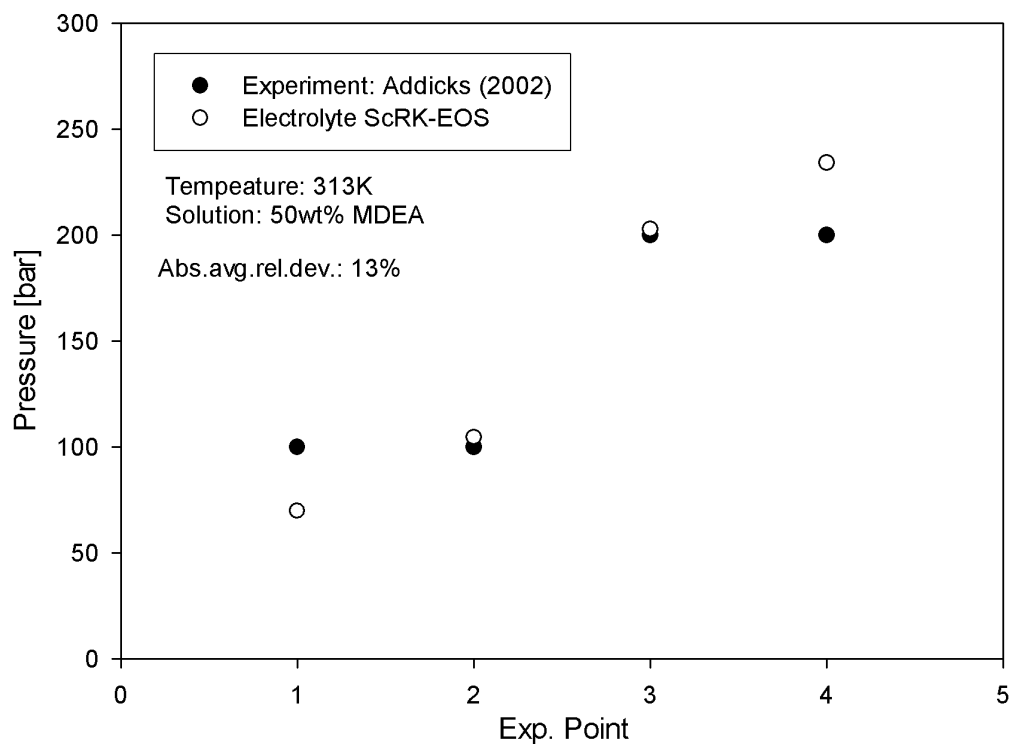
Figure 8-18 Experimental (Addicks, 2002) and calculated (electrolyte-ScRK) bubble point pressures of methane, CO₂, MDEA (50wt% in water) and water solutions at 313K. *Script: pubp_amine.py, p. 315*
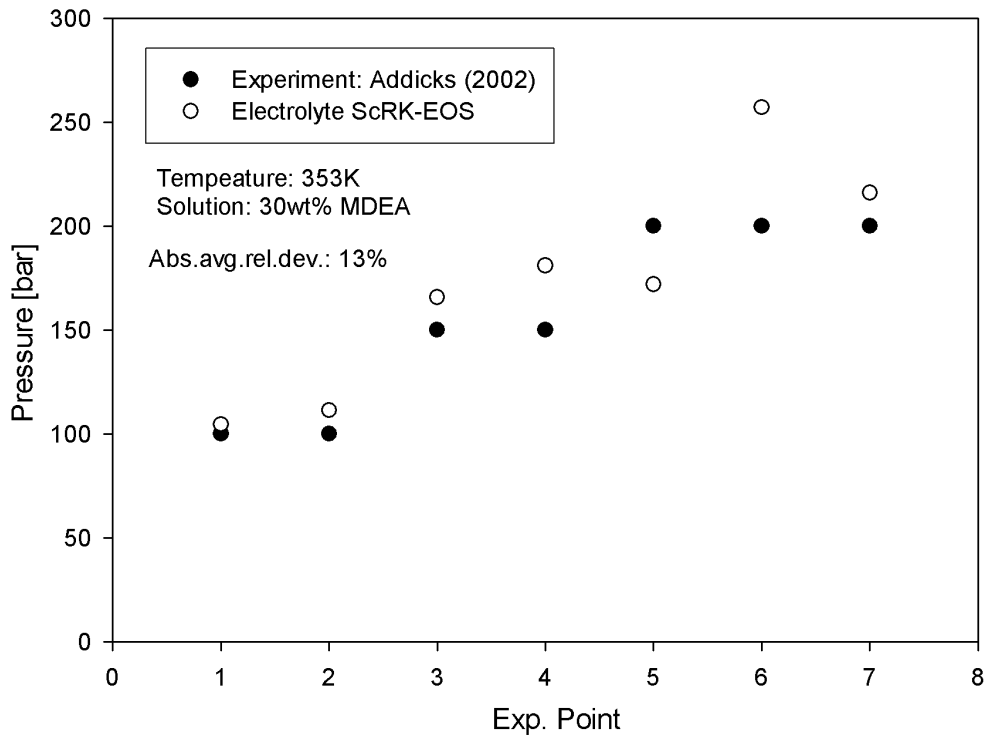
Figure 8-19 Experimental (Addicks, 2002) and calculated (electrolyte-ScRK) bubble point pressures of methane, CO₂, MDEA (30wt% in water) and water solutions at 353K. *Script: pubp_amine.py, p. 315*
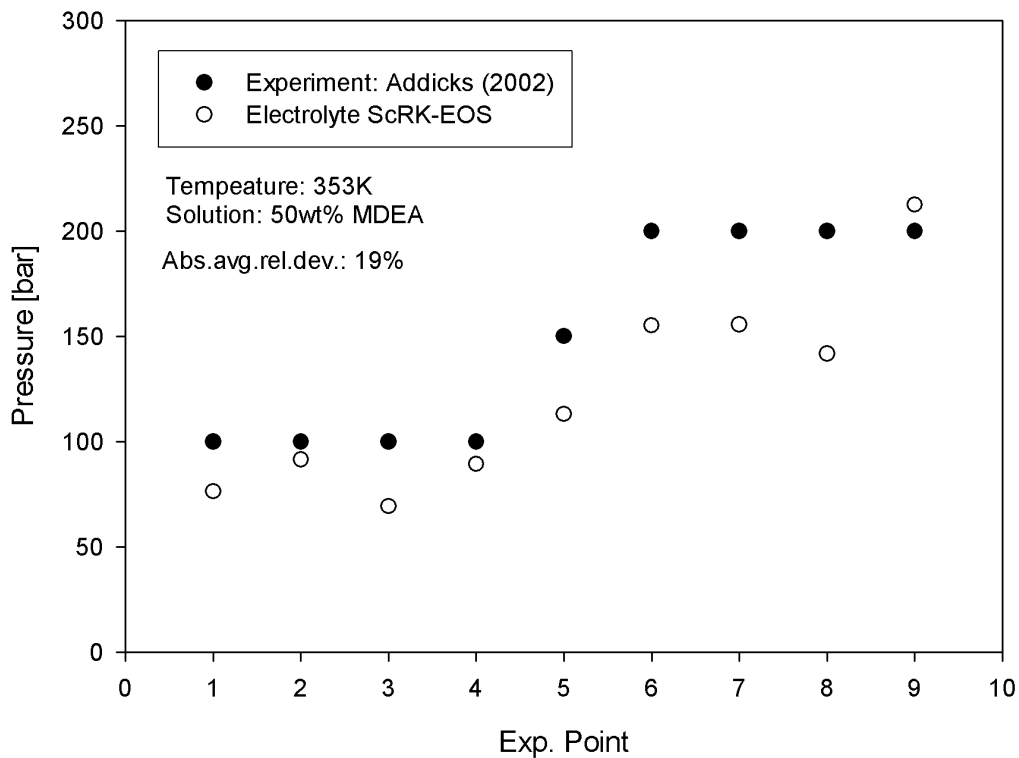
Figure 8-20 Experimental (Addicks, 2002) and calculated (electrolyte-ScRK) bubble point pressures of methane, CO₂, MDEA (50wt% in water) and water solutions at 353K. *Script: pubp_amine.py, p. 315*
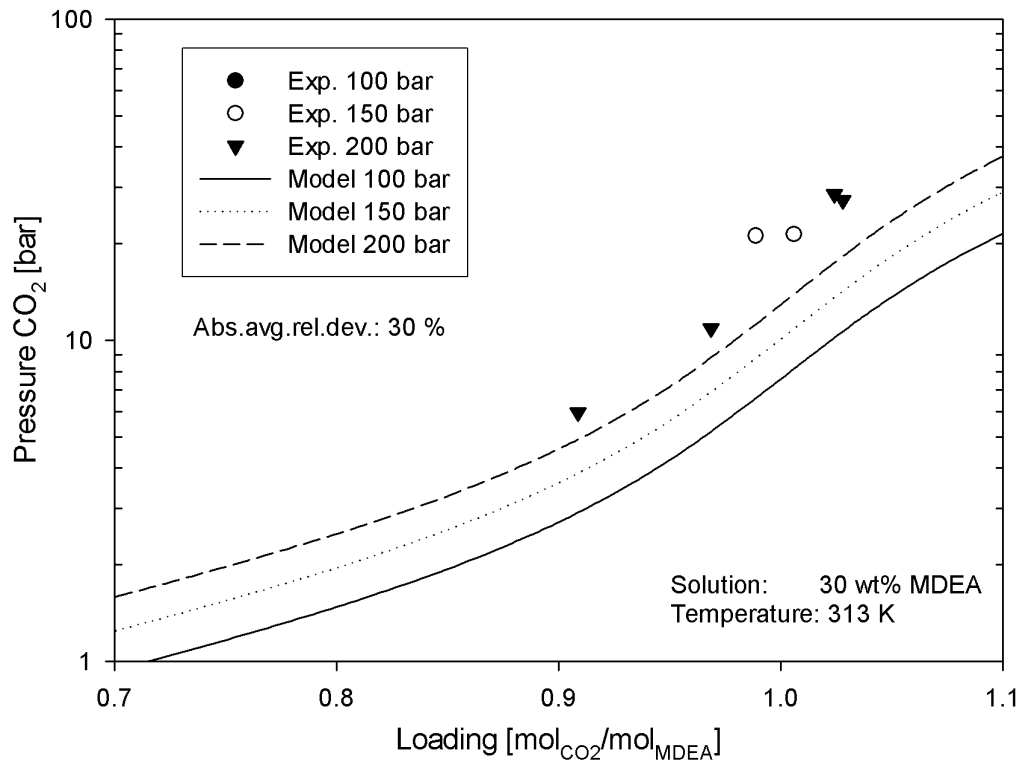
Figure 8-21 Experimental (Addicks, 2002) and calculated (electrolyte-ScRK) partial pressures of CO_2 for methane, CO_2, MDEA (30wt% in water) and water solutions at 313K. *Script: pubp_amine.py, p. 315*
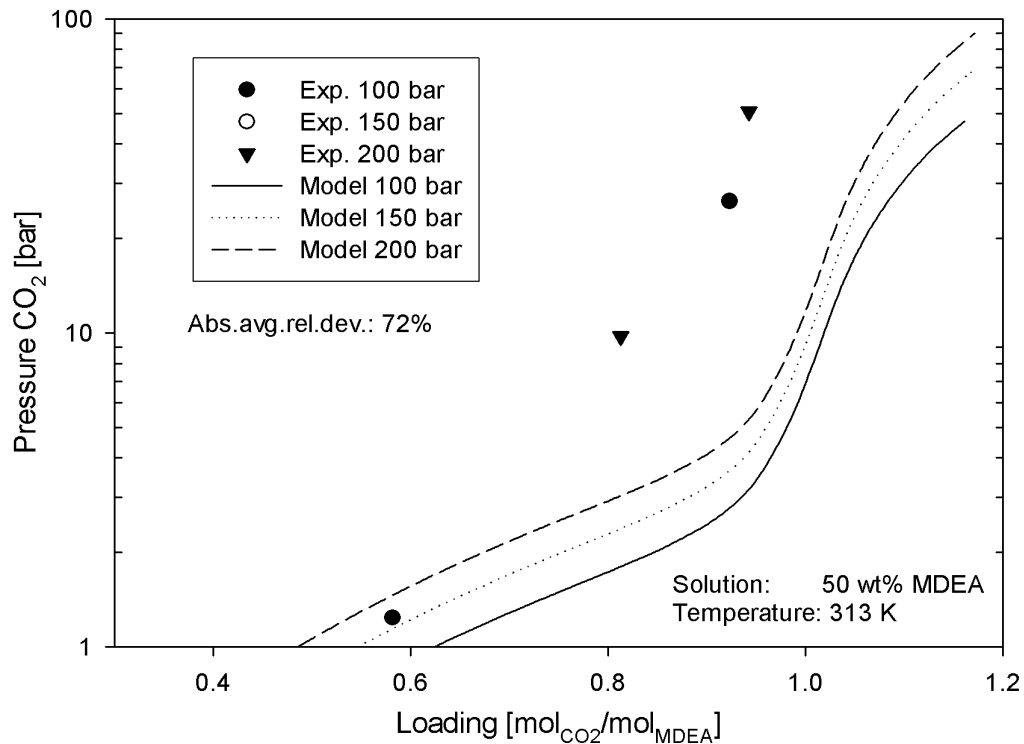
Figure 8-22 Experimental (Addicks, 2002) and calculated (electrolyte-ScRK) partial pressures of CO_2 for methane, CO_2, MDEA (50wt% in water) and water solutions at 313K. *Script: pubp_amine.py, p. 315*
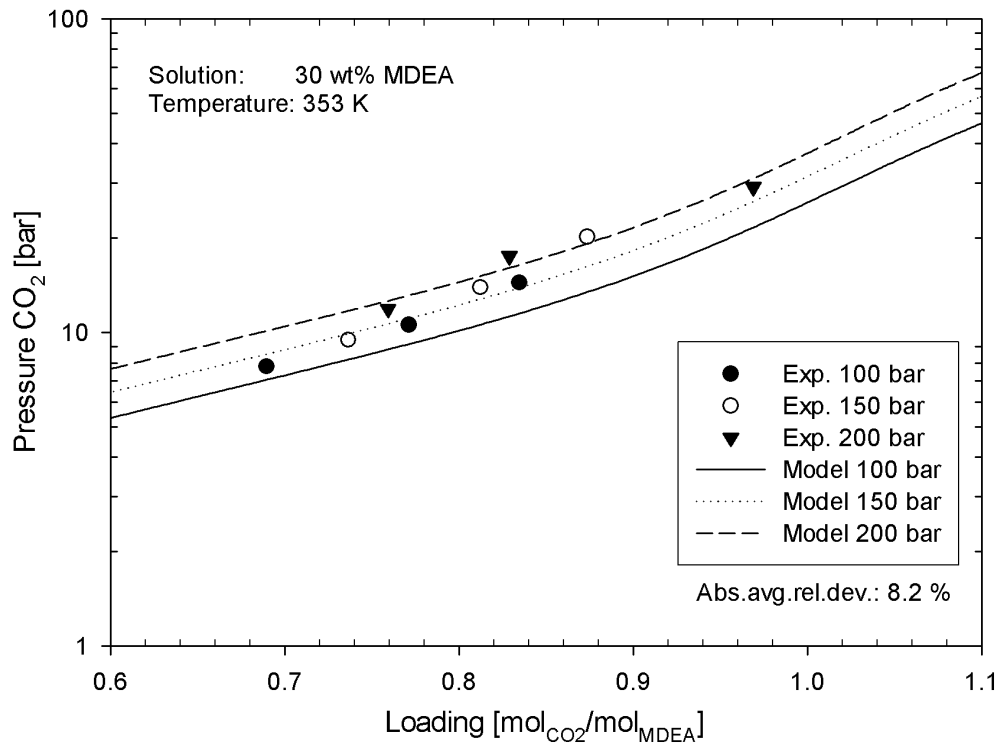
Figure 8-23 Experimental (Addicks, 2002) and calculated (electrolyte-ScRK) partial pressures of CO₂ for methane, CO₂, MDEA (30wt% in water) and water solutions at 353K. *Script: pubp_amine.py, p. 315*
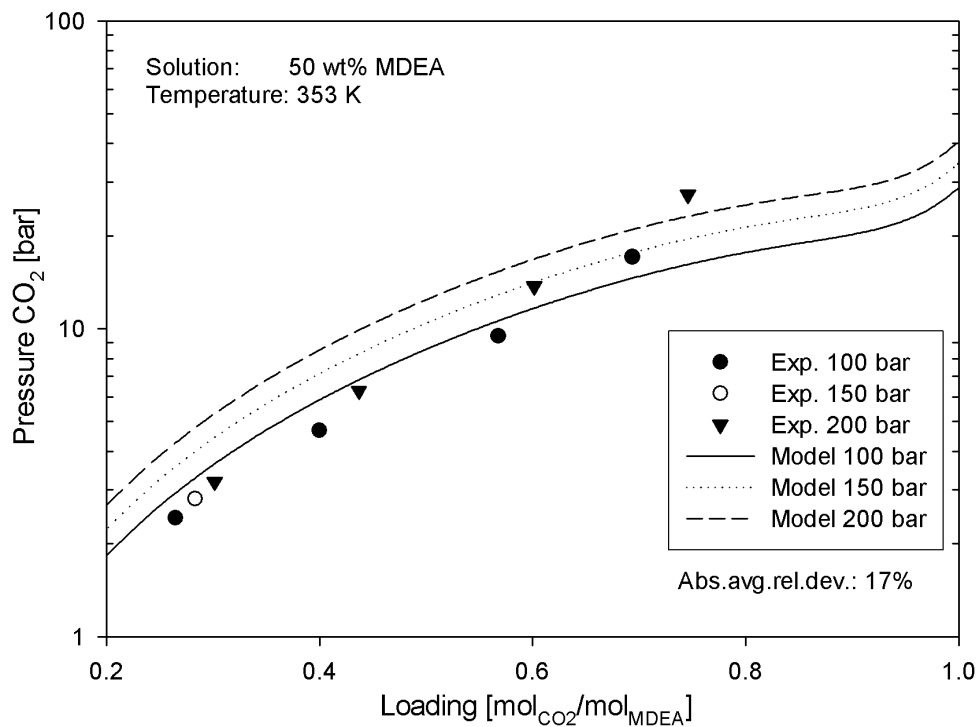
Figure 8-24 Experimental (Addicks, 2002) and calculated (electrolyte-ScRK) partial pressures of CO₂ for methane, CO₂, MDEA (50wt% in water) and water solutions at 353K. *Script: pubp_amine.py, p. 315*
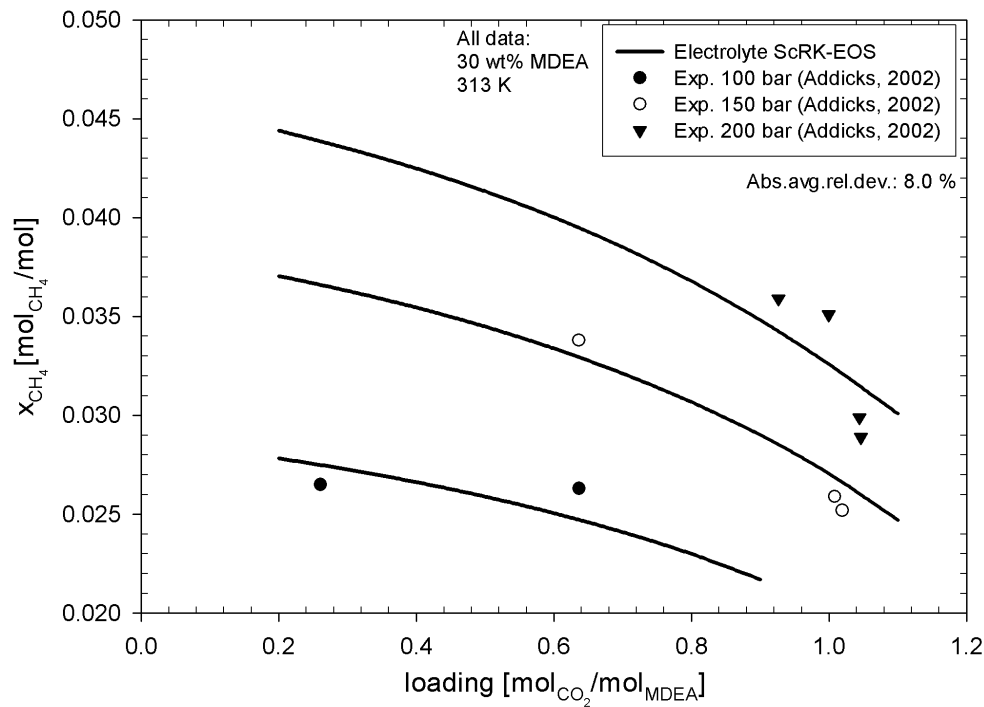
Figure 8-25 Experimental (Addicks, 2002) and calculated (electrolyte-ScRK) liquid solubility of methane for a methane, CO₂, MDEA (30wt% in water) and water system at 313K. *Script: TPflash_amine.py, p. 316*
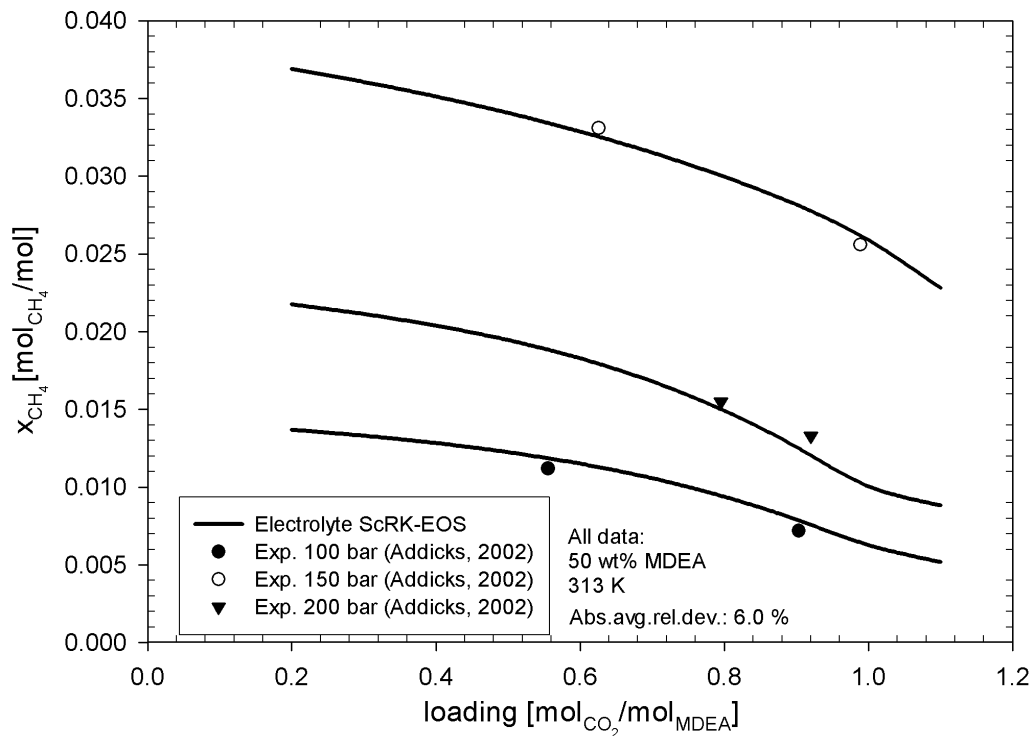
Figure 8-26 Experimental (Addicks, 2002) and calculated (electrolyte-ScRK) liquid solubility of methane for a methane, CO₂, MDEA (50wt% in water) and water system at 313K. *Script: TPflash_amine.py, p. 316*

By fitting the ionic interaction parameter $W_{methane-MDEA^+}$ to the data of Addicks (2002) and by using the classical one-parameter mixing rule for methane and CO_2 interactions, the experimental data of Addicks could be calculated with an acceptable accuracy. It should however be noted that relatively few data points were used when fitting the parameters, and that more experimental data should be obtained.

No literature data for the solubility of heavier hydrocarbons in CO_2, MDEA and water solution were found. The ionic interaction coefficients between $MDEA^+$ and heavy hydrocarbons can thus not be estimated at this time. Experimental solubility data of heavy hydrocarbons in MDEA solutions are needed – and experiments on such systems should be done.

8.7 Final Thermodynamic Model

A thermodynamic model that can be used for ideal and non-ideal molecular and ionic systems has been developed. By regressing the model to experimental data, the parameters needed to model the thermodynamics of acid gas treating with MDEA solutions have been estimated. Together with the models developed for calculating physical properties of MDEA solutions this thermodynamic model forms the basis of the mass transfer model that has been developed for simulating gas treating operations. The models used for calculating physical properties of gasses and liquids during gas treating operations are described in appendix D.

Figure 8-27 gives an illustration of the activity coefficient and composition of the liquid phase of a CO_2, MDEA and water system as calculated from the electrolyte ScRK-EOS. No experimental data is available to justify these calculations – but the well known salting out effect is observed.
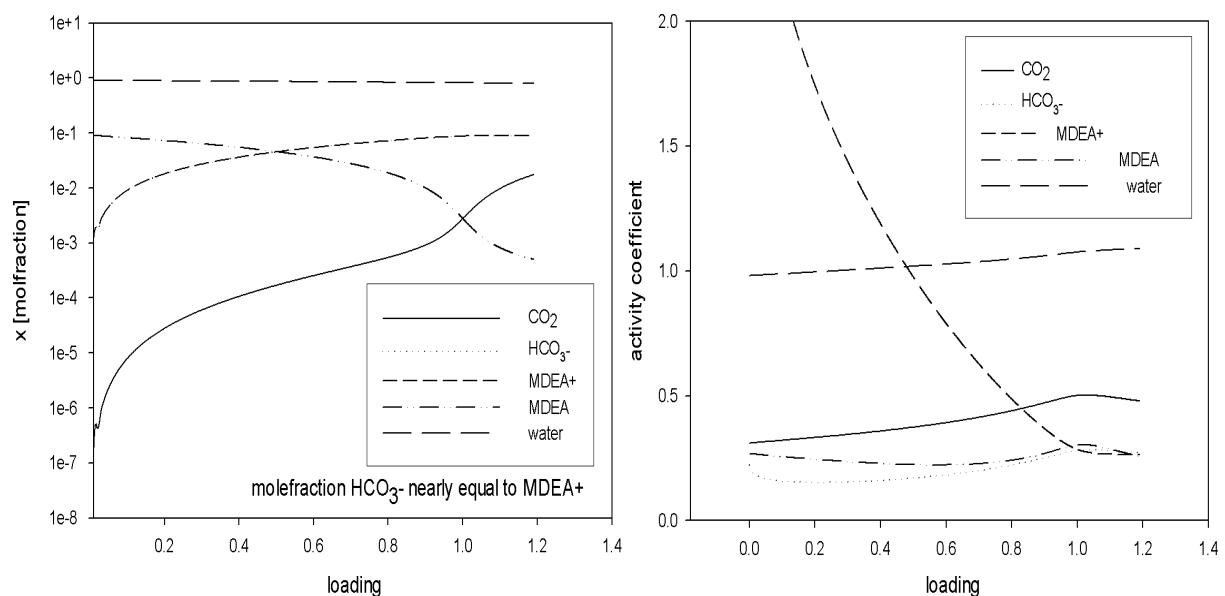
Figure 8-27 Activity coefficient of a CO_2-water-MDEA solution as function of loading [mol_{CO2}/mol_{MDEA}].
Script: bubp_amine.py, p. 315

8.8 Summary and Discussions

In this chapter the electrolyte ScRK-EOS and the electrolyte CPA-EOS have been fitted to relevant experimental data from the open literature.

The electrolyte ScRK-EOS with the Huron-Vidal mixing rule is able to simulate the solubility of CO_2 and methane in water over a large temperature and pressure range. The electrolyte terms in these equations were fitted to experimental data of strong and weak electrolyte solutions. The electrolyte ScRK-EOS model is able to represent the CO_2-MDEA-water data found in the open literature with a high accuracy. The model was fitted to the experimental high pressure equilibrium data of methane, CO_2, MDEA and water solutions from Addicks (2002). The model was able to correlate the bubble point pressure and CO_2 partial pressure data with an acceptable accuracy. It was also able to correlate the methane solubility in aqueous MDEA-solutions with CO_2 with a high accuracy. Only one ionic interaction parameter per inert component in the system has to be fitted. Using the electrolyte ScRK-EOS with the parameters obtained in this chapter we are able to predict the physical hydrocarbon loss (methane) to the amine solution with a high accuracy. This is an important achievement in the modelling and design of high pressure acid gas treating process plants.

The electrolyte CPA-EOS was fitted to 28 aqueous salt solutions. The model was able to reproduce experimental osmotic coefficient and activity coefficient data with a good accuracy. A simple mixing rule was used to describe molecular interactions (classical Van der Waals mixing rule) – but the model was not able to reproduce the experimental CO_2 solubility data in water over a large temperature range. This could probably be corrected for by introducing a more advanced mixing rule. The electrolyte CPA-EOS is expected to be able to reproduce the densities of ionic solutions in an accurate way – but this was not investigated in this work. Further development of the electrolyte CPA-EOS is planned for future modelling work.

9 Experimental Equipment – Design of a High Pressure Wetted Wall Column

Mass transfer experiments give important information about how fast components will be transported between phases. The mass transfer can occur by both molecular diffusion and convective mass transfer. Dependent on which type of mass transfer (pure molecular diffusion or convective mass transfer) we want to study we generally use two different kinds of experimental equipment to evaluate mass transfer in fluid systems. In the first type of equipment we study pure molecular diffusive mass transfer. In the second type of equipment we study convective mass transfer.

In this chapter a general introduction to experimental equipment used in mass transfer studies is given. The experimental equipment designed, constructed and used in this work is also presented.

9.1 Experimental Equipment Used to Study Mass Transfer

To be able to verify and develop models for convective mass transfer we must know how to model the fluid mechanics and have a well-defined gas-liquid interface. The requirement of a well-defined interface and known fluid mechanics is the reason that it is not suitable to do experiments in conventional process equipment (e.g. packed towers). In this kind of equipment many of the physical parameters, such as interphase area, turbulent forces in gas and liquid and liquid distribution influence the mass transfer and are generally unknown.

Accurate experimental measurements of convective mass transfer are difficult to carry out. It is hard to isolate the effects of the parameters we want study. A typical situation is when we want to study the effects of turbulent forces (high Reynolds numbers) on the mass transfer – and at the same time we want to keep the interface smooth and free of ripples. Convective mass transfer with a smooth interface is often hard to fulfil.

The final goal of all kinds of experimental work on mass transfer is to be able to understand the physical mechanisms that are important in non-equilibrium situations. To obtain this understanding it is of crucial importance to select the best type of experimental equipment.

Many types of laboratory equipment for studying convective mass transfer have been used. We can divide these equipments into three types:

a. Experimental equipment where the interphase area is known and where the mass transfer coefficient can be estimated based on the known fluid mechanics. An example of such experimental equipment is the short wetted wall column – where a liquid film and a gas are in contact in a pipe (Figure 9-1a).
b. Experimental equipment where the interfacial area is known, but where the fluid mechanics is such that the mass transfer coefficient can not be estimated mathematically from basic theory. An example of such experimental equipment is the stirred vessel (Figure 9-1b). The fluid flow in the stirred vessel is 3-dimensional and analytical expressions for the mass transfer coefficient are impossible to derive.
c. Experimental equipment where neither the interphase area nor the mass transfer coefficient can be estimated. An example of this type of equipment is a gas-liquid

194

wheel (Petreco-wheel, Figure 9-1c). In this type of equipment the fluid mechanics is so complicated that neither the interphase area nor the mass transfer coefficient can be analytically estimated.

a) Wetted wall column   b) The stirred tank   c) The Petreco Wheel
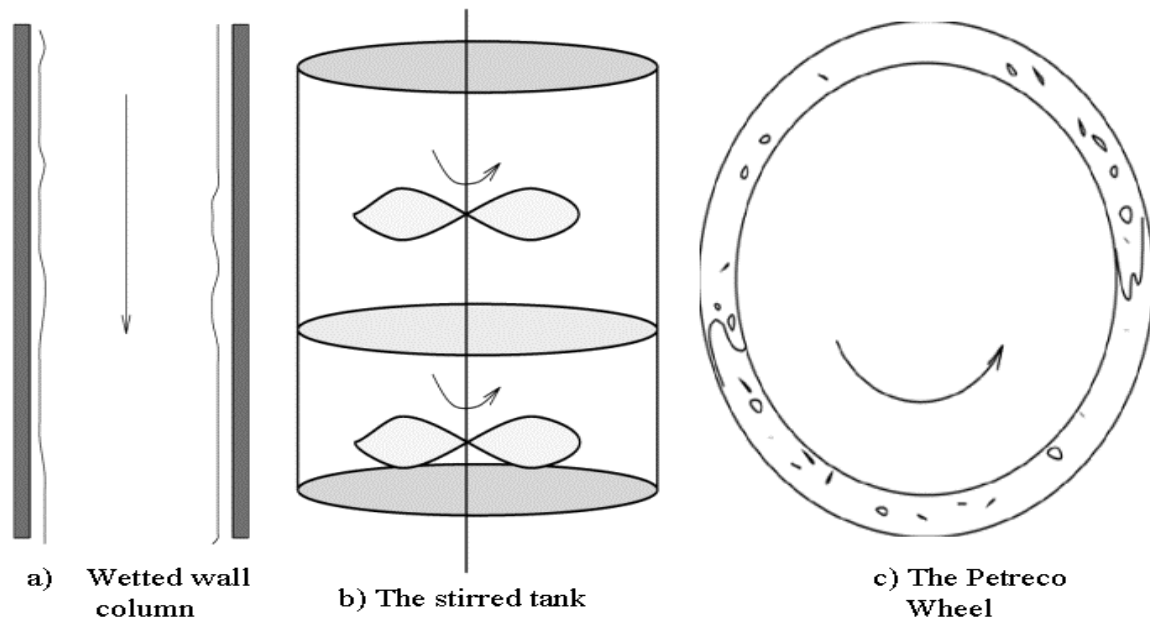
Figure 9-1 Experimental equipment used in mass transfer experiments

The selection of type of experimental equipment must be based on a number of considerations, but generally type a is preferable compared to type b, and type b is preferable to type c. A guide for the selection of experimental equipment is given by Astarita et.al. (1983).

In this work a variable length high-pressure wetted wall column was designed and built. This experimental equipment can be of type a) or type b) dependent on the contact length between the gas and liquid. For short ($<\sim$20 cm) contact lengths between the liquid and gas it is of type a) while for long ($>\sim$20 cm) contact lengths it will be of type b). The reason for this is that the liquid film will form waves and ripples in long wetted wall towers, and mathematical models for mass transfer will be empirical. In this work the experimental equipment was always operated as a long wetted wall column (1.5 meter gas-liquid contact length).

The "high pressure wetted wall tower" was designed and built at the Statoil research centre in Trondheim during the winter 1999-2000. It is placed in the HPU-lab (high-pressure-unit-laboratory), a laboratory specially design for high pressure experimental equipment.

9.2   *The High Pressure Wetted Wall Tower*

A variable length wetted wall column is an ideal experimental equipment used to study convective mass transfer. For short contact lengths between liquid and gas, fundamental parameters such as reaction-rate constants can be measured, while for long contact lengths the influence of waves, convective- and turbulent forces can be studied.

The high-pressure wetted wall tower designed in this work could operate at pressures up to 200 bar. A simple flowsheet for the experimental equipment is given in Figure 9-2. A photo of the experimental equipment is given in Figure 9-3. Detailed flow diagrams and sketches of the experimental equipment are given in appendix F.

Wetted wall columns have traditionally been used for laboratory studies of fundamental phenomena related to heat and mass transfer. Because of the large contact area between the liquid and the pipe wall, it has also been used as processes equipment where the heat of reaction is large (temperature can be controlled by cooling the wall). The basic operational principle of a wetted wall column is a thin liquid film completely wetting the wall on a vertical pipe flowing in co-or counter-current contact with a gas. The relatively simple and defined fluid mechanics, interphase conditions and known interphase area makes us able to formulate mathematical models from fundamental theory of fluid mechanics (short wetted wall columns) or empirical models based on large amounts of experimental data (long wetted wall columns).

The main parts of the high-pressure wetted wall column are:

- The wetted wall column/pipe
- The gas circulation loop
- The liquid circulation system

An important component of the experimental equipment is the pipe where the liquid film and the gas are in contact. A lot of mechanical and electronic equipment are needed to circulate the gas and liquid at high pressures. The equipment used in the main parts of the high-pressure wetted wall column is described in the following sections.

Window

Film distributor

Liquid in

1.5 meter

Inner pipe

Gas Booster

Nitrogen

CO$_2$

Liquid out
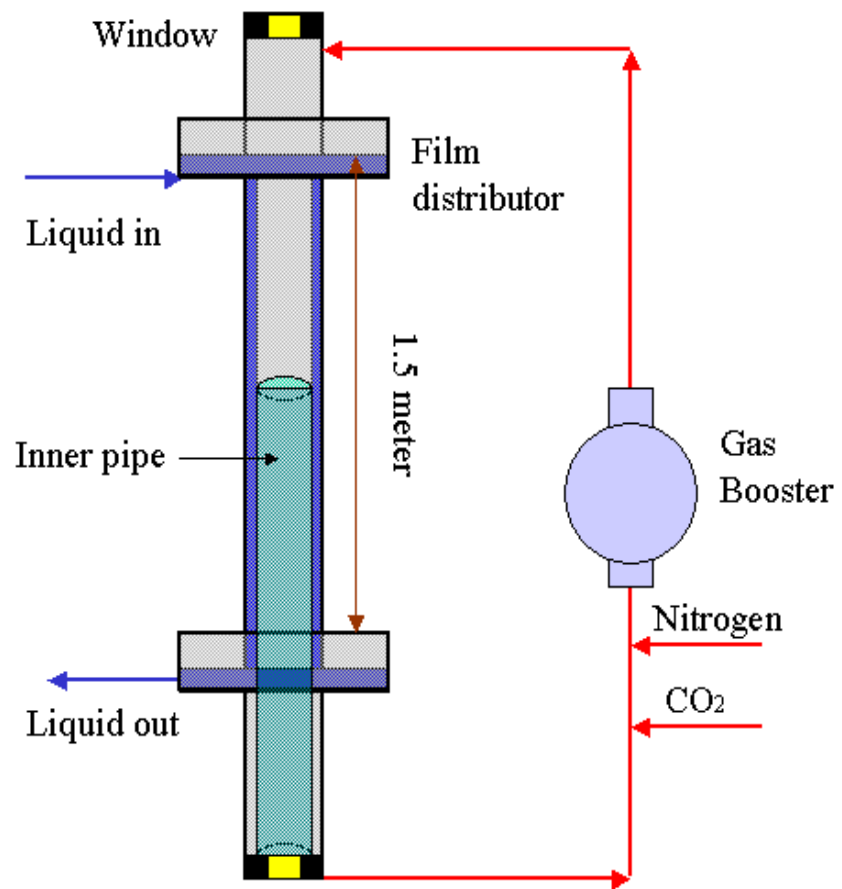
Figure 9-2 The high pressure wetted wall column

The experimental equipment consists of a wetted wall column made of a temperature controlled stainless steel pipe with sapphire glass windows in each end, so that visual inspection is possible. To avoid rippling and entrainment of the liquid film, the liquid and gas flow cocurrent down the pipe. A specially designed distributor creates a thin liquid film on the inner pipewall. An internal pipe is used to separate the liquid film and the gas core. The liquid film flows on the outside of the inner pipe while the gas flows inside. The maximum length where the liquid film and the gas can be in contact in the wetted wall column is 1.5 meter. By changing the length of the inner pipe, the contact length between liquid and gas can be varied between 0.1 and 1.5 meter. The inner diameter of the wetted wall column is 25.2 mm.

In this work a mixture of CO_2 and nitrogen was used in the gas circulation loop. Nitrogen functioned as an inert gas while CO_2 was absorbed into the liquid solution. A gas booster was used to circulate the gas.

The wetted wall column operates batch wise with respect to the liquid solution. The inlet and outlet liquid storage tanks have a capacity of 60 litres. These tanks operate at atmospheric pressure. The liquid was pressurized using a liquid pump. The liquid was saturated with nitrogen before entering the wetted wall column.
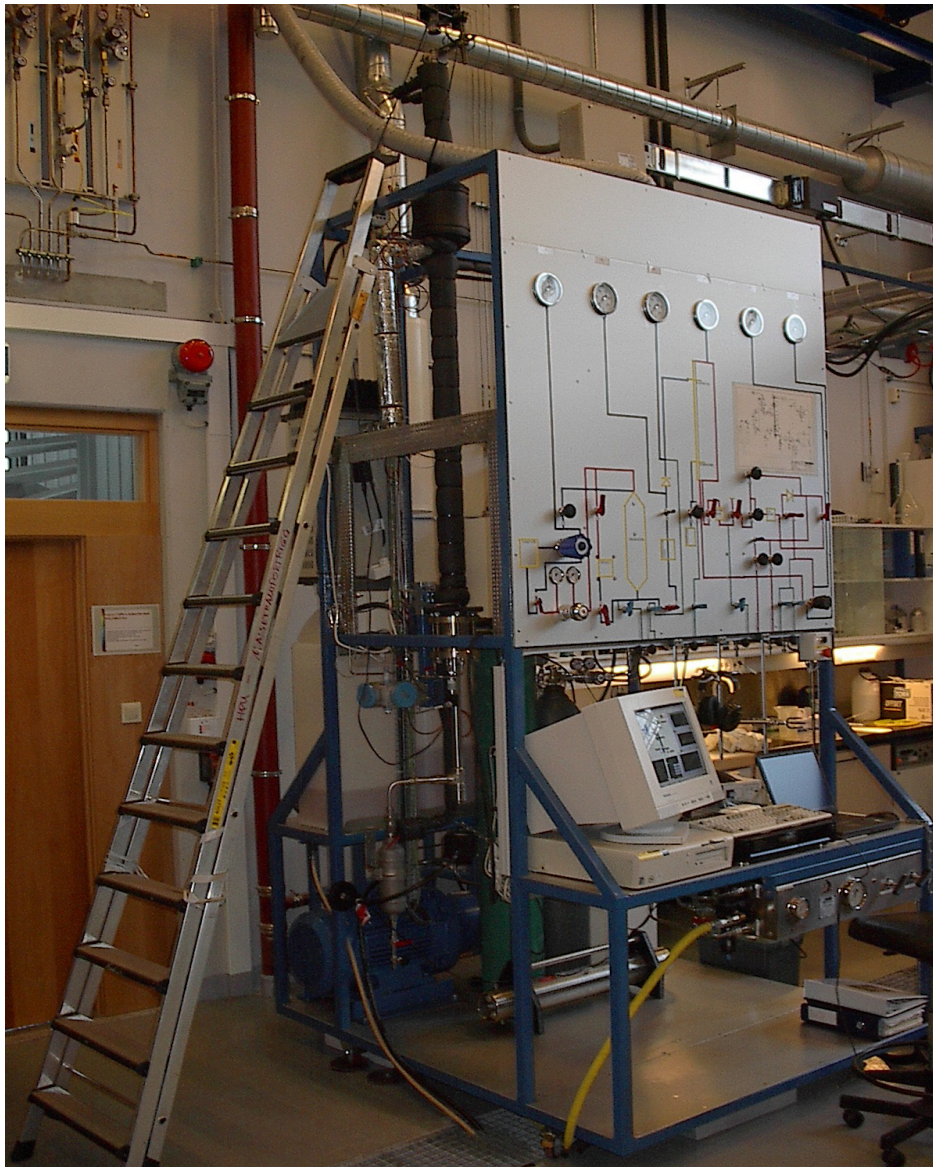
Figure 9-3 Picture of the high pressure wetted wall tower

9.2.1 The Wetted Wall Pipe

A 2.5 meter long and 25.2 mm inner diameter stainless steel pipe was used as the main component of the high-pressure wetted wall column. Because of the need for a calming section at the inlet and outlet (both 0.5 meter long), only 1.5 meter of the total length could be used to contact the liquid and gas. The inner wall of the pipe was polished so a smooth liquid film could easily form and flow as a continuous film down the wall. By varying the length of the inner pipe the contact length between liquid and gas could be varied from 0.1 to 1.5 meter

The temperature of the wetted wall column was controlled by heating tapes mounted on the outside of the pipe. The heating effect of the heating tape was regulated with a Eurotherm regulator. A layer of isolation material was placed on the outside of the heating tape.

In Figure 9-4 a picture taken from the top of the wetted wall column is given. We can see the distribution point of the liquid film – and the inner pipe. Separation of gas and liquid will be obtained when the liquid film flows on the outside of the inner pipe and the gas flows on the

inside of this pipe. The gap between the inner pipe and the wall of the wetted wall column is about 1.5 mm. A very small and normally negligible amount of liquid will flow into the inner pipe (as droplets). It was important that the pipe was placed in a totally vertical position for the liquid film to distribute correct and flow evenly down the pipewall.
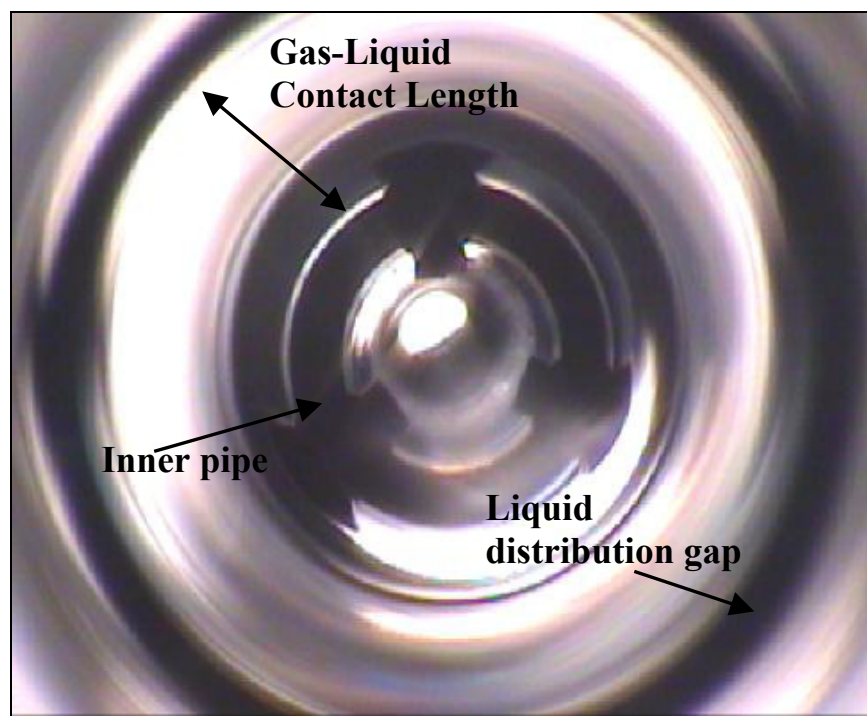
Figure 9-4 A picture taken from the top of the wetted wall column

Inner pipes with three different lengths were fabricated during this work. These three thin walled pipes gave contact lengths between liquid and gas of respectively 0.1, 1.0 and 1.5 meter. Only the inner pipe, which gave a gas-liquid contact length of 1.5 meter, was used in the experiments presented in this thesis.

Table 9-1 Characteristic data for the wetted wall column

Inner Diameter [mm]	Gas-Liquid Contact length [m]	Relative Roughness [ra]	Material	Temperature range	Pressure range
25.2	0.1 - 1.5 m	0.1-0.15	Stainless Steel	Up to 100°C (at 200 bar)	Up to 200 bar

9.2.2 Gas Circulation System

The gas circulation was carried out using a Haskel gas-booster. The booster can operate at pressures up to 275 bar and circulate 35 actual litres of gas pr minute (independent of total pressure). A picture of the gas-booster is given in Figure 9-6.

Nitrogen and CO_2 were supplied to the gas loop from separate gas bottles. The pressure of CO_2 on the gas bottle (about 60 bar at 298 K) can be lower than the operating pressure of the wetted wall column (up to 200 bar). The supply point of CO_2 is therefore placed between a pressure reduction valve, that reduces the pressure to approximately 50 bar, and the gas

booster (see Figure 9-5 and flow diagram in appendix F). A Sulzer gas mixer is placed directly after the injection point of CO_2 and nitrogen.
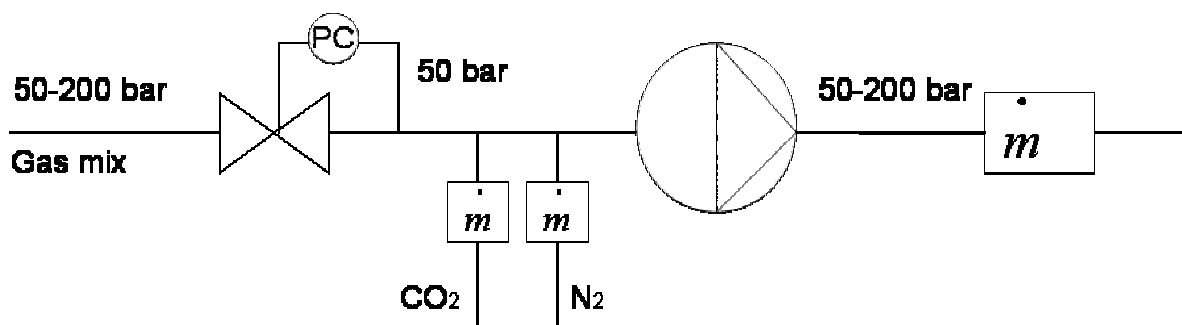
Figure 9-5 Gas injection and mixing system

Before an experiment was started - the inert gas was circulated for long enough time to become saturated with the liquid solution (water and amine).

A Bronkhorst thermal mass-flow meter with a capacity of 0-1000 Nlitres/min was used to measure the total gas circulation rate. The CO_2 supply rate was measured by a thermal-mass flow meter with a capacity of 0-100 Nlitres/min.

Temperature controlled heating tapes wrapped around the piping regulated the gas temperature. The temperature was measured with PT100 elements placed at the inlet and outlet of the wetted wall column. The pressure was measured at two different sites on the wetted wall column (at the top and bottom).

Calibration curves and error analysis for the measurement equipment used – are given in appendix H.
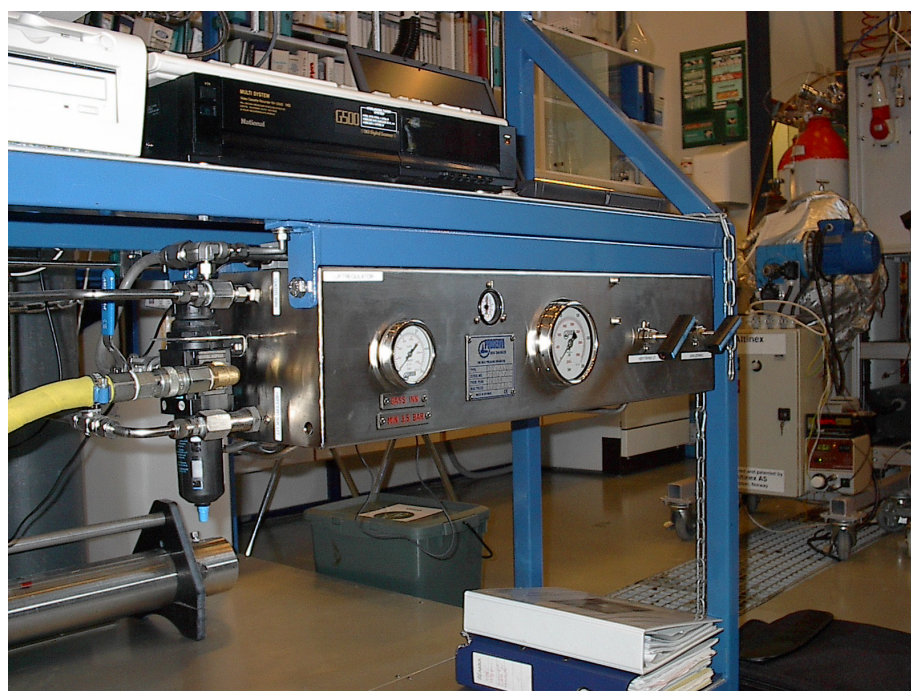
Figure 9-6 Haskel gas-booster used for gas circulation

The main specifications for the gas circulation system are listed in Table 9-2.

Table 9-2 Technical specification for gas circulation system

Equipment	Type	Capacity
Haskel gas booster	ProServ type AGD-32	32 Al/min
Bronkhorst Mass Flow meter for CO_2	F-112AC-HD-44-V Thermal Mass Flow Meter	100 Nl/min
Bronkhorst Mass Flow Meter for nitrogen and CO_2 mixture	Thermal Mass flow meter	1000 Nl/min
Temperature regulation	Heating tapes with Eurotherm PID controllers	20-60°C

9.2.3 Liquid Circulation System

The liquid solution was operated in a batch wise manner. Fresh liquid was supplied from a 60-litre plastic storage tank and pressurized by a liquid circulation pump. A backpressure regulator regulated the pressure, and a custom made liquid accumulator dampened the pressure variations/pulses and created a constant and smooth liquid supply. This accumulator also functioned as a saturator, where the liquid was saturated with the inert gas at the operating pressure before entering the wetted wall column. The liquid pump system is illustrated in Figure 9-7. In the experiments done in this work the liquid flow rate was typically 0.2-1.5 litre/min.

The liquid flow rate was measured by a turbine-meter with a capacity of 0 - 10 litre/min. Heating tapes on the piping from the pump to the liquid distributing system heated the liquid to the desired operation temperature. The liquid inlet temperature could be regulated between ambient and 60°C.

Table 9-3 Technical specification for liquid circulation system

Equipment	Type	Capacity
Liquid pump	Øwre-Johnsen	20 liters/min
Turbine Flow Meter	Swissflow 800/6	0.2-10 l/min
Liquid Accumulator	Custom-made by ProServ	1 litre
Temperature regulation	Heating tapes with Eurotherm PID controllers	up to 60°C
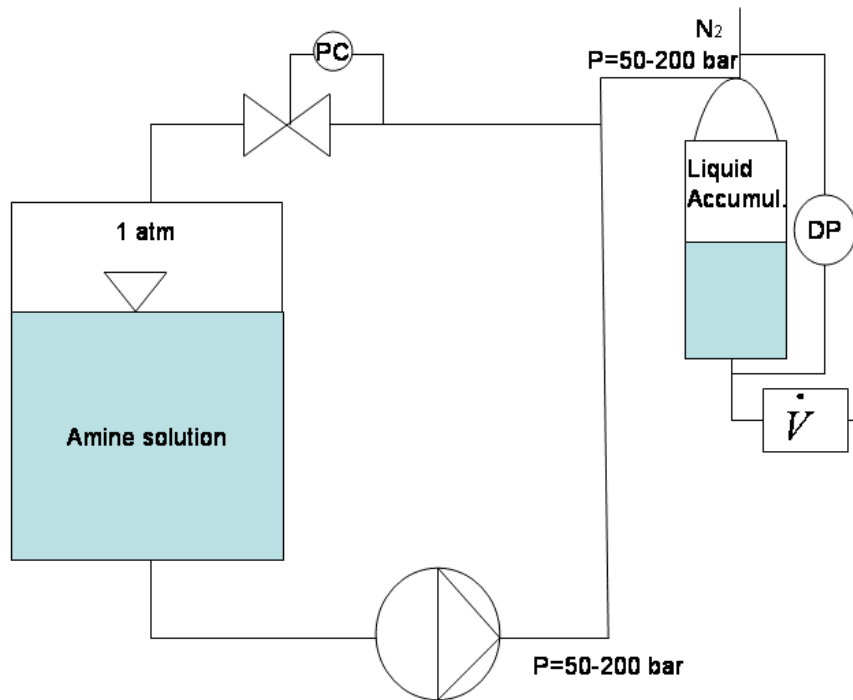
Figure 9-7 Liquid pump and gas saturation system

9.2.4 Liquid Distribution System

The liquid distribution was carried out with a custom-made liquid film distributor designed and made in the mechanical workshop at the Statoil research centre. A sketch of the liquid distribution chamber is given in Figure 9-8.

The liquid film was distributed evenly and effectively by regulating the gap between the distribution chamber and the wetted wall pipe (see Figure 9-8). The film distribution system was able to create a smooth liquid film over a large range of liquid flow rates. The distribution gap could be varied with valve handles on the top of the distribution chamber. In Figure 9-9 photographs of the liquid film flowing down the wetted wall column at different operation pressures are given. There was no gas circulation when these pictures were taken. Video recordings of liquid film flow at varying pressures and flow rates are available on the web (www.stud.ntnu.no/~solbraa/thesis/video).

At high pressures and large gas circulation rates the insight into the column was poor. At these conditions it was difficult to visually control that the liquid film wetted the pipewall completely. A large amount of video-recordings of the liquid film were taken during the experiments. In this work no attempt was made to analyse pressure effects on droplet- and fluid ripple formation.
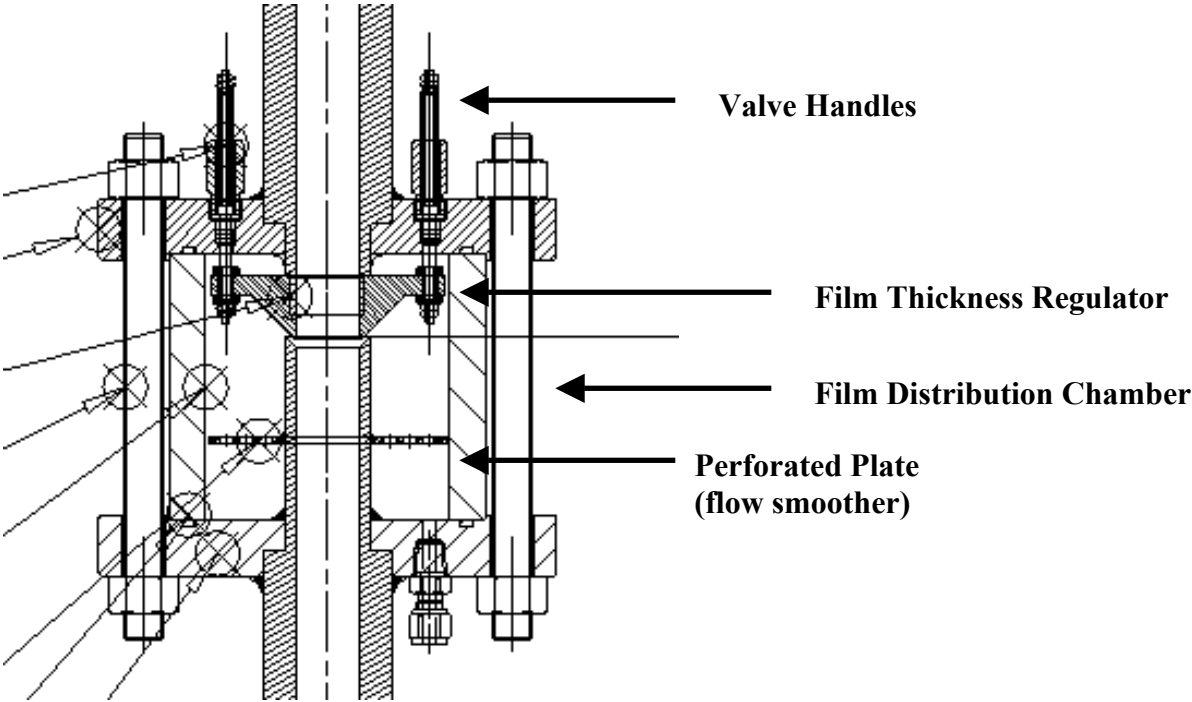
Figure 9-8 Liquid film distributor
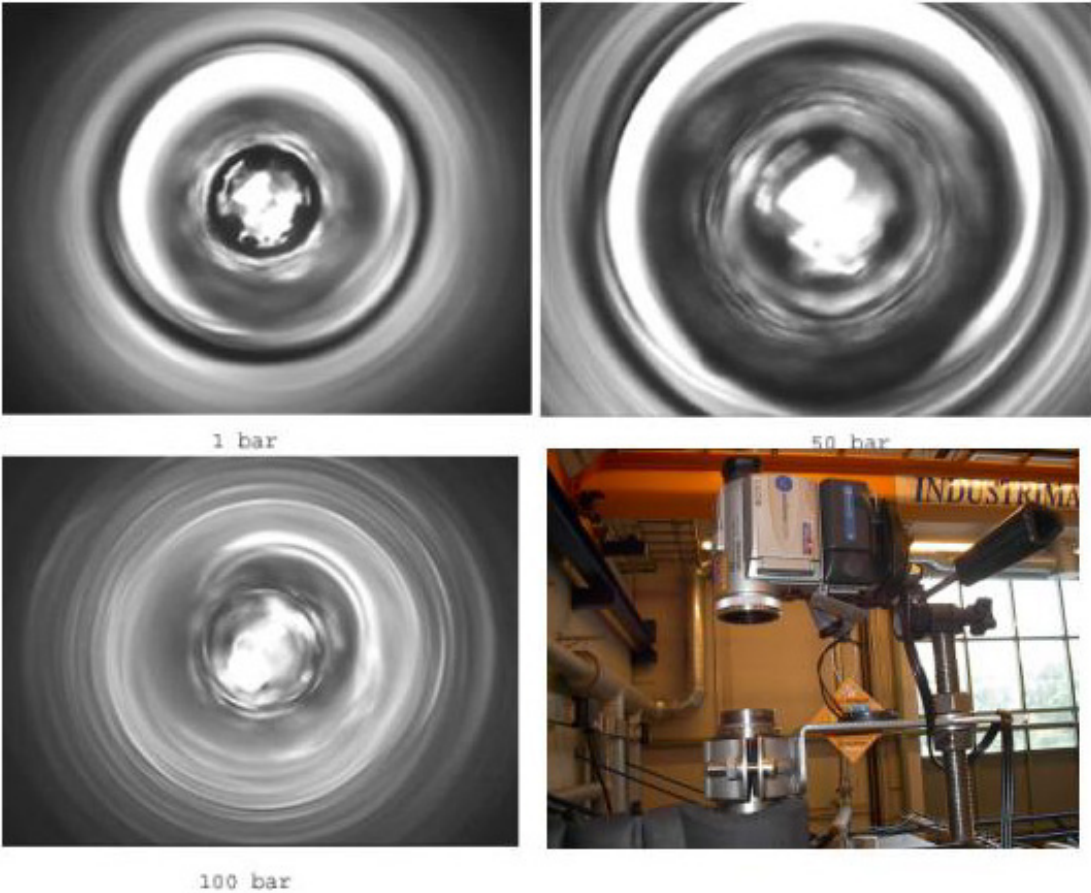
Figure 9-9 Pictures of the liquid film distribution at varying pressures

Ripple formation on the liquid film, as seen in Figure 9-9, was observed at all operating conditions. This ripple formation will eventually disappear for very short contact lengths and with low liquid circulation rates. In this work the only contact length used was 1.5 meter – and ripples always formed.

Typical liquid and gas velocities, Reynolds numbers and phase fractions for the experiments done in this work are given in Figure 9-11 and Figure 9-12. These data were calculated using the two-fluid model as described in chapter 5. The characteristic numbers will vary dependent on viscosities of the liquid (temperature in the system) and will thus be different for water and MDEA (higher viscosity). At the moment no measuring devices for velocity and holdup are installed on the experimental equipment.

From Figure 9-11 and Figure 9-12 we can see that for a gas circulation rate of 200 Nlitres/min the gas flow will be turbulent at all operational pressures (Re>5000). A gas circulation rate of 200 Nlitres/min was used in all experiments done in this work. The gas velocity would typically be between 2-10 cm/sec at this circulation rate. The liquid film velocity was typically 20-50 cm/sec for the liquid circulation rates used in this work.

The liquid droplets formed in the wetted wall column were collected in a droplet collector at the bottom of the column (see Figure 9-10). No analysis was made on the droplet formation rate during experiments, but the amount of liquid transported as droplets was always small (typically 1 dl of droplets formed per 10 liter of circulated liquid).
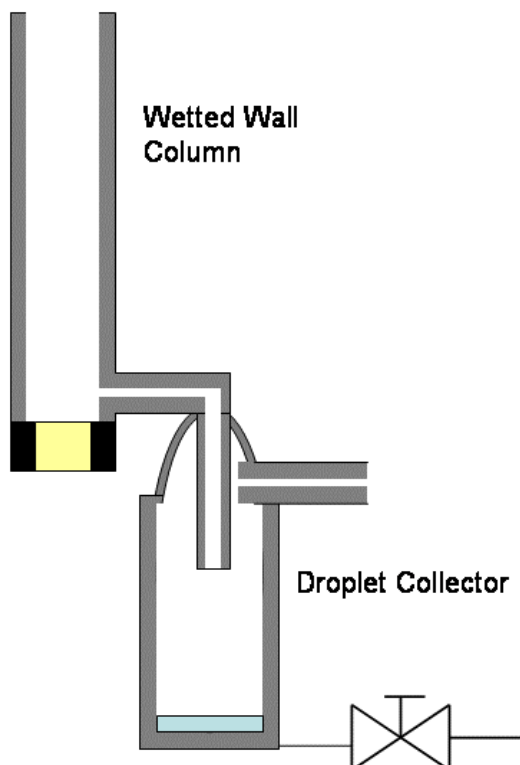
Figure 9-10 Droplet collection system
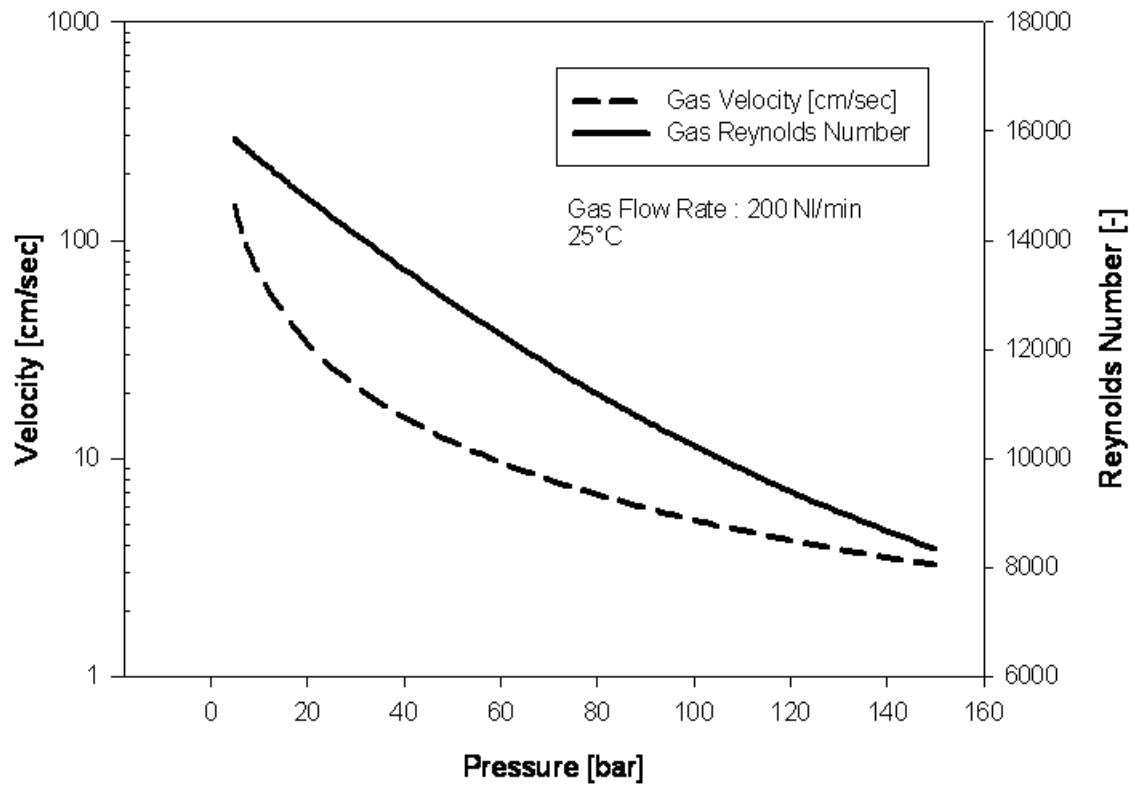
Figure 9-11 Velocity and Reynolds number of gas
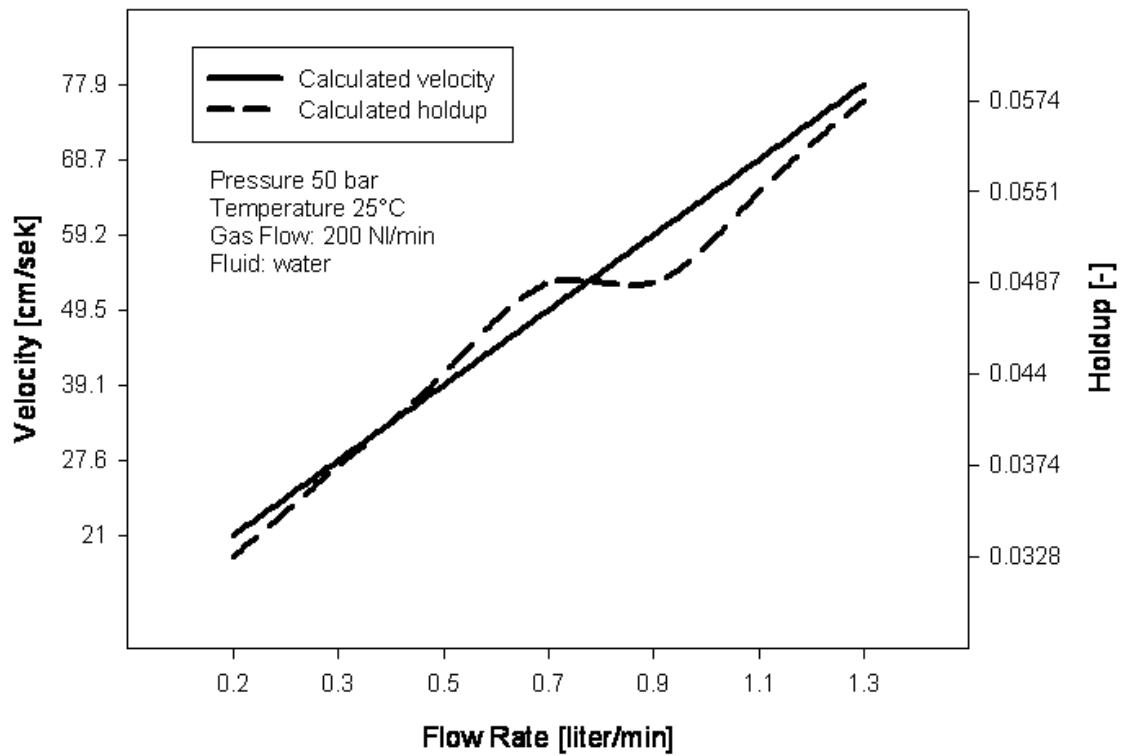
Figure 9-12 Typical liquid holdup and velocity for water

9.2.5 Regulation and Control

The computer program LabView from National Instruments was used for data logging, control and regulation of the electronic equipment used in the wetted wall column. Temperature set points, logging and plotting intervals were specified through this user interface. A screenshot of the graphical user interface is given in Figure 9-13.

All of the electrical equipment are placed in a cabinet on the experimental rig. Safety controllers for temperature and emergency stop buttons are placed in this cabinet.
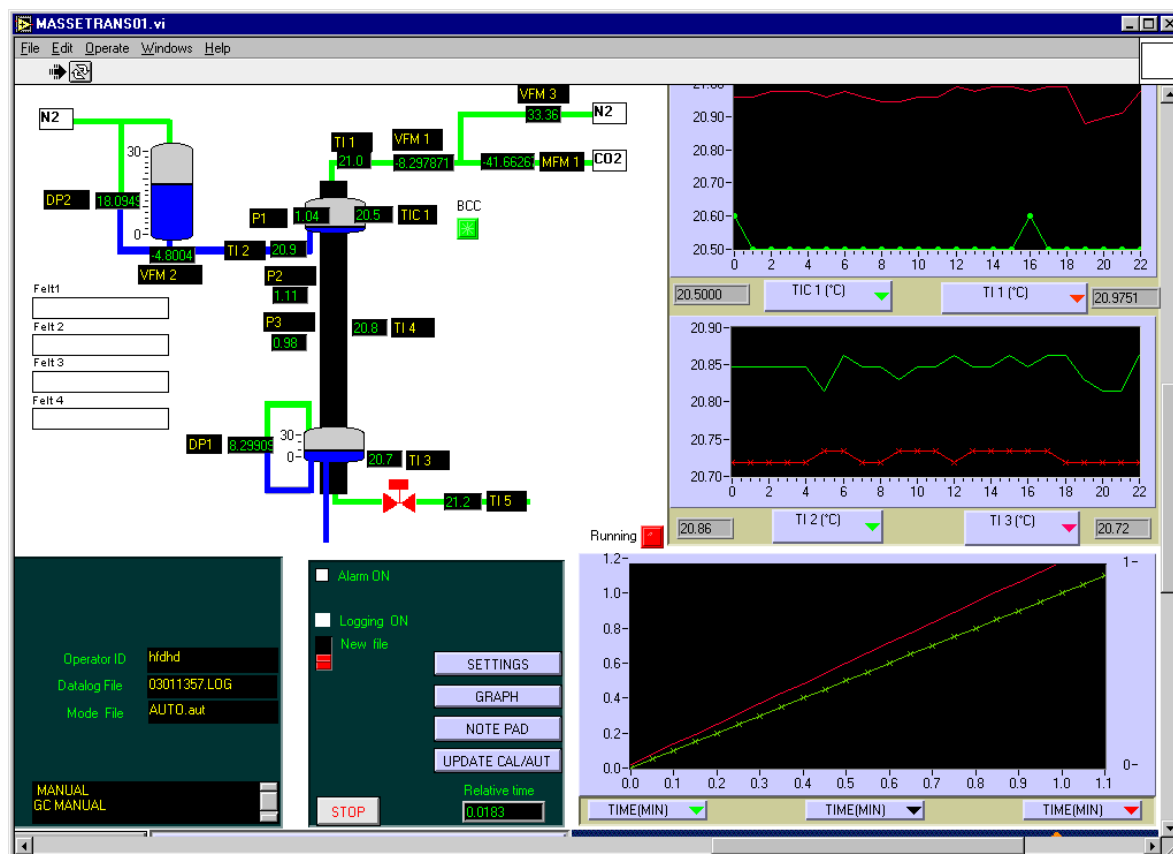
Figure 9-13 LabView logging and regulation user interface

9.2.6 Gas and Liquid Sampling Points

Many gas and liquid sampling points are placed on the experimental equipment. Gas and liquid samples will typically be taken from points at the inlet and outlet of the wetted wall column. The composition of the liquid was analysed before it was filled into the liquid supply tank. The liquid was analysed by a Gas Chromatography technique described by Addicks (2002). The liquid composition at the outlet could be calculated from the total mass balance from knowledge of flow rates and inlet liquid and gas compositions. Analyses of liquid-samples taken at the liquid-outlet were done infrequently and were only used for control.

Sampling bags (1 litre) were used for gas sampling. Gas samples were taken from both the inlet and outlet of the column. The outlet gas composition was used for control since it also could be calculated from the knowledge of the CO_2 supply rate (in a steady state situation). A

picture of a gasbag is shown in Figure 9-14 where we see a gas sample being taken at the gas outlet. The gas was analysed with a gas chromatograph.

Figure 9-14 Gas sampling on wetted wall column

9.2.7 Test Fluids

The specifications of the test fluids used in this study are given in Table 9-4.

Table 9-4 Fluid specifications

Fluid	Supplier	Quality
Nitrogen	Hydro Gas	5.0
CO_2	Hydro Gas	5.0
MDEA	DYNEA	> 98 wt% MDEA
Water	Distilled water	-

MDEA-solutions of 30 and 50 wt% were made by weighing up specified amounts of water and MDEA. Typically 30 litres of a solution of a given composition were made at the time and filled into the liquid supply tank.

9.2.8 Gas and Liquid Analysis

Both gas and liquid analysis were done using a gas chromatograph technique. The gas chromatograph used for gas analysis was calibrated against a calibration gas from Norsk

Hydro (90% Nitrogen and 10% CO_2). The results from these calibrations are given in appendix H.

The liquid analysis was done with a gas chromatograph calibrated against results from a precipitation titration technique (using NaOH and BaCl) for analysing the CO_2 content in liquid samples. For a detailed explanation of the analysis techniques used, the reader is referred to Addicks (2002).

Table 9-5 gives the specifications for the gas chromatographs used in this work.

Table 9-5 Gas Chromatograph Specifications

Analysis Type	Equipment	Supplier	Components
Gas Analysis	Gas Chromatograph	Hewlet Packard 6890 series	CO_2 and nitrogen
Liquid Analysis	Gas Chromatograph	Hewlet Packard 6890 series	CO_2, MDEA and water

9.3 Experimental Method

An experiment started by filling the apparatus to the desired partial pressure of CO_2 and nitrogen. The gas booster and a regulating valve were used to circulate the gas at a specified flow-rate. Heating tapes on the gas piping heated the gas to the set point of the temperature controller.

The liquid circulation was started and regulated to a specified flow rate. The liquid was heated to the desired temperature using heating elements on the liquid accumulator and a heating tape near the liquid inlet on the wetted wall column. The liquid flow rate was regulated using a metering valve (and a frequency regulated engine for the liquid pump).

After the temperatures and flow rates had stabilized in the column, the CO_2 supply rate was regulated until the pressure stabilized at a specified initial pressure. The CO_2 suply rate was now equal to the absorption rate into the liquid (only CO_2 was assumed to be absorbed since the liquid was saturated with nitrogen and the gas was saturated with water).

The experiments could be done in two ways:
1. During experiments CO_2 was supplied into the gas loop at constant rate. When the rate of absorption of CO_2 from the gas was equal to the supply rate (the pressure was stable) gas samples were taken at the inlet and outlet.
2. The CO_2 supply was stopped and the pressure drop was measured as a function of time. The absorption rate could be calculated from the measured pressure drop in the column. This kind of experiment gives a lot of data – since the process is dynamic and the concentration of CO_2 in the gas is constantly changing.

Both of these methods were tested during this work. The first experimental method has the advantage that the absorption rate is measured directly, while in the second method it has to be calculated from the pressure drop rate. The second method has the advantage that a large number of different data points with varying CO_2 partial pressure are measured in single experiments. The disadvantage is that the absorption rate has to be calculated (using an equation of state) from knowledge of pressure drop rate, volume of the total equipment and

temperatures in the system. Both methods seemed to give reasonable results. In Figure 9-15 the pressure is given for an experiment where CO_2 first was supplied at constant rate (method 1) and then suddenly stopped (method 2). The experimental data presented in this work were measured using the first method, where CO_2 was supplied at constant pressure and rate.
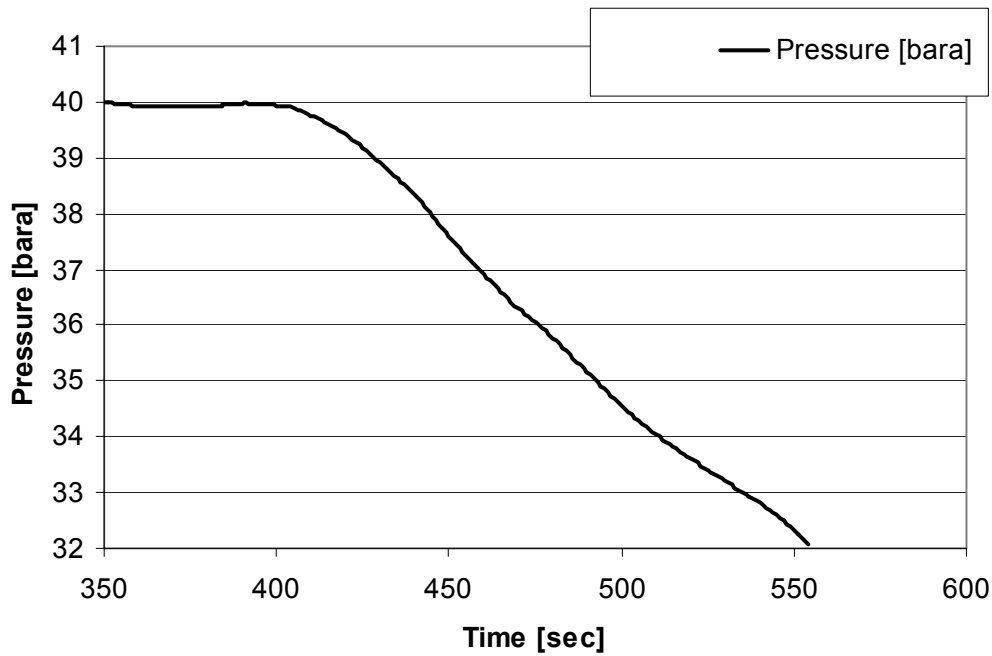
Figure 9-15 Pressure-log during an experiment
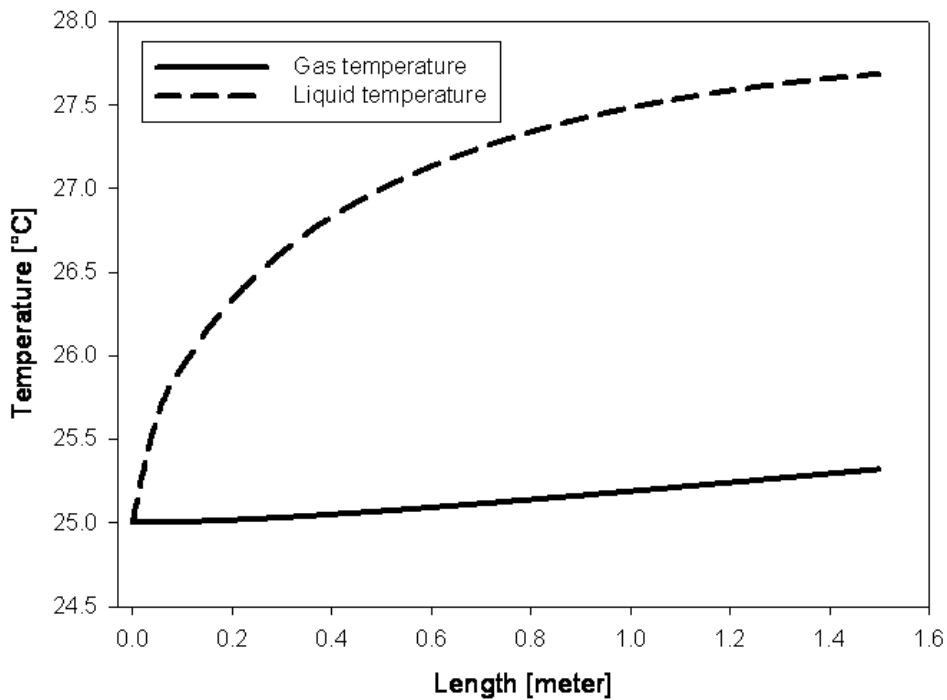
Figure 9-16 Temperature rise due to chemical reaction (CO_2 and MDEA) in the wetted wall column

When performing experiments with CO_2 and amines – reactions will occur in the liquid. The temperature of the liquid will rise due to the exothermic reaction. The effect of the chemical reactions was typically a temperature difference of 1-3°C for the liquid in the top and bottom of the column. A typical case was simulated using NeqSim – and the temperature profile is given in Figure 9-16.

9.4 Calibration and Error Analysis

Calibration of the measurement equipment used in the wetted wall column was done regularly. Calibration results are given in appendix H.

The error analysis related to the experiments done during this work is presented in the last part of appendix H. The estimated error contributions from erroneous temperature, pressure, liquid flow rate and gas flow rate measurements were maximum 4-5% of the measured absorption rate. The error in the measured absorption rate of CO_2 is about 2% of measured value (contribution from thermal mass flow meter). The absorption rate of CO_2 could be measured with a total uncertainty of 6-7% of measured value.

9.5 Mathematical Modeling of Wetted Wall Columns

Gas absorption in a long wetted-wall column differs in several aspects from the conventional packed column or bubble column. The interfacial area for mass transfer in a wetted-wall column is fixed and known. Waves on the free surface of a falling film contribute only a small increase in interfacial area by a few percent. Thus the mass transfer can be determined directly in terms of the flow and physical properties. Because of this, the wetted-wall column has been used as a model equipment for studying the transport mechanism at a turbulent gas-liquid interface.

Modeling of turbulent and wavy transport with chemical reaction has been conducted eg. by Menez and Sandall (1975) and Yih and Chen (1982). A number of investigators such as Kamei and Oishi (1955), Emmert and Pigford (1954), Lamourelle and Sandall (1972), Chung and Mills (1976) have studied gas absorption rates in wavy and turbulent falling films. Yih and Chen (1982) collected and systematized much of the experimental data obtained (data from 11 different experimental works), and were able to create general equations for the mass transfer coefficient of falling films with a standard deviation of 15% (regressed to available experimental data from wetted wall columns).

The mathematical model obtained by Yih and Chen was based on the viscosity-dampened turbulence model (VDTM) proposed originally by Henstock and Hanratty (1978). The model and the references to the experimental data used by Yih and Chen are given in Table 9-6. The experimental data used in the modeling work was found from experiments where CO_2, oxygen, hydrogen and helium were absorbed in water. All experimental data were obtained at pressures less than 10 bar.

Table 9-6 Correlation obtained by Yih and Chen (1982) regressed to available experimental data[1]

Reynolds Number	Number of exp. Data Points	Correlating Equation $k_L^* = \left(\dfrac{k_L}{D}\right)\cdot\left(\dfrac{v^2}{g}\right)^{1/3}$	Standard Deviation	Temperature
49 - 300	121	$k_L^* = 1.099\cdot10^{-2}\,\mathrm{Re}^{0.3995}\,Sc^{1/2}$	18.2 %	8.5-50°C
300 - 1600	364	$k_L^* = 2.995\cdot10^{-2}\,\mathrm{Re}^{0.2134}\,Sc^{1/2}$	13.2 %	8.5-50°C
1600 - 10500	361	$k_L^* = 9.777\cdot10^{-2}\,\mathrm{Re}^{0.6804}\,Sc^{1/2}$	12.3 %	8.5-50°C

1) Yih and Chen(1982), Kamei and Oishi (1955), Emmert and Pigford (1954), Lamourelle and Sandall (1972), Chung and Mills (1976)

The correlating equation found by Yih and Chen will be described in detail in next chapter.

In the experimental work done during this work the resistance to mass transfer in the gas phase was always negligible. Gas phase resistance can be important in systems with very fast reactions in the liquid phase. This could happen if fast reacting activators were added to the amine solution (e.g. piperazine). The model used to calculate binary mass transfer coefficients in the gas phase in this work is equation (4.48)

$$St = \frac{1}{2} f \cdot Sc^{-2/3}$$

where f is the fanning friction factor and can be calculated from equation (5.8) for two phase flow. This equation reduces to equation (4.50) for a smooth surface and turbulent gas flow.

9.6 Simulation of Absorption Processes in the Wetted Wall Column Using NeqSim

In this work the simulation, modeling and parameter regression to the experimental data measured in the wetted wall column were done using NeqSim. The script used to simulate a typical absorption process in the experimental equipment is given below (HP-masstrans.py). The calculated CO_2 absorbed as function of column length is given in Figure 9-17.

```python
# HP-masstrans.py
# created by:   Even Solbraa, January 2002

temperature = 298.15
pressure = 50.0
wtmdea = 30.0
flow = 0.5

systemName = thermo('electrolyte', temperature, pressure)
systemName.addComponent('methane', 160.0, 'Nlitre/min',0)
systemName.addComponent('CO2', 40.0, 'Nlitre/min', 0)
systemName.addComponent('MDEA', (wtmdea/100.0*flow), 'kg/min', 1)
systemName.addComponent('water', ((100.0-wtmdea)/100.0*flow), 'kg/min', 1)
reactionCheck(systemName)
newdatabase(systemName)
systemName.setPhysicalPropertyModel(3)
mixingRule(systemName,4)
stream1 = neqstream(systemName)

legHeights =            [0,0]
legPositions =          [0.0, 0.5]
pipeDiameters =         [0.025, 0.025]
outerTemperature =      [295.0, 295.0]
pipeWallRoughness =     [1e-5, 1e-5]
pipe = twophasepipe(stream1, legPositions, pipeDiameters, legHeights,
outerTemperature, pipeWallRoughness)
pipe.setInitialFlowPattern("annular")
pipe.setOutputFileName("c:/labsim/exp04.nc")

run()
processTools.view()
```
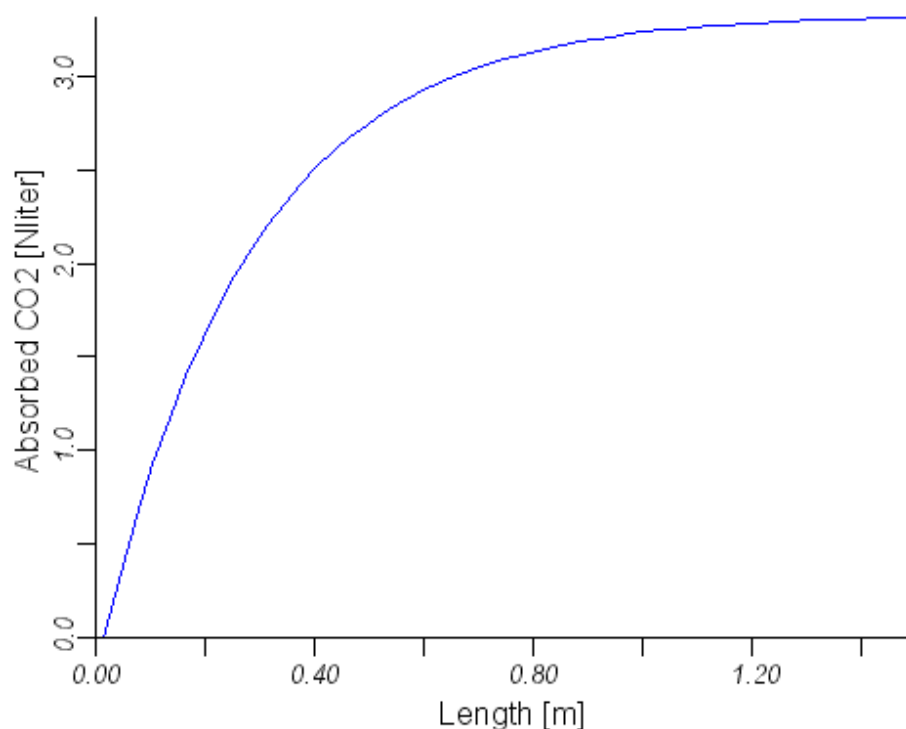
Figure 9-17 Calculated absorbed CO$_2$ as function of gas-liquid contact length.
            Script: HP-masstrans.py, p. 212

9.7 Experiments

An overview of the experiments done during this work is given in Table 9-6.

Table 9-6 Experiments done in this work

Experiment Type	Number of Experiments	Comments	Temperature [°C]	Pressure [bar]	Purpose
Water-CO$_2$-nitrogen	12	Low pressure experiments	25, 40	20	Study physical mass transfer – compare to exciting low pressure data
Water-CO$_2$-nitrogen	35	High pressure experiments	25, 40	50, 100,150	Measure new high pressure data
MDEA-water-CO$_2$-nitrogen	48	High pressure experiments	25, 40	50, 100,150	High pressure absorption data of CO$_2$ in MDEA solutions

The detailed experimental results are presented in the next chapter.

9.8 Summary

A high pressure wetted wall column experimental equipment has been designed and built. The experimental equipment can operate at pressures up to 200 bar and at temperatures between ambient and 60°C. The wetted wall column was made of a polished stainless steel pipe and visual inspection was possible through high-pressure windows in each end. The contact length between the liquid and the gas can be varied between 10 and 150 cm. In this work all experiments were done using the longest gas-liquid contact length.

The wetted wall column is unique of its kind because of the possibility to carry out experiments at very high pressures (up to 200 bar). New experimental high pressure absorption data of CO_2 in aqueous MDEA solutions have been measured during this work and will be presented in the next chapter.

10 Experimental Data and Mass Transfer Modeling

In this chapter the experimental data obtained from experiments with the high-pressure wetted wall column are presented. Two types of experiments were done. In introductory experiments nitrogen, CO_2 and water systems were used to analyse pure physical mass transfer of CO_2 into water. In later experiments mass transfer of nitrogen and CO_2 into aqueous MDEA solutions were studied - to look at reactive mass transfer in amine systems. The experiments were done at pressures between 20 and 150 bar and at temperatures 25 and 40°C.

The nitrogen, CO_2 and water experimental data were used to evaluate and tune the physical mass transfer model described in earlier chapters. The nitrogen, CO_2, MDEA and water data were used to regress the parameters describing the reaction kinetics (rate constants and enhancement factor) used in the modelling of reactive mass transfer.

The non-equilibrium two-fluid model described in chapter 5 is the basis of the modelling work to the experimental data obtained from the wetted wall column. When we calculate the fluid mechanical state of a system it is important to be able to calculate thermodynamic- and physical properties correct. In the mass transfer model described in chapter 4 we assumed local equilibrium at the interface as well as chemical equilibrium in the liquid bulk. This means that an accurate equilibrium model is important. The thermodynamic model used in the modelling work in this chapter is the electrolyte ScRK-EOS described in chapter 3 with the parameters regressed in chapter 8. Physical properties such as viscosities and diffusivities are important parameters in the non-equilibrium two fluid model. The physical property models used in this work are described in appendix D.

It is important to notice that when we fit parameters to a new model - the parameters will be strictly valid only in combination with the other models used. In this work parameter fitting was done for all the fundamental models (thermodynamic-, physical properties-, mass transfer- and fluid mechanical models). It is important to note that an error in one of the fundamental models - would give an error when fitting parameters in models that are based on this model.

10.1 Physical Mass Transfer - Experiments and Modelling

It is important to be able to simulate and predict pure physical mass transfer in the experimental equipment before we start to study reactive mass transfer. Pure physical mass transfer is easier to model than reactive mass transfer. In this work the parameters in the model used to calculate binary mass transfer coefficients were fitted to the physical mass transfer data. The model used to calculate the reaction rate constant (and enhancement factor) between MDEA and CO_2 was fitted to the reactive mass transfer data of this work.

All experiments in this work were done with a 10 bar partial pressure of CO_2 in the gas phase and with a gas circulation rate of 200 Nliter/min. The gas-liquid contact length was 1.5 meter in all experiments. The gas flow was turbulent and resistance to mass transfer in the gas phase was always negligible. The wetted wall column was first evacuated – and CO_2 was filled to a pressure of 10 bar. Nitrogen was then filled into the system until the wanted total pressure was obtained. The gas and liquid circulation rates were regulated to specified set points. New CO_2 was supplied to the wetted wall column at equal rate as the absorption rate in the liquid.

The total pressure in the system should then be stable. The absorption rate was measured directly by a thermal mass flow meter.

10.1.1   Experimental Data for Nitrogen, CO₂ and Water Systems

The experimental data obtained in this work with nitrogen, CO_2 and water are presented in Table 10-1. The columns in Table 10-1 are:

Experiment	Name identifier of the experiment
P_{CO_2}	The partial pressure of CO_2 in the gas
P_{total}	The total pressure in the wetted wall column
Temperature	The temperature of the liquid and gas in °C
$\dot{V}_{water}$	The liquid flow rate measured as liter/min
$\dot{V}_{total\,gas-circulation}$	The total gas circulation rate (circulated with the gas booster)
$\dot{V}_{CO_2\,absorption,exp.}$	The absorption rate of CO_2 measured as Nliter/min
$\dot{V}_{CO_2\,absorption,model}$	The calculated absorption rate using the model developed in this chapter
Re_{liq}	The Reynolds number of the liquid film (calculated)
Sc_{liq}	The Schmidt number of the liquid film (based on CO_2)
$\dfrac{k_{liq,exp}^*}{Sc_{liq}^{0.5}}$	A dimensionless mass transfer coefficient (calculated from measured data)
$\dfrac{k_{liq,model}^*}{Sc_{liq}^{0.5}}$	A dimensionless mass transfer coefficient calculated from the model
abs.rel.dev	The deviation between the measured dimensionless mass transfer coefficient and the one calculated with the model

The reference experiments were done at 25 and 40°C with liquid circulation rates of 0.3, 0.5, 0.7, 0.9, 1.1 and 1.3 liter/min. By varying the liquid flow rate the effect of liquid Reynolds number can be evaluated.

The dimensionless mass transfer coefficient is calculated from

$$k_L^* = \left(\frac{k_L}{D}\right)\cdot\left(\frac{\nu^2}{g}\right)^{1/3}$$

where k_l is the mass transfer coefficient, D the diffusion coefficient, and ν the kinematic viscosity. The relation by Yih et.al (1982) described in last chapter was used to calculate the mass transfer coefficient k_l for the experimental equipment. The experimental measured mass transfer coefficient can be calculated from the equation

$$k_l = \frac{\dot{V}_{liq}}{2\pi RL}\left(\frac{R}{R+\delta}\right)\ln\frac{C_s-C_{1b}}{C_s-C_{2b}} \tag{10.1}$$

where R is the radius of the pipe and δ is the liquid film thickness (calculated from the two-fluid model). C_s is the concentration of CO_2 in the liquid in equilibrium with the gas. C_{1b} and C_{2b} are the actual concentrations of CO_2 in the liquid at the inlet and at the outlet.

For the experiments done the water film absorbed from 50 to 100% of the maximum capacity of CO_2 in water at the operation conditions. It was important to prevent complete saturation (or close to saturation) of the liquid phase, since extraction of kinetic information from such data will be impossible. For some of the experiments done the contact time was too long – and almost complete saturation was obtained. Most of the experimental points were obtained under suitable conditions for mass transfer experiments.

A comparison between experimental data and calculated values is presented in graph 10-1 to 10-3. From the experimental data we see higher mass transfer rates with increasing liquid circulation rates and with higher partial pressure of CO_2. This is in agreement with theories on turbulent mass transfer – where driving forces and turbulence intensity contributes to the mass transfer.

These experimental data will be used for data regression in the next section.

Table 10-1 Experimental data from Wetted –Wall-Column for the system nitrogen, CO₂ and water

Exp.	P_{CO_2} [bar]	P_{total} [bar]	Temp. [°C]	$\dot{V}_{water}$ [liter/min]	$\dot{V}_{total\,gas-circulation}$ [Nliter/min]	$\dot{V}_{CO_2,absorption,}$ exp. [Nliter/min]	$\dot{V}_{CO_2,absorption,}$ model [Nliter/min]	Re_{liq} [-]	Sc_{liq} [-]	$\dfrac{k^*_{liq,exp}}{Sc_{liq}^{0.5}}$	$\dfrac{k^*_{liq,model}}{Sc_{liq}^{0.5}}$	abs.rel.dev [%]
ref01	10	20	25	0.3	200	2.2	1.93	238	585	0.135	0.103	23.8
ref02	10	20	25	0.5	200	2.8	2.75	480	584	0.123	0.112	9.1
ref03	10	20	25	0.7	200	3.5	3.36	672	584	0.132	0.120	8.9
ref04	10	20	25	0.9	200	3.8	3.84	865	584	0.130	0.127	2.3
ref05	10	20	25	1.1	200	4	4.22	1057	584	0.127	0.132	-4.4
ref06	10	20	25	1.3	200	4.6	4.56	1249	584	0.145	0.137	5.7
ref07	10	20	40	0.3	200	1.6	1.40	397	299	0.088	0.107	-22.0
ref08	10	20	40	0.5	200	2.3	2.00	663	299	0.119	0.120	-0.8
ref09	10	20	40	0.7	200	2.6	2.81	929	299	0.101	0.129	-27.3
ref10	10	20	40	0.9	200	3.1	3.28	1194	299	0.114	0.136	-19.0
ref11	10	20	40	1.1	200	3.5	3.66	1460	299	0.123	0.142	-15.3
ref12	10	20	40	1.3	200	4.1	4.12	1725	299	0.144	0.156	-7.8
ref13	10	50	25	0.3	200	1.7	1.64	288	583	0.135	0.103	23.7
ref14	10	50	25	0.5	200	2.4	2.32	481	583	0.131	0.112	14.8
ref15	10	50	25	0.7	200	2.8	2.82	673	583	0.120	0.120	-0.3
ref16	10	50	25	0.9	200	3.2	3.21	866	582	0.139	0.127	8.7
ref17	10	50	25	1.1	200	3.4	3.53	1059	582	0.140	0.132	5.4
ref18	10	50	25	1.3	200	3.7	3.79	1251	582	0.151	0.137	9.1
ref19	10	50	40	0.3	200	1.4	1.29	398	299	0.094	0.107	-14.5
ref20	10	50	40	0.5	200	2	1.92	663	299	0.123	0.120	2.3
ref21	10	50	40	0.7	200	2.4	2.41	928	299	0.120	0.129	-7.5
ref22	10	50	40	0.9	200	2.8	2.80	1193	299	0.131	0.136	-4.0
ref23	10	50	40	1.1	200	3.0	3.12	1459	299	0.133	0.142	-6.2
ref24	10	50	40	1.3	200	3.4	3.51	1724	299	0.147	0.156	-5.8
ref25	10	100	25	0.3	200	1.4	1.30	289	581	0.085	0.103	-22.0
ref26	10	100	25	0.5	200	1.8	1.83	482	581	0.119	0.112	6.1
ref27	10	100	25	0.7	200	2.2	2.21	674	580	0.142	0.120	15.1
ref28	10	100	25	0.9	200	2.5	2.50	867	580	0.148	0.127	14.3
ref29	10	100	25	1.1	200	2.6	2.73	1060	580	0.147	0.132	9.7
ref30	10	100	25	1.3	200	2.9	2.93	1253	580	0.168	0.137	18.1
ref31	10	100	40	0.3	200	1.1	1.05	397	298	0.074	0.107	-46.1
ref32	10	100	40	0.5	200	1.6	1.56	662	298	0.119	0.120	-0.4

ref33	10	100	40	0.7	200	1.8	1.94	927	298	0.106	0.129	-21.8
ref34	10	100	40	0.9	200	2.1	2.23	1192	298	0.120	0.136	-13.4
ref35	10	100	40	1.1	200	2.3	2.48	1457	298	0.127	0.142	-11.4
ref36	10	100	40	1.3	200	2.6	2.78	1722	299	0.147	0.156	-6.1
ref37	10	150	25	0.3	200	1.1	1.07	289	579	0.086	0.103	-19.8
ref38	10	150	25	0.5	200	1.6	1.48	482	579	0.128	0.112	12.3
ref39	10	150	25	0.7	200	1.7	1.79	675	579	0.133	0.120	9.4
ref40	10	150	25	0.9	200	2.2	2.02	868	579	0.172	0.127	26.0
ref41	10	150	25	1.1	200	2.1	2.21	1061	578	0.178	0.132	25.6
ref42	10	150	25	1.3	200	2.3	2.36	1254	578	0.190	0.137	27.6
ref43	10	150	40	0.3	200	0.9	0.88	397	298	0.077	0.107	-40.3
ref44	10	150	40	0.5	200	1.4	1.30	662	298	0.143	0.120	16.2
ref45	10	150	40	0.7	200	1.6	1.61	926	298	0.124	0.129	-3.8
ref46	10	150	40	0.9	200	1.8	1.85	1191	298	0.131	0.136	-3.8
ref47	10	150	40	1.1	200	2	2.05	1456	298	0.144	0.142	1.3
ref48	10	150	40	1.3	200	2	2.01	1720	298	0.147	0.155	-5.6
Abs. Average:												**13.0 %**

10.1.2   Parameter Regression to the Physical Mass Transfer Model

For a liquid film in a wetted wall column we usually get an expression for the mass transfer coefficient on the form

$$k_L^* = \left(\frac{k_L}{D}\right) \cdot \left(\frac{v^2}{g}\right)^{1/3} = K \cdot \text{Re}^a \, Sc^b \qquad (10.2)$$

Where the constants K, a and b are dependent on which kind of fluid mechanical model we apply. The coefficients K, a and b in equation (10.2) are dependent on the turbulence intensity and wave formation on the liquid film. As was described in last chapter Yih et.al (1982) regressed the constants in equation (10.2) to experimental mass transfer data obtained in different wetted wall columns with varying gasses and liquids. The fitted parameters as given by Yih are given in Table 10-2. The standard deviation reported by Yih was about 15 % (see Table 9-6).

Table 10-2 Constants regressed in equation (10.2) by Yih et.al. (1982)

Regime	Reynolds Number	K	a	b
Laminar	Re<300	$1.099 \cdot 10^{-2}$	0.3955	0.5
Laminar-Wavy	300<Re<1600	$2.995 \cdot 10^{-2}$	0.2134	0.5
Turbulent-Wavy	1600<Re	$9.77 \cdot 10^{-4}$	0.6804	0.5

In Figure 10-1 the dimensionless mass transfer coefficient calculated from equation (10.2) are compared to the ones calculated from the experimental data obtained in this work (calculated from equation (10.1)). The absolute relative deviation between the model of Yih and Chen and the experimental data of this work is 13.0%. This is comparable to the deviations between the model and the experimental data used by Yih.

The coefficients in (10.2) were fitted to the experimental data of this work. The objective function used for regression was

$$\chi^2 = \sum_{i=1}^{n} \left(\frac{\dot{V}_{CO_2,\exp} - \dot{V}_{CO_2,calc}\left(T, P_{CO_2}, m_{liq}\right)}{\sigma_{i,\exp}} \right)^2 \qquad (10.3)$$

The standard deviation in the experimental data measured in this work was discussed and estimated in chapter 9. All the physical mass transfer experimental data obtained in this work were measured in the Laminar-Wavy regime. In Table 10-3 the parameters obtained from regression are compared to the parameters presented by Yih et.al. (1982).

Table 10-3 Regressed constants and absolute average deviation to experimental data of this work

Reference	Reynolds Number	K	a	b	Abs.rel.dev. [%]
Yih et.al. (1982)	300<Re<1600	$2.995 \cdot 10^{-2}$	0.2134	0.50	13.0
This work	230<Re<1750	$3.101 \cdot 10^{-2}$	0.2201	0.50	10.5

When the parameters of equation 10.2 were fitted to the experimental data of this work - the best possible fit was an absolute relative deviation of 10.5 %. The accuracy of calculated mass transfer coefficients with the optimised model is illustrated in Figure 10-1. The parameters reported by Yih et.al (1982) were used for further modelling in this work – since they were based on a large range of liquid film Reynolds numbers and could be reproduced using the high-pressure wetted wall column with an acceptable accuracy. The Reynolds number range of the experimental data reported here was limited because only water was used as liquid and the experimental equipment restricted the liquid circulation rate range. High liquid circulation rates could lead to problems with gas-liquid separation in the column, while low circulation rates could lead to incomplete wetting of the wall.

All the high-pressure data measured for the nitrogen, CO_2 and water systems could be represented with an acceptable accuracy with equation (10.2) and the parameters given in Table 10-2. From Table 10-1 and Figure 10-1 to Figure 10-3 we can see that the deviations between experimental data and the model are relatively independent of the total pressure in the system. We can conclude that the mass transfer model with parameters regressed by Yih et.al. (1982) seems to be able to predict high pressure data with a good accuracy.
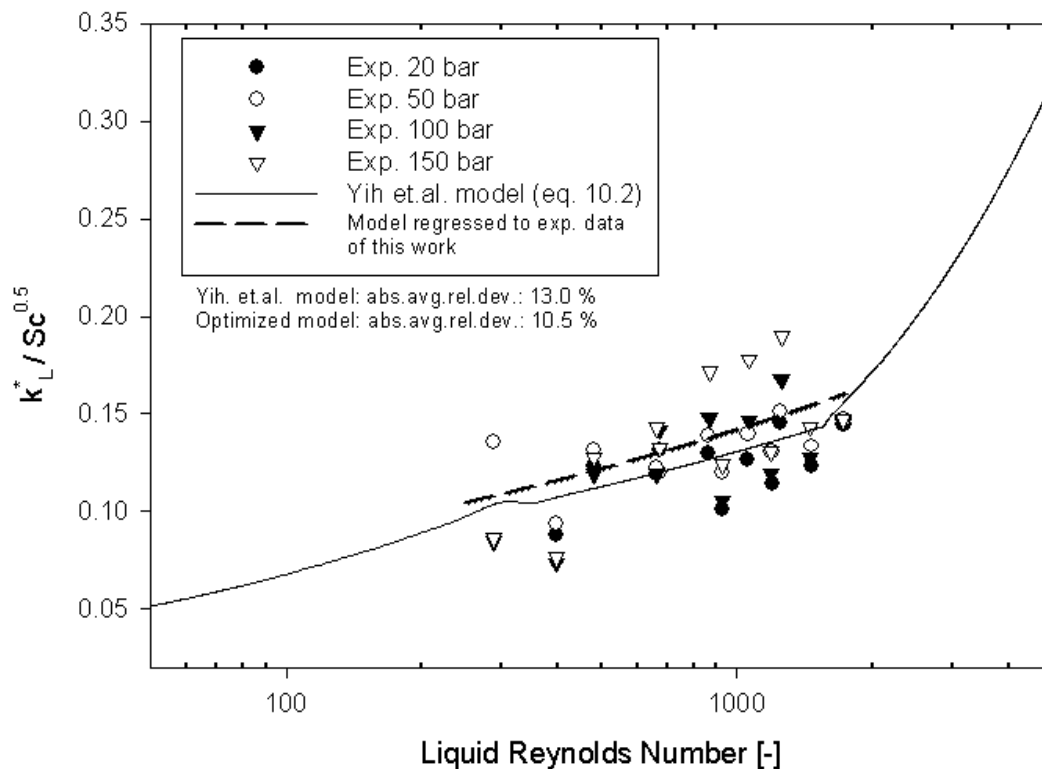
Figure 10-1 Calculated and experimental dimensionless mass transfer coefficients
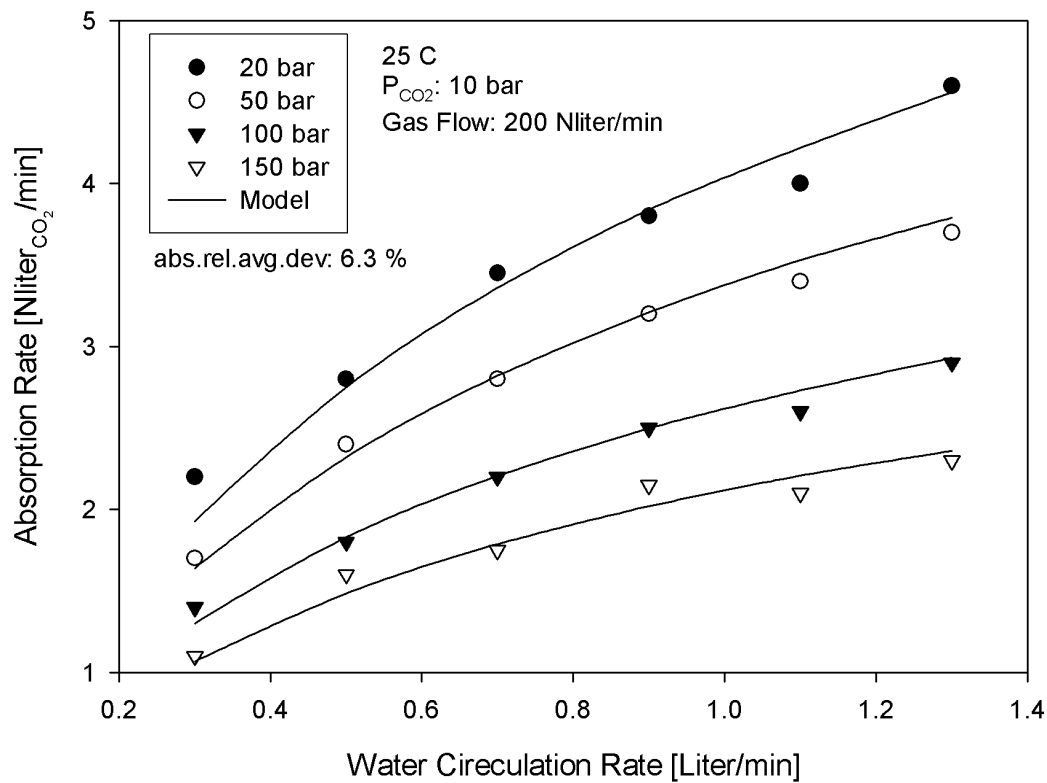
Figure 10-2 Measured and calculated absorption rates of CO$_2$ in water at 25°C.
Script: HP-masstrans.py, p. 212
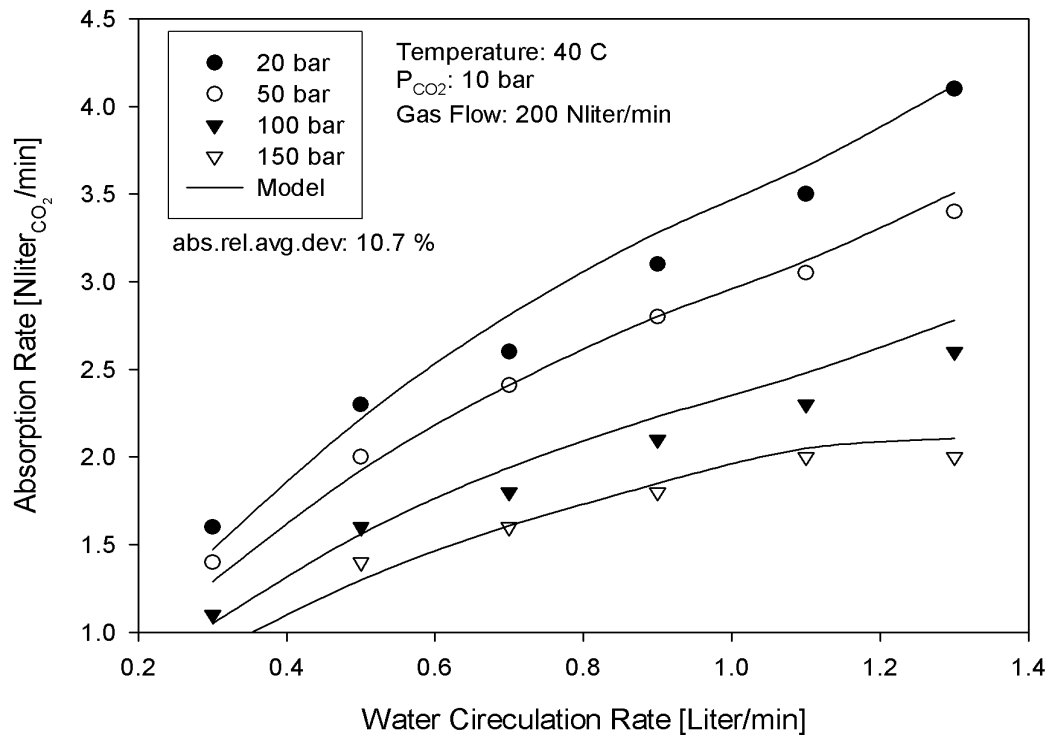
Figure 10-3 Measured and calculated absorption rates of CO$_2$ in water at 40°C.
Script: HP-masstrans.py, p. 212

10.2 Reactive Mass Transfer - Experiments and Modelling

Reactive mass transfer is normally modelled using a physical mass transfer coefficient multiplied by an enhancement factor that is dependent on the kinetics of the reactions. The absorption of CO_2 into MDEA solutions is a reactive mass transfer process, and we thus have to introduce kinetic models (enhancement factor models). The calculation of reactive mass transfer for multicomponent solutions was discussed in chapter 4.

In this work experiments with 30 and 50 wt% MDEA solutions were done. Experiments were run at 50, 100 and 150 bar pressure and at 25 and 40°C. The liquid circulation rate was varied between 0.2 and 0.5 litre/min. The partial pressure of CO_2 in the gas was 10 bar in all experiments.

The mass transfer model described in chapter 4 was used to fit to the experimental data. The Maxwell-Stefan equations were used for the calculation of physical mass transfer in both gas and liquid. The enhancement factor of CO_2 was calculated from an analytical equation using effective mass transfer coefficients and diffusivities. This method was described in chapter 4.

10.2.1 Experimental Mass Transfer Data for CO_2, Nitrogen, MDEA and Water

The experimental data obtained in the experiments with nitrogen-CO_2-MDEA-water are presented in Table 10-4 (no CO_2 in the inlet amine solution).

The columns in Table 10-4 are:

Experiment	Name identifier of the experiment
wt % MDEA	Weight % MDEA in water
P_{CO_2}	The partial pressure of CO_2 in the gas
P_{total}	The total pressure in the wetted wall column
Temperature	The temperature of the liquid and gas
$\dot{V}_{solvent}$	The liquid flow rate measured as liter/min
$\dot{V}_{total\,gas-circulation}$	The total gas circulation rate (circulated with the gas booster)
$\dot{V}_{CO_2\,absorption,\exp.}$	The absorption rate of CO_2 measured as Nliter/min
$\dot{V}_{CO_2\,absorption,\text{mod}el}$	The calculated absorption rate using the model developed in this chapter
abs.rel.dev	The deviation between experimental absorption rates of CO_2 and the ones calculated from the model

The experimental results are presented and compared to calculated values in Figure 10-5 and Figure 10-6. We see that we get a higher mass transfer rate with increasing liquid circulation rate, with higher partial pressure of CO_2 and with increasing temperature. The reaction rate will increase at rising temperatures and will lead to higher mass transfer rates.

These experimental data will be used for data regression in the next section.

Table 10-4 Experimental data from Wetted –Wall-Column for the system CO$_2$, nitrogen, MDEA and water (inlet loading 0.0)

Experiment	wt% MDEA	P_{CO_2} [bar]	P_{total} [bar]	Temperature [°C]	$\dot{V}_{solvent}$ [liter/min]	$\dot{V}_{total\ gas-circulation}$ [Nliter/min]	$\dot{V}_{CO_2,absorption,exp.}$ [Nliter/min]	$\dot{V}_{CO_2,absorption,model}$ [Nliter/min]	Abs.rel.dev [%]
exp01	30	10	50	25	0.25	200	12.5	12.20	2.40
exp02	30	10	50	25	0.3	200	13.2	12.93	2.02
exp03	30	10	50	25	0.4	200	14	14.10	-0.71
exp04	30	10	50	25	0.5	200	15	15.00	0.00
exp05	30	10	50	40	0.25	200	12.6	12.50	0.79
exp06	30	10	50	40	0.3	200	13.4	13.34	0.47
exp07	30	10	50	40	0.4	200	14.5	14.63	-0.90
exp08	30	10	50	40	0.5	200	15.5	15.64	-0.90
exp09	30	10	100	25	0.25	200	7.4	7.21	2.57
exp10	30	10	100	25	0.3	200	7.6	7.70	-1.32
exp11	30	10	100	25	0.4	200	8.8	8.70	1.14
exp12	30	10	100	25	0.5	200	9.2	9.33	-1.41
exp13	30	10	100	40	0.25	200	7.9	7.86	0.51
exp14	30	10	100	40	0.3	200	8.6	8.24	4.19
exp15	30	10	100	40	0.4	200	8.9	8.91	-0.11
exp16	30	10	100	40	0.5	200	9.5	9.44	0.66
exp17	30	10	150	25	0.25	200	4.9	4.73	3.51
exp18	30	10	150	25	0.3	200	5	4.97	0.53
exp19	30	10	150	25	0.4	200	5.4	5.37	0.56
exp20	30	10	150	25	0.5	200	5.5	5.69	-3.53
exp21	30	10	150	40	0.25	200	5.5	5.38	2.24
exp22	30	10	150	40	0.3	200	5.7	5.65	0.88
exp23	30	10	150	40	0.4	200	6.1	6.08	0.33
exp24	30	10	150	40	0.5	200	6.6	6.43	2.58
exp25	50	10	50	25	0.25	200	7.8	7.74	0.73
exp26	50	10	50	25	0.3	200	8.2	8.16	0.52
exp27	50	10	50	25	0.4	200	8.8	8.87	-0.74
exp28	50	10	50	25	0.5	200	9.4	9.46	-0.64
exp29	50	10	50	40	0.25	200	9.3	9.12	1.95
exp30	50	10	50	40	0.3	200	9.6	9.61	-0.06
exp31	50	10	50	40	0.4	200	10.3	10.43	-1.24
exp32	50	10	50	40	0.5	200	11.3	11.11	1.66

Experimental Mass Transfer Data

exp33	50	10	100	25	0.25	200	4.5	4.61	-2.49
exp34	50	10	100	25	0.3	200	4.8	4.86	-1.33
exp35	50	10	100	25	0.4	200	5.2	5.29	-1.67
exp36	50	10	100	25	0.5	200	5.6	5.64	-0.66
exp37	50	10	100	40	0.25	200	5.6	5.69	-1.59
exp38	50	10	100	40	0.3	200	5.8	5.99	-3.21
exp39	50	10	100	40	0.4	200	6.5	6.48	0.29
exp40	50	10	100	40	0.5	200	6.9	6.89	0.19
exp41	50	10	150	25	0.25	200	3	3.00	-0.12
exp42	50	10	150	25	0.3	200	3.1	3.17	-2.34
exp43	50	10	150	25	0.4	200	3.5	3.46	1.27
exp44	50	10	150	25	0.5	200	3.7	3.69	0.30
exp45	50	10	150	40	0.25	200	3.8	3.89	-2.26
exp46	50	10	150	40	0.3	200	4.1	4.09	0.21
exp47	50	10	150	40	0.4	200	4.5	4.43	1.52
exp48	50	10	150	40	0.5	200	4.8	4.71	1.90
							Mean.err.:	1.2%

10.2.2   Parameter Regression to the Reactive Mass Transfer Data

Reactive mass transfer is usually modelled using an enhancement factor approach as was described in chapter 4. The mass transfer was modelled from the equation

$$\dot{m} = E_{CO_2} \cdot k_{CO_2} \cdot \Delta x_{CO_2}$$

(10.4)

where k is the physical mass transfer coefficient as regressed in the last section, and E is the enhancement factor. For multicomponent mass transfer we have (equation (4.97))

$$(N\ ) = c_t(E)\left[k^* \right](x_b - x_i)$$

where E is a vector of enhancement factors, k^* is the matrix of finite flux mass transfer coefficients. In the current work the enhancement factor for all components but CO_2 was set to 1. The finite flux mass transfer matrix is calculated from equation (4.54)

$$\left[k^* \right] = [\Gamma][\Xi][R]^{-1}$$

where $[\Gamma]$ is the non-ideality corrections, $[\Xi]$ is the finite flux correction matrix and $[R]$ is the Maxwell-Stefan mass transfer coefficient matrix. For irreversible (pseudo-) first order reactions we can model the enhancement factor for CO_2 as (see equation (4.98) chapter 4)

$$E_{CO_2} = \sqrt{1 + \frac{\left(k_{2t} \left[MDEA \right] \right) D_{CO_2,eff}}{k_{CO_2,eff}^{\,2}}}$$

(10.5)

The reaction rate for CO_2 in a MDEA-solution can be calculated from

$$r_{CO_2} = k_{2t}\left[CO_2 \right]\left[MDEA \right] - \frac{K_1}{k_{2t}}\left[HCO_3^- \right]\left[MDEA + \right]$$

(10.6)

where k_{2t} is the second order reaction rate constant and K is the chemical equilibrium constant for the reaction between CO_2 and MDEA-solutions. The reversibility of the reactions is accounted for by using thermodynamic models as is described in chapter 4 and appendix E. The reaction rate constant is normally given using an Arrenihus type of equation

$$k_{2t} = k_{2t(T=313K)} \exp\left\{ -\frac{E_a}{R}\left(\frac{1}{T} - \frac{1}{313K} \right) \right\}$$

(10.7)

When all experimental data for absorption of CO_2 in aqueous MDEA done in this work were regressed, the following correlation was found (only reaction rate constant was regressed)

$$k_{2t(T=313.15K)} = 6.45\,m^3 / kmol\,s$$

$$E_a = 50.0\,{}^{kJ}\!\!/\!_{mol}$$

(10.8)

The objective function used for regression of parameters was

$$\chi^2 = \sum_{i=1}^{n} \left(\frac{\dot{V}_{CO_2,\exp} - \dot{V}_{CO_2,calc}\left(T, P_{CO_2}, \dot{m}_{liq}\right)}{\sigma_{i,\exp}} \right)^2$$

The results of the regression of parameters to the experimental data at 25 and 40°C are given in Table 10-5. In Figure 10-4 to Figure 10-7 the experimental measured absorption rates are compared to values calculated with the model using equation (10.7) for the reaction rate constant for CO_2 in MDEA solutions.

Since no equilibrium data for the system nitrogen, CO_2, MDEA and water are available, the ionic interaction coefficient $W_{nitrogen-MDEA^+}$ in the electrolyte ScRK-EOS had to be fitted to the mass transfer data. The regressed values of the ionic interaction coefficient at 25 and 40°C are given in Table 10-5.

Table 10-5 Reaction rate constants fitted to experimental data of this work

Temperature [K]	r $[m^3 / kmol\, s]$	$W_{nitrogen-MDEA^+} \cdot 10^4$ $[-]$	AAD [%]
298.15	2.45	0.96	2.4
313.15	6.45	1.12	3.1

From Table 10-4 and Figure 10-5 and Figure 10-6 we see that the mass transfer model used are able of representing the experimental data of this work with high accuracy.
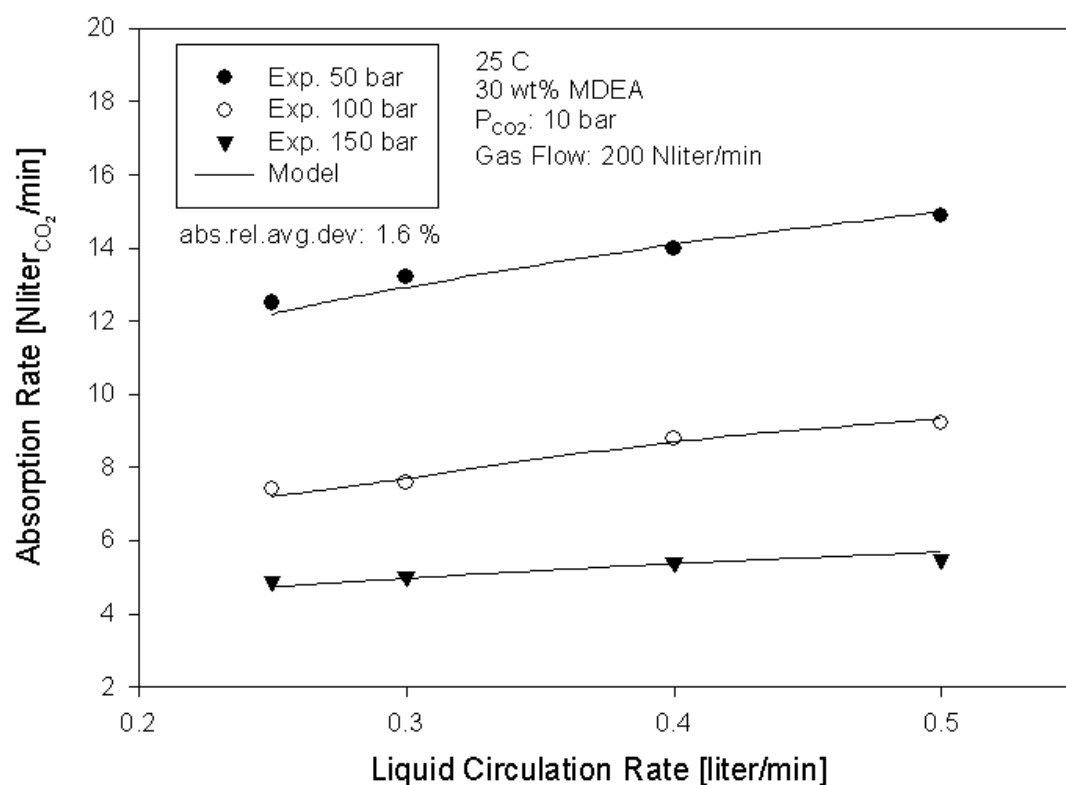
Figure 10-4 Measured and calculated absorption rates of CO₂ in a 30wt% MDEA-solutions at 25°C.
Script: HP-masstrans.py, p. 212
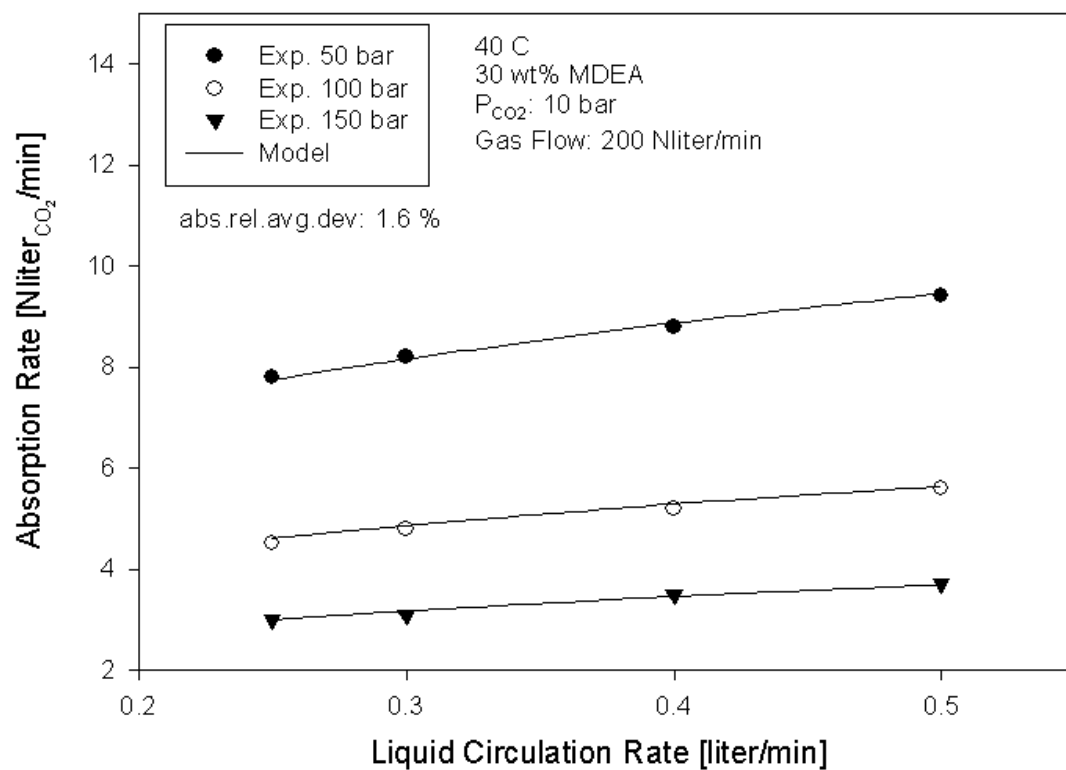
Figure 10-5 Measured and calculated absorption rates of CO₂ in a 30wt% MDEA-solutions at 40°C.
Script: HP-masstrans.py, p. 212
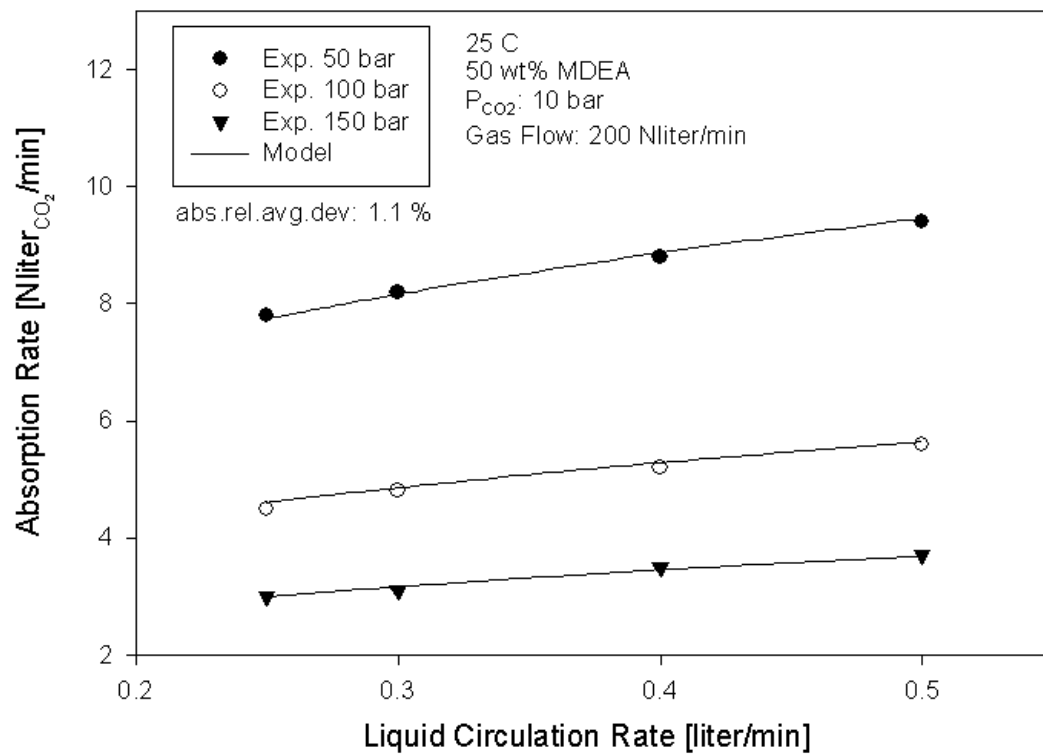
Figure 10-6 Measured and calculated absorption rates of CO_2 in a 50wt% MDEA-solutions at 25°C.
Script: HP-masstrans.py, p. 212
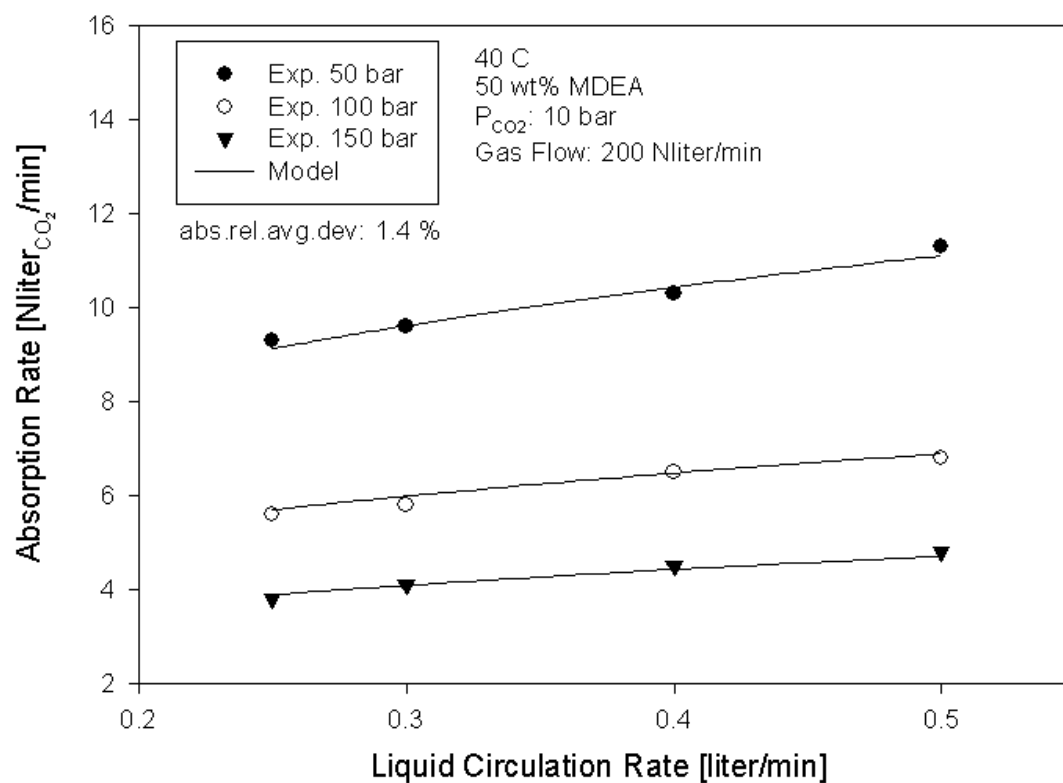
Figure 10-7 Measured and calculated absorption rates of CO_2 in a 50wt% MDEA-solutions at 40°C.
Script: HP-masstrans.py, p. 212

The main reason for the observed decrease in absorption rate of CO_2 with increasing pressure is the non-ideality of the gas phase. The physical solubility of CO_2 in the amine solution decreases with increasing pressures – and the driving force for mass transfer is reduced.

10.3 Summary and Discussions

Two kinds of high-pressure experiments have been done during this work. Reference experiments were done with nitrogen, CO_2 and water – where CO_2 was absorbed in the water phase at pressures between 20 and 150 bar. The physical mass transfer model was fitted to these data. The mass transfer data could be correlated using a model based on the equations published by Yih et.al (1982) with a good accuracy (13% AAD). The results indicate that the mass transfer analogies developed from low-pressure experiments – also seems to be able to represent the data obtained at high pressures in this work. However, it is important to use accurate thermodynamic models for the calculation of CO_2 solubility in the aqueous phase.

In the second kind of experiment done CO_2 was absorbed into aqueous MDEA solutions. In these experiments CO_2 was absorbed into the amine solutions by chemical reactive absorption. The experimental data could be represented by the mass transfer model described in chapter 4 by fitting the model for the second order rate constant for the reaction between CO_2 and MDEA to the experimental data. The rate constants obtained in this work at 25 and 40°C are comparable to the rate constants obtained by other authors from low-pressure experiments. Figure 10-8 shows a comparison of the second order rate constant obtained in this work (equation (10.7)) to the one obtained by Pacheco (1998) from low-pressure experiments (equation (2.9)). We see that the values of the rate constants calculated by the two models are comparable. It should however be noticed that the ionic interaction coefficient $W_{nitrogen-MDEA^+}$ used in the electrolyte ScRK-EOS had to be fitted to the mass transfer data in order to obtain all necessary parameters.
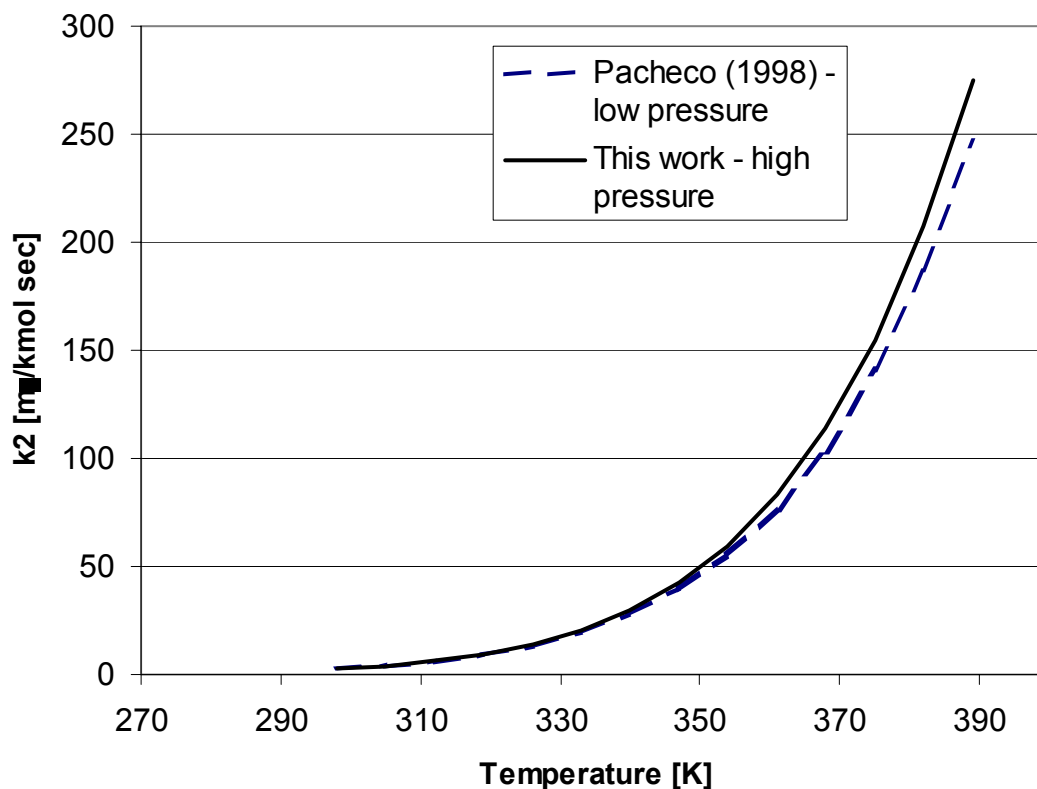
Figure 10-8 Reaction rate constant fitted to the experimental data and to the data of Pacheco (1998)

From this work it is not possible to conclude that the absolute pressure of the system will have a large influence on the reaction rate between CO_2 and MDEA. It rather seems that the high pressure effects can be corrected for by using thermodynamic and mass transfer models that corrects for these effects in a consistent way (equations of state and advanced mass transfer models). This is opposite to the thermodynamic modelling where we concluded that the liquid phase properties were affected in a considerable degree by the total pressure. We should however keep in mind that nitrogen has been used as inert gas in the mass transfer measurements. Nitrogen has a more ideal behaviour at high pressures than methane and is less soluble (typically by one order of magnitude) in the aqueous phase. We would therefore expect the pressure effects of nitrogen to be less important than the pressure effects of methane.

The expression for the rate constant between CO_2 and MDEA obtained from this work – will form the basis when we simulates high pressure gas treating processes using MDEA-water solutions as solvent.

11 Simulation of High Pressure Non-Equilibrium Processes

To demonstrate and test the process simulation model developed in this work and implemented in the NeqSim simulation tool – some case studies have been done. Four of these case studies are presented in this chapter.

In the first case study we track the composition of the natural gas in a pipeline as function of time and position when the composition of the gas varies at the pipe inlet. Such calculations are important when we want to follow specific components in a pipeline in transient operation of the pipe.

In the second case study we simulate a small process plant – where two gasses are mixed – and water starts to condense in a pipeline. The water condensation rate and holdup in the pipeline are calculated along the pipeline using the mass transfer model developed in this work.

In the third case study free water and natural gas containing CO_2 are contacted in a pipeline. Because of the reactions with carbon dioxide the water becomes acidic. The non-equilibrium model developed in this work is used to calculate the pH of the water film as function of position in the pipeline.

In the final case studied we simulate an acid gas treating process where CO_2 is absorbed into a MDEA solution in a packed bed. Composition and temperature profiles in the liquid and gas along the absorption tower are calculated using the mathematical models developed in this work.

The figures presented in this chapter are automatically generated by NeqSim – and will sometimes use unsuitable units on the axis. The results of the examples presented in this chapter can be reproduced by running the scripts in the NeqSim simulation program.

11.1 Case 1. Compositional Tracking of CO_2 in a Natural Gas Pipeline

The first case we have simulated using the non-equilibrium model implemented in NeqSim – is a case where the inlet natural gas composition of a pipeline is changing in time. The reason for such changes could be accidental releases of gases, downtime of the gas processing plant or other unexpected happenings. In the case studied we simulate a situation where the concentration of carbon dioxide in the gas suddenly is increased for some time – and then comes back to normal again. We want to simulate the distribution of CO_2 in the pipe as function of time and position.

We will look at a 720 km long pipe with an inner diameter of 1.0 meter. In steady state operation the gas composition will be 99 mol% methane and 1% CO_2. The inlet pressure will be 200 bar and the total gas flow rate is 50.5 MSm^3/day. The inlet gas temperature was 25°C and the surrounding temperature was 5°C. The pipe was made of steel (1 cm wall thickness) with an outer concrete isolation cap (20 cm). The heat transfer was calculated considering contributions from the gas, walls and surroundings.

The NeqSim script for the case simulated is given below.

```
# Simulates transient flow in a pipeline: pipeflow.py
#
# Written by: Even Solbraa, nov. 2001
#

systemName = SystemSrkEos(298.0, 200.0)
systemName.addComponent("methane", 50, "MSm^3/day")
systemName.addComponent("CO2", 0.5, "MSm^3/day")
stream1 = stream(systemName,"stream 1")

legHeights =            [0,0]
legPositions =          [0.0, 720000.0]
pipeDiameters =         [1.025, 1.025]
outerTemperature =      [278.0, 278.0]
pipeWallRoughness =     [1e-5, 1e-5]
pipe = pipeline(stream1, legPositions, pipeDiameters, legHeights,
outerTemperature, pipeWallRoughness)
pipe.setNumberOfNodesInLeg(100)
pipe.setOutputFileName('c:/steadysim.nc')
run()

times = [0, 60000, 120000, 180000, 250000, 320000]
systemName2 = systemName.clone()
systemName2.addComponent("CO2",  2.0, "MSm^3/day")
systems = [systemName, systemName2, systemName2, systemName, systemName,
systemName]
pipe.setTimeSeries(times,systems,50)
pipe.setOutputFileName('c:/transsim.nc')

runtrans()
```

11.1.1   Stationary Results of Gas Flow in Pipeline

The steady state solution was calculated and used as initial condition for the transient simulations. The pressure, temperature and velocity profiles along the pipeline for the steady state operation are given in Figure 11-1 to Figure 11-3. We see that the pressure drops to about 120 bar and that the temperature falls to a temperature below the surroundings (because of the well known Joule-Thomson cooling effect). The gas velocity will first drop because of the temperature fall in the gas and then rise because of the decreasing gas density/pressure.
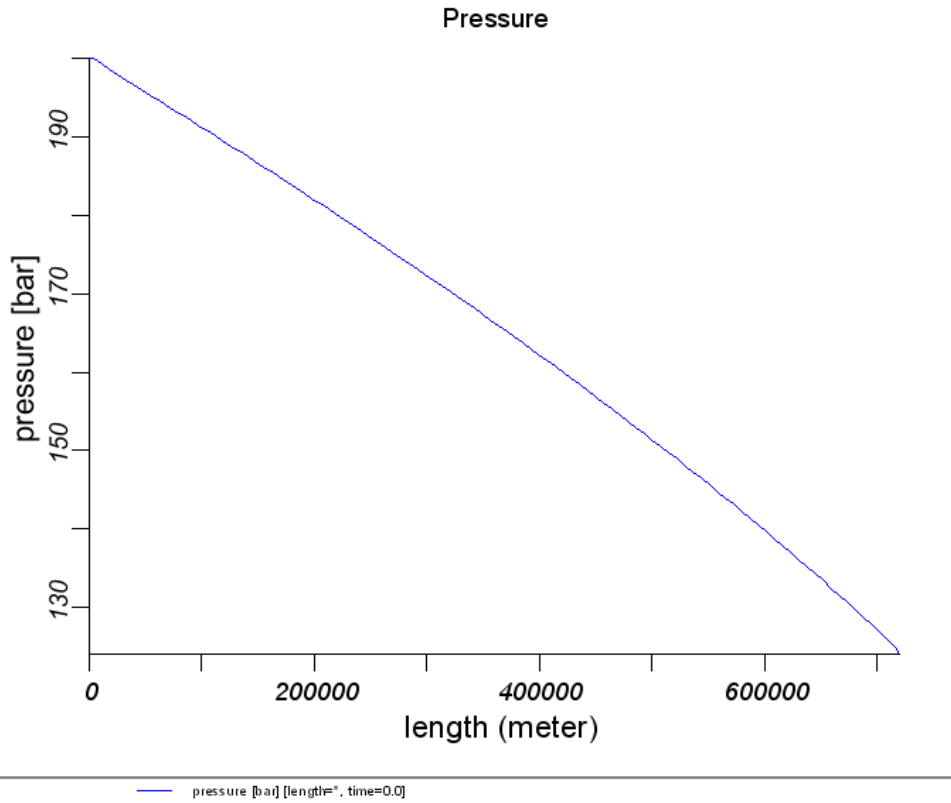
Figure 11-1 Steady state pressure profile for case 1
Script: pipeflow.py, p. 233
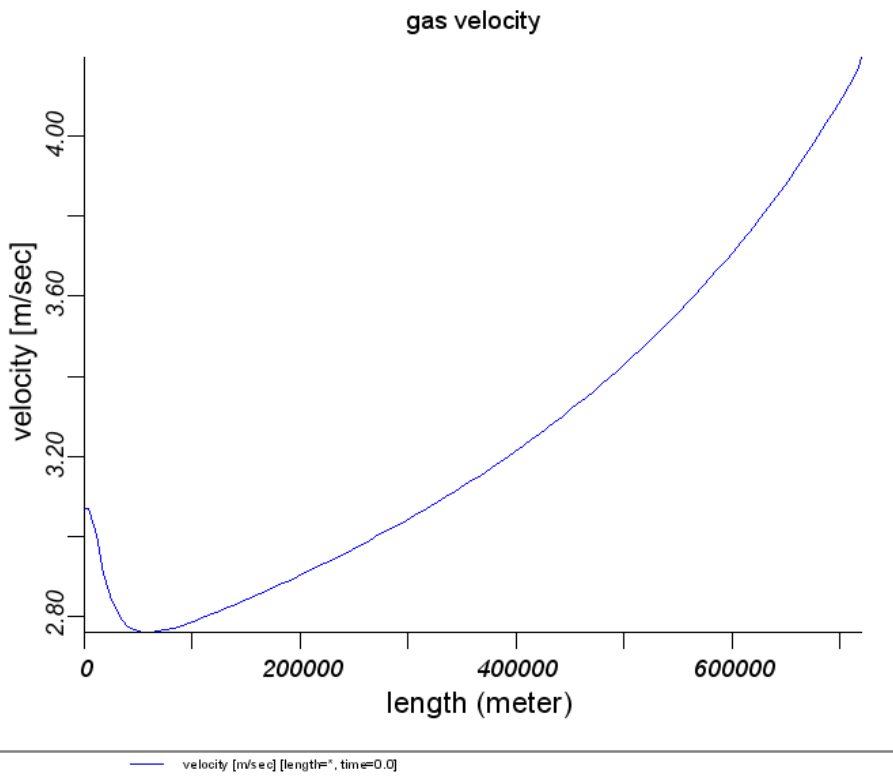
Figure 11-2 Initial gas velocity profile for case 1
Script: pipeflow.py, p. 233
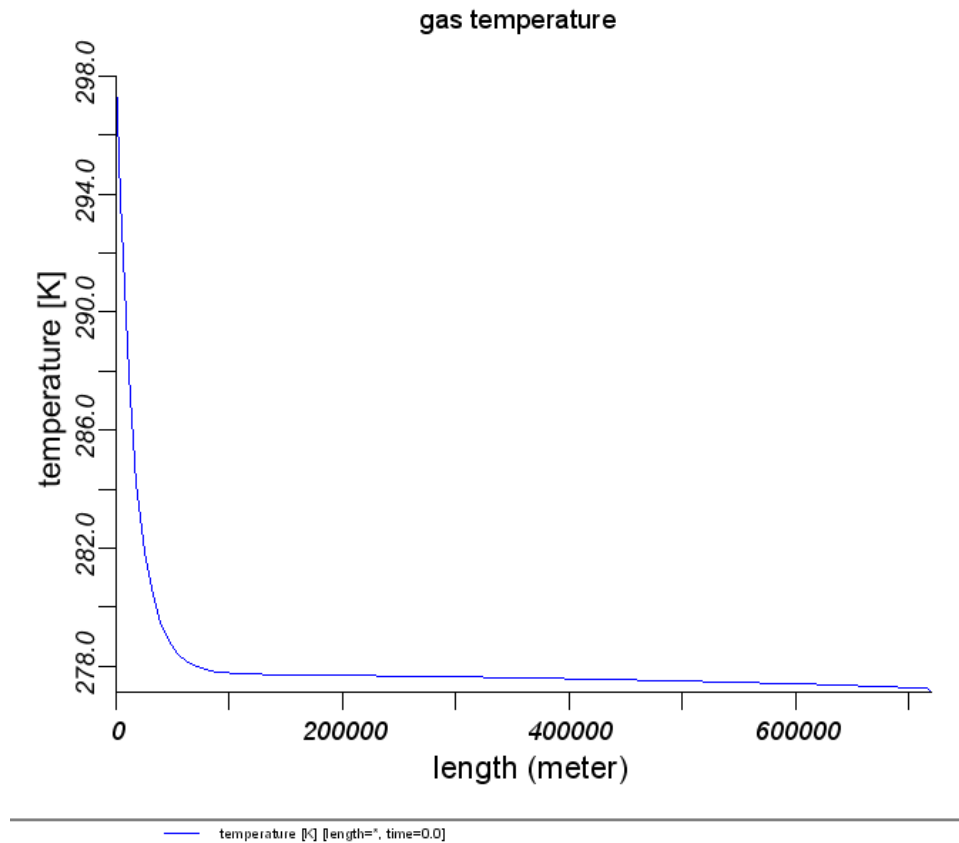
Figure 11-3 Steady state gas temperature profile for case 1
            Script: pipeflow.py, p. 233

11.1.2   Dynamic Results of Transient Flow in Pipeline

In the transient situation, it was assumed that the inlet CO_2 concentration suddenly was raised to 5 mol% (total gas flow rate 52 MSm^3/day) for 33 hours. The velocity and concentration of CO_2 along the pipeline as function of time are given in Figure 11-4 and Figure 11-5.

Axial mixing will occur because of the diffusion and dispersion effects. Because of a high Reynolds number (>1·10^7), the gas will be transported in the pipe in almost plug flow (Levenspiel, 1999). The mixing of the low- and high concentration regions of CO_2 will happen because of dispersion.

Simulations like the one done in this case can be useful in many situations. It is however important to eliminate the effects of numerical dispersion in this type of simulations. The importance of numerical dispersion has not been evaluated for the case simulated here.

From Figure 11-5 we see how the high CO_2 concentration area slowly spreads out as the gas is transported through the pipeline.
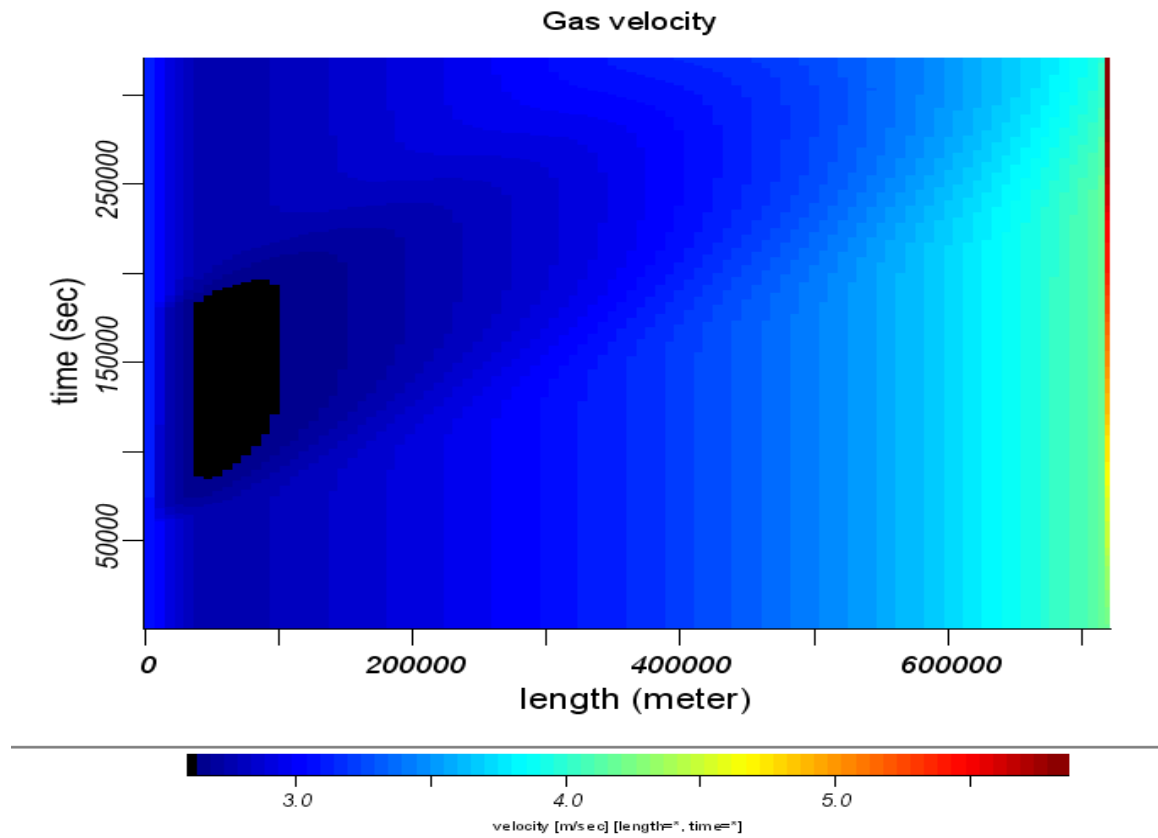
Gas velocity

Figure 11-4 Gas velocity vs. time.
Script: pipeflow.py, p. 233

Molfraction CO2 in gas
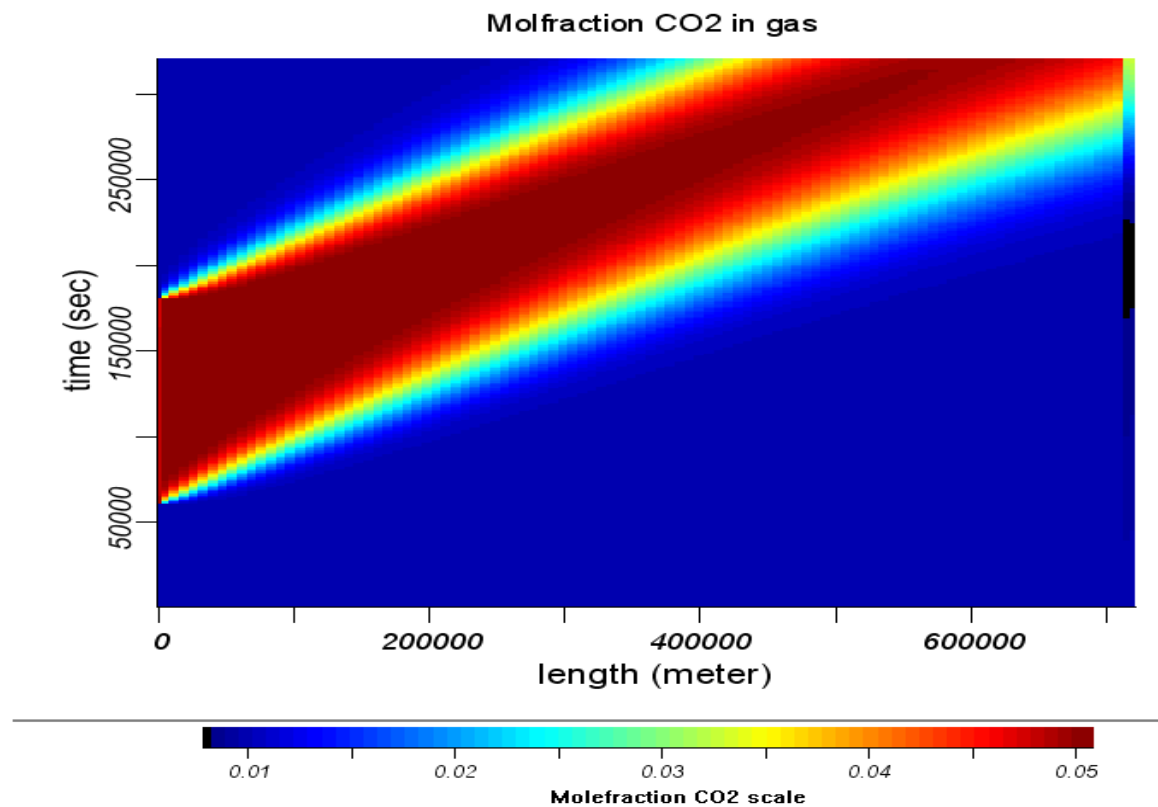
Figure 11-5 Mole fraction CO$_2$ vs. time.
Script: pipeflow.py, p. 233

11.2 Case 2. Condensation of Water in a Pipeline

The next case we will consider is the condensation of water from gas after mixing of two gasses and a fast cooling process. The process we want to simulate is illustrated in Figure 11-6. Such situations can occur in real gas systems when different gasses are mixed and sent into a pipeline.
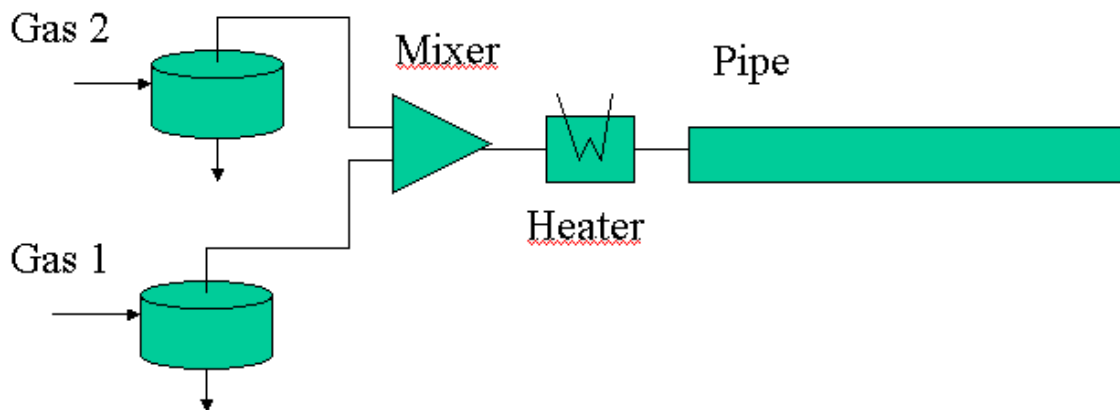
Figure 11-6 Illustration of the mixing process of two gasses

We assume that we have two gases containing methane, ethane, nitrogen, and water. The gas out of the separators in Figure 11-6 is saturated with water. The temperature of gas 1 is 48°C and 4.3°C for gas 2. The gases are mixed in a mixer – and then cooled fast 2.5°C in a cooler. We assume that the cooling process is so fast that no mass transfer will happen in the cooler. The water will start to condense in the pipe. We want to simulate how long time it will take for the system to come to equilibrium in the pipe. For data describing the gas flow rates and the process equipment – see the corresponding NeqSim script.

The velocity and holdup along the pipe are given in Figure 11-7 and Figure 11-8. From the figures we can conclude that it will take about 150 meter (or 20 seconds) for the system to come to equilibrium in the pipe. The final liquid fraction (holdup) will be about $4 \cdot 10^{-4}$. In the case simulated it was assumed that the liquid was transported as a stratified liquid film in the bottom of the pipe.

Simulations like the one demonstrated here will be important in situations where an accurate knowledge of water condensation is important. This will typically be in equipment not designed for two-phase flow or in cases we want to evaluate the condensation rate in process equipment (eg. in cases we want to evaluate condensation of water from the gas between absorption towers and dry gas compressors).

```
# Simulates condensation of water after mixing two gasses: mixing.py
#
# Written by: Even Solbraa, nov. 2001
#

MSm_day_stream1 = 100.0e6 / 2.0
MSm_day_ stream2 = 10.0e6 / 2.0
mol_sec_ stream1 = MSm_day_stream1 *40.0/(3600.0*24.0)
mol_sec_ stream2 = MSm_day_ stream2 *40.0/(3600.0*24.0)

systemName = SystemSrkEos(321.0, 92.6)
systemName.addComponent("nitrogen", 0.0178*mol_sec_ stream)
systemName.addComponent("methane", 0.95*mol_sec_ stream1)
systemName.addComponent("ethane", 0.035*mol_sec_ stream1)
systemName.addComponent("water",  0.01*mol_sec_ stream1)
systemName.setMixingRule(2)
newdatabase(systemName)

systemName2 = SystemSrkEos((273.15+4.3), 92.6)
systemName2.addComponent("nitrogen",  0.01678*mol_sec_ stream2 )
systemName2.addComponent("methane",  0.9465*mol_sec_ stream2)
systemName2.addComponent("ethane", 0.0365*mol_sec_ stream2)
systemName2.addComponent("water",  0.01*mol_sec_ stream2 )
systemName2.setMixingRule(2)

stream1 = stream(systemName,"stream 1")
stream2 = stream(systemName2,"stream 2")

separator1 = separator(stream1)
separator2 = separator(stream2)

stream3 = stream(separator1.getGasOutStream(),"gasOut")
stream4 = stream(separator2.getGasOutStream(),"gasOut")

mixer1 = mixer("mixer1")
mixer1.addStream(stream3)
mixer1.addStream(stream4)

stream5 = stream(mixer1.getOutStream(),"mixerOut")

neqheater1 = neqheater(stream5, "heater1")
neqheater1.setdT(-2.5)

stream6 = stream(neqheater1.getOutStream(),"heaterOutEqui")
stream7 =  neqstream(neqheater1.getOutStream(),"heaterOutNeq")

legHeights =            [0,0]
legPositions =          [0.0, 150.0]
pipeDiameters =         [1.025, 1.025]
outerTemperature =      [295.0, 295.0]
pipeWallRoughness =     [1e-5, 1e-5]
pipe = twophasepipe(stream7, legPositions, pipeDiameters, legHeights,
outerTemperature, pipeWallRoughness)

run()
processTools.view()
```
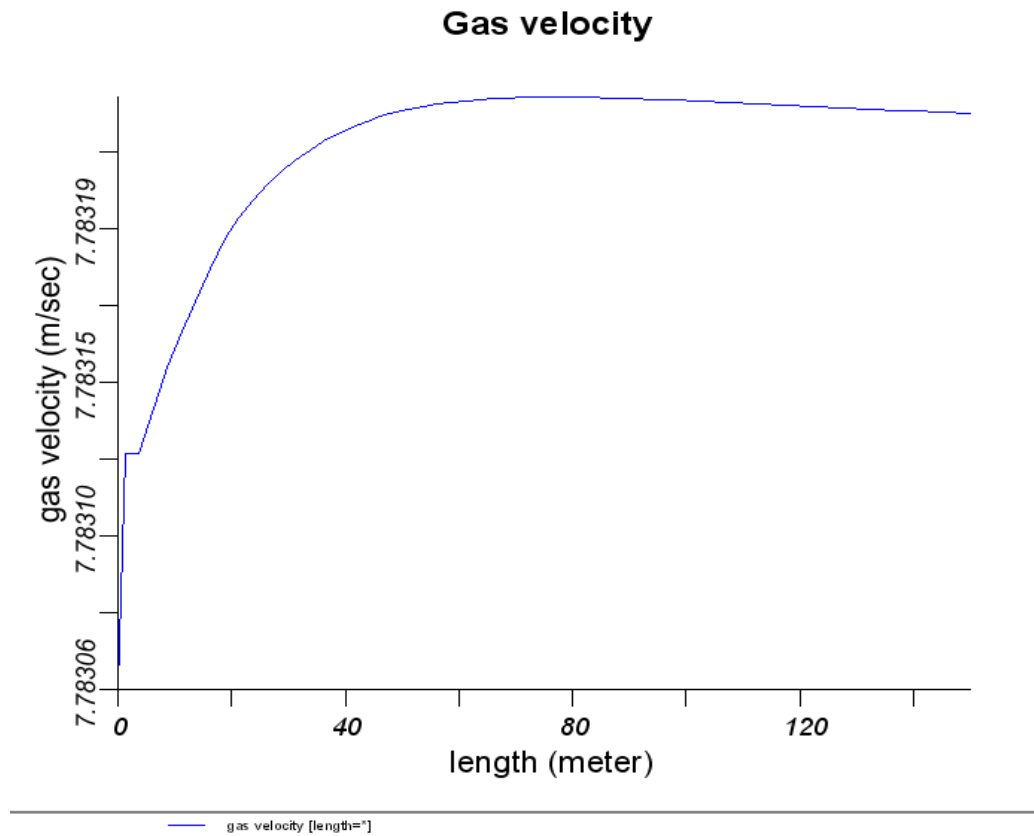
Gas velocity

Figure 11-7 Velocity of gas in pipe after mixing gas 1 and gas 2 for case 2
             Script: mixing.py, p. 238
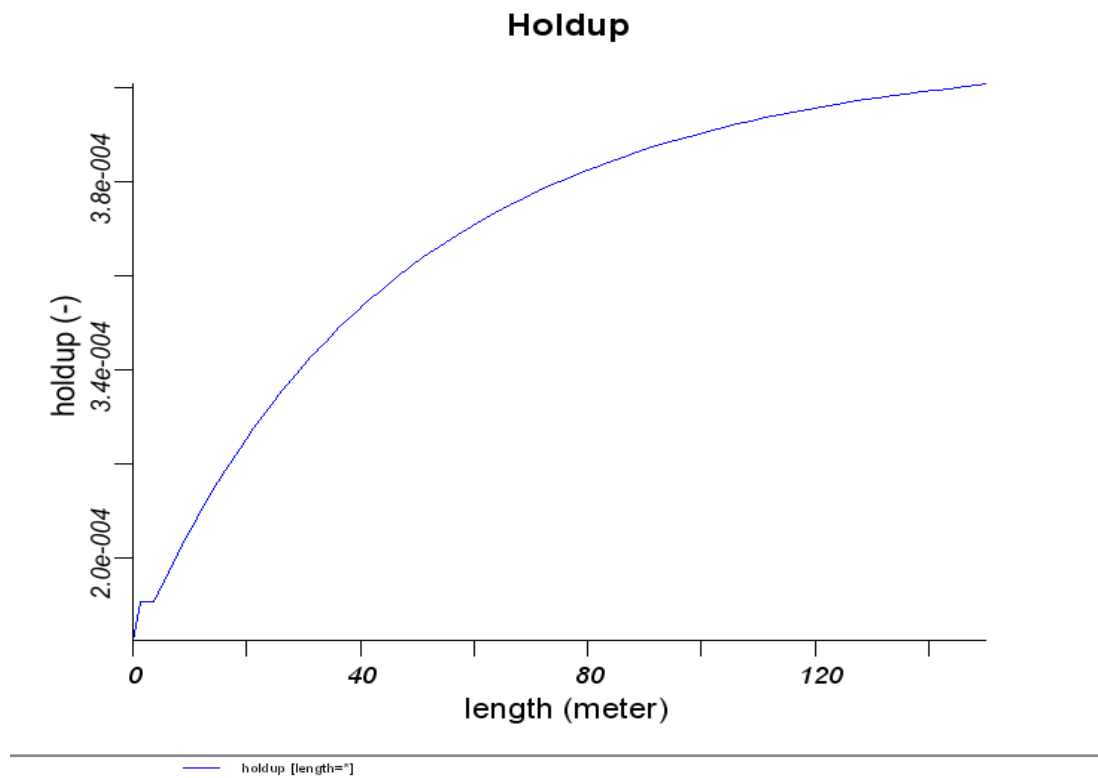
Holdup

Figure 11-8 Holdup along pipe for case 2.
             Script: mixing.py, p. 238

11.3 Case 3. pH of Water in Contact with CO_2

Corrosion of pipelines is a big and costly problem we often see in the petroleum industry. Corrosion of offshore pipelines can lead to uncertainties in daily operations with large maintenance and repair costs. An accurate prediction of pH-values and ionic concentrations along pipelines will help us to find optimal operation conditions and predict positions with a high corrosion potential.

Figure 11-9 Water-CO_2 corrosion of pipelines

The case studied here is illustrated in Figure 11-9. A gas containing CO_2 comes into contact with a water film, and reactions in the liquid phase leads to acidic water. We have used NeqSim with the electrolyte CPA-EOS developed in this work to calculate the pH as a function of position along the pipeline. We have considered a situation were 11000 NL/min of gas with 10% CO_2 flows in a 25 cm diameter pipe at 25°C and 10 bar. The water injection rate was 10.5 kg/min. In Figure 11-10 the calculated pH as function of position is given.

From Figure 11-9 we can see that the pH of the solution drops very fast once the gas and liquid comes in contact (pH of 5 after about 4 meter). The acidity of the water stabilizes around a pH value of 4.7.
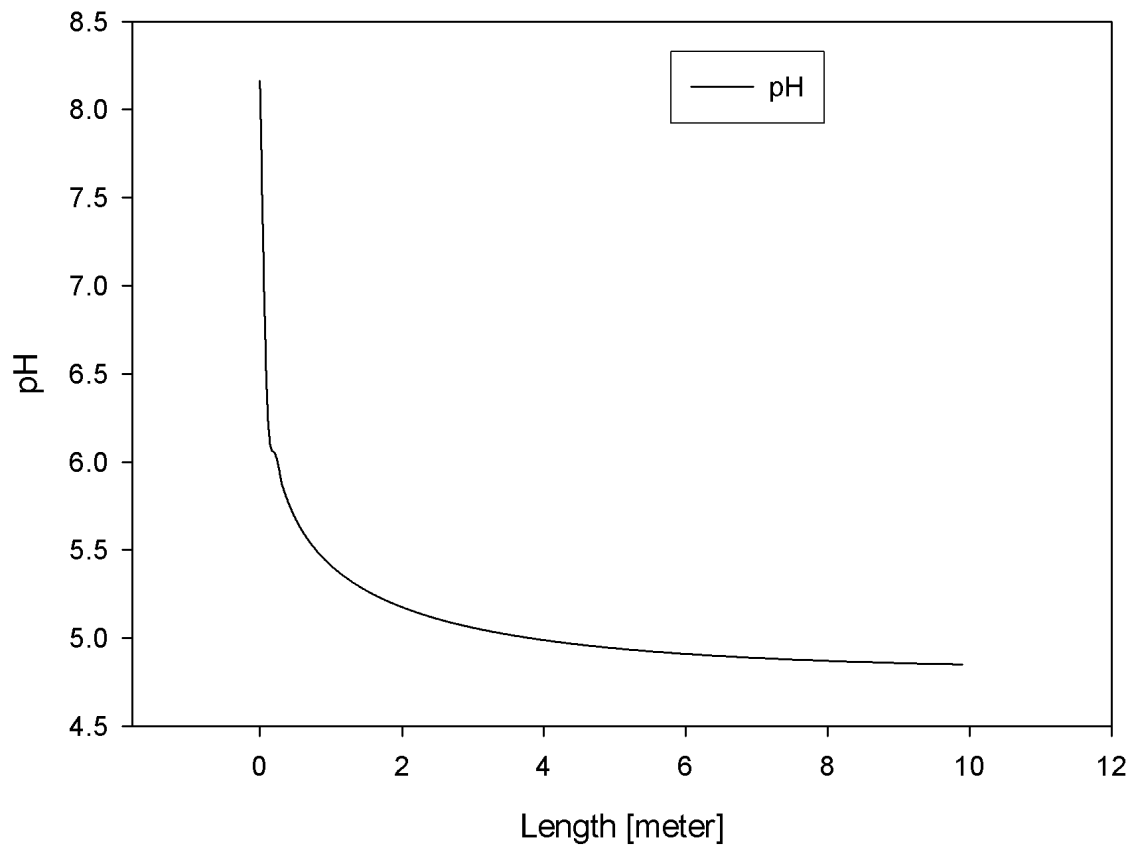
Figure 11-10 pH of water film along the pipeline.
Script: pH.py, p. 241

The NeqSim script for calculating pH along the pipe is given below.

```
system = thermo('electrolyte', 298.15, 10.0)
addComponent(system,'methane', 10000.000, 'Nlitre/min', 0)
addComponent(system,'CO2', 1000.0000010, 'Nlitre/min', 0)
addComponent(system,'water', 10.5, 'kg/min', 1)
reactionCheck(system)
newdatabase(system)
system.setPhysicalPropertyModel(4)
system.initPhysicalProperties()

geometry2 = geometry.pipe(0.25, 0.005)
flowtest = node.twophase(system,geometry2,'stratified')
flowtest.setLengthOfNode(0.1)
for i in range(100):
        flow.solve(flowtest,1,0,1)
        flow.show(flowtest)
        print 'length ', i*0.1,' pH
',flowtest.getBulkSystem().getPhase(1).getpH()
        flowtest.update()
```

11.4 Case 4. Simulation of a High Pressure CO$_2$ Absorption Process

In the last case studied in this work a high pressure CO$_2$ absoprtion process was simulated. We assumed that the gas was contacted counter-current with a 50wt% MDEA solution in a 12 meter high packed absorption tower with diameter 1.0 meter. The internal packing used was pall rings (12 mm) with an interphase area of 250 m^2/m^3 (see Table 5-1). The mass transfer coefficient was calculated using the correlations given in chapter 4. The inlet gas had a CO$_2$ concentration of 7% and the absorber operated at a total pressure of 50 bar and an inlet amine solution temperature of 40°C. The inlet gas circulation rate was 40000 NL/min and the inlet amine circulation rate was 200 kg/min. The NeqSim script is presented in appendix G, p. 317.

The results from the simulation are given in Figure 11-11, Figure 11-12 and Figure 11-13. We can see the typical temperature bulge in the lower part of the absorption tower. The highest temperature will be about 60°C in the liquid and 57°C in the gas. The enhancement factor for absorption of CO$_2$ into the aqueous MDEA solution was calculated as function of the vertical position in the tower. We can see that the enhancement factor will be in the range between 3.0 and 5.5. The reason for the relatively low enhancement factors is the slow reaction rates of CO$_2$ in aqueous MDEA solution. Larger enhancement factors will be obtained by addition of activators to the amine solution (e.g. AEEA or piperazine).

From Figure 11-13 we see that we are able to reduce the CO$_2$ content to a mole fraction of about 2.5% in the absorber. This will in many cases be a sufficient quality for transportation of the gas in pipelines. If the gas should be used for LNG production a much lower CO$_2$ concentration had to be obtained (typically 50 ppm) – because of the risk of freezing out CO$_2$.
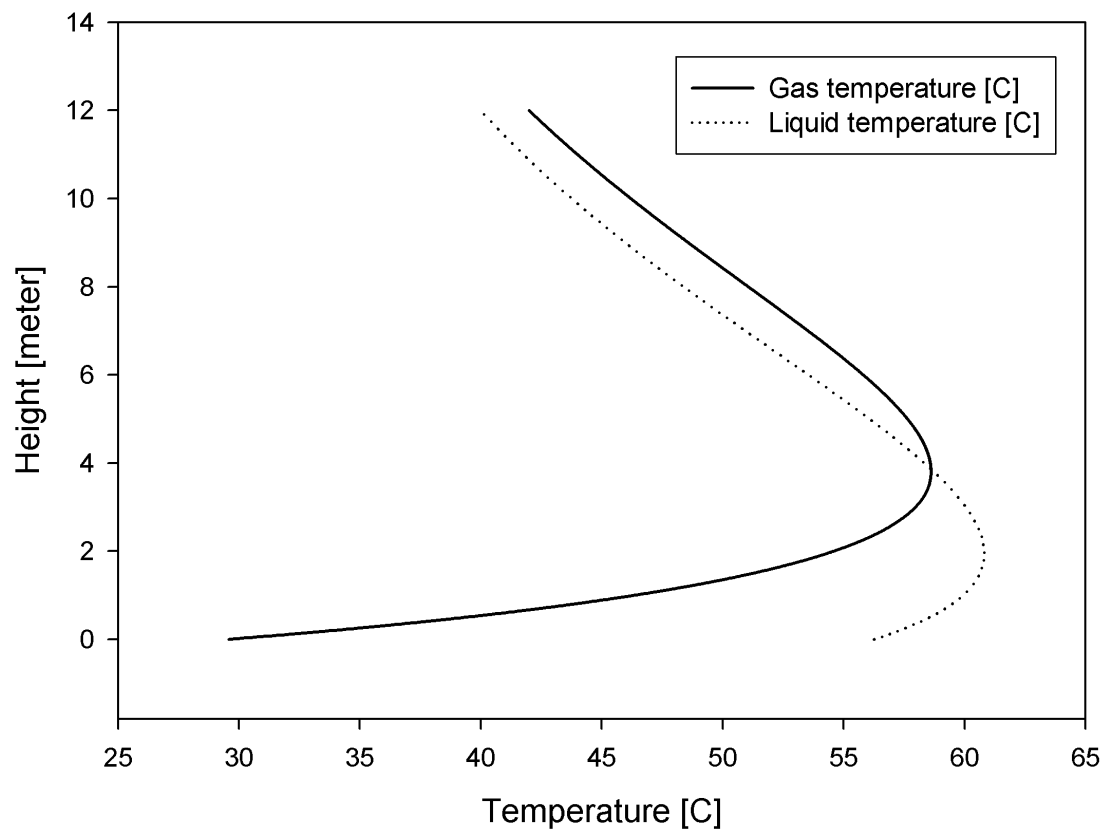
Figure 11-11 Temperature profile of gas and liquid in absorber.
Script: reactive-absorption, p. 317
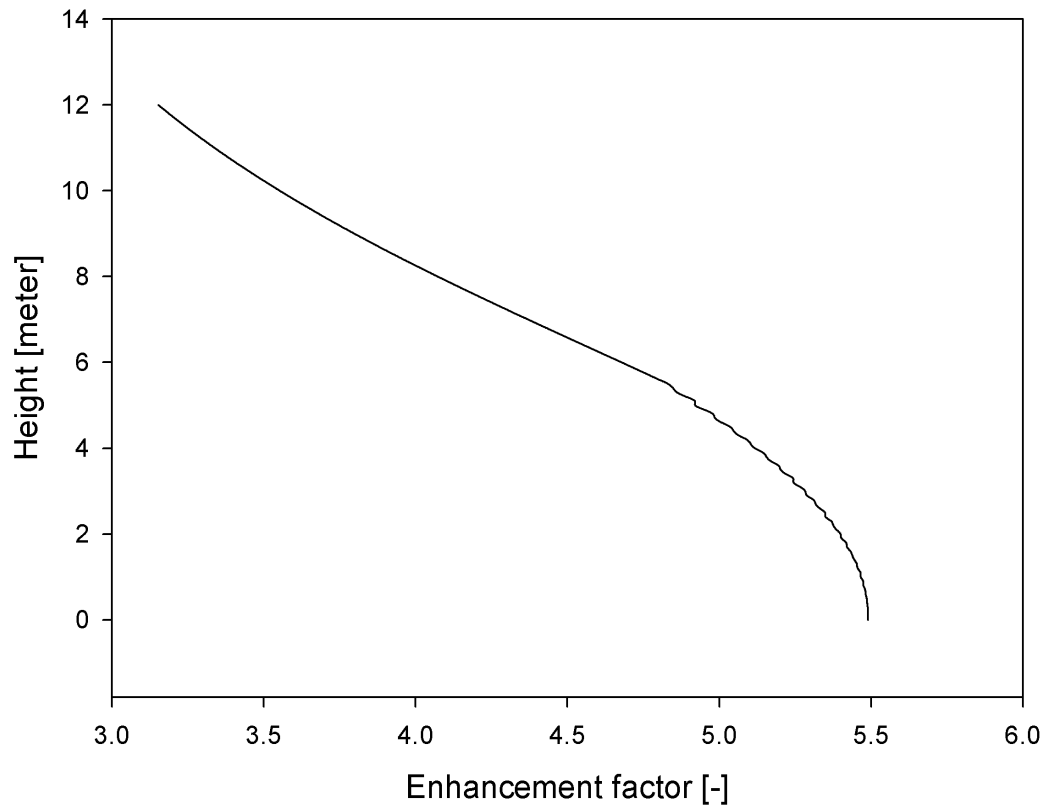
Figure 11-12 Enhancement factor for CO_2 in the absorber
Script: reactive-absorption, p. 317
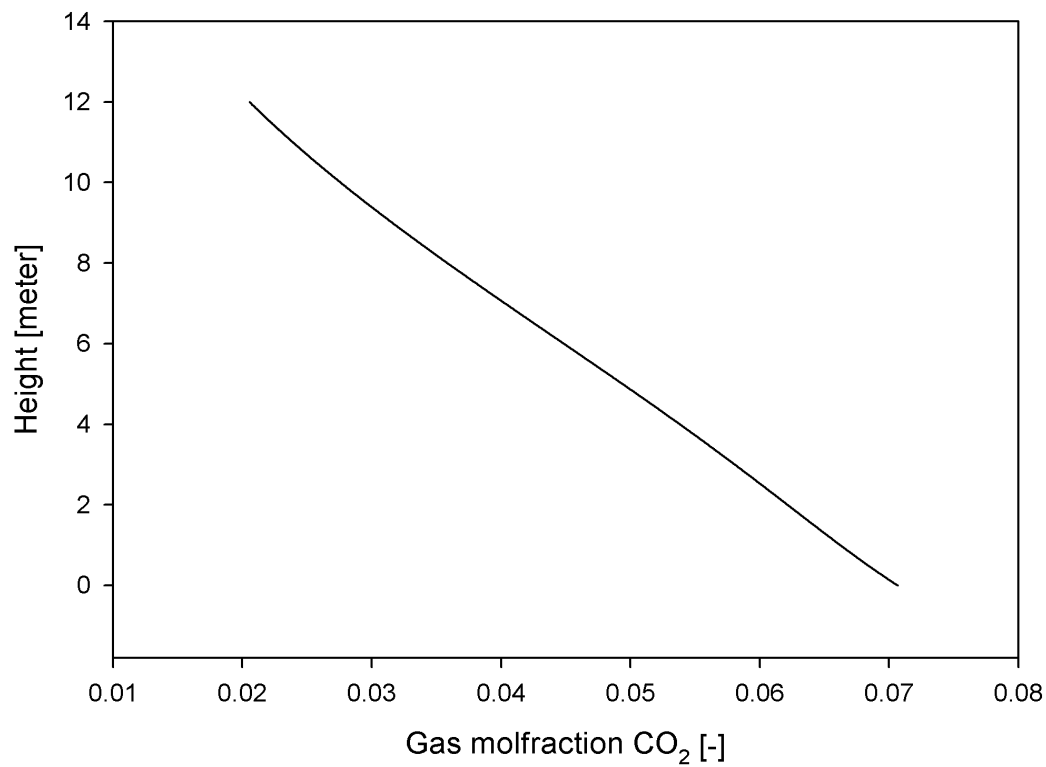
Figure 11-13 Mol fraction CO_2 in gas.
Script: reactive-absorption, p. 317

11.5 Summary and Discussions

In this chapter some cases studies using the mass transfer model developed in this work have been presented. The models developed in this work are able to simulate many different types of mass transfer processes.

At present the process plant simulation model (network model) is only able to simulate stationary cases. For future development of the model it would be advantageous to implement dynamic network models – so transient processes can be solved. Such transient model will make NeqSim able to track components through both pipelines and process plants (from field to market).

The simulation of a CO_2 absorption process using MDEA was demonstrated in this chapter. It would be interesting to simulate a high pressure CO_2 absorption process – and compare the economics with conventional moderate-pressure CO_2 absorption processes. Process optimizing routines should then be added to the simulation model.

NeqSim is based on rigorous thermodynamic and fluid mechanic routines. The calculations can be time-consuming and convergence problems will often occur. The stability of the mathematical models should be worked on to make the model more robust.

12 Summary, Conclusions and Further Work

The aim of this work has been to study non-equilibrium processes commonly found in the process industry – and to develop simulation models for these processes. A second and more specific goal was to study absorption of CO_2 into solvents at high pressures. Both these goals were achieved to some degree. It is the hope of the author that the work will not stop with this dissertation. Still a lot of work on high-pressure mass transfers modeling and experimental measurements should be done.

The modeling of mass transfer in multi-phase fluid systems is normally extremely complicated. Very often the fluid mechanics of such systems is unknown – and we have no simple way to estimate mass transfer coefficients. Anyway, we are often forced to do predictions of non-equilibrium processes – and models have to be used. These models are based on experimental data for systems with simple fluid mechanics and thermodynamics. Such mass transfer data have been measured in thus work – where it is shown that rigorous mass transfer models are capable of correlating the experimental data with a good precision.

12.1 Summary

This work can be divided into two parts

- An experimental part – where a high pressure wetted wall column has been designed and built and used to study mass transfer and kinetics of absorption of CO_2 in MDEA solutions at high pressures. New mass transfer data have been measured for absorption of CO_2 at very high pressures.
- A modeling part - where thermodynamic, non-equilibrium and fluid mechanic models have been developed and implemented in a computer program written in the Java programming language.

The experimental work has been unique because mass transfer experiments have been conducted at pressures up to 150 bar. The experimental data obtained have been reported in this thesis.

The modeling work has been concentrated around developing a general non-equilibrium model that can simulate most of the typical non-equilibrium processes we will find in the petroleum industry. The simulation program is at the time of writing this thesis still in active development.

The thermodynamic model developed in this work was used to evaluate the effect of system pressure on the capacity of MDEA solutions. Methane will have a considerable effect on the fugacity of CO_2 in high pressure natural gas systems. For a given partial pressure of CO_2 in the natural gas, calculations show a decreased CO_2 capturing capacity of aqueous MDEA solutions at increased natural gas system pressure. In Figure 12-1 and Figure 12-2 the equilibrium partial pressure of CO_2 for a 50wt% MDEA solution at 40 and 70°C is given for low and high pressures (0-200 bar) where methane is the inert gas. We see that the equilibrium partial pressure of CO_2 in the gas is increaed at high system pressures. In a practical situation, the partial pressure of CO_2 in the natural gas will be proportional to the total pressure. In these situations we can see from Figure 12-1 and Figure 12-2 that the CO_2 capturing capacity of the MDEA solution will be increased at rising total pressures.

246
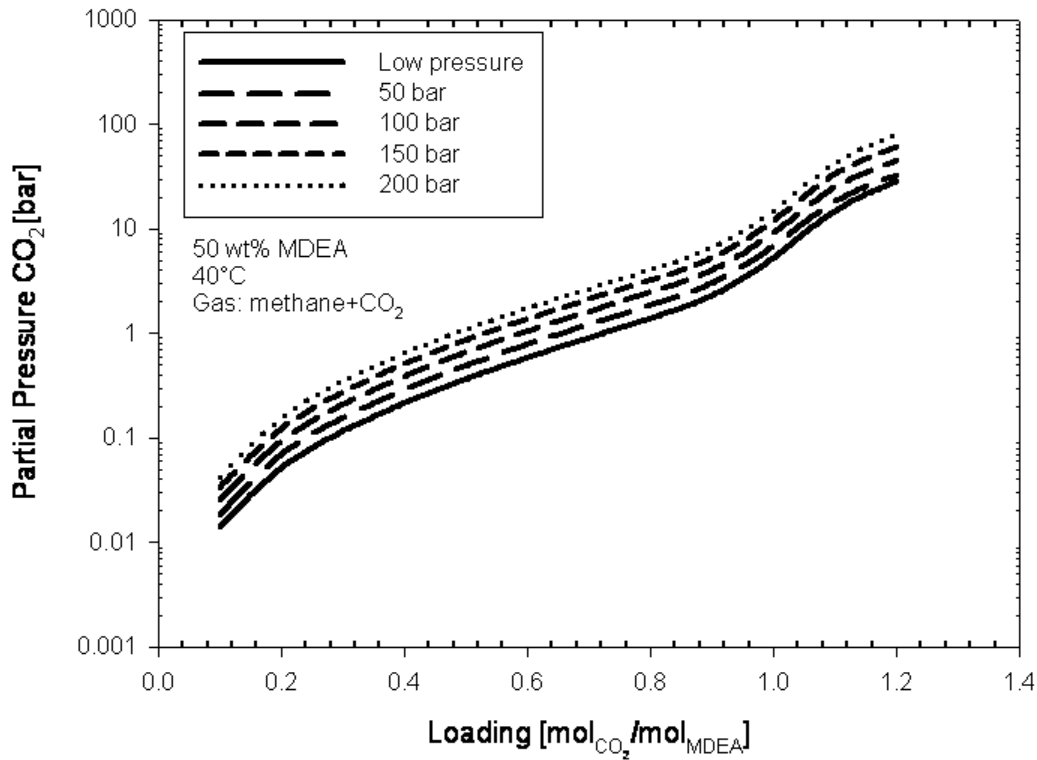
Figure 12-1 Partial pressure of CO$_2$ for a solution of 50wt% MDEA at 40°C.
      Script: partpres.py, p. 320.
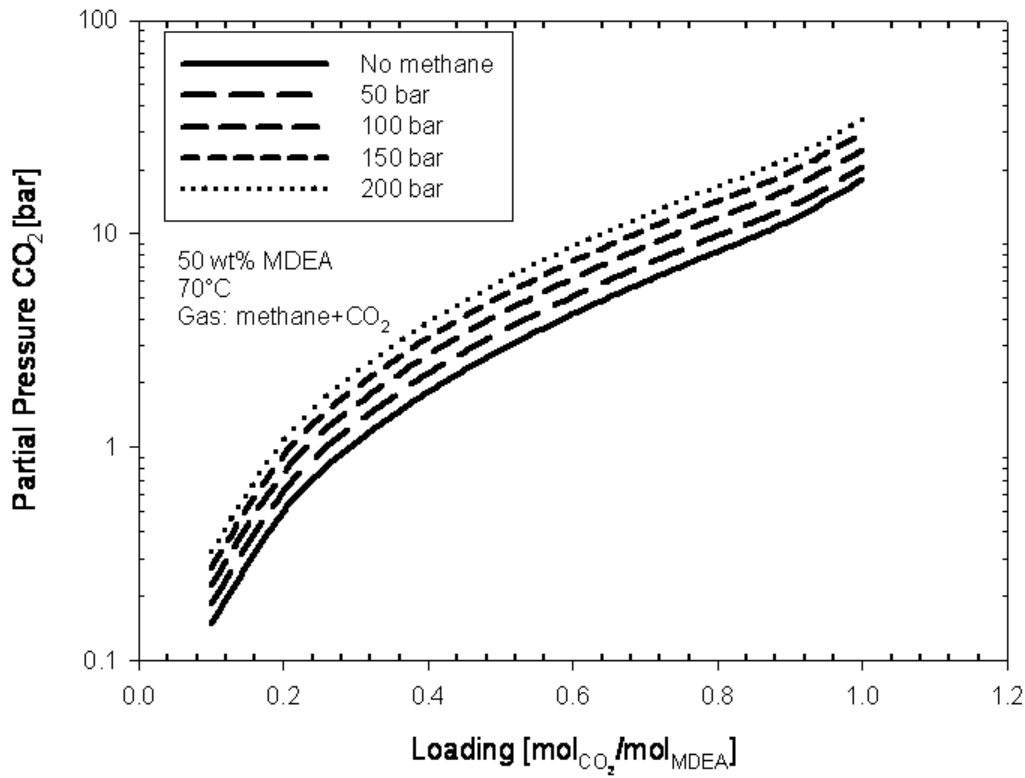
Figure 12-2 Partial pressure of CO$_2$ for a solution of 50wt% MDEA at 70°C.
      Script: partpres.py, p. 320.

As we have seen, for a given partial pressure of CO_2 in the natural gas, the CO_2 capturing capacity of aqueous MDEA solutions will decrease with increased natural gas system pressure. The decrease in CO_2 capturing capacity of the solvent can be evaluated by comparing to the capacity for a low pressure system (no methane). This has been done in Figure 12-3 and Figure 12-4. From the figures we see that the capacity of the 50wt% MDEA solution generally will be considerably reduced at high pressures. The decrease in capacity is estimated to be as high as 40% at 200 bar and 40°C for low partial pressures of CO_2. A 40% decrease in capacity can also be observed at 70°C but this will happen at a partial pressure of around 2 bar in the gas phase. This is important since the cleanup specifications often will be close to this partial pressure of CO_2 in the gas. Generally we find a reduced capacity up to 40% (at 200 bar) compared to low pressure capacity. The pressure effects can be modelled correctly by using suitable thermodynamic models for the liquid and gas.

In a practical situation, the partial pressure of CO_2 in the natural gas will be proportional to the total pressure. In these situations we can see from Figure 12-1 and Figure 12-2 that the CO_2 capturing capacity of the MDEA solution will be increased at rising total pressures. However, the increased capacity is not as large as we would expect from the higher CO_2 partial pressure in the gas.

The reaction kinetics of CO_2 with MDEA was shown to be relatively unaffected by the total pressure when nitrogen was used as inert gas. However, it was important that the effects of thermodynamic and kinetic non- ideality in the gas and liquid phase were modelled in a consistent way. The reaction rate of CO_2 in high pressure aqueous MDEA solutions could be represented well by the model developed in this work. The reaction rate model found here was compared to the low pressure model of Pacheco (1998) in Figure 10-8. We see that the second order reaction rate constants regressed in this work are comparable to the values found by other experimenters from low pressure data. We can conclude that the reaction kinetics probably won't be affected in a large degree by the total pressure.

Generally we see:
- For a given partial pressure CO_2, the capacity of MDEA solutions is lowered at increasing pressures. The capacity can be reduced up to 40% at 200 bar total pressure (inert gas methane)
- For a specified natural gas, the capacity of MDEA solutions will increase with increasing gas stream pressures. This increase is not as high as we would expect from only consideration of the increased partial pressure of CO_2
- The reaction kinetics is not considerable affected by the total pressure (up to 150 bar with nitrogen as inert gas)

The measurements of the reaction kinetics should however be done in systems where methane is used as inert gas. Methane is more soluble in the MDEA solution and will affect the fugacity of CO_2 in the gas more than nitrogen.
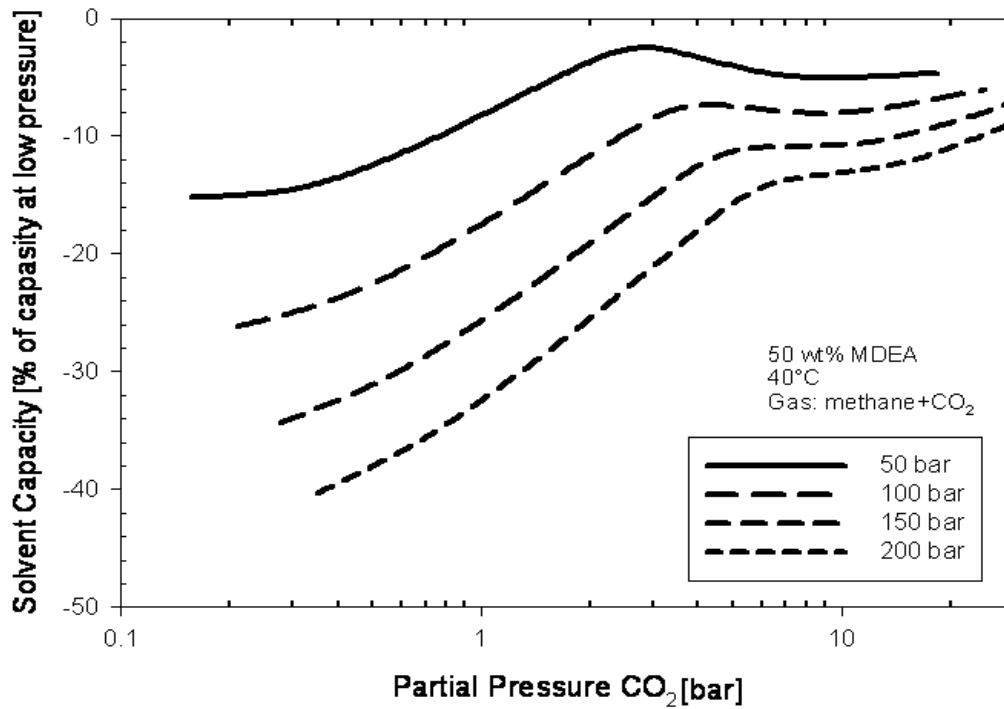
Figure 12-3 Relative CO₂ removal capacity (percent of low pressure capacity) at high pressures for a 50wt% MDEA solution at 40°C. *Script: partpres.py, p. 320.*
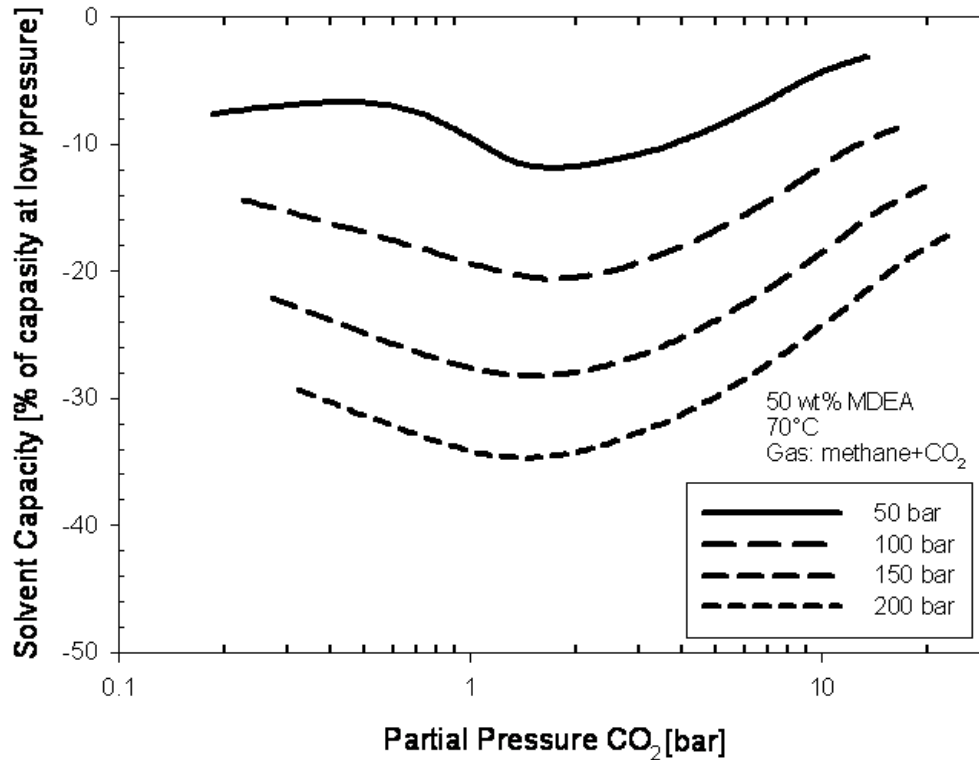
Figure 12-4 Relative CO₂ removal capacity percent of low pressure capacity) at high pressures for a 50wt% MDEA solution at 70°C. *Script: partpres.py, p. 320.*

12.2 Conclusions

- A high pressure wetted wall column was designed and constructed
- New mass transfer data were obtained for absorption of CO_2 into MDEA-solutions at pressures between 50 and 150 bar
- An electrolyte EOS (electrolyte ScRK-EOS) was used to model the thermodynamics of the CO_2-MDEA-water systems
- The electrolyte EOS was able to represent the experimental data for the systems CH_4-CO_2-MDEA-water with good accuracy
- A general non-equilibrium mass transfer model was developed
- A non-equilibrium simulator – NeqSim – was implemented in a Java code
- Examples of how to do non-equilibrium process simulations were presented
- The non-equilibrium model developed is able to represent the experimental mass transfer data of this work with a good precision.

12.3 Suggestions for Further Work

Some suggestions for future work are
- Conduct absorption experiments where activators are used in combination with MDEA (some have been done but are not yet published)
- Implement a dynamic network solver in the NeqSim simulation tool
- Put in more electronic equipment into the wetted wall column – so that more parameters can be measured (film velocity, hold up, online gas analyser)
- Install an online GC on the wetted wall column – so gas sampling and compositional analysis will be easier and faster
- Develop and implement numerical and fundamental models for calculation of the enhancement factors in reactive mass transfer
- Develop and implement a dynamic and stable non-equilibrium two-fluid model

Finally the economics of operating gas processing equipment at high pressures should be evaluated with the model developed here. Process optimisation routines should be implemented and a high pressure CO_2 removal process should be designed based on these models.

12.4 Acid Gas Treating at 200 bar ?

In this work the mass transfer during absorption of CO_2 in amine solution have been studied and modelled. From the experiments and modelling work done we can conclude

- For a given gas stream, the CO_2 capturing capacity of anaqeous MDEA solution is increased with increasing system pressure (and increasing CO_2 pressure)
- The high pressure does not affect the reaction kineticks of CO_2 in MDEA solutions considerably
- Finally the thermodynamic and mass transfer of the high pressure MDEA solution can be simulated with the rigorous models described in this work

All these three conclusions give positive contributions to the development of high pressure gas processing solutions.

It will be important to study high-pressure fluid mechanical effects in gas processing equipment. Liquid and gas interactions will increase at rising pressures. Entrainment of liquid, bubble formation and foaming could therefore become a big problem.

The present work has contributed thermodynamic and mass transfer models for gas processing. To be able to develop new high pressure gas processing equipment – more fundamental work have to be done related to thermodynamics, physical properties and fluid mechanics of high pressure systems. Such experimental work is in progress at Statoil Research centre at the moment. As more experimental data are becoming available – and more experience are obtained from existing process equipment, the better fundamental understanding we have to come up with new high pressure gas processing solutions (Figure 12-5).
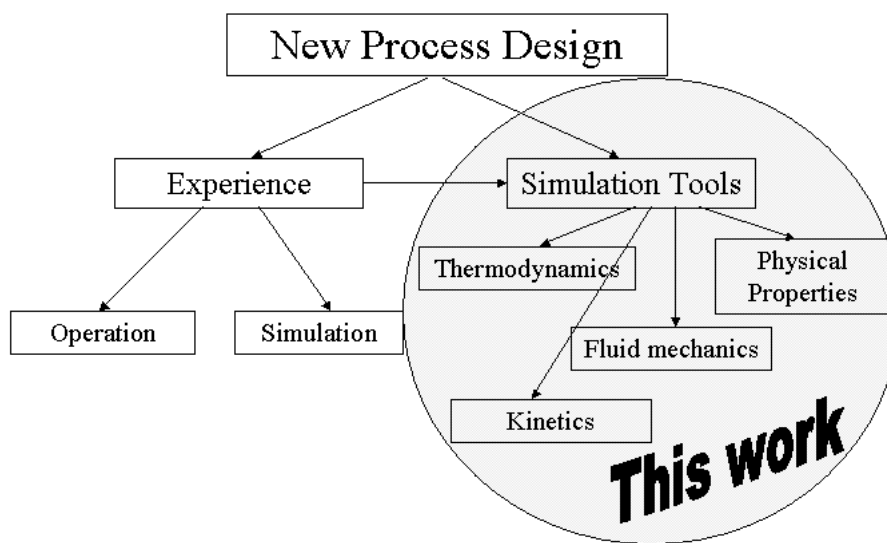
Figure 12-5 The contributions from this work

Bibliography

Abbott, M.M., *Cubic Equation of State:An Interpretive Review, Equations of State in Engineering and Research*, Adv. in Chemistry Ser., Vol. 182, K.C.Chao, and R.L. Robinson eds., American Chemical Society, Washington DC, p. 47, 1979.

Adachi, Y., Sugie, H., *A New Mixing Rule-Modified Conventional Mixing Rule*, Fluid Phase Equilibria, Vol. 28, p. 103, 1986.

Addicks, J., Owren, G.A., Fredheim, A.O., Tangvik, K., *Solubility of Carbon Dioxide and Methane in Aqueous Methyldiethanolamine Solutions*, J.Chem. Eng. Data, 2002b.

Addicks, J., *Solubility of Carbon Dioxide and Methane in Aqueous N-Methyldiethanolamine Solutions at Pressures between 100 and 200 bar*, Ph.D thesis, Norwegian University of Science and Technology, 2002.

Akhadow (1981)

Al-Ghawas, H.A., Hagewiesche, D.P., Ruiz-Ibanez, G., Sandall, O.C., Physiochemical Properties Important for Carbon Dioxide Absorption in Aqeous Methyldiethanolamine, J.Chem.Eng.Data, Vol. 34, p. 385, 1989.

Astarita, G., Savage, D.W., Bisio, B., *Gas Trating With Chemical Solvents*, Wiley, New York, 1983.

Atwood, K., Arnold, M.R., Kindrick, R.C., *Equilibria for the System, Ethanolamines - Hydrogen Sulfide - Water*, Ind.Eng.Chem., Vol. 49, p. 1439, 1957.

Austgen, D.M., *A Model of Vapor-Liquid Equilibria for Acid Gas-Alkanolamine-Water Systems*, Ph.D Dissertation, The University of Texas at Austin, 1989.

Austgen, D.M., Rochelle, G.T., Chen, C.C., *Model of Vapour-Liquid Equilibria for Aqueous Acid Gas-Alkanolamine Systems, 2. Representation of H_2S and CO_2 solubility in Aqueous MDEA and CO_2 Solubility in Aqueous Mixtures of MDEA with MEA and DEA*, Ind.Eng.Chem.Res., Vol. 30, p. 543, 1991.

Bahiri, A.M, *Experimental Equilibrium Between Acid Gases and Ethanolamine Solutions*, Ph.D. dissertation of Oklahoma Stat University, 1984.

Ball, F.X, Planche, H., Furst, W., Renon, H., *Representation of Deviation from Idelatiy in Concentrated Aqueous Solutions of Electrolytes Using a Mean Spherical Approximation Molecular Model*, AIChE Journal, Vol. 31, p. 1233, 1985.

Banaszak, M., Chiew, Y.C., o'Lenick, R., Radosz, M., *Thermodyanmic Perturbation Theory: Lennard Jones Chains*, J.Chem.Phys., Vol. 100, p. 3803, 1994.

Barth, D., Tonde, C., Lappai, G., Delpuech, J.J., *Kinetic Study of Carbon Dioxide Reaction with Ternary Amines in Aqueous Solution*, J. Phys. Chem., Vol. 85, p. 3660-3667, 1981.

Bejan, A., *Heat Transfer*, John Wiley and Sons, 1993

Bendiksen, K.H., Malnes, D., Moe, R., Nuland, S., *The Dynamic Two-Fluid Model OLGA: Theory and Application*, SPE Production Engineering, May, 1991.

Beret, S., Prausnitz, J.M., *Perturbed Hard-Chain Theory: An Equation of State for Fluids Containing Small or Large Molecules*, AIChE J., Vol. 26, p.1123, 1975.

Billet, R., *Packed Towers in Processing and Environmental Technology*, English Version, VCH Verlagsgesellschaft mbH , 1995.

Bird, R., Curtis, C.F., *Multicomponent Diffusion*, Ind.Eng.Chem.Res., Vol. 38, p. 2551, 1999.

Bird, R.B., Stewart, W.E., Lightfoot, E.N., Transport Phenomena, Second Ed., John Wiley & Sons Inc., 2002.

Bjerrum, N., *A New Form for the Electrolyte Dissociation Theory*, Proceeding of the Seventh International Congress of Applied Chemistry, London, 1909.

Blauhoff, P.M.M., Versteeg, G.F., Van Swaaij, W.P.M., *A Study of the Reaction Between CO_2 and Alkanolamines in Aqueous Solutions*, Chem.Eng.Sci., Vol. 39, p. 207, 1984.

Blum, L., Høye, J.S., *Mean Spherical Model for Asymmetric Electrolytes. 2 Thermodynamic Properties and the Pair Correlation Function*, J.Phys.Chem , Vol. 81, p.1311, 1977.

Blum, L., *Mean Spherical Model for Asymmetric Electrolytes I. Method of Solution*, Mol. Phys., Vol. 30, p. 1529, 1975.

Bolles, W.L., Fair, J.R, Chem. Eng., Vol. 89, July 12, p. 109, 1982.

Borgnakke, C., Sonntag, R.E., *Thermodynamic and Transport Properties*, John Wiley & Sons, 1997

Box, G.E.P., Hunter, W.G., Hunter, J.S., *Statistics for Experimenters*, John Wiley & Sons, 1978.

Bravo, J.L., Fair, J.R., Ind.Eng.Chem.Process Des.Dev., Vol 21, no. 1., p. 162, 1982.

Bromley, L.A., *Approximate Individual Ion Values of β (or B) in Extended Debye-Huckel Theory for Uni-Univalent Aqueous Solutions at 298.15K*, J. Chem.Thermo, Vol. 4, p. 669, 1972.

Bromley, L.A., *Thermodynamic Properties of Strong Electrolytes in Aqueous Solutions*, AIChE J., Vol. 19, p. 313, 1973.

Button, J.K., Gubbins, K.E., *SAFT Prediction of Vapour-Liquid Equilibria of Mixtures Containing Carbon Dioxide and Aqueous Monoethanolamine or Diethanolamine*, AIChE J., Vol. 18, p. 1239, 1999.

Carnahan, N.F., Starling, K.E., *Intermolecular Repulsion and the Equation of State for Fluids*, AIChE Journal, Vol. 18, p. 1184, 1972.

Castier, M., Rasmussen, P., Fredenslund, Aa., *Calculation of Simultaneous Chemical and Phase Equilibrium in Nonideal Systems*, Chem.Eng.Sci., Vol. 44, p. 237, 1988.

Chakma, A., Meisen, A., *Solubility of Aqueous Methyldiethanolamine and N,N-Bis(hydroxyethyl) piperazine Solutions*, Ind.Eng.Chem.Res., Vol. 26, p.2461, 1987.

Chakravarty, T., *Solubility Calculations for Acid Gases in Amine Blends*, Ph.D Dissertation, Clarkson College, Portsdam NY, 1985.

Chang, H.T., Posey, M., Rochelle, G.T., *Thermodynamics of Alkanolamine-Water Solutions from Freezing Point Measurement*, Ind.Eng.Chem.Res., Vol. 32, p. 2324, 1993.

Chang, H.T., Posey, M., Rochelle, G.T., *Thermodynamics of Alkanolamine-Water Solutions from Freezing Point Measurements*, Ind.Eng.Chem., Vol. 32, p. 2324, 1993.

Chapman, W.G., Gubbins, K.E., Jackson, G., Radosz, M., *New Reference Equation of State for Associating Liquids*, Ind.Eng.Chem.Res., Vol.29, p.1709, 1990.

Chapman, W.G., Jackson, G., Gubbins, K.E., *Phase Equilibria of Associating Fluids: Chain Molecules with Multiple Bounding Sites*, Mol.Phys, Vol. 65, p.1057, 1988.

Chen, C.C., Britt, H.I., Boston, J.F., Evans, L.B., *Local Composition Model for Excess Gibbs Energy of Electrolytes Systems, Part I: Single Solvent, Single Completely Dissociated Electrolyte Systems*, AIChE J., Vol. 28, p. 588, 1982.

Chen, C.C., Britt, J.F., Boston, J.F., Evans, L.B., *Extension and Application of th Pitzer Equation for Vapor-Liquid Equilibrium of Aqueous Electrolyte Systems with Molecular Solutes*, AIChE J., Vol. 25, p. 820, 1979.

Christiansen, C., *High-Pressure Natural Gas Liquefaction and Adsorption Pre Treatment*, Ph.D thesis, NTNU, 2001.

Chung, D.K., Mills, A.F., *Experimental Study of Gas Absorption into Turbulent Falling Films of Water and Ethylene Glycol-Water Mixtures*, Int.J. Heat Mass Transfer, Vol. 19, p. 51, 1976.

Chunxi, L., Furst, W., *Representation of CO_2 and H_2S Solubility in Aqueous MDEA Solutions Using an Electrolyte Equation of State*, Chem.Eng.Sci., Vol. 55, p. 2975-2988, 2000.

Colburn, A.P., *A Method for Correlating Forced Convection Heat Transfer Data and a Comparison with Fluid Friction*, Trans. Am.Inst.Cham.Eng., Vol. 29, 1933, p. 17, reprinted in Int.J.Heat Mass Transfer, Vol. 7, p.1359, 1964.

Cooper, J.W., *Java Design Patterns - A Tutorial*, Addison-Wesley, 2000.

Crichfeld, J.E., Rochelle, G.T., *CO_2 Absorption into Aqueous MDEA and MDEA/MEA Solutions*, Presented at the AIChE National Meeting, Huston, Texas, 1987.

Crichfield, J.E., *CO_2 Absorption/desoorption in Methyldiethanolamine Solution Promoted with Monoethanolamine and Diethanolamine: Mas Transfer and Reaction Kinetics*, Ph.D. Dissertation, The University of Texas at Austin, 1988.

Culberson, O., McKetta, *The Solubility of Methane in Water at Pressures to 10000 psia*, Petrol. Trans. AIME, Vol. 192, p. 223, 1951.

Curtiss, C.F., Bird, R.B., *Multicomponent Diffusion*, Ind. Eng. Chem. Res., Vol. 38, p. 2515, 1999.

Dahl, S.A., Michelsen, M.L., *High Pressure Vapour Liquid Equilibrium with a Modified UNIFAC-Based Equation of State*, AIChE J., Vol. 36, p. 1829, 1990.

Danckwerst, P.V., *The Reaction of CO_2 with Ethanolamines*, Chem.Eng.Sci., Vol. 34, p. 443, 1979.

Danckwerts, P.V., *Gas-Liquid Reactions*, McGraw-Hill NY, 1970.

Dankwerst, G.C., McNeil, K.M., *The Absorption of Carbon Dioxide Into Aqueous Amine Solutions and the Effects of Catalysis*, Trans. Inst.Chem.Eng., Vol. 45, p.32, 1967.

de Groot, S.R., Mazur, P., *Non-Equilibrium Thermodynamics*, republication corrected version of book from 1962, Dover Ed., 1984.

Debye, P., Huckel, E., *Zur Theorie der Electrolyte*, Physik. Z., Vol. 25, p. 185, 1923.

DeCoursey, W.J., *A Simpler Approximation for Enhancement of Mass Transfer by Second-Order Reversible Reaction*, IChemE.Symp.Ser., 128, B269, 1992.

DeCoursey, W.J., Thring, R.W., *Effects of Unequal Diffusivities on Enhancement Factors for Reversible and Irreversible Reaction*, Chem.Eng.Sci., Vol. 44, p. 1715, 1989.

Deshmukh, R.D., Mather, A.E., *A Mathematical Model for Equilibrium Solubility of Hydrogen Sulfide and Carbon Dioxide in Aqueous Alkanolamine Solutions*, Chem.Eng.Sci., Vol. 36, p.355, 1981.

Donaldson, T.L., Nguyen, Y.N., *Carbon Dioxide Reaction Kinetics and Transport in Aqueous Amine Membranes*, Ind.Eng.Chem.Fundam., Vol. 19, p.260, 1980.

Donohue, M.D., Prausnitz, J.M, *Perturbed Hard Chain Theory for Fluid Mixtures: Thermodynamic Properties for Mixtures in Natural Gas and Petroleum Technology*, AIChE. J., Vol.24, p. 849, 1978.

Eckert, J.S., Chem.Eng.Prog., Vol 66, no. 3, p. 39, 1970.

Edwards, T.J., Maurer, G., Newman, J., Prausnitz, J.M., *Vapor-Liquid Equilibria in Multicomponent Aqueous Solution of Weak Electrolytes*, AIChE J., Vol. 24, p. 966, 1978.

Edwards, T.J., Maurer, G., Newman, J., Prausnitz, J.M., *Vapor-Liquid Equilibria in Multicomponent Aqueous Solutions of Weak Electrolytes*, AIChE J., Vol. 24, p.966, 1978.

Edwards, T.J., Newman, J., Prausnitz, J.M., *Thermodynamics of Aqueous Solutions Containing Volatile Weak Electrolytes*, AIChE J., Vol. 21, p. 248, 1975.

Elliot, J.R., Daubert, T.E., *Evaluation of an Equation of State Method for Calculating the Critical Properties of Mixtures*, Ind.Eng.Chem.Res., Vol. 26, p. 1686, 1985.

Elliot, J.R., Daubert, T.E., *Revised Procedures for Phase Equilibrium Calculations with the Soave Equation of State*, Ind.Eng.Chem.Process Des.Dev., Vol. 24, p. 743, 1985.

Emmert, R.E., Pigford, R.L., Chem. Eng. Prog., Vol. 50, p. 87, 1954.

Fair, J.R., Chap. 15 in Design of Equilibrium Stage Processes, B.D. Smith, Ed., NY, 1963.

Fair, J.R., Petro/Chem.Eng., Vol. 33, no. 19, October, p. 45, 1961.

Flory, P.J., *Statistical Thermodyanmics of Liquid Mixtures*, J.Amer.Chem.Soc., Vol. 87, p1833, 1965.

Frank, M.J., Kuipers, J.A.M., Versteeg, G.F., Van Swaaij, W.P.M., *Modelling of Simultaneous Mass and Heat Transfer with Chemical Reaction Using the Maxwell-Stefan Theory-I. Model Development and Isothermal Study*, Chem.Engng.Sci., Vol. 50, p. 1645, 1995a.

Frank, M.J.W., Kuipers, J.A.M., Krishna, R., Van Swaaij, W.P.M., *Modelling of Simultaneous Mass and Heat Transfer with Chemical Reaction Using the Maxwell-Stefan Theory-II. Non-Isothermal Study*, Vol. 50, p. 1661, 1995b.

Fuchs, P., *Flerfase Rørstrømning*, Kompendium, Inst. for Klima- og Kuldeteknikk, NTNU, 1997.

Fuller, E.N., J. Phys. Chem., vol. 75, p. 3679, 1969.

Fuller, E.N., P.D. Schettler, and J.C. Giddings. 1966. *A new method for prediction of binary gas-phase diffusion coefficients*. Ind. Eng. Chem*., Vol. 58, p.19, 1966.

Furst, W., Renon, H., *Representation of Excess Properties of Electrolyte Solutions Using a New Equation of State*, AIChE Journal, Vol. 39, p. 2, 1993.

Gamma, E., Helm, R., Johnson, R., Vlissides, J., *Design Patterns: Elements of Reusable Object -Oriented Software*, Addison-Wesley, 1995.

Geankoplis, C.J., *Transport Processes and Unit Operations*, Third Edition, Prentice Hall, 1993.

Gillespie, P.C., Wilson, G.M., *Vapor-Liquid and Liquid-Liquid Equilibria: Water-Methane, Water-Carbon Dioxide, Water-Hydrogen Sulfide, Water-nPentane, Water-methane-nPentane*, res.rep. RR-48, GPA, Tulsa, 1982.

Gill-Villegas, A., Galindo, P.J., Whitehead, S.J., Mills, G., Jackson, G., Burgess, A.N., *Statistical Associating Fluid Theory for Chain Molecules with Attractive Potentials of Variable Range*, J.Chem.Phys., Vol.106, p.4168, 1997.

Glasscock, D.A., Modelling and Experimental Study of Carbon Dioxide Absorption into Aqueous Alkanolamines, Ph.D Dissertation, The University of Texas at Austin, 1990.

Glasscock, D.A., Rochelle, G.T., *Numerical Solution of Theories for Gas Absorption with Chemical Reaction*, Vol. 35, p. 1271, 1989.

Greiner, H., *An Efficient Implementation of Newton's Method for Complex Nonideal Chemical Equilibria*, Computers Chem.Eng., Vol. 15, p. 115, 1991.

Guggenheim, E.A., *The Specific Thermodynamic Properties of Aqueous Solutions of Strong Electrolytes*, Phil. Mag., Vol. 19, p. 588, 1935.

Guggenheim, E.A., Turgeon, J.C., *Specific Interaction of Ions*, Trans. Faraday Soc., Vol. 51, p. 747, 1955.

Guntelberg, E., *Untersuchungen Uber Ioneninteraktion*, Z.Physik.Chem., Vol. 123, p. 199, 1926.

Hagewieche, D.P., Ashour, S.S., Al-Ghawas, H.A., Sandall, O.C., *Absorption of Carbon Dioxide into Aqueous Blens of Monoethanolamine and N-Methyldiethanolamine*, Chem.Eng.Sci., Vol. 50, p. 1071, 1995.

Håland, S.E., *Simple and Explicit Formulas for the Friction Factor in Turbulent Pipe Flow*, J.Fluids Eng., Vol. 105, p. 89, 1983.

Harismiadis, V.I, Koutras, N.K., Tassios, D.P., Panagiotopoulos, A.Z., *Gibbs Ensemble Simulations of Binary Lennard-Jones Mixtures. How Good is Conformal Solutions Theory for Phase Equilibrium Predictions*, Fluid Phase Equilibria, Vol. 65, p. 1, 1991.

Heidemann, R.A, Rizvi, S.S.H., *Correlation of Ammonia-Water Equilibrium Data with Various Peng-Robinson Equation of State*, Fluid Phase Equilibria, Vol. 29, p. 439, 1986.

Heidemann, R.A., Kokal, S., *Combined Excess Free Energy Models and Equations of State*, Fluid Phase Equilibria, Vol. 56, p. 17, 1990.

Henstock, W.H., Hanratty, T.J., *Gas Absorption by a Liquid Layer Flowing on the Wall of a Pipe*, AIChE J., Vol. 25, p. 122, 1978.

Holderbaum and Gmehling, Fluid Phase Equilibria, Vol. 70, p. 251, 1991.

Houghton, G., McLean, A.M., Ritchie, P.D., *Compressibility, fugacity, and water solubility in the region 0-36 atm. and 0-100 C*, Chem.Eng.Sci., Vol. 6, p. 132, 1957.

Huang, S.H., Radosz, M., *Equation of State for small Large and Polydisperse, and Associating Molecules*, Ind.Eng.Chem.Res., Vol. 29, p. 2284, 1990.

Hughmark G.A., o'Connell, H.E., Chem.Eng.Prog, Vol. 53, no. 3, p. 127, 1957.

Huron, M.K., Vidal, J., *New Mixing Rules in Simple Equation of State for Representing Vapour-Liquid Equilibria of Strongly Nonideal Mixtures*, Fluid Phase Equilibria, Vol. 3, p.255, 1979.

Ikonomu, G.D., Donohue, M.D., *Thermodynamics of Hydrogenbounded Molecules: The Associated Perturbed Anisotropic Chain Theory*, AIChE J., Vol. 32,p. 1716, 1986.

Ishi, *Thermo-fluid dynamic theory of two-phase flow*, 1975.

Jason and Homme,...,1984.

Jou, F.Y., Carrol, J.J., Mather, A.E., Otto, F.D., *The Solubility of Carbon Dioxide and Hydrogen Sulfide in 35wt% Aqueous Methyldiethanolamine solutions*, Can. J.Chem.Engr., Vol. 71, p.264, 1993.

Jou, F.Y., Mather, A.E., Otto, F.D., *Solubility of H₂S and CO₂ in aqueous MDEA solutions*, Ind.Eng.Chem., Proc.Design.Dev., Vol. 21, p. 539, 1982.

Kamei, S., Oishi, J., *Mass and Heat Transfer in a Falling Liqid Film of Wetted-Wall Tower*, Mem.Fac.Kyoto.Univ., Vol. 17, p. 277, 1955.

Kent, R.L., Eisenberg, B., *Better Data for Amine Treating*, Hydrocarbon Process., Vol. 55, p. 87, 1976.

Kessler, D.P, Wankat, P.C., Chem.Eng., Vol. 95, no. 13, p. 72, 1988.

Kiepe, J., Horstmann, S., Fisher, K., Gmehling, J., *Experimental Determination and Prediction of Gas Solubility Data for CO₂+H₂O Mixtures Containing NaCl or KCl at Temperatures between 313 and 393 K and Pressures up to 10 MPa*, Ind.Eng.Chem.Res., Vol. 41, p. 4393, 2002.

Kjelstrup, S., Bedaux, D., *Irreversible Thermodynamics of Heterogeneous Systems*, Book to be published, Norwegian University of Science and Technology, 2002.

Klyamer, S.D., Kolesnikova T.L., *General Mathematical Description of Experimental Data for the Thermodynamic Equilibrium in Carbon Dioxide-Monoethanolamine (Diethanolamine)-Water Systems*, Russian J.Phys.Chem., Vol. 46, p.620, 1972.

Klyamer, S.D., Kolesnikova, T.L., Rodin, Y.A., Gazov.Prom. Vol. 18, p. 44, 1973.

Kobayashi et.al., 1953

Kohl, A.L, Nielsen, R.B., *Gas Purification*, 5.th ed., Gulf Publishing Company, 1997.

Kontogeorgis, G.M., Voutsas, E.C., Yakoumis, I.V., Tassios, D.P., *An Equation of State for Associating Fluids*, Ind.Eng.Chem.Res., Vol. 35, p. 4310, 1996.

Krishna, R., *A Film Model Analysis of Non-Equimolar Distillation of Multicomponent Mixures*, Chem.Eng.Sci., Vol. 32, p. 1197, 1977.

Krishna, R., Wesselingh, J.A., *The Maxwell-Stefan Approach to Mass Transfer*, Chem.Eng.Sci., Vol. 52, p.861, 1997.

Krishnamarthy, R., Taylor, R., Ind.Eng.Chem.Process Des. Dev., Vol. 24, no. 3, p. 513, 1985B.

Krishnamurthy, R., Taylor, R., Absorber Simulation and Design Using a Nonequilibrium Stage Model, Can.J.Chem.Eng., Vol. 64, p. 96, 1986.

Krishnamurthy, R., Taylor, R., AIChE Journal, Vol. 2, p. 449-465, 1985A.

Kuranov, G., Rumpf, G., Smirnova, N.A., Maurer, G., *Solubility of Single Gases Carbon Dioxide and Hydrogen Sulfide in Aqueous Solutions of N-Methyldiethanolamine in Temperature Range 313-413K at Pressures up to 5 MPa*, Ind.Eng.Chem.Res., Vol. 71, p.264, 1996.

Lamourelle, A.P., Sandall, O.C., *Gas Absorption into a Turbulent Liquid*, Chem.Eng.Sci., Vol. 27, p. 1035, 1972.

Lee, *Molecular Thermodynamics of Nonideal Fluids*, Buttherworths Series in Chemical Engineering, 1988.

Levenspiel, O., *Chemical Reaction Engineering*, New York, Wiley, 1999.

Li, Y.G., Mather, A.E., *Correlation and Prediction of the Solubility of Carbon Dioxide in a Mixed Alkanolamine Solution*, Ind.Eng.Chem.Res, p. 2006, 1994.

Mac Gregor, R.J., Mather, A.E., *Equilibrium Solubility of H₂S and CO₂ and their Mixtures in a Mixed Solvent*, Can.J.Che.Engr., Vol. 69, p. 1357, 1991.

Marquardt, D.W., Journal of the Society for Industrial and Applied Mathematics, Vol. 11, p. 431-441, 1963.

Mason, J.W., Dodge, B.F., Trans.Am.Inst.Chem.Engr., Vol. 32, p. 27, 1936.

Mathias, P.M.A., *Versatile Phase Equilibrium Equation of State*, Ind.Eng.Chem, Process Des.Dev., Vol. 22, 1983.

Menez, F., Sandall, O.C., *Gas Absorption Accompanied by Instantaneous Bimolecular Reaction in Turbulent Liquids*, AIChE Jornal, Vol. 21, p. 534, 1975.

Michelsen, M., *Calculation of Multiphase Equilibrium*, Computers Chem. Engng., Vol. 18, p. 545, 1994.

Michelsen, M., Hendriks, E., Physical Properties from Association Models, Vol. 180, p. 165, 2001

Michelsen, M., Mollerup, J., *Derivatives of Thermodynamic Properties*, AIChE Journal, Vol. 32, p. 1389, 1986

Michelsen, M., The Isothermal Flash Problem I. Stability Analysis, Fluid Phase Equilibria, Vol. 16, p. 57, 1982b.

Michelsen, M., *The Isothermal Flash Problem. Part II. Phase Split Calculation*, Fluid Phase Equilibria, Vol. 9, p. 19, 1982a.

Michelsen, M.L, Mollerup, J.M., *Thermodynamic Models, Fundamentals and Computational Aspects*, Course notes, Technical University of Denmark, 2000.

Michelsen, M.L., *A Modified Huron-Vidal Mixing Rule for Cubic Equations Of State*, Fluid Phase Equilibria, Vol. 60, p. 213, 1990.

Michelsen, M.L., Kistenmacher, H., *On Composition-Dependent Interaction Coefficients*, Fluid Phase Equilibria, Vol. 58, p. 229, 1990.

Mollerup, J., *A Note on the Derivation of Mixing Rules from Excess Gibbs Energy Models*, Fluid Phase Equilibria, Vol. 25, p. 323, 1986.

Mollerup, J., Michelsen, M., *Calculation of Thermodynamic Equilibrium Properties*, Fluid Phase Equilibria, Vol. 74, p. 1, 1992

Muller, E.A., Gubbins, K.E., *Molecular-Based Equations of State for Associating Fluids: A Review of SAFT and Related Approaches*, Ind.Eng.Chem.Res., Vol. 40, p. 2193, 2001.

Myers, A.K., Myers, A.L., *Numerical Solution of Chemical Equilibria With Simultaneous Reactions*, J.Chem.Phys., Vol. 84, p. 5787, 1986.

Noll, O., Valtz, A., Richon, D., Getachew-Sawaya, T., Mokbel, I., Jose, J., *Vapor Pressures and Liquid Densities of N-Methylethanolamine, Diethanolamine, and N-methyldiethanolamine*, The Int. Elec. Journ. of Phys.Chem. Data, Vol. 4, p. 105, 1998.

O'Connell, H.E., Trans.Am.Inst.Chem.Enrs.Journal, Vol. 42, p. 741, 1946.

Onda, K., Takeuchi, H., Okumoto, Y., Journal of ChE Japan, Vol 1, no. 1, p. 56, 1968.

Onsager, L., Phys.Rev., Vol. 37, p. 405, 1931.

Orbey, N., Sandler, S.I., *Reformulation of Wong-Sandler Mixing Rule for Cubic Equations of State*, AIChE J., Vol. 41, p. 683, 1995.

Oscarson et.al. (1995)

Pacheco, M.A., *Mass Transfer, Kinetics and Rate-Based Modelling of Reactive Absorption*, Dissertation, University of Austin Texas, 1998.

Pacheco, M.A., *Mass Transfer, Kinetics and Rate-Based Modelling of Reactive Absorption*, Dissertation, University of Austin, Texas, 1998.

Patankar,S.V., *Numerical Heat Transfer and Fluid Flow*, Taylor and Francis, 1980.

Peneloux, A, Rauzy, E., *A Consistent Correction For Redlich-Kwong-Soave Volumes*, Fluid Phase Equilibria, Vol. 8, p. 7, 1982.

Peng, D.Y., Robinson, D.B., *A new Cubic Equation Of State*, Ind.Eng.Chem.Fundam., Vol. 15, p.50, 1976.

Perry, R.H, Green, D.W, *Perry's Chemical Engineers' Handbook*, Seventh Edition, McGraw-Hill Int.Ed., 1998.

Pfohl O., Budich, M., *About Prediction of Phase Equilibria for CO_2-C_2H_5OH-H_2O Systems Using the SAFT Equation of State*, Fluid Phase Equilibria, Vol. 189, p. 179, 2001.

Pitzer, K.S., *Activity Coefficient in Electrolyte Solution*, 2.nd edition, CRC Press, Boca Raton Ann Arbor Boston London, 1991.

Pitzer, K.S., *Electrolytes. From Dilute Solutions of Fused Salts*, J.Am.Chem.Soc., Vol. 102, p. 2902, 1980.

Pitzer, K.S., Kim, J.J., *Thermodynamics of Electrolytes. IV. Activity and Osmotic Coefficients for Mixed Electrolytes*, J.Am.Chem.Soc., Vol. 96, p. 5701, 1974.

Pitzer, K.S., *Thermodynamics of Electrolytes. I. Theoretical Basis and General Equations*, J.Phy.Chem., Vol. 77, p. 268, 1973.

Planche, H., Renon, H., *Mean Spherical Approximation Applied to a Simple but Nonprimitive Model of Interaction for Electrolyte Solutions and Polar Substances*, Am.Chem.Soc., Vol. 85, p. 3924, 1981.

Posey and Rochelle (1994)

Posey, M.L., *Thermodynamic Model for Acid Gas Loaded Aqueous Alkanolamine Solutions*, Dissertation, Univ. of Texas, 1995.

Prausnitz, J.M., Lichtentaler, R.N., de Azevedo, E.G., *Molecular Thermodynamics of Fluid-Phase Equilibria*, Prentice Hall Int., Third ed., 1999.

Press, W.H., Teukolsky, S.A., Vetterling, W.T., Flannery, B.P., *Numerical Recipes in C*, Cambridge University Press, 1999.

Prigogine, I., *The Molecular Theory of Solutions*, North-Holland, Amsterdam, 1957.

Raal, J.D., Khurnana, M.K., *Gas Absorption with Large Heat Effects in Packed Columns*, Can.J.Chem.Eng., Vol. 51, p.162, 1973.

Redlich, O., Kwong, J.N.S., *On the Thermodynamics of Solutions V: An Equation of State. Fugacities of Gaseous Solutions*, Chem. Rev., Vol. 44, p.233, 1949.

Reid, R.C, Prausnitz, J.M., Poling, B.E., *The Properties of Gases and Liquids*, McGraw-Hill, fourth edition, 1988.

Renon, H., Prausnitz, J.M., *Local Composition in Thermodynamics Excess Functions for Liquid Mixtures*, Am.Inst.Chem.Eng.J., Vol. 14, p. 135, 1968.

Reynolds, O., *On the Extent and Action of the Heating Surface for Steam Boilers*, Proc.Manchester Lit.Phil.Soc., Vol. 14, p.7, 1874.

Rho, S.W., Yoo, K.P., Lee, J.S., Nam, S.C., Son, J.E., Min, B.M., *Solubility of CO$_2$ in Aqueous Methyldiethanolamine Solutions*, J.Chem.Eng.Eng.Data, Vol. 42, p.1161, 1997.

Rinker, E.B., Ashour, S.S., Sandall, O.C., *Kinetics and Modelling of Carbon Dioxide Absorption into Aqueous Solutions of N-metyldiethanolamine*, Chem.Eng.Sci., Vol. 50, p. 755, 1995.

Robinson, R.A., Stokes, R.H., *Electrolyte Solutions*, Ed. Butterworths, London, 1952.

Rojey, A., Jaffret, C., *Natural Gas Production Processing and Transport*, Institut Francais Du Petrole Publications, 1997.

Sada, E., Kumazawa, H., Butt, M.A., *Solubility and Diffusivity of Gases in Aqueous Solutions of Amines*, J.Chem.Eng.Data, Vol. 23, p. 161, 1978.

Sandler, S.I. ed., *Models for Thermodyanmic and Phase Equilibria Calculations*, Marcel Dekker, New York, 1994.

Sandler, S.I., *Chemical Engineering Thermodynamics*, 2nd Edition, Wiley, New York, 1989.

Schwarzebtruber, J., Renon, H., *Extension of UNIFAC to High Pressures and Temperatures by the use of a Cubic Equation of State*, Ind. Eng.Chem.Res., Vol 28, p. 1049, 1989.

Scwarzentruber, J., Renon, H., Watanasiri, S., *Developement of a New Equation of State for Phase Equilibrium Calculations*, Fluid Phase Equilibria, Vol. 52, p. 127, 1989.

Sherwood et.al., *Mass Transfer*, 1975

Smith, W.R., Missen, R.W., *Chemical Reaction Equilibrium Analysis: Theory and Algorithms*, Wiley, New York, 1991

Snijder, E.D., Riele, M.J.M, Versteeg, G.F., Van Swaaij, W.P.M., *Diffusion Coefficients of Several Aqueous Alkanolamine Solutions*, J.Chem.Eng.Data, Vol. 38, p. 475, 1993.

Soave, 1992

Soave, G., *Equilibrium Constants from a Modified Redlich-Kwong Equation Of State*, Chem.Eng.Sci., Vol. 27, p.1197, 1972.

Soave, G., *Improvements of the Van der Waals Equation of State*, Chem.Eng.Sci., Vol. 39, p. 357, 1984.

Solbraa, E., Tangvik, K., *Removal of Carbondioxide from Natural Gas at Well Stream Pressures*, IGRC conference 2001, Amsterdam, 2001.

Solbraa, E:, Tangvik, K., *Mass Transfer and Kinetics of Absorption of Carbondioxide into Methyldiethanolamine Solutions at High Pressures*, AICHE Annual Meeting 2000, Los Angeles, 2000.

Taylor, J.R., *Error Analysis - The Study of Uncertainties in Physical Measurements*, University Science Books, 1997.

Taylor, R., Krishna, R., *Multicomponent Mass Transfer*, Wiley Series in Chemical Engineering, 1993.

Teng, T.T., Maham, Y., Hepler, L.G. and Mather, A.E., *Viscosity of Aqueous Solutions of N-Methyldiethanolamine and of Diethanolamine,* Journal of Chemical and Engineering Data, Vol. 39, p. 290, 1994.

Toman, J.J., Rochelle, G.T., Carbon Dioxide Absorption Rates and Physical Solubility in 50% Aqueous Methyldiethanolamine Partially Neutralized with Sulfuric Acid, Presented at the AIChE Spring Meeting. Paper No. 56c, Huston, 1989.

Valerio, S., Vanni, M., *Interfacial Mass Transfer and Chemical Reaction in Non-Ideal Multicomponent Systems*, Chem.Eng.Sci., Vol. 49, p. 3297, 1994.

Vallee, G., Mougin, P., Jullian, S., Furst, W., *Representation of CO₂ and H₂S Absorption by Aqueous Solutions of Diethanolamine Using an Electrolyte Equation of State*, Ind.Eng.Chem.Res., Vol. 38, p. 3473, 1999.

Van Krevlen, D.W., Hoftijzer, P.J., Huntjens, F.J., *Composition and Vapour Pressures of Aqueous Solutions of Ammonia, Carbon Dioxide and Hydrogen Sulfide*, Recueil, Vol. 68, p. 191, 1949.

Vanni, M., Baldi, G., *Mass Transfer and Chemical Reaction with Multicomponent Diffusion*, Chem.Eng.Sci., Vol. 46, p. 2465, 1991.

Versteeg, G.F., Kuipers, J.A.M., Van Beckum, F.P.H., va Swaaij, W.P.M., *Mass Transfer with Complex Reversible Chemical Reactions-II. Parallel Reversible Chemical Reactions*, Chem.Eng.Sci., Vol. 45, p. 183, 1990.

Versteeg, G.F., Ph.D Dissertation, University of Twente, Enshede, The Netherlands, 1986.

Versteeg, G.F., Van Swaaij, W.P.M., *Solubility and Diffusivity of Acid Gases (CO₂ and N₂O) in Aqueous Alkanolamines Solutions*, J.Chem.Eng.Data, Vol. 33, p. 29, 1988.

Versteeg, H.K, Malalasekera, W., *An Introduction to Computational Fluid Dynamics*, Addison Wesley, 1995.

Vilmalchand, P., Donohue, M.D., *Thermodynamics of Quardopolar Molecules: The perturbed-Anisotropic-Chain Theory*, Ind.Eng.Chem.Fundam., Vol. 24, p. 246, 1985.

Voutsas, E.C., Yakoumis, I.V., Tassios, D.P., *Prediction of phase equilibria in water/alcohol/alkane systems*, Fluid Phase Equilibria, Vol. 158, p. 151, 1999.

Waisman, E., Lebowitz, J.L., *Mean Spherical Model Integral Equation for Charged Hard Spheres I. Method of Solution*, J.Chem.Phys., Vol. 56, p. 3086, 1972.

Wallis, G.B., *One-Dimensional Two Phase Flow*, New York, McGraw-Hill, 1969.

Wang, P., Anderko, A., *Computation of Dielectric Constants of Solvent Mixtures and Electrolyte Solutions*, Fluid Phase Equilibria, Vol. 186, p. 103, 2001.

Wei , Y.S., Sadus, R.J., *Equations of State for the Calculation of Fluid-Phase Equilibria*, AIChE Journal, Vol. 46, p. 169, 2000

Weiland, R.H., Chakravarty, T., Mather, A.E., *Solubility of Carbon Dioxide and Hydrogen Sulfide in Aqueous Alkanolamines*, Ind.Eng.Chem.Res., Vol. 32, p.1419, 1993.

Wertheim, M.S., *Fluids with Highly Directional Attractive Forces: 1. Statistical Thermodynamics*, J.Stat.Phys., Vol. .35, p. 19, 1984a.

Wertheim, M.S., *Fluids with Highly Directional Attractive Forces: II. Thermodynamics of Perturbation Theory and Integral Equations*, J.Stat.Phys., Vol. 35, p.34, 1984b.

Wong, S.S.H., Sandler, S.I., *A Theoretical Correct Mixing Rule for Cubic Equations Of State*, AIChE J., Vol. 38, p. 671, 1992.

Wu, J., Prausnitz, J.M., Ind.Eng.Chem.Res, Vol. 37, p. 1634, 1998.

Wu, J., Prausnitz, J.M., *Phase Equilibria for Systems Containing Hydrocarbons, Water, and Salt: An Extended Peng-Robinson Equation of State*, Ind.Eng.Chem.Res., Vol. 37, p. 1634, 1998.

Yakoumis, I.K., Kontogeorgis, G.M., Voutsas, E.C., Hendriks, E., Tassios, D.P., *Prediction of Phase Equilibria in Binary Aqueous Systems Containing Alkanes, Cycloalkanes, and Alkenes with the Cubic-plus-Association Equation of State*, Ind.Eng.Chem.Res., Vol. 27, p. 4175, 1998.

Yih, S.M., Chen, K.Y., *Gas Absorption into Wavy and Turbulent Falling Liquid Films in a Wetted Wall Column*, Chem.Eng.Commun., Vol. 17, p. 123, 1982.

Zarzycki, R., Chacuk, A., *Absorption, Fundamentals and Applications*, Pergamon Prss. Oxford, Great Britain, 1993.

Zuo, Y.X., Furst, W., *Use of an Electrolyte Equation of State for the Calculation of Vapour-Liquid Equilibria and Mean Activity Coefficients in Water-Alcohol Systems*, Fluid Phase Equilibria, Vol. 150, p. 567, 1998.

Appendix A   Calculation of Thermodynamic Properties in the Michelsen and Mollerup Framework

Calculation of thermodynamic properties from an equation of state may appear a trivial problem which only requires adherence to basic definitions as outlined in Chapter 3. The increasing complexity of thermodynamic models, however calls for a systematic approach in order to avoid inefficient or even incorrect computer codes. To generate a fast and thermodynamically consistent computer code for calculations of the thermodynamic properties of mixtures it is essential to take a modular approach which enables modification of single features of the model, e.g. a mixing rule for one of the model parameters, without rewriting the entire computer code. This calls for a formalism where the properties and its derivatives are calculated by combining the partial derivatives of the state function which ensures a consistent set of relations and leads to an efficient code. This appendix describes such a method – which has been developed by Mollerup and Michelsen (2000).

As was discussed in chapter 6 it is advantageous to implement the model in an object-oriented language – where we can extend and change the models through inheritance. An object-oriented structure for implementing thermodynamic models was developed in this work (chapter 6).

In this chapter the thermodynamic relations used for calculating thermodynamic properties from an equation of state are derived – and all the derivatives needed are given. The method presented here is similar to the one given by Mollerup and Michelsen (2000).

A.1   Introduction

The pressure equation is often denoted an equation of state. Given a pressure equation

$$P = P(T,V,\mathbf{n}) \tag{A.1}$$

where V is the total volume and $\mathbf{n}$ is the vector of mixture mole numbers. The fugacity coefficients can be calculated from

$$
\begin{aligned}
RT \ln \varphi_i &= -\frac{\partial}{\partial n_i} \int_\infty^V \left(P - \frac{nRT}{V} \right) dV - RT \ln Z \\
&= \frac{\partial A^r(T,V,\mathbf{n})}{\partial n_i} - RT \ln Z
\end{aligned} \tag{A.2}
$$

where

$$A^r(T,V,\mathbf{n}) = -\int_\infty^V \left(P - \frac{nRT}{V} \right) dV \tag{A.3}$$

$A^r(T,V,n)$ is the residual Helmholtz function, i.e. the Helmholtz function of the mixture given as a function of temperature T, total volume V, and the vector of mixture mole numbers minus that of the equivalent ideal gas mixture at the same state variables (T,V,n).

The expression for the residual Helmholtz energy is the key equation in equilibrium thermodynamics because all other residual properties are calculable as partial derivatives in the independent variables T,V and n.

A.2 The Calculation of Thermodynamic Properties From the Derivatives of the Reduced Residual Helmholtz Function

The residual Helmholtz function is calculable from equation (A.3), but it is in many cases more convenient to use the partial derivatives of the reduced residual Helmholtz function F,

$$F = \frac{A^r(T,V,\mathbf{n})}{RT} \tag{A.4}$$

In this section we give the general equations relating the thermodynamic properties to the partial derivatives of F. In the following sections we in detail give the derivatives of the F function for cubic equation of states. In appendix C we give the derivatives needed for the electrolyte terms of the Furst and Renon equation of state and the electrolyte models implemented in this work. In appendix B the equations used to implemented advanced mixing rules are given.

The pressure and its derivatives, calculated as partial derivatives of F are

$$P = -RT\left(\frac{\partial F}{\partial V}\right)_{T,n} + \frac{nRT}{V} \tag{A.5}$$

$$Z = \frac{PV}{nRT} \tag{A.6}$$

$$\left(\frac{\partial P}{\partial V}\right)_{T,n} = -RT\left(\frac{\partial^2 F}{\partial V^2}\right)_{T,n} - \frac{nRT}{V^2} \tag{A.7}$$

$$\left(\frac{\partial P}{\partial T}\right)_{V,n} = -RT\left(\frac{\partial^2 F}{\partial T\partial V}\right)_n + \frac{P}{T} \tag{A.8}$$

$$\left(\frac{\partial P}{\partial n_i}\right)_{T,V} = -RT\left(\frac{\partial^2 F}{\partial V\partial n_i}\right)_{T,n_j} + \frac{RT}{V} \tag{A.9}$$

$$\left(\frac{\partial V}{\partial n_i}\right)_{T,P} = \bar{V}_i = -\frac{\left(\frac{\partial P}{\partial n_i}\right)_{T,V,n_j}}{\left(\frac{\partial P}{\partial V}\right)_{T,n}} \tag{A.10}$$

The fugacity coefficient and its derivatives are calculated from

$$\ln \varphi_i = \left(\frac{\partial F}{\partial n_i} \right)_{T,V,n_j} - \ln Z \tag{A.11}$$

$$\left(\frac{\partial \ln \varphi_i}{\partial T} \right)_{P,n} = \left(\frac{\partial^2 F}{\partial T \partial n_i} \right)_{V,n_j} + \frac{1}{T} - \frac{\bar{V}_i}{RT} \left(\frac{\partial P}{\partial T} \right)_{V,n} \tag{A.12}$$

$$\left(\frac{\partial \ln \varphi_i}{\partial P} \right)_{T,n} = \frac{\bar{V}_i}{RT} - \frac{1}{P} \tag{A.13}$$

$$\left(\frac{\partial \ln \varphi_i}{\partial n_j} \right)_{T,P} = \left(\frac{\partial^2 F}{\partial n_j \partial n_i} \right)_{T,V} + \frac{1}{n} - \frac{\bar{V}_i}{RT} \left(\frac{\partial P}{\partial n_j} \right)_{T,V,n_k} \tag{A.14}$$

The residual bulk properties

$$\frac{S^r (T,V,n)}{R} = -T \left(\frac{\partial F}{\partial T} \right)_{V,n} - F \tag{A.15}$$

$$\frac{C_V^r (T,V,n)}{R} = -T^2 \left(\frac{\partial^2 F}{\partial T^2} \right)_{V,n} - 2T \left(\frac{\partial F}{\partial T} \right)_{V,n} \tag{A.16}$$

$$\frac{C_P^r - C_V^r}{R} = -\frac{T}{R} \frac{\left(\frac{\partial P}{\partial T} \right)_{V,n}^2}{\left(\frac{\partial P}{\partial V} \right)_{T,n}} - n \tag{A.17}$$

$$H^r (T,P,n) = A^r (T,V,n) + TS^r (T,V,n) + PV - nRT \tag{A.18}$$

$$G^r (T,P,n) = A^r (T,V,n) + PV - nRT - nRT \ln Z \tag{A.19}$$

$$S^r (T,P,n) = S^r (T,V,n) + nR \ln Z = \left(H^r (T,P,n) - G^r (T,P,n) \right) / T \tag{A.20}$$

The sound of speed can be calculated from

$$W^2 = \frac{V}{\beta_s M_W} \tag{A.21}$$

$$M_W = \sum_i n_i M_{W_i} \tag{A.22}$$

$$\beta_s = -\frac{1}{V}\left(\frac{\partial V}{\partial P}\right)_s = -\frac{1}{V}\frac{C_V}{C_P}\bigg/\left(\frac{\partial P}{\partial V}\right)_{T,n} \tag{A.23}$$

The Joule-Thomson coefficient is calculated from

$$\eta = \left(\frac{\partial T}{\partial P}\right)_{H,n} = -\frac{1}{C_P}\left(V + T\left(\frac{\partial P}{\partial T}\right)_{V,n}\bigg/\left(\frac{\partial P}{\partial V}\right)_{T,n}\right) \tag{A.24}$$

The partial molar enthalpy, gibbs energy and entropy are calculated from

$$\frac{\bar{H}_i^r\left(T,P,n\right)}{RT} = -T\left(\frac{\partial \ln \varphi_i}{\partial T}\right)_{P,n} \tag{A.25}$$

$$\frac{\bar{G}_i^r\left(T,P,n\right)}{RT} = \ln \varphi_i \tag{A.26}$$

$$\bar{S}_i^r\left(T,P,n\right) = \left(\bar{H}_i^r\left(T,P,n\right) - \bar{G}_i^r\left(T,P,n\right)\right)\bigg/T \tag{A.27}$$

A.3 Calculation of the Reduced Residual Helmholtz Function of the Generic Equation of State

The cubic equation of state has two or three adjustable parameters and are thus easy to generalize and apply to fluids where little experimental information is available. The generic cubic equation of state is given as

$$P = \frac{RT}{v-b} - \frac{a\left(T\right)}{\left(v+\delta_1 b\right)\left(v+\delta_2 b\right)} \tag{A.28}$$

where $\delta_1 = 1$ and $\delta_2 = 0$ yields the Redlich-Kwong equation of state (and the ScRK-EOS), and $\delta_1 = 1+\sqrt{2}$ and $\delta_2 = 1-\sqrt{2}$ yields the Peng-Robinson equation of state.

The reduced residual Helmholtz function of the generic equation of state can be calculated as

$$F\left(T,V,\mathbf{n}\right) = \frac{A^r\left(T,V,\mathbf{n}\right)}{RT} = -n\ln\left(1-B/V\right) - \frac{D}{RTB\left(\delta_1 - \delta_2\right)}\ln\left(\frac{1+\delta_1\,B/V}{1+\delta_2\,B/V}\right) \tag{A.29}$$

where V is the total volume of the mixture. It is assumed that a_{mix} and b_{mix} are quadratic sums of their pure component values, then

$$D = n^2 a_{mix} = \sum_{i=1}^{n} n_i \sum_{j=1}^{n} n_j a_{ij} \tag{A.30}$$

with

$$a_{ij} = a_{ji} = \sqrt{a_i a_j} \left(1 - k_{ij}\right) \tag{A.31}$$

and

$$B = \sum_{i=1}^{n} n_i b_i \tag{A.32}$$

The binary interaction coefficient k_{ij} is normally treated as a constant.

The total differential of F is

$$dF = F_n dn + F_T dT + F_V dV + F_B dB + F_D dD \tag{A.33}$$

where

$$F_n = \left(\frac{\partial F}{\partial n}\right)_{T,V,B,D} , \quad F_T = \left(\frac{\partial F}{\partial T}\right)_{n,V,B,D} \quad etc... \tag{A.34}$$

$$n = \sum_{i=1}^{n} n_i \tag{A.35}$$

The second order total differential of F is

$$
\begin{aligned}
d^2 F = &\left(F_{nn} dn + F_{nT} dT + F_{nV} dV + F_{nB} dB + F_{nD} dD\right) dn + F_n d^2 n + \\
&\left(F_{Tn} dn + F_{TT} dT + F_{TV} dV + F_{TB} dB + F_{TD} dD\right) dT + F_T d^2 T + \\
&\left(F_{Vn} dn + F_{VT} dT + F_{VV} dV + F_{VB} dB + F_{VD} dD\right) dV + F_V d^2 V + \\
&\left(F_{Bn} dn + F_{BT} dT + F_{BV} dV + F_{BB} dB + F_{BD} dD\right) dB + F_B d^2 B + \\
&\left(F_{Dn} dn + F_{DT} dT + F_{DV} dV + F_{DB} dB + F_{DD} dD\right) dD + F_D d^2 D
\end{aligned}
\tag{A.36}
$$

where

$$F_{XY} = F_{YX} = \frac{\partial^2 F}{\partial X \partial Y} = \frac{\partial^2 F}{\partial Y \partial X} \tag{A.37}$$

A.4   Derivatives of the Helmholtz Function

To calculate the thermodynamic properties of a fluid we must calculate the partial derivatives as outlined in section A.2 and A.3. The reduced residual Helmholtz function of the generic equation of state (eq. (A.28)) can be written

$$F = F\left(n, T, V, B, D\right) = -n\, g\left(V, B(\mathbf{n})\right) - \frac{D(\mathbf{n}, T)}{T} f\left(V, B(\mathbf{n})\right) \tag{A.38}$$

where

$$g = \ln\left(1 - B/V\right) = \ln\left(V - B\right) - \ln V \tag{A.39}$$

$$f = \frac{1}{RB\left(\delta_1 - \delta_2\right)} \ln \frac{1 + \delta_1 \, B/V}{1 + \delta_2 \, B/V} = \frac{1}{RB\left(\delta_1 - \delta_2\right)} \ln \frac{V + \delta_1 B}{V + \delta_2 B} \tag{A.40}$$

$$n = \sum_{i=1}^{n} n_i \tag{A.41}$$

$$nB = \sum_{i=1}^{n} n_i \sum_{j=1}^{n} n_j b_{ij} \tag{A.42}$$

$$D(T) = \sum_{i=1}^{n} n_i \sum_{j=1}^{n} n_j a_{ij}(T) = \frac{1}{2} \sum_{i=1}^{n} n_i D_i \tag{A.43}$$

where D_i is defined in equation (A.79).

The appropriate derivatives of the reduced Helmholtz energy are straightforward to calculate. The partial derivatives needed for calculation of all thermodynamic properties are:

The first order partial derivatives

$$\left(\frac{\partial F}{\partial n_i}\right)_{T,V,n_j} = F_n + F_B B_i + F_D D_i \tag{A.44}$$

$$\left(\frac{\partial F}{\partial T}\right)_{n,V} = F_T + F_D D_T \tag{A.45}$$

$$\left(\frac{\partial F}{\partial V}\right)_{n,T} = F_V \tag{A.46}$$

The second order partial derivatives

$$\left(\frac{\partial^2 F}{\partial n_i \partial n_j}\right)_{T,V} = F_{nB}\left(B_i + B_j\right) + F_{BD}\left(B_i D_j + B_j D_i\right) + F_B B_{ij} + F_{BB} B_i B_j + F_D D_{ij} \tag{A.47}$$

$$\left(\frac{\partial^2 F}{\partial n_i \partial T}\right)_{V,n_j} = \left(F_{BT} + F_{BD} D_T\right) B_i + F_{DT} D_i + F_D D_{iT} \tag{A.48}$$

$$\left(\frac{\partial^2 F}{\partial n_i \partial V}\right)_{T,n_j} = F_{nV} + F_{BV}B_i + F_{DV}D_i \tag{A.49}$$

$$\left(\frac{\partial^2 F}{\partial T^2}\right)_{n,V} = F_{TT} + 2F_{DT}D_T + F_D D_{TT} \tag{A.50}$$

$$\left(\frac{\partial^2 F}{\partial T \partial V}\right)_n = F_{TV} + F_{DV}D_T \tag{A.51}$$

$$\left(\frac{\partial^2 F}{\partial V^2}\right)_{n,T} = F_{VV} \tag{A.52}$$

The first order partial derivatives of F, g, and f

$$F_n = -g \tag{A.53}$$

$$F_T = \frac{D}{T^2}f \tag{A.54}$$

$$F_V = -ng_V - \frac{D}{T}f_V \tag{A.55}$$

$$F_B = -ng_B - \frac{D}{T}f_B \tag{A.56}$$

$$F_D = -\frac{f}{T} \tag{A.57}$$

$$g_V = \frac{1}{V-B} - \frac{1}{V} = \frac{B}{V(V-B)} \tag{A.58}$$

$$g_B = -\frac{V}{B}g_V = -\frac{1}{V-B} \tag{A.59}$$

$$\begin{aligned} f_V &= \frac{1}{RB(\delta_1 - \delta_2)}\left(\frac{1}{(V+\delta_1 B)} - \frac{1}{(V+\delta_2 B)}\right) \\ &= -\frac{1}{R(V+\delta_1 B)(V+\delta_2 B)} \end{aligned} \tag{A.60}$$

$$f_B = -\frac{f + Vf_V}{B} \tag{A.61}$$

The second order partial derivatives of F, g, and f

$$F_{nV} = -g_V \tag{A.62}$$

$$F_{nB} = -g_B \tag{A.63}$$

$$F_{TT} = -2\frac{F_T}{T} \tag{A.64}$$

$$F_{BT} = \frac{Df_B}{T^2} \tag{A.65}$$

$$F_{DT} = \frac{f}{T^2} \tag{A.66}$$

$$F_{BV} = -ng_{BV} - \frac{D}{T}f_{BV} \tag{A.67}$$

$$F_{BB} = -ng_{BB} - \frac{D}{T}f_{BB} \tag{A.68}$$

$$F_{DV} = -\frac{f_V}{T} \tag{A.69}$$

$$F_{BD} = -\frac{f_B}{T} \tag{A.70}$$

$$F_{TV} = \frac{D}{T^2}f_V \tag{A.71}$$

$$F_{VV} = -ng_{VV} - \frac{D}{T}f_{VV} \tag{A.72}$$

$$g_{VV} = -\frac{1}{(V-B)^2} + \frac{1}{V^2} \tag{A.73}$$

$$g_{BV} = -\frac{g_V + Vg_{VV}}{B} = \frac{1}{(V-B)^2} \tag{A.74}$$

$$g_{BB} = -\frac{g_B + Vg_{BV}}{B} = -\frac{1}{(V-B)^2} \tag{A.75}$$

$$f_{VV} = \frac{1}{RB(\delta_1 - \delta_2)}\left(-\frac{1}{(V+\delta_1 B)^2} + \frac{1}{(V+\delta_2 B)^2}\right) \tag{A.76}$$

$$f_{BV} = -\frac{2f_V + Vf_{VV}}{B} \tag{A.77}$$

$$f_{BB} = -\frac{2f_B + Vf_{BV}}{B} \tag{A.78}$$

The partial derivatives of D

$$D_i = 2\sum_{i=1}^{n} n_j a_{ij} \tag{A.79}$$

$$D_{iT} = 2\sum_{j=1}^{n} n_j \frac{\partial a_{ij}}{\partial T} \tag{A.80}$$

$$D_{ij} = 2a_{ij} \tag{A.81}$$

$$D_T = \frac{1}{2}\sum_{i=1}^{n} n_i D_{iT} \tag{A.82}$$

$$D_{TT} = \sum_{i=1}^{n} n_i \sum_{j=1}^{n} n_j \frac{\partial^2 a_{ij}}{\partial T^2} \tag{A.83}$$

The derivatives of B are,

$$B_i = \frac{2\sum_{j=1}^{n} n_j b_{ij} - B}{n} \tag{A.84}$$

$$B_{ij} = \frac{2b_{ij} - B_i - B_j}{n} \tag{A.85}$$

It might look making a simple problem complex by splitting such a simple model in so many contributions. However, adoption of the procedure described here does not only lead to an easier and better structured approach for deriving thermodynamic properties but also is very likely to provide an efficient code in particular when derivatives of fugacity coefficients are required. It is also much easier to modify the model using this modular approach. This is easily seen when we extend the model to electrolyte solutions in appendix C.

Appendix B   Incorporating Excess Gibbs Energy Models In Equations of State

In this work advanced mixing rules were used and implemented in the Michelsen and Mollerup F-function framework described in appendix A. In this appendix the derivatives needed to implement Gibbs Excess Energy model based mixing rules such as the Huron-Vidal or the Wong-Sandler mixing rules are derived.

B.1 Basic Equations

We shall consider a cubic equation of state of the general form

$$P = \frac{RT}{v-b} - \frac{a}{(v+\delta_1 b)(v+\delta_2 b)} \tag{B.1}$$

Where a and b are mixture parameters and δ_1 and δ_2 are constants. For convenience we replace the mixture parameter a by α, where $a = \alpha b R T$. Equation (B.1) thus becomes

$$\frac{P}{RT} = \frac{1}{v-b} - \alpha \frac{b}{(v+\delta_1 b)(v+\delta_2 b)} \tag{B.2}$$

The mixture fugacity f_{mix} is given by

$$\ln\left(\frac{f_{mix} b}{RT}\right) = \frac{Pv}{RT} - 1 - \ln\left(\frac{v-b}{b}\right) - \frac{\alpha}{\delta_2 - \delta_1} \ln\left(\frac{v+\delta_2 b}{v+\delta_1 b}\right) \tag{B.3}$$

The mixture fugacity for component i f_i is given by

$$\ln\left(\frac{f_i b_i}{RT}\right) = \frac{Pv_i}{RT} - 1 - \ln\left(\frac{v_i - b_i}{b_i}\right) - \frac{\alpha_i}{\delta_2 - \delta_1} \ln\left(\frac{v_i + \delta_2 b_i}{v_i + \delta_1 b_i}\right) \tag{B.4}$$

For a mixture of composition z the reduced excess Gibbs energy thus becomes

$$\frac{g_E}{RT}(T,P,z) = \ln f_{mix}(T,P,z) - \sum_i z_i \ln f_i(T,P) \tag{B.5}$$

When $P \rightarrow \infty$, $v \rightarrow b$ and $v_i \rightarrow b_i$ we get after some algebra (Michelsen et. al, 2000)

$$g_{P\rightarrow\infty}^E = \frac{P}{RT}\left(b - \sum_i z_i b_i\right) - \Delta\left(\alpha - \sum_i z_i \alpha_i\right) \tag{B.6}$$

Where

$$\Delta = \frac{1}{\delta_2 - \delta_1} \ln\frac{1+\delta_2}{1+\delta_1} \tag{B.7}$$

Provided we use a linear mixing rule $b = \sum_i z_i b_i$ we get

$$\alpha = \sum_i z_i \alpha_i - \frac{1}{\Delta} g_\infty^E \tag{B.8}$$

B.2 Derivatives

To get the equations on the right form we need the derivatives of B and D.

$$B = n_t b$$
$$D = n_t^2 a = n_t^2 \alpha b RT$$

Derivatives of D
We get

$$\frac{\partial D}{\partial n_i} = n_t^2 \frac{\partial \alpha}{\partial n_i} bRT + n_t^2 \alpha \left(\frac{\partial b}{\partial n_i} \right) RT \tag{B.9}$$

$$\frac{\partial D}{\partial n_i \partial T} = n_t^2 \left(\frac{\partial \alpha}{\partial n_i \partial T} \right) bRT + n_t^2 \left(\frac{\partial \alpha}{\partial n_i} \right) bR + n_t^2 \left(\frac{\partial \alpha}{\partial T} \right) \left(\frac{\partial b}{\partial n_i} \right) RT + n_t^2 \alpha \left(\frac{\partial b}{\partial n_i} \right) R \tag{B.10}$$

$$\frac{\partial D}{\partial n_i \partial n_j} = n_t^2 \frac{\partial \alpha}{\partial n_i \partial n_j} bRT + n_t^2 \frac{\partial \alpha}{\partial n_i} \frac{\partial b}{\partial n_j} RT + n_t^2 \frac{\partial \alpha}{\partial n_j} \left(\frac{\partial b}{\partial n_i} \right) RT + n_t^2 \alpha \left(\frac{\partial b}{\partial n_i \partial n_j} \right) RT \tag{B.11}$$

$$\frac{\partial D}{\partial T} = n_t^2 \frac{\partial \alpha}{\partial T} bRT + n_t^2 \alpha \left(\frac{\partial b}{\partial T} \right) RT + n_t^2 \alpha bR \tag{B.12}$$

$$\frac{\partial^2 D}{\partial T^2} = n_t^2 \frac{\partial^2 \alpha}{\partial T^2} bRT + n_t^2 \frac{\partial \alpha}{\partial T} \frac{\partial b}{\partial T} RT + n_t^2 \frac{\partial \alpha}{\partial T} bR + n_t^2 \frac{\partial \alpha}{\partial T} \left(\frac{\partial b}{\partial T} \right) RT + n_t^2 \alpha \left(\frac{\partial^2 b}{\partial T^2} \right) RT + n_t^2 \alpha \left(\frac{\partial b}{\partial T} \right) R$$
$$+ n_t^2 \frac{\partial \alpha}{\partial T} bR + n_t^2 \alpha \frac{\partial b}{\partial T} R \tag{B.13}$$

The derivatives of α are calculated from equation (B.8). The derivatives of α with respect to temperature and mole numbers are

$$\frac{\partial \alpha}{\partial T} = \sum_i z_i \frac{\partial \alpha_i}{\partial T} - \frac{1}{\Delta} \frac{\partial g_\varpi^E}{\partial T}$$

$$\frac{\partial \alpha}{\partial n_i} = \alpha_i - \frac{1}{\Delta} \frac{\partial g_\infty^E}{\partial n_i}$$

We see that it is necessary to calculate the derivatives of the gibbs excess energy model with respect to temperature and mole numbers. In this work the NRTL-GE-model was used and the derivatives of this model had to be calculated.

Derivatives of B

$$\frac{\partial B}{\partial n_i} = b + n_t \frac{\partial b}{\partial n_i} \tag{B.14}$$

$$\frac{\partial B}{\partial n_i \partial n_j} = \frac{\partial b}{\partial n_j} + \frac{\partial b}{\partial n_i} + n_t \frac{\partial b}{\partial n_i \partial n_j} \tag{B.15}$$

All models have been checked for thermodynamic consistency following the procedures suggested by Michelsen and Mollerup (2000).

Appendix C   The Electrolyte Equation of State

The electrolyte equation of state published in 1993 by Furst and Renon was used as the basis for modelling thermodynamic properties of electrolyte solutions in this work. The electrolyte equation of state was implemented in the modelling framework of Michelsen and Mollerup as was described in appendix A and B. The electrolyte equation of state consists of non-electrolyte- and electrolyte terms. The non-electrolyte terms are the same as those derived in appendix A and B, and can be used in the electrolyte equation of state without modifications. The derivatives of the electrolyte terms are derived and presented in this appendix.

C.1   Basic Equations of the Modified Furst-Renon Electrolyte EOS

The Furst and Renon electrolyte equation of state is based on an expression of the Helmholtz Energy $A(T,V,n_i)$. The advantage of such an approach is that all thermodynamic functions can be derived from that expression. The molar Helmholtz Energy is developed as the sum of:

$$\left(\frac{A-A^0}{RT}\right) = \left(\frac{A-A^0}{RT}\right)_{RF} + \left(\frac{A-A^0}{RT}\right)_{SR1} + \left(\frac{A-A^0}{RT}\right)_{SR2} + \left(\frac{A-A^0}{RT}\right)_{LR} + \left(\frac{A-A^0}{RT}\right)_{BORN} \qquad (C.1)$$

where,

$$\left(\frac{A-A^0}{RT}\right)_{RF} + \left(\frac{A-A^0}{RT}\right)_{SR1} = -n \cdot g(V,B(n)) - \frac{D(n,T)}{T} f(V,B(n)) \qquad (C.2)$$

For cubic equations of state the expressions for the different terms in this equation and its derivatives were derived in appendix A and B. The last three terms (ionic contributions) of equation (C.1) and its derivatives are derived in this appendix.

The short range ionic term is calculated from

$$\left(\frac{A-A^0}{RT}\right)_{SR2} = -\sum_k \sum_l \frac{n_k n_l W_{kl}}{V(1-\varepsilon_3)} \qquad (C.3)$$

Where ε_3 is calculated from,

$$\varepsilon_3 = \frac{N\pi}{6} \sum_k \frac{n_k \sigma_k^3}{V} \qquad (C.4)$$

where k is over all species. The ion-molecule/ion-ion interaction parameter W_{kl} is an adjustable parameter. A model for calculating the values of these interaction parameters from characteristic ionic diameters was described in chapter 7.

The long-range ion-ion interaction term is given by a simplified MSA term (Planche et.al 1980, Ball et. al. 1985),

$$\left(\frac{A-A^0}{RT}\right)_{LR} = -\frac{\alpha_{LR}^2}{4\pi}\sum_i \frac{n_i Z_i^2 \Gamma}{1+\Gamma\sigma_i} + \frac{\Gamma^3 V}{3\pi N} \tag{C.5}$$

where N is the avagadro number and Γ the shielding parameter. Γ is given implicitly by the equation

$$4\Gamma^2 = \alpha_{LR}^2 \sum_i \frac{n_i}{V}\left(\frac{Z_i}{1+\Gamma\sigma_i}\right)^2 \tag{C.6}$$

with,

$$\alpha_{LR}^2 = \frac{e^2 N}{\varepsilon_0 DRT} \tag{C.7}$$

and

$$D = 1 + (D_s - 1)\frac{(1-\varepsilon_3)}{\left(1+\dfrac{\varepsilon_3}{2}\right)} \tag{C.8}$$

The shielding parameter is calculated by a Newton approach, and is normally found in a few iterations with 0 as an initial guess. The solvent dielectric constant is given as

$$D_s = \frac{\sum_i n_i D_i}{\sum_i n_i} \tag{C.9}$$

where i is only over molecular components.

The Born term is given as,

$$\left(\frac{A-A^0}{RT}\right)_{BORN} = \frac{Ne^2}{4\pi\varepsilon_0 RT}\left(\frac{1}{D_s}-1\right)\sum_i \frac{n_i Z_i^2}{\sigma_i^*} \tag{C.10}$$

The ionic volume (σ^*) in this equation is not the same as given earlier (solvent dependent). In this work the ionic diameters σ^* were set equall to the characteristic ionic diameters defined in chapter 7 (Pauling anionic- and Stokes cationc diameter). The Born term does not give contribution to the activity coefficient of ions in single solvent systems (e.g. pure water). It does however give a contribution to the activity of ions in mixed solvent systems – when the reference state is that of infinite dilution in a pure water phase. It gives a large contribution to the fugacity coefficient of ions – and is mathematically the reason for the low ionic consentration in the gas phase and phases with low dielectric constants (e.g condensate). Furst and Renon did not use the Born term in their original publication (1993) – though it has been added in a later article on LLE in electrolyte systems.

C.2   Calculation of First and Second Order Derivatives of the Furst and Renon Electrolyte Model

This section gives the expressions for all the derivatives needed to implement the aqueous electrolyte equation of state (AEEOS) presented in last section in a computer code. In order to calculate all thermodynamic properties and its derivatives, we would have to specify the following derivatives (see eqs. (A.5)-(A.27)) of the F-function (reduced Helmholtz energy)

$$\left(\frac{\partial F}{\partial T}\right)_{n,V} \qquad \left(\frac{\partial^2 F}{\partial T\partial V}\right)_{n} \qquad \left(\frac{\partial^2 F}{\partial T^2}\right)_{n,V} \qquad \left(\frac{\partial F}{\partial n_i}\right)_{T,V,n} \qquad \left(\frac{\partial F}{\partial V}\right)_{T,n}$$

$$\left(\frac{\partial^2 F}{\partial n_i \partial n_j}\right)_{T,V} \qquad \left(\frac{\partial^2 F}{\partial n_i \partial T}\right)_{V,n} \qquad \left(\frac{\partial^2 F}{\partial n_i \partial V}\right)_{T,n} \qquad \left(\frac{\partial^2 F}{\partial^2 V}\right)_{T,n} \qquad \left(\frac{\partial^2 F}{\partial^3 V}\right)_{T,n}$$

In the first sections we give the derivatives needed to calculate the fugacity coefficient (which for simple flash calculations are sufficient). In the second section we give the rest of the derivatives needed to calculate all thermodynamic properties and the corresponding derivatives as calculated from equations (A.5)-(A.27).

C.3   Derivatives of the Ionic Short Range Term

The short-range ionic term is given as

$$F_{SR2} = -\sum_k \sum_l \frac{n_k n_l W_{kl}}{V(1-\varepsilon_3)} = \frac{W}{V(1-\varepsilon_3)} \tag{C.11}$$

where we have defined the function

$$W = -\sum_k \sum_l n_k n_l W_{kl} \tag{C.12}$$

We got the function

$$F_{SR2} = F_{SR2}(T,V,n,W,\varepsilon_3) \tag{C.13}$$

The first order differential of this function is

$$dF_{SR2} = \left(\frac{\partial F_{SR2}}{\partial n}\right)_{T,V,W,\varepsilon} \partial n + \left(\frac{\partial F_{SR2}}{\partial V}\right)_{n,W,T,\varepsilon} \partial V + \left(\frac{\partial F_{SR2}}{\partial W}\right)_{n,V,T,\varepsilon} \partial W$$

$$+ \left(\frac{\partial F_{SR2}}{\partial T}\right)_{n,V,W,\varepsilon} \partial T + \left(\frac{\partial F_{SR2}}{\partial \varepsilon}\right)_{n,V,W,T} \partial \varepsilon \tag{C.14}$$

The second order differential is given as

$$d^2 F_{SR2} = \left(F_{nn}dn + F_{nT}dT + F_{nV}dV + F_{n\varepsilon}d\varepsilon + F_{nW}dW \right)dn + F_n d^2 n$$
$$\left(F_{Tn}dn + F_{TT}dT + F_{TV}dV + F_{T\varepsilon}d\varepsilon + F_{TW}dW \right)dT + F_T d^2 T$$
$$\left(F_{Vn}dn + F_{VT}dT + F_{VV}dV + F_{V\varepsilon}d\varepsilon + F_{VW}dW \right)dV + F_V d^2 V \qquad (C.15)$$
$$\left(F_{\varepsilon n}dn + F_{\varepsilon T}dT + F_{\varepsilon V}dV + F_{\varepsilon\varepsilon}d\varepsilon + F_{\varepsilon W}dW \right)d\varepsilon + F_\varepsilon d^2 \varepsilon$$
$$\left(F_{Wn}dn + F_{WT}dT + F_{WV}dV + F_{W\varepsilon}d\varepsilon + F_{WW}dW \right)dW + F_W d^2 W$$

To calculate the fugacity coefficient we need the derivative $\left(\dfrac{\partial F_{SR2}}{\partial n_i} \right)_{T,V,n}$. Some of the terms

in equation (C.14) cancel out, and we get

$$\left(\frac{\partial F_{SR2}}{\partial n_i} \right)_{T,V,n} = \left(\frac{\partial F_{SR2}}{\partial W} \right)_{n,V,T,\varepsilon} \left(\frac{\partial W}{\partial n_i} \right)_{T,V,n} + \left(\frac{\partial F_{SR2}}{\partial \varepsilon_3} \right)_{n,V,W,T} \left(\frac{\partial \varepsilon_3}{\partial n_i} \right)_{T,V,n} \qquad (C.16)$$

$$\left(\frac{\partial F_{SR2}}{\partial \varepsilon_3} \right)_{n,V,W,T} = \frac{W}{V\left(1 - \varepsilon_3\right)^2}$$

$$\left(\frac{\partial \varepsilon_3}{\partial n_i} \right)_{T,V,n} = \frac{N\pi\sigma_i^3}{6V}$$

$$\left(\frac{\partial F_{SR2}}{\partial W} \right)_{n,V,T,\varepsilon} = \frac{1}{V\left(1 - \varepsilon_3\right)}$$

$$\left(\frac{\partial W}{\partial n_i} \right)_{T,V} = W_i = -2\sum_k n_k W_{ki}$$

From the equations above and equation (C.14), we see that the ionic short-range term gives the following contribution to the fugacity coefficient

$$\left(\frac{\partial F_{SR2}}{\partial n_i} \right)_{T,V,n_j} = \frac{N\pi\sigma_i^3}{6} \frac{W}{V^2\left(1-\varepsilon_3\right)^2} + \frac{W_i}{V\left(1-\varepsilon_3\right)} \qquad (C.17)$$

Which is equal to the expression presented by Furst and Renon (1993).

C.3.1 More Derivatives of the Ionic Short Range Term

All the derivatives for the SR2 term are given in this section. As long as we assume temperature independent mixing rules for W (W_{ij} was assumed constant in this work), we get

$$\left(\frac{\partial F_{SR2}}{\partial T} \right)_{n,V} = \left(\frac{\partial F_{SR2}}{\partial W} \right)_{n,V,T,\varepsilon} \left(\frac{\partial W}{\partial T} \right)_{n,V} \qquad (C.18)$$

$$\left(\frac{\partial^2 F_{SR2}}{\partial T^2}\right)_{n,V} = \left(\frac{\partial F_{SR2}}{\partial W}\right)_{n,V,T,\varepsilon}\left(\frac{\partial^2 W}{\partial T^2}\right)_{n,V} \tag{C.19}$$

$$\left(\frac{\partial F_{SR2}}{\partial n_i \partial T}\right)_V = \left(\frac{\partial F_{SR2}}{\partial W}\right)_{n,V,T,\varepsilon}\left(\frac{\partial^2 W}{\partial n_i \partial T}\right)_V + \left(\frac{\partial F_{SR2}}{\partial W \partial \varepsilon}\right)_{n,V,T}\left(\frac{\partial \varepsilon}{\partial n_i}\right)_V\left(\frac{\partial W}{\partial T}\right)_V \tag{C.20}$$

$$\left(\frac{\partial F_{SR2}}{\partial V \partial T}\right)_n = \left(\frac{\partial F_{SR2}}{\partial W \partial V}\right)_{n,V,T,\varepsilon}\left(\frac{\partial W}{\partial T}\right)_n + \left(\frac{\partial F_{SR2}}{\partial W \partial \varepsilon}\right)_{n,V,T}\left(\frac{\partial \varepsilon}{\partial V}\right)_n\left(\frac{\partial W}{\partial T}\right)_n \tag{C.21}$$

$$\left(\frac{\partial F_{SR2}}{\partial V}\right)_{T,n} = \left(\frac{\partial F_{SR2}}{\partial V}\right)_{n,W,T,\varepsilon} + \left(\frac{\partial F_{SR2}}{\partial \varepsilon_3}\right)_{n,V,W,T}\left(\frac{\partial \varepsilon_3}{\partial V}\right)_{T,n} \tag{C.22}$$

$$\left(\frac{\partial^2 F_{SR2}}{\partial V^2}\right)_{T,n} = \left(\frac{\partial^2 F_{SR2}}{\partial V^2}\right)_{n,W,T,\varepsilon} + 2\cdot\left(\frac{\partial^2 F_{SR2}}{\partial \varepsilon \partial V}\right)\left(\frac{\partial \varepsilon_3}{\partial V}\right)_{T,n}$$
$$+ \left(\frac{\partial^2 F_{SR2}}{\partial \varepsilon_3{}^2}\right)_{n,V,W,T}\left(\left(\frac{\partial \varepsilon_3}{\partial V}\right)_{T,n}\right)^2 + \left(\frac{\partial F_{SR2}}{\partial \varepsilon}\right)_{n,W,T,V}\left(\frac{\partial^2 \varepsilon_3}{\partial V^2}\right)_{T,n} \tag{C.23}$$

$$\left(\frac{\partial^3 F_{SR2}}{\partial V^3}\right)_{T,n} = \left(\frac{\partial^3 F_{SR2}}{\partial V^3}\right)_{n,W,T,\varepsilon} + 3\cdot\left(\frac{\partial^3 F_{SR2}}{\partial \varepsilon_3 \partial \varepsilon_3 \partial V}\right)\left(\left(\frac{\partial \varepsilon_3}{\partial V}\right)_{T,n}\right)^2$$
$$+ 3\cdot\left(\frac{\partial^3 F_{SR2}}{\partial \varepsilon_3 \partial V \partial V}\right)\left(\frac{\partial \varepsilon_3}{\partial V}\right)_{T,n} + \left(\frac{\partial^3 F_{SR2}}{\partial \varepsilon_3{}^3}\right)\left(\left(\frac{\partial \varepsilon_3}{\partial V}\right)_{T,n}\right)^3 \tag{C.24}$$

$$\left(\frac{\partial^2 F_{SR2}}{\partial n_i \partial n_j}\right)_{T,V} = \left(\frac{\partial^2 F_{SR2}}{\partial \varepsilon_3{}^2}\right)_{n,V,W,T}\left(\frac{\partial \varepsilon_3}{\partial n_i}\right)_{T,V}\left(\frac{\partial \varepsilon_3}{\partial n_j}\right)_{T,V} + \left(\frac{\partial^2 F_{SR2}}{\partial \varepsilon \partial W}\right)_{n,V,T}\left(\frac{\partial W}{\partial n_i}\right)_{T,V}\left(\frac{\partial \varepsilon_3}{\partial n_j}\right)_{T,V}$$
$$+ \left(\frac{\partial F_{SR2}}{\partial \varepsilon}\right)_{n,V,T,W}\left(\frac{\partial^2 W}{\partial n_i \partial n_j}\right)_{T,V} + \left(\frac{\partial^2 F}{\partial W \partial \varepsilon}\right)_{n,T,V}\left(\frac{\partial \varepsilon}{\partial n_i}\right)_{T,V}\left(\frac{\partial W}{\partial n_j}\right)_{T,V} \tag{C.25}$$

$$\left(\frac{\partial^2 F_{SR2}}{\partial n_i \partial V}\right)_{T,n} = \left(\frac{\partial^2 F_{SR2}}{\partial V \partial \varepsilon}\right)_{n,W,T}\left(\frac{\partial \varepsilon}{\partial n_i}\right)_{T,n} + \left(\frac{\partial^2 F_{SR2}}{\partial V \partial W}\right)_{n,T,\varepsilon}\left(\frac{\partial W}{\partial n_i}\right)_{T,n} + \left(\frac{\partial^2 F_{SR2}}{\partial V^2}\right)_{n,T,W,\varepsilon}\left(\frac{\partial V}{\partial n_i}\right)_{T,n} +$$
$$\left(\frac{\partial^2 F_{SR2}}{\partial \varepsilon^2}\right)_{n,W,T,V}\left(\frac{\partial \varepsilon}{\partial n_i}\right)_{T,n}\left(\frac{\partial \varepsilon}{\partial V}\right)_{T,n} + \left(\frac{\partial^2 F_{SR2}}{\partial \varepsilon \partial W}\right)_{n,T,V}\left(\frac{\partial W}{\partial n_i}\right)_{T,n}\left(\frac{\partial \varepsilon}{\partial V}\right)_{T,n} +$$
$$\left(\frac{\partial^2 F_{SR2}}{\partial \varepsilon \partial V}\right)_{n,T,W}\left(\frac{\partial V}{\partial n_i}\right)_{T,n}\left(\frac{\partial \varepsilon}{\partial V}\right)_{T,n} + \left(\frac{\partial F_{SR2}}{\partial \varepsilon}\right)_{n,T,V,W}\left(\frac{\partial^2 \varepsilon}{\partial n_i \partial V}\right)_{n,T} \tag{C.26}$$

The individual partial derivative terms of equations (C.18) to (C.26) are calculated from

$$\left(\frac{\partial F_{SR2}}{\partial V}\right)_{n,W,T,\varepsilon} = -\frac{W}{V^2(1-\varepsilon_3)} \tag{C.27}$$

$$\left(\frac{\partial \varepsilon_3}{\partial V}\right)_{T,n} = -\frac{N\pi}{6}\sum_k \frac{n_k \sigma_k}{V^2} = -\frac{\varepsilon_3}{V} \tag{C.28}$$

$$\left(\frac{\partial^2 F_{SR2}}{\partial V^2}\right)_{n,W,T} = \frac{2W}{V^3\left(1-\varepsilon_3\right)} \tag{C.29}$$

$$\left(\frac{\partial^2 F_{SR2}}{\partial \varepsilon_3 \partial V}\right)_{n,W,T} = -\frac{W}{V^2(1-\varepsilon_3)^2} \tag{C.30}$$

$$\left(\frac{\partial^2 F_{SR2}}{\partial \varepsilon \partial W}\right)_{n,V,T} = \frac{2W}{V\left(1-\varepsilon_3\right)^2} \tag{C.31}$$

$$\left(\frac{\partial^2 \varepsilon_3}{\partial V^2}\right)_{T,n} = \frac{2N\pi}{6}\sum_k \frac{n_k \sigma_k}{V^3} = 2\frac{\varepsilon_3}{V^2} \tag{C.32}$$

$$\left(\frac{\partial^2 F_{SR2}}{\partial \varepsilon_3^{\;2}}\right)_{n,V,W,T} = \frac{2W}{V\left(1-\varepsilon_3\right)^3} \tag{C.33}$$

$$\left(\frac{\partial^2 F_{SR2}}{\partial V^3}\right)_{n,W,T} = -\frac{6W}{V^4\left(1-\varepsilon_3\right)} \tag{C.34}$$

$$\left(\frac{\partial^3 F_{SR2}}{\partial \varepsilon_3 \partial \varepsilon_3 \partial V}\right)_{n,V,W,T} = -\frac{2W}{V^2(1-\varepsilon_3)^3} \tag{C.35}$$

$$\left(\frac{\partial^3 F_{SR2}}{\partial \varepsilon_3 \partial V \partial V}\right)_{n,T,W} = \frac{2W}{V^3(1-\varepsilon_3)^2} \tag{C.36}$$

$$\left(\frac{\partial^3 F_{SR2}}{\partial \varepsilon_3^{\;3}}\right)_{n,V,W,T} = \frac{6W}{V\left(1-\varepsilon_3\right)^4} \tag{C.37}$$

C.4   Derivatives of the Long Range MSA-Term (ion-ion interaction term)

The ion-ion interaction term is derived from the Mean Spherical Approximation (Blom and Høye, 1980), and is given as

$$F_{LR} = -\frac{\alpha_{LR}^2}{4\pi} \sum_i \frac{n_i Z_i^2 \Gamma}{1 + \Gamma \sigma_i} + \frac{\Gamma^3 V}{3\pi N} = -\frac{\alpha_{LR}^2}{4\pi} X + \frac{\Gamma^3 V}{3\pi N} \tag{C.38}$$

where we have defined X as

$$X = \sum_i \frac{n_i Z_i^2 \Gamma}{1 + \Gamma \sigma_i} \tag{C.39}$$

The first- and second order differentials of the MSA term are given as

$$dF_{LR} = \left(\frac{\partial F_{LR}}{\partial n}\right)_{T,V,\alpha_{LR},X,\Gamma} \partial n + \left(\frac{\partial F_{LR}}{\partial T}\right)_{n,V,\alpha_{LR},X,\Gamma} \partial T + \left(\frac{\partial F_{LR}}{\partial V}\right)_{n,T,\alpha_{LR},X,\Gamma} \partial V$$
$$+ \left(\frac{\partial F_{LR}}{\partial \alpha_{LR}^2}\right)_{n,T,V,X,\Gamma} \partial \alpha_{LR}^2 + \left(\frac{\partial F_{LR}}{\partial X}\right)_{n,T,V,\alpha_{LR},\Gamma} \partial X + \left(\frac{\partial F_{LR}}{\partial \Gamma}\right)_{n,T,V,\alpha_{LR},X} \partial \Gamma \tag{C.40}$$

$$d^2 F_{LR} = \left(F_{nn} dn + F_{nT} dT + F_{nV} dV + F_{n\alpha^2} d\alpha^2 + F_{nX} dX + F_{n\Gamma} d\Gamma\right) dn + F_n d^2 n$$
$$\left(F_{Tn} dn + F_{TT} dT + F_{TV} dV + F_{T\alpha^2} d\alpha^2 + F_{TX} dX + F_{T\Gamma} d\Gamma\right) dT + F_T d^2 T$$
$$\left(F_{Vn} dn + F_{VT} dT + F_{VV} dV + F_{V\alpha^2} d\alpha^2 + F_{VX} dX + F_{V\Gamma} d\Gamma\right) dV + F_V d^2 V$$
$$\left(F_{\alpha^2 n} dn + F_{\alpha^2 T} dT + F_{\alpha^2 V} dV + F_{\alpha^2 \alpha^2} d\alpha^2 + F_{\alpha^2 X} dX + F_{\alpha^2 \Gamma} d\Gamma\right) d\alpha^2 + F_{\alpha^2} d^2 \alpha^2 \tag{C.41}$$
$$\left(F_{Xn} dn + F_{XT} dT + F_{XV} dV + F_{X\alpha^2} d\alpha^2 + F_{XX} dX + F_{X\Gamma} d\Gamma\right) dX + F_X d^2 X$$
$$\left(F_{\Gamma n} dn + F_{\Gamma T} dT + F_{\Gamma V} dV + F_{\Gamma \alpha^2} d\alpha^2 + F_{\Gamma X} dX + F_{\Gamma \Gamma} d\Gamma\right) d\Gamma + F_\Gamma d^2 \Gamma^2$$

Due to its importance in equilibrium calculations, we give the detailed derivations of the $\left(\frac{\partial F_{LR}}{\partial n_i}\right)_{T,V,n}$ term. We see that

$$\left(\frac{\partial F_{LR}}{\partial n_i}\right)_{T,V,n} = \left(\frac{\partial F_{LR}}{\partial \alpha_{LR}^2}\right)_{n,T,V,X,\Gamma} \left(\frac{\partial \alpha_{LR}^2}{\partial n_i}\right)_{T,V,n} + \left(\frac{\partial F_{LR}}{\partial X}\right)_{n,T,V,\alpha_{LR},\Gamma} \left(\frac{\partial X}{\partial n_i}\right)_{T,V,n} + \left(\frac{\partial F_{LR}}{\partial \Gamma}\right)_{n,T,V,\alpha_{LR},X} \left(\frac{\partial \Gamma}{\partial n_i}\right)_{T,V,n}$$

where we have

$$\left(\frac{\partial F_{LR}}{\partial \alpha_{LR}^2}\right)_{n,T,V,X,\Gamma} = -\frac{X}{4\pi}$$

$$\left(\frac{\partial \alpha_{LR}^2}{\partial n_i}\right)_{T,V,n} = -\frac{e^2 N}{\varepsilon_0 D^2 RT} \left(\frac{\partial D}{\partial n_i}\right)_{T,V,n}$$

the derivative of F_{LR} with respect to X is,

$$\left(\frac{\partial F_{LR}}{\partial X}\right)_{n,T,V,\alpha_{LR},\Gamma} = -\frac{\alpha_{LR}^2}{4\pi}$$

$$\left(\frac{\partial X}{\partial n_i}\right)_{T,V,n} = \frac{Z_i^2 \Gamma}{1+\Gamma\sigma_i}$$

The derivative F_Γ is

$$\left(\frac{\partial F_{LR}}{\partial \Gamma}\right)_{n,T,V,\alpha_{LR},X} = \frac{3\Gamma^2 V}{3\pi N}$$

and the derivative of the shielding parameter is

$$8\Gamma\left(\frac{\partial \Gamma}{\partial n_i}\right)_{T,V,n} = \alpha_{LR}^2 \frac{n_i}{V}\left(\frac{Z_i}{1+\Gamma\sigma_i}\right)^2 + \frac{\partial \alpha_{LR}^2}{\partial n_i}\frac{n_i}{V}\left(\frac{Z_i}{1+\Gamma\sigma_i}\right)^2 - 2\sigma_i\alpha_{LR}^2 \sum_i \frac{n_i}{V}\left(\frac{Z_i}{1+\Gamma\sigma_i}\right)^2 \left(\frac{1}{1+\Gamma\sigma_i}\right)\left(\frac{\partial \Gamma}{\partial n_i}\right)_{T,V,n}$$

which rearranged is an explicit equation for the derivative of the shielding parameter. This derivative has normally a small contribution to the fugacity coefficient. We will neglects it in the equations that follow (this was also done by Furst & Renon, 1993). (It can be turned on as an option in the computer code).

From the equations derived above and equation (C.40), we see that the ionic long-range term gives the following contribution to the fugacity coefficient

$$\left(\frac{\partial F_{LR}}{\partial n_i}\right)_{T,V,n_j} = \left(\frac{\partial F_{LR}}{\partial \alpha_{LR}^2}\right)_{n,T,V,X,\Gamma}\left(\frac{\partial \alpha_{LR}^2}{\partial n_i}\right)_{T,V,n} + \left(\frac{\partial F_{LR}}{\partial X}\right)_{n,T,V,\alpha_{LR},\Gamma}\left(\frac{\partial X}{\partial n_i}\right)_{T,V,n}$$

$$= \frac{1}{4\pi}\frac{e^2 N}{\varepsilon_0 D^2 RT}\left(\frac{\partial D}{\partial n_i}\right)_{T,V,n} X - \frac{\alpha_{LR}^2}{4\pi}\frac{Z_i^2 \Gamma}{1+\Gamma\sigma_i} \qquad \text{(C.42)}$$

$$= \frac{\alpha_{LR}^2}{4\pi D}\left(\frac{\partial D}{\partial n_i}\right)_{T,V,n} X - \frac{\alpha_{LR}^2}{4\pi}\frac{Z_i^2 \Gamma}{1+\Gamma\sigma_i}$$

which is equal to the expression given by Furst & Renon (1993).

C.4.1 More Derivatives of the Ionic Long Range Term

The other derivatives of the ionic long-range term are,

$$\left(\frac{\partial F_{LR}}{\partial V}\right)_{T,n} = \left(\frac{\partial F_{LR}}{\partial V}\right)_{n,T,\alpha_{LR},X,\Gamma} + \left(\frac{\partial F_{LR}}{\partial \alpha_{LR}^2}\right)_{n,T,V,X,\Gamma}\left(\frac{\partial \alpha_{LR}^2}{\partial V}\right)_{T,n} \qquad \text{(C.43)}$$

$$\left(\frac{\partial^2 F_{LR}}{\partial V^2}\right)_{T,n} = \left(\frac{\partial F_{LR}}{\partial \alpha_{LR}{}^2}\right)_{n,T,V,X,\Gamma} \left(\frac{\partial^2 \alpha_{LR}{}^2}{\partial^2 V}\right)_{T,n} \tag{C.44}$$

$$\left(\frac{\partial^3 F_{LR}}{\partial V^3}\right)_{T,n} = \left(\frac{\partial F_{LR}}{\partial \alpha_{LR}{}^2}\right)_{n,T,V,X,\Gamma} \left(\frac{\partial^3 \alpha_{LR}{}^2}{\partial^3 V}\right)_{T,n} \tag{C.45}$$

$$\left(\frac{\partial F_{LR}}{\partial T}\right)_{V,n} = \left(\frac{\partial F_{LR}}{\partial \alpha_{LR}{}^2}\right)_{n,T,V,X,\Gamma} \left(\frac{\partial \alpha_{LR}{}^2}{\partial T}\right)_{V,n} \tag{C.46}$$

$$\left(\frac{\partial^2 F_{LR}}{\partial T^2}\right)_{n,V} = \left(\frac{\partial F_{LR}}{\partial \alpha_{LR}{}^2}\right)_{n,T,V,X,\Gamma} \left(\frac{\partial^2 \alpha_{LR}{}^2}{\partial T^2}\right)_{n,V} \tag{C.47}$$

$$\left(\frac{\partial^2 F_{LR}}{\partial T \partial V}\right)_{n} = \left(\frac{\partial F_{LR}}{\partial \alpha_{LR}{}^2}\right)_{n,T,V,X,\Gamma} \left(\frac{\partial \alpha_{LR}{}^2}{\partial T \partial V}\right)_{n} \tag{C.48}$$

$$\left(\frac{\partial^2 F_{LR}}{\partial n_i \partial n_j}\right)_{T,V} = \left(\frac{\partial^2 F_{LR}}{\partial \alpha_{LR}{}^2 \partial X}\right)_{n,T,V,\Gamma} \left(\frac{\partial X}{\partial n_i}\right)_{T,V} \left(\frac{\partial \alpha_{LR}{}^2}{\partial n_j}\right)_{T,V} + \left(\frac{\partial F_{LR}}{\partial \alpha_{LR}{}^2}\right)_{n,T,V,X,\Gamma} \left(\frac{\partial^2 \alpha_{LR}{}^2}{\partial n_i \partial n_j}\right)_{T,V} +$$
$$\left(\frac{\partial^2 F_{LR}}{\partial X \partial \alpha_{LR}{}^2}\right)_{n,T,V,\Gamma} \left(\frac{\partial \alpha_{LR}{}^2}{\partial n_i}\right)_{T,V} \left(\frac{\partial X}{\partial n_j}\right)_{T,V} \tag{C.49}$$

$$\left(\frac{\partial^2 F_{LR}}{\partial n_i \partial T}\right)_{V} = \left(\frac{\partial^2 F_{LR}}{\partial \alpha_{LR} \partial X}\right)_{n,T,V,\Gamma} \left(\frac{\partial X}{\partial n_i}\right)_{V} \left(\frac{\partial \alpha_{LR}{}^2}{\partial T}\right)_{V} + \left(\frac{\partial F_{LR}}{\partial \alpha_{LR}{}^2}\right)_{n,T,V,X,\Gamma} \left(\frac{\partial^2 \alpha_{LR}{}^2}{\partial n_i \partial T}\right)_{V} \tag{C.50}$$

$$\left(\frac{\partial^2 F_{LR}}{\partial n_i \partial V}\right)_{T} = \left(\frac{\partial^2 F_{LR}}{\partial \alpha^2 \partial X}\right)_{n,T,V,\Gamma} \left(\frac{\partial X}{\partial n_i}\right)_{T} \left(\frac{\partial \alpha^2}{\partial V}\right)_{T} + \left(\frac{\partial F_{LR}}{\partial \alpha_{LR}{}^2}\right)_{n,T,V,X,\Gamma} \left(\frac{\partial^2 \alpha^2}{\partial n_i \partial V}\right)_{T} \tag{C.51}$$

The individual partial derivative terms of equations (C.43) to (C.51) are calculated from

$$\left(\frac{\partial F_{LR}}{\partial V}\right)_{n,T,\alpha_{LR},X,\Gamma} = \frac{\Gamma^3}{3\pi N} \tag{C.52}$$

$$\left(\frac{\partial^2 F_{LR}}{\partial \alpha^2 \partial X}\right)_{n,T,V,\Gamma} = -\frac{1}{4\pi} \tag{C.53}$$

$$\left(\frac{\partial \alpha_{LR}{}^2}{\partial T}\right)_{n,V} = -\left(\frac{e^2 N}{\varepsilon_0 D R T^2}\right) - \left(\frac{e^2 N}{\varepsilon_0 D^2 R T}\right)\left(\frac{\partial D}{\partial T}\right) \tag{C.54}$$

$$\left(\frac{\partial \alpha_{LR}^2}{\partial T \partial V}\right)_n = \left(\frac{e^2 N}{\varepsilon_0 D^2 R T^2}\right)\left(\frac{\partial D}{\partial V}\right)_n + \left(\frac{2e^2 N}{\varepsilon_0 D^3 R T}\right)\left(\frac{\partial D}{\partial V}\right)_n\left(\frac{\partial D}{\partial T}\right)_n - \left(\frac{e^2 N}{\varepsilon_0 D^2 R T}\right)\left(\frac{\partial D}{\partial T \partial V}\right)_n \quad (C.55)$$

$$\left(\frac{\partial^2 \alpha_{LR}^2}{\partial^2 V}\right)_n = \left(\frac{2e^2 N}{\varepsilon_0 D^3 R T}\right)\left(\frac{\partial D}{\partial V}\right)_n^2 - \left(\frac{e^2 N}{\varepsilon_0 D^2 R T}\right)\left(\frac{\partial^2 D}{\partial^2 V}\right)_n \quad (C.56)$$

$$\left(\frac{\partial^2 \alpha_{LR}^2}{\partial T^2}\right)_{n,V} = \left(\frac{2e^2 N}{\varepsilon_0 D R T^3}\right) + \left(\frac{e^2 N}{\varepsilon_0 D^2 R T^2}\right)\left(\frac{\partial D}{\partial T}\right)_{n,V} - \left(\frac{e^2 N}{\varepsilon_0 D^2 R T}\right)\left(\frac{\partial^2 D}{\partial T^2}\right)_{n,V} +$$
$$\left(\frac{e^2 N}{\varepsilon_0 D^2 R T^2}\right)\left(\frac{\partial D}{\partial T}\right)_{n,V} + \left(\frac{2e^2 N}{\varepsilon_0 D^3 R T}\right)\left(\frac{\partial D}{\partial T}\right)_{n,V}^2 \quad (C.57)$$

$$\left(\frac{\partial \alpha_{LR}^2}{\partial V}\right)_{T,n} = -\frac{e^2 N}{\varepsilon_0 D^2 R T}\left(\frac{\partial D}{\partial V}\right)_{T,n} \quad (C.58)$$

$$\left(\frac{\partial \alpha_{LR}^2}{\partial n_i}\right)_{T,V} = -\frac{1}{D}\alpha_{LR}^2\left(\frac{\partial D}{\partial n_i}\right)_{T,V} \quad (C.59)$$

$$\left(\frac{\partial \alpha_{LR}^2}{\partial n_i \partial T}\right)_V = -\frac{1}{D}\alpha_{LR}^2\left(\frac{\partial D}{\partial n_i \partial T}\right)_V + \frac{2}{D^2}\alpha_{LR}^2\left(\frac{\partial D}{\partial n_i}\right)_V\left(\frac{\partial D}{\partial T}\right)_V + \frac{1}{T \cdot D}\alpha_{LR}^2\left(\frac{\partial D}{\partial n_i}\right)_V \quad (C.60)$$

$$\left(\frac{\partial \alpha_{LR}^2}{\partial n_i \partial V}\right)_T = -\frac{1}{D}\alpha_{LR}^2\left(\frac{\partial D}{\partial n_i \partial V}\right)_T + \frac{2}{D^2}\alpha_{LR}^2\left(\frac{\partial D}{\partial n_i}\right)_T\left(\frac{\partial D}{\partial V}\right)_T \quad (C.61)$$

$$\left(\frac{\partial \alpha_{LR}^2}{\partial n_i \partial n_j}\right)_{T,V} = -\frac{1}{D}\alpha_{LR}^2\left(\frac{\partial D}{\partial n_i \partial n_j}\right)_{T,V} + \frac{2}{D^2}\alpha_{LR}^2\left(\frac{\partial D}{\partial n_i}\right)_{T,V}\left(\frac{\partial D}{\partial n_j}\right)_{T,V} \quad (C.62)$$

C.4.2 Derivatives of the Dielectric Constant

The dielectric constant can be written as (equation (C.8))

$$Y = (D_s - 1)$$
$$X = \frac{1 - \varepsilon_3}{1 + \varepsilon_3/2}$$
$$D = 1 + Y \cdot X$$
$$(C.63)$$

The general first order derivative of the dielectric constant is

$$\frac{\partial D}{\partial a} = \frac{\partial D}{\partial X}\bigg|_Y \cdot \frac{\partial X}{\partial a} + \frac{\partial D}{\partial Y}\bigg|_X \cdot \frac{\partial Y}{\partial a}$$

We have

$$\left.\frac{\partial D}{\partial Y}\right|_X = \frac{\partial \varepsilon}{\partial n_i} \frac{3/2}{\left(\varepsilon/2 + 1\right)^2}$$

$$\left.\frac{\partial D}{\partial X}\right|_Y = D_s$$

we get

$$\left(\frac{\partial D}{\partial n_i}\right)_{T,V} = \left.\frac{\partial D}{\partial X}\right|_Y \cdot \left(\frac{\partial X}{\partial n_i}\right)_{T,V} + \left.\frac{\partial D}{\partial Y}\right|_X \cdot \left(\frac{\partial Y}{\partial n_i}\right)_{T,V} \tag{C.64}$$

and

$$\left(\frac{\partial D}{\partial T}\right)_{n,V} = \left.\frac{\partial D}{\partial X}\right|_Y \cdot \left(\frac{\partial X}{\partial T}\right)_{n,V} + \left.\frac{\partial D}{\partial Y}\right|_X \cdot \left(\frac{\partial Y}{\partial T}\right)_{n,V}$$

$$\left(\frac{\partial D}{\partial V}\right)_{n,T} = \left.\frac{\partial D}{\partial X}\right|_Y \cdot \left(\frac{\partial X}{\partial V}\right)_{n,T} + \left.\frac{\partial D}{\partial Y}\right|_X \cdot \left(\frac{\partial Y}{\partial V}\right)_{n,T} \tag{C.65}$$

The derivative of the shielding parameter with respect to volume is set to zero. The partial derivatives of X and Y are calculated from equation (C.63).

C.5 Derivatives of the Born Term

The Born term is given as

$$F_{BORN} = \frac{Ne^2}{4\pi\varepsilon_0 RT}\left(\frac{1}{D_s} - 1\right)\sum_i \frac{n_i Z_i^2}{\sigma_i^*} = \frac{Ne^2}{4\pi\varepsilon_0 RT}\left(\frac{1}{D_s} - 1\right)X_{Born} \tag{C.66}$$

where X is

$$X_{Born} = \sum_i \frac{n_i Z_i^2}{\sigma_i^*} \tag{C.67}$$

This gives us the total differential

$$dF_{BORN} = \left(\frac{\partial F_{BORN}}{\partial n}\right)_{T,V,D_s,X}\partial n + \left(\frac{\partial F_{BORN}}{\partial V}\right)_{T,n,D_s,X}\partial V + \left(\frac{\partial F_{BORN}}{\partial T}\right)_{V,n,D_s,X}\partial T$$
$$+ \left(\frac{\partial F_{BORN}}{\partial D_s}\right)_{V,n,T,X}\partial D_s + \left(\frac{\partial F_{BORN}}{\partial X_{Born}}\right)_{V,n,T,D_s}\partial X_{Born} \tag{C.68}$$

and the second order differential

$$d^2F_{Born} = \left(F_{nn}dn + F_{nT}dT + F_{nV}dV + F_{nD}dD + F_{nX}dX \right)dn + F_n d^2 n$$
$$\left(F_{Tn}dn + F_{TT}dT + F_{TV}dV + F_{TD}dD + F_{TX}dX \right)dT + F_T d^2 T$$
$$\left(F_{Vn}dn + F_{VT}dT + F_{VV}dV + F_{VD}dD + F_{VX}dX \right)dV + F_V d^2 V \qquad \text{(C.69)}$$
$$\left(F_{Dn}dn + F_{DT}dT + F_{DV}dV + F_{DD}dD + F_{DX}dX \right)dD + F_D d^2 D$$
$$\left(F_{Xn}dn + F_{XT}dT + F_{XV}dV + F_{XD}dD + F_{XX}dX \right)dX + F_X d^2 X$$

Again, due to its importance in equilibrium calculations, we give the detailed derivations of the $\left(\dfrac{\partial F_{LR}}{\partial n_i} \right)_{T,V,n}$ term,

$$\left(\frac{dF_{BORN}}{\partial n_i} \right)_{T,V,n} = \left(\frac{\partial F_{BORN}}{\partial X_{Born}} \right)_{V,n,T,D_s} \left(\frac{\partial X}{\partial n_i} \right)_{T,V,n} + \left(\frac{\partial F_{BORN}}{\partial D_s} \right)_{V,n,T,X} \left(\frac{\partial D_s}{\partial n_i} \right)_{T,V,n} \qquad \text{(C.70)}$$

we have,

$$\left(\frac{\partial F_{BORN}}{\partial X_{Born}} \right)_{V,n,T,D_s} = \frac{Ne^2}{4\pi\varepsilon_0 RT}\left(\frac{1}{D_s} - 1 \right)$$

$$\left(\frac{\partial X_{Born}}{\partial n_i} \right)_{T,V,n} = \frac{Z_i^2}{\sigma_i^*}$$

For the partial derivative with respect to the dielectric constant of the solvent we get

$$\left(\frac{\partial F_{BORN}}{\partial D_s} \right)_{V,n,T,X} = -\frac{Ne^2}{4\pi\varepsilon_0 RTD_s^2} \cdot X_{Born}$$

$$\left(\frac{\partial D_s}{\partial n_i} \right)_{T,V,n} = \frac{1}{\sum\limits_j n_j}\left(\frac{\partial D_s}{\partial n_i} - D_s \right)$$

which gives us the final expression,

$$\left(\frac{dF_{BORN}}{\partial n_i} \right)_{T,V,n} = \frac{Ne^2}{4\pi\varepsilon_0 RT}\left(\frac{1}{D_s} - 1 \right)\frac{Z_i^2}{\sigma_i^*} - \frac{Ne^2}{4\pi\varepsilon_0 RTD_s^2}X\frac{1}{\sum\limits_j n_j}\left(\frac{\partial D_s}{\partial n_i} - D_s \right) \qquad \text{(C.71)}$$

C.5.1 More Derivatives of Born term
The rest of the derivatives of the Born term are calculated from

$$\left(\frac{\partial F_{Born}}{\partial V}\right)_{T,n} = \left(\frac{\partial^2 F_{Born}}{\partial V^2}\right)_{T,n} = \left(\frac{\partial^3 F_{Born}}{\partial V^3}\right)_{T,n} = 0 \tag{C.72}$$

$$\left(\frac{\partial F_{Born}}{\partial T}\right)_{V,n} = \left(\frac{\partial F_{Born}}{\partial T}\right)_{V,n,D,X} + \left(\frac{\partial F_{BORN}}{\partial D_s}\right)_{V,n,T,X}\left(\frac{\partial D_s}{\partial T}\right)_{V,n} \tag{C.73}$$

$$\left(\frac{\partial^2 F_{Born}}{\partial T \partial T}\right)_n = \left(\frac{\partial^2 F_{Born}}{\partial T \partial T}\right)_{V,n,X,D_s} + \left(\frac{\partial^2 F_{Born}}{\partial D_s \partial T}\right)_{V,n,T,X}\left(\frac{\partial D_s}{\partial T}\right)_n \tag{C.74}$$

$$\left(\frac{\partial^2 F_{Born}}{\partial T \partial V}\right)_n = 0 \tag{C.75}$$

$$\left(\frac{\partial^2 F_{Born}}{\partial n_i \partial T}\right)_V = \left(\frac{\partial^2 F_{Born}}{\partial T \partial D}\right)_{V,n,X}\left(\frac{\partial D_s}{\partial n_i}\right)_V + \left(\frac{\partial^2 F_{Born}}{\partial T \partial X}\right)_{V,n,D_s}\left(\frac{\partial X}{\partial n_i}\right)_V + $$
$$\left(\frac{\partial^2 F_{Born}}{\partial^2 D_s}\right)_{V,n,T,X}\left(\frac{\partial D_s}{\partial n_i}\right)_V\left(\frac{\partial D_s}{\partial T}\right)_V + \left(\frac{\partial^2 F_{Born}}{\partial D_2 \partial X}\right)_{V,n,T,D_s}\left(\frac{\partial X}{\partial n_i}\right)_V\left(\frac{\partial D_s}{\partial T}\right)_V + \tag{C.76}$$
$$\left(\frac{\partial F}{\partial D_s}\right)_V\left(\frac{\partial^2 D_s}{\partial n_i^2}\right)_V$$

$$\left(\frac{\partial^2 F_{Born}}{\partial n_i \partial V}\right)_T = 0 \tag{C.77}$$

$$\left(\frac{\partial^2 F_{Born}}{\partial n_i \partial n_j}\right)_{T,V} = \left(\frac{\partial^2 F}{\partial^2 D_s}\right)_{V,n,X}\left(\frac{\partial D_s}{\partial n_i}\right)\left(\frac{\partial D_s}{\partial n_j}\right) + \left(\frac{\partial^2 F}{\partial D_s \partial X}\right)_{V,n}\left(\frac{\partial X}{\partial n_i}\right)\left(\frac{\partial D_s}{\partial n_j}\right) + \left(\frac{\partial F}{\partial D_s}\right)_{V,n,X}\left(\frac{\partial^2 D_s}{\partial n_i \partial n_j}\right)$$
$$+ \left(\frac{\partial^2 F_{Born}}{\partial X \partial D_s}\right)_{V,n}\left(\frac{\partial D_s}{\partial n_i}\right)\left(\frac{\partial X}{\partial n_j}\right) + \left(\frac{\partial^2 F_{Born}}{\partial X \partial X}\right)_{V,n,D}\left(\frac{\partial X}{\partial n_i}\right)\left(\frac{\partial X}{\partial n_j}\right) + \left(\frac{\partial F_{Born}}{\partial X}\right)_{V,n,D}\left(\frac{\partial^2 X}{\partial n_i \partial n_j}\right) \tag{C.78}$$

The other derivatives are given as

$$\left(\frac{\partial F_{Born}}{\partial T}\right)_{V,n,D,X} = -\frac{Ne^2}{4\pi\varepsilon_0 RT^2}\left(\frac{1}{D_s}-1\right)X \tag{C.79}$$

$$\left(\frac{\partial F_{Born}}{\partial D}\right)_{V,n,T,X} = -\frac{Ne^2}{4\pi\varepsilon_0 RT}\frac{1}{D_s^2}X \tag{C.80}$$

$$\left(\frac{\partial F_{Born}}{\partial X}\right)_{V,n,T,D} = \frac{Ne^2}{4\pi\varepsilon_0 RT}\left(\frac{1}{D_s}-1\right) \tag{C.81}$$

$$\left(\frac{\partial^2 F_{Born}}{\partial T^2}\right)_{V,n,D,X} = \frac{Ne^2}{2\pi\varepsilon_0 RT^3}\left(\frac{1}{D_s}-1\right)X \tag{C.82}$$

$$\left(\frac{\partial^2 F_{Born}}{\partial D^2}\right)_{V,n,T,X} = \frac{Ne^2}{2\pi\varepsilon_0 RT}\frac{1}{D_s^3}X \tag{C.83}$$

$$\left(\frac{\partial^2 F_{Born}}{\partial D\partial T}\right)_{V,n,X} = \frac{Ne^2}{4\pi\varepsilon_0 RT^2}\frac{1}{D_s^2}X \tag{C.84}$$

$$\left(\frac{\partial^2 F_{Born}}{\partial T\partial X}\right)_{V,n,D} = -\frac{Ne^2}{4\pi\varepsilon_0 RT^2}\left(\frac{1}{D_s}-1\right) \tag{C.85}$$

$$\left(\frac{\partial^2 F_{Born}}{\partial D\partial X}\right)_{V,n,T} = -\frac{Ne^2}{4\pi\varepsilon_0 RT}\frac{1}{D_s^2} \tag{C.86}$$

$$\left(\frac{\partial^2 F_{Born}}{\partial X^2}\right)_{V,n,T,D} = 0 \tag{C.87}$$

The electrolyte equation of state derived in this appendix was checked for thermodynamic consistency (all thermodynamic models used was checked), and the calculated fugacity and its derivatives were checked with a procedure proposed by Michelsen and Mollerup (2000). The analytical derivatives were compared to numerically calculated values. All tests were passed with success, and we concluded that the models were implemented correct.

Appendix D   Physical Property Models

If errors are introduced in fundamental thermodynamic or physical property models, the parameters fitted in higher level models such as fluid mechanical models will be inaccurate. Therefore, it is important to use accurate thermodynamic and physical property models when we want to model fluid mechanic and mass transfer operations. The derivation of the thermodynamic models for MDEA, water and CO_2 systems was done in chapter 3 and 8. The multiphase fluid mechanic model was explained in chapter 5. In this appendix we will regress parameters to the models used to calculate physical properties of MDEA-water-CO_2 solutions.

The models used in NeqSim by default (standard physical property models from Reid et.al, 1988) are not able to correlate or predict physical properties of amine solutions with a high precision. Such amine systems are highly non-ideal – and more specialized and often pure empirical models have to be applied. The models used to calculate viscosity and diffusivity in the liquid phase will be described in section D.1 to D.4. The physical properties of the gas phase can be calculated with an acceptable precision by the standard methods presented in Reid et.al (1988). These models will be presented in section D.5.

The models used to calculate physical properties are summarized in table D.1.

Table D.1 Models used to calculate physical properties of natural gas – aqueous MDEA systems

Property	Correlation/Data
Liquid Viscosity	Empirical model of Glasscock (1990)
Liquid and Gas Density	Equation of State with volume correction
Effective Diffusivity of CO_2 in aqueous MDEA solution	N_2O-CO_2 analogy
Effective Diffusivity of MDEA in liquid	Snijder et.al. (1993)
Maxwell Stefan Diffusivities in liquid	Assumed to be equal to effective diffusivities
Liquid Conductivity	Standard method from Reid et.al (1988)
Gas Viscosity	Standard method from Reid et.al (1988)
Maxwell Stefan Diffusivities in Gas	Method of Fuller et.al. (1966, 1969)
Gas Conductivity	Standard method from Reid et.al (1988)

The models used to calculate gas phase physical properties will be described only briefly in this appendix.

D.1   Modelling of the Viscosity of CO_2, Water and MDEA Solutions

Viscosities of pure component liquids can normally be calculated by simple equations, such as $\ln \mu = A + B/T$. For liquid mixtures we normally apply some kind of mixing rules to calculate the viscosity of the solution. An alternative (but less general) method is to let the parameters A and B be dependent on the liquid composition. Such a method is used for calculating the viscosity of aqueous amine solutions in this work.

D.1.1 Pure Component Liquid Viscosities of MDEA and Water

The viscosity of the unloaded solution was calculated by the correlation developed by Glasscock et.al. (1990) based upon the data of Al-Ghawas et.al. (1989), Critchfeld (1988) and Sada et.al. (1978). Using these experimental data for viscosity of different amine solutions; Glasscock obtained the following correlation for viscosity of MDEA solution;

$$\ln \mu = A + \frac{B}{T} + CT \tag{D.1}$$

where

$$
\begin{aligned}
A &= -19.52 - 23.40 wf_{MDEA} - 31.24 wf_{MDEA}{}^2 + 36.17 wf_{MDEA}{}^3 \\
B &= 3912 + 4894 wf_{MDEA} + 8477 wf_{MDEA}{}^2 - 8358 mf_{MDEA}{}^3 \\
C &= 0.02112 + 0.03339 wf_{MDEA} + 0.02780 wf_{MDEA}{}^2 - 0.04202 wf_{MDEA}{}^3
\end{aligned}
\tag{D.2}
$$

where wf_{MDEA} is the weight fraction of total MDEA in the solution, T is the temperature in Kelvin and μ is the viscosity in cP. The correlation is considered to be valid in the range of 20 to 50°C and for MDEA concentration up to 50 wt%. This range is large enough for the systems considered in this work.

A comparison between the viscosity model and experimental data is given in figure D-1. We see that equation (D.1) gives relative accurate results when compared to the experimental data of Teng et.al. (1994).
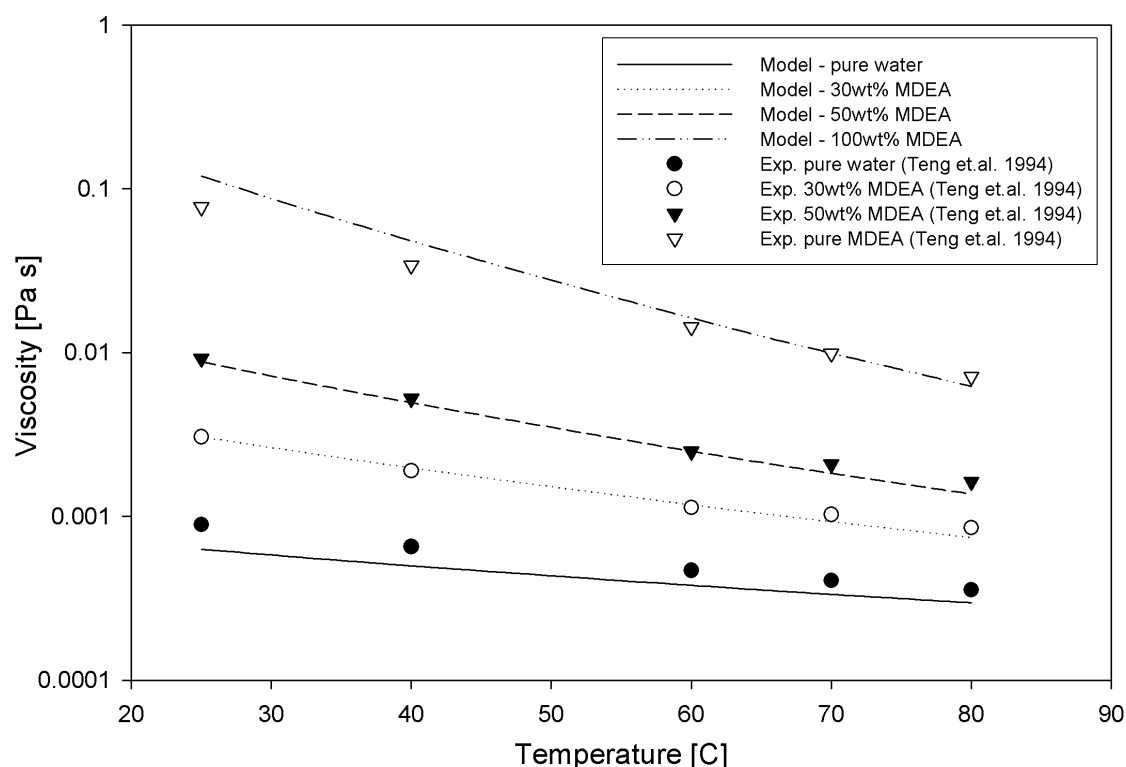
Figure D.1 Calculated and experimental viscosity of aqueous MDEA solutions.

D.1.2 Viscosities of Solutions of MDEA, Water and CO_2

The viscosity of MDEA-water solutions with dissolved/reacted CO_2 was in this work assumed to be the same as the unloaded solution of MDEA-water solution (equation (D.1)). This is a crude approximation – but since we have few experimental points – we have to use this simplification.

Toman (1989) determined the effect of CO_2 loading in the viscosity of 50 wt% MDEA at 298K (loading range 0.001 to 0.76). Glasscock (1990) fit them by a second order equation $r_{MDEA} = 1.0 + 0.8031 \cdot loading + 0.35786 \cdot loading^2$. Where r_{MDEA} is the relative viscosity compared to an unloaded solution. More data and at higher temperatures should be measured to generate a general correlation for the viscosity of aqueous MDEA solution with reacted CO_2.

D.2   Modelling of the Density of CO_2 – Water - MDEA Solutions

The density of the solution is calculated directly from the equation of state (ScRK-EOS or CPA-EOS described in chapter 3). For the ScRK-EOS we have to use a volume shift parameter in the equation of state to get a correct representation of the pure component densities in polar systems. For the CPA-EOS we generally obtain accurate density predictions for all components without volume corrections (see chapter 3).

D.2.1 Densities of Pure Components

The densities of pure components were calculated by introducing a volume shift parameter in the ScRK equation of state. The Penelux-volum correction method was used (see equation (3.32))

$$\bar{V} = \bar{V}_{ScRK} + c \qquad (D.3)$$

and the constant c was fitted to available experimental data for the pure component density. The results from this regression are given in table D-2.

Table D-2 Penloux parameters for the ScRK-EOS fitted to atmospheric density data for MDEA and water

Component	Penloux parameter (ScRK-EOS)	AAD [%]	Exp. data
Water	0.2	3.1	Perry (1998)
MDEA	0.22	4.4	Noll et.al. (1998)

A comparison between calculated densities using the ScRK-EOS model and the experimental data of Noll et.al. (1998) for MDEA is presented in figure D-2.

Density of MDEA
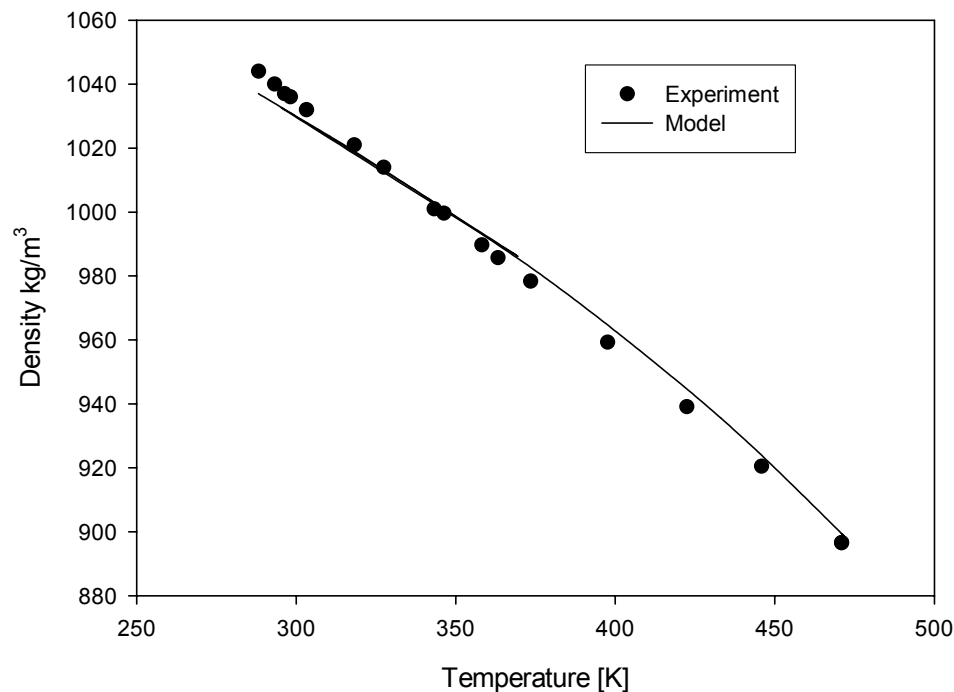
Figure D-2 Experimental and calculated density of MDEA using the ScRK-EOS with volume correction
Script: penloux.py, p. 318

D.2.2 Densities of Mixtures

The densities of mixtures are calculated directly from the equation of state. We use a linear mixing rule for the volume correction parameter ($c = \sum_i x_i c_i$) so that no new binary interaction parameters are needed. The effect of ions on the liquid density is handled by the electrolyte terms of the electrolyte equation of state. A comparison between experimental densities of an aqueous NaCl solution and predictions with the electrolyte equation of state was given in chapter 3 (Figure 3-18).

D.3   Effective Diffusivity of CO_2 in Aqueous MDEA Solutions

The diffusivity of CO_2 in MDEA solutions was estimated using the N_2O-analogy, data and correlations for the diffusivity of N_2O in the chemical solvent. According to the N_2O-CO_2 analogy, the diffusion coefficients of N_2O and CO_2 in the aqueous amine solutions and in pure water (represented by the superscript °) are related by the following expression:

$$\frac{D_{CO_2}}{D_{CO_2}^{\circ}} = \frac{D_{N_2O}}{D_{N_2O}^{\circ}} \tag{D.4}$$

Versteeg et. al. (1988) measured the diffusion coefficient of N_2O in aqueous solutions up to around 35 wt% MDEA and from 20 to 60°C. Al-Ghawas et.al. (1989) report measurements of diffusion coefficients of N_2O in aqueous solutions from 10 to 50 wt% MDEA and from 15 to 50°C.

The diffusivity of CO_2 and N_2O in water can be represented by the equations

$$D_{CO_2}^{\circ} \left(cm^2 / sek \right) = 0.02397 \exp\left(-\frac{2122.2}{T(K)} \right) \quad Versteeg\ et.al.(1988) \tag{D.5}$$

$$D_{N_2O}^{\circ} \left(cm^2 / sek \right) = 0.0404 \exp\left(-\frac{2288.4}{T(K)} \right) \quad Versteeg\ et.al.(1988) \tag{D.6}$$

A comparison between experimental data and these equations is given in figures D-3 and D-4.

The diffusivity of N_2O in MDEA-water solutions can be calculated from a modified Stokes Einstein relation

$$D_{N_2O} \left(cm^2 / sec \right) = 5.533 \cdot 10^{-4} \frac{T}{\mu_L^{0.545}} \tag{D.7}$$

where the viscosity if the liquid μ_L is in cP and the temperature in K. The calculated diffusivities compared to experimental data are given in figures D-3 and D-4.

From this development it can be seen that knowing the viscosity of the solution, equation (D.7) can be used to predict the diffusion coefficient of N_2O in the chemical solvent, then the diffusion coefficients of N_2O and CO_2 in water can be estimated from the correlations presented above and the diffusion coefficient of CO_2 in the MDEA-solution can be calculated through the N_2O-CO_2 analogy (equation (D.4)).
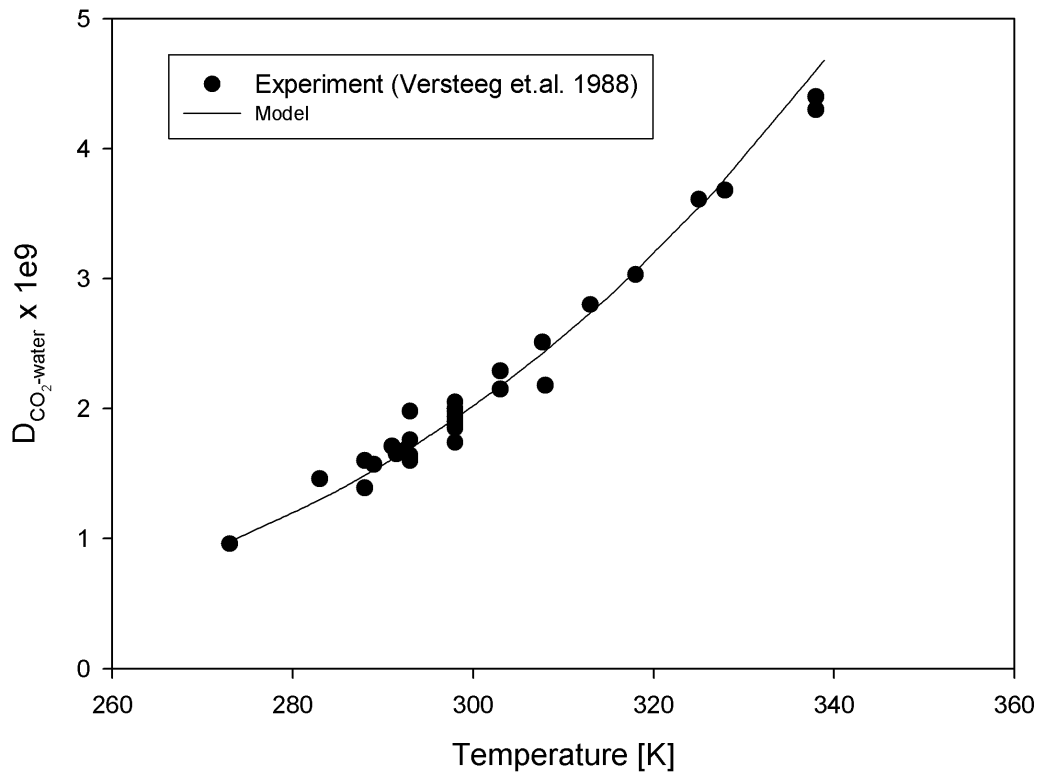
Figure D-3 Calculated (equation (D.5)) and experimental diffusion coefficients of CO_2 in water
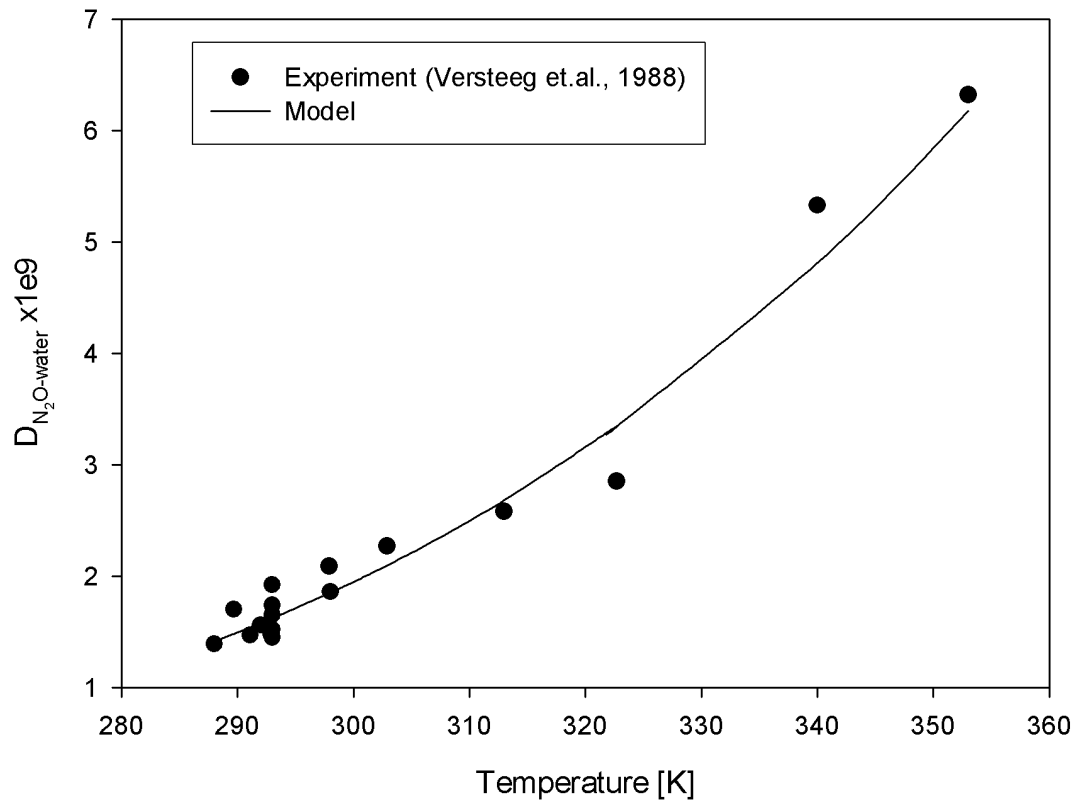

Figure D-4 Calculated (equation (D.6)) and experimental diffusion coefficients of N_2O in water

D.3.1   Modelling of the Diffusivity of MDEA in Solution

Snijder and co-workers (1993) measured the diffusion coefficient of MEA, DEA, MDEA and DIPA in the corresponding aqueous alkanolamine solutions using the Taylor dispersion method. This technique is based on the fact that due to a combination of axial laminar convection and radial diffusion, axial dispersion takes place when a solute is introduced in a solvent flowing slowly through a long capillary tube. By solving the mass balance for such a system, the diffusion coefficient can be related to the measured axial dispersion coefficient.

The correlation for the diffusion coefficient of MDEA in water obtained by Snijder and coworkers was

$$D_{MDEA}\left(cm^2/\sec\right)=0.0207\exp\left(-\frac{2360.7}{T(K)}-24.727\cdot10^{-5}C_{MDEA}\right) \qquad (D.8)$$

where C_{MDEA} is the concentration of MDEA in the solution in moles/m^3. This correlation was developed based on diffusivity data for MDEA solutions up to 48 wt% MDEA and for a range of temperatures from 25 to 75°C.

D.3.2   Calculation of Maxwell Stefan Diffusion Coefficients

Maxwell Stefan diffusion coefficients were introduced in chapter 3 and are used in the mathematical model developed in this work. It is not available any general and accurate model for prediction of Maxwell-Stefan diffusion coefficients in liquids. The Maxwell Stefan binary diffusion coefficients must obey the general rule

$$\DJ_{12}=\DJ_{21} \qquad (D.9)$$

In this work the following assumptions were made:
- All binary Maxwell-Stefan diffusion coefficients involving MDEA were assumed to be equal to the effective diffusion coefficient D_{MDEA} calculated from equation (D.8)
- All other binary diffusion coefficients were estimated equal to the effective diffusion coefficient of CO_2 in the solution, D_{CO_2} calculated from the N_2O-CO_2 analogy (equation (D.4)).

This means that $\DJ_{MDEA-j}=\DJ_{j-MDEA}=D_{MDEA}\ \ j=1..n$ and $\DJ_{CO_2-i}=\DJ_{i-CO_2}=D_{CO_2}\ i\neq MDEA$. The effect of this assumption will be that the coupling effects introduced by differences in the numerical value of the Maxwell Stefan diffusion coefficients will be uncertain and eventually not corrected for.

D.4   Modelling of the Liquid Conductivity of CO$_2$, Water and MDEA Solutions

The conductivity of MDEA-water solutions was calculated using a standard method from Reid et.al (1988). It was not considered important in this work – so no attempt was done to test the model.

D.5   Physical Properties of the Gas Phase

The physical properties (conductivity, viscosity and Maxwell-Stefan diffusivities) of the gas phase are calculated by standard methods taken from Reid et.al (1988). In this subsection, the methods used will be described very briefly. In the experimental work described in this thesis the gas phase resistance was negligible – and the gas phase diffusivities were therefore unimportant. The gas diffusivities can however be important in many other non-equilibrium situations and are therefore important to estimate as accurate as possible.

D.5.1 Gas Viscosity

Method of Chung et al. [p. 426 in Reid et.al (1988)]
Chung et.al. modified equation for dense gases is on the form

$$\eta = \eta^* \frac{36.344 \left(M T_c \right)^{1/2}}{V_c^{2/3}} \tag{D.10}$$

where
η=viscosity
M=molecular weight
T_c=critical temperature
V_c=critical volume

The parameter η^* was calculated by a method described by Reid et.al (1988).

D.5.2 Maxwell-Stefan Diffusivity for Gas

The Maxwell-Stefan diffusivities in the gas phase were calculated by a method developed by Fuller et.al.(1966, 1969);

$$D_{12} = C T^{1.75} \frac{\sqrt{\left(M_1 + M_2 \right) / M_1 M_2}}{P \left\{ \sqrt[3]{V_1} + \sqrt[3]{V_2} \right\}^2} \tag{D.11}$$

where T is in Kelvin, P is in pascals, M in grams per mole and C=0.013. V is the molecular diffusion volumes and numerical values are given in Reid et.al. (1988). The diffusion coefficients calculated from equation (D.11) have dimension m^2/sec.

D.5.3 Gas Conductivity

The gas conductivity was estimated by a standard method described in Reid et.al (1988).

Appendix E Chemistry and Reaction Mechanisms and Reaction Rates of CO$_2$ in Alkanolamine Systems

In aqueous solution CO$_2$ reacts with hydroxide and water to form bicarbonate and carbonic acid, respectively:

$$CO_2 + OH^- \underset{k_1}{\overset{k_2}{\rightleftharpoons}} HCO_3^- \tag{E.1}$$

$$CO_2 + H_2O \underset{k_1}{\overset{k_2}{\rightleftharpoons}} H_2CO_3 \tag{E.2}$$

The water reaction is usually negligible compared to the hydroxide reaction for alkaline solutions. However, it has been shown conclusively to be catalysed by "anions of weak acids or by molecules having a high affinity for protons" (Sherwood et.al., 1975).
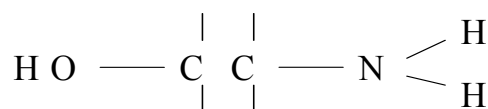
Monoethanolamine (MEA)
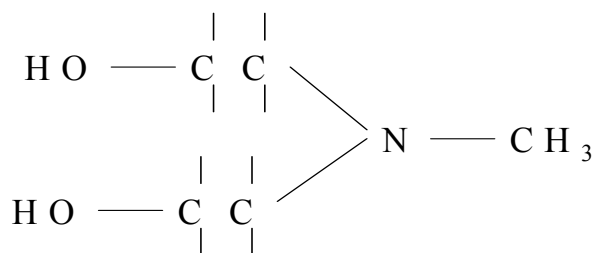
Methyldiethanolamine (MDEA)

Figure E-1 Molecular structure of Monoethanolamine and Methydiethanolamine

E.1 CO$_2$ Reaction Mechanism and Reaction Rate with MDEA

Some of the early research into ternary amines was concerned with whether or not the enhanced CO$_2$ absorption rate could be explained by the hydroxide reaction. It has been demonstrated by numerous authors that this reaction alone does not account for the enhanced absorption rates. It has been proposed, however, that the amine serves to catalyse the CO$_2$ hydrolysis reaction rate. This is not the only possibility, however. Barth et.al. (1981) provide a thorough discussion of the possible mechanism for the reaction of CO$_2$ with alkanolamines.

The ternary amine Methyldiethanolamine (MDEA) is in widespread use due the fact it has relatively low heat of reaction with CO$_2$ as compared with MEA, and it can be used for selective removal since its reaction rate with CO$_2$ is relatively low. The structural forms of MEA and MDEA are illustrated in Figure E-1. There is much discrepancy in the literature for the reaction rate of CO$_2$ with MDEA, most likely due to the fact that the reaction mechanism

is more complex than which most authors assume. The generally accepted reaction of CO_2 with MDEA is a base catalysis of the direct reaction of CO_2 with water ending with formation of bicarbonate

$$CO_2 + MDEA + H_2O \underset{k_1}{\overset{k_2}{\rightleftarrows}} MDEAH^+ + HCO_3^- \tag{E.3}$$

In order to explain both absorption and desorption, reversibility of the reaction should be considered. The approximate rate expression is

$$Rate = \left([CO_2] - [CO_2]_{eq} \right) [MDEA]_{int} \, k_{MDEA} \tag{E.4}$$

The variable $[CO_2]_{eq}$ refers to the CO_2 concentration in chemical equilibrium with HCO_3^- and $[MDEA]_{int}$ is the interface concentration of MDEA. The effective second order rate constant k_{MDEA} was regressed from the absorption data of this work for 30 and 50 wt% MDEA solutions at 25 and 40°C.

The second order reaction rate constant is normally given using an Arrenihus type of equation

$$k_{MDEA} = k_{MDEA(T=298K)} \exp \left\{ -\frac{E_a}{R} \left(\frac{1}{T} - \frac{1}{298K} \right) \right\} \tag{E.5}$$

When experimental data from the literature are regressed to experimental mass transfer data the rate coefficient can be calculated. Some of the published experimental data for the second order rate constant in reaction (E.5) are given in the table below.
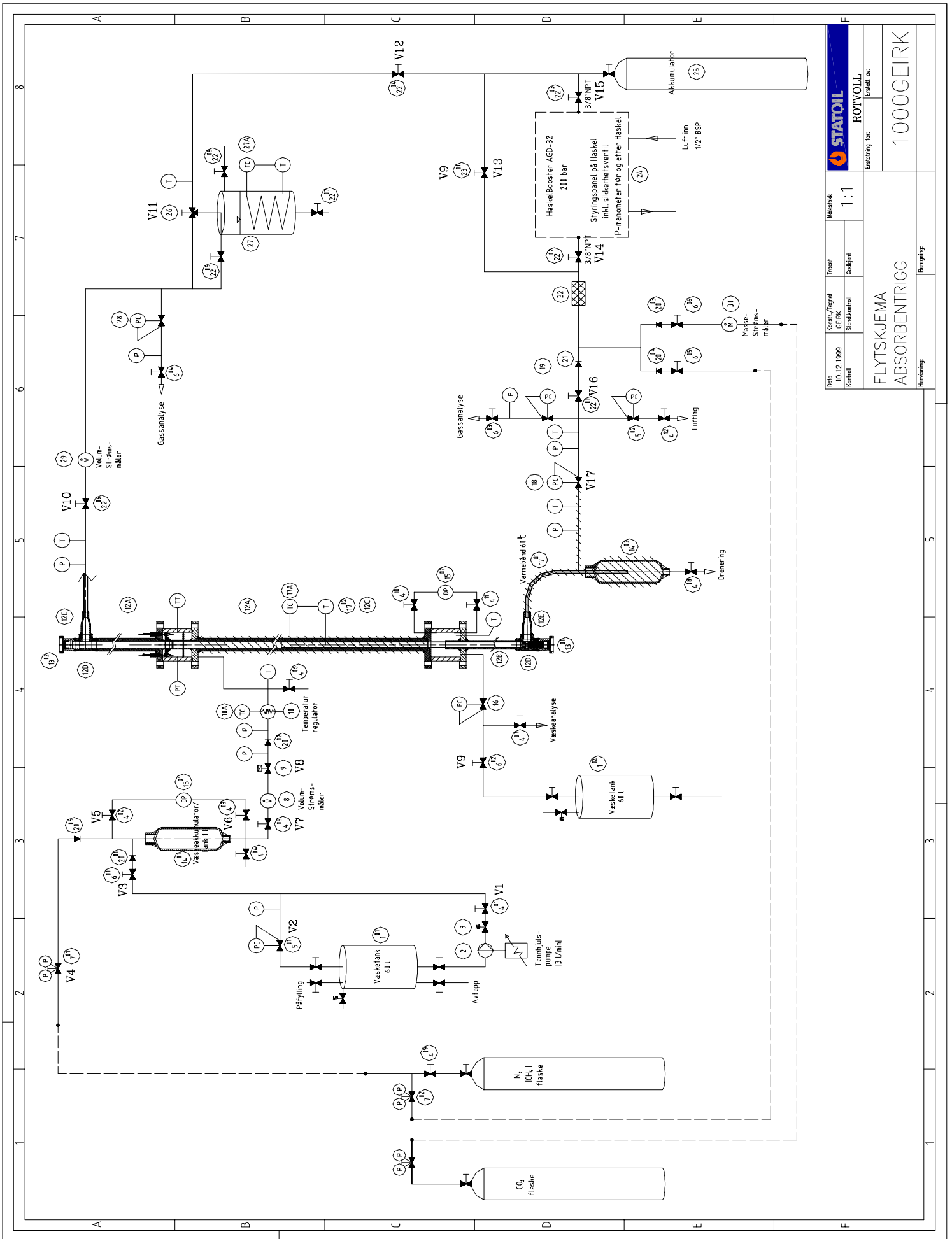
Table E-2 Reaction rate data for CO_2-MDEA solutions

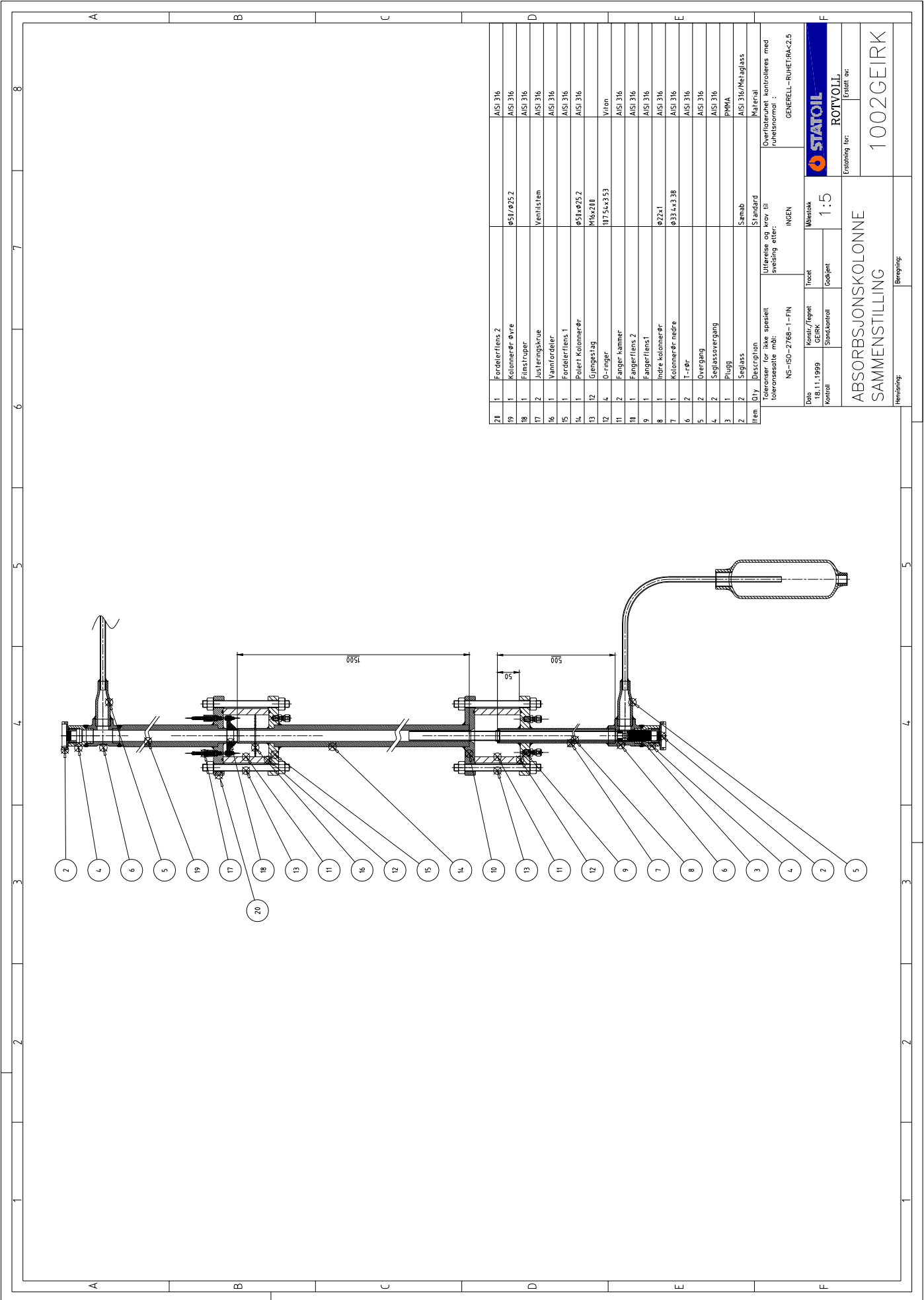| Reference	Temperature [K]	[MDEA] $\left[\dfrac{kmoles}{m^3} \right]$	P_{CO2} [atm]	$k_{MDEA,Tref}$ $\left[\dfrac{m^3}{kmol\,s} \right]$	T_{ref}	Activation energy E_a $\left[\dfrac{kcal}{gmole} \right]$	Method
Barth et.al. (1981)	293-313	293-313	0.003-0.03	2.85	298	-	stopped flow
Barth et.al. (1984)	293	293	0.003-0.03	3.2	298	-	stopped flow
Versteeg and van Swaaij (1988)	293-333	293-333	<1	4.4	298	10.1	stirred tank
Glasscock (1990)	298	1.7	0.1-1	3-10	298	6.5-10	stirred tank
Little et.al. (1990)	298	0.2-2.7	<1	5.2	298	11.5	stirred tank

Appendix F.   Experimental Equipment

Figure 1. Flow-diagram of High Pressure Wetted Wall Column
Figure 2. Detail sketch of wetted wall column

299

FLYTSKJEMA ABSORBENTRIGG

STATOIL
ROTVOLL

1000GEIRK

Akkumulator

HaskelBooster AGD-32
201 bar
Styringspanel på Haskel
inkl. sikkerhetsventil
P-manometer før og etter Haskel

Luft inn
1/2" BSP

3/8"NPT V15
3/8"NPT V14

V9 V13
V12
V11

Gassanalyse

Volum-
Strøms-
måler

V10

Masse-
Strøms-
måler

Gassanalyse

Lufting

Varmebånd 61t

V16
V17

Drenering

Temperatur
regulator

Volum-
Strøms-
måler

V8

Vaskeakkumulator/
tank 1 l

V5 V6 V7

V3

Vaskeanalyse

V9

Vasketank
6 l l

V2 V1

Vasketank
6 l l

Tannhjuls-
pumpe
[3 l/min]

Påfylling   Avtapp

V4

N₂
[CH₄]
flaske

CO₂
flaske

Dato 10.12.1999   Konstr./Tegnet GEIRK   Tracet   Målestokk 1:1
Kontroll   Standkontroll   Godkjent
Henvisning: Beregning: Erstatter for: Erstatt. av:

URN:NBN:no-3363

Item	Qty	Description		Material
20	1	Fordelerflens 2		AISI 316
19	1	Kolonnerør Øvre	Ø51/Ø25.2	AISI 316
18	1	Filmstruper		AISI 316
17	2	Justeringskrue		AISI 316
16	1	Vannfordeler	Ventilstem	AISI 316
15	1	Fordelerflens 1		AISI 316
14	1	Polert Kolonnerør	Ø51/Ø25.2	AISI 316
13	12	Gjengestag	M16x200	AISI 316
12	4	O-ringer		Viton
11	2	Fanger kammer	1075.4x353	AISI 316
10	1	Fangerflens 2		AISI 316
9	1	Fangerflens1		AISI 316
8	1	Indre kolonnerør	Ø22x1	AISI 316
7	1	Kolonnerør nedre	Ø33.4x3.38	AISI 316
6	2	T-rør		AISI 316
5	2	Overgang		AISI 316
4	2	Seglassovergang		AISI 316
3	1	Plugg		PMMA
2	2	Seglass		AISI 316/Metaglass
Item	Qty	Description	Standard	Material

Toleranser for ikke spesielt toleransesatte mål:
NS–ISO–2768–1–FIN

Overflateruhet kontrolleres med ruhetsnormal :
GENERELL–RUHET:RAK2.5

Utførelse og krav til sveising etter:
INGEN

Dato 18.11.1999	Konstr./Tegnet GEIRK	Trocet	Målestokk
Kontroll	Stand.kontroll	Godkjent	1:5

ABSORBSJONSKOLONNE
SAMMENSTILLING

Henvisning: Beregning:

STATOIL
ROTVOLL

Erstatning for: Erstatt av:

1002GEIRK

URN:NBN:no-3363

Appendix G. NeqSim – Scripts

The scripts presented in this appendix are downloadable from the NeqSim homepage (www.stud.ntnu.no/~solbraa/neqsim). By copying a script directly from the web and paste it into the NeqSim editor – the calculation can be redone fast and easily.

tray.py

```python
# Construction of a physical absorption process
# in a trayed column
# By Even Solbraa, 2002

temperature = 313.0  # Kelvin
pressure   =  30.0  # Bar

gasIn = thermo('srk',temperature,pressure)
addComponent(gasIn, 'methane', 95, 'Nlitre/min')
addComponent(gasIn,'CO2',50, 'Nlitre/min')
newdatabase(gasIn)
TPflash(gasIn)

liqIn = thermo('srk',temperature,pressure)
addComponent(liqIn, 'water', 200.2, 'kg/min')
newdatabase(liqIn)
TPflash(liqIn)

# Calciulating equilibrium-line
eqsyst = thermo('srk',temperature,pressure)
addComponent(eqsyst, 'methane', 200.0)
addComponent(eqsyst, 'CO2',0.0000001)
addComponent(eqsyst, 'water', 200.0)
newdatabase(eqsyst)
TPflash(eqsyst)

xeq = []
yeq = []
for i in range(60):
    xeq.append(molefrac(eqsyst,1)[2])
    yeq.append(molefrac(eqsyst,1)[1])
    addComponent(eqsyst,'CO2',1.0)
    addComponent(eqsyst,'methane',-1.0)
    TPflash(eqsyst)

# Calculation operational-line
Lrate = moles(liqIn)
Grate = moles(gasIn)
Yin = molefrac(gasIn,1)[0]
Xin = 0
```

```python
Yout = molefrac(gasIn,1)[0]/20.0
print 'yin ' , Yin
print 'yut ' , Yout

xop = xeq
yop = []
for i in range(len(xeq)):
    yop.append(Lrate/Grate*xeq[i] - Lrate/Grate*Xin)
    #print yop[i]

#Find the number of transfer steps

eqpoly = polyfit.polyfit(yeq,xeq,5)
oppoly = polyfit.polyfit(xeq,yop,5)
xstep = []
ystep = []
ystep.append(Yout)
xstep.append(Xin)
i = 0
while(ystep[i]<Yin):
    print i
    xstep.append(eqpoly.gety([ystep[i]])[0])
    ystep.append(oppoly.gety([xstep[i]])[0])
    i = i

graph = graph2D.graph2D("Absorption modelling")
graph.setxy(xeq,yeq,"equilibrium line")
graph.setxy(xeq,yop,"operation line")
graph.setxy(xstep,ystep,"step-line")
graph.setXaxisTitle("x-CO2  [-]")
graph.setYaxisTitle("y-CO2  [-]")
graph.show()
```

tray-amine.py

```python
tray-amine.py
# Construction of a amine absorption process
# in a trayed column
# By Even Solbraa, 2002

temperature = 313.0 # Kelvin
pressure =   20.0  # Bar

gasIn = thermo('srk',temperature,pressure)
addComponent(gasIn, 'methane', 100, 'Nlitre/min')
addComponent(gasIn,'CO2', 10, 'Nlitre/min')
newdatabase(gasIn)
TPflash(gasIn)

liqIn = thermo('srk',temperature,pressure)
addComponent(liqIn, 'water', 0.5, 'kg/min')
newdatabase(liqIn)
TPflash(liqIn)

# Calciulating equilibrium-line
eqsyst = thermo('electrolyte',temperature,pressure)
addComponent(eqsyst, 'methane', 0.5)
addComponent(eqsyst, 'CO2',0.0000001)
addComponent(eqsyst, 'water', 200.0)
addComponent(eqsyst, 'MDEA', 10.0)
reactionCheck(eqsyst)
newdatabase(eqsyst)
mixingRule(eqsyst,4)
TPflash(eqsyst)

xeq = []
yeq = []
for i in range(21):

xeq.append(molefrac(eqsyst,1)[2]+molefrac(eqsyst,4)[2])
    yeq.append(molefrac(eqsyst,1)[1])
    addComponent(eqsyst,'CO2',0.5)
    #addComponent(eqsyst,'methane',-1.0)
    TPflash(eqsyst)
    print 'eq ' ,i
```

```python
# Calculation operational-line
Lrate = moles(liqIn)
Grate = moles(gasIn)
print 'Lrate ' , Lrate
print 'Grate ' , Grate
Yin = molefrac(gasIn,1)[0]
Xin = 0
Yout = molefrac(gasIn,1)[0]/100.0
print 'yin ' , Yin
print 'yut ' , Yout

xop = xeq
yop = []
for i in range(len(xeq)):
    yop.append(Lrate/Grate*xeq[i]+Yout-Lrate/Grate*Xin)

#Find the number of transfer steps

eqpoly = polyfit.polyfit(yeq,xeq,10)
oppoly = polyfit.polyfit(xeq,yop,10)
xstep = []
ystep = []
ystep.append(Yout)
xstep.append(Xin)
i = 0
while(ystep[i]<Yin):
    print i
    xstep.append(eqpoly.gety([ystep[i]])[0])
    ystep.append(oppoly.gety([xstep[i]])[0])
    i = i+1
    print 'eq ' ,i

graph = graph2D.graph2D("Chemical Absorption Modelling")
graph.setxy(xeq,yeq,"equilibrium line")
graph.setxy(xeq,yop,"operation line")
graph.setxy(xstep,ystep,"step-line")
graph.setXaxisTitle("x-CO2 [-]")
graph.setYaxisTitle("y-CO2 [-]")
graph.show()
```

bubp.py

bubp.py

```
#
# Script bubp.py - calculation of saturated properties
of pure components
# Even Solbraa, 2001
#

# Create a thermodynamic system - using the preferred
equation of state (eg. srk,cpa,pr)
system = thermo('srk', temperature=300, pressure=1.01)
# Add a component to the system
addComponent(system,'water',1.0)
# Import molecular properties from database
newdatabase(system)
# set volume correction off - default is on
system.useVolumeCorrection(0)
# do a bubble point pressure flash
bubp(system)
# display system
show(system)
```

TPflash.py

```
#
# Script TPflash.py - calculation of saturated
properties of pure components
# Even Solbraa, 2001
#

# Create a thermodyanmic system - using the preferred
equation of state (eg. srk,cpa,pr)
system = thermo('srk', temperature=300.0,
pressure=10.0)
# Add a component to the system
addComponent(system,'CO2',1.0)
addComponent(system,'water',1.0)
# Import molecular properties from database
newdatabase(system)
# Select mixing rule classic/HV/WS/no
mixingRule(system,'classic')
# do a flash at constant temperature and pressure
TPflash(system)
# display system
show(system)
```

electrolyte.py

electrolyte.py

```
# electrolyte.py
# Fitting Calculation of osmotic and mean ionic activity coefficients
#
# test osmotic coefficient of a stron electrolyte solution

system = thermo('electrolyte',298.15,1.01325)
addComponent(system,'Na+',  0.00310498)
addComponent(system,'Cl-',  0.00310498)
addComponent(system,'water',1.0-2*0.00310498)
newdatabase(system)
system.init(0)
system.init(1)

print 'Osmotic Coefficient ',   system.getPhase(1).getOsmoticCoefficientOfWater()
print 'Mean Ionic coefficient ',  system.getPhase(1).getMeanIonicActivity(0,1)
```

Electrolyte-MDEA.py

electrolyte-MDEA.py

```python
# electrolyte-MDEA.py
# Fitting Calculation of activity coefficients n CO2-water-MDEA solution
#

system = thermo('electrolyte', (273.0+40.0), 100.15)
addComponent(system, 'CO2', 0.08)
addComponent(system, 'MDEA', 0.1)
addComponent(system, 'water', 1.0)
reactionCheck(system)
newdatabase(system)

mixingRule(system, 4)
print bubp(system)
print system.getPhase(1).getActivityCoefficient(1)
```

enhancement.py

```python
enhancement.py
#
# Script enhancement.py - calculation of saturated
properties of pure components
# Even Solbraa, 2001
#
#
# Create a thermodyanmic system - using the prefered
equation of state (eg. srk,cpa,pr)
# Add components to the system
system = thermo('electrolyte', 313.15, 5.0)
#addComponent(system,'methane', 80.00, 'Nlitre/min', 0)
#addComponent(system,'ethane', 10.00, 'Nlitre/min', 0)
addComponent(system, 'CO2', 10.00, 'Nlitre/min', 0)
addComponent(system, 'water', 0.10, 'kg/min', 1)
addComponent(system, 'MDEA', 0.10, 'kg/min', 1)

mixingRule(system, 'HV')
# Checking for possible chemical rections
reactionCheck(system)
# Imports parameters from database
newdatabase(system)
# Initializing physical properties
system.initPhysicalProperties()
# Setting amine-physical property model
system.setPhysicalPropertyModel(3)
# Creates a stirred cell object with diameter (meter)
# Adding the thermodynamic system to the cell
cellgeometry = geometry.stirredcell(0.074)
cell = node.stirredcell(system,cellgeometry)
# Setting stirrer speed (rpm)
cell.setStirrerSpeed(100.0/60.0)
# Setting stirrer diameter (meter)
cell.setStirrerDiameter(0.074)

#cell.initFlowCalc()
# Setting the time step
cell.setDt(10.00)
# Specify corrections to use
cell.getFluidBoundary().useFiniteFluxCorrection(0)
cell.getFluidBoundary().useThermodynamicCorrections(0)
# Iterates a specified number of time-steps

#cell.update()

flow.solve(cell,noneq=1,heattrans=0,masstrans=1)

print
cell.getFluidBoundary().getEnhancementFactor().getEnhan
cementVec(0)
print cell.display("testnode6");
print cell.getFluidBoundary().display('test')
```

```python
# thermoModel.py
# Example:    Creating a new thermodyanic model
# By:         Even Solbraa, 2001
# Create a ideal gas model and a liquid model based on Raults
# law
#

class idealgascomponent(ComponentDefault):
    def __init__(self):
        ComponentDefault()

    def fugcoef(self, phase):
        fugcalc = 1.0
        self.setFugacityCoefficient(fugcalc)
        return fugcalc

class idealliquidcomponent(ComponentDefault):
    def __init__(self):
        ComponentDefault()

    def fugcoef(self, phase):
        fugcalc =
self.getAntoineVaporPressure(phase.getTemperature())/phase.get
Pressure()
        self.setFugacityCoefficient(fugcalc)
        return fugcalc

class idealgasphase(PhaseDefault):
    def __init__(self):
        PhaseDefault()
        self.tempcomp = idealgascomponent()
        self.setComponentType(self.tempcomp)

    def getMolarVolume(self):
        return self.R*self.temperature/self.pressure

class idealliquidphase(PhaseDefault):
    def __init__(self):
        PhaseDefault()
        self.tempcomp = idealliquidcomponent()
        self.setComponentType(self.tempcomp)

    def getMolarVolume(self):
        return
    self.R*self.temperature/self.pressure/100.0

    def getGibbsEnergy(self):
        print 'gibbs ',
        PhaseDefault.getGibbsEnergy(self)
        return PhaseDefault.getGibbsEnergy(self)

class idealgasystem(SystemDefault):
    def __init__(self, T, P):
        SystemDefault.__init__(self, T,P)
        self.phasess = idealgasphase()
        self.setPhase(self.phasess)
        self.setTemperature(T)
        self.setPressure(P)

# some test code...

idgas = idealgasphase()
idliq = idealliquidphase()
tests = idealgasystem(390,1)
#tests = thermo('srk', 340,1)
tests.setPhase(idgas,0)
tests.setPhase(idliq,1)
#mixingRule(tests,2)

addComponent(tests, 'methanol',1)
addComponent(tests, 'water',1)
bubp(tests)
show(tests)
```

310

```python
#natgas-chart.py
systemName = thermo('srk',290,1.0)
addComponent(systemName, 'methane', 1.0)
addComponent(systemName, 'ethane', 1.0)
newdatabase(systemName)

#func = enthalpy
func = beta

b = phaseenvelope(systemName)
dewT = b.get('dewT')
dewP = b.get('dewP')
dewH = b.get('dewH')
bubT = b.get('bubT')
bubP = b.get('bubP')
bubH = b.get('bubH')

# Setter inn verdier i system
temp = graph.makeRealType('temperature')
pres = graph.makeRealType('pressure')
ent = graph.makeRealType('enthalpy')
temp_pres_tuple = RealTupleType(temp, pres)

# T-dewP-ent curve
func_temp_dewpres = FunctionType(temp, pres)
dewtemp_vals = []
dewtemp_vals.append(list(dewT))
dewtemp_set = Irregular1DSet(temp, dewtemp_vals)

dewpres_vals = []
dewpres_vals.append(list(dewP))

dewvals_ff = FlatField(func_temp_dewpres, dewtemp_set)
dewvals_ff.setSamples(dewpres_vals)

dewdata_ref = DataReferenceImpl("data_ref")
dewdata_ref.setData( dewvals_ff )

# T-bubP-ent curve
func_temp_bubpres = FunctionType(temp, pres)
bubtemp_vals = []
bubtemp_vals.append(list(bubT))
bubtemp_set = Irregular1DSet(temp, bubtemp_vals)
bubpres_vals = []
bubpres_vals.append(list(bubP))
bubvals_ff = FlatField(func_temp_bubpres, bubtemp_set)
bubvals_ff.setSamples(bubpres_vals)

bubdata_ref = DataReferenceImpl("data_ref")
bubdata_ref.setData( bubvals_ff )

# 2-D isocurve
#func = enthalpy

z = []
for pres2 in range(1,21):
    for temp2 in range(1,21):

z.append(func(systemName,(temp2*10.0+100.0),pres2*4)[0])

bef = []
bef.append(z)

func_temp_pres_ent = FunctionType(temp_pres_tuple, ent)
temp_pres_set = Linear2DSet(temp_pres_tuple, 100.0, 300.0, 20, 1.0, 80.0, 20)
entvals_ff = FlatField(func_temp_pres_ent, temp_pres_set)
entvals_ff.setSamples(bef)

entdata_ref = DataReferenceImpl("data_ref")
entdata_ref.setData(entvals_ff )

# Lager display og legger til akser
display = DisplayImplJ2D("display1")
tempMap = ScalarMap(temp, Display.XAxis )
presMap = ScalarMap(pres, Display.YAxis )
entMap = ScalarMap(ent, Display.IsoContour)
entMapCol = ScalarMap(ent, Display.RGB)
display.addMap(tempMap)
display.addMap(presMap)
display.addMap(entMap)
display.addMap(entMapCol)

display.addReference( bubdata_ref )
display.addReference( dewdata_ref )
display.addReference( entdata_ref )

display.getGraphicsModeControl().setScaleEnable(1)
isoControl = entMap.getControl()
#isoControl.setContourInterval(0.1, 0, 1.0, 0);
isoControl.enableLabels(1)

jframe = JFrame("My first VisAD application")
jframe.getContentPane().add(display.getComponent())
jframe.setSize(300, 300)
jframe.setVisible(1)
```

#CPA-fit.py
Script available from NeqSim-homepage
Script to long for inclusion in thesis

312

```python
# ActivityCalc.py
#
# Script ActivityCalc.py - calculation of saturated
properties of pure components
# Even Solbraa, 2001
#

# Create a thermodyanmic system - using the preferred
equation of state (eg. srk,cpa,pr)
system = thermo('srk', temperature=300.0,
pressure=10.0)
# Add a component to the system
addComponent(system,'MDEA',1.0)
addComponent(system,'water',1.0)
# Import molecular properties from database
newdatabase(system)
# Select mixing rule classic/HV/WS/no
mixingRule(system,'HV')
# do a flash at constant temperature and pressure
TPflash(system)
# display system
system.getPhase(1).getActivityCoefficient(0)
show(system)
```

freeze.py

```
#freeze.py
# freezing-pint calculation using an EOS
a = thermo('srk-s', 273.15, 1.0)
addComponent(a,'MDEA',0.01,'kg/min')
addComponent(a,'water',0.9,'kg/min')
newdatabase(a)
mixingRule(a,'HV')
solid(a)
freeze(a)
show(a)
```

314

pubp_amine.py

```
# bubp_amine.py
# Calculation of pubble point calculation in a CO2-
# MDEA-water system
system = thermo('electrolyte',310.0, 10.101)
addComponent(system,'CO2',0.041)
addComponent(system,'MDEA',0.1)
addComponent(system,'water',1.0)
reactionCheck(system)
newdatabase(system)
mixingRule(a,'HV')
bubp(system)
show(system)
```

TPflash_amine.py

```
#TPflash_amine.py
system = thermo('electrolyte',310.0, 10.1)
addComponent(system,methane,0.1)
addComponent(system,'CO2',0.041)
addComponent(system,'MDEA',0.1)
addComponent(system,'water',1.0)
reactionCheck(system)
newdatabase(system)

mixingRule(system,4)
TPflash(system)
show(system)
```

reactive-absorption.py

```python
#reactive-absoprtion.py
# Simulation of a chemical absorption process in MDEA
# in a packed column
# By Even Solbraa, Jan. 2002

testSystem = SystemFurstElectrolyteEos(313.315, 50.01325)
testOps = ThermodynamicOperations(testSystem)

pipe1 = ReactorData(0.25, 0.025)
pipe1.setPackingType("pallring","metal",50)

testSystem.addComponent("methane", 00000.11152187,"Nlitre/min",
0)
testSystem.addComponent("CO2", 3000.511152181 , "Nlitre/min",0)
testSystem.addComponent("water", 100.50220476 , "kg/min", 1)
testSystem.addComponent("MDEA", 100.502204876, "kg/min", 1)
testSystem.chemicalReactionInit()
testSystem.createDatabase(true)
testSystem.setMixingRule(4)
testOps.TPflash()
testSystem.addComponent("CO2", 2000.11152181 , "Nlitre/min", 0)
testSystem.setPhysicalPropertyModel(3)
testSystem.init_x_y()
testSystem.getPhases()[1].setTemperature(313.0)
testSystem.getPhases()[0].setTemperature(325.0)

test = TwoPhasePackedBedFlowNode(testSystem, pipe1)
test.setLengthOfNode(0.1)
test.setInterphaseModelType(1)
test.getFluidBoundary().useFiniteFluxCorrection(false)
test.getFluidBoundary().useThermodynamicCorrections(false)
test.setFlowDirection(-1.0)
test.initFlowCalc()
fileName = "c:/labsim/exp-abs-heat.txt";
test.write("node 0",fileName,true);

for i in range(120):
    test.calcFluxes()
    test.update()
    test.display()
    test.write(("node " +i ),fileName,false)
```

penloux.py

```
# penloux.py
# Calculates the density of the liquid using the Penloux
# volume correction model.
#

system = thermo(srk-s,298.15,1.01325)
addComponent(system,MDEA,1.0)
newdatabase(system)
system.init(0)
system.init(1)
volumecorrection(system,1)
show(system)
```

MonteCarlo.py

```python
MonteCarlo.py
# Calculation of uncertainties related to experiments in
# the HP-wetted wall column
# Created: Even Solbraa, 2002
#

temperature = 273.15+40.0
dt = 0.1
pressure = 100.0
dp = pressure/100.0
totalgasflow = 200.0
dgf = totalgasflow/50.0
totalliqflow = 0.35
dlf = totalliqflow/50.0
pipediameter = 0.025
dpd = pipediameter/100.0
pipelength = 1.0
pl = pipediameter/100.0
gascomp = 0.1
dgc = gascomp/50.0

for i in range(10):
    temp =
jet.random.Normal.staticNextDouble(temperature,dt)
    pres = jet.random.Normal.staticNextDouble(pressure,dp)
    gasflow =
jet.random.Normal.staticNextDouble(totalgasflow,dgf)
    liqflow =
jet.random.Normal.staticNextDouble(totalliqflow,dlf)
    pipediam =
jet.random.Normal.staticNextDouble(pipediameter,dpd)
    pipelen =
jet.random.Normal.staticNextDouble(pipelength,pl)
    co2frac =
jet.random.Normal.staticNextDouble(gascomp,dgc)
    system = thermo('electrolyte', temp, pres)
```

NeqSim scripts

```python
    addComponent(system,'nitrogen', gasflow* (1.0-co2frac),
'Nlitre/min', 0)
    addComponent(system,'CO2', gasflow*co2frac,
'Nlitre/min', 0)
    addComponent(system,'water', liqflow, 'kg/min', 1)
    addComponent(system,'MDEA', liqflow, 'kg/min', 1)
    reactionCheck(system)
    newdatabase(system)
    system.setPhysicalPropertyModel(3)
    mixingRule(system,'HV')
    geometry2 = geometry.pipe(pipediam, 0.005)
    flowtest = node.twophase(system,geometry2,'annular')
    flowtest.setLengthOfNode(pipelen)
    flow.solve(flowtest,heattrans=0,masstrans=1)
    print 'flux ',
flowtest.getFluidBoundary().getInterphaseMolarFlux(1)
    #show(flowtest)
```

```
# partpres.py
#
# This script is used to find the amount of methane (or
other component) giving a specified pressure
#
# Written by: Even Solbraa
#

# Correct system pressure
pressure = 100.0

# Sample point specifications
temperature = 273.15+40.0
molCO2 = 0.7
molMDEA = 1.0
#molWater = 15.433805160
molWater = 6.61448792672

systemName = thermo('electrolyte',temperature,pressure)
systemName.addComponent('methane', 0.1001)
systemName.addComponent('CO2', molCO2)
systemName.addComponent('MDEA', molMDEA)
systemName.addComponent('water', molWater)
mixingRule(systemName,'HV')
reactionCheck(systemName)
#newdatabase(systemName)

def testFunc(x):
    systemName.addComponent('methane',-
systemName.getPhase(0).getComponent(0).getNumberO
    fmoles())
    systemName.addComponent('methane', x)
    err = bubp(systemName)-pressure
    print 'err: ', err
    return err

print newton.newton(testFunc,0.00222738)
show(systemName)
```

Appendix H   Calibration of Experimental Equipment

The high-pressure wetted wall column designed and built during this work contained many different measurement devices. In this appendix the calibration curves for these devices are presented.

H.1   Temperature Measurement Accuracy

The temperature was measured with PT100 elements. The PT100 elements measure the temperature directly and were calibrated on installation. The accuracy of the temperature measurements is approximately 0.1 K.

H.2   Pressure Transmitter Calibration

The absolute pressure was measured using two pressure transducers (Digibar) giving a mV signal as a function of pressure. The pressure transducers were calibrated using a reference pressure transducer from ProServ. The accuracy of the pressure measurements is better than ± 1% of measured pressure. The calibration and scatter curve for the pressure transducer P1 are given in figure H.1 and H.2.
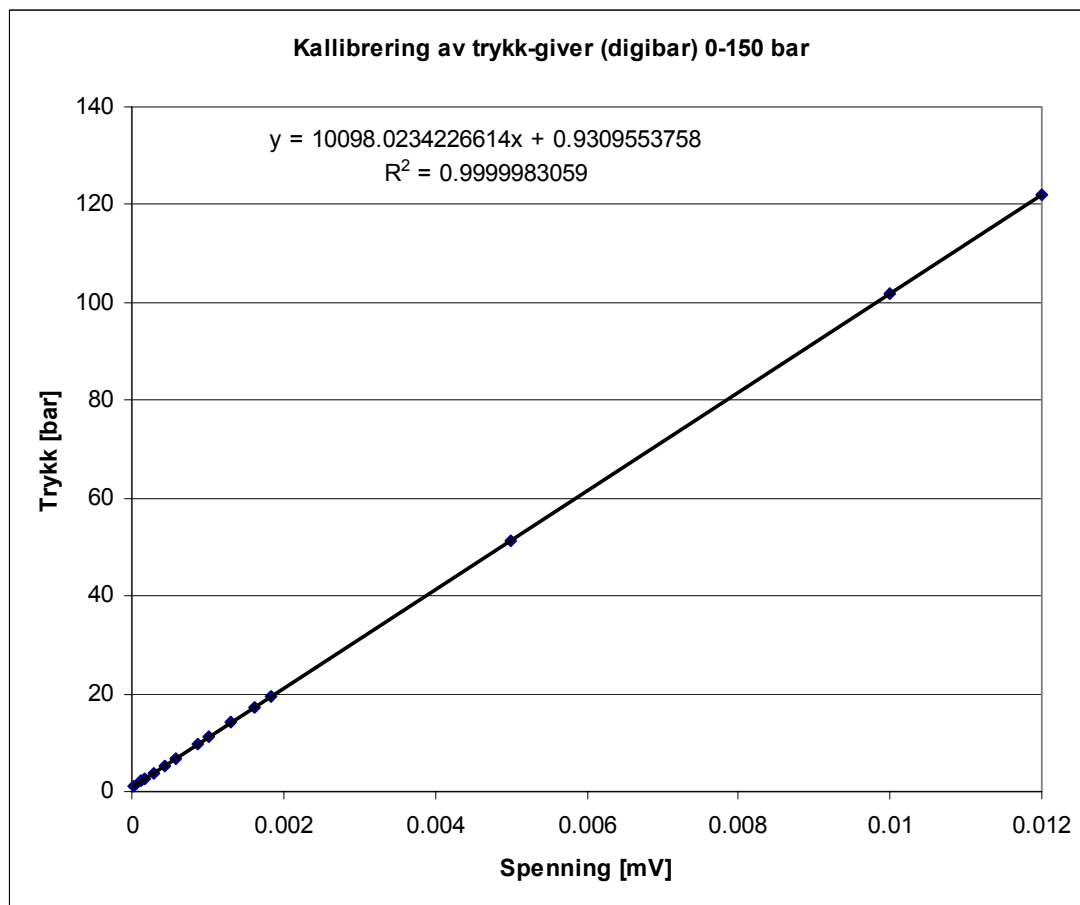
Figure H.1 Pressure transducer P1

Data scatter (digibar P1)
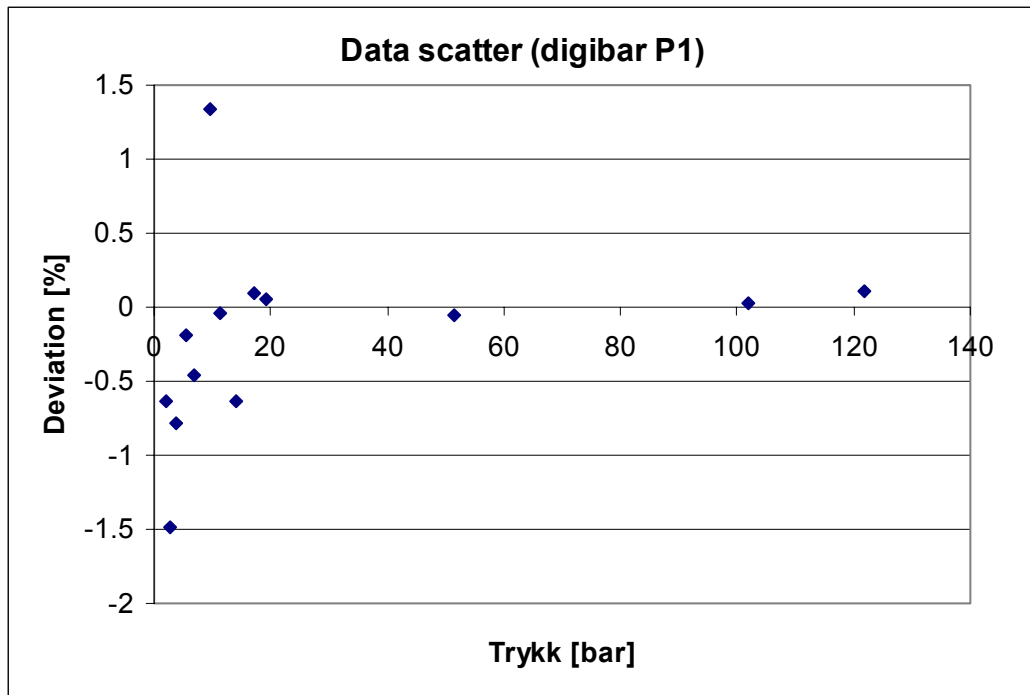
Figure H.2 Accuracy of pressure transducer P1

H.3   Liquid Turbine Flow Meter Calibration

The liquid flow rate was measured using a liquid turbine flow meter of type Swissflow 800/6. The calibration and scatter curve for the turbine flow meter are given in figure H.3 and H.4. The accuracy of the measurements was better than 2% of measured value.
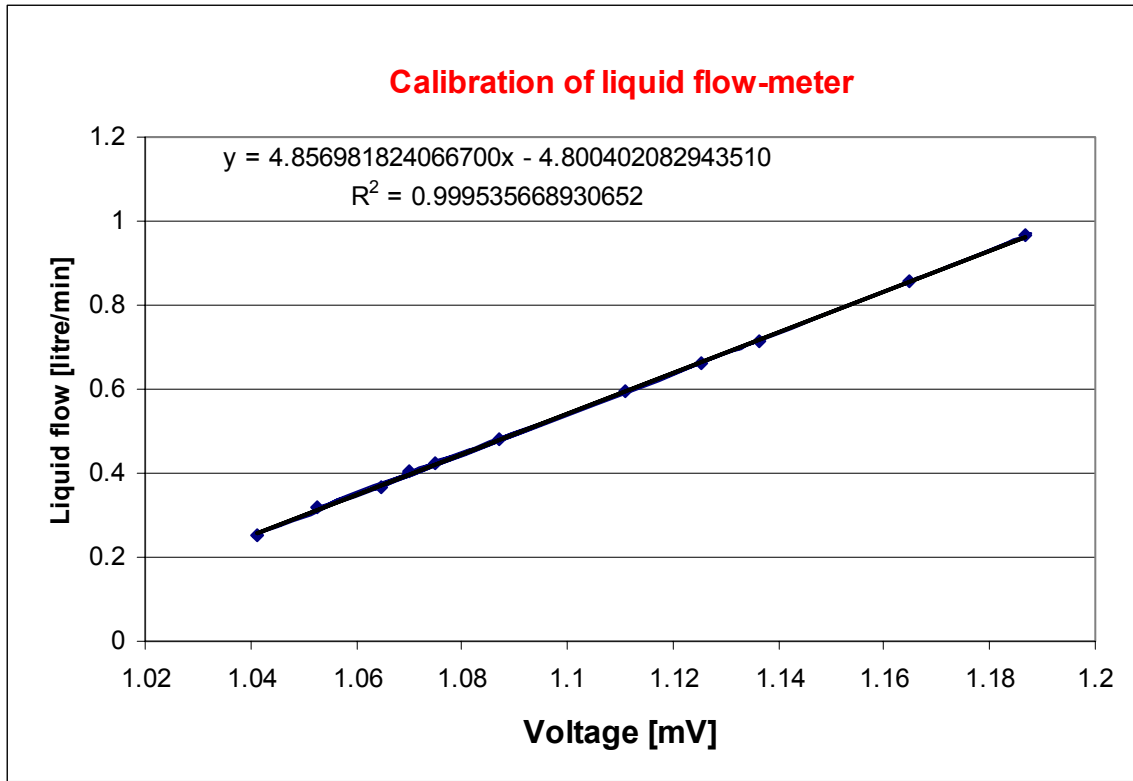
Figure H.3 EMO turbine liquid flow meter
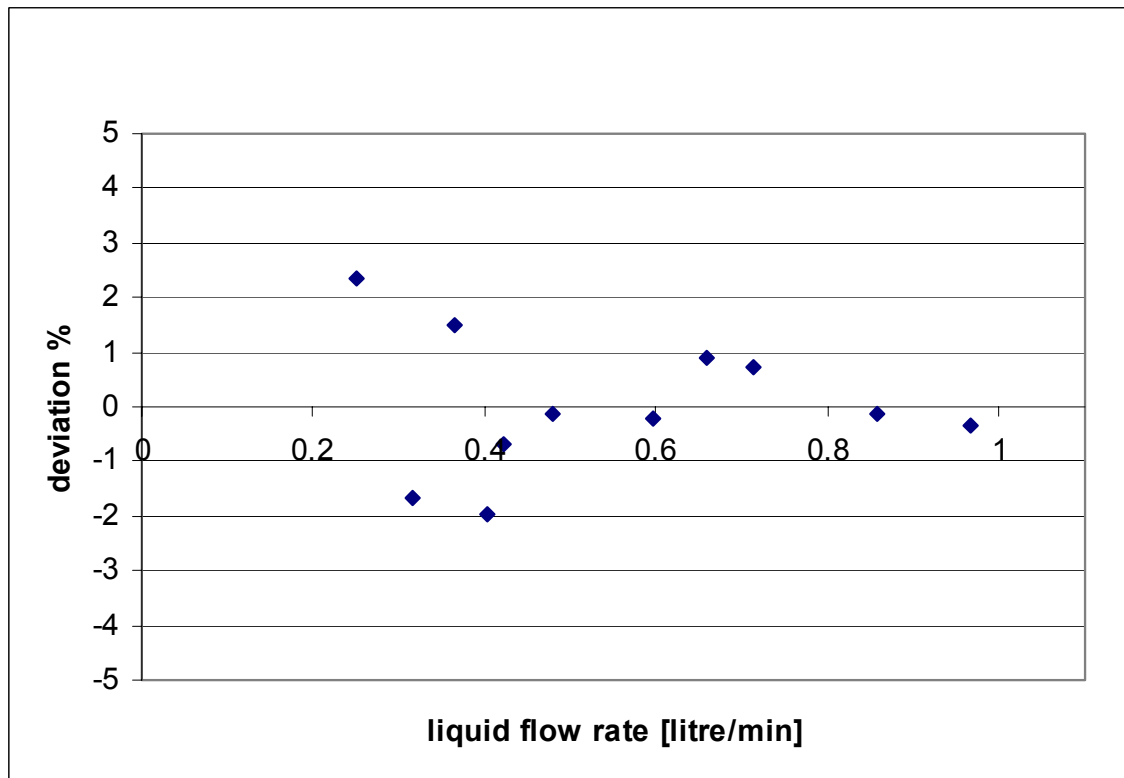
Figure H.4 Scatter for EMO turbine liquid flow meter

H.4 Gas Flow Meters

The gas flow meters were of type Bronkhorst Mass Flow Meter type F-112AC-HD-44-V for CO_2 and Bronkhorst Mass Flow Meter type F for the total gas flow. The gas flow meters were calibrated using a standard gas calibrator from Flow Teknikk. The calibration curve for the CO_2 flow meter is given in figure H-5 and the total flow meter in figure H-6. The accuracy of the flow meters was less than ±1.5 % of measured value.

Calibration of CO_2 flow meter

$$y = 42.5061514030x - 42.3275497215$$
$$R^2 = 0.9994139895$$
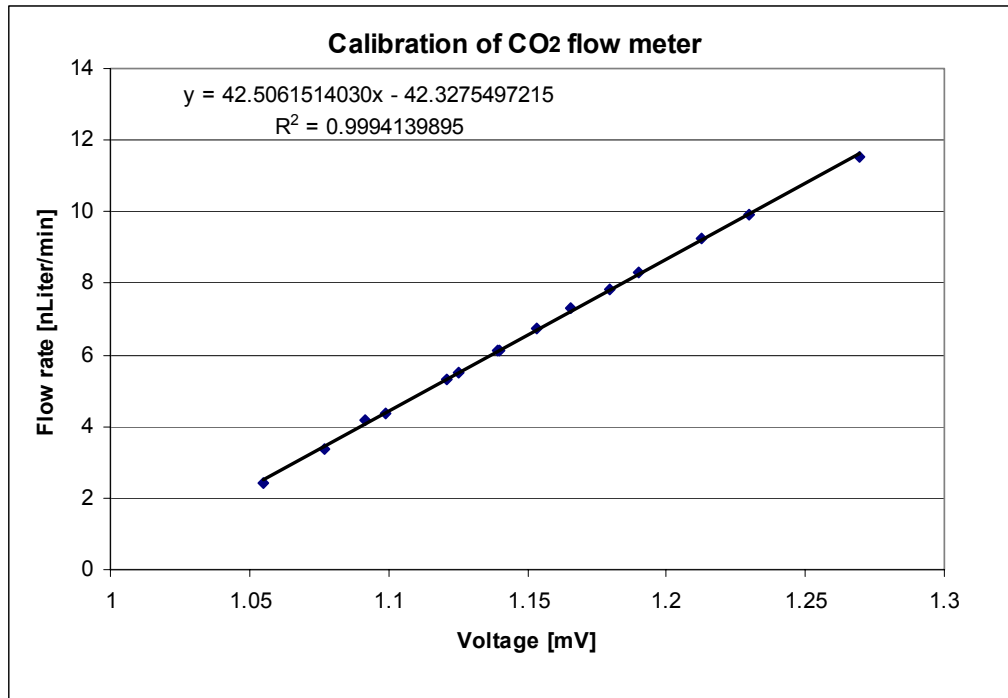
Figure H-5 Calibration curve of the CO_2 flow meter
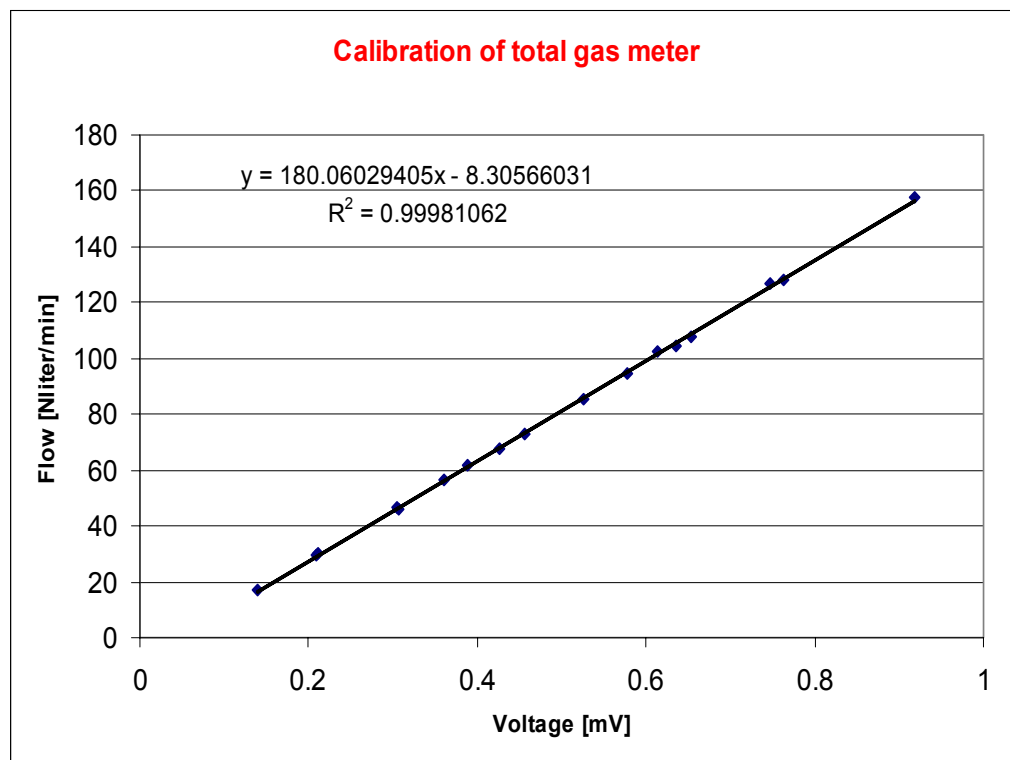
Figure H-6 Calibration of total gas flow meter

H.5   Gas Chromatograph Analysis

The gas composition was analyzed using a standard gas chromatograph technique. The chromatograph was calibrated using a standard calibration gas from Hydro Gas (90.1 % N_2+ 9.9 % CO_2). The calibration points (repeated experiments) are given in figure H-7 and H-8 for CO_2 and nitrogen.
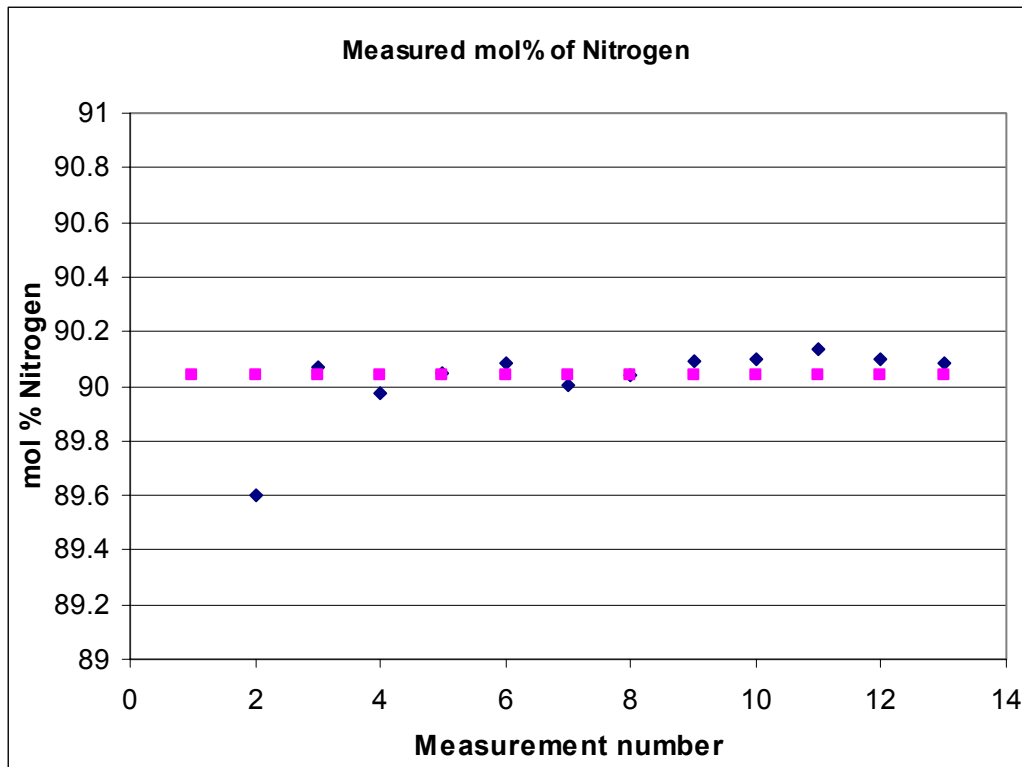
Figure H-7 Measured mol% nitrogen for repeated experiments
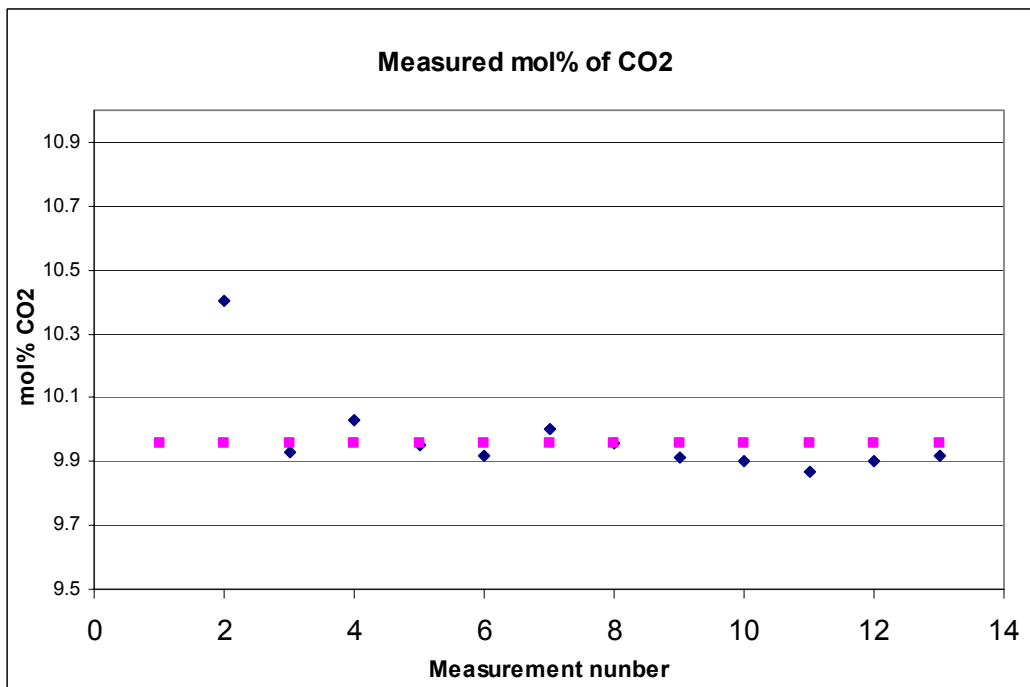
Figure H-8 Measured mol% CO$_2$ for repeated experiments

H.6   Volume of the Wetted Wall Column

The total gas volume in the high-pressure wetted wall column was measured from differential pressure evaluations when filling a known amount of gas into the wetted wall column. The results from 7 independent measurements are given in figure H-9.
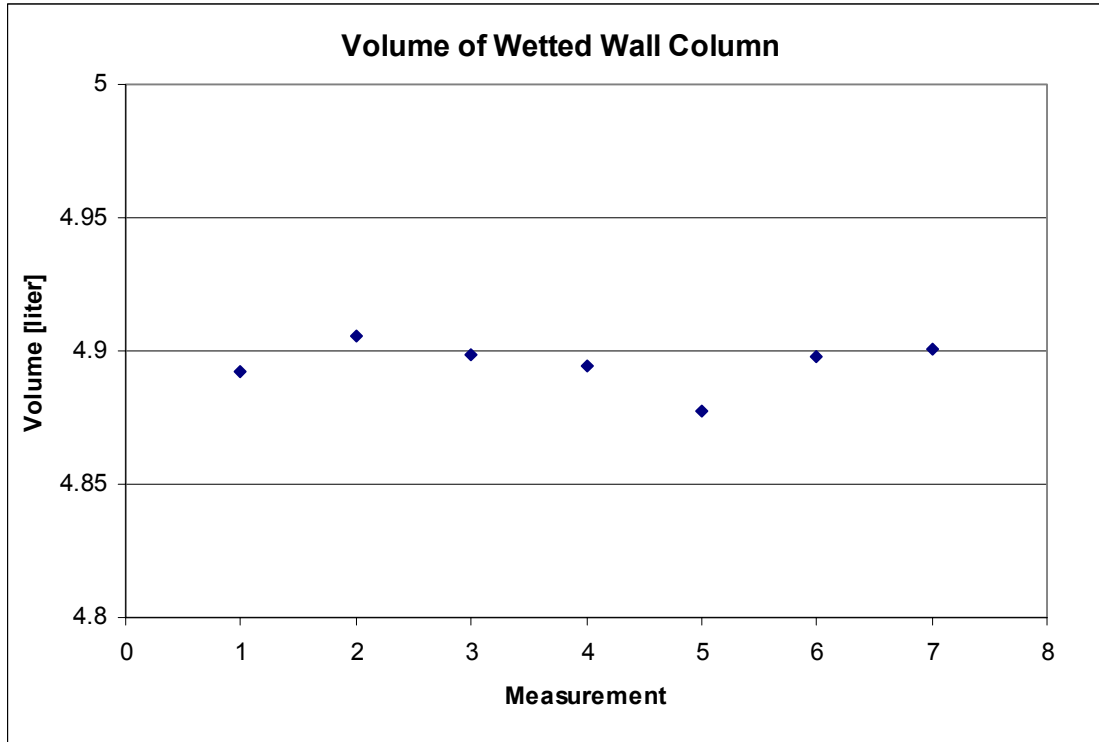
Figure H-9 Measurement of total gas volume in wetted wall column

H.7   Estimation and treatment of uncertainty in measurements

Estimation of errors and uncertainties in measurements can be calculated from the techniques described in chapter 7. The uncertainty in the measured absorption rate can be estimated from the individual uncertainties in the measurement devices from the relation

$$\delta Q_{CO_2} = \frac{\partial Q_{CO_2}}{\partial P}\Delta P_{\exp} + \frac{\partial Q_{CO_2}}{\partial T_{gas}}\Delta T_{\exp,gas} + \frac{\partial Q_{CO_2}}{\partial T_{liq}}\Delta T_{\exp,liq} + \frac{\partial Q_{CO_2}}{\partial Q_{liq}}\Delta Q_{liq} + \frac{\partial Q_{CO_2}}{\partial Q_{gas}}\Delta Q_{gas} +$$

$$\frac{\partial Q_{CO_2}}{\partial d_{pipe}}\Delta d_{\exp,pipe} + \frac{\partial Q_{CO_2}}{\partial L_{pipe}}\Delta L_{\exp} + \frac{\partial Q_{CO_2}}{\partial y_{CO_2}}\Delta y_{CO_2}$$

(H.1)

where Q_{CO2} is the measured gas flow rate of CO_2 (absorption rate). In this equation we have assumed that the main contributions to the errors comes from measurements errors in pressure, temperature, inner pipe diameter(d), contact length(L) liquid flow rate, the total gas flow rate and the gas composition (y_{CO2}).

The uncertainties in the pressure, temperate and flow measurements are estimated as:

$$\Delta P_{exp} = \frac{P}{100} \quad \Delta T_{gas} = 0.1 \quad \Delta T_{liq} = 0.1 \quad \Delta Q_{gas} = \frac{Q_{exp}}{50} \quad \Delta Q_{liq} = \frac{Q_{exp}}{50}$$

$$\Delta d_{pipe} = \frac{d_{pipe}}{100} \quad \Delta L_{pipe} = \frac{L_{pipe}}{100} \quad \Delta y_{CO_2} = \frac{y_{CO_2}}{50}$$

Estimated uncertainties in calculated absorption rates of CO_2 in the amine solution can be calculated by introducing these values in equation (H.1). A problem we are facing is however calculating the derivatives in equation (H.1). Since we are working with very complicated mathematical models – these derivatives can not be represented by analytical expressions.

An alternative method to calculate the experimental uncertainties is the use of the Monte Carlo methods as described in chapter 7. In these methods we will have to know the standard deviations of the dependent values in the mathematical models. These standard deviations must be estimated from the calibrations curves and the uncertainty analysis of each measurement.

In this work the standard deviations of the measured values are (conservative estimates)

$$\sigma_{P_{exp}} = \frac{P}{100} \quad \sigma_{T_{gas}} = 0.1 \quad \sigma_{T_{liq}} = 0.1 \quad \sigma_{Q_{gas}} = \frac{Q_{exp}}{50} \quad \sigma_{Q_{liq}} = \frac{Q_{exp}}{50}$$

$$\sigma_{d_{pipe}} = \frac{d_{pipe}}{100} \quad \sigma_{L_{pipe}} = \frac{L_{pipe}}{100} \quad \sigma_{CO_2} = \frac{y_{CO_2}}{50}$$

By calculating the absorption rate of CO_2 at varying pressures, temperatures and flow rates – uncertainties can be calculated. This was done in this work – and the results from the Monte Carlo simulations are presented in Table H-1 (physical mass transfer of CO_2 into water) and Table H-2 (reactive mass transfer of CO_2 into MDEA solutions). The NeqSim script used to do these calculations is presented in the script: MonteCarlo.py, p. 319. The results from the Monte Carlo simulations are presented in figures H-1 to H-4. All measured errors were assumed to be randomly distributed (normal distribution), and the values were picked using the Java-Colt statistical library. The errors seems to always be lower than 4% for physical mass transfer and lower than 4-5% for reactive mass transfer into MDEA solutions. It should be remarked that such an uncertainty analysis is difficult – and should therefore be treated only as estimates.

Table H-1 Estimated experimental errors in experiments with nitrogen, CO_2 and water (physical mass transfer). In all estimates the partial pressure of CO_2 was 10 bar and the total gas circulation rate was 200 NL/min.

Case	Average Calculated Absorption Flux CO_2 [mol/m^2sec]	Gas /Liquid Temperature [°C]	Total Pressure [bar]	Liquid Circulation rate [L/min]	Estimated Uncertanty[1] [%]
1	0.03465	25	100	1.0	± 4%
2	0.03764	25	100	1.5	± 4%
3	0.0358	40	100	1.0	± 4-5%
4	0.4337	40	100	1.5	± 4-5%

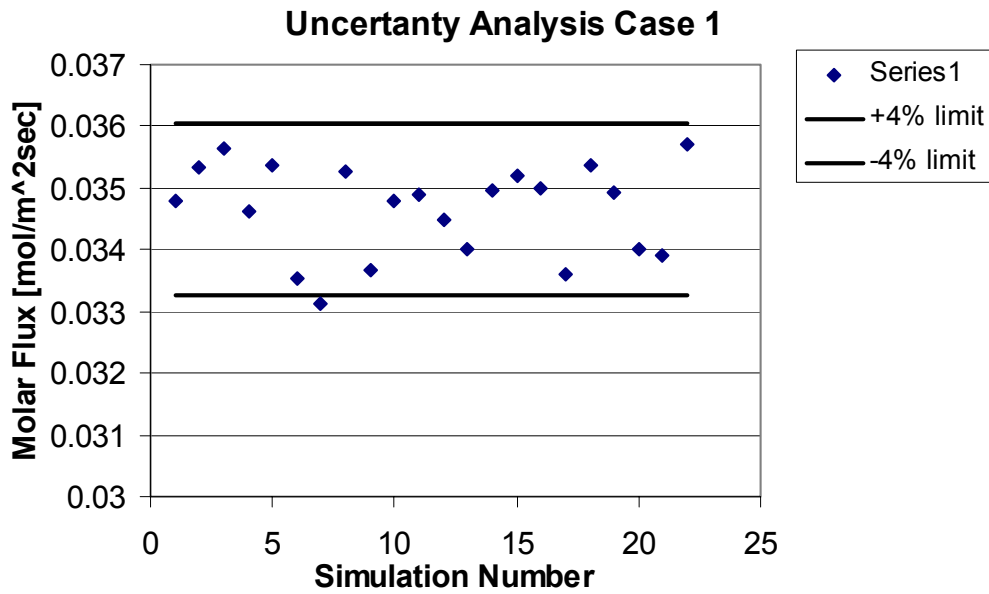1) About 97% confidence interval. See figure H-1 and H-2

Figure H-1. Monte Carlo simulation of physical mass transfer in a nitrogen, CO$_2$ and water system (case 1 from table H-1). *Script: MonteCarlo.py, p. 319*
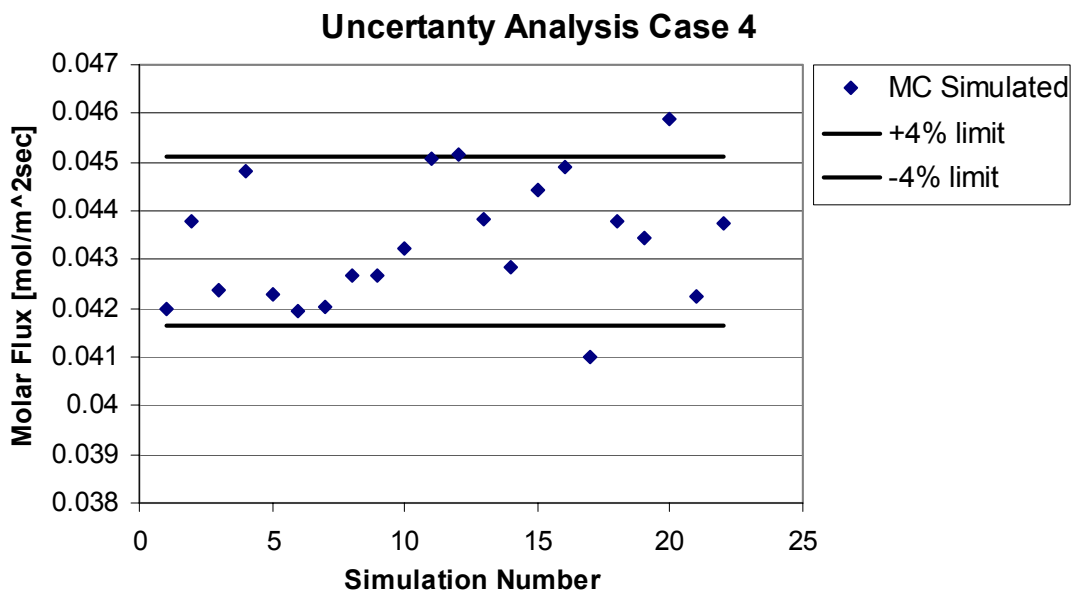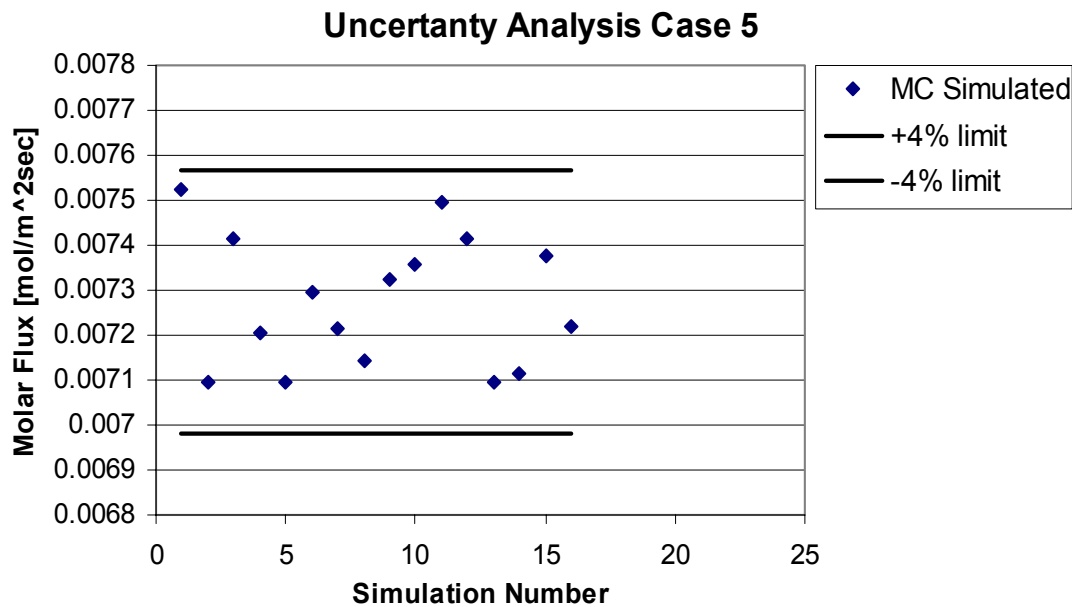

Figure H-2. Monte Carlo simulation of physical mass transfer in a nitrogen, CO$_2$ and water system (case 3 from table H-1). *Script: MonteCarlo.py, p. 319*

Table H-2 Estimated experimental errors in experiments with nitrogen, CO₂ , MDEA (50wt%) and water (reactive mass transfer). In all estimates the partial pressure of CO₂ was 10 bar and the total gas circulation rate was 200 NL/min.

Case	Average Calculated Absorption Flux CO$_2$ [mol/m^2sec]	Gas /Liquid Temperature [°C]	Total Pressure [bar]	Liquid Circulation rate [L/min]	Estimated Error [%]
5	0.00727	25	100	0.5	± 4%
6	0.00731	25	100	0.7	± 4%
7	0.00878	40	100	0.5	± 4%
8	0.00890	40	100	0.7	± 4%

1) About 97% confidence interval. See figure H-3 and H-4

Figure H-3. Monte Carlo simulation of reactive mass transfer in a nitrogen, CO₂, MDEA and water system in a wetted wall column (case 5 from table H-2). *Script: MonteCarlo.py, p. 319*
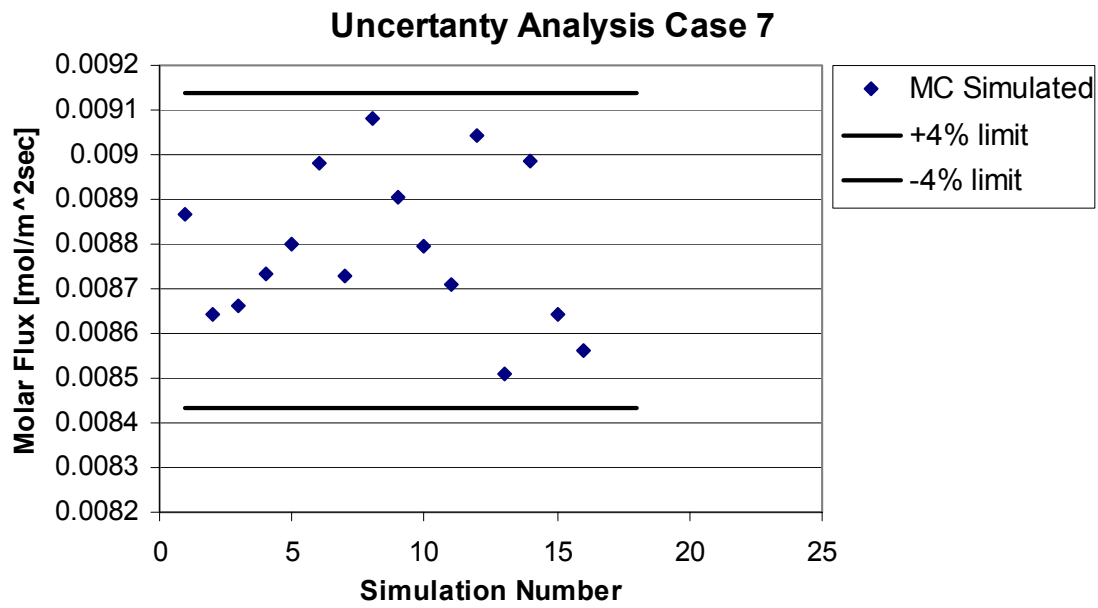
Figure H-4. Monte Carlo simulation of reactive mass transfer in a nitrogen, CO_2, MDEA and water system in a wetted wall column (case 7 from table H-2). *Script: MonteCarlo.py, p. 319*

Appendix I   NeqSim Users Guide

The users guide can be downloaded from the NeqSim homepage at:

www.stud.ntnu.no/~solbraa/neqsim